

AD-A169 964

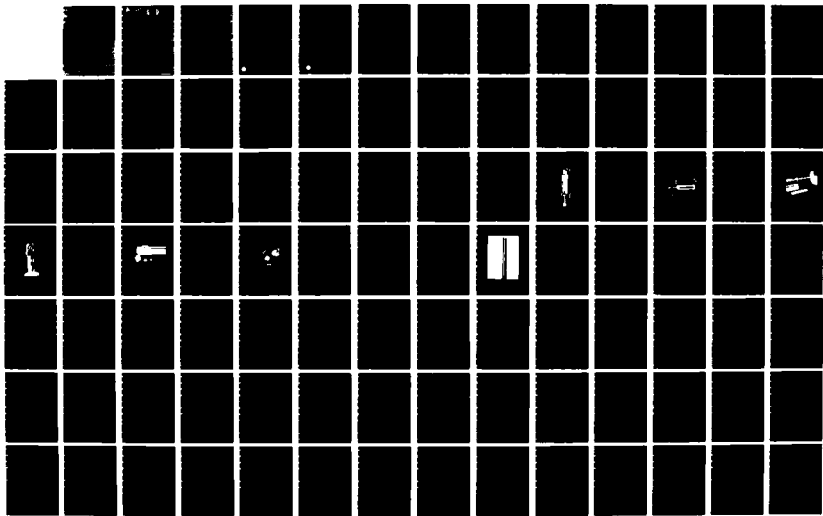
HIGH SPECIFIC HEAT DIELECTRICS AND KAPITZA RESISTANCE  
AT DIELECTRIC BOUND (U) WESTINGHOUSE RESEARCH AND  
DEVELOPMENT CENTER PITTSBURGH PA P W ECKELS ET AL

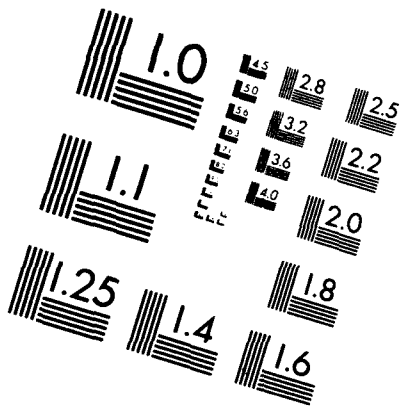
1/5

UNCLASSIFIED

30 SEP 85 AFOSR-TR-86-0477 F49620-83-C-0129 F/G 20/13

NL





MICROCOPY RESOLUTION TEST CHART  
NATIONAL BUREAU OF STANDARDS-1963-A

**UNCLASSIFIED**

**DTIC ELECTE**

JUL 24 1986

2

REPORT DOCUMENTATION PAGE

**AD-A169 964**

1b. RESTRICTION MARKINGS

3. DISTRIBUTION AVAILABILITY OF REPORT  
Approved for public release  
Distribution unlimited

2b. DECLASSIFICATION DOWNGRADING SCHEDULE

4. PERFORMING ORGANIZATION REPORT NUMBER(S)

5. MONITORING ORGANIZATION REPORT NUMBER(S)

**AFOSR-TR-83-0014-77**

6a. NAME OF PERFORMING ORGANIZATION  
Westinghouse Research and  
Development Center

6b. OFFICE SYMBOL  
(If applicable)

7a. NAME OF MONITORING ORGANIZATION  
DCASMA; Pittsburgh S3111A

6c. ADDRESS (City, State and ZIP Code)  
1310 Beulah Road  
Pittsburgh, Pennsylvania 15235

7b. ADDRESS (City, State and ZIP Code)  
1610 - S Federal Bldg.  
1000 Liberty Ave.  
Pittsburgh, PA 15222

8a. NAME OF FUNDING SPONSORING  
ORGANIZATION  
AFOSR

8b. OFFICE SYMBOL  
(If applicable)

9. PROCUREMENT INSTRUMENT IDENTIFICATION NUMBER  
F49620-83-C-0129

8c. ADDRESS (City, State and ZIP Code)  
Bolling Air Force Base  
Building 410  
Washington, DC 20332

10. SOURCE OF FUNDING NOS

PROGRAM ELEMENT NO.	PROJECT NO.	TASK NO.	WORK UNIT NO.
61102F	2301	A7	

11. TITLE (Include Security Classification)  
(See reverse side, No. 11)

12. PERSONAL AUTHOR(S)  
Eckels, P.W., Lawless, W.N., Parker, J.H., Jr., Patton, B.R., Clark, C.F. & Arenz, R.W.

13a. TYPE OF REPORT  
Final

13b. TIME COVERED  
FROM 8/1/83 TO 9/30/85

14. DATE OF REPORT (Yr., Mo., Day)  
1985, Sept. 30

15. PAGE COUNT  
413

16. SUPPLEMENTARY NOTATION

Prepared in cooperation with Subcontract CeramPhysics, Inc., P.O. Box 346, Westerville, Ohio with support from B. R. Patton at Ohio State.

17. COSATI CODES		
FIELD	GROUP	SUB GR

18. SUBJECT TERMS (Continue on reverse if necessary and identify by block number)

19. ABSTRACT (Continue on reverse if necessary and identify by block number)

This program has two efforts: Kapitza and thermal properties studies. Two separate Kapitza conductance test facilities have been designed and fabricated for both solid+solid and for solid+liquid He II measurements. Preliminary data has been obtained for copper to TlCl interface conductance and also for KBr and LiF thermal conductance to Helium II. For the latter two materials, the test dewars were designed to allow cleaving of the samples under liquid helium. The Kapitza conductance of both samples was very near the phonon radiation limit providing strong evidence that the anomalous Kapitza conductance is not the result of surface contamination. (Continued on reverse side.)

20. DISTRIBUTION AVAILABILITY OF ABSTRACT  
UNCLASSIFIED/UNLIMITED  SAME AS RPT  DTIC USERS

21. ABSTRACT SECURITY CLASSIFICATION  
Unclassified

22a. NAME OF RESPONSIBLE INDIVIDUAL  
**MAJ BRUCE L. Smith**

22b. TELEPHONE NUMBER  
(Include Area Code)  
**202/767-4908**

22c. OFFICE SYMBOL  
**RF**

DD FORM 1473, 83 APR

EDITION OF 1 JAN 73 IS OBSOLETE

**UNCLASSIFIED**

DTIC FILE COPY

UNCLASSIFIED

SECURITY CLASSIFICATION OF THIS PAGE

11. High Specific Heat Dielectrics and Kapitza Resistance at Dielectric Boundaries.

19. (Cont'd)

Thermal properties work has included the measurement of the specific heat and thermal conductivity of the  $\text{CdCr}_2\text{O}_4$  spinels and of several CsCl structure heavy metal halides in the temperature range of 1.5 to 35K. The specific heat data for the spinels was analyzed in terms of both lattice phonons and magnetic contributions. The dependence of the spinels' thermal conductivity on magnetic fields up to 15T was studied and magnetocaloric data has been obtained. For both the Zn and Cd spinels, the latter results showed a paramagnetic behavior with demagnetization cooling and magnetization heating. Theory has been developed to explain some of the magnetocaloric effects in the new spinels,  $\text{CdCr}_2\text{O}_4$  and  $\text{ZnCr}_2\text{O}_4$ .

SECURITY CLASSIFICATION OF THIS PAGE

**AFOSR-TR- 86-0477**

Final Report

August 1, 1983 to September 30, 1985

**HIGH SPECIFIC HEAT DIELECTRICS AND  
KAPITZA RESISTANCE AT DIELECTRIC  
BOUNDARIES**

by

P. W. Eckels, W. N. Lawless,  
J. H. Parker, Jr., B. R. Patton,  
C. F. Clark and R. W. Arenz

Westinghouse Electric Corporation  
Research and Development Center  
Pittsburgh, Pennsylvania 15235

AFOSR Contract No. F49620-83-C-0129

Research sponsored by the Air Force  
Office of Scientific Research, Air Force  
Systems Command, United States Air Force



**Westinghouse R&D Center  
1310 Beulah Road  
Pittsburgh, Pennsylvania 15235**

Approved for public release;  
distribution unlimited.

86 7 23 0 90

**Final Report**

**August 1, 1983 to September 30, 1985**

**HIGH SPECIFIC HEAT DIELECTRICS AND  
KAPITZA RESISTANCE AT DIELECTRIC  
BOUNDARIES**

by

**P. W. Eckels, W. N. Lawless,  
J. H. Parker, Jr., B. R. Patton,  
C. F. Clark and R. W. Arenz**

**Westinghouse Electric Corporation  
Research and Development Center  
Pittsburgh, Pennsylvania 15235**

**AFOSR Contract No. F49620-83-C-0129**

**Research sponsored by the Air Force  
Office of Scientific Research, Air Force  
Systems Command, United States Air Force**

**AIR FORCE OFFICE OF SCIENTIFIC RESEARCH (AFOSR)  
NOTICE OF TRANSMITTAL TO PUBLIC  
This technical report has been reviewed and is  
approved for public release IAW AFR 190-12.  
Distribution is unlimited.  
MATTHEW J. KEEPER  
Chief, Technical Information Division**



**Westinghouse R&D Center  
1310 Beulah Road  
Pittsburgh, Pennsylvania 15235**

Qualified requesters may obtain additional copies from the Defense Documentation Center; all others should apply to the Clearinghouse for Federal Scientific and Technical Information.

Accession For	
NTIS CRA&I	<input checked="" type="checkbox"/>
DTIC TAB	<input type="checkbox"/>
Unannounced	<input type="checkbox"/>
Justification .....	
By .....	
Distribution /	
Availability Codes	
Dist	Avail and/or Special
A-1	



Reproduction, transition, publication, use and disposal in whole or in part by or for the United States Government is permitted.

TABLE OF CONTENTS

	<u>Page</u>
1. TITLE PAGE . . . . .	1
2. ABSTRACT . . . . .	2
3. PROGRAM OBJECTIVES . . . . .	3
4. SUMMARY AND CONCLUSIONS. . . . .	4
4.1 Kapitza Studies . . . . .	4
4.1.1 Kapitza Conductance of LiF and KBr Cleaved Under He II. . . . .	5
4.1.2 Kapitza Research: Solid-Solid. . . . .	7
4.1.3 References. . . . .	11
4.2 Experimental Thermal Properties Studies . . . . .	11
4.2.1 Heavy-metal Ion Alkali Halides. . . . .	11
4.2.2 Cadmium and Zinc Chromite Spinel . . . . .	13
Specific Heat . . . . .	13
Magnetocaloric Effects. . . . .	15
Thermal Conductivity. . . . .	15
4.2.3 Magnetic Columbite Studies. . . . .	16
4.2.4 Discussion. . . . .	16
4.2.5 Conclusions . . . . .	17
4.3 Theoretical Thermal Properties Studies. . . . .	18
5. PUBLICATIONS . . . . .	21
6. PERSONNEL. . . . .	22
Appendix A: SOLID TO HE II KAPITZA STUDIES. . . . .	A-1
KAPITZA CONDUCTANCE OF CRYSTALS CLEAVED UNDER HE II	
ABSTRACT. . . . .	A-2

TABLE OF CONTENTS (Cont'd)

	<u>Page</u>
1. INTRODUCTION . . . . .	A-3
2. EXPERIMENTAL APPARATUS . . . . .	A-5
3. SAMPLE PREPARATION . . . . .	A-12
4. EXPERIMENTAL PROCEDURE . . . . .	A-16
5. DATA REDUCTION . . . . .	A-19
6. REFERENCES . . . . .	A-22
Appendix B: SOLID-SOLID KAPITZA STUDIES. . . . .	B-1
Kapitza Studies I. Probe Design and Construction, 1/5/84. .	B-2
Kapitza Studies II. Preliminary Tests, 10/10/84 . . . . .	B-8
Kapitza Studies III. CsI - Copper Interfaces, 2/15/85 . . .	B-16
Kapitza Studies IV. Low Thermal Conductivity Interfaces, 8/8/85 . . . . .	B-23
Appendix C: ALKALI HALIDE THERMAL PROPERTIES STUDIES. . . . .	C-1
Specific heat and thermal-conductivity measurements on cesium and thalious halide crystals at low temperatures, 11/15/84 . . . . .	C-2
Alkali Halide Studies, I. Experimental Studies, 11/1/83. .	C-12
Alkali Halide Studies, II. Data Analyses, 12/15/83 . . . .	C-29
Alkali Halide Studies, III. Magnetoelectric Measurements on CsBr at Low Temperatures, 7/31/84 . . . . .	C-48
Appendix D: SPINEL THERMAL PROPERTIES STUDIES . . . . .	D-1
Spinel Studies, I. Broad Temperature Range Thermal Measurements, 9/2/83 . . . . .	D-2

TABLE OF CONTENTS (Cont'd)

	<u>Page</u>
Spinel Studies, II. Spinel Specific Heats, 10/1/83 . . . .	D-10
Spinel Studies, III. Analyses of Spinel Specific Heats, 1/23/84. . . . .	D-21
Spinel Studies, IV. Magnetic Entropies and Enthalpies, 3/14/84. . . . .	D-30
Spinel Studies, V. Literature Survey, 4/17/84. . . . .	D-40
Spinel Studies, VI. Critical Exponents, 6/14/84. . . . .	D-53
Spinel Studies VII. Magnetocaloric Effects, 5/18/84. . . .	D-72
Spinel Studies VIII. Thermal Conductivities in Intense Magnetic Fields, 5/7/84. . . . .	D-87
Spinel Studies XI. Spin Densities, 8/15/84 . . . . .	D-104
Spinel Studies XII. Re-examination of Critical Exponents, 3/1/85 . . . . .	D-115
Spinel Studies XIII. Doping Studies, 4/1/85. . . . .	D-126
Spinel Studies XIV. Careful Measurements of Thermal Conductivities in the Neighborhood of $T_N$ , 5/3/85 . . . .	D-134
Spinel Studies XV. $Fe^{3+}$ Doping in C(9/1)--Specific Heat Measurements, 7/17/85. . . . .	D-141
Spinel Studies XVI. $Fe^{3+}$ Doping in C(9/1)--Thermal Conductivity Measurements, 8/8/85. . . . .	D-146
Columbite Studies I. Critical Exponents, 6/3/85. . . . .	D-150

TABLE OF CONTENTS (Cont'd)

	<u>Page</u>
Appendix E: THEORETICAL THERMAL PROPERTIES STUDIES . . . . .	E-1
Spinel Studies I. Structural Studies, 5/7/84. . . . .	E-2
Spinel Studies II. Theoretical Models, 7/12/84. . . . .	E-14
Spinel Studies III. Thermal Properties. . . . .	E-29
Spinel Studies IV. Thermal Conductivity, 11/15/84 . . . . .	E-37
Spinel Studies V. Comparison with Experiment:	
Specific Heat, 8/15/85. . . . .	E-48
Spinel Studies VI. Comparison with Experiment:	
Thermal Conductivity, 8/30/85 . . . . .	E-68
Spinel Studies VII. Impurity Models, 9/7/85 . . . . .	E-84

1. Final Report, Fundamental Physics Studies on High-Specific-Heat Dielectrics and Kapitza Resistance at Dielectric Boundaries

AFOSR Contract No. F49620-83-C-0129

P. W. Eckels, J. H. Parker Jr., W. N. Lawless, C. F. Clark,  
R. W. Arenz and B. R. Patton

## 2. ABSTRACT

This program is divided into two separate parts: Kapitza and thermal properties studies. Two separate Kapitza conductance test facilities have been designed and fabricated for both solid-solid and for solid-liquid He II measurements. Data has been obtained for copper to TlCl, Helium II.

The Kapitza conductance of LiF and KBr single crystals has been measured immediately after cleaving under pure He II. Heating techniques were used to evaluate the Conductance and it approaches the phonon radiation limit for these materials. Cleaving LiF under He II reduced the Kapitza conductance compared to an aged, cleaved surface by only a small fraction. Despite the very good cleaved surface obtained with LiF crystals, the results suggest that sufficient *micro-fracturing* of the surface occurs upon cleaving to significantly increase the Kapitza conductance over the acoustic mismatch theory values. These results are in contradiction to results obtained by phonon reflection techniques.

Thermal properties work has included the measurement of the specific heat and thermal conductivity of the  $\text{CdCr}_2\text{O}_4$  and  $\text{ZnCr}_2\text{O}_4$  spinels and of several CsCl structure heavy metal halides in the temperature range of 1.5 to 35K. The specific heat data for the spinels was analyzed in terms of both lattice phonons and magnetic contributions. The dependence of the spinels' thermal conductivity on magnetic fields up to 15T was studied and magnetocaloric data has been obtained. For both the Zn and Cd spinels, the latter results showed a paramagnetic behavior with demagnetization cooling and magnetization heating.

### 3. PROGRAM OBJECTIVES

- Carry out experimental studies on solid-solid and solid-liquid helium Kapitza conductance.
- Study the effect of surface defect centers and surface roughness on the solid-liquid helium Kapitza conductance for alkali halide materials.
- Analyze the Kapitza conductance data in terms of existing theoretical models.
- Obtain and analyze specific heat data for spinel-columbite and alkali halide materials.
- Obtain and analyze thermal conductivity data for spinel-columbite and alkali halide materials.
- Study the effect of magnetic fields on both the specific heat and thermal conductivity.
- Develop theoretical models to interpret the above experimental results.

#### 4. SUMMARY AND CONCLUSIONS

The long-range purpose of this program is to study insulating materials having potential as low-temperature superconducting wire insulations. The insulations are agglomerates and the thermal conductivity of agglomerates at low temperature is to a great extent controlled by the Kapitza conductance of the species' interface. Our approach to this study is to gain understanding of the material parameters affecting the Kapitza conductance. In describing our progress in this program we have reported the Kapitza studies and the other thermal properties work in separate sections starting with the Kapitza conductance studies.

##### 4.1 Kapitza Studies

The Kapitza resistance at the interface of a superconductor surrounded by an insulator can become significant under several different conditions. For instance at the beginning of a transient heat pulse the effective heat transfer coefficient in a homogeneous material may be of the same size as the Kapitza conductance at its surface. Another condition when the Kapitza resistance can be the limiting factor in heat flow occurs in composite materials when a large number of particles of one material are mixed into another material. In this case the number of surface interfaces between the particles is so large that the total Kapitza resistance in the composite becomes large.

Both of these conditions occur for the materials presently being considered as a new generation of superconductor insulators and therefore there is a motivation for studying the Kapitza resistance of both solid-liquid and solid-solid interfaces in order to develop a basic physical understanding as well as to provide engineering numbers for design purposes.

At low temperatures, heat is transmitted by phonons and the limiting rate of transfer can be computed as the phonon radiation limit (PRL).<sup>(1)</sup> Various acoustic transmission theories predict phonon transmission rates that may be several orders of magnitude less than the PRL. Khalatnikov originated the first of these theories and others extended the acoustic mismatch theories (AM) attempting to explain the anomalously high interface thermal resistance measured in the laboratory. Typically the measured values are found to lie nearer the PRL than the acoustic predictions. The anomalously large transmission is attributed to solid material effects by some researchers and to superfluid liquid effects by others. We have approached this study by concentrating upon the material effects and by evaluating the Kapitza conductance using heat transmission into superfluid helium and into solids.

Since the Kapitza conductance is a phonon transmission phenomena some experimenters have evaluated the conductance as the ratio of reflected to incident phonon energy from the material surface. The conductance is then presented as a fraction of the PRL. Of particular interest to this study is phonon data reported by Weber et al.<sup>(2)</sup> that indicates the absence of the anomalous Kapitza conductance in single crystals of NaF and LiF which were cleaved under liquid helium. Apparently contaminate and strain free smooth surfaces obtained by cleaving under liquid helium could be produced for study.

Kapitza measurements must be made under a variety of experimental conditions such as solid-to-solid and solid-to-liquid helium interfaces (and possibly solid-to-gaseous helium interfaces). The temperature conditions can vary from the critical point of liquid helium (5.25K) to below 1.5K and with pressures up to at least 2.26 atm. (the critical pressure of He<sup>4</sup>).

#### 4.1.1 Kapitza Conductance of LiF and KBr Cleaved Under He II

After an extensive literature search, an optical dewar was prepared in which a single crystal could be cleaved under He II. Considerable effort was expended in developing a solid sample support system

that had acceptable heat leak characteristics and which was compatible with cooldown contraction. The present design surrounds a right circular cylindrical crystal with a teflon canister that uniformly shrinks onto the crystal at low temperature. The diameter of the cylinder is 1 cm and the length is about 2 cm. Support is provided for the teflon by the metal dewar walls. Carbon resistors are used as temperature sensors, and they are placed in holes drilled into the crystals. Copper leads to the thermometers are coiled inside the holes in the crystals and actually make the thermal contact to the crystal. The thermometers are calibrated during each run at each experimental point using the saturation temperature-pressure relation for helium. A heater (wire wound) is applied to the recessed end of the crystal with GE lacquer. Heat fluxes in excess of  $1 \text{ W/cm}^2$  can be generated by the heater. Two carbon resistors are positioned along the sample to provide redundancy and establish the temperature gradient in the sample. A third carbon resistor indicates the bath temperature.

Initial tests were performed with copper to prove the experimental apparatus. These tests yielded Kapitza values that have been found by others. Subsequently KBr and LiF crystals were tested. The measured values for all of the crystals cleaved under liquid helium were 33% of the PRL or higher. We have not been able to reproduce the phonon propagation results of Weber et al. It should be noted that Wyatt,<sup>(3)</sup> in a postscript to his paper in the 1980 NATO Summer Workshop on Nonequilibrium Phonons, indicates that the reflection technique may not give any useful information on the anomalous transmission of phonons across interfaces. We appear to have confirmed that speculation.

Summarizing the results, the Kapitza conductance of LiF and KBr single crystals have been measured immediately after cleaving under pure He II. Heating techniques were used to evaluate the conductance and it approaches the phonon radiation limit for these materials. Cleaving LiF under He II reduced the Kapitza conductance compared to an aged, cleaved surface by only a few percent. Despite the very good cleaved surface obtained with LiF crystals, the results suggest that sufficient

micro-fracturing of the surface occurs upon cleaving to significantly increase the Kapitza conductance over the acoustic mismatch theory values.

It is evident that surface contamination is a small part of the "anomalous" Kapitza conductance for LiF. The Kapitza conductance of cleaved LiF is two orders of magnitude above the acoustic mismatch theory prediction,  $0.0009 \text{ W/cm}^2\text{-K}^4$ , and more than one order of magnitude larger than any modification of that theory. These results, obtained by heating, are remarkably different from those reported using phonon reflection techniques and it appears that further effort in trying to resolve the difference between the two measuring techniques would be useful.

Because of our inability to significantly reduce the Kapitza conductance of LiF toward the acoustic limit by conventional techniques, further study of LiF may be useful in fundamental Kapitza conductance experiments. In the absence of any other theories, we conclude that surface microstructure is primarily responsible for the anomalous Kapitza conductance in LiF since surface impurities and volumetric imperfections in these tests were minimal. In particular, surface microstructure studies coordinated with theoretical analysis of the type published by Shiren appear to be an appropriate next step.

#### 4.1.2 Kapitza Research: Solid-Solid

For summary purposes, the reports documenting this research are collected in Appendix B and are referenced below by date [e.g., (1-2-85) refers to the Report of Jan. 2, 1985].

A low temperature probe specifically designed for Kapitza measurements was constructed at CeramPhysics during the first phase of the contract and was described in the report of 1-5-84. The probe has a copper block acting as a thermal reservoir and is attached to a liquid helium subpot. The reservoir is surrounded by an adiabatic shield also anchored to the subpot. This entire assembly is thermally isolated from a flange which is also the attachment point for a vacuum can surrounding

the entire low-temperature end of the probe. Temperature control is achieved by either pumping on the subpot through a mechanical regulator valve or with a heater connected to an electronic temperature controller.

The working space inside the adiabatic shield was large enough for two Kapitza-interface samples each 10-12 cm long including support. Since the solid-solid Kapitza interfaces were all pressure contacts, the supports consisted of a nylon yoke bolted to a copper platform which in turn was attached to the reservoir. Since nylon thermally contracts more than metals or the other dielectrics used in these experiments, the yoke applied large pressures to the Kapitza interfaces at low temperatures. The error introduced by the extra heat path of the nylon yoke was negligible due to the lower thermal conductivity of the nylon.

In solid-solid Kapitza interface measurements, there are two basic experimental arrangements determined by the thermal conductivity of the materials involved. The first of these is described and used in the reports of 10-10-84 and 2-15-85 and the second is described in the report of 8-8-85. The two methods differ in the physical arrangement of high and low thermal conductivity materials. The simplest arrangement measures the Kapitza resistance at the interface between two high conductivity materials. The proper experimental method for these types of measurements is to place two thermometers on each of the two materials which are then pressed together to form a Kapitza interface. A heat flow is established along the materials and across the interface by powering an electrical heater at the end of the samples farthest from the reservoir. Two thermometers on the material permit the temperature gradient along the material to be measured and extrapolated to the interface. If this is done in both materials, the Kapitza resistance can be directly calculated from the temperature drop across the interface.

This method works well in practice for two materials with large thermal conductivities, but a problem arises if one of the materials has a small thermal conductivity (e.g.,  $10^{-3}$  W/cm·K). In this case it is impossible to know the position of the thermometers well enough to

extrapolate to the interface temperature,  $T$ , with enough accuracy to make the measurement. That is, the uncertainty of the temperature at the interface is much larger than the temperature drop due to the Kapitza resistance.

This problem can be overcome with a different physical arrangement. A thin section ( $\sim 50$  microns) of the low thermal conductivity material is placed between two rods of high thermal conductivity material and the temperature gradient along each of these is extrapolated to the nearest interface. The temperature drop due to the thermal conductivity of the slice is then subtracted from the total drop, leaving the Kapitza drop across two interfaces.

Once the Kapitza resistance,  $R_K$ , is found, it was fit to an equation of the form

$$R_K = DT^{-n} \quad (\text{cm}^2\text{-K/W})$$

where  $D$  and  $n$  are constants. A number of experiments were run with different interfaces. Without exception  $R_K$  was described very well by the above equation. Initial tests (10-10-84) were run between bare copper and thallium chloride (TlCl). The fitted results were  $D = 3.1 \times 10^4$  and  $n = 2.16$ . The value of  $n$  is well within the range of typical values for solid-solid interfaces but  $D$  is extremely high. However, neither interface surface was polished which led to a large overestimate of the surface area in contact which led to the large  $D$  value.

For all further measurements, all the interface surfaces were polished to optical flatness.  $D$  was thereby lowered by at least two orders of magnitude, but in fact was probably still too high because even polished surfaces are in contact over only a small fraction of their areas.

Another set of experiments was performed on CsI versus copper interfaces (2-15-85). CsI (and TlCl) have higher thermal conductivities than any other dielectrics (with the exception of sapphire) that have

been used in Kapitza measurements. The CsI rods were interfaced with both Ni-plated and bare copper rods. Note that the copper sheathing on superconductors will be nickel-plated before an insulation coating is applied. The results were  $n = 2.76$ ,  $D = 144$  and  $n = 2/82$ ,  $D = 411$  for the unplated and plated interfaces respectively. The  $n$  values are practically identical and the values of  $D$  are within the range of uncertainty due to the uncertainty of contact area.

Finally, a series of experiments were performed using slices of low thermal conductivity material between either Ni-plated copper rods or CsI rods (8-8-85). The first low-thermal conductivity material was SC1C which is the probable material of choice for incorporation in superconductor insulators because of its excessively high specific heat at low temperatures. This material has been extensively investigated in other Air Force programs. A second material was 50%/50% (by weight) cdramic/glass mixture of SC1C and 3072 glass which is the favored glass (and mixing ratio) for the Westinghouse superconductor insulation procedure. A third material was SC1D which is a chemical analog of SC1C, both having B-site spinel structures. The final material was a 50%/50% ceramic/glass mixture of SC1A and 3072 glass. SC1A has also been thoroughly investigated in the Air Force insulation programs, primarily as a high thermal conductivity additive to the glass insulators.

The results of these measurements were: for a Cu-SC1C interface,  $n = 2.58$  and  $D = 244$ ; for a Cu-SC1D interface,  $n = 2.38$  and  $D = 778$ ; for a Cu-SC1A/3072 interface,  $n = 2.27$  and  $D = 673$ ; for a CsI-SC1C/3072 interface,  $n = 1.92$  and  $D = 12720$ . The value of  $D$  for the last measurement is anomalously higher than the rest probably because the CsI interfaces could not be polished as well as the Cu interfaces, thus increasing the over-estimate of the interface area.

The temperature dependences are very consistent with a wealth of previous data by other workers on a wide variety of different interfaces. The well-accepted acoustical mismatch theory of Kapitza resistance predicts a temperature dependence of  $n = 3$  for ideal surfaces, but most real surfaces differ from this because of imperfections of many types at

the interface, and these imperfections usually lower  $n$ , as was found in these experiments. No attempt (other than Ni-plating the copper rods) was made to lower the imperfections of the surfaces in these experiments. Thus the results here (especially the temperature dependences) should be accurate representations of the Kapitza resistance of real insulators on Ni-plated superconducting wire.

#### 4.1.3 References

1. Snyder, N. S., Heat Transport through Helium II: Kapitza Conductance, *Cryogenics*, V. 10:2, 1970, p. 89.
2. Weber, J. et al., Absence of Anomalous Kapitza Conductance on Freshly Cleaved Surfaces, *Phys. Rev. Lett.*, V. 40:22, May 29, 1978, p. 1469.
3. Wyatt, A. F. G., Kapitza Conductance of Solid-Liquid He Interfaces, "Nonequilibrium Superconductivity, Phonons, and Kapitza Boundaries," K. E. Gray, Ed., Plenum Press, 1981, p. 69.

#### 4.2 Experimental Thermal Properties Studies

The purpose of this part of the program is to determine and understand the thermal properties (specific heat and thermal conductivity) of a recently formulated group of compounds having potential as superconducting wire insulation in the future.

##### 4.2.1 Heavy-metal Ion Alkali Halides

Specific-heat and thermal-conductivity measurements in the temperature range of 1.7 to 20 K were made on single crystals of CsBr, CsI, TlBr, and TlCl and on a polycrystalline sample of TlI. All crystals display minima in the effective Debye temperatures which are reflected in maxima in  $C/T^3$  versus  $T$  curves, and these extrema are especially pronounced for TlCl. Comparisons are made with the predictions of existing lattice dynamics calculations, and the specific heat of TlBr is in very good agreement with the shell-model calculations of Cowley and Okazaki.

A Schottky specific heat term is resolved in the cesium halides at the lowest temperatures and attributed to hydroxyl ions; by adopting the zero-field splitting for  $\text{OH}^-$  in KCl, hydroxyl concentrations  $\sim 10^{20} \text{ cm}^{-3}$  are estimated in CsBr and CsI. The  $C/T^3$  maxima are fitted with Einstein terms added to the Debye backgrounds, and these fittings (together with the Schottky fits for CsBr and CsI) yield the following Debye temperatures: CsBr, 145 K; CsI, 124 K; TlBr, 116 K; TlCl 120 K; and TlI, 103 K. Thermal conductivity data for all crystals display maxima at  $\sim 4\text{-}5$  K and an apparent  $T^3$  boundary-scattering regime at the lowest temperatures. Phonon mean free paths at the higher temperatures are analyzed according to the Peierls relation, and for CsBr and TlCl it is found that the Debye modes are the dominant heat carriers. For the remaining crystals, The Einstein modes also carry heat. The Einstein modes at these higher temperatures dominate the specific heats, contributing up to 75% in the case of TlCl. Thermal conductivity measurements were also made on thin crystals ( $\sim 0.05$  cm) of CsBr, TlBr, and TlCl to examine the boundary-scattering region. It is found that in this region the limiting phonon mean free path for CsBr scales with the crystal dimension, and it is suggested that the suppression of the thermal conductivity may be due to the hydroxyl concentration. For TlBr and TlCl, the limiting phonon mean free path is  $\sim 0.01$  cm and is independent of the crystal thickness; this behavior is attributed to a mosaic structure within these crystals.

These results have been published [W. N. Lawless, Phys. Rev. B30, 6057 (1984)], and a reprint is attached in Appendix C.

In addition to the above published studies, interesting new magnetic phenomena were discovered in a CsBr single crystal at low temperatures (7-31-84, see below). Namely, the thermal conductivity displays a maximum at  $\sim 8$  T, rising  $\sim 35\%$  above the zero-field value, and the dielectric constant is suppressed by  $\sim 4\%$  in a field of 15 T. The implication here is that both the acoustic and optic modes in CsBr are H-field dependent, due possibly to vibronic effects.

#### 4.2.2 Cadmium and Zinc Chromite Spinel

For convenience, the reports documenting the research here are collected in Appendix D and are referenced below by date. For example, a reference in parentheses such as (1-2-85) refers to the Letter Report of January 2, 1985 titled Spinel Studies.

The spinels studied here at low temperatures are  $\text{CdCr}_2\text{O}_4$  and  $\text{ZnCr}_2\text{O}_4$ , and a literature survey (4-17-84) revealed that the low-temperature properties of these spinels have not previously been explored due in part to the difficulty of preparing bulk samples.

##### Specific Heat

High precision specific heat data on the  $\text{CdCr}_2\text{O}_4$  and  $\text{ZnCr}_2\text{O}_4$  spinels (9-2-83, 10-1-83) were analyzed according to simple models (1-23-84), taking into account the minor columbite phases present that act as mineralizers in the ceramic formation. The Debye temperatures for  $\text{CdCr}_2\text{O}_4$  and  $\text{ZnCr}_2\text{O}_4$  so determined (420 and 463 K, respectively) agree very well with the predictions of the Lindemann relation (414 and 469 K).

These Cd and Zn spinels display enormous specific heat maxima ( $T_c = 8$  and  $10.5$  K, respectively) of technological importance. At temperatures well below  $T_c$ , antiferrimagnetic spin waves contribute a  $T^3$  term to the specific heat, and these spin waves are characterized by

$$\begin{aligned} \text{CdCr}_2\text{O}_4 : J_s/c_a &= 5.943 \times 10^{-16} \text{ erg} \\ \text{ZnCr}_2\text{O}_r : J_s/c_a &= 9.651 \times 10^{-16} \text{ erg} \end{aligned} \quad (1)$$

where  $c_a$  is a lattice geometry factor.

The magnetic contribution to the specific heat arising from the transition at  $T_c$  was determined for each of the spinels by subtracting the remaining contributions, and by numerical integration the magnetic entropies which were found (3-14-84)

$$\begin{aligned}
\text{CdCr}_2\text{O}_4 : S_m/R &= 2.340 \\
\text{ZnCr}_2\text{O}_4 : S_m/R &= 1.434
\end{aligned}
\tag{2}$$

Careful measurements of the specific heat near  $T_C$  were performed by a slow drift method (<10 mK between points in the range  $T_C \pm 2$  K) to study critical exponents (6-14-84, 3-1-85). These measurements also yielded high precision transition temperatures,

$$\begin{aligned}
\text{CdCr}_2\text{O}_4 : T_C &= 7.958 \text{ K} \\
\text{ZnCr}_2\text{O}_4 : T_C &= 10.637 \text{ K}
\end{aligned}
\tag{3}$$

Analyses of these drift data according to renormalization group theoretical models yielded critical exponents  $\alpha = 9.8 \times 10^{-3}$  and  $7.8 \times 10^{-3}$  for  $\text{CdCr}_2\text{O}_4$  and  $\text{ZnCr}_2\text{O}_4$ , respectively, in the range  $1 \text{ mK} < |T - T_C| < 50 \text{ mK}$  (3-1-85). At larger temperature differences, the specific heat data show considerable rounding and an  $\alpha \sim 2$  regime is seen in both spinels. This latter behavior may be due to correlation-length effects in the ceramic grains.

These drift measurements also established that there is no latent heat associated with the transition in either spinel.

Composition studies were undertaken to see if the specific heat maxima in  $\text{CdCr}_2\text{O}_4$  and  $\text{ZnCr}_2\text{O}_4$  could be altered by solid solutions or by doping. Solid solutions of  $(\text{Cd}_{0.5}\text{Zn}_{0.5})\text{Cr}_2\text{O}_4$  poisoned all specific heat structure (4-1-85), but  $\text{Fe}^{3+}$ ,  $\text{Gd}^{3+}$ , and  $\text{Pb}^{2+}$  doping in  $\text{CdCr}_2\text{O}_4$  reduced both  $T_C$  and the height of the specific heat maximum (4-1-85). This finding was pursued further with a series of  $\text{Fe}^{3+}$  doped  $\text{CdCr}_2\text{O}_4$  samples (7-17-85), and it was found that the trend of suppressed  $T_C$  and  $C_{\text{max}}$  with doping followed a regular behavior and above 3%  $\text{Fe}^{3+}$  on the  $\text{Cr}^{3+}$  site the specific heat maximum was completely suppressed.

### Magnetocaloric Effects

At temperatures well below  $T_c$  in both spinels, adiabatic demagnetization cooling and magnetization heating effects were measured (5-18-84). No hysteretic effects were observed, and the magnetocaloric effects are very large (e.g.,  $\Delta T \sim 1$  K at 9 T) considering how large the specific heats are at these temperatures. Magnetization measurements at 4.2 K revealed that both spinels are linear paramagnets up to 7 T.

The specific heat and magnetic data for these spinels are understandable in terms of a simple model of two spin densities. That is, some fraction of the  $\text{Cr}^{3+}$  spins order antiferromagnetically at  $T_c$ , and the remaining spins are unordered below  $T_c$ . The former spins contribute the  $T^3$  spin-wave term to the specific heat below  $T_c$ , and the latter spins account for the linear-paramagnet behavior below  $T_c$ . However, under adiabatic conditions the ordered spins show demagnetization heating whereas the unordered spins show demagnetization cooling and dominate the overall effect. Model calculations based on two, non-interacting spin densities (8-15-84) were reasonably successful in explaining and correlating the specific heat data [Eqs. (1) and (2)], magnetocaloric data, and magnetization data, and the estimated ordered and unordered spin densities are  $\sim 84$  and  $16\%$  for  $\text{CdCr}_2\text{O}_4$ ,  $\sim 52$  and  $48\%$  for  $\text{ZnCr}_2\text{O}_4$ . The exchange constants from Eq. (1) are estimated to be  $J/k = 3.42$  and  $4.72$ , respectively.

### Thermal Conductivity

Thermal conductivity ( $k$ ) measurements on the spinels (9-2-83) revealed very large jumps in  $k$  below  $T_c$ , and these data were measured in fine detail in the neighborhood of  $T_c$  (5-3-85). Both spinels have small thermal conductivities ( $\sim 1 \text{ mW cm}^{-1} \text{ K}^{-1}$ ), and the jump below  $T_c$ ,  $\Delta k/k$ , is much larger for  $\text{ZnCr}_2\text{O}_4$  ( $\sim 100\%$ ) than for  $\text{CdCr}_2\text{O}_4$  ( $\sim 30\%$ ). According to the above two-spin-system model, the ordering of a portion of the  $\text{Cr}^{3+}$  spins at  $T_c$  removes a phonon-scattering mechanism.

The thermal conductivities of the spinels in the neighborhood of the jump in  $k$  were measured as a function of magnetic field up to 15 T (5-7-84). Interestingly, an H-field quenches the  $k$ -anomaly in  $\text{CdCr}_2\text{O}_4$ , but the effect in  $\text{ZnCr}_2\text{O}_4$  is unaffected.

Finally, the thermal conductivities of  $\text{Fe}^{3+}$  doped  $\text{CdCr}_2\text{O}_4$  were measured, 2-10 K, with particular attention paid to the jump in  $k$  below  $T_c$  (8-8-85). Recall from the above that  $T_c$  and  $C_{\text{max}}$  are quenched by increasing  $\text{Fe}^{3+}$  doping, and this same trend is observed in  $\Delta k$ . At the 3%  $\text{Fe}^{3+}$  doping level where structure in the specific heat vanishes, the jump in  $k$  also disappears.

#### 4.2.3 Magnetic Columbite Studies

Although this program has concentrated on the  $\text{CdCr}_2\text{O}_4$  and  $\text{ZnCr}_2\text{O}_4$  spinels because of the technological importance of the former spinel, there are two other high-specific-heat ceramics that have entered previous Air Force applied programs:  $\text{MnNb}_2\text{O}_6$ ,  $T_c = 4.3$  K, and  $\text{NiNb}_2\text{O}_6$ ,  $T_c = 5.5$  K, both columbite materials.

Because the above mentioned drift method for measuring specific heat had been perfected for the spinels, a minor effort was devoted to determining critical exponents for these two columbites using this method. These studies (6-3-85) yielded the following:

$$\text{MnNb}_2\text{O}_6 \quad T_c = 4.332 \text{ K}, \alpha = 0.00532$$

$$\text{NiNb}_2\text{O}_6 \quad T_c = 5.497 \text{ K}, \alpha = 0.00145$$

#### 4.2.4 Discussion

The primary goals of this portion of the AFOSR contract were to study the physics of the heavy-metal-ion alkali halides and of the new spinels  $\text{CdCr}_2\text{O}_4$  and  $\text{ZnCr}_2\text{O}_4$ , and these goals have been fulfilled as originally proposed. A separate portion of this contract was devoted to theoretical studies of these spinels based on the measurements here, and these theoretical studies are summarized below.

#### 4.2.5 Conclusions

The following conclusions can be drawn from the research described above:

1. The thermal properties of the Cs and Tl halides at low temperatures are now well understood in terms of simple models, and these studies have been published.
2. The substantial H-field dependence of the thermal and dielectric properties of CsBr discovered here, while a minor part of this program, is a rich new area for future research.
3. A great deal of low temperature data on the new spinels,  $\text{CdCr}_2\text{O}_4$  and  $\text{ZnCr}_2\text{O}_4$ , have been generated in this program, including data measured in intense magnetic fields. Unexpected magnetocaloric effects have been measured, and the simple model of two, non-interacting spin systems appears to explain some, but not all, of the data. Future research here should concentrate in part on the time dependence of the magnetocaloric phenomena as an experimental means for separating the two spin systems.
4. Limited doping studies have shown that the thermal phenomena in  $\text{CdCr}_2\text{O}_4$  can be influenced and eventually quenched, and this finding has significant theoretical implications. Future research here should expand into other doping systems.
5. Although not emphasized above, the  $\text{CdCr}_2\text{O}_4$  and  $\text{ZnCr}_2\text{O}_4$  spinels do not form as ceramic bodies unless the "mineralizers"  $\text{CdNb}_2\text{O}_6$  and  $\text{ZnNb}_2\text{O}_6$  are present, but these mineralizers do not enter into solid solution with, or otherwise dope, the spinels. Future research should address this phenomenon of formation (epitaxial growth?). In fact, our lack of understanding of how these new spinels form has hindered our ability to publish the studies to date.

### 4.3 Theoretical Thermal Properties Studies

The theoretical phase of the research on this contract was carried out in a series of reports which are collected in Appendix E: Spinel Studies I through VII, and are referenced accordingly below. The theoretical results so far have developed an attractive and suggestive picture for the ordering phenomena in the B-site spinels,  $\text{CdCr}_2\text{O}_4$  and  $\text{ZnCr}_2\text{O}_4$ . A systematic program of increasing theoretical complexity has been followed to insure that an accurate understanding of these materials is constructed from the ground up, with the gross features properly interpreted with simple mean-field models before the details are addressed. The results have shown that at least two types of magnetic correlations are present, and that frustration and the presence of strong spin-lattice coupling play an important role in the anomalously large specific heats and thermal conductivities. A paper on this work is in preparation, and will be submitted for publication shortly.

The theoretical approach started with a basic examination of the structure of the spinel phases of  $\text{CdCr}_2\text{O}_4$  and  $\text{ZnCr}_2\text{O}_4$ . This study (Structural Studies, Report I) revealed an interesting pattern among the B-site spinels, which suggests that additional systems of considerable interest might be made by filling in a table of materials constructed by replacing the A-site atom (Zn or Cd) by isoelectronic mixtures of Cu and In, or Ag and In. In addition, the transitions in these materials were seen to have a peculiar nature in which the spins order weakly in a lattice which has a high degree of frustration. This has great importance for our understanding of these systems, since it means that large numbers of spins can remain unordered below the transition, resulting in anomalously large specific heats, and, furthermore, that distortions of the lattice, which remove the frustration, can couple strongly to the spins, thus leading to large thermal conductivities due to spin energy being transported through the spin-phonon interaction.

The first attempt (Report II: Theoretical Models) toward a theoretical understanding of the properties of these systems was to derive

the Hamiltonian describing the interaction of the spins on the spinel lattice sites. From this we extracted a simple model in which we kept only two possible sublattice magnetizations, an antiferromagnetic one which orders at the transition, and a ferromagnetic one coupled to it, which is polarized in a magnetic field, giving rise to spin-flop like effects. In the mean-field approximation, this model already gives interesting effects, including a temperature dependent magnetization linear in field and a magnetic field dependent specific heat which increases with field. These results are in good qualitative agreement with the experimental data and indicate the basic correctness of our approach.

The renormalization effects due to fluctuations were examined (Report III: Thermal Properties) which led to the novel feature that the non-ordering spins give rise to a large contribution to the specific heat even well below the ordering temperature of the antiferromagnetic spins. This is not possible in a simpler system with only one order parameter, again suggesting our model has correct general properties. Detailed results were obtained in the gaussian fluctuation approximation for the specific heat as a function of temperature and magnetic field both above and below the transition.

Next (Report IV: Thermal Conductivity) a theory for the thermal conductivity in this class of materials was developed. The thermal conductivity depends on both the specific heat and the scattering rate. We showed that the scattering rate involved, in addition to the usual phonon and antiferromagnetic spin wave contributions, a spin fluctuation term which limits the thermal conductivity in the vicinity of the transition. Fits were made to the specific heat and thermal conductivity data using the same set of fitting parameters, which revealed that the peak in the thermal conductivity at the transition arises from the peak in the specific heat, but that the former is typically a factor of three or so smaller than the latter due to the spin scattering near transition.

Detailed fits of our theoretical model to specific heat data on  $\text{CdCr}_2\text{O}_4$  as a function of temperature were carried out (Report V:

Comparison with Experiment: Specific Heat). Good fits were obtained and values of some key parameters in the theory were deduced. The best fit over the entire temperature range gave large values for the specific heat exponent, which suggested the importance of disorder, as discussed in Report III. In addition, values of the ferromagnetic-antiferromagnetic coupling were obtained which correlated well with the value found in the  $\text{Fe}^{3+}$  impurity substitution experiments. In Report VI the thermal conductivity data were fit to the theoretical calculation we carried out in our Report IV. From this analysis the parameters that characterize the spin scattering near the transition were obtained and were found to be consistent with the theory developed.

Finally, a theory of the effects of substitutional impurities was worked out (Report VII: Impurity Models) and compared with the experimental measurements involving the effects of  $\text{Fe}^{3+}$  doping. The comparison gives strong evidence for the interaction between the two order parameters that is an essential feature of the theoretical model we have proposed, and allows us to determine the magnitude of the coupling. This work is being written up for publication along with the model we have developed for the frustrated B-site spinels.

5. PUBLICATIONS

"Specific Heat and Thermal Conductivity Measurements on Cesium and Thallous Halide Crystals at Low Temperature,"  
W. N. Lawless, accepted for publication in the Physical Review.

6. PERSONNEL

Westinghouse: P. W. Eckels, Co-Principal Investigator

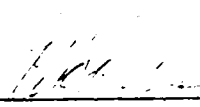
J. H. Parker Jr.

A. Patterson

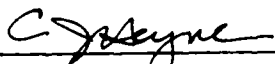
CeramPhysics: W. N. Lawless, Co-Principal Investigator

C. F. Clark

Ohio State: B. R. Patton

  
\_\_\_\_\_  
P. W. Eckels  
Electromagnetic Devices

Approved:

  
\_\_\_\_\_  
C. J. Heyne, Manager  
Electromagnetic Devices

  
\_\_\_\_\_  
C. J. Mole, Manager  
Electrotechnology Department

Appendix A

SOLID TO HE II KAPITZA STUDIES

## KAPITZA CONDUCTANCE OF CRYSTALS CLEAVED UNDER HE II

### ABSTRACT

The Kapitza conductance of LiF and KBr single crystals has been measured immediately after cleaving under pure He II. Heating techniques were used to evaluate the Conductance and it approaches the phonon radiation limit for these materials. Cleaving LiF under He II reduced the Kapitza conductance compared to an aged, cleaved surface by only a few percent. Despite the very good cleaved surface obtained with LiF crystals, the results suggest that sufficient micro-fracturing of the surface occurs upon cleaving to significantly increase the Kapitza conductance over the acoustic mismatch theory values. These results are in contradiction to results obtained by phonon reflection techniques.

## 1. INTRODUCTION

It is well known that the measured values of thermal resistance between solids and liquid helium are frequently found to be an order of magnitude larger than acoustic mismatch (AM) theoretical calculations indicate they should be [1, 2]. The AM theory is based on the transmission of acoustic phonons across the solid-liquid interface. In fact the Kapitza conductance is frequently found to be nearer to the phonon radiation limit than to even the AM theories that have been modified for solid-liquid molecular attraction, etc. Snyder [3] discusses the existing uncertainty in the scientific community as to whether the anomalous conductance is attributable to solid, liquid or combined processes and is unable to reach a definitive conclusion. Clearly more experiments directed at defining and characterizing the interface under very controlled conditions are warranted.

Our objective in these experiments was to determine the Kapitza conductance of a nearly contaminate free surface that had the minimum possible surface restructuring and roughness. The small number of surface dislocations reported [4] for LiF cleaved in the 100 plane and the small number of volumetric dislocations reported [5] in single crystal LiF led us to experiment with LiF cleaved under He II.

Our intuitive approach was supported by Weber's data reporting [6] variations in surface impedances of 2 - 6% between acoustic phonon reflections to vacuum and reflections to He II. Clearly implied is that the vacuum reflection is near to the Khalatnikov limit (perfect acoustic mismatch) and, therefore, that the He II reflection is within 2 - 6% of the theoretical acoustic limit of 0.09% for LiF. The present results do not support the foregoing conclusions.

# OPTICAL SUPERFLUID DEWAR

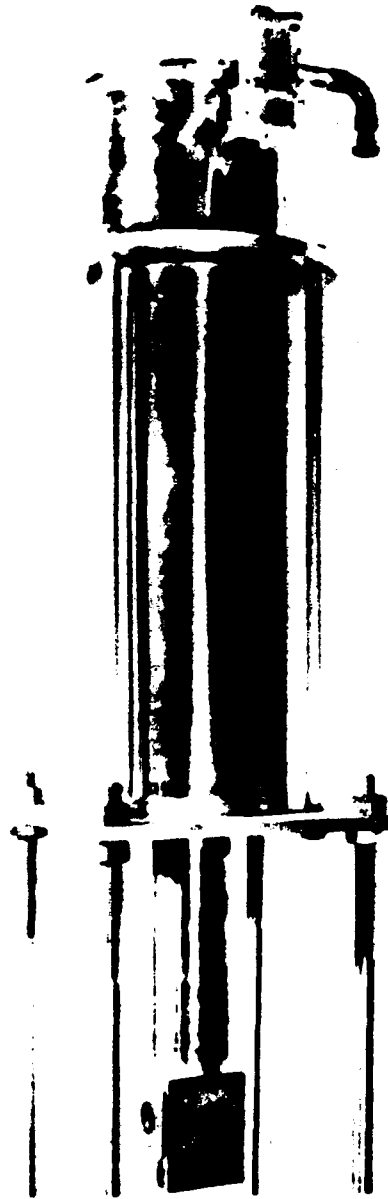


Figure 1. The optical superfluid dewar.

## 2. EXPERIMENTAL APPARATUS

Figure 1 shows the Dewar used in these experiments. The test chamber is seen extending below the main He II reservoir and is equipped with three quartz optical ports. The optical ports allow observation of the sample and controlled disruption of the subsurface structure with LASERS by the formation of "F" centers. "F" center formation with "UV" LASERS is a well documented [7] process allowing prediction of the distribution and density of a type of lattice defect. The test chamber is isolated from the main He II reservoir so that pure He gas can be condensed into the test chamber. Figure 2 shows various interior components of the dewar. The function of these components is best determined by reference to Figure 3, a schematic diagram of the dewar and test section. It is a vacuum insulated, gold plated dewar that uses  $\text{LN}_2$  to provide intermediate radiant heat shielding. The inner He II reservoir is pumped directly to obtain superfluid conditions. A vertical 2.54 cm tube runs through the center of the reservoir and located at its lower end is the test chamber. Heat generated during the experiment and radiant heat are transported up the superfluid column, through the tube wall and into the He II reservoir. A rod (see Figure 2) extends from the warm end of the tube into the test chamber and to it are attached the cleaving blade and the internal IR shields that can be rotated over the windows on the superfluid side. The purpose of the isolated test chamber is to allow pure He gas to be condensed into the test volume and to allow control of its pressure independent from the reservoir.

Figure 4 is a picture of the Kapitza test chamber of the dewar showing the low temperature radiant heat shield and instrumentation leads attached to the central tube. Figure 5 shows an enlarged view of the test sample case fitted into one of the windows. In this photograph a copper sample is ready for test having been mounted in one of the viewing

## SUPERFLUID DEWAR COMPONENTS

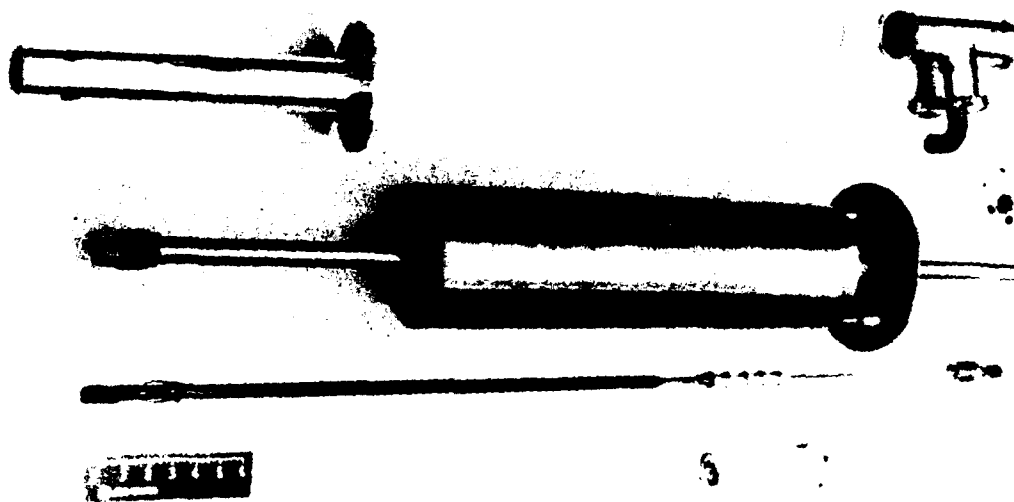


Figure 2. Components of the superfluid dewar.

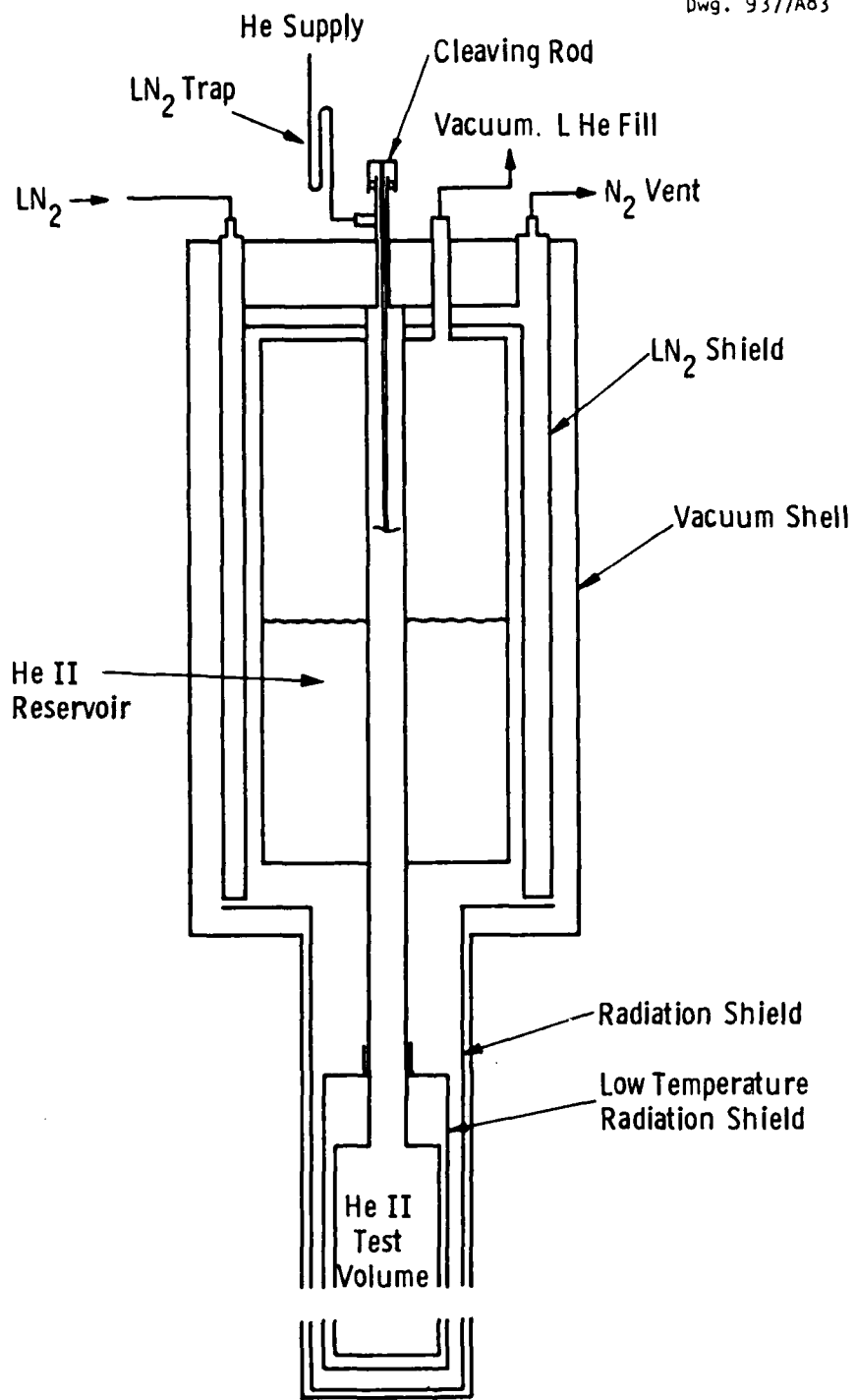


Fig. 3 - Schematic diagram of the optical superfluid dewar

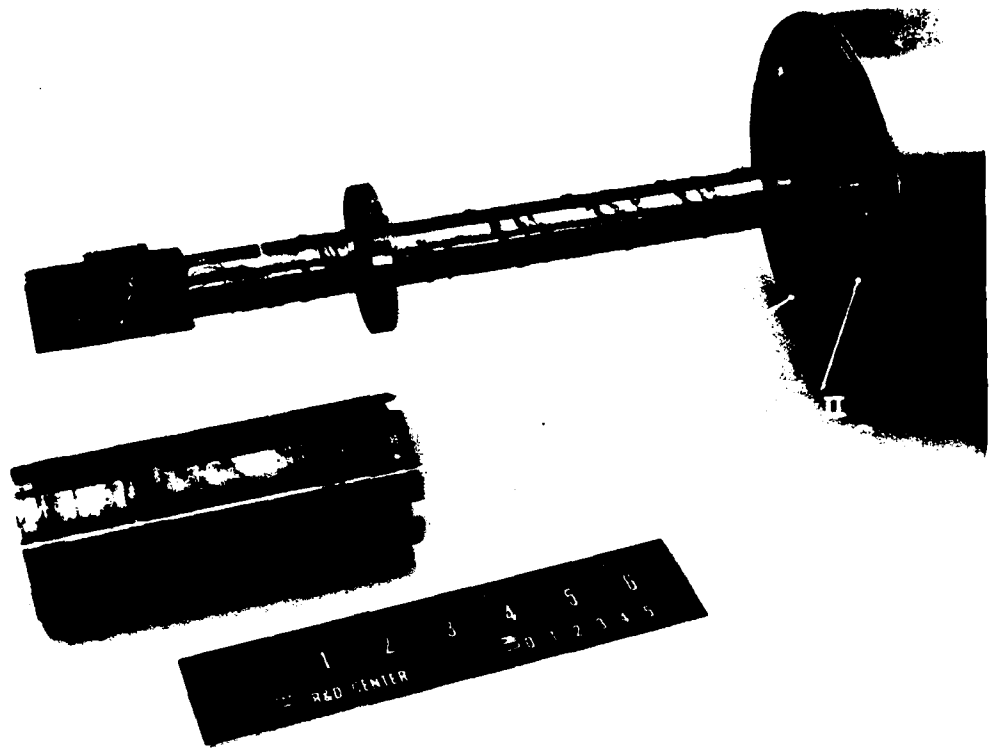


Figure 4. The Kapitza test chamber.

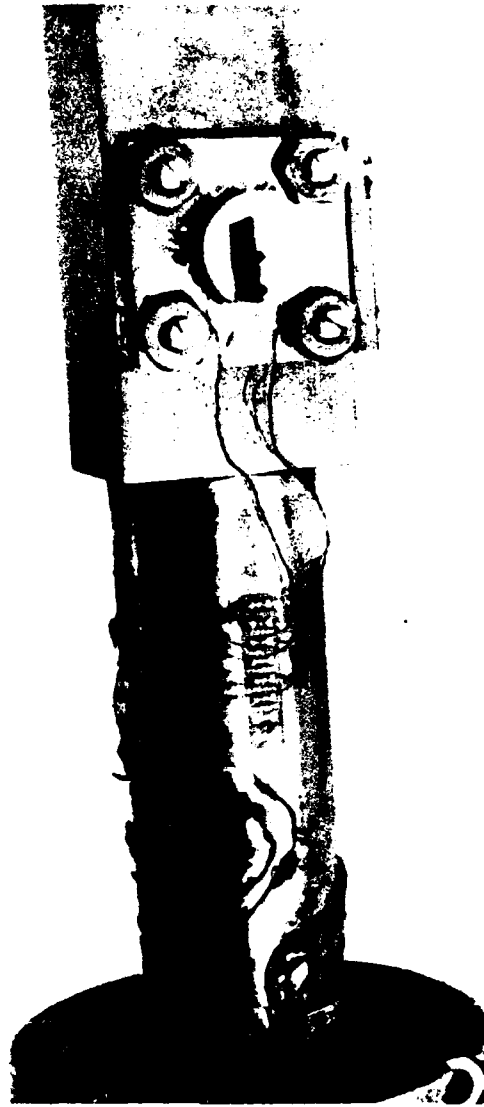


Figure 5. A detail of the test sample case and lead arrangement.

ports and sealed with an indium "O" ring around its periphery. In this case the heater and leads are within the vacuum space on the back of the sample. Figure 6 shows the copper proof sample, its mounting fixture, a typical heater and two carbon resistors of the type that are prepared as thermometers. A slightly different arrangement is used during a crystal test. During a crystal test, one of the windows holds the sample and another contains a glass ceramic feed-through for the heater and thermometer leads. The test setup for crystal testing has the 12  $\mu\text{m}$  thermometer leads and 0.25 mm heater leads running for 2.54 cm through the He II test chamber to the feed-through.

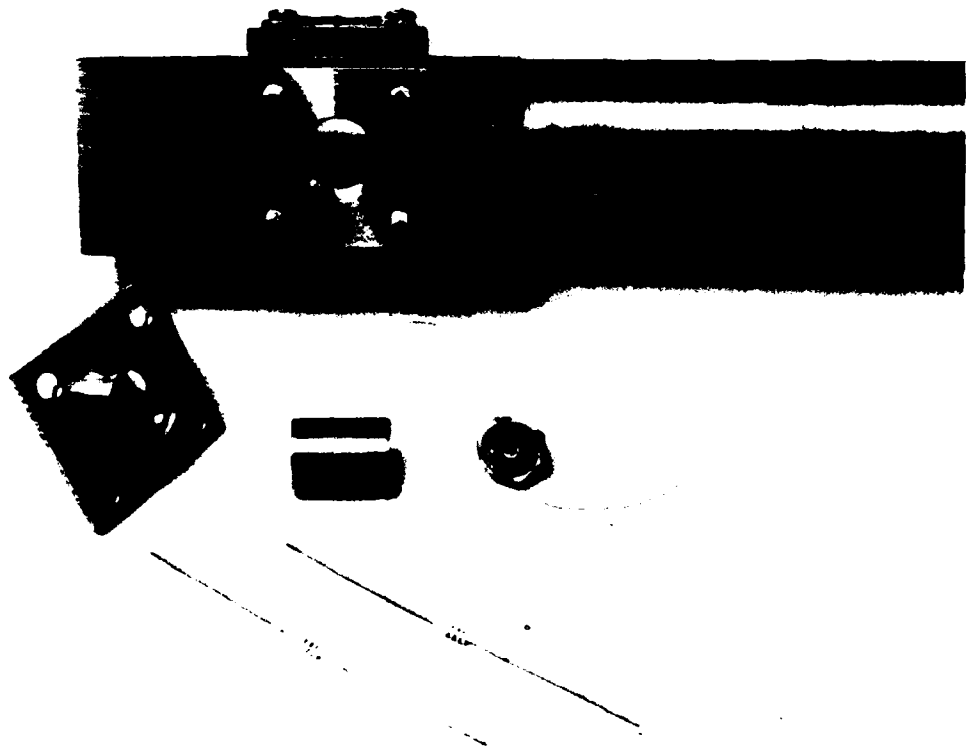


Figure 6. The brass sample holder is shown with a bifilar wound heater.

### 3. SAMPLE PREPARATION

Figure 7 shows a LiF crystal prepared for installation of the heater and thermometer in the same picture. The preparation starts with machining a Harshaw single crystal to the proper diameter. Surface cracks in the KBr were removed by washing with an alcohol-water mixture containing about 3 - 5% water. Next holes were drilled into the crystal body for thermometer insertion. Drilling was done with an alcohol-water solution lubricant to prevent fracture. The heater, a manganin wire coiled on Kapton adhesive tape, was bonded to the back of the crystal with GE lacquer.

The thermometers were made by sanding Allen-Bradley carbon radio resistors to a small diameter and heat sinking them by attaching a coil of copper wire to one lead as shown in Figure 7. The coil was twisted tight and inserted into the crystal where it expanded to form a good thermal contact with the crystal. Tests were run both with the thermometer well packed with jeweler's rouge and without. The intent was to determine if the heat capacity of the He II in the open well or the additional impurities in the rouge influenced the data. The same results were obtained in each case indicating adequate lead thermal contact was achieved. The thermometer leads were wrapped around the crystal as a further heat sink. As seen in Figure 7, two axially distributed thermometers indicated the crystal temperature gradient and these measurements were in agreement with thermal conductivity data in the literature [8]. This aspect of the test was used to assign a quality to the heat run data. Those data whose computed axial heat flux, as indicated by temperature gradient, did not agree with the  $I^2R$  heater flux, were discarded.

Crystal support and sealing were a major problem in this experiment. Sealing of the ports was accomplished by indium "O" ring seals

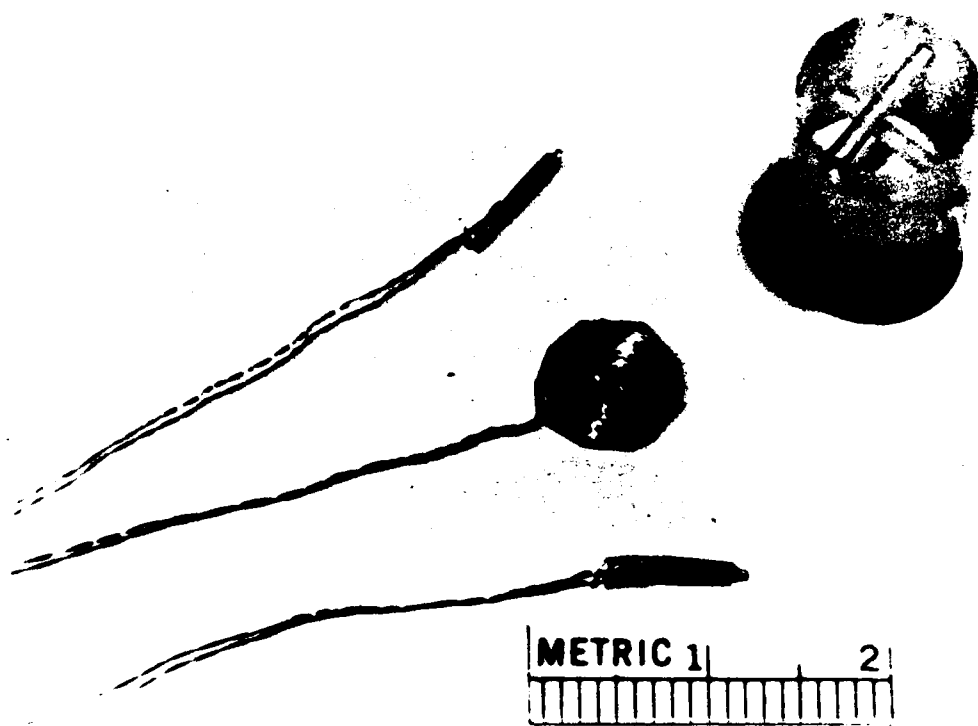


Figure 7. A LiF test sample with the heater and carbon thermometers.

and indium soldering. Efforts to seal around the crystal cylindrical body were unsuccessful, apparently because any three dimensional stress field would crack the crystal. Matching the thermal contraction of the crystal to a support is problematic because of the large cooldown contraction of the alkali-halide ionic crystals [8]. It is more than twice the value for most metals. Because of the differential contraction, no seal was permanent. Each had to be replaced after several cooldown cycles. Ultimately, the crystal was fitted into a teflon container that shrunk down on the sample to support and thermally insulate it. The teflon container had to be made from simple geometric shapes to assure that there were no three dimensional stress fields. For example, if the clearance was not proper around the crystal, the cylindrical teflon shell would cleave the crystal at the end of the shell during cooldown. Also, if the disk end of the teflon container was integral with the cylindrical shell section, the stress pattern would cleave the crystal axially. The container has to provide rim stress relief, sealing and controlled venting of the heater space. If these criteria are met, simple computation shows that the heat penetration and storage in the teflon are negligible compared to the heat flow through the crystal.

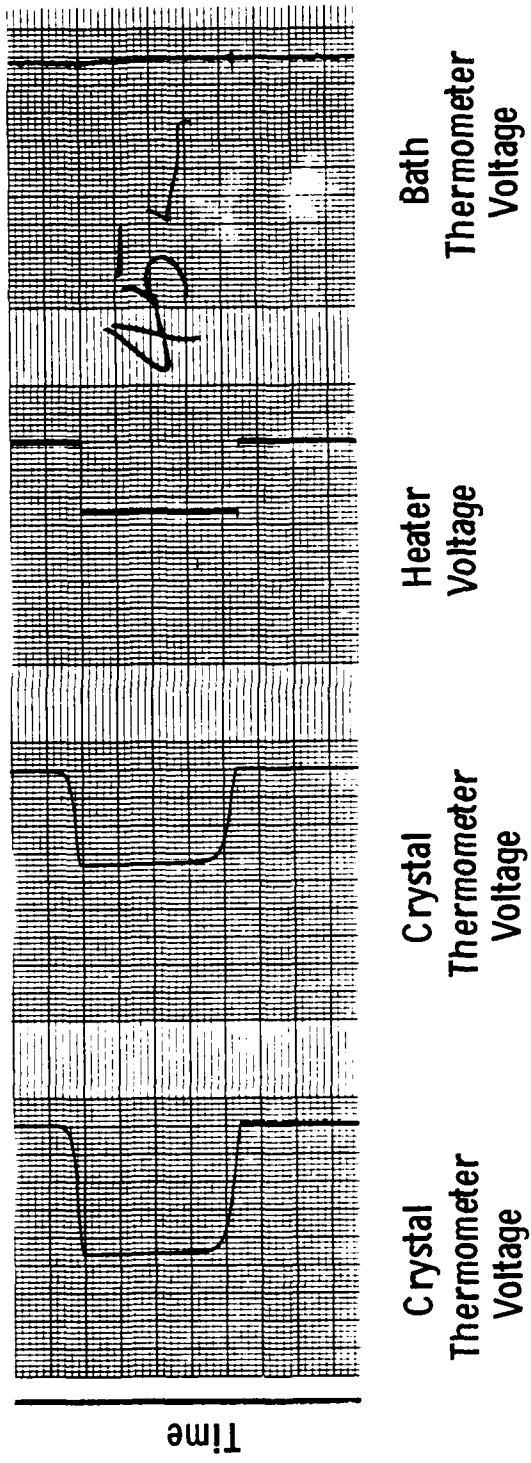


Fig. 8—Sample voltage trace during testing of a LiF sample

#### 4. EXPERIMENTAL PROCEDURE

After sample installation and assembly of the dewar, the test chamber and tubing were cleaned with acetone and alcohol. The chamber was flushed with helium and pumped down to clean and check vacuum. Liquid nitrogen was introduced into the jacket and the dewar was cooled overnight to about 100 K by conduction and radiation. Subsequently LHe was introduced into the reservoir and the cooldown continued by conduction and radiation. After topping off the reservoir, the reservoir was pumped to about 3.0 K and boil-off He gas was admitted to the test chamber at about atmospheric pressure through a liquid nitrogen trap and metering valve. At this point, slow admission of the helium was required to prevent cracking the crystal even though it was at 80 K.

When the central tube was filled, it was sealed and the first calibration point on the thermometers was recorded along with the pressure in the test chamber. In this way, the thermometers were calibrated as the dewar temperature was reduced. To start the test series, the crystal was cleaved and testing commenced immediately. Judging from visual observation the quality of the surface was excellent. Data taken immediately after cleaving was indistinguishable from data taken after several hours below 4 K; leading to the conclusion that the surface condition did not change with time -- that is, the He II environment was indeed clean at low temperature. Figure 8 is a sample data trace of the two crystal thermometers, the bath thermometer and heater current shunt voltage. The thermometer signals have been processed through a dc amplifier and biased so that only the top, varying voltage is displayed. Very good sensitivity is obtained in this way. The thermometer voltage is produced by a current of 10  $\mu$ A. Accuracy and repeatability of the recording method was verified by comparison to ac bridge and current reversal techniques. Figure 9 is a picture of the test apparatus. To

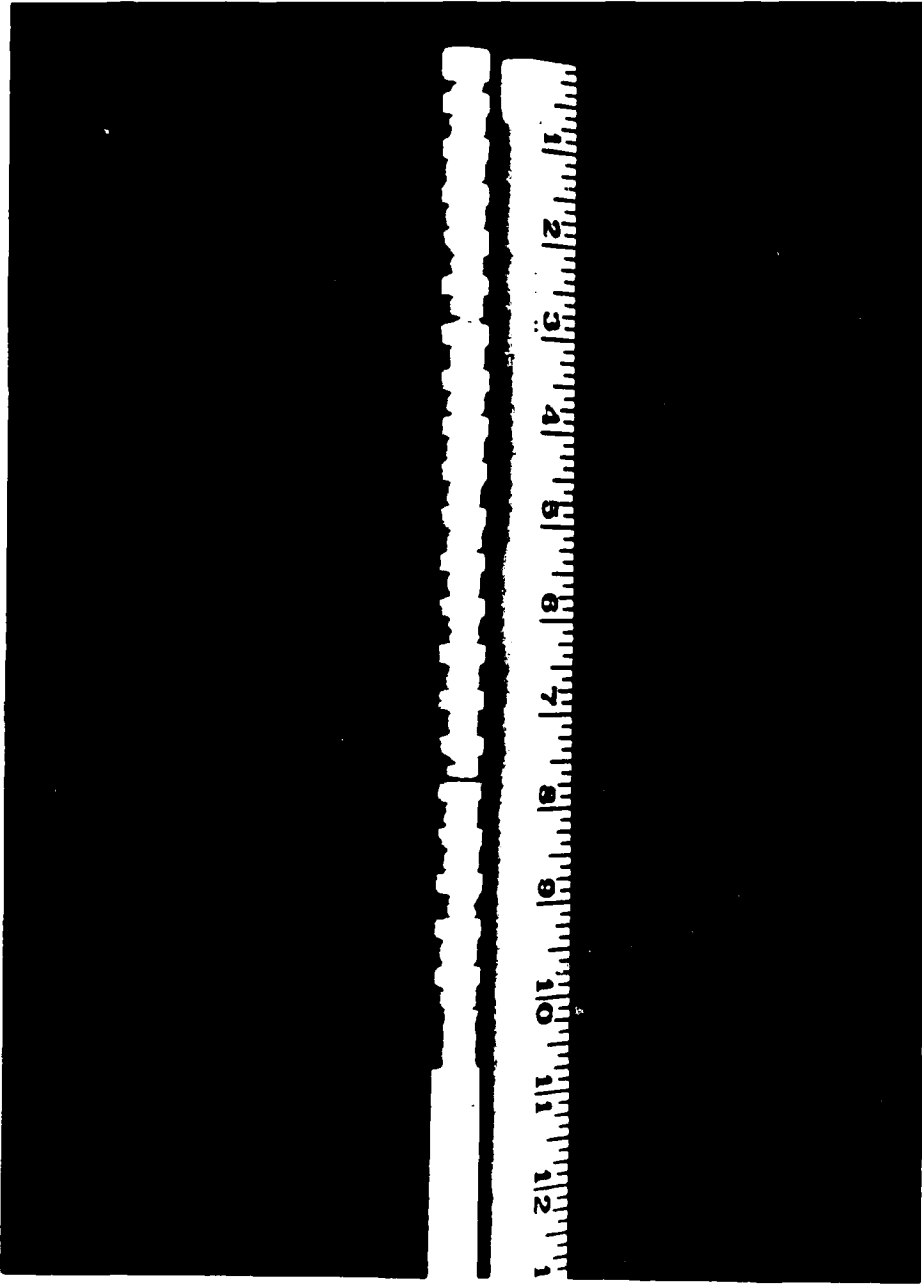


Figure 9. The Kapitza conductance test apparatus.

obtain a single data point, all of the voltage traces were read at the same time in the linear, steady rise portion of the time interval. In each case, the temperature rise of the bath and both thermometers was the same, allowing the data to be considered "quasi-steady". The different slopes in Figure 8 are due to different amplification factors required for optimum thermometer sensitivity. The factors are determined experimentally.

A typical test sequence would start at a bath temperature of 2.1 K and the heater would be energized at intervals when the bath was stable. The heating rate was increased for each interval until the thermometers indicated that normal He I boiling was occurring. The bath temperature was then reduced to 2.0, 1.9, ..., 1.5 K and the increasing heat rate procedure was followed at each temperature level.

## 5. DATA REDUCTION

The data was reduced to coefficient form using the relation [9]

$$h_k = q'' / [f(\delta T)T^3]$$

where:

$$f = 1 + 1.5(\delta T/T) + (\delta T/T)^2 + 0.25(\delta T/T)^3$$

Figure 10 shows the Kapitza conductance vs fluid temperature for LiF and KBr along with the phonon radiation limit for each. In each case the conductance is only slightly less than the phonon radiation limit and about two orders of magnitude above the perfect acoustic mismatch theories. Several crystals were cleaved and tested and the data was found to repeat within the data error band shown. The repeatability of the data lends high confidence that these are representative results for single crystals cleaved under helium. Johnson and Little's data [10] for air cleaved LiF are very comparable to this data as shown in Figure 10.

Also shown in Figure 10 is the conductance of a surface before cleaving. The conductance exceeds the PRL slightly, probably because the actual three dimensional temperature gradient in the uncleaved crystal is greater than the calculated two-dimensional gradient for which the interface temperature difference is projected.

Another test was also run with the cleaved sample. While under the He cover gas, the sample was allowed to warm up to 60 K and then it was recooled and retested. These data are also shown in Figure 10 where it is seen that the conductance increased to midway between the aged surface and fresh cleaved level. The same time interval of storage at 4 K produces no change in the conductance. It seems likely that some

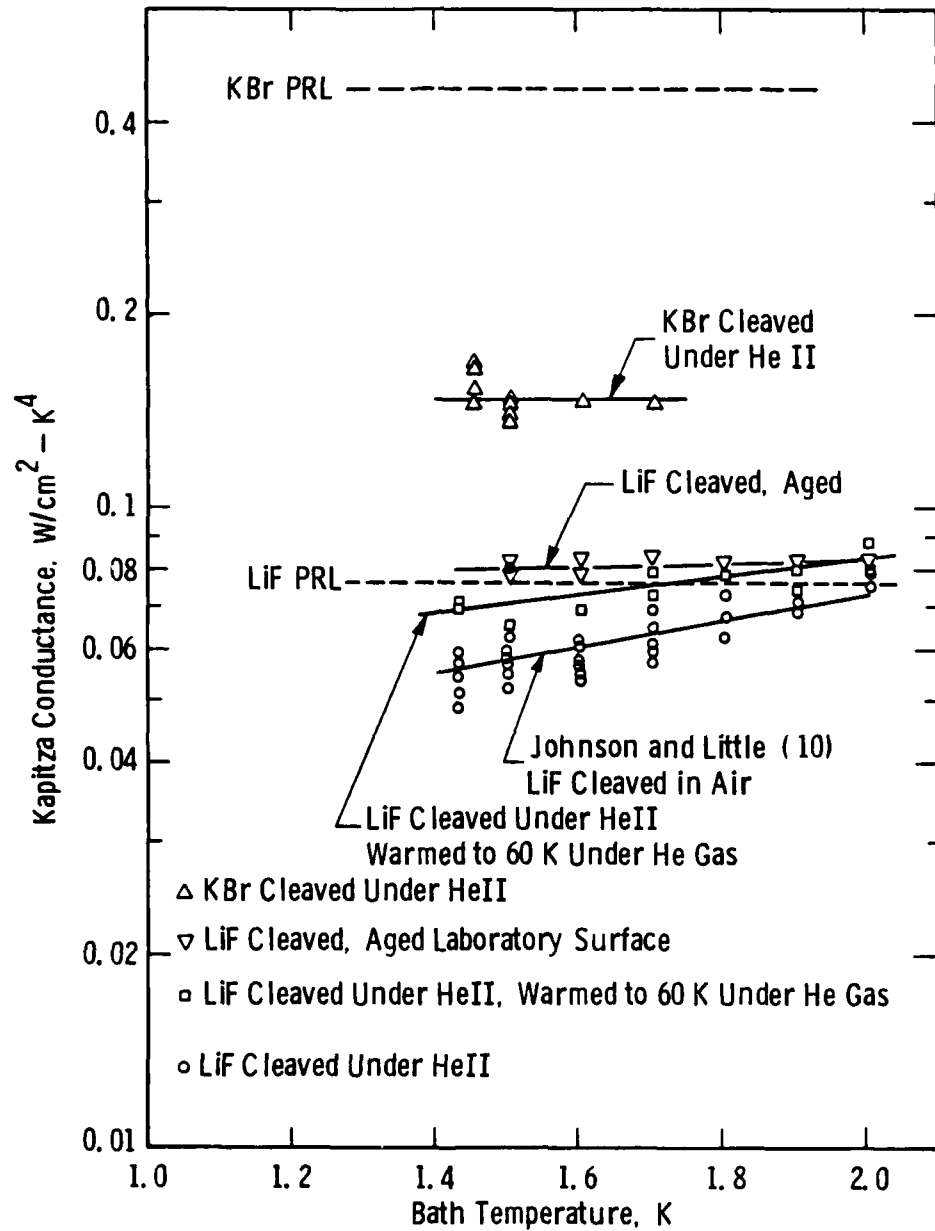


Fig. 10—Kapitza conductance as a function of bath temperature for LiF and KBr

Figure 10. A Summary of the Kapitza Conductance Data.

contaminant increased in vapor pressure enough to contaminate the surface during the warm-up but the possibility of other effects cannot be eliminated.

Analysis of the surface cleaved under helium using a moving stylus (Sloan Dektak II) showed the existence of 1 - 2  $\mu$  steps in the surface but the surface was generally of good quality. The anomalous conductance cannot be attributed to surface roughness but may be attributable to micro-fracturing.

Summarizing the results, it is evident that surface contamination is a small part of the "anomalous" Kapitza conductance for LiF. The Kapitza conductance of cleaved LiF is two orders of magnitude above the acoustic mismatch theory prediction,  $0.0009 \text{ W/cm}^2\text{K}^4$ , and more than one order of magnitude larger than any modification of that theory [10]. These results, obtained by heating, are remarkably different from those reported using phonon reflection techniques and it appears that further effort in trying to resolve the difference between the two measuring techniques would be useful.

Because of our inability to significantly reduce the Kapitza conductance of LiF toward the acoustic limit by conventional techniques, further study of LiF may be useful in fundamental Kapitza conductance experiments directed at identifying the source of the anomalous conductance. In the absence of any other theories, we conclude that surface microstructure is primarily responsible for the anomalous Kapitza conductance in LiF since surface impurities and volumetric imperfections in these tests were minimal. In particular, surface microstructure studies coordinated with theoretical analysis of the type published by Shiren [11] appear to be an appropriate next step.

## 6. REFERENCES

1. O. Pfothenhauer, J. M. and Donnelly, R. J., "Heat Transfer in Liquid Helium," Advances in Heat Transfer, Vol. 17, Edited by J. P. Hartnett and T. F. Irvine, Jr., Academic Press, 1985, Pg. 65.
2. Frost, W., Heat Transfer at Low Temperatures, Plenum Press, 1975.
3. Snyder, N. S., Heat Transport Through Helium II: Kapitza Conductance, Cryogenics, V. 10:2, 1970, Pg. 89.
4. Gilman, J. J. and Johnston, W. G., "Observations of Dislocation Glide and Climb in Lithium Fluoride Crystals," Jo. Applied Physics, Vol. 27, No. 9, Sept. 1956, Pg. 1018.
5. Childs, G. E., Thermal Conductivity of Solids at Room Temperature and Below, NBS Monograph 131, Sept. 1973, Pg. 443.
6. Weber, J. et. al., Absence of Anomalous Kapitza Conductance on Freshly Cleaved Surfaces, Phys. Rev. Lett., V. 40:22, May 29, 1978, Pg. 1469.
7. Parker, J. H., Jr., Exciton-Induced F-Center Growth in KI and KBr Crystals, Physical Review, Vol. 124, No. 3, Nov. 1, 1961, Pg. 703.
8. Yates, B. and Panter, C. H., Thermal Expansion of Alkali Halides at Low Temperatures, Proc. Phys. Soc., Vol. 80, 1962, Pg. 380.
9. Mittag, K., Kapitza Conductance and Thermal Conductivity of Copper, Niobium and Aluminum in the Range from 1.3 to 2.1 K, Cryogenics, Vol. 13, No. 2, Feb. 1973, Pg. 94.
10. Johnson, R. C. and Little, W. A., Experiments on the Kapitza Resistance, Physical Review, Vol. 130, No. 2, Apr. 15, 1963, Pg. 596.
11. Shiren, N. S., Surface Roughness Contribution to Kapitza Conductance, Phys. Rev. Lett., V. 47:20, Nov. 16, 1981, Pg. 1466.

Appendix B

SOLID-SOLID KAPITZA STUDIES

Progress Report  
AFOSR Contract #F49620-83-C-0129

Fundamental Physics Studies on High-Specific-Heat  
Dielectrics and Kapitza Resistance at Dielectric Boundaries

Kapitza Studies I. Probe Design and Construction

by

C.F. Clark *CFC*

CeramPhysics, Inc.

Westerville, Ohio 43081

January 5, 1984

Distribution:

J.H. Parker, Sr.

~~P.~~W. Eckels

T.K. Gupta

M. Ashkin

W.N. Lawless

The initial months of the contract have been used to design a low-temperature probe for doing Kapitza experiments. The probe is neither simple to design nor build because of the different types of experiments it must accommodate. First and foremost there should be no paths for heat flow other than directly through the Kapitza samples. Even when this requirement cannot be strictly met, any extra heat paths should be small and measurable. An example will be discussed below. In any case, heat paths due to poor vacuums and/or radiation loads should be eliminated by correct design. In particular, a high vacuum needs to be maintained around the sample and all experiments need to be done inside an adiabatic shield maintained at the temperature of the heat reservoir.

This heat reservoir presents a problem because of the typical temperature ranges over which most of the experiments will be performed, i.e. from 1.5 K to 6-8 K. This range implies that a  $\text{He}^4$  subpot would be ideal rather than a mass of metal which is thermally linked to a pumped helium bath. However a probe with a subpot is more complicated to build.

A subpot of some kind is necessary for Kapitza experiments between a solid and liquid or gaseous helium. The alternative is to have one end of the sample opened directly to a pumped bath - an impractical solution both in probe design and from the standpoint of being able to control a subpot environment more than a bath. The probe also needs to accommodate solid-solid interface experiments which have no direct need for a subpot (other than as a possible heat reservoir). The requirement for different types of interface (solid-solid, solid-liquid, solid-gas) experiments with different requirements for the geometry of each is a problem in the design of the probe. Other experimenters have built probes to do either solid-solid or solid-fluid interfaces, but not both.<sup>1-3</sup>

The probe shown in Figures 1 and 2 is designed for maximum flexibility and should be useful for all Kapitza experiments (except those in high magnetic fields). Figure 1 is a schematic of the overall design. Pumping tubes (A and B) support a vacuum can (F) which is attached to a flange (D) with an indium o-ring. Pumping tube A leads to the vacuum space at the lower end and a diffusion pump at the upper end. Pumping tube B is attached to a large mechanical pump at the upper end and the subpot (G) at the lower end. The subpot temperature can be controlled two ways: either by a heater (attached to a controller) around the subpot, or by a vacuum regulator valve placed between the mechanical pump and probe. The subpot is filled using a fill line valve which enters the probe through another tube (C). The actual valve seats immediately above flange D where there is a small opening in tube C. When the valve is opened, helium from the bath space flows through the fill line (E) into the subpot. The valve can then be closed before pumping on the subpot. All experiments will be conducted inside an adiabatic can (H) anchored to the subpot.

Electrical leads enter through a vacuum tight feedthru at the top and go down in another tube (not shown) through the flange D and are heat-sunk both at the flange and on the subpot. Enough leads are provided to accommodate several samples in one run.

An enlargement of the experimental space is shown in Fig. 2. The adiabatic can (H) is threaded onto the bottom of the subpot (G). There are two primary places to attach experiments. A threaded post (J) provides good mechanical support and intimate thermal contact to the reservoir. There is also a port (I) into the subpot. This port is shown plugged with an insert sealed with an indium o-ring. If required, the plug may be removed and another tube attached which in turn would lead to a small reservoir that would

provide the helium side of a solid-liquid interface. The flexibility and interchangeability of the experiment hanging from the subpot bottom means that decisions on methods for sealing samples into this small helium reservoir do not have to be made immediately. This support necessarily provides a small extra heat path and it may be necessary to try several designs for this support in order both to minimize the heat loss and to seal the sample. The probe design makes it easy to test different methods.

At present engineering drawings have been done for the probe, the materials have been ordered and received and most of the parts have been machined. Construction of the probe will start shortly, followed by initial Kapitza measurements.

#### References

1. Curt Schmidt, Phys. Rev. B 15, 4187 (1977).
2. C.L. Reynolds, Jr. and A.C. Anderson, Phys. Rev. B 14, 4114 (1976).
3. J.C.A. van der Sluijs and A.E. Al Naimi, Cryogenics 16, 161 (1976).

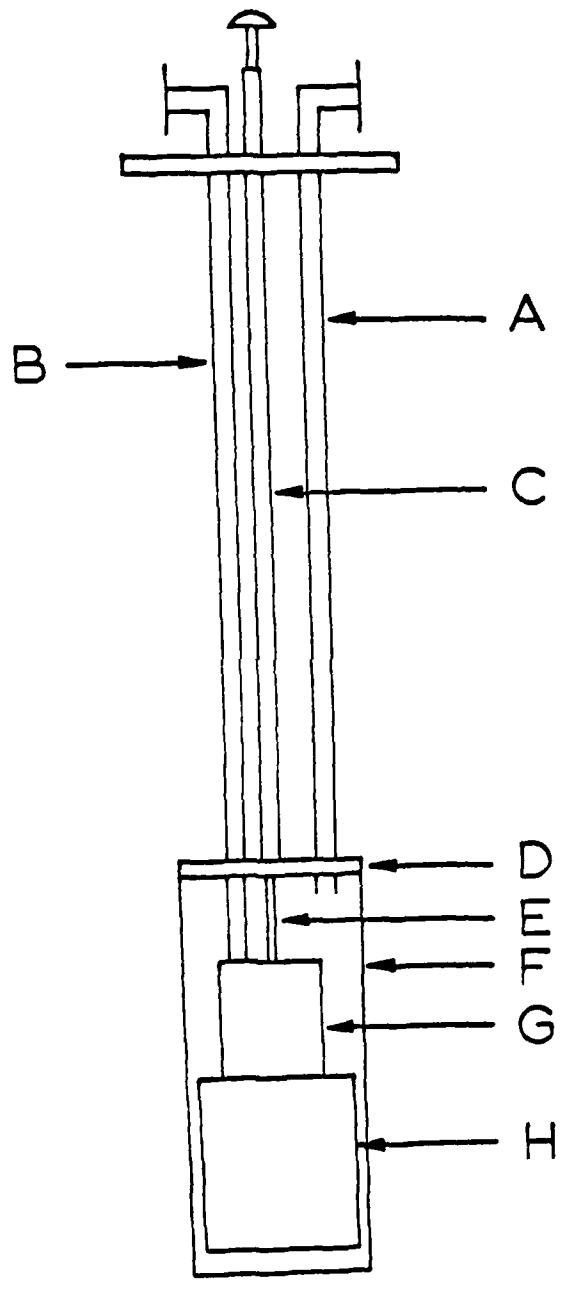


Figure 1.

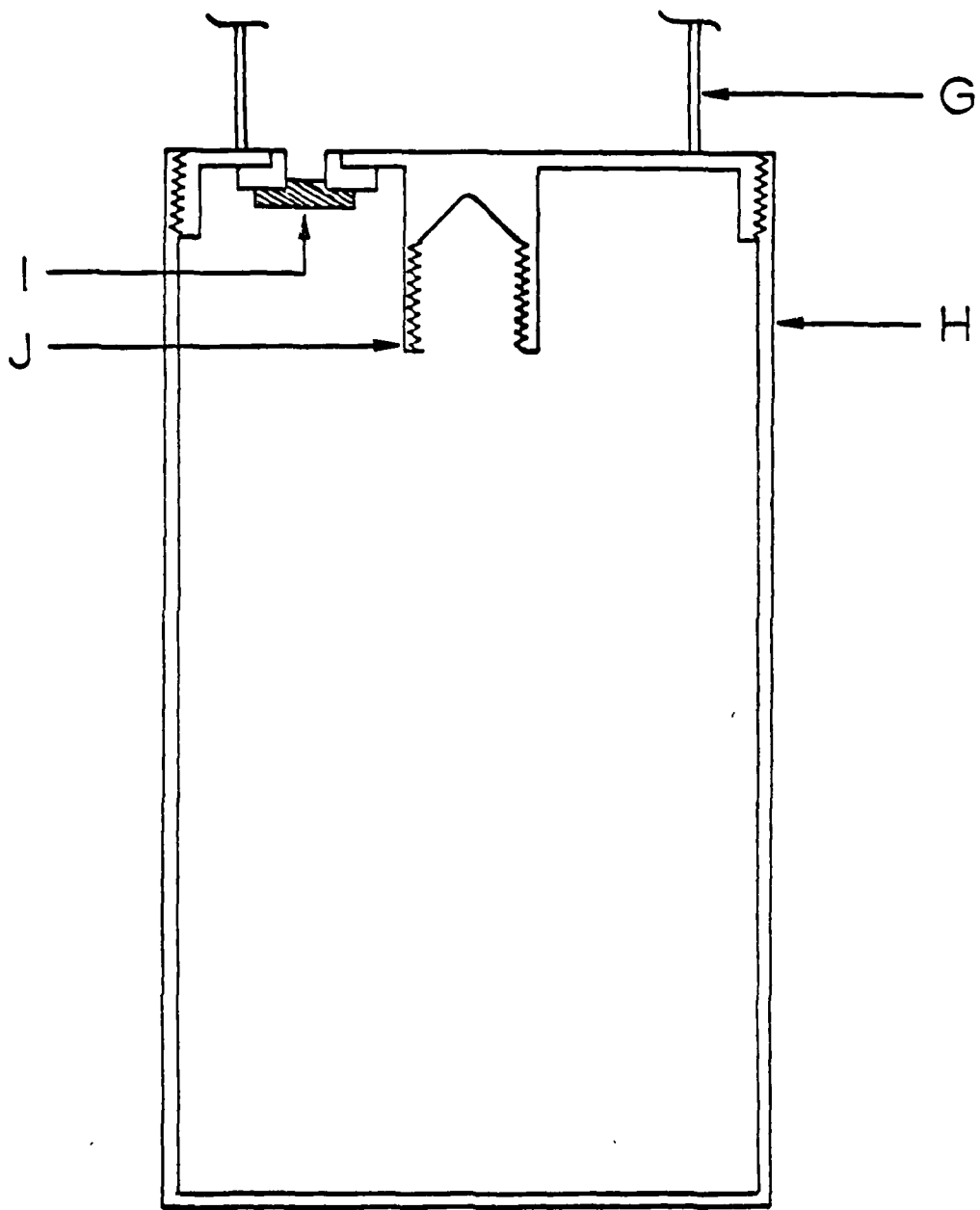


Figure 2.

B-7

Progress Report

AFOSR Contract #F49620-83-C-0129

Fundamental Physics Studies on High-Specific-Heat  
Dielectrics and Kapitza Resistance at Dielectric Boundaries

Kapitza Studies II. Preliminary Tests

by

C.F. Clark

CeramPhysics, Inc.

Westerville, Ohio 43081

October 10, 1984

Distribution:

J.H. Parker, Sr.

P.W. Eckels

T.K. Gupta

M. Ashkin

W.N. Lawless

This report summarizes the results of recent tests using the specially-built probe for studying Kapitza resistances. The purpose of the tests was three-fold: (1) to evaluate the performance of the probe under real operating conditions, (2) to develop experimental techniques of measurement, and (3) to obtain some preliminary Kapitza resistance data.

Since the last report, the probe has been machined, assembled and leak-checked at room and liquid nitrogen temperatures. The only problem was in accurately machining a needle valve and seat at the opening to the subpot. The valve is located immediately above the vacuum can flange in the liquid helium bath space. When the valve is opened by using a stem which runs out the top of the probe, liquid helium can run into the subpot from the bath space. The valve has to seal completely when shut, but the channel into which the valve has to seat is only .015" in diameter which implies a high accuracy not only in machining parts, but also in assembling them. After some testing, a valve was developed which seals completely and reliably and should last as long as the probe.

For these first experiments, an interface of TlC<sub>2</sub> to copper was chosen. TlC<sub>2</sub> has a large thermal conductivity (comparable to copper at helium temperatures) and is one of the principal materials being considered as a superconducting coating material. A piece of TlC<sub>2</sub> ceramic with convenient dimensions (0.17 cm<sup>2</sup> cross-sectional area and approximately 3.5 cm in length) was chosen and placed in the fixture pictured in Figure 1. The copper fixture was machined from a single piece of ETP copper and attached at the bottom to the probe reservoir.

The T&C $\lambda$  was held in place by placing a piece of nylon horizontally across the top of the T&C $\lambda$ . This piece was screwed into two vertical pieces of nylon which were anchored at their bottom end to the two horizontal wings of the copper fixture.

A 400 ohm manganin heater was wrapped around the top of the T&C $\lambda$  sample and attached with GE 7031 varnish. Two thermometers were placed in thermal contact on each sample by taking a doubled strand of small gauge copper wire, wrapping it around the sample, twisting the free ends together, wrapping the free ends around the thermometers and lightly varnishing the wrap to the sample. This method provides a much more precise knowledge of the relative positions of the thermometers as compared to directly attaching each thermometer to the sample.

Each thermometer was an Allen-Bradley 1/8 watt, 220 ohm (nominal) carbon resistor with the outer plastic coating removed. The thermometers were wired in series and were isolated from each other with a short length of 100 ohm/ft manganin between each one. A voltage lead pair for each thermometer provided a potentiometric measurement of each device. An accurate room temperature resistance measurement was made of the heater and a correction formula was used for the resistance at low temperatures. A small correction was also made for the heater's connecting lead lengths. The nylon supports provide an additional heat path, but since the thermal conductivity of nylon is so low, a correction for the nylon would be less than 0.1% and was therefore ignored.

After the probe was loaded, sealed, and leak-tested at room temperature, it was cooled overnight to liquid nitrogen temperatures.

The next morning, the bath space surrounding the probe was filled with liquid helium while helium exchange gas in the subpot allowed the sample to cool in a short time. As soon as subpot and sample were near 4.2 K, the subpot valve was opened and the subpot was filled with liquid helium.

The subpot can be pumped through a mechanical regulator valve which is capable of maintaining stable temperatures for a long period of time. The lower limit of the subpot temperature is below 1.5 K. To obtain reservoir temperatures at temperatures above 4.2 K, the subpot can be pumped dry and the temperature controlled with an electronic regulator using a silicon diode as a temperature sensor.

Once a particular reservoir temperature is established, the entire reservoir and sample assembly is allowed to come to temperature equilibrium with no current flowing through the sample heater. Each of the four sample thermometers are calibrated at this temperature against a germanium resistance thermometer attached to the reservoir. This thermometer has been previously calibrated against another thermometer calibrated at the National Bureau of Standards. Next the sample heater is turned on and the sample thermometers are monitored until a steady-state temperature gradient is established in the samples. Each sample thermometer is then read. If necessary a different heater power is established and the thermometers are read again. A good rule-of-thumb seems to be establishing a temperature differential between the two thermometers on a sample of 3-5% of the sample temperature.

After all the measurements are completed, each of the four sample thermometers are calibrated using the equation

$$\log R = A + BT^{-P}$$

where R is resistance, T the temperature, and A,B,P are the fitting parameters. Then the thermal conductivity of each sample can be calculated as function of temperature (with the sample temperature defined as the average temperature between the two sample thermometers). The Kapitza resistance can be calculated from the equation

$$R_K = (A/\dot{Q}) \Delta T$$

where A is the interface area,  $\dot{Q}$  is the heat flow and  $\Delta T$  is the temperature differential across the interface which is obtained by direct extrapolation of the temperature gradient of each sample to the interface.

In the first series of experiments with TlC<sub>2</sub> and copper, the experimentally determined thermal conductivities were more than an order of magnitude lower than the known values. However the isolating manganin links between each of the four sample thermometers was very short (< 1cm). For a second experiment, these lengths were increased to 5-6 cm each. This time, experimental thermal conductivities were very close to accepted values. A plot of the Kapitza resistances from this same run are shown in Figure 2. The data can be analyzed according to the equation:

$$R_K = D T^{-n}$$

Using a least-square fit for all the points shown,  $D = 3.14 \times 10^4$  and  $n = 2.16$ .

Anyone familiar with typical Kapitza resistance numbers will recognize that the exponent n is well within reason (especially for "dirty" surfaces), but that D is much too high. The problem appears to

be in the calculation of the area of the interface, i.e., the contact area occurs not across the entire interface, but is instead only at a few small points across face.

No special care was taken to control the interface surfaces of the copper and TlCl for the experiment. The copper face was machined "flat" but then allowed to oxidize in air. The TlCl was ground (by hand) to a "flat" surface using fine-grained emery paper. Obviously at least one and maybe both surfaces are rough enough (or uneven enough) to limit the contact area. A different method must be found for the future.

A small contact area at the interface also explains the average sample temperatures observed during these experiments. All the data shown in Figure 2 was taken with a nominal reservoir temperature of 4.2 K. The heater power was changed in several steps from about .09 mWatts to 16 mWatts. At each of these power levels, the average copper temperature (i.e., the sample nearest the reservoir) rose only slightly (tenths of a Kelvin at most) while the TlCl temperature climbed to over 19 K at the highest power level. However TlCl has about the same thermal conductivity as copper which means there was a large temperature change across the interface.

In summary, two of the three goals of these experiments were met. The probe performed flawlessly and according to design expectations. The experimental methods appear to be adequate to provide the accuracy necessary for Kapitza measurements. However, because the interface area between the samples was not known, it was impossible to obtain an absolute value for the Kapitza resistance.

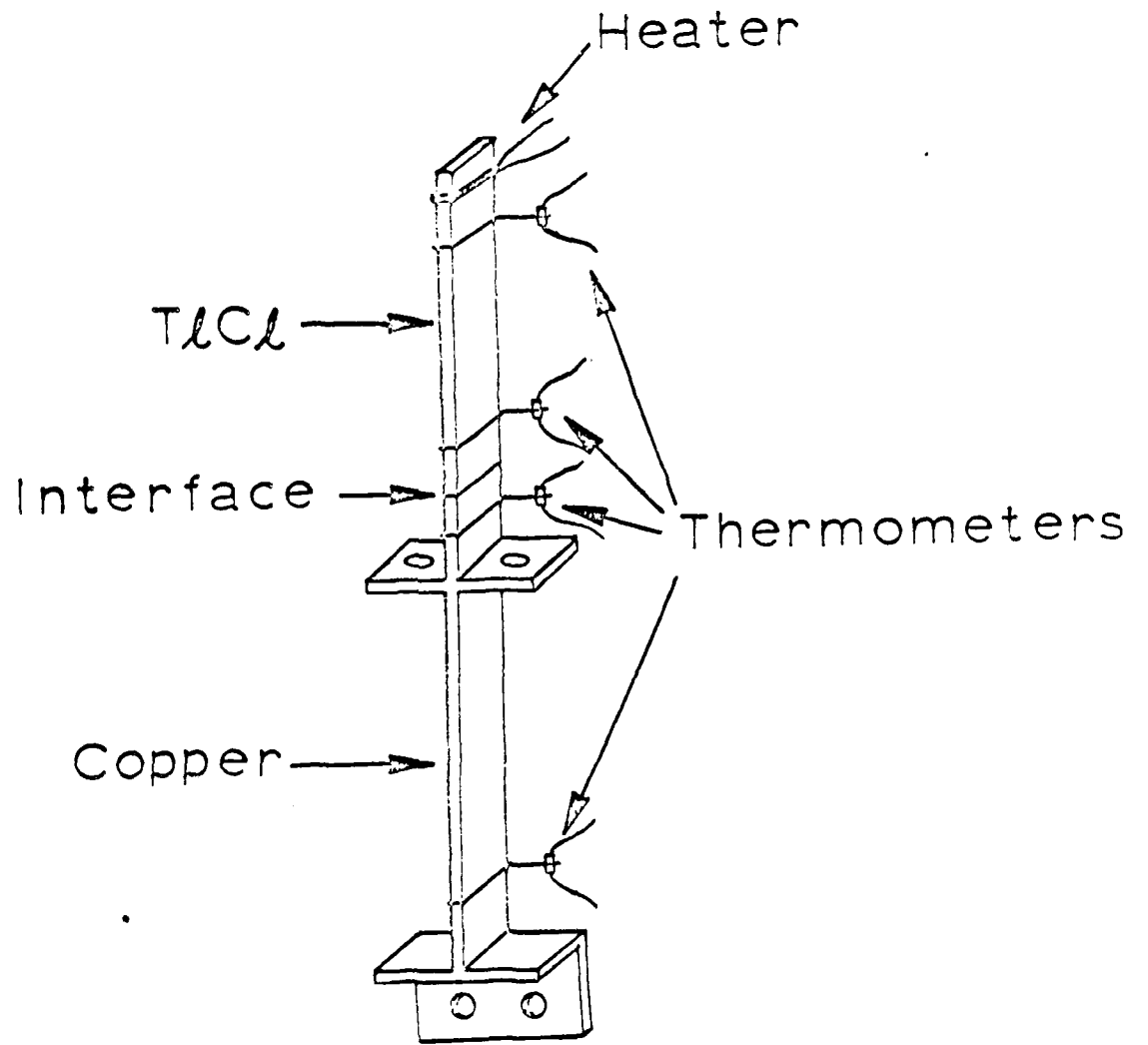


Figure 1: Physical Arrangement of Kapitza Measurement

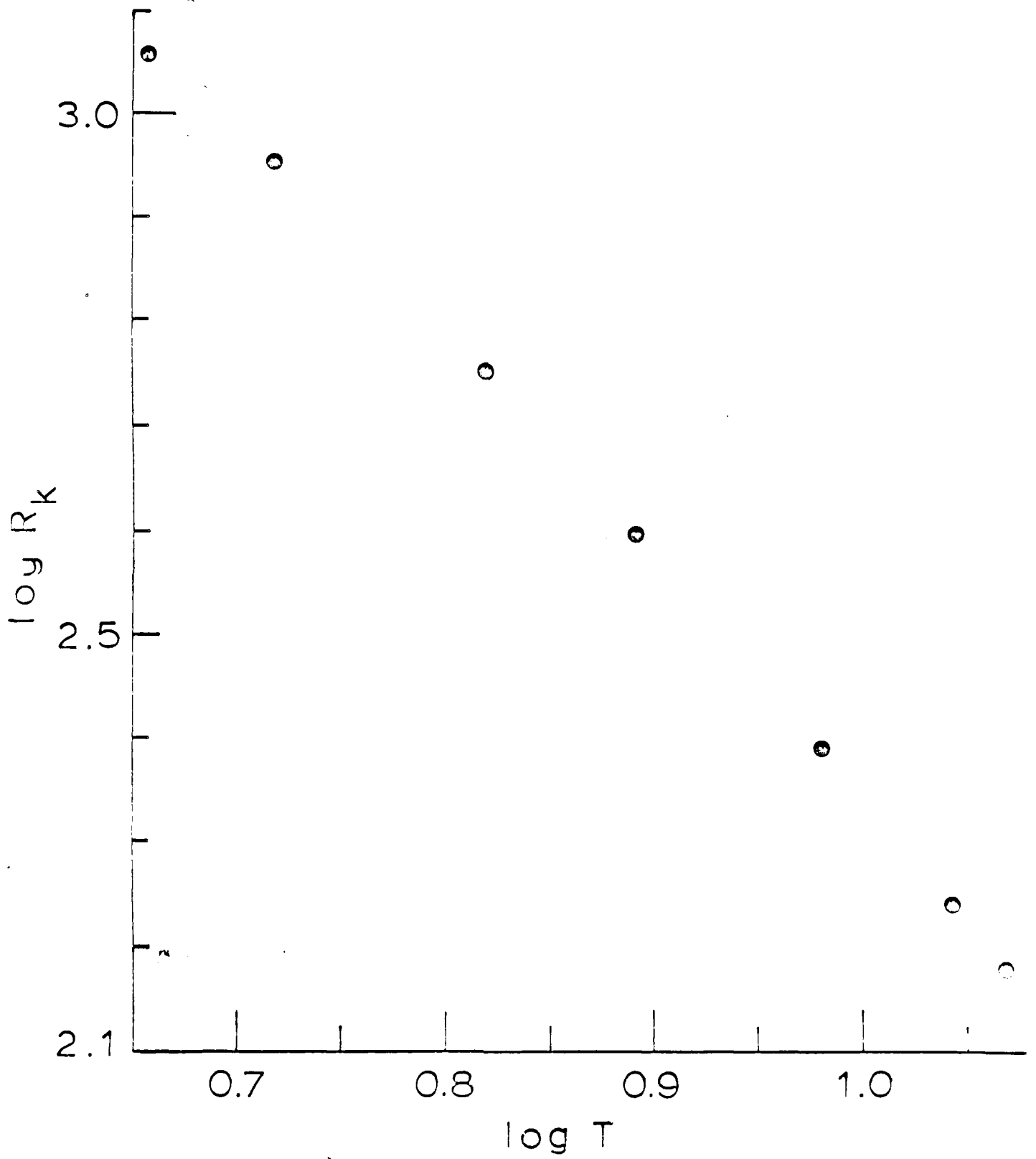


Figure 2: Kapitza Resistance at a  $TaO_2$ -Copper Interface

Progress Report

AFOSR Contract #F49620-83-C0129

Fundamental Physics Studies on High-Specific-Heat  
Dielectrics and Kapitza Resistance at Dielectric Boundaries

Kapitza Studies III. CsI - Copper Interfaces

by

C.F. Clark *CFC*

CeramPhysics, Inc.  
Westerville, Ohio 43081

February 15, 1985

Distribution:

P.W. Eckels  
T.K. Gupta  
M. Ashkin  
W.N. Lawless

Kapitza resistance measurements have recently been completed on interfaces between CsI crystals and metal. CsI belongs to a group of halides which exhibit unusually large thermal conductivities<sup>1</sup> (~1.0 W/cm-k) for dielectrics. Most solid-solid Kapitza measurements have been between metals and low thermal conductivity materials, except for a couple measurements on sapphire-metal interfaces.<sup>2-5</sup>

In the last report on Kapitza measurements, the interpretation of the results on a TlCl-copper interface was ambiguous (in the magnitude of the resistance) because of the uncertainty in the contact area between the samples. For these measurements each of the matching faces was polished optically-flat in order to maximize the contacted surface area.

The CsI crystals were purchased from Harshaw/Filtrol (Solon, Ohio) as an "off-the-shelf" item in single-crystal rods each about .21" in diameter and about 1" long. Each face was polished by Harshaw but nothing was done to the cylindrical walls of the rods. For the metal part of the interface, two rods of 1/4" ETP copper were cut about 1.5" in length. One end of each rod was polished optically-flat at Westinghouse R&D Center (Pittsburgh). One rod was nickel-plated to simulate the nickel-plating on the copper sheath of a superconductor as used in the CeramPhysics/Westinghouse dielectric insulation coating program funded by Wright-Patterson Air Force Base. This latter copper rod was chemically cleaned immediately before it was plated. No other attempts were made to remove surface oxidation, etc. from any samples.

The measurements were done in the probe previously made and described in this program. Two sets of measurements were made simultaneously in the probe: (1) A CsI-unplated copper interface and (2) A CsI-Ni-plated copper interface. Each interface was formed as a pressed contact between a CsI and metal rod with the metal being the closest to the probe reservoir. The pieces were held in place by a yoke of nylon attached with screws to a copper platform which in turn was bolted directly to the probe reservoir. The nylon yoke was made of two "posts" of nylon which

stood on either side of the sample and were parallel to the axis of the sample. These nylon pieces were slightly shorter than the combined length of the two sample rods (CsI + copper). The two nylon posts were bridged by a third nylon piece (a "lintel") and secured to them with screws. This lintel piece thus pressed down onto the sample rods, holding the rods on the platform and against each other. Since the CsI rod was slightly smaller in diameter than the copper rod, there was no problem with the axial alignment of the two rods; it was easy to keep the CsI completely on the face of the copper rod. A slight bit of indium was placed between the copper rod and the platform to ensure good thermal contact at that point.

Calculations show that the nylon conducts less than .1% of the heat. Therefore, this correction was ignored in the calculations.

Two carbon resistance thermometers (nominal 220  $\Omega$ , 1/8 watt Allen-Bradley) were attached to each copper and CsI sample. In order to minimize the uncertainty in the measurement of thermometer positioning, a single strand of Formvar-insulated copper wire was wrapped around a rod for each thermometer. The ends were twisted to draw the wire tightly against the rod and GE 7031 varnish was painted on the wire to ensure good thermal contact. One free end of the wire was then wrapped and varnished to the thermometer.

The thermometers were placed in series in order to minimize the number of lead wires needed (resistance measurements were always four-lead). The thermometers were thermally isolated from each other and from the external leads with about six inches of ~100 ohm/ft manganin between each thermometer and in front of each external lead. The heaters were about 500 ohms of the same manganin wrapped around the free end of the CsI rods.

The results of the Kapitza measurements are shown in Fig. 1 for both interfaces. The methodology consisted of establishing a reservoir temperature at various temperatures 4.2 K and lower. At each of these points, the heater power was turned off and thermometer calibration points were made using a germanium

thermometer in the reservoir. Then heater power was applied, the system was allowed to stabilize, and the measurements were recorded. Usually several different heater powers were applied at each reservoir setting which would drive the sample temperatures a little higher at each increase in power and therefore provide data points at temperatures in between each reservoir setting.

At times, the heater power was either too high or too low as judged by the ratio of  $\Delta T/T$  on the CsI samples, where  $\Delta T$  is the temperature difference between the two sample thermometers and  $T$  is their average temperature. In general  $\Delta T/T$  values less than 1% or more than 6% were eliminated from the data in Fig. 1. Within this range, however, the Kapitza resistance was not affected by the power levels as shown in several places by comparing data at different power levels and different reservoir temperatures. That is, the highest power setting at one reservoir temperature often brought the interface temperature above the temperature from the lowest power setting at the next highest reservoir temperature. The points always were consistent with each other.

The data in Fig. 1 were fit to the equation:

$$R_K = AT^n.$$

For the unplated copper - CsI interface,  $n = -2.76$  and  $A = 144$ , for the plated copper - CsI,  $n = -2.72$ ,  $A = 411$  with units of  $R_K$  of  $(\text{cm}^2\text{-K/W})$ . The slopes are consistent with each other and very typical for solid-solid Kapitza measurements. The values of  $A$  are somewhat higher than usual which probably indicates that even with optically-flat surfaces pressed against each other, the pieces are not in complete contact, (i.e., the cross-sectional area of the CsI rod) is too large and in fact only a fraction of this area was actually in intimate contact with the copper. This area of contact should be somewhat dependent on the pressure applied to the contact which in this case is provided by the nylon post and lintel arrangement. It is not possible to measure

this force directly especially at 4.2 K (recall nylon contracts much more than copper at low temperatures). The difference in the applied force could account for the difference between the two samples in the absolute magnitudes of the Kapitza resistances. Qualitatively, the unplated copper - CsI combination was clamped more tightly and this interface has the lower Kapitza resistance, as would be expected.

As a comparison, consider the measurements of Schmidt and Umlauf<sup>5</sup> on an interface of indium and sapphire. They found a temperature dependence of  $n \sim 2.5$  and a magnitude of  $R_K \sim 0.6-0.8$  ( $\text{cm}^2\text{-K/W}$ ) at 4.0 K compared to values of 3.0 and 10.0 found here. They used vacuum evaporation and casting to form their interface. Their results for  $R_K$  are greater at 4.0 K by a factor of two above that predicted by the acoustical mismatch theory.<sup>6</sup>

When the data is analyzed, the temperature at the interface is found directly by extrapolating the temperature between the two thermometers of any one sample to the interface, i.e., it is not assumed that the thermal conductivity of the sample is known. It can be calculated from the measurements, however, and can be used as a check on the methodology. For instance, in this case the thermal conductivity of both copper pieces was found to be  $\sim 4.5$  W/cm-K at 4.2 K and had a linear temperature dependence. Not only is the magnitude correct, but so is the temperature dependence, which lends credence to the experimental method. The thermal conductivity of the CsI was somewhat depressed compared to the expected value of 5-7 W/cm-K at 4.2 K.<sup>1</sup> Both samples had a positive temperature dependence indicating measurements in the boundary scattering regime. If the peak in the thermal conductivity of these samples occurs at about 10 K, then the depressed thermal conductivity could be explained by boundary scattering from grains with dimensions on the order of a micron. Grains this small are however unlikely in a sample sold by Harshaw as a single crystal.

A more likely explanation is found in Ref. 1. The cesium halides are fairly hygroscopic and there was good evidence in Ref. 1 for the presence of  $\text{OH}^-$  ions in crystals of CsI also

purchased from Harshaw. The crystals used here were "off-the-shelf" and it is not known under what conditions, or for how long they were stored. The presence of  $\text{OH}^-$  ions could provide scattering centers responsible for lowering the sample thermal conductivity.

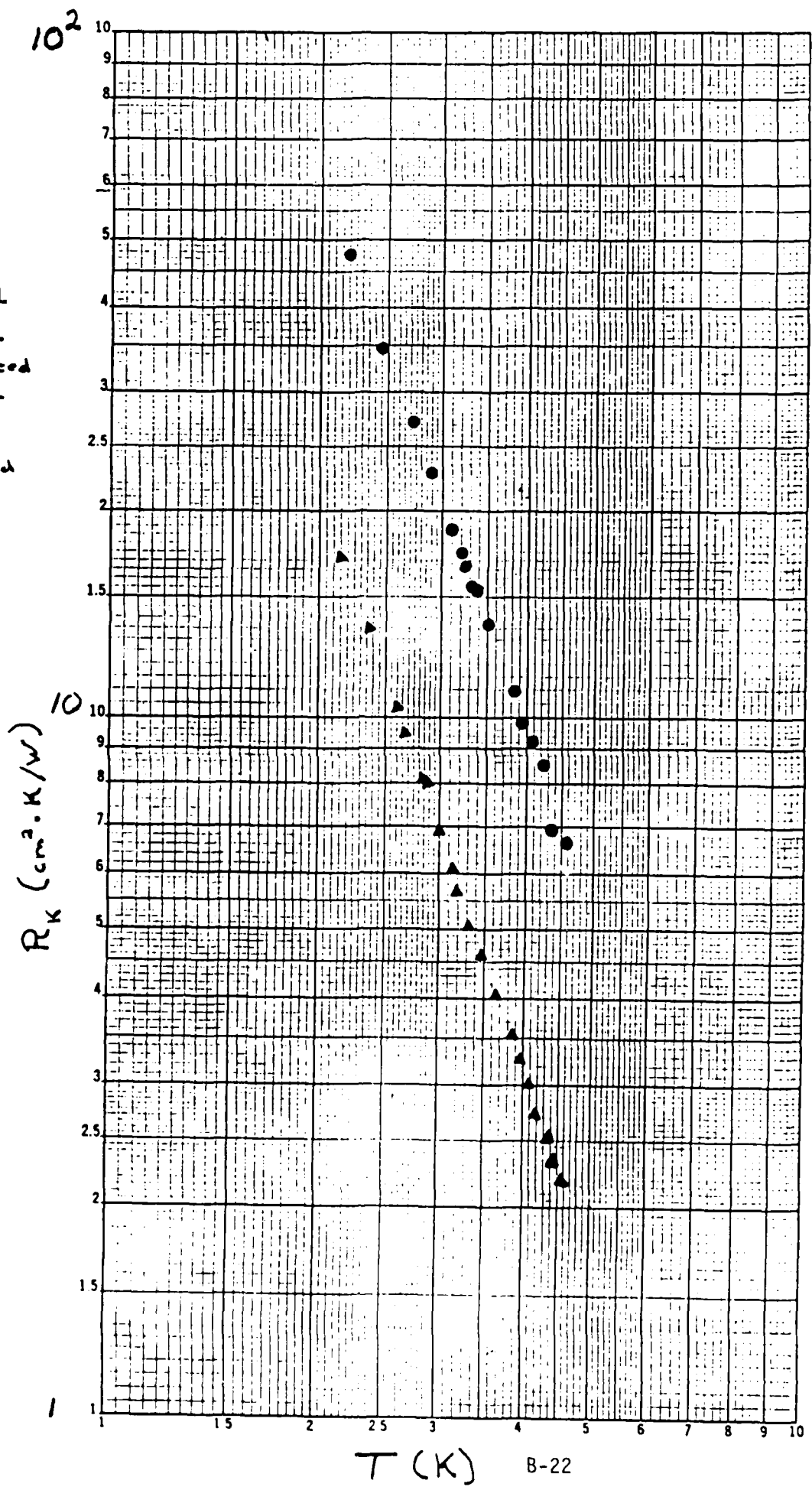
In conclusion, the present measurements are an excellent indication of the temperature dependence of "real" CsI-metal interfaces, i.e., interfaces that would actually be used in the process of coating superconducting wire. Nickel-plating the wire does not change the temperature dependence and probably does not change the magnitude of the resistance.

#### REFERENCES:

1. W.N. Lawless, Phys. Rev. B 30, 6057 (1984).
2. D.A. Neeper and J.R. Dillinger, Phys. Rev. 135, A1028 (1964).
3. M.W. Wolfmeyer, G.T. Fox, and J.R. Dillinger, Phys. Lett. 31A, 401 (1970).
4. B.S. Park and Y. Narahara, J. Phys. Soc. Jap. 30, 760 (1971).
5. C. Schmidt and E. Umlauf, J. Low Temp. Phys. 22, 597 (1976).
6. A.C. Anderson in Nonequilibrium Superconductivity, Phonons and Kapitza Boundaries, Ed. Ken Gray Plenum Press.

FIGURE 1

- CsI - Ni-plated Copper
- ▲ CsI - unplated Copper



Progress Report

AFOSR Contract #F49620-83-C0129

Fundamental Physics Studies on High-Specific-Heat  
Dielectrics and Kapitza Resistance at Dielectric Boundaries

Kapitza Studies IV. Low Thermal Conductivity Interfaces

by

C.F. Clark *CFC*  
CeramPhysics, Inc.  
Westerville, Ohio 43081

August 8, 1985

Distribution:

P.W. Eckels  
W.N. Lawless

## Introduction

A series of measurements has been completed on the Kapitza resistances between high thermal conductivity materials (nickel-plated copper and cesium iodide, CsI), and low thermal conductivity materials. The normal procedure for measuring the Kapitza resistance between two high thermal conductivity materials as detailed in previous reports and reviewed below, must be modified so that uncertainties in the temperature drop across the low thermal conductivity material do not swamp the temperature drop due to the Kapitza resistance.

Four different low thermal conductivity ceramic wafers were measured and are listed in Table I. SClC (also known as CCN(9/1)) has been the subject of previous investigation for use as the high-specific heat component of a ceramic/glass insulator for superconductors and is the present material of choice along with 3072 glass for use in the Westinghouse wire-coating process. As seen in Table I, a 50%/50% (by weight) ceramic/glass mixture was another of the thin wafers measured here. SClD (also known as ZCN(9/1)) is a chemical analog of SClC, both having oxygen-octahedral structures. SClA has also been thoroughly investigated in the Air Force insulation programs, primarily as a higher-thermal conductivity material.

To review, the Kapitza resistance is defined as a temperature difference across a boundary of surface area (A) when heat ( $\dot{Q}$ ) is flowing across that boundary, i.e.,

$$R_k = (A/\dot{Q})\Delta T \quad . \quad (1)$$

The temperature drop occurs because the acoustical mismatch at the interface causes some reflection of phonons from the surface, i.e., not all the phonons incident on the surface are transmitted through it. Experimentally, the best way to measure  $R_k$  is to join two bars of dissimilar material together at their ends. A heat flow is established by a heater at the opposite end of one material and the opposite end of the other material is attached to a constant temperature reservoir. Two thermometers are

attached to each material allowing a measurement of the temperature gradient along the material. The temperature can be extrapolated to each side of the interface thus establishing  $\Delta T$  and  $R_k$  across the interface. This is the method used in the measurements of the previous two reports.

The primary uncertainty in this type of measurement is the uncertainty in the distances between thermometers and from the thermometers to the interface. This uncertainty in length is equivalent to an uncertainty in temperature at the interface. For high thermal conductivity materials this uncertainty in temperature is not as significant as in low thermal conductivity materials. For instance, a temperature uncertainty of 1 mK in a 1/4" copper rod with a thermal conductivity of 1 W/cm-K and a heat flow of 1 mW corresponds to an uncertainty of  $\sim 0.3$  cm in the distance between thermometers, i.e., the total uncertainty in the thermometer positions must be less than 3 mm to know the temperature at any point to within a millikelvin. This accuracy is easy to achieve. However, if the thermal conductivity of a material is lowered by a factor of  $10^3$  (typical for dielectrics), then the position of the thermometers must be known to within three microns in order to preserve the same accuracy under these same conditions, which is an impossible task.

The solution to this problem is to place a thin ( $\sim 50$  microns) disk of low thermal conductivity material between two bars of high thermal conductivity material. Each bar of this high thermal conductivity material has the usual two thermometers. Thus the temperature within these materials may be extrapolated to the nearest interface with the low conductivity material, i.e., the result is a measurement of the total temperature drop across the disk due to the two Kapitza interfaces plus the thermal conductivity of the disk. If the thickness and thermal conductivity of the disk are known, the calculated temperature drop across the disk can be subtracted from the total to yield the Kapitza resistance across the two interfaces.

### Sample Preparation

The high thermal conductivity bars had been previously prepared and were used in making the measurements of the previous report. These are rods of nickel-plated copper and CsI. Each had been polished optically flat on one end. Thermometers were attached by looping a single strand of 30 gauge copper wire around the sample, twisting the ends to hold it tightly and then looping one long end of the wire around the thermometer (a nominal 220  $\Omega$ , 1/8 watt Allen-Bradley carbon resistor). The uncertainty in the placement of loop was  $\pm 0.025$  cm including non-uniformities due to the plane of the loop not being perpendicular to the axis of the rod. GE 7031 varnish was sparingly used on the loop to insure good thermal contact to the rod. Each thermometer lead was thermally isolated from the terminal block by a coiled 1 foot link of .0015" manganin ( $\sim 100$   $\Omega$ /ft).

The thermometers were wired in series to minimize the number of required leads and a voltage lead was attached between each pair of thermometers and at each end of the series so that each voltage measurement was a four-lead (potentiometric) measurement across one Allen-Bradley and two thermal isolation manganin links. The manganin links are ohmic and their resistance is temperature independent over the range used so they are effectively included as a change in a constant in the calibration equation and may be ignored.

The heater on each sample was a nominal 500 ohm manganin heater, the resistance of which was accurately measured at room temperature. There is a known correction for the resistance at helium temperatures, so it was only necessary to measure the heater current to know the heater power.

Each thin disk of low thermal conductivity material was prepared by starting with materials whose thermal conductivity had been previously independently measured. Initial "thick" disks (nominal 100 microns thick) were cut at CeramPhysics using a Buehler "Isomet" cutting saw. They were then sent to the Westinghouse R&D Center where they were polished on each side and

their thickness was measured. Their final thicknesses ended up varying from 35 to over 70 microns. Dr. Phil Eckels was instrumental in getting this work done and his help and care is gratefully acknowledged.

The entire assembly of high thermal conductivity rods with a wafer between them was loaded into a yoke (described in the last report) made of nylon which clamped the assembly tightly against a copper platform which was in turn bolted to the probe reservoir. The probe has also been previously described. Two samples could be run simultaneously, although in most runs a problem occurred which limited the run to one sample. Since nylon shrinks much more than metals when it is cooled, there were large stresses on the nylon yoke at low temperatures. Twice one part of the yoke snapped where it was attached to another part with a screw, thus releasing the sample. The differential shrinking of the nylon also put large pressure on the samples, squeezing them together. This was beneficial in that it increased the contact area at each interface, but it also caused an unexpected problem with the CsI rods. These rods are much more malleable than metals and the large pressures from the nylon bent the rods after no more than two or three runs, i.e., the rods would end up curved by 15°-20°. During a run, this bending would sometimes separate the two pieces of CsI so the upper piece (farthest from the reservoir) was in contact with the lower material on only one edge and would therefore never cool below ~ 40-50 K.

#### Experimental Procedure

The experimental procedure started with an overnight cooldown with liquid nitrogen in the bath space. In the morning this was pumped out and the bath space filled with liquid helium. As it was designed to do, the subpot and reservoir would then cool slowly to 4.2 K over about three hours with the main thermal link being gaseous helium in the subpot and pumping line. After the system was stabilized at 4.2 K measurements were taken by holding the subpot (with a mechanical regulator temperature controller) while heat was applied to the samples. Increasing

the heat flow in small steps effectively raised the temperature of the sample in small steps, so that the reservoir temperature did not have to be reset for each point. A good compromise in the trade-off between minimizing the number of reservoir settings and keeping the heat flow in a reasonable range was to change the reservoir temperature by  $\sim 0.3$  K downward and take 6-8 points (at different power levels) within each reservoir setting.

At 4.2 K, the typical heat flow ranged from  $\sim 1.5$  mW to 10 mW. This range gave a typical  $\Delta T/T$  of  $\sim 1.5\%$ - $10\%$  and this range was maintained at all temperatures. Here  $\Delta T$  is the total temperature drop across the two interfaces and low thermal conductivity disk and  $T$  is the average temperature in the thin disk (which is also assumed to be the Kapitza temperature).

At each reservoir temperature, each of the Allen-Bradley thermometers were calibrated against a previously calibrated germanium thermometer which in turn had been calibrated directly against an NBS calibrated standard. The set of 8-10 calibration points for each Allen-Bradley was then fit to the equation:

$$\log R = A + BT^{-P} \quad . \quad (2)$$

Since only temperature differences are required, the fitted value of  $A$  was not retained. Instead it was recalculated each time there was a zero-power point and this  $A$  was used for each of the thermal conductivity points made at that reservoir setting. This effectively means that in the Kapitza calculations, only temperature differences for each thermometer were used, which increases the accuracy as long as the differences do not become excessively large.

#### Experimental Results

The experimental results are shown in the graphs of Figs. 1-4. Each of the sets of data has been fit to a straight line of the form  $\log R_k = \log D + n \log T$ , i.e., the functional form

$$R_k = DT^n \quad (3)$$

was assumed. The results of the fittings are shown in Table I.

Table I  
Fitting parameters of Equation 3 (units of  $R_k \sim \text{cm}^2\text{-K/W}$ )

Material	D	n
Cu vs. SC1C	244	-2.58
Cu vs. SC1D	778	-2.38
Cu vs. SC1A/3072 (50/50)	673	-2.27
CsI vs. SC1C/3072 (50/50)	12720	-1.92

For the Cu versus SC1C sample only, the fitting was limited to the temperature range  $2 < T < 4$  K since  $R_k$  seems to turn up slightly at each temperature end. All the other fittings include all the points shown on the graphs.

There are no error bars shown, but an estimate can be made of the measurement uncertainty and other errors. For instance, at 4.2 K, the error in absolute temperatures is estimated to be less than 10 mK and is due primarily to error in transferring the calibrations. Typical fits to Eq.(2) gave residuals (squared) on the order of .9999 which corresponded to temperature residuals on the order of 2-3 mK. Kapitza resistances were calculated from temperature differences and these are much more accurate than the absolute temperature uncertainty. For instance the reading error of the resistance was  $\pm 0.1 \Omega$  which corresponds to a temperature uncertainty of  $\sim 0.13$  mK at 4.2 K and decreases rapidly at lower temperatures since  $dR/dT$  increases. From the discussion above, the uncertainty in the thermometer placement also corresponds to an uncertainty in the temperature at the interfaces, but this uncertainty is constant as is the uncertainty in the area measurement and would therefore not affect the error bars on each points, but would raise or lower the entire curve. The heater current uncertainty is the only other uncertainty which would add to the error bar at each point. The lowest heater current was  $\sim 400 \mu\text{amps}$  and it could be read to  $\pm 1 \mu\text{amps}$  or to .025%. There are thus five sources of error for each  $R_k$  measurement: four reading errors from thermometers and the heater current (which is

squared). Thus, the maximum root-mean-square reading uncertainty of each point near 4.2 K is  $\sim .035\%$ . The absolute uncertainty in constants (especially the interface area) dominates all others and is discussed below.

### Discussion

Over the years, there have been many measurements of Kapitza resistance, most of which have been fit to Eq.(3).<sup>1,2</sup> Typical values of  $D$  range from 5-60 (units of  $R_k$  in  $\text{cm}^2\text{-K/W}$ ) while  $n$  ranges from -2 to -3. The acoustic mismatch theory predicts  $n = -3$  and a value for  $D$  which depends on sound velocities (as a function of frequency) and the transmission coefficients of phonons across an interface among other things<sup>2</sup>. Since sound velocities are not available for any of these materials it was impossible to predict what  $D$  should be.

In all cases  $D$  is higher than the typical values. As suggested in the last two reports, this is almost surely due to the necessity of using pressed contacts (even though highly polished) compared to measuring the Kapitza resistance across boundaries of materials which can be bonded to each other. In fact, it is this uncertainty in the contact areas which has probably led most investigators to limit themselves to materials which are either easily deformed and highly malleable (e.g. indium) or to materials which can be directly bonded to metals (e.g. epoxies). One exception was a series of pressed materials measured by A.C. Anderson under very similar conditions to those used in this study.<sup>3</sup> He estimated that for his surfaces (unpolished) only  $\sim 0.01\%$  of the area was making contact. Polishing the surfaces should make a difference and probably does according to Table I. All of the thin wafers seemed to polish about the same judging from how much diffusion of reflected light there was from the surfaces. Of the high thermal conductivity bars, the nickel-plated copper was more highly polished than the CsI rods. These differences account for the large value of  $D$  in Table I for the CsI-SCIC/3072 interfaces since the value of the contact area was probably overestimated more for this surface

than for the copper surfaces since the surface roughness was greater for the CSI surfaces.

The values of D for the copper surfaces are all within a factor of three of each other. It is not known whether these differences reflect (at least partially) real differences in the Kapitza resistance or whether they reflect only differences in the surface roughness and contact pressure (i.e., contact surface area). If the lower value of D for the Cu-SCLC surface reflects a real tendency for SCLC to have a lower Kapitza resistance than SCLA, it would explain an anomalous set of data discovered during previous investigation of SCLC and SCLA in glass for use as insulators on superconductors.<sup>4</sup> The anomalous data occurred when it was noted that when SCLA was added to different glasses the thermal conductivity of the mixtures are depressed by factors on the order of ~ 10-100 below that of bulk SCLA ( $\kappa \sim 10$  mW/cm-K). In fact, there is evidence the composite thermal conductivities are lower than those of the base glasses. This is shown in Fig. 5 for three different glasses with 50/50 (weight) mixtures.

Furthermore, Fig. 6 shows the effect of adding the (relative) high thermal conductivity SCLA in increasing amounts to 3072 glass. The thermal conductivity decreases as more SCLA is added. These results along with the slopes of the thermal conductivity curves are consistent with bulk thermal conductivity of the composite material being limited by a large Kapitza resistance between the grains of SCLA and the glass, and in fact this Kapitza resistance dominates more and more as the percentage of SCLA increases.

An anomaly occurs, however, when the same procedure is followed with SCLC as shown in Fig. 7. In this case the SCLC thermal conductivity is smaller than that of the 3072 glass and has a pronounced dip near 8 K associated with the specific heat maximum. As SCLC is added in decreasing amounts to the glass, the thermal conductivity moves consistently from that of bulk SCLC to that of the glass and the dip disappears. There is no evidence that increasing the SCLC content increases the Kapitza-limiting thermal resistance. Yet both SCLA and SCLC are

refractory oxides with oxygen-octahedral structures and had about the same particle-size distribution in the ceramic/glass mixtures. The anomaly can be explained if the Kapitza resistance of SClC/glass is significantly less than SClA/glass as possibly indicated in Table I.

Even though the values of  $D$  in Table I depend on the contact area, the exponent  $n$  does not, and the exponents calculated here can be taken as accurate for the interfaces measured. As stated above, the predicted value of  $n$  by the acoustic-mismatch theory is  $-3$ , but it is very common to find lower absolute values of  $n$ . The difference between experiment and theory arises from the dominant role of added phonon scattering centers near the interface due to such things as adsorbed gases, oxide layers, dislocations, impurities, etc. These conditions are very hard to control and characterize, and beyond keeping the surfaces clean and protecting the copper surfaces with nickel-plating, no attempt to do so was made here. Recall that one of the primary purposes here was to obtain engineering numbers for the Kapitza resistance which implies using real (non-ideal surfaces) as would be used in the manufacturing process.

With the idea that the data in Table I can be used as the upper limits of the Kapitza resistance, it can be noted that the Kapitza resistance for the Cu versus SClA/3072 interface is  $\sim 25 \text{ cm}^2\text{-K/W}$  at 4.2 K and the thermal conductivity of SClA/3072 is  $10^{-3} \text{ W/cm-K}$  at 4.2 K. This means that the Kapitza resistance at a Cu-SClA/3072 interface is at most equal to an extra 250 microns of SClA/3072 in the length of the heat flow path. Since (judging from the value of  $D$  in Table I) the value of  $R_k$  is probably at least 10 times lower, it can be seen that under most conditions the value of  $R_k$  is negligible compared to variations in thickness of an SClA/3072-coated superconducting wire.

A number of attempts were made to seal one of the CsI rods into a fixture which would allow a Kapitza measurement between the CsI and superfluid helium (i.e., helium with high thermal conductivity). The rod must be sealed against superleaks yet the sealing itself must not add a significant parallel heat path

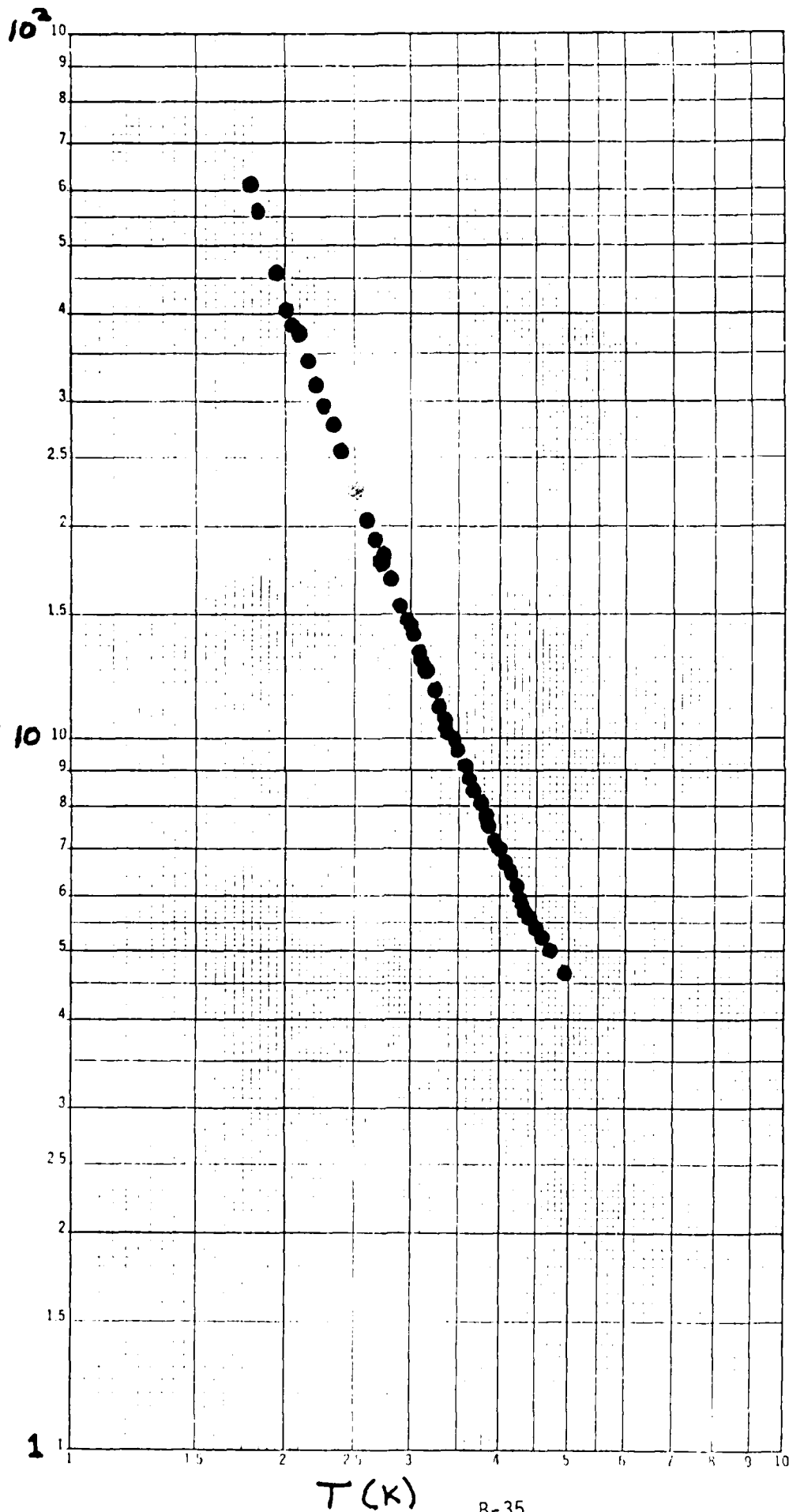
along the rod which would cause measurement error. Several different fixtures were tried with several different sealing methods including indium, several epoxies, and fired-on silver paste with solder applied. None would seal because of the mismatch in thermal contraction between the CSI, the fixture, and the sealing material.

References:

1. Snyder, N.S., Cryogenics 10, 89(1970).
2. Anderson, A.C., in Nonequilibrium Superconductivity, Phonons and Kapitza Resistance, ed by K.E. Gray (plenum, New York, 1981) p. 1.
3. Yoo, K.H. and Anderson, A.C., Cryogenics 23, 531 (1983).
4. Wright-Patterson Air Force Base Contract F33615-82-R-2227, CeramPhysics Letter Reports dated April 7, 1983 and May 25, 1983.

LOGARITHMIC 40 7083  
REUPPEL & EBNER CO

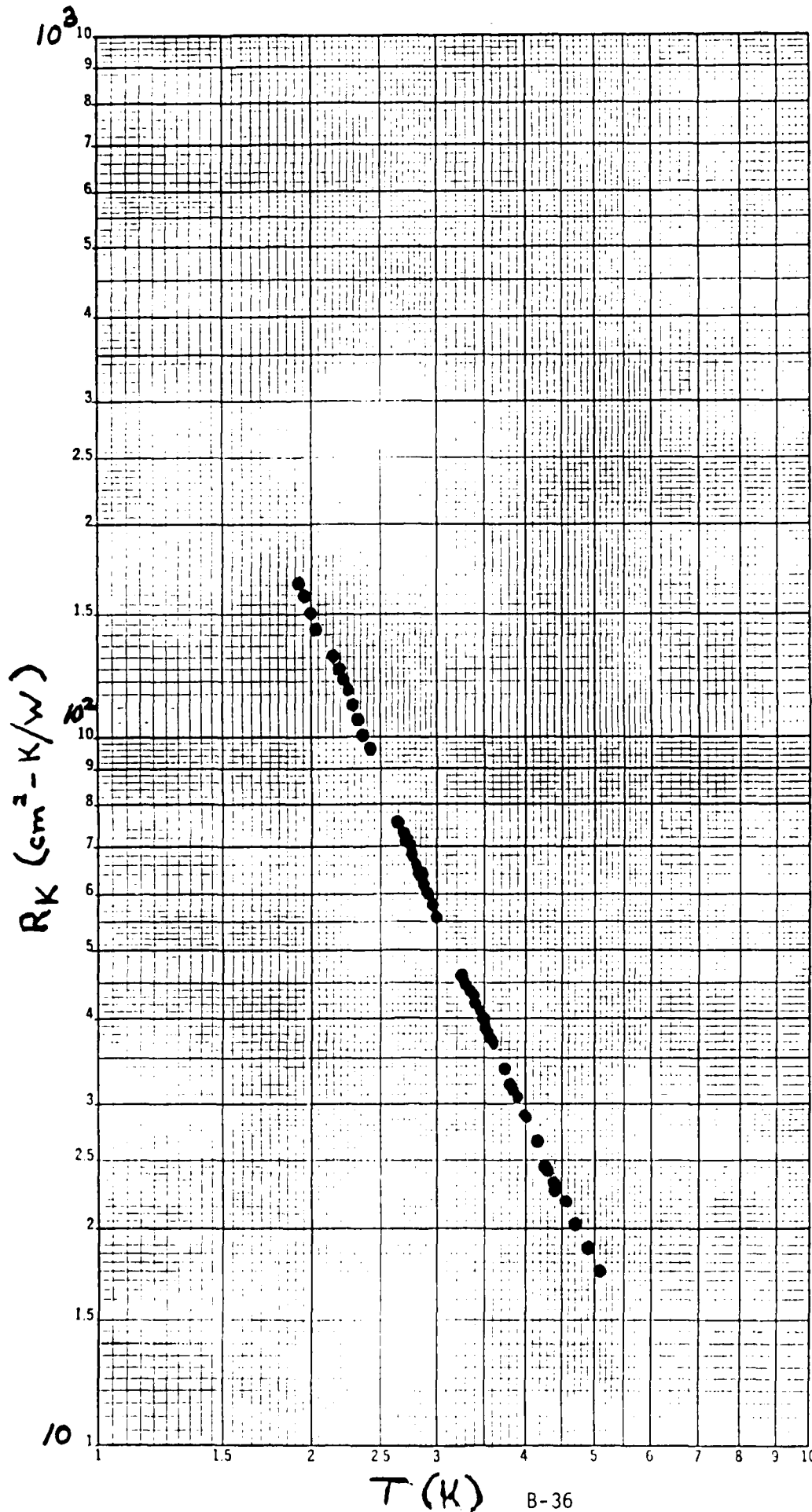
$R_K (cm^2 - K/W)$



Cu vs.  
CCN (9/1)  
(SCIC)

Fig. 1

K&E LOGARITHMIC 46 7083  
2 X 1 CUBES  
MADE IN U.S.A.  
KEUFFEL & ESSER CO



Cu vs  
ZCN(9)  
(SCID)

Fig. 2

Cu vs SCIA/3072 50/50

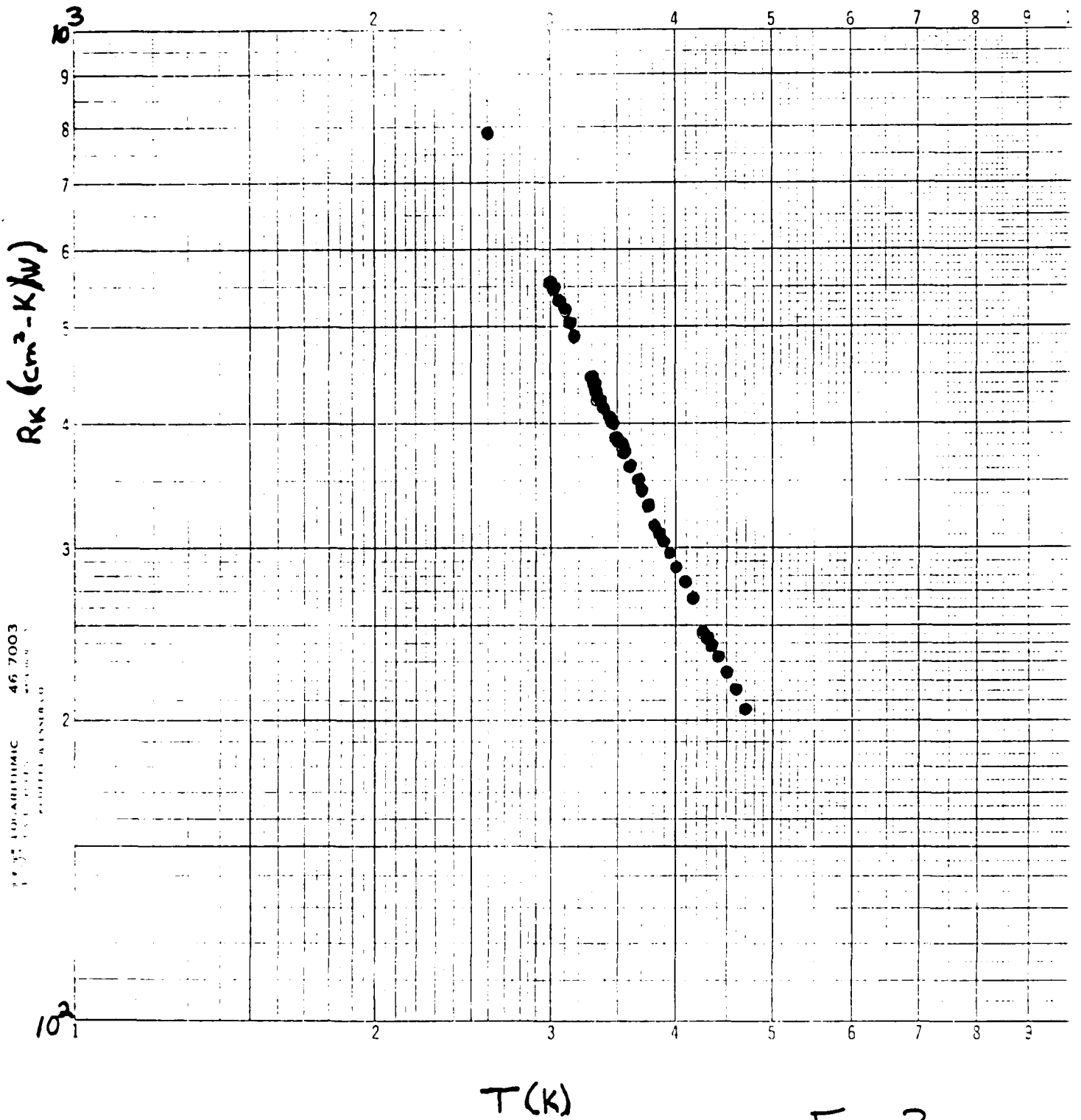
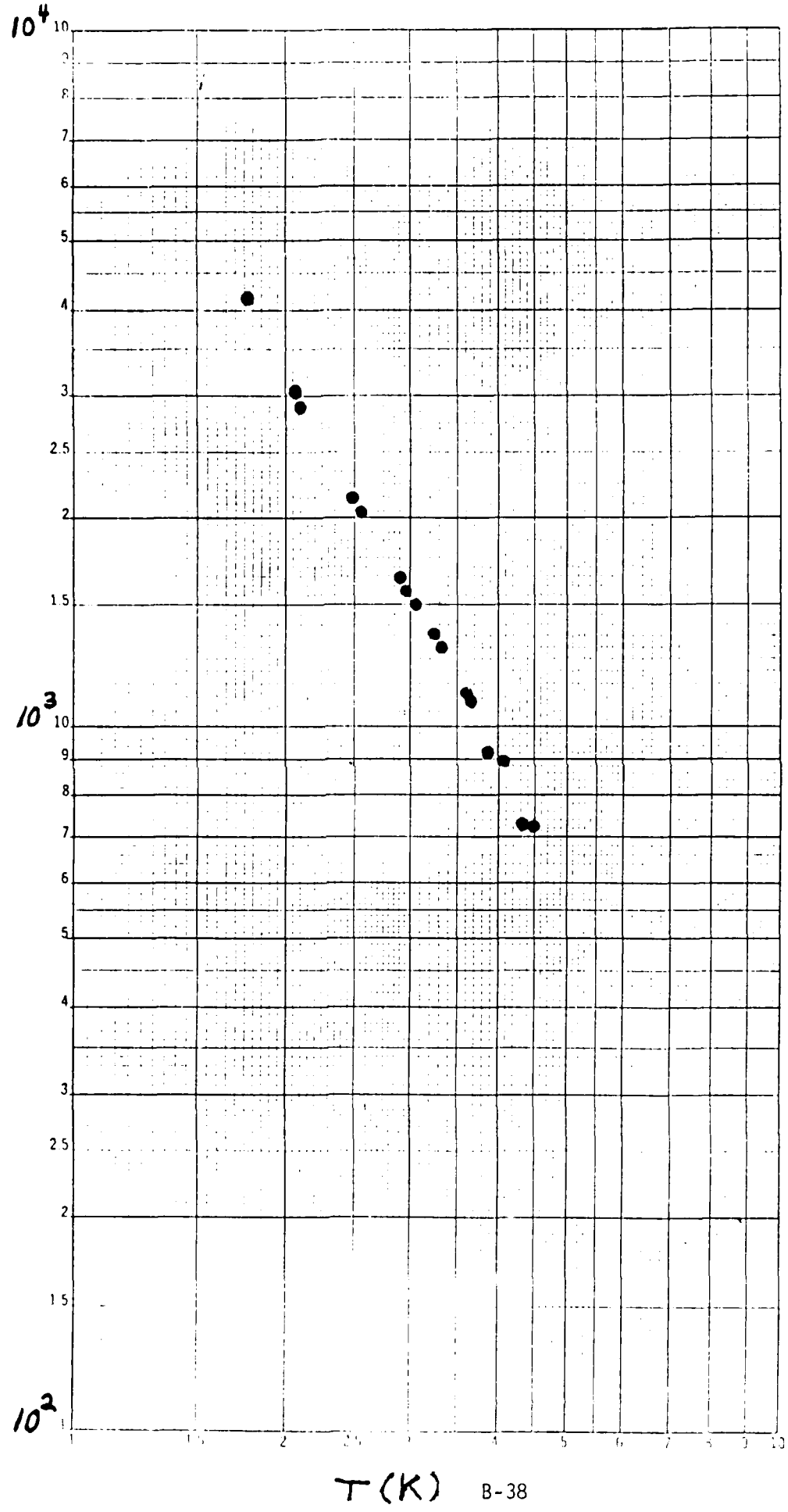


Fig. 3

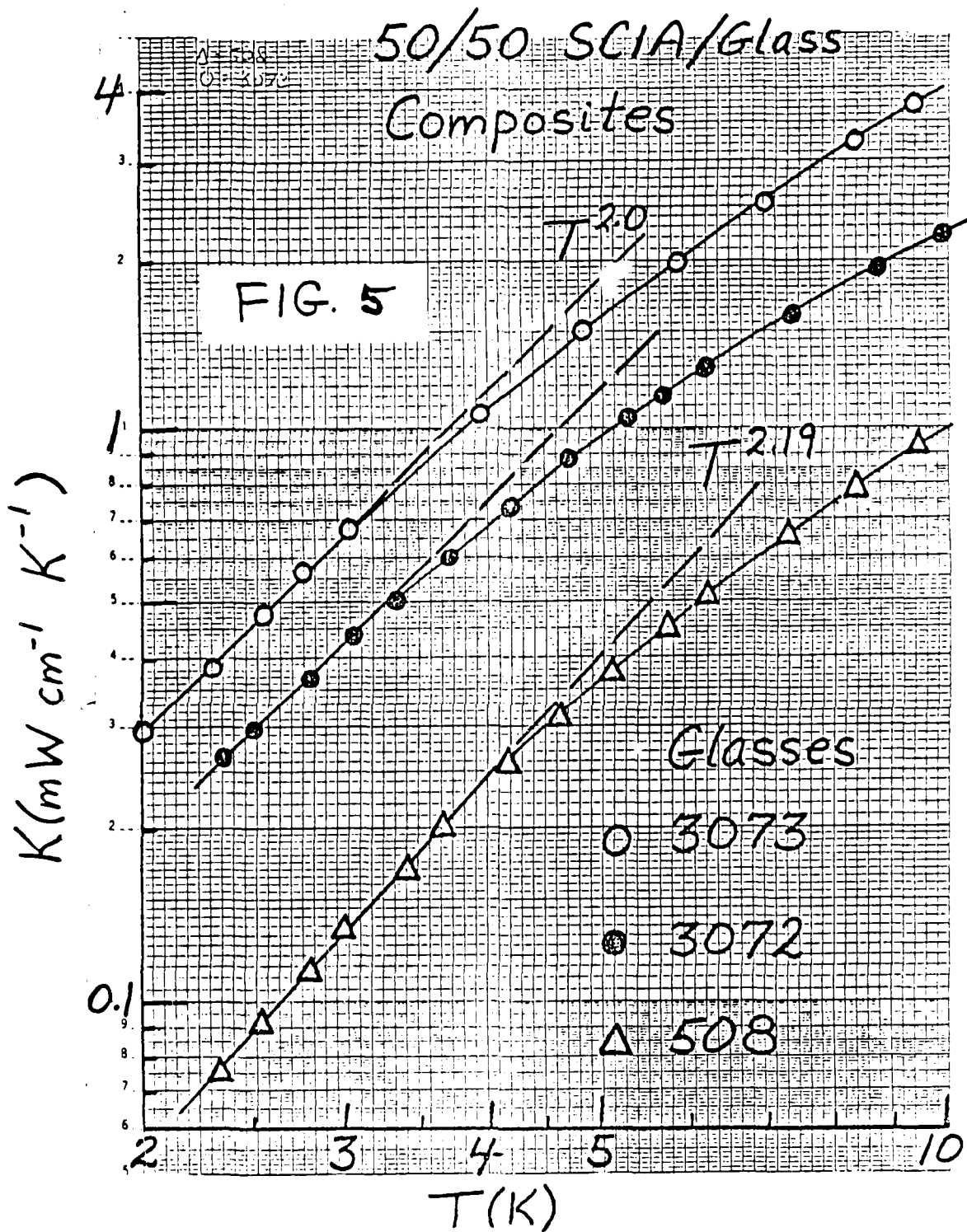
KE LOGARITHMIC 40 7083  
REDFORD & ESSER D

$R_K (cm^2 - K/W)$



CsI ✓  
SCIC/307  
50/50

Fig. 4



SCIA/3072  
Composites

$K(\text{mW cm}^{-1} \text{K}^{-1})$

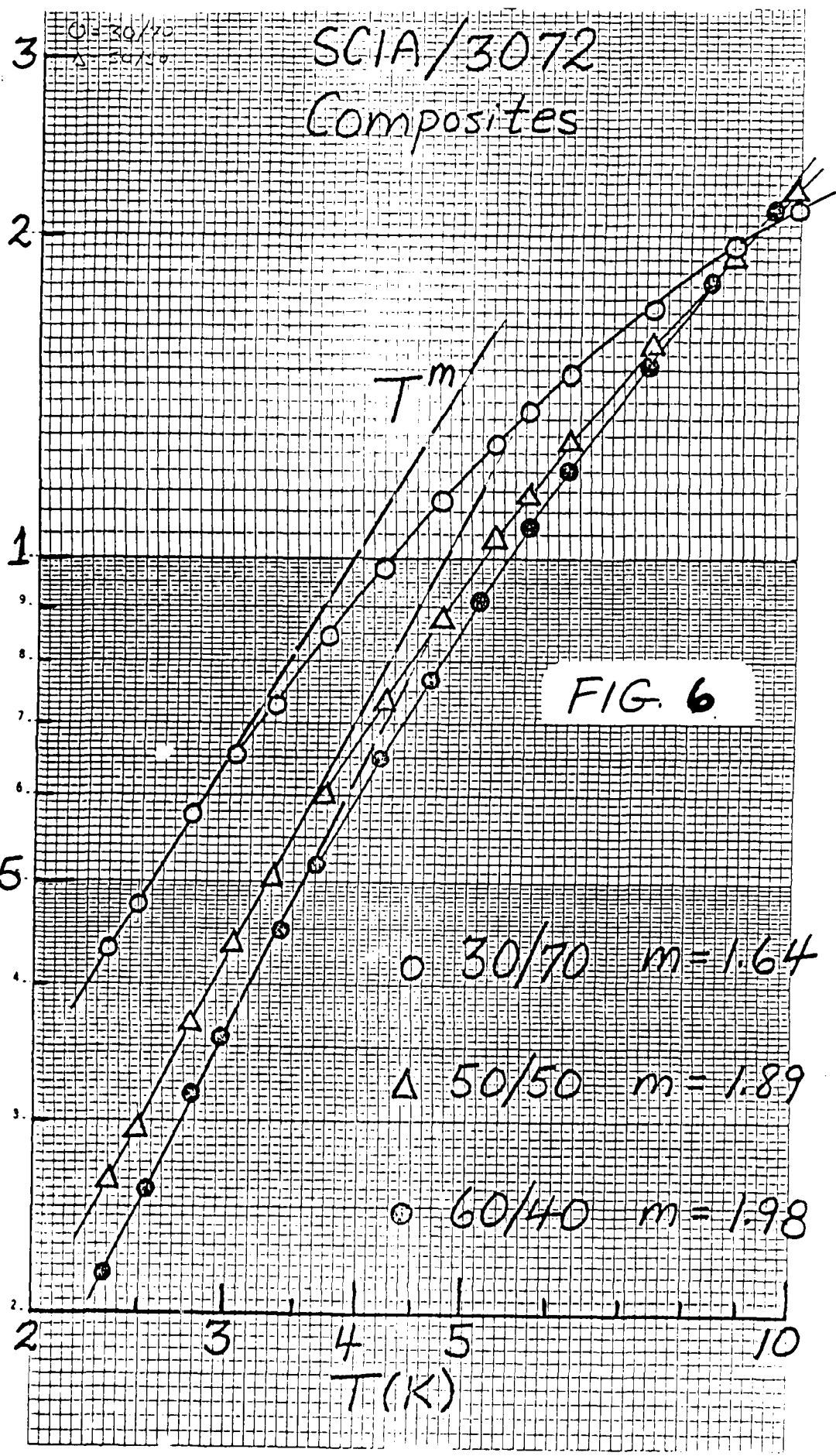
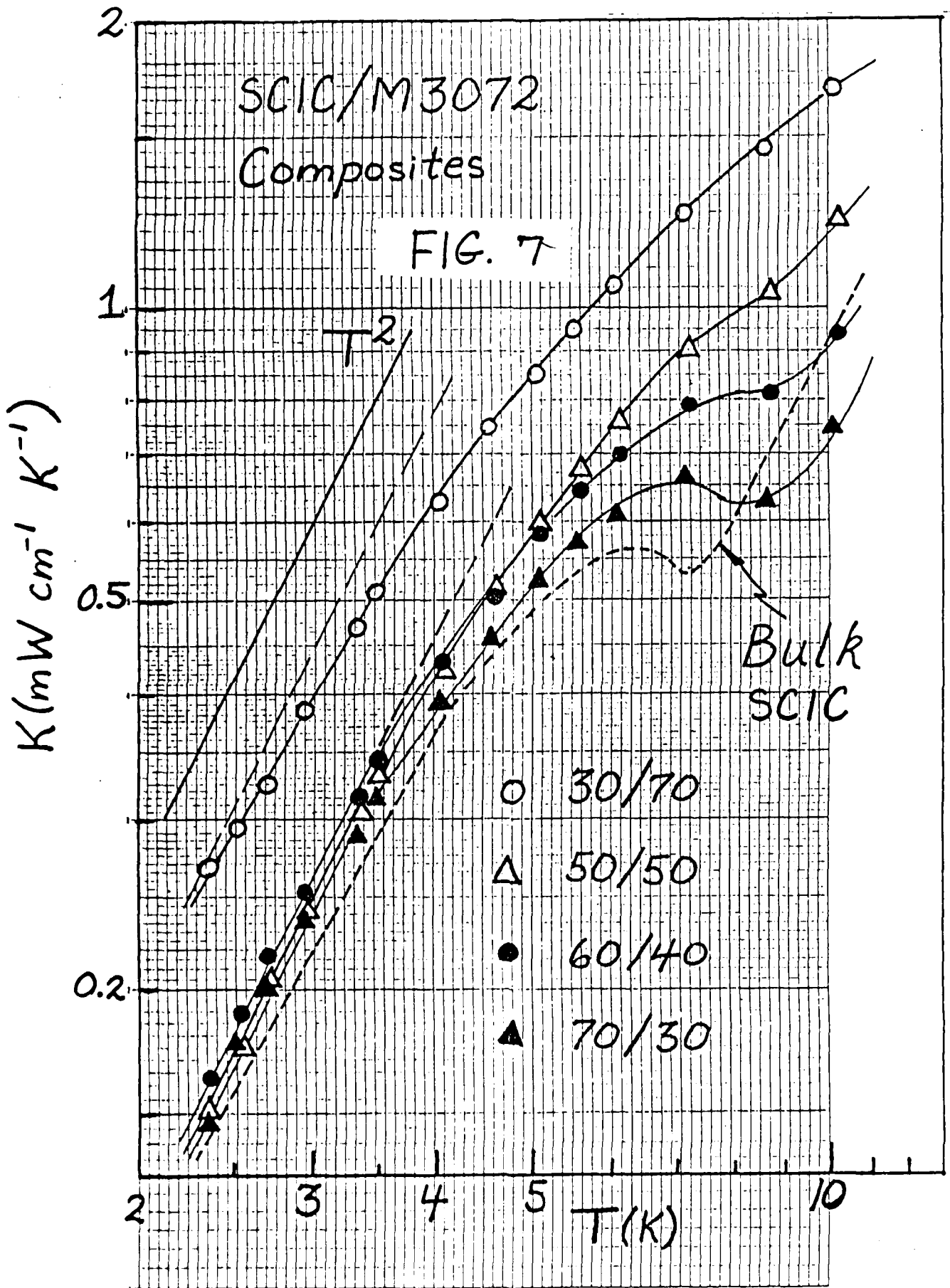


FIG. 6



## Specific heat and thermal-conductivity measurements on cesium and thallos halide crystals at low temperatures

W. N. Lawless

*CeramPhysics, Inc., Westerville, Ohio 43081*

(Received 28 December 1983; revised manuscript received 12 July 1984)

Specific-heat and thermal-conductivity measurements in the temperature range of 1.7 to 20 K are reported on single crystals of CsBr, CsI, TlBr, and TlCl and on a polycrystalline sample of TlI. All crystals display minima in the effective Debye temperatures which are reflected in maxima in  $C/T^3$ -versus- $T$  curves, and these extrema are especially pronounced for TlCl. Comparisons are made with the predictions of existing lattice-dynamics calculations, and the specific heat of TlBr is in very good agreement with the shell-model calculations of Cowley and Okazaki. A Schottky specific-heat term is resolved in the cesium halides at the lowest temperatures and attributed to hydroxyl ions; by adopting the zero-field splitting for  $\text{OH}^-$  in KCl, hydroxyl concentrations  $\sim 10^{20} \text{ cm}^{-3}$  are estimated in CsBr and CsI. The  $C/T^3$  maxima are fitted with Einstein terms added to the Debye backgrounds, and these fittings (together with the Schottky fits for CsBr and CsI) yield the following Debye temperatures: CsBr, 145 K, CsI, 124 K, TlBr, 116 K, TlCl, 120 K, and TlI, 103 K. Thermal-conductivity data for all crystals display maxima at  $\sim 4$ –5 K and an apparent  $T^3$  boundary-scattering regime at the lowest temperatures. Phonon mean free paths at the higher temperatures are analyzed according to the Peierls relation, and for CsBr and TlCl it is found that the Debye modes are the dominant heat carriers. For the remaining crystals, the Einstein modes also carry heat. (The Einstein modes at these higher temperatures dominate the specific heats, contributing up to 75% in the case of TlCl.) Thermal-conductivity measurements were also made on thin crystals ( $\sim 0.05 \text{ cm}$ ) of CsBr, TlBr, and TlCl to examine the boundary-scattering region. It is found that in this region the limiting phonon mean free path for CsBr scales with the crystal dimension, and it is suggested that the suppression of the thermal conductivity may be due to the hydroxyl concentration. For TlBr and TlCl, the limiting phonon mean free path is  $\sim 0.01 \text{ cm}$  and is independent of the crystal thickness; this behavior is attributed to a mosaic structure within these crystals.

### I. INTRODUCTION

Alkali halides are representative ionic crystals with simple-cubic structures and relatively simple interatomic potentials, and as such have been the subject of a great deal of experimental and theoretical work. It has been natural to concentrate on the NaCl-structure crystals, and, by comparison, the CsCl-type halides have been relatively unexplored from an experimental (and, to a lesser extent, from a theoretical) viewpoint.

There are significant structure-sensitive differences in some of the properties of the NaCl- and CsCl-type crystals. For example, the Grüneisen parameters for the cesium halides are practically temperature independent down to low temperatures,<sup>1</sup> whereas the NaCl-type crystals display a marked temperature dependence of this parameter. In the thallos halides, the elastic anisotropy,  $2C_{44}/(C_{11}-C_{12})$ , has a negative temperature dependence,<sup>2</sup> in contrast to the NaCl-type crystals. Other differences have been reported in the temperature and pressure dependences of the dielectric constants<sup>3</sup> and in thermal-expansion coefficients.<sup>4</sup>

The dielectric properties of the thallos halides are especially unique in that the dielectric constants are large ( $\sim 30$ ) and follow a Curie-Weiss law below room temperature,<sup>5</sup> suggestive of a dominant soft-optic mode. However, Samara<sup>6</sup> has shown from pressure and temperature

measurements of the dielectric constants that the explicit temperature dependence of the polarizability is responsible for the Curie-Weiss behavior, rather than a soft mode. Subsequent neutron-scattering and infrared measurements on TlBr confirmed the absence of a dominant soft mode.<sup>7</sup>

The lattice dynamics of several CsCl-type crystals have been calculated based on various models (shell model, rigid-ion model, etc.).<sup>8</sup> These calculations predict the temperature dependence of the Debye temperature ( $\Theta_D$ ) at low temperatures, and two central results are obtained: (1)  $\Theta_D$  at  $T \rightarrow 0$  for comparison with  $\Theta_D$  from elastic constant measurements, and (2) the position of a minimum in  $\Theta_D$  in the helium-temperature range. The former property is not very model dependent because  $\Theta_D(0)$  is determined primarily from the elastic continuum. On the other hand, the position and depth of the minimum in  $\Theta_D$  results from the first rapid rise in the density of states (i.e., above the  $\omega \propto k^2$  Debye background) and so is very model dependent. However, there do not appear to be adequate specific-heat data in the literature for the CsCl-type crystals in the neighborhood of these predicted minima in the  $\Theta_D$ 's. In addition, no measurements of the thermal conductivities of CsCl-type crystals at low temperatures have been reported.

The purpose of the studies here was to measure the specific heats and thermal conductivities of several CsCl-type crystals at low temperatures, namely TlBr, TlCl, TlI,

AD-A169 964

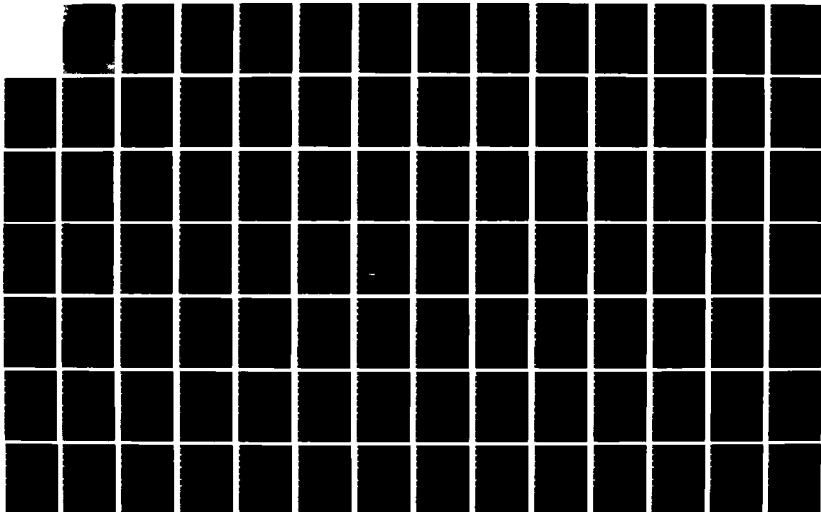
HIGH SPECIFIC HEAT DIELECTRICS AND KAPITZA RESISTANCE  
AT DIELECTRIC BOUND (U) WESTINGHOUSE RESEARCH AND  
DEVELOPMENT CENTER PITTSBURGH PA P W ECKELS ET AL

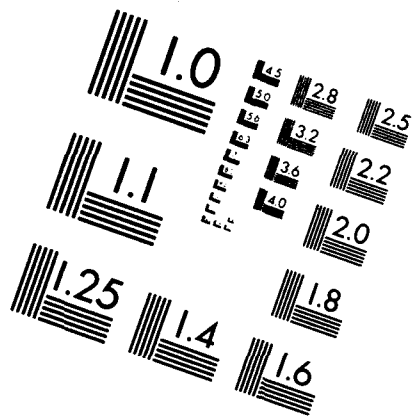
2/5

UNCLASSIFIED

30 SEP 85 AFOSR-TR-86-0477 F49620-83-C-0129 F/G 20/13

NL





MICROCOPY RESOLUTION TEST CHART  
NATIONAL BUREAU OF STANDARDS-1963-A

## Specific heat and thermal-conductivity measurements on cesium and thallos halide crystals at low temperatures

W. N. Lawless

*CeramPhysics, Inc., Westerville, Ohio 43081*

(Received 28 December 1983; revised manuscript received 12 July 1984)

Specific-heat and thermal-conductivity measurements in the temperature range of 1.7 to 20 K are reported on single crystals of CsBr, CsI, TlBr, and TlCl and on a polycrystalline sample of TlI. All crystals display minima in the effective Debye temperatures which are reflected in maxima in  $C/T^3$ -versus- $T$  curves, and these extrema are especially pronounced for TlCl. Comparisons are made with the predictions of existing lattice-dynamics calculations, and the specific heat of TlBr is in very good agreement with the shell-model calculations of Cowley and Okazaki. A Schottky specific-heat term is resolved in the cesium halides at the lowest temperatures and attributed to hydroxyl ions; by adopting the zero-field splitting for  $\text{OH}^-$  in KCl, hydroxyl concentrations  $\sim 10^{20} \text{ cm}^{-3}$  are estimated in CsBr and CsI. The  $C/T^3$  maxima are fitted with Einstein terms added to the Debye backgrounds, and these fittings (together with the Schottky fits for CsBr and CsI) yield the following Debye temperatures: CsBr, 145 K; CsI, 124 K; TlBr, 116 K; TlCl, 120 K; and TlI, 103 K. Thermal-conductivity data for all crystals display maxima at  $\sim 4\text{--}5$  K and an apparent  $T^3$  boundary-scattering regime at the lowest temperatures. Phonon mean free paths at the higher temperatures are analyzed according to the Peierls relation, and for CsBr and TlCl it is found that the Debye modes are the dominant heat carriers. For the remaining crystals, the Einstein modes also carry heat. (The Einstein modes at these higher temperatures dominate the specific heats, contributing up to 75% in the case of TlCl.) Thermal-conductivity measurements were also made on thin crystals ( $\sim 0.05$  cm) of CsBr, TlBr, and TlCl to examine the boundary-scattering region. It is found that in this region the limiting phonon mean free path for CsBr scales with the crystal dimension, and it is suggested that the suppression of the thermal conductivity may be due to the hydroxyl concentration. For TlBr and TlCl, the limiting phonon mean free path is  $\sim 0.01$  cm and is independent of the crystal thickness; this behavior is attributed to a mosaic structure within these crystals.

### I. INTRODUCTION

Alkali halides are representative ionic crystals with simple-cubic structures and relatively simple interatomic potentials, and as such have been the subject of a great deal of experimental and theoretical work. It has been natural to concentrate on the NaCl-structure crystals, and, by comparison, the CsCl-type halides have been relatively unexplored from an experimental (and, to a lesser extent, from a theoretical) viewpoint.

There are significant structure-sensitive differences in some of the properties of the NaCl- and CsCl-type crystals. For example, the Grüneisen parameters for the cesium halides are practically temperature independent down to low temperatures,<sup>1</sup> whereas the NaCl-type crystals display a marked temperature dependence of this parameter. In the thallos halides, the elastic anisotropy,  $2C_{44}/(C_{11}-C_{12})$ , has a negative temperature dependence,<sup>2</sup> in contrast to the NaCl-type crystals. Other differences have been reported in the temperature and pressure dependences of the dielectric constants<sup>3</sup> and in thermal-expansion coefficients.<sup>4</sup>

The dielectric properties of the thallos halides are especially unique in that the dielectric constants are large ( $\sim 30$ ) and follow a Curie-Weiss law below room temperature,<sup>5</sup> suggestive of a dominant soft-optic mode. However, Samara<sup>6</sup> has shown from pressure and temperature

measurements of the dielectric constants that the explicit temperature dependence of the polarizability is responsible for the Curie-Weiss behavior, rather than a soft mode. Subsequent neutron-scattering and infrared measurements on TlBr confirmed the absence of a dominant soft mode.<sup>7</sup>

The lattice dynamics of several CsCl-type crystals have been calculated based on various models (shell model, rigid-ion model, etc.).<sup>8</sup> These calculations predict the temperature dependence of the Debye temperature ( $\Theta_D$ ) at low temperatures, and two central results are obtained: (1)  $\Theta_D$  at  $T \rightarrow 0$  for comparison with  $\Theta_D$  from elastic constant measurements, and (2) the position of a minimum in  $\Theta_D$  in the helium-temperature range. The former property is not very model dependent because  $\Theta_D(0)$  is determined primarily from the elastic continuum. On the other hand, the position and depth of the minimum in  $\Theta_D$  results from the first rapid rise in the density of states (i.e., above the  $\omega \propto k^2$  Debye background) and so is very model dependent. However, there do not appear to be adequate specific-heat data in the literature for the CsCl-type crystals in the neighborhood of these predicted minima in the  $\Theta_D$ 's. In addition, no measurements of the thermal conductivities of CsCl-type crystals at low temperatures have been reported.

The purpose of the studies here was to measure the specific heats and thermal conductivities of several CsCl-type crystals at low temperatures, namely TlBr, TlCl, TlI,

CsBr, and CsI. There were several motivations for these measurements: (1) to provide specific-heat data for comparisons with theoretical predictions, (2) to investigate the nature of heat conduction in these crystals, and (3) to gain a better understanding of these materials, because, owing to their unusual thermal properties, they are becoming technologically important for enthalpy stabilization in superconducting windings.<sup>9</sup>

Large single crystals of CsBr, CsI, TlBr, and TlCl of optical quality are available commercially. TlI can be grown in the CsCl structure at elevated temperatures, but upon cooling transforms to a polycrystalline mass at 170°C with a double-layered orthorhombic structure ( $D_{2h}^{17}-Cmcm$ ).<sup>10</sup> Similarly, CsCl can be grown in the CsCl structure, but at 450°C transforms to a mechanically unstable NaCl structure. Finally, CsF and TlF are difficult to study experimentally as they are both extremely hygroscopic and the latter fluoride is hazardous.

## II. EXPERIMENTAL METHODS AND RESULTS

Single crystals of CsBr, CsI, TlBr, and TlCl of good optical quality were obtained from Harshaw Chemical Co. (Solon, Ohio), and the typical impurity levels (e.g., Fe, Na, etc.) are reported to be <0.1 ppm.<sup>11</sup> A polycrystalline sample of TlI was also obtained from Harshaw. Some specific-heat data on these thallos halides were previously measured<sup>12</sup> on crystals of comparable quality (see below).

Specific-heat measurements here were performed by a pulse method in the adiabatic calorimeter described elsewhere.<sup>12</sup> Briefly, the addenda were kept to a minimum by fixturing the heater ( $\sim 200 \Omega$ ) and a carbon-chip thermometer ( $\sim 10$  mg) directly on the sample, and the  $\Delta T/T$  values were maintained at  $\approx 2\%$ . The addenda contribution to the specific heat is largest at the lowest temperature (1.7 K), and in the measurements here this maximum addenda contribution varied from 4.2% for TlBr to 9.2% for TlI. Owing to the small addenda corrections, the uncertainty in the method is believed to be less than  $\pm 5\%$ .

Thermal-conductivity measurements were made on bars cut from the crystals (and on thin sections; see below). All cutting operations were done slowly under oil using a thin diamond saw, and all cut samples were annealed in Grafoil for 24 h at 350°C or 450°C for the thallos and cesium halides, respectively. No effort was made to polish the cut surfaces which appeared smooth.

Owing to the large thermal conductivities of these crystals, the "two-heater, one-thermometer" linear-heat-flow method was used.<sup>13</sup> The primary advantage of this method is that only one thermometer calibration is required, since, for these crystals, the  $\Delta T$  values tend to be relatively small. The main uncertainty in the method stems from measuring the separation of the heaters ( $\leq \pm 5\%$ ).

The thermal conductivities of thin ( $\sim 0.5$ -mm) bars were also measured, and samples were assembled by loading 25–30 bars (or fibers; see below) into a thin-walled plastic straw (3.2 mm diam) for mechanical support. Actually, sections of a straw were used to allow gaps for winding the two heaters, and a tight-packing arrangement

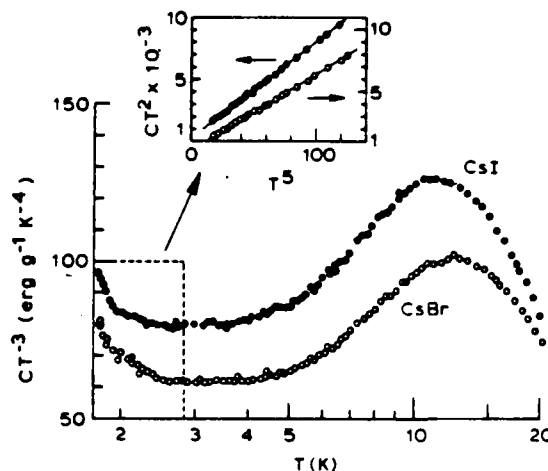


FIG. 1. Specific heats of CsBr and CsI plotted as  $C/T^3$  vs  $T$ . Both crystals display maxima in  $C/T^3$  at about 12 K and a sharp rise in  $C/T^3$  below 3 K. The latter features follow a Schottky term as shown in the inset and are believed due to hydroxyl impurities.

was obtained to ensure efficient transverse heating at the heater locations. The free end of the bundle of bars was potted with silver epoxy through which several thin copper wires were threaded; these wires, in turn, were wrapped around, and varnished to, a carbon-chip thermometer. In all the thermal-conductivity measurements here, the overall  $A/l$  ratios were  $\sim 0.1$ – $0.2$  cm, and these measurements were also made in the adiabatic calorimeter mentioned above.

Specific-heat data, 1.7–20 K, on the cesium and thallos halides are shown in Figs. 1 and 2, respectively. The data are plotted as  $C/T^3$  to illustrate the departure from

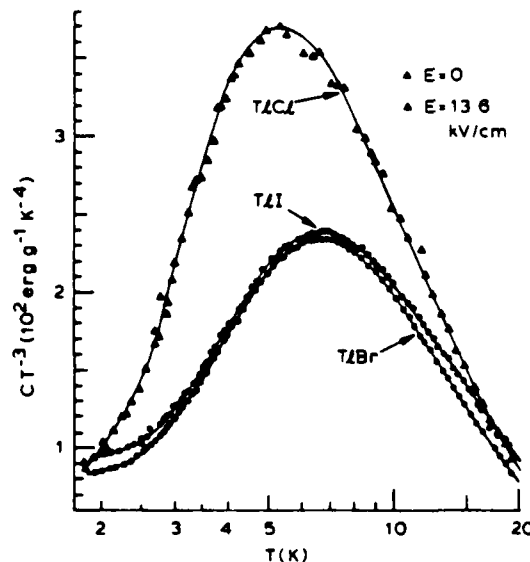


FIG. 2. Specific heats of the thallos halides plotted as  $C/T^3$  vs  $T$ . All crystals display pronounced maxima in  $C/T^3$  at 5–7 K, especially TlCl. The electric field dependence of the specific heat of TlCl is shown in the neighborhood of the maximum in  $C/T^3$ .

Debye behavior. For the cesium halides in Fig. 1, an additional excitation contributes to the specific heat below about 3 K, and the inset of Fig. 1 indicates that this excitation follows a Schottky term very well (see below).

The data in Fig. 2 for the thallos halides include the data reported previously.<sup>12</sup> There are two major additions in Fig. 2 compared to the previously reported data: (1) data are extended in Fig. 2 down to 1.7 K, and (2) data for TlCl are shown measured with an applied electric field of 13.6 kV/cm.

The reason for extending the thallos halide measurements to 1.7 K was to look for an additional excitation, as occurs in the cesium halides (Fig. 1). The reason for the electric field measurements was as follows: The  $C/T^3$  maximum for TlCl in Fig. 2 represents such a dominating effect (the Debye contribution to this maximum is only 25%; see below) and the depth of the minimum in the effective  $\Theta_D$  for TlCl (76 K, Fig. 3) disagrees so substantially with lattice-dynamics calculations (127 K; see below), that it was logical to question whether some portion of this  $C/T^3$  maximum may be due either to a polar impurity or to an optic mode that becomes low lying in the helium-temperature range (note that neutron-scattering data<sup>7</sup> on TlBr were not measured below 100 K). In either case, an  $E$  field is expected to alter the specific heat.<sup>14</sup> However, as seen in Fig. 2, the applied electric field does not affect the position or height of the maximum in  $C/T^3$  of TlCl,<sup>15</sup> and we conclude that this is an intrinsic effect.

The effective Debye temperatures of the cesium and thallos halides are derivable directly from the (smoothed) specific-heat data in Figs. 1 and 2 using published tables

for the Debye function,<sup>16</sup> and these  $\Theta_D - T$  data are shown in Fig. 3. Here, and throughout this paper, the reported Debye temperatures are normalized to one atom per formula weight. In arriving at these data in Fig. 3 the specific-heat data for the cesium halides below 3 K have been deleted due to the Schottky-type excitation (Fig. 1). The  $\Theta_D$  intercept values at  $T=0$  in Fig. 3 result from the data fittings discussed below. As seen,  $\Theta_D$  for TlCl displays the deepest minimum (from 120 K at  $T=0$  to 76 K at 5.4 K) of all the halides measured.

Thermal-conductivity data measured on bars [(~0.15 × 1.0)-cm<sup>2</sup> cross section] of the cesium and thallos halides are shown in Figs. 4 and 5, respectively. For all materials, the thermal conductivity ( $K$ ) passes through a maximum, and, at the lowest temperatures, a  $K \propto T^3$  boundary-scattering limit is apparently reached. Some data from separate runs on TlBr and TlCl are also shown in Fig. 5.

Although the crystals in Figs. 4 and 5 have relatively large maximum  $K$  values (2–7 W cm<sup>-1</sup> K<sup>-1</sup>), it is surprising that the TlBr and TlCl crystals do not have much larger thermal conductivities because the specific heats and densities of these crystals are very large (Fig. 2). That is, if we adopt the kinetic expression,

$$K = \frac{1}{3} C \rho \bar{v} \lambda, \quad (1)$$

where  $\rho$  is the density,  $\bar{v}$  is the average sound velocity, and  $\lambda$  is the phonon mean free path, then in the boundary-scattering limit,  $\lambda \approx d$ , where  $d$  is the minimum crystal thickness. For TlBr and TlCl,  $\rho = 7.557$  and  $7.000$  g/cm<sup>3</sup>, respectively, and Morse and Lawson<sup>2</sup> report  $\bar{v} = 1.82 \times 10^5$

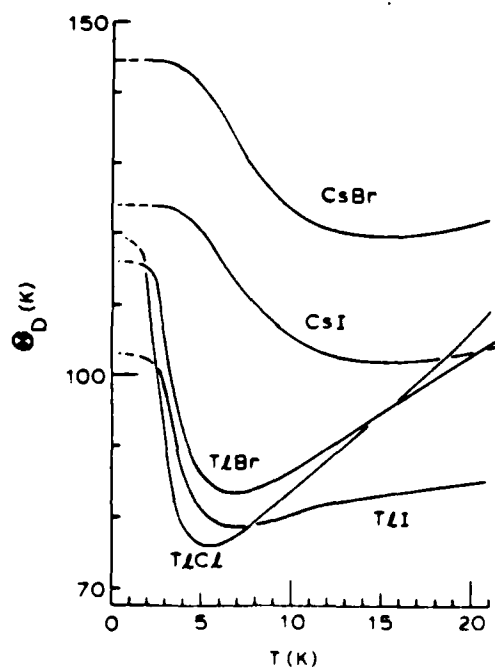


FIG. 3. Temperature dependences of the effective Debye temperatures of the cesium and thallos halides derived from the data in Figs. 1 and 2. The  $\Theta_D$  values shown at  $T=0$  K result from the fittings described in the text.

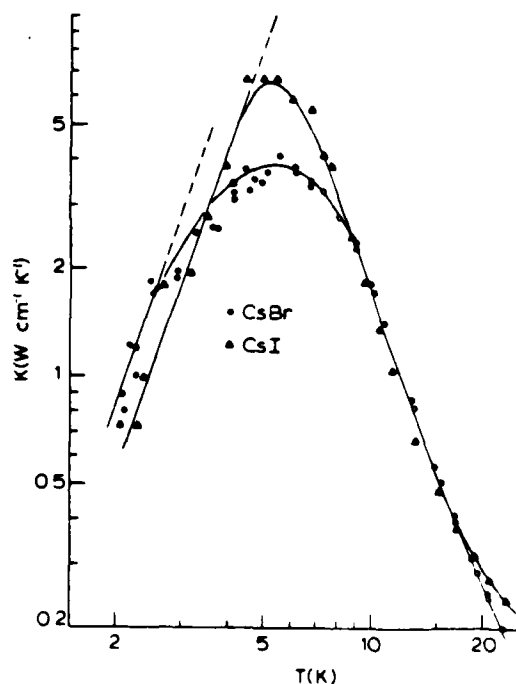


FIG. 4. Thermal-conductivity data measured on crystals of CsBr and CsI. The dashed lines represent the  $T^3$  boundary-scattering regions.

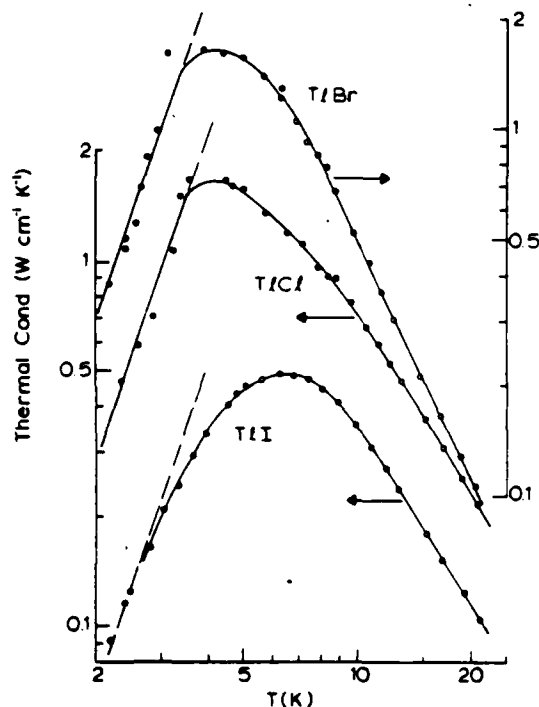


FIG. 5. Thermal-conductivity data measured on crystals of TlBr and TlCl, and on a polycrystalline sample of TlI. The dashed lines represent the  $T^3$  boundary-scattering regions, and some duplicate data for TlBr and TlCl are shown (solid points).

cm/sec for TlBr. Using the  $C$  data in Fig. 2 for these crystals, Eq. (1) predicts that  $K \sim 50 \text{ W cm}^{-1} \text{ K}^{-1}$  for  $d \sim 0.15 \text{ cm}$  near the maximum in  $K$ . Conversely, for CsBr and CsI ( $\rho = 4.440$  and  $4.526$ ) the same exercise yields  $K \sim 10 \text{ W cm}^{-1} \text{ K}^{-1}$ , which agrees somewhat better with the measured data, Fig. 4.

The Casimir relation

$$K = 4.076 \times 10^{10} T^3 A^{1/2} / (\bar{v})^2$$

is useful for judging homogeneous boundary scattering, where  $A$  is the cross-sectional area of the bar and  $\bar{v}$  is the average sound velocity. Applying this relation to the crystals here, we find that at 2 K the predicted thermal conductivities for the thallous halides are at least an order of magnitude larger than the measured values in Fig. 5. For the cesium halides the comparison is somewhat better, the predicted values being about 4 times larger than the experimental values at 2 K in Fig. 4. These results indicate that the scattering of phonons by defects is important in these crystals despite the very small impurity levels quoted above.

Phonon scattering in these CsCl-structure crystals was pursued further by measuring thermal conductivities on thin samples. Thin bars of TlCl ( $0.64 \times 0.64 \text{ mm}^2$ ) and CsBr ( $0.64 \times 0.64 \text{ mm}^2$ ) were cut from the crystals as described above, and thin fibers of TlBr (0.49 mm diam) were obtained from Harshaw (The CsI crystal proved too brittle to cut). The results of these measurements for CsBr, and for TlBr and TlCl, are shown in Figs. 6 and 7, respectively; also shown are the "bulk" thermal conduc-

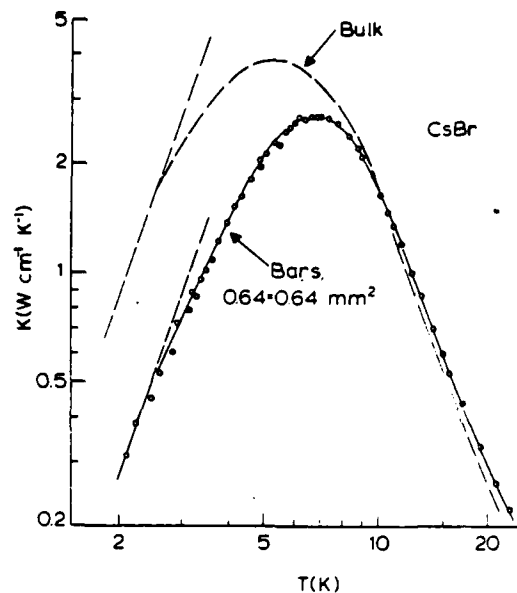


FIG. 6. Thermal-conductivity data measured on thin crystals of CsBr compared to the "bulk" data from Fig. 4.

ivities for these crystals from Figs. 4 and 5 for comparison.

The thin-crystal data in Figs. 6 and 7 also approach the  $K \propto T^3$  limit at the lowest temperatures, but there is a striking difference between CsBr and the thallous halides: The  $T^3$  limit is depressed for CsBr, whereas this limit is

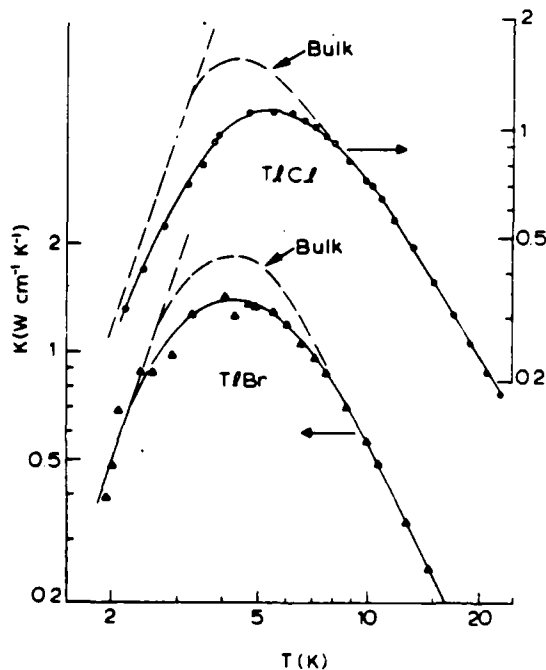


FIG. 7. Thermal-conductivity data measured on thin crystals ( $\sim 0.05 \text{ cm}$ ) of TlBr and TlCl compared to the "bulk" data from Fig. 5. In contrast to CsBr (Fig. 6), the thick- and thin-sample data for these thallous halides approach the same limiting values in the  $T^3$  boundary-scattering regions.

approximately the same for thick and thin crystals of the thallos halides. At the higher temperatures, the thick- and thin-sample thermal-conductivity data converge for all three crystals.

### III. DATA ANALYSES

The thermal data above reveal significant differences between the cesium and thallos halides: The effective Debye temperatures for the cesium salts are larger than those for the thallos salts, and go through broad minima compared to the deep and narrow minima for the thallos salts. The scattering of phonons in CsBr appears to scale approximately with the crystal thickness, but the scattering in TlBr and TlCl appears to be independent of the crystal thickness. In this section we will pursue analyses of these thermal data according to simple models.

The specific-heat data for the cesium halides in Fig. 1 show that an excitation makes a significant contribution to  $C/T^3$  below about 3 K. Attempts were made to fit these data to various specific-heat functionals, and excellent fits were obtained with the high-temperature form of the Schottky term,  $C_{Sch} \propto T^{-2}$ , added to a  $T^3$  Debye background. These  $CT^2$ -versus- $T^3$  fits are shown in the inset of Fig. 1. Debye temperatures for CsBr and CsI are obtained from the slopes of these fits, and are 146.0 and 125.1 K, respectively.

The general, multilevel Schottky term has a  $T^{-2}$  dependence at temperatures larger than the level splitting, so the presence of this term says nothing about the responsible excitation. An impurity effect is suggested, which, however, is absent in the thallos halides. Since the cesium halides are far more hygroscopic than the thallos halides, this Schottky term may be due to hydroxyl ions. It is known that  $\text{OH}^-$  ions occupy halogen sites in NaCl-type crystals (e.g., KCl and KBr) and have six equilibrium orientations along [100].<sup>17</sup> The ground state is tunneling-split into a singlet  $A_{1g}$  of energy  $-2\delta$ , a triplet  $T_{1g}$  of zero energy, and a doublet  $E_g$  of energy  $\delta$ , where  $\delta$  is the zero-field splitting.<sup>18</sup> The Schottky contribution to the specific heat from these tunneling states is<sup>19</sup>

$$C_{Sch} = \frac{6Nky^2(2e^{-2y} + 3e^{-3y} + e^{-5y})}{(1 + 3e^{-2y} + 2e^{-3y})^2}, \quad y = \delta/T \quad (2)$$

where  $N$  is the  $\text{OH}^-$  concentration in  $\text{cm}^{-3}$ . At  $T \gg \delta$ , Eq. (2) reduces to  $C_{Sch} = Nk(\delta/T)^2$ . Assuming this form applies to the CsCl structure and using the fitted data for CsBr and CsI, we find that  $N\delta^2 = 1.13 \times 10^{19}$  and  $9.68 \times 10^{18} \text{ K}^2 \text{ cm}^{-3}$ , respectively. In the NaCl-type crystals,  $\delta \approx 0.34 \text{ K}$ ,<sup>20</sup> which implies  $\text{OH}^-$  concentrations in these cesium halide crystals of  $N \approx 10^{20} \text{ cm}^{-3}$ . These concentrations are comparable to those found in KCl crystals,<sup>18</sup> but apparently were not detected in the chemical analyses for Fe, Na, etc. in these cesium salts. (An alternate suggestion<sup>11</sup> is the  $\text{CN}^-$  ion; however, the splitting for this ion is so small,  $\delta \approx 0.07 \text{ K}$ ,<sup>21</sup> that unrealistically large concentrations,  $N \sim 2 \times 10^{21} \text{ cm}^{-3}$ , are needed to satisfy the fitting parameters.)

Phonon scattering by the (suspected) hydroxyl ions in the cesium halides would be most pronounced at temperatures near the zero-field splitting ( $\sim 0.3 \text{ K}$ ), and this may

prove to be a useful area for future research. We can speculate here that the hydroxyl impurities may be responsible for the depressed thermal conductivities of these cesium salts in the  $T^3$  limit, as discussed above.

The specific-heat data in Figs. 1 and 2 show large maxima in  $C/T^3$ , and it has been found<sup>12</sup> that such maxima can often be described very accurately by a single Einstein-oscillator term added to the Debye background,

$$C = 3nRD(T/\Theta_D) + 3Rrx^2e^x/(e^x - 1)^2, \quad x = \Theta_E/T \quad (3)$$

where  $n$  is the number of atoms per formula weight,  $D(\Theta_D/T)$  and  $\Theta_D$  are the Debye function and temperature, respectively,  $r$  is the number of Einstein oscillators per formula weight, and  $\Theta_E$  is the Einstein temperature. In the general case, if one has knowledge of optical modes and if such modes are approximately independent of the wave vector, then these modes can be represented by appropriate Einstein terms.<sup>22</sup> In our case here, the Einstein term can be thought of as representing the first rapid rise in the density of states above the Debye background, and the analyses according to Eq. (3) have the particular advantage of yielding the Debye temperatures.

The specific-heat data for the cesium and thallos halides were fitted to Eq. (3) using a three-level-fitting regime (i.e., for  $\Theta_D$ ,  $\Theta_E$ , and  $r$ ) which incorporated a table of the Debye function.<sup>16</sup> The cesium halide data below 4 K were not used in these fits to avoid the tail of the Schottky term (Fig. 1). These fitted data are shown in Fig. 8 for the cesium halides. In these plots,  $C_{ex}$  is the excess specific heat,  $C_{ex} = C_{exp} - C_{Debye}$ , and excellent fits to the data are obtained over several orders of magnitude in  $T^2C_{ex}/3R$  [the slight curvature in Fig. 8 is due to the

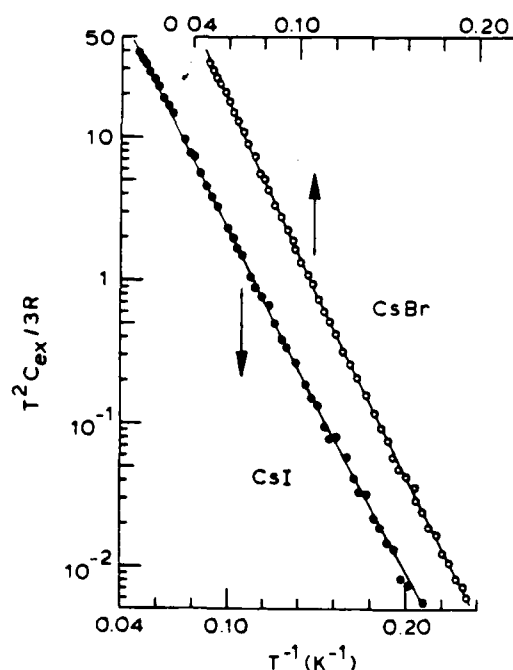


FIG. 8. Fittings of the CsBr and CsI specific-heat data to the single Einstein-oscillator model, Eq. (3). Data below 4 K were not included in these fittings to avoid the tail of the Schottky term, Fig. 1.

TABLE I. Fitting parameters, Eq. (3).

Crystal	$\Theta_D$ (K)	$\Theta_E$ (K)	$\omega_E$ (cm <sup>-1</sup> )	$r$	$N_E/N_D$
TlCl	120.4	26.14	18.17	0.239	23.31
TlBr	115.7	31.34	21.78	0.251	12.64
TlI	103.2	33.97	23.61	0.353	9.89
CsBr	143.2	60.09	41.76	0.331	4.49
CsI	122.7	56.36	39.17	0.397	4.10

$T \ll \Theta_E$  form of Eq. (3) used for plotting]. Similar fits for limited data on the thallos halides were reported previously;<sup>12</sup> the fits obtained here are equivalent, and only the fitting parameters are reported (Table I). The correlation coefficients for these fits were  $\approx 99.6\%$  and the fitting parameters are given in Table I. Also given in Table I is an approximate estimate of the ratio of the number of Einstein modes ( $N_E$ ) to Debye modes ( $N_D$ ) excited at the Einstein temperature,<sup>23</sup>

$$N_E/N_D \approx r(\Theta_D/\Theta_E)^3. \quad (4)$$

The Debye contribution to the specific heat of these crystals can be estimated directly from the Debye temperatures in Table I and compared to the experimental data. At the maximum in  $C/T^3$  it is found that the Debye contribution varies from 25% for TlCl to 64% for CsI. Thus, the Einstein modes *dominate* the specific heats of these halides, particularly so in the case of the thallos halides, and this is also seen in the  $N_E/N_D$  values in Table I. A similar dominance has been found in the hexagonal tungsten bronzes<sup>23</sup> and in ferroelectrics.<sup>12</sup>

The agreement between the Debye temperatures for the cesium halides from the Schottky and Einstein fits is quite good: CsBr,  $(144.6 \pm 0.97\%)K$ ; CsI,  $(123.9 \pm 0.97\%)K$ . These uncertainties in the Debye temperatures translate into uncertainties in  $C/T^3$  of  $\pm 2.9\%$ , which is commensurate with the experimental inaccuracy. Furthermore, the fitting parameters demonstrate that the Schottky term makes a negligible contribution in the fitting temperature range of the Einstein term, and vice versa.

It has recently been pointed out by Pederson and Brewer<sup>24</sup> that a linear relationship exists between  $\Theta_D$  and the reduced mass ( $\mu$ ) for cubic crystals, and this relation holds very well for the halides in Table I. Going further, the Einstein frequencies  $\omega_E$  scale with  $\mu^{-1/2}$  for the cesium halides; for the thallos halides, the  $\omega_E$  values in Table I do not scale with  $\mu^{-1/2}$ , but tend to increase as the mass of the halogen ion increases.

Turning next to the thermal-conductivity data, the primary question is what are the heat-carrying modes in these crystals? This question deserves special consideration since, as seen above, the Einstein term *dominates* the specific heat in these halides at low temperatures. One approach to this problem of determining the heat-carrying phonons is to employ the well-known result due to Peierls,<sup>25</sup>

$$\lambda = \lambda_0 e^{\Theta_D/2T}, \quad (5)$$

for the phonon mean free path, which has been verified in several dielectric crystals. This relation pertains to the

temperature region well above the maximum in the thermal conductivity and has been derived on the assumption that the Debye phonons are the dominant heat carriers. What is important here is that if  $\lambda \propto K/C_D$  [i.e., from Eq. (1)] follows Eq. (5), at these higher temperatures, where  $C_D$  is the Debye contribution to the specific heat, and if there is internal consistency between the  $\Theta_D$ 's from Eq. (5) and from Table I, then it can reasonably be concluded that the Debye phonons carry heat and the Einstein modes do not.

Consequently, plots of  $\ln \lambda$  versus  $T^{-1}$  were constructed from the experimental data using Eq. (1) in two ways: (1) using the experimental specific-heat data (i.e., Debye plus Einstein contributions), and (2) using only the Debye contribution to the specific heat *via* the Debye temperatures in Table I. In constructing these plots, the data for  $\rho$  and  $\bar{v}$  quoted above were used, but we note that these data do

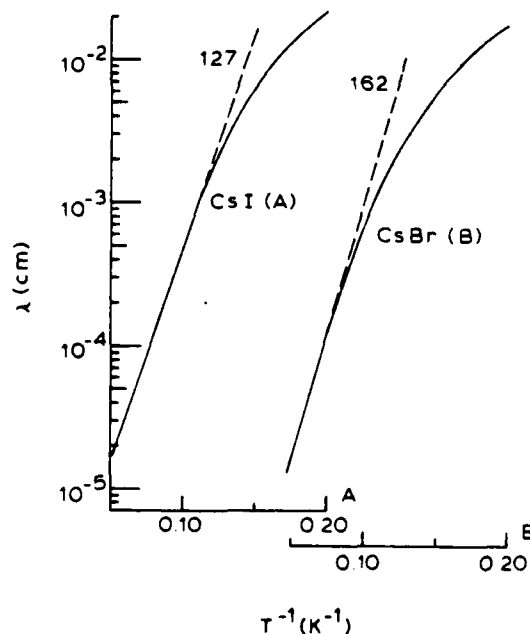


FIG. 9. Plots of the temperature dependence of the phonon mean free paths in CsBr and CsI. These plots were constructed using Eq. (1) and the thermal-conductivity data from Fig. 4 (and from Fig. 6 in the overlap region) and specific-heat data from Fig. 1. Similar plots were constructed using just the Debye specific-heat data obtained from the  $\Theta_D$ 's in Table I. According to the Peierls relation, Eq. (5), the slopes of the linear portions of these curves are simply related to  $\Theta_D$ , and the dashed curves correspond to the  $\Theta_D$  values shown. Note that the  $\Theta_D$  value shown for CsI agrees well with the calorimetric value, Table II (also see text).

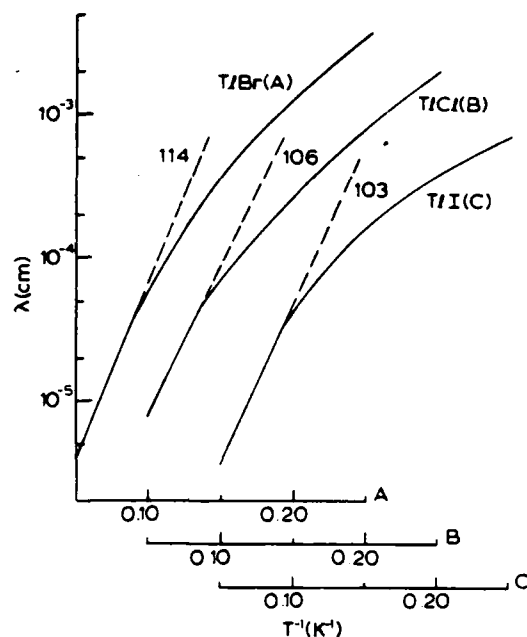


FIG. 10. Phonon mean-free-path data for the thallous halides, analogous to the Fig. 10 plot for the cesium halides. Note that the  $\Theta_D$  values shown for TlBr and TlI agree well with the calorimetric values in Table II.

not affect the  $\Theta_D$  values according to Eq. (5). Thermal-conductivity data at the higher temperatures on both thick and thin crystals (Figs. 6 and 7) were used, and examples of these  $\lambda$  plots are shown in Figs. 9 and 10 for the cesium and thallous halide crystals, respectively. For these plots, the Debye plus Einstein specific heats were used, and at the higher temperatures, well removed from the  $K \propto T^3$  region, a linear  $\ln \lambda$  versus  $T^{-1}$  region is reached from which  $\Theta_D$  can be determined according to Eq. (5). The results of these linear-region fittings are summarized in Table II.

The Table II data reveal some interesting contrasts: (1) For TlCl and CsBr, there is excellent agreement with the calorimetric  $\Theta_D$ 's if the Einstein modes are assumed *not* to carry heat, whereas (2) for TlBr, TlI, and CsI, the excellent agreement between the  $\Theta_D$ 's suggests that the Einstein modes do carry heat in these crystals. The latter agreement is probably fortuitous since, if non-Debye modes carry heat, the basic assumptions leading to Eq. (5)

TABLE II. Debye temperatures from mean-free-path fits.

Crystal	$\Theta_D$ (calorimetric) <sup>a</sup> (K)	$\Theta_D(D)$ <sup>b</sup> (K)	$\Theta_D(D+E)$ <sup>b</sup> (K)
TlBr	116	135	114
TlCl	120	120	106
TlI	103	123	103
CsBr	145	148	162
CsI	124	144	127

<sup>a</sup>Average  $\Theta_D$ 's from Schottky and Einstein fits to cesium halide data.

<sup>b</sup> $D$ , Debye specific heat only used in Eq. (1);  $D+E$ , experimental specific heat used in Eq. (1).

TABLE III. Boundary-scattering mean free paths.

Crystal	Minimum crystal thickness (cm)	$\lambda_c$ (cm)
TlBr	0.145	0.016
TlBr	0.049	0.016
TlCl	0.155	0.0084
TlCl	0.064	0.0077
TlI <sup>a</sup>	0.169	0.0020
CsBr	0.172	0.063
CsBr	0.064	0.020
CsI	0.156	0.032

<sup>a</sup>Fused polycrystalline sample.

are violated. We remark in this regard, however, that the Einstein terms make such a large contribution in the temperature ranges involved here that the analyses are very sensitive to whether the  $D$  or  $D+E$  contributions are used in Eq. (1).

Returning to the apparent boundary-scattering regions seen in the thermal conductivities at the lowest temperatures in Figs. 4–7, we shall employ Eq. (1) to find  $\lambda_c$ , the limiting phonon mean free path in these crystals. The heat-carrying modes identified above are assumed to be correct, and the appropriate specific heats are used in Eq. (1). The average sound velocity  $\bar{v}$  quoted above for TlBr will be used for all crystals (see below), and the Schottky term in the specific heat of the cesium halides is assumed to be localized (i.e., this excitation does not carry heat). Using smoothed thermal-conductivity data in the boundary-scattering range,  $\lambda_c$  data were determined, and these data are given in Table III compared to the crystal thicknesses. The Table III data demonstrate a marked contrast between the cesium and thallous halides: For CsBr, the limiting phonon mean free path  $\lambda_c \approx d/3$ , where  $d$  is the crystal thickness, whereas for TlBr and TlCl,  $\lambda_c \approx 0.016$ – $0.008$  cm, respectively, independent of  $d$ .

#### IV. DISCUSSION

In the above section, specific-heat data at constant pressure have been analyzed, whereas data at constant volume are more suitable for comparisons with theories. This correction involves the thermal-expansion coefficient and the adiabatic compressibility, and estimates of this correction by Sorai<sup>26</sup> show that it is smaller than the experimental inaccuracy; hence, it has been ignored here.

##### A. Cesium halides

Specific-heat data on CsBr and CsI below room temperature have been reported by several authors over the following temperature ranges. For CsBr: 20–300,<sup>27</sup> 1.14–5.62,<sup>28</sup> and 3–9 K.<sup>29</sup> For CsI: 2.1–10 K (Ref. 30) and 30–100 K (Ref. 31). Where possible, comparisons with the experimental data reported here are very good. However, as alluded to previously, none of these reported data sets spans the temperature range where the minimum in  $\Theta_D$  is pronounced.

Some of the above measurements on CsBr and CsI extend to temperatures<sup>28,30</sup> sufficiently low where the

Schottky term reported here would make a noticeable contribution, and the crystals measured are reportedly the same quality Harshaw crystals measured here. These authors (Refs. 28–30) did not report this Schottky term; on the other hand, they did not look for it. In fact, it is apparent in these other data that  $C/T^3$  increases with decreasing temperature at the lowest temperatures, as in Fig. 1, but analyses of these data were not pursued.

The Debye temperatures for CsBr (145 K) and CsI (124 K) reported above from the Schottky and Einstein fittings are in good agreement with the  $\Theta_D$ 's at  $T \rightarrow 0$  K reported from other calorimetric studies and from elastic constant measurements. From the former measurements,  $\Theta_D$  values of 150.9 K (Ref. 28) and 127.7 K (Ref. 30) have been reported for CsBr and CsI, respectively. From elastic constant data,  $\Theta_D$ 's for CsBr of 149.0 K (Ref. 32) and 148.8 K (Ref. 33) and for CsI of 129.4 K (Ref. 30) have been reported.

Turning to theoretical studies, Karo and Hardy<sup>34</sup> have published detailed calculations of the frequency distributions and dispersion curves for CsBr, CsCl, and CsI according to three models: the rigid-ion, polarization-dipole, and deformation-dipole models. These authors present curves of the predicted temperature dependence of the effective Debye temperature according to each model, and these data can be compared directly with the curves in Fig. 3. First, these lattice-dynamics calculations all locate the minima in the  $\Theta_D$ 's for CsBr and CsI at about 15 K, in good agreement with the experimental data. The depth of these minima increase upon going from the rigid-ion to the deformation-dipole to the polarization-dipole model, and for both CsBr and CsI the best agreement with experimental data results from the deformation-dipole model. For example, the predicted  $\Theta_D$  minima are 120 and 107 K, compared to the Fig. 3 minima of 120 and 102 K for CsBr and CsI, respectively. From the limited data available to Karo and Hardy, they also concluded tentatively that the deformation-dipole model appeared to give the best representation of the cesium halides.

As mentioned above, the Einstein-oscillator model, Eq. (3), is a convenient representation of the maximum in  $C/T^3$  above the Debye background, and can be thought of as reflecting the first rapid rise in the density of states. Accordingly, the Einstein frequencies  $\omega_E$  in Table I might be expected to correspond to the calculated positions of the first Van Hove singularities in the frequency distributions from the lattice-dynamics models. For CsBr and CsI, Karo and Hardy<sup>34</sup> report these calculated positions at about 5 THz  $\sim$  170  $\text{cm}^{-1}$ . However, from Table I the  $\omega_E$ 's for CsBr and CsI are smaller by a factor of 4. As will be seen below, the agreement for the thallous halides is much better.

### B. Thallous halides

Turning next to the thallous halides, there have been fewer reported specific-heat measurements than for the cesium halides: Specific-heat data from 5 to 300 K have been reported for TlBr (Ref. 35) and for TlCl and TlI (Ref. 36); data for TlCl from 15 to 310 K have also been

reported.<sup>37</sup> As with the cesium halides, complete specific-heat data in the neighborhood of the minima have not previously been published. The specific-heat data reported here agree well with published data, although the latter data are reported at such widely spaced temperature intervals that detailed comparisons are difficult.

With one exception, all of the experimentally determined Debye temperatures quoted in the literature for the thallous halides come from elastic constant measurements: For TlCl, both Haussühl<sup>38</sup> and Joshi *et al.*<sup>39</sup> report  $\Theta_D = 125$  K, which is in good agreement with the fitted value in Table I (120 K). For TlBr, elastic Debye temperatures of 132 K (Ref. 2) and 128 K (Ref. 40) have been reported, together with values of 115 K (Ref. 38) and 114 K (Ref. 39), which are in better agreement with the Table I value (116 K). From calorimetric measurements above 5 K, Brade and Yates<sup>35</sup> report  $\Theta_D = 128$  K for TlBr. For TlI, no quoted Debye temperatures appear in the literature.

Turning to lattice-dynamics treatments, Cowley and Okazaki<sup>7</sup> have reported a detailed study of TlBr wherein the normal modes of vibration were measured at 100 and 300 K using neutron-scattering methods and the results were fitted to various rigid-ion and shell models. According to a shell model which yielded the most satisfactory agreement with the neutron data, these authors derived a curve of the temperature dependence of the effective Debye temperature for TlBr. This predicted curve demonstrated a minimum in  $\Theta_D$  at about 7 K of depth 87 K, in excellent agreement with the experimental data in Fig. 3. The model also yielded  $\Theta_D = 132$  K at  $T \rightarrow 0$  K, which is in reasonably good agreement with the value reported here. Of particular significance, Cowley and Okazaki report a first rapid rise in the density of states for TlBr at about 0.65 THz  $\approx$  22  $\text{cm}^{-1}$ , in excellent agreement with the Einstein frequency in Table I.

The phonon vibrational frequencies of TlCl have been calculated by Kamal and Mendiratta<sup>41</sup> using a shell model. These authors report a minimum in the effective  $\Theta_D$  of about 127 K at 13 K, which is significantly different than the experimental values (Fig. 3) of 76 K at 5.4 K. However, this shell model predicts the first rapid rise in the density of states at about 6 THz  $\approx$  20  $\text{cm}^{-1}$ , which agrees reasonably well with the  $\omega_E$  for TlCl in Table I.

Finally, turning to the new thermal-conductivity data on these halide crystals, it has long been recognized that in dielectric crystals the critical phonon mean free path ( $\lambda_c$  above) rarely equals the actual sample dimension. Differences are commonly ascribed to specular versus diffuse phonon scattering at crystal boundaries, and scattering by dislocations has been extensively studied.<sup>42</sup> In the annealed, CsCl-type crystals measured here under identical conditions, the  $\lambda_c$  values for CsBr scale approximately uniformly with the crystal dimensions (Table III), whereas for TlCl and TlBr, the  $\lambda_c$  values are ostensibly crystal-dimension independent. It is admittedly true that the data in Table III are dependent on the assignment of heat-carrying modes, as discussed above, but for a given crystal these qualitative conclusions are independent of these mode assignments. It is also true that the average sound velocity<sup>2</sup> for TlBr has been used for all crystals in arriving

at the Table III data; however, this assumption is believed to introduce a very small error, and, moreover, does not affect the conclusions regarding a particular crystal. For example, the elastic constant data for CsI (Ref. 30) indicate that  $\bar{v} = 1.92 \times 10^3$  cm/sec, a value within 5% of the value used above.

The picture that emerges for CsBr and CsI is that although boundary scattering is clearly indicated by the scaling of  $\lambda_c$  to the crystal dimension, the magnitude of the thermal conductivity is reduced by the hydroxyl content inferred from the Schottky term in the specific heat.

The independence of  $\lambda_c$  on crystal dimension for TlBr and TlCl may be due to the "mosaic" structure within these crystals. That is, the results of small-angle x-ray-diffraction studies have shown that, regardless of the care in growing these crystals, there always exists a mosaic structure such that a mosaic spread of about  $0.2^\circ$ – $0.3^\circ$  is found in these crystals regardless of composition.<sup>11,43</sup> Moreover, the physical dimension of these mosaics is reportedly  $\approx 0.01$  cm, a value which agrees well with the critical mean free paths for TlBr and TlCl in Table III.

## V. CONCLUSIONS

A large amount of new thermal data for certain cesium and thallos halides between 1.7 and 20 K has been presented. Specific-heat data have been compared with existing lattice-dynamics models, where possible, and it is perhaps significant that only in the case of TlBr, where neutron-scattering data are available, is there satisfactory agreement between the experimental and predicted behavior of the effective Debye temperature. Fitted values of the Debye temperatures at  $T \rightarrow 0$  K are presented, and these values compare favorably with literature values. Minima in the effective Debye temperature are reflected in maxima in  $C/T^3$ , and these maxima can be fitted very accurately with a single Einstein-oscillator term. For TlBr and TlCl, the resulting Einstein frequencies agree very well with the positions of the first Van Hove singularities in the density of states, as predicted by vari-

ous lattice-dynamics models. For CsBr, the corresponding agreement is poor.

The specific-heat data reported here represent the first complete set of data, to our knowledge, measured on the cesium and thallos halides in the temperature range of the minima in the effective Debye temperatures, and it is hoped that these data may stimulate refinements of the lattice-dynamics models.

A Schottky term in the specific heats of CsBr and CsI at the lowest temperatures has been resolved and tentatively attributed to  $\text{OH}^-$  ions occupying halogen sites, by analogy with  $\text{OH}^-$  ions in NaCl-type crystals. Adopting the zero-field splitting for KCl:OH, the Schottky terms in these cesium halides yield hydroxyl-ion concentrations that are comparable to the concentrations found in NaCl-type crystals.

The thermal-conductivity data reported here for the cesium halides are understandable in a straightforward fashion: The heat-carrying modes are identified in a self-consistent fashion from analyses of the temperature dependence of the phonon mean free path using the specific-heat data, and in the apparent boundary-scattering region the limiting mean free path is about one-third of the crystal thickness. The magnitude of the thermal conductivity of the cesium salts at the lowest temperatures is alleged to be uniformly reduced by the hydroxyl content. The heat-carrying modes are similarly identified in the thallos halide crystals, but in the boundary-scattering region the limiting mean free path is determined by a mosaic structure within the crystals rather than the crystal dimensions. No evidence is found for appreciable hydroxyl contents in the thallos halides.

## ACKNOWLEDGMENTS

Portions of this research were supported by the U. S. Air Force Office of Scientific Research. The author is grateful to C. F. Clark and R. W. Arenz for technical assistance, and to A. C. Anderson and G. A. Samara for helpful discussions.

- <sup>1</sup>A. J. Kirkham and B. Yates, *J. Phys. C* **1**, 1162 (1968); A. C. Bailey and B. Yates, *Philos. Mag.* **16**, 1241 (1967).
- <sup>2</sup>G. E. Morse and A. W. Lawson, *J. Phys. Chem. Solids* **28**, 939 (1967).
- <sup>3</sup>E. E. Havinga and A. J. Bosman, *Phys. Rev.* **140**, A292 (1965).
- <sup>4</sup>G. K. White, *Proc. R. Soc. London, Ser. A* **286**, 204 (1965).
- <sup>5</sup>K. V. Rao and A. Smakula, *J. Appl. Phys.* **36**, 3953 (1965); R. P. Lowndes, *Phys. Lett.* **21**, 26 (1966).
- <sup>6</sup>G. A. Samara, *Phys. Rev.* **165**, 959 (1968).
- <sup>7</sup>E. R. Cowley and A. Okazaki, *Proc. R. Soc. London, Ser. A* **300**, 45 (1967); R. P. Lowndes, *Phys. Rev. Lett.* **27**, 1134 (1971).
- <sup>8</sup>See S. Bijanki and R. J. Hardy, *J. Phys. Chem. Solids* **38**, 147 (1977), and references therein.
- <sup>9</sup>W. N. Lawless, C. F. Clark, and R. W. Arenz, *IEEE Trans. Magn. MAG-19*, 432 (1983).
- <sup>10</sup>G. A. Samara, L. C. Walters, and D. A. Northrop, *J. Phys. Chem. Solids* **28**, 1875 (1967).

- <sup>11</sup>C. Swinehart, Harshaw Chemical Co. (private communication).
- <sup>12</sup>W. N. Lawless, *Phys. Rev. B* **14**, 134 (1976); **17**, 1458 (1978).
- <sup>13</sup>See, for example, M. P. Zaitlin and A. C. Anderson, *Phys. Rev. B* **12**, 4475 (1975).
- <sup>14</sup>W. N. Lawless, *Phys. Rev. B* **16**, 433 (1977); **18**, 2394 (1978).
- <sup>15</sup>In the course of these measurements, the electric field was also quickly (adiabatically) cycled between 0 and 13.6 kV/cm in the range 4–15 K. No adiabatic polarization-heating or depolarization-cooling effects were observed in TlCl.
- <sup>16</sup>E. S. R. Gopal, *Specific Heats at Low Temperatures* (Plenum, New York, 1966).
- <sup>17</sup>U. Kuhn and F. Lüty, *Solid State Commun.* **3**, 31 (1965); F. Lüty, *J. Phys. (Paris) Colloq. Suppl.* **8-9**, **28**, C4-120 (1967).
- <sup>18</sup>I. W. Shepherd, *J. Phys. Chem. Solids* **28**, 2027 (1967).
- <sup>19</sup>W. N. Lawless, *J. Phys. Chem. Solids* **30**, 1161 (1969).

- <sup>20</sup>G. Fegerm, I. W. Sherpherd, and H. Shore, *Phys. Rev. Lett.* **16**, 500 (1966).
- <sup>21</sup>J. P. Harrison, P. P. Peressini, and R. O. Pohl, *Phys. Rev.* **167**, 856 (1968).
- <sup>22</sup>See, for example, G. D. Khattak, H. Akbarzadeh, and P. H. Keesom, *Phys. Rev. B* **23**, 2911 (1981).
- <sup>23</sup>A. J. Bevolo, H. R. Shanks, P. H. Sidles, and G. C. Danielson, *Phys. Rev. B* **9**, 3220 (1974).
- <sup>24</sup>D. O. Pederson and J. A. Brewer, *Phys. Rev. B* **16**, 4546 (1977).
- <sup>25</sup>R. Peierls, *Ann. Phys. (Leipzig)* **3**, 1055 (1929); C. Herring, *Phys. Rev.* **95**, 954 (1954).
- <sup>26</sup>M. Sorai, *J. Phys. Soc. Jpn.* **25**, 421 (1968).
- <sup>27</sup>A. J. Kirkham and B. Yates, *J. Phys. C* **1**, 1162 (1968).
- <sup>28</sup>R. A. Robbins and B. J. Marshall, *J. Appl. Phys.* **42**, 2562 (1971).
- <sup>29</sup>M. Sorai, H. Suga, and S. Seki, *Bull. Chem. Soc. Jpn.* **41**, 312 (1968).
- <sup>30</sup>B. J. Marshall and J. R. Kunkel, *J. Appl. Phys.* **40**, 5191 (1969).
- <sup>31</sup>A. R. Taylor, T. E. Gardner, and D. F. Smith, *U. S. Bur. Mines, Rept. Invest.* 6157 (1963).
- <sup>32</sup>T. K. H. Barron and J. A. Morrison, *Phys. Rev.* **115**, 1439 (1959).
- <sup>33</sup>D. Vallin, O. Beckman, and K. Salama, *J. Appl. Phys.* **35**, 1222 (1964).
- <sup>34</sup>A. M. Karo and J. R. Hardy, *J. Chem. Phys.* **48**, 3173 (1968).
- <sup>35</sup>R. M. Brade and B. Yates, *J. Phys. C* **4**, 417 (1971).
- <sup>36</sup>Y. Takahashi and E. F. Westrum, *J. Chem. Eng. Data* **10**[3], 244 (1965).
- <sup>37</sup>I. R. Bartky and W. F. Giaque, *J. Am. Chem. Soc.* **81**, 4169 (1959).
- <sup>38</sup>S. Haussuhl, *Acta Crystallogr.* **13**, 685 (1960).
- <sup>39</sup>S. K. Joshi and S. S. Mitra, *Proc. Phys. Soc. London* **76**, 295 (1960).
- <sup>40</sup>J. Vallin, K. Marklund, and J. O. Sikström, *Ark. Phys.* **33**, 345 (1966).
- <sup>41</sup>R. Kamal and R. G. Mendiratta, *J. Phys. Soc. Jpn.* **26**, 621 (1969).
- <sup>42</sup>See, for example, S. G. O'Hara and A. C. Anderson, *Phys. Rev. B* **10**, 574 (1974).
- <sup>43</sup>A. Smakula and M. W. Klein, *J. Opt. Soc. Am.* **39**, 445 (1949).

PROGRESS REPORT

AFOSR Contract #F49620-83-C-0129

Fundamental Physics Studies on High-Specific-Heat  
Dielectrics and Kapitza Resistance at Dielectric Boundaries

Alkali Halide Studies, I. Experimental Studies

by

W.N. Lawless *WNL*  
CeramPhysics, Inc.  
Westerville, Ohio 43081

November 1, 1983

Distribution:  
J.H. Parker, Sr.  
✓ W. Eckels  
T.K. Gupta  
M. Ashkin  
C.F. Clark  
B.R. Patton

## INTRODUCTION

This is the first in a series of reports devoted to the thalious and cesium halides, which in previous programs have been labelled as SC-2 and SC-3 materials, respectively (here "SC" means superconductor coating). These materials are of practical interest as dielectric insulations for superconductors owing to their very large specific heats and thermal conductivities at low temperatures. Indeed, in one of the previous programs,<sup>1</sup> about 5m of NbTi wire was coated with TlC<sub>2</sub> in a continuous hot-extrusion process.

Historically, the fundamental thermal properties of the thalious and cesium halides at low temperatures were measured on single crystals by the author in unsupported research, and subsequent sponsored research<sup>1-3</sup> was based on these original measurements. Specifically, an Air Force program<sup>1</sup> incorporated these materials in studies of dielectric insulations for superconductors; a Jet Propulsion Lab program<sup>2</sup> was devoted to studying mixtures of thalious halides as regenerator-matrix materials; and a National Bureau of Standards program<sup>3</sup> was devoted to in situ studies of practical regenerators loaded with extruded rods of a certain mixture of thalious halides.

Therefore, a considerable amount of new low-temperature data has been measured on single crystals of these halides (including mixtures), but these data have neither been analyzed nor published in the scientific literature. The present AFOSR program affords us the opportunity to do both.

The purpose of this first report is to collect the considerable amount of data measured on the thalious and cesium halides. Subsequent reports will deal with analyses of these data using simple models and with a literature survey on these materials.

#### EXPERIMENTAL DATA - THALLOUS HALIDES

The  $Tl_2Cl_2$  and  $Tl_2Br_2$  materials are cubic  $CsCl_2$ -type structures available in single-crystal form from Harshaw Chemical.  $TlI$  is available only in fused, polycrystalline form with a double-layered orthorhombic structure (at room temperature).

The specific heats of these thallos halides were measured in the calorimeter reported previously.<sup>4</sup> As a percentage of the total heat capacity, the addenda contribution in these measurements was as follows:  $Tl_2Cl_2$ , < 9%;  $Tl_2Br_2$ , < 9%; and  $TlI$ , < 8%.

Specific heat data for these halides are shown in Fig. 1 where the data are plotted as  $C/T^3$  to illustrate the non-Debye behavior. A maximum in  $C/T^3$  indicates a significant specific-heat contribution from a low-lying vibrational mode, and  $Tl_2Cl_2$  is especially noteworthy in this respect as  $C/T^3$  varies by more than a factor of three between 2-10 K.

Pursuing this further, the  $Tl_2Cl_2$  crystal in Fig. 1 was also measured under an applied electric field of 13.6 kV/cm, and as seen in Fig. 1 the specific heat of  $Tl_2Cl_2$  is E-field independent in the neighborhood of the maximum in  $C/T^3$ . The purpose of this E-field measurement was to investigate the nature of the low-lying mode responsible for the  $C/T^3$  maximum (i.e., an optic mode is expected to be E-field dependent).

Thermal conductivity data were measured on bar samples of the three thallos halides (approx. cross section area,  $0.16 \times 0.5 \text{ cm}^2$ ). Owing to the large thermal conductivities of these materials (see Fig.2), the "two heater-one thermometer" method of measuring thermal conductivity was employed. In this method, a thermometer is attached to the free end of the bar and two heaters are attached to the bar at separate locations. First one, and then the other, heater is activated by a heater current, and if the heater power is maintained the same in the

two heaters, the thermal conductivity is obtained from the temperature difference at the free end of the bar. The advantage of this technique resides largely in the fact that only one thermometer calibration is involved, since for large thermal conductivity materials, small  $\Delta T$ 's are usually involved.

Measured thermal conductivity data on the three thalious halides are shown in Fig. 2, and for TlBr and TlCl data points are also shown from a duplicate run. The data for the TlBr and TlCl crystals are practically identical in Fig. 2 (note different scales), whereas the data for polycrystalline TlI are somewhat depressed. All three halides approach the  $T^3$  boundary-scattering limit at the lowest temperatures, as indicated in Fig. 2.

The  $T^3$  limits in Fig. 2 are puzzling at first sight, for the following reason: One expects that

$$K = C\bar{v}\lambda\rho/3 \quad (1)$$

where  $C$  is the specific heat,  $\bar{v}$  the average sound velocity,  $\lambda$  the (dominant) phonon mean free path, and  $\rho$  the density. The  $K \propto T^3$  limit follows directly from Eq. (1): At sufficiently low temperatures,  $C \propto T^3$  and  $\lambda = d$ , the smallest sample dimension. For sound velocities,  $\bar{v} \sim 2 \times 10^5$  cm/sec, and for TlBr,  $d \sim 0.2$  cm,  $\rho = 7.453$ , and  $C \sim 7.8 \times 10^3$  erg g<sup>-1</sup> K<sup>-1</sup> from Fig. 1. Consequently, from Eq. (1) one expects  $K \sim 50$  W cm<sup>-1</sup> K<sup>-1</sup>, whereas the experimental data are about 25 times smaller than this value. Stated differently, the very large specific heats of the thalious halides (Fig. 1) indicate that very large thermal conductivities should be attained given the sample dimensions involved and the sound velocities usually found in solids.

To address this problem, the thermal conductivities of thin samples of TlCl and TlBr were measured. For TlCl, thin bars (0.64 x 0.64 mm<sup>2</sup>,

cross section) were cut from the crystal on a diamond saw using oil. For TlBr, thin fibers (0.49 mm diameter) were obtained from Harshaw Chemical Co. The bars and fibers were annealed for 24 hours at 350°C in grafoil and a thermal-conductivity sample was constructed by loading about 25-30 bars (or fibers) into a thin-walled plastic straw for mechanical support. Actually, sections of a straw were used to allow gaps for winding the two heaters (see above).

The results of these thin-sample thermal conductivity measurements on TlCl and TlBr are shown in Fig. 3 where the bulk data from Fig. 2 are also shown. The data for both crystals converge above ~ 7 K which lends credence to the experimental techniques. The data also converge at the lowest temperatures and approach the same  $T^3$  limit, indicating that the actual boundary scattering in these crystals is due to some entity within the crystal rather than the crystal dimensions.

Finally, the thermal properties of the TlBr and TlCl crystals were measured in intense magnetic fields at low temperatures.

Specific heat data were measured on the two crystals by a calibrated-wire, transient method employing capacitance thermometry,<sup>5</sup> and in the temperature range 3-13 K it was found that the specific heats were H-field independent up to 5T to within  $\pm 5\%$  of the zero-field specific heats.

For thermal conductivity measurements in magnetic fields, the "two heater-one thermometer" method was employed in a way that yielded relative data under isothermal conditions. The copper reservoir (to which the samples were attached) was temperature-controlled, and the heaters on the samples were wound bifilarly to cancel inductive effects (the heater wire was manganin which has a negligible magnetoresistance). A capacitance thermometer was attached to the free end of the crystal.

At zero field, the heater power was determined to give a favorable  $\Delta T$  ( $\Delta T/T \sim 2\%$ ), and the thermometer reading with the lower heater activated was noted. Under an applied field, the set point of the controller was adjusted to give the same thermometer reading with the same power applied to the lower heater. With the same power applied to the upper heater, the  $\Delta T$  was measured, and in this fashion thermal conductivity data were measured under essentially isothermal conditions relative to the zero-field value.

These thermal conductivity data for  $TlBr$  and  $TlCl$  are shown in Fig. 4 at various H-fields up to 12.5T. At each field level, between 4 and 8 points were taken, and the error bars in Fig. 4 reflect the spread in the data.

The Fig. 4 data indicate a negative slope for  $TlBr$  ( $d\kappa/dH = -0.47\% T^{-1}$ ) and a positive slope for  $TlCl$  ( $= +0.61\% T^{-1}$ ). The samples and measuring conditions here were identical (the two crystals were measured in the same run), and the fact that the two crystals behave oppositely suggests that the effects are real.

#### EXPERIMENTAL DATA - CESIUM HALIDES

The cesium halides also have  $CsCl$ -type crystal lattices, and single crystals of  $CsBr$  and  $CsI$  from Harshaw were studied ( $CsCl$  proved too hygroscopic for reliable measurements). The measurement methods discussed above for the thallos halides were also used for these cesium halides. In the specific heat measurements the addenda contributed  $< 5\%$  for  $CsBr$ ,  $< 4\%$  for  $CsI$ , as a percentage of the total heat capacity.

Specific heat data measured from 1.7 to 20 K on  $CsBr$  and  $CsI$  are shown in Fig. 5 plotted as  $C/T^3$ . The cesium halides also display maxima in  $C/T^3$ , and, as with the thallos halides, the  $C/T^3$  maxima are about twice as large as what might be judged as the Debye background.

However, the  $C/T^3$  maxima for the cesium salts are about 2-3 times smaller than the corresponding maxima in the thallos salts (Fig. 1).

In contrast to the thallos halides, the cesium halides in Fig. 5 display increases in  $C/T^3$  with decreasing temperature below about 3 K. These latter data follow a  $T^{-2}$  Schottky term very well, as shown in the inset in Fig. 5. We shall return to a discussion of this Schottky term in a subsequent report.

Thermal conductivity data measured by the two heater-one thermometer method on CsBr and CsI crystals are shown in Fig. 6. As with the thallos halides, the data display the  $T^3$  boundary scattering limit at the lowest temperatures. It is interesting to note that CsI displays a remarkably large thermal conductivity maximum at 6 K,  $\approx 7 \text{ W cm}^{-1} \text{ K}^{-1}$ .

Boundary scattering in CsBr was pursued further by measuring thin bars ( $0.64 \times 0.64 \text{ mm}^2$  cross section) cut from the original crystal (CsI proved too brittle to cut). The CsBr bars were annealed at 400 C for 24 hours in grafoil and measured. These thin-section thermal conductivity data for CsBr are shown in Fig. 7 where the bulk data from Fig. 6 are reproduced.

In contrast to  $\text{Tl}_2\text{Br}$  and  $\text{Tl}_2\text{Cl}$  (Fig. 3), reducing the thickness of the CsBr crystal has a dramatic effect on the boundary scattering, as seen in Fig. 7. The data above about 10 K are in reasonably good agreement ( $\sim \pm 10\%$ ). The  $T^3$  limit is approached at the lowest temperatures as indicated in Fig. 7.

The data in the  $T^3$  regime of Fig. 7 are in reasonably good agreement with the predictions of Eq. (1). For example, at 2 K,  $C = 500 \text{ erg g}^{-1} \text{ K}^{-1}$  (Fig. 5),  $\rho = 4.44$ ,  $\bar{v} \sim 2 \times 10^5 \text{ cm/sec}$ , and for the thin bars  $\lambda = 0.06 \text{ cm}$ , and from Eq. (1)  $K \sim 0.8 \text{ W cm}^{-1} \text{ K}^{-1}$  which agrees with the experimental value (Fig. 7) within a factor of two.

Finally, we report an interesting measurement of the thermal conductivity of CsBr in intense magnetic fields using the two heater-one thermometer method (capacitance thermometer) described above. These data are shown in Fig. 8 ( $T = 10.45$  K), and the thermal conductivity display a maximum at  $\sim 9T$ , and the height of the maximum is 33% larger than the zero-field value.

The experimental data in Fig. 8 were measured under identical conditions as the data in Fig. 4 and about six measurements were made at each H-field. The error bars in Fig. 8 reflect the spread in the data at each field level, and the noise conditions were very favorable. The uncertainty in the temperature in Fig. 8 ( $\pm 40$  mK) is far too small to explain the anomaly in the thermal conductivity of CsBr at  $\sim 9T$ .

#### DISCUSSION

Analyses of these experimental data for the thallous and cesium halides in zero magnetic field will concentrate on two areas: (1) The nature of the low-lying vibrational modes causing the maxima in  $C/T^3$ ; the E-field measurement on TlCl in Fig. 1 suggests acoustic modes; and (2) The nature of the phonon mean free paths in these materials. This latter problem also bears on which modes carry heat; i.e., do the low-lying modes that dominate the specific heat also contribute to the thermal conductivity.

The effects of intense magnetic fields on the thermal conductivities at low temperatures appear to be real effects. The data in Fig. 4 are particularly convincing as the effects in TlBr and TlCl behave oppositely. Going further, the data in Fig. 4 appear to have an oscillatory behavior, and this observation is lent some credence by the data in Fig. 8 on CsBr which were measured under essentially noise-free

conditions (note that the dramatic effect in Fig. 8 has an amplitude about an order of magnitude larger than the uncertainty in the data).

These magnetothermal effects require a coupling mechanism between the magnetic field and the phonon field via an intermediate agent (nuclear spin?). Measurements of the dielectric constant in intense fields would be interesting as the (static) dielectric constant is simply related to phonon frequencies through the Lyddane-Sachs-Teller relation.

The data in Fig. 8 should be repeated. Also, the specific heat of CsBr should be measured in intense fields, as the data in Fig. 8 indicate significant effects on the specific heat near 9T from Eq. (1).

#### REFERENCES

- <sup>1</sup>W.N. Lawless, C.F. Clark, and R.W. Arenz, Final Report, WPAFB Contract 33615-80-C-2022, "Enthalpy-Improved Dielectric Insulation for Superconducting Wires," May, 1982.
- <sup>2</sup>W.N. Lawless, Final Report, JPL Contract 955446, "Evaluation of High Specific Heat Ceramic for Regenerator Use at Temperatures Between 2-30 K," Dec. 1979.
- <sup>3</sup>W.N. Lawless and R.W. Arenz, Final Report, NBS Contract NB82RAA20923, "Evaluation of a Packed-Rod Regenerator," March 1982.
- <sup>4</sup>W.N. Lawless, Phys. Rev. B14, 134 (1976).
- <sup>5</sup>W.N. Lawless, C.F. Clark, and R.W. Arenz, Rev. Sci. Instrum. 53, 1647 (1982).

FIG. 1

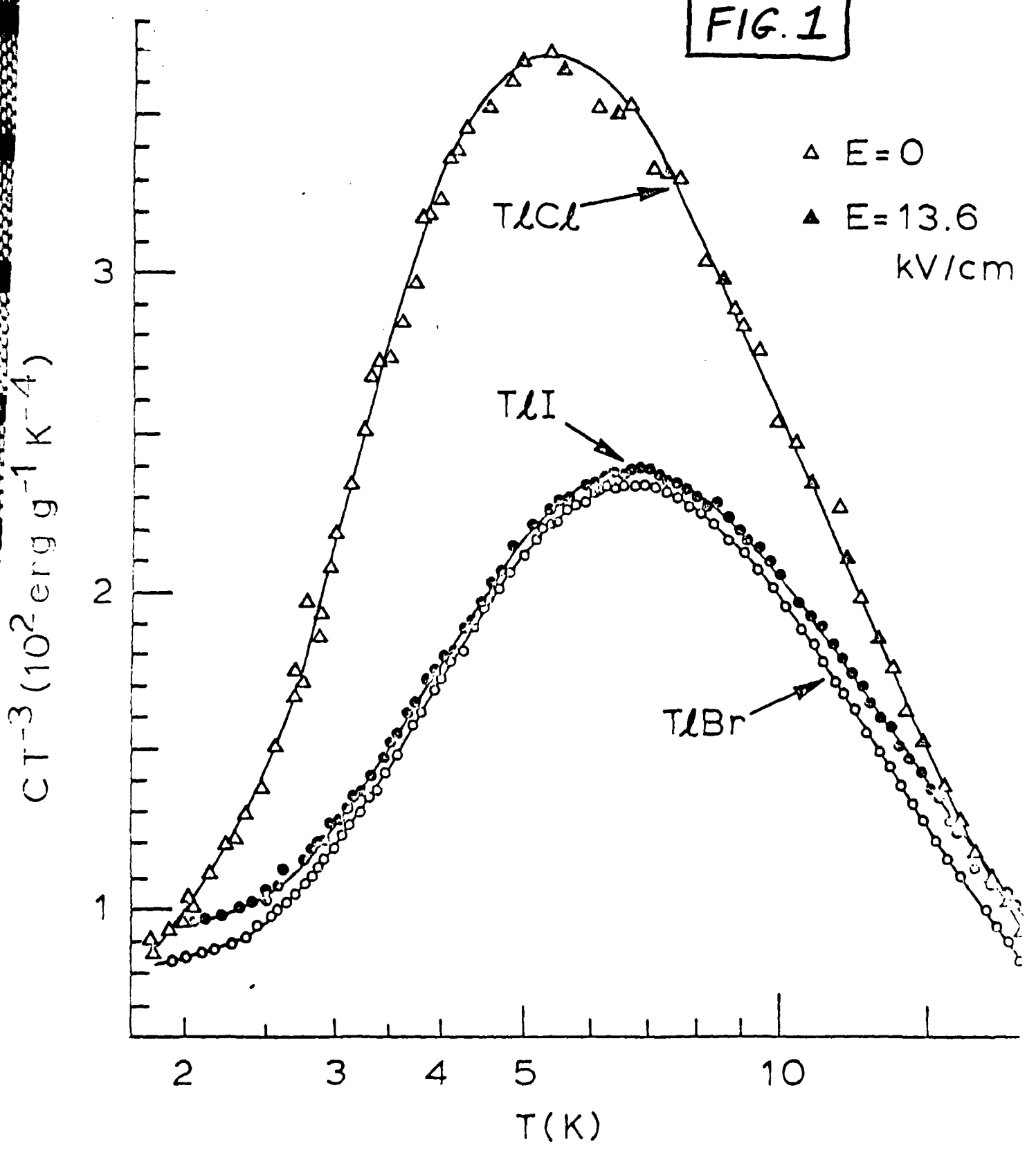


FIG. 2

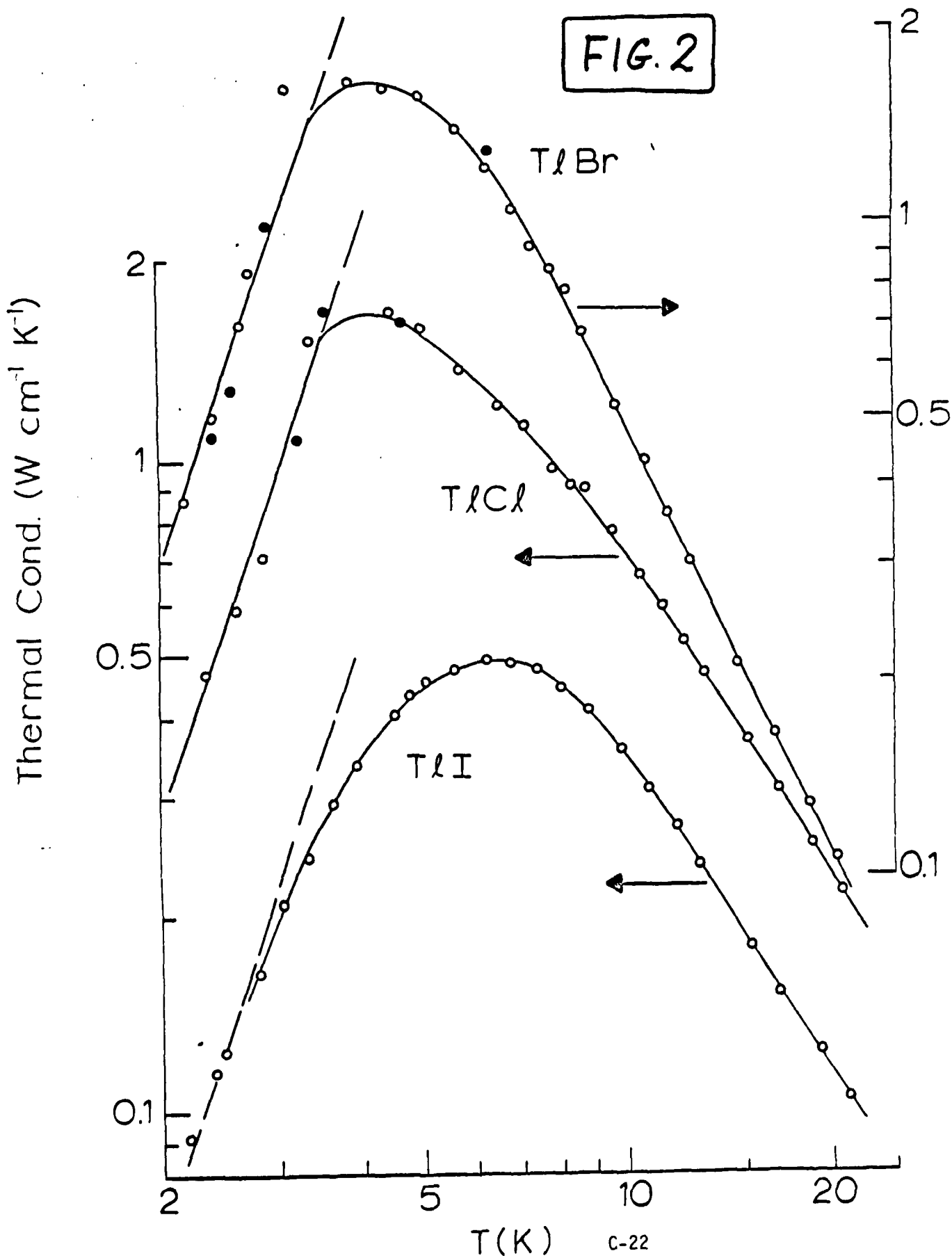
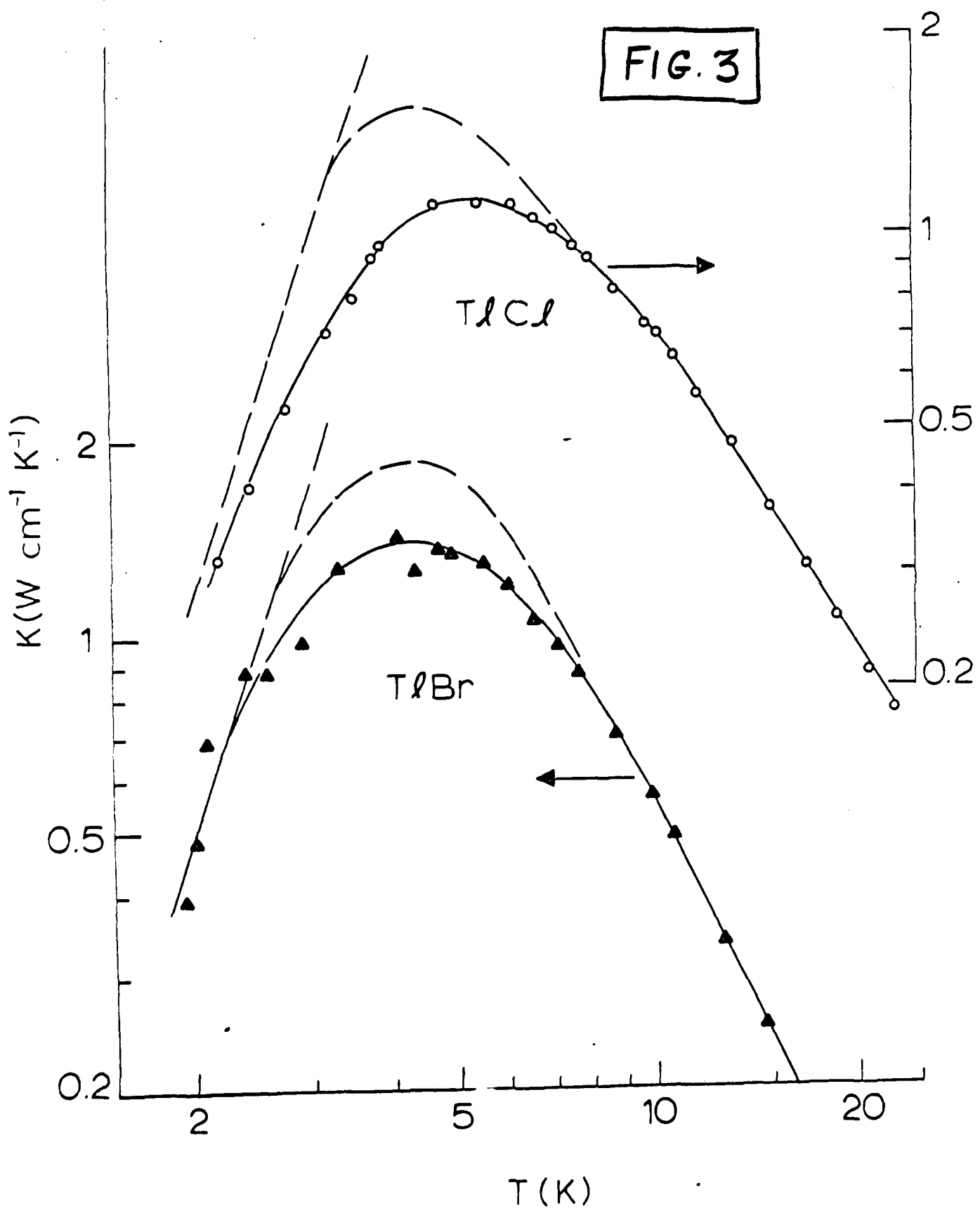


FIG. 3



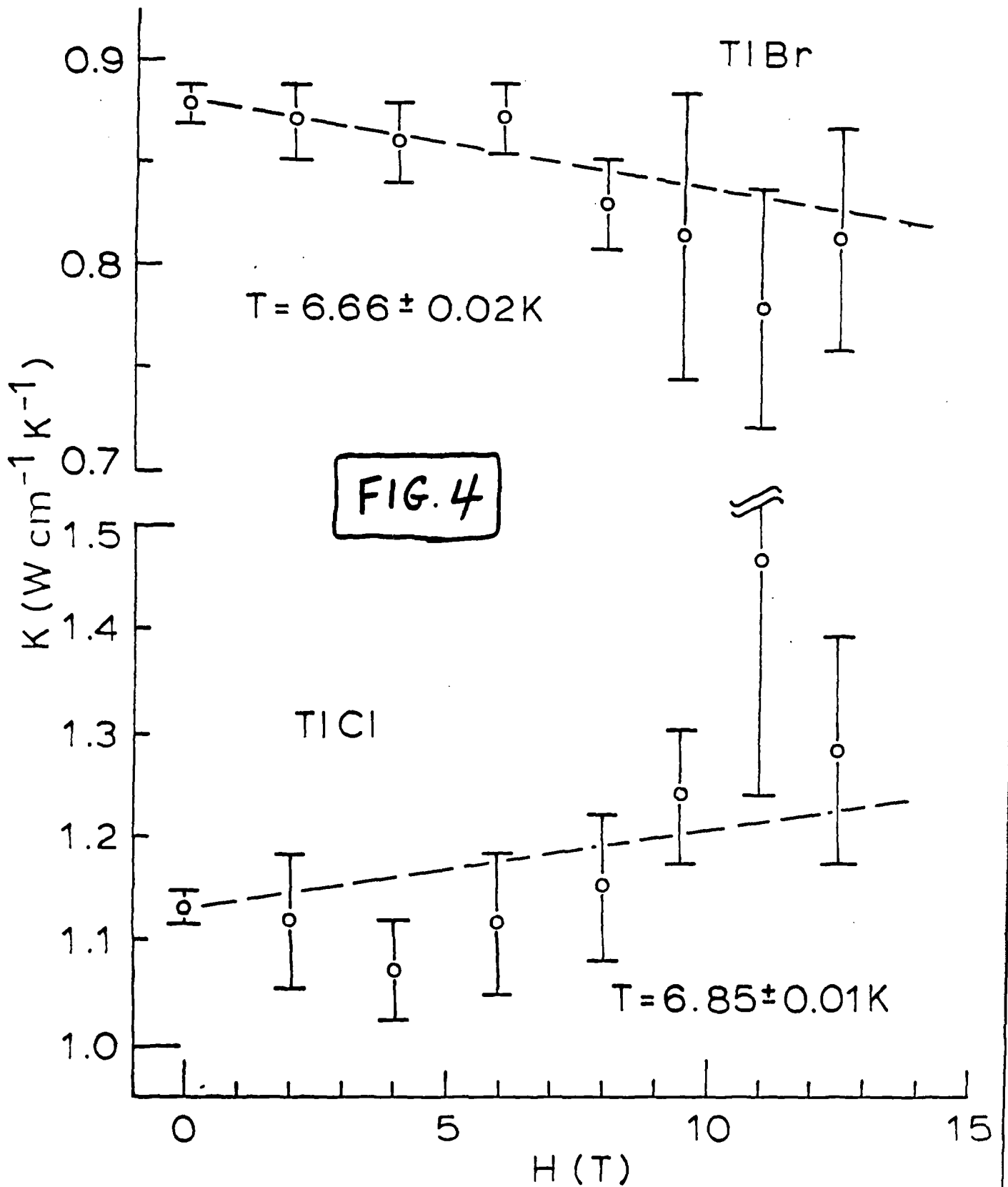
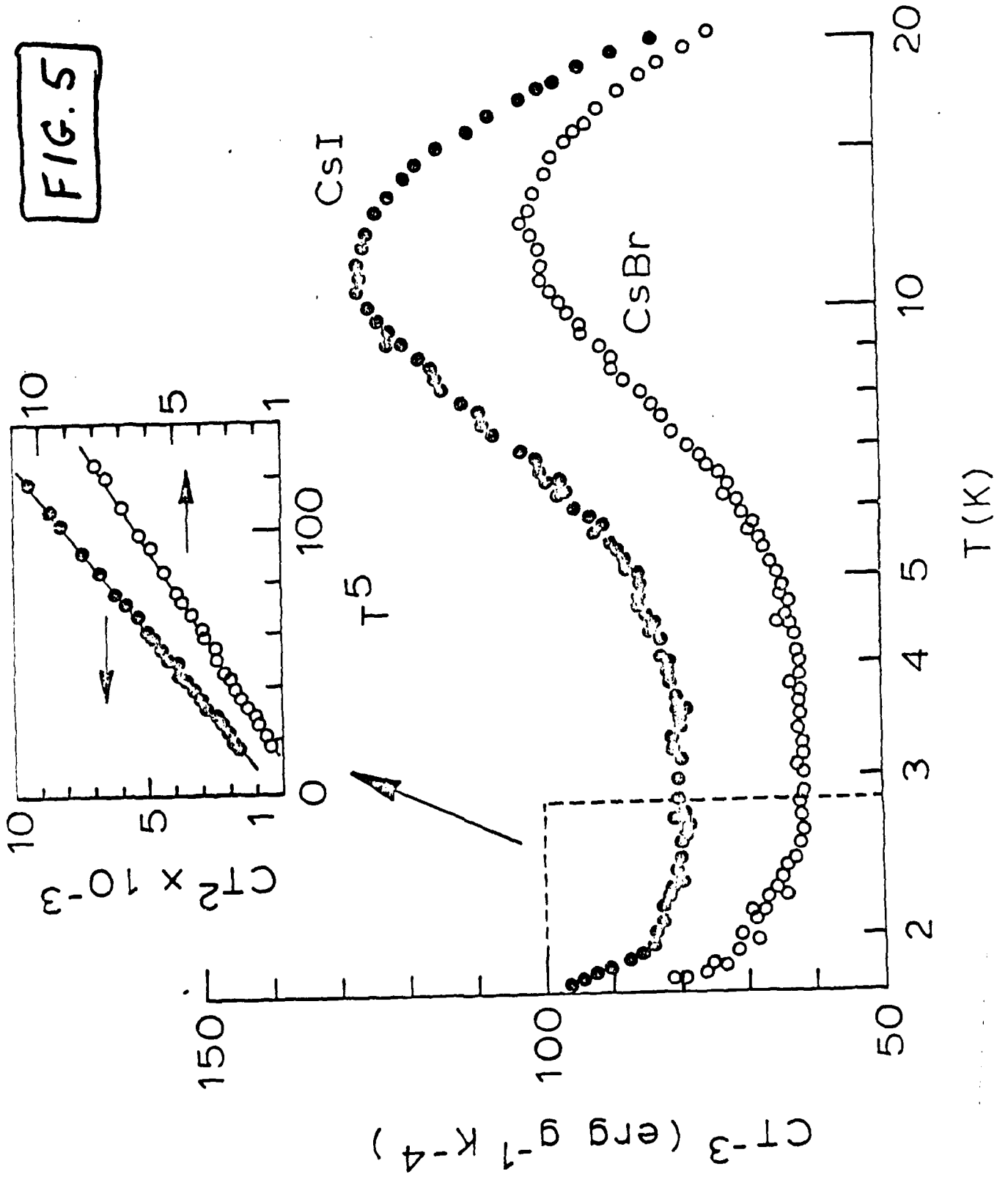


FIG. 5



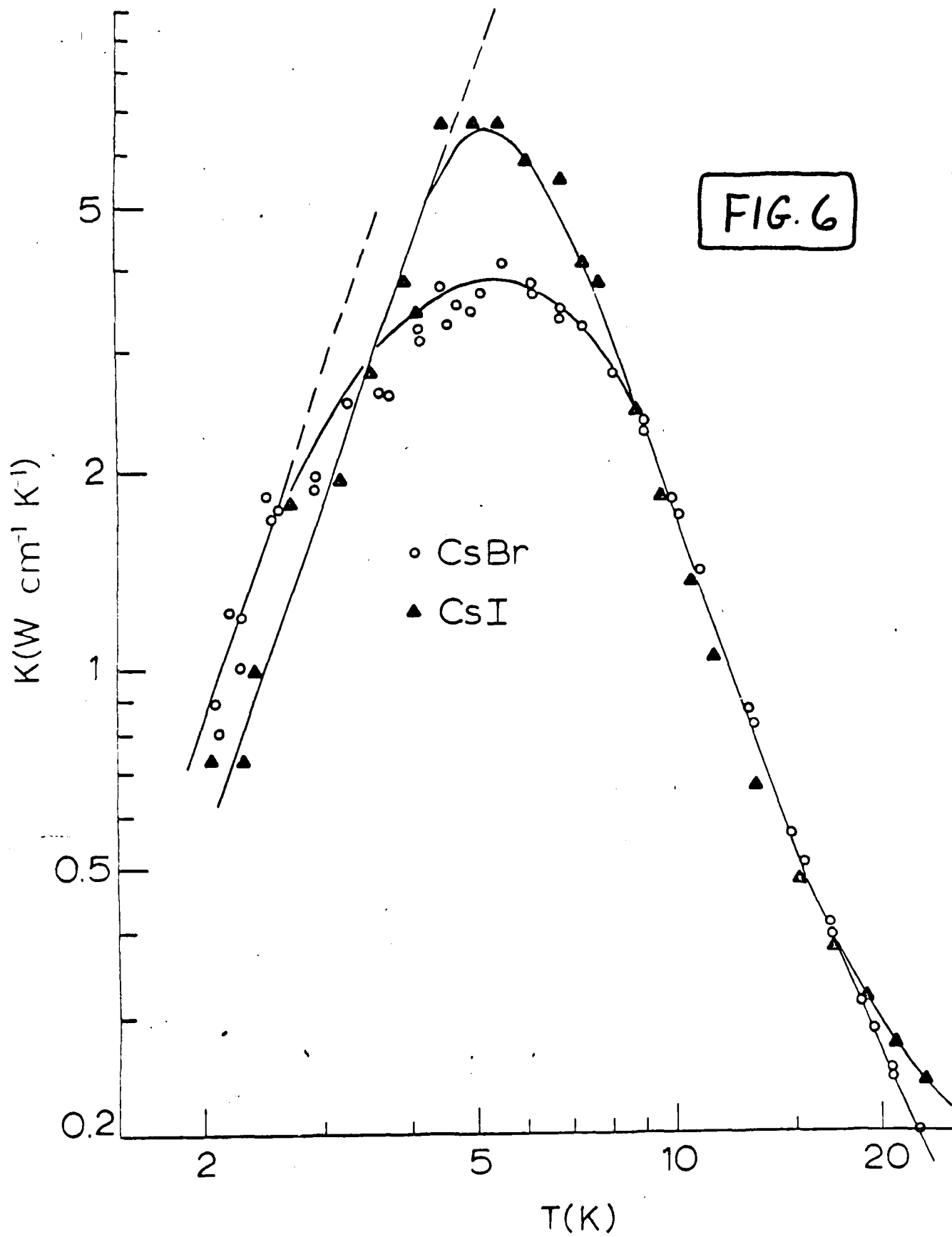
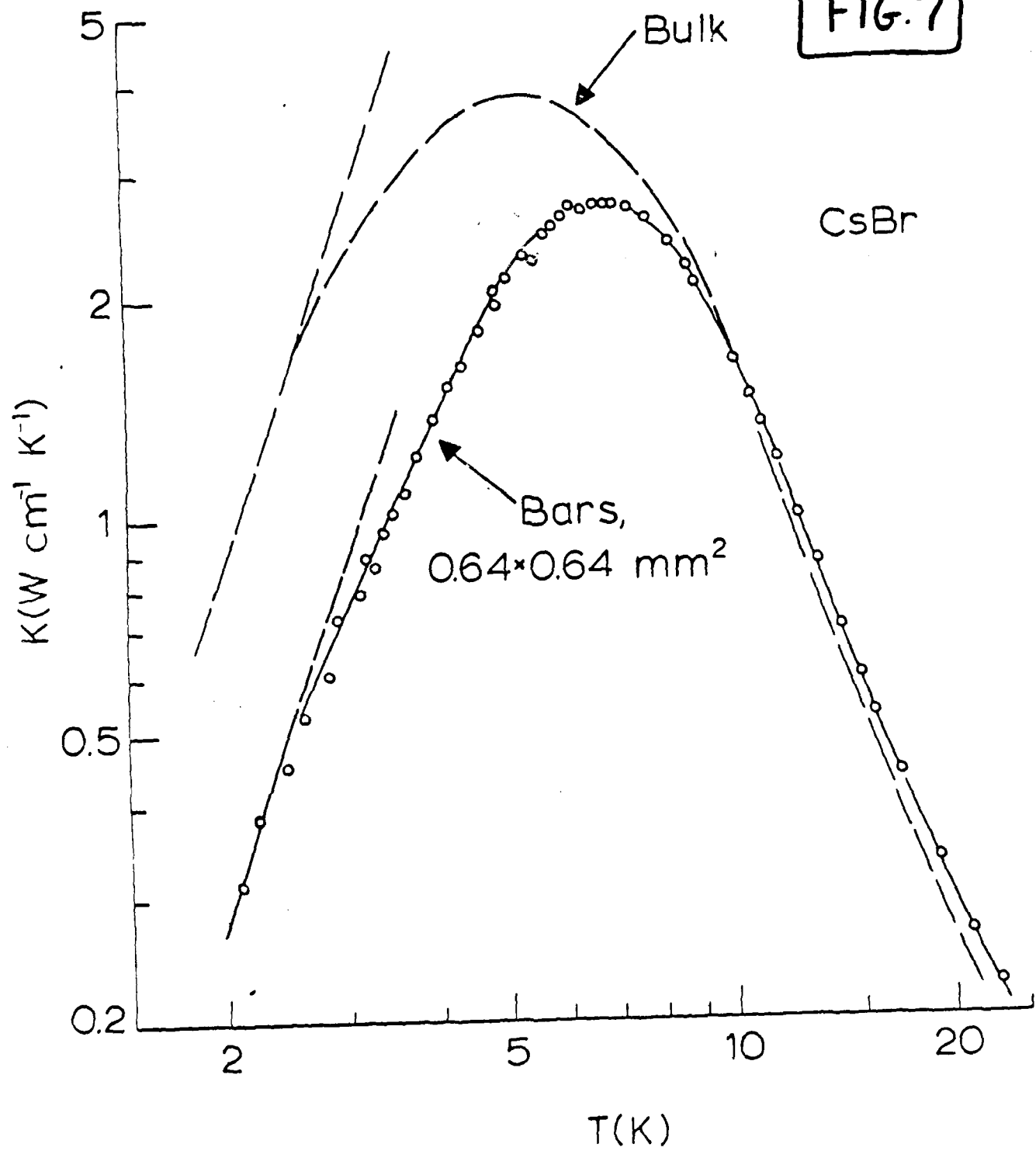
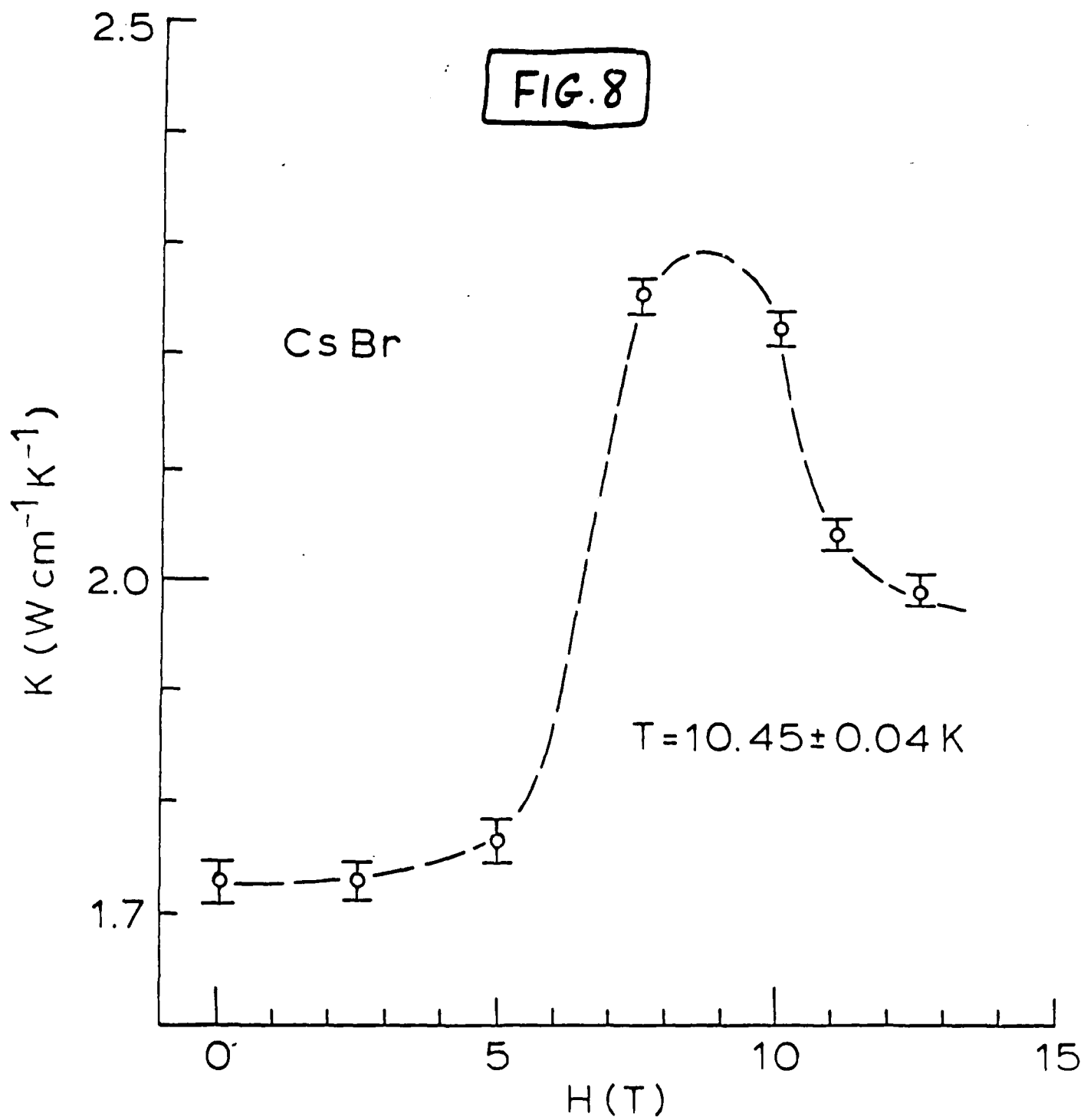


FIG. 7





PROGRESS REPORT

AFOSR Contract #F49620-83-C-0129

Fundamental Physics Studies on High-Specific-Heat  
Dielectrics and Kapitza Resistance at Dielectric Boundaries

Alkali Halide Studies, II. Data Analyses

by

W.N. Lawless *WNL*  
CeramPhysics, Inc.  
Westerville, Ohio 43081

December 15, 1983

Distribution:

✓ J.H. Parker, Sr.  
P.W. Eckels  
T.K. Gupta  
M. Ashkin  
C.F. Clark  
B.R. Patton

## INTRODUCTION

This is the second in a series of reports devoted to the thallos and cesium halides. In the first report, all of the experimental data measured to date on these halides was collected, including thermal-property data measured in intense magnetic fields up to 12.5 T. With the exception of TlI, all of the halides measured were single crystals.

The salient experimental findings are summarized below:

1. For all halides, the specific heat is significantly non-Debye,  $C/T^3$  displaying maxima in the range 5-15K which are ~ 2-5 times larger than the apparent Debye backgrounds.
2. In contrast to the thallos halides, the cesium halides display a Schottky-like excitation at the lowest temperatures in that  $C/T^3$  rises sharply with decreasing temperature below about 3 K.
3. For bulk samples, the thermal conductivities of all the halides display  $T^3$  boundary scattering below about 3-4 K. For thin samples (~ 0.5mm thickness), the thermal conductivity of CsBr is suppressed in the  $T^3$  region, as expected, but the are not.
4. Although the specific heats of TlCl and TlBr are unaffected by intense magnetic fields, the thermal conductivities of these crystals are changed by intense fields but in opposite ways. The effects are relatively small,  $d\kappa/dH = -0.47$  and  $+ 0.61\%$   $T^{-1}$  for TlBr and TlCl, respectively.

5. In contrast to the thallos halides, the thermal conductivity of CsBr in intense magnetic fields displays a large maximum at  $\sim 9T$ . The effect here is significant: The change in  $K$  between zero field and  $9T$  is 33%. The effect of intense magnetic fields on the specific heat of CsBr has not yet been measured.

The purpose of this report is to present analyses of the zero-magnetic-field, thermal-properties data for these halides according to simple models. More experimental work is called for on the magnetic-field-dependent properties; these experiments are in progress and will be reported in subsequent report.

#### DATA ANALYSES - SPECIFIC HEATS

The large and dominating maxima in  $C/T^3$  for the thallos and cesium halides are reminiscent of similar maxima found universally in amorphous<sup>1</sup> and ferroelectric<sup>2</sup> solids. Such phenomena have been described by a single Einstein-oscillator term added to the Debye background,<sup>2</sup>

$$C = 3nRD(T/\theta_D) + 3Rrx^2e^x (e^x-1)^{-2}, \quad x = \theta_E/T \quad (1)$$

where  $n$  is the number of atoms per formula weight,  $D(T/\theta_D)$  is the Debye function where  $\theta_D$  is the Debye temperature,  $r$  is the number of (dispersionless) Einstein oscillators per formula weight, and  $\theta_E$  is the Einstein temperature. The form of Eq. (1) is common in analyzing specific heat data, and generally if one has information on low-lying modes from Raman data, these frequencies are used in Eq. (1) by adding appropriate Einstein terms. For the case of a single Einstein term, it is straightforward to show from Eq. (1) that in the  $D(T/\theta_D) \approx T^3$  region,

$C/T^3$  will have a maximum at a temperature  $T_{\max} = \omega_E/3$  where  $\omega_E$  is the Einstein frequency (in  $\text{cm}^{-1}$ ).<sup>2</sup>

The specific heat data for the thallos and cesium halides were fitted to Eq. (1) using a three-level fitting scheme (for  $\theta_D$ ,  $\theta_E$ , and  $r$ ) which incorporated a tabulation of the Debye function.<sup>3</sup> For the thallos halides, the data from 2-20 K were fitted. For the cesium halides, the  $C/T^3$  data increase with decreasing temperature below 3 K (see Fig. 3) indicating a separate excitation. Consequently, the cesium halide data between 4 and 20 K were fitted to Eq. (1) because, as is evident from Fig. 3, the lower temperature excitation appears not to contribute above about 4 K (see below also).

The fitted data according to Eq. (1) for the thallos and cesium halides are shown in Figs. 1 and 2, respectively. The data in these figures are plotted according to the  $T \ll \theta_E$  form of Eq. (1), and this imparts a curvature to the data at the higher temperatures. In these figures  $C_{\text{ex}}$  is the excess specific heat,  $C_{\text{ex}} = C_{\text{exp}} - C_{\text{Debye}}$ , and excellent fits to the data are obtained over several orders of magnitude in  $T^2 C_{\text{ex}}/3R$ . The correlation coefficients for these fits varied from 98.7% for  $\text{TlCl}$  to 99.6% for  $\text{CsI}$ , and the fitted parameters are given in Table I. Also listed in Table I is the ratio of the number of Einstein modes,  $N_E$ , to Debye modes,  $N_D$ , given by<sup>4</sup>

$$N_E/N_D = r(\theta_D/\theta_E)^3. \quad (2)$$

Table I  
Fitting Parameters, Einstein Fits

Crystal	$\theta_D(K)$	$\theta_E(K)$	$\omega_E(\text{cm}^{-1})$	$r$	$N_E/N_D$
TlCl	120.4	26.14	18.17	0.2387	23.31
TlBr	115.7	31.34	21.78	0.2509	12.64
TlI	103.2	33.97	23.61	0.3533	9.89
CsBr	143.2	60.09	41.76	0.3314	4.49
CsI	122.7	56.36	39.17	0.3972	4.10

The Debye contribution to the specific heat can be estimated directly from the Debye temperatures in Table I and compared to the experimental specific heat at the maximum in  $C/T^3$ . When this is done it is found that the Debye contribution varies from 25.0% for TlCl to 63.8% for CsI. Thus, the Einstein modes dominate the specific heats in these halides, and this can also be seen in the  $N_E/N_D$  values in Table I. A similar dominance has been observed in the hexagonal tungsten bronzes<sup>4</sup> and ferroelectrics.<sup>2</sup>

It has recently been pointed out by Pederson and Brewer<sup>5</sup> that a linear relationship exists between  $\theta_D$  and the reduced mass for cubic crystals, and indeed the Debye temperatures in Table I do follow this relationship for the thallous and cesium halides.

The number of Einstein oscillators per formula weight,  $r$  in Table I, are quite large and this rules out an impurity effect. For the Cs halides, the Einstein frequencies  $\omega_E$  scale exactly with  $\mu^{-1/2}$ , where  $\mu$  is the reduced mass. For the thallous halides, however, the frequencies  $\omega_E$  in Table I do not scale well with any function of the masses of the thallous and halogen ions, although there is a general tendency for  $\omega_E$  to

scale with the mass of halogen ion. These findings suggest that the low-lying excitation responsible for the Einstein contribution is different in the cesium halides compared to the thalious halides.

The cesium halides display another non-Debye contribution to the specific heat below about 3 K as seen in Fig. 3. Various specific heat functionals were tried in attempts to fit these data, and excellent fits were found to the high-temperature form of the Schottky term,

$$C_{\text{exp}} = mT^3 + n'Rg_0g_1 (g_0+g_1)^{-2} (\delta/T)^2 \quad (3)$$

where the  $T^3$  term is the Debye contribution,  $n'$  are the number of excitations per formula weight,  $\delta$  is the level splitting (of a two-level system), and  $g_0, g_1$  are the degeneracies of the system. We have no reason to select a two-level system; what is important is the  $T^{-2}$  temperature dependence which is common to the general Schottky term.

The data below 3 K for CsBr and CsI are plotted according to Eq. (3) in the inset in Fig. 3, and satisfactory fits are obtained. Assuming  $g_0 = g_1$  and  $n' = 1$  in Eq. (1) (the latter assumption puts an upper limit on  $\delta$ ), the fitted parameters are given in Table I where  $\theta_D$  is obtained from  $m$  in Eq. (3).

Table II  
Fitting Parameters, Schottky Fits

Crystal	$\theta_D$ (K)	$\delta$ (mK)
CsBr	146.0	61.0
CsI	125.1	60.7

The similarity of the level splittings  $\delta$  in Table II indicates that the same mechanism is responsible for these low-lying excitations in both CsBr and CsI. The agreement between the Debye temperatures in Tables I and II is satisfactory: CsBr,  $144.6 \pm 0.97\%$  K; CsI,  $123.9 \pm 0.97$  K. These variations in the Debye temperatures translate into uncertainties in  $C/T^3$  of  $\pm 2.9\%$ , which are commensurate with the experimental inaccuracies. Finally, the fitted parameters in Tables I and II show that the Schottky term makes a negligible contribution in the fitting temperature range of the Einstein term, and vice versa.

It is difficult to identify the mechanism responsible for the Schottky excitation in the cesium halides which is missing in the thallos halides. Such excitations have been seen previously in crystalline insulators and attributed to the interaction of electric quadrupole moments with local electric-field gradients.<sup>6</sup> However, in these cubic CsCl lattices there are no such gradients. An impurity effect (e.g.,  $Fe^{3+}$ ) may be responsible, but the manufacturer of the crystals believes that the kind and amounts of impurities in the cesium and thallos halides should be comparable. Alternately, the cesium halides are far more hygroscopic than the thallos halides, and it is well-known that hydroxyl groups in alkali halides give rise to Schottky specific heat contributions at low and very low temperatures.<sup>7</sup>

#### DATA ANALYSES - THERMAL CONDUCTIVITIES

There are two questions to address regarding the thermal conductivities of the thallos and cesium halides: (1) Do the Einstein modes carry heat, and (2) What is the nature of boundary scattering in these crystals.

The former question deserves special consideration since, as seen above, the Einstein terms dominate the specific heats of these halides at low temperatures. In applying the perfect-gas approximation,

$$\kappa = \frac{1}{3} C \bar{v} \rho \lambda, \quad (4)$$

only those specific-heat contributions from heat-carrying modes can be used in Eq. (4), where  $\bar{v}$  is the average sound velocity,  $\rho$  is the density, and  $\lambda$  is the mean-free path of the dominant phonon.

To investigate the heat-carrying phonons, we adopt the well-known result due to Peierls,<sup>8</sup>

$$\lambda = \lambda_0 e^{\theta_D/2T} \quad (5)$$

which has been verified in several dielectric crystals. This relation does not, of course, pertain to the boundary scattering region.

Combining Eqs. (4) and (5),

$$\kappa/C = e^{\theta_D/2T}, \quad (6)$$

so that the scheme involves examining whether the total specific heat (Debye + Einstein) or the Debye specific heat yields the correct  $\theta_D$  from Eq. (6) when combined with the experimental thermal conductivity data at temperatures above the boundary scattering region.

For calculation purposes, the average sound velocity reported by Morse and Lawson<sup>9</sup> for TlBr was adopted for all the halides,  $\bar{v} = 1.82 \times 10^5$  cm/sec, and the densities of the crystals are: TlBr, 7.557; TlCl, 7.000; TlI, 7.090; CsBr, 4.440; and CsI, 4.526 [note that these parameters enter the pre-exponential factors in Eq. (6)]. Examples of the  $\lambda$  vs.  $T^{-1}$  plots for the thallos and cesium halides are shown in Figs. 4 and 5,

respectively. These plots were generated using smoothed thermal conductivity and specific heat data where the total specific heat data were used. The plots are linear for  $T \gtrsim 10$  K, and this agrees with the temperature range for TlBr, TlCl, and CsBr where the thick-and thin-sample thermal conductivity data converge. For these latter crystals, both sets of K-data were used above 10 K to construct the plots in Figs. 4 and 5.

From the linear portions of the plots,  $\theta_D$ -values were found by least-squares fits, and these values are shown in Figs. 4 and 5. The results of these studies are summarized in Table III.

Table III  
Debye Temperatures from Mean-Free-Path Studies

Crystal	$\theta_D$ (calor.)(a)	$\theta_D(D)$ (b)	$\theta_D(D+E)$ (b)
TlBr	116	135	114
TlCl	120	120	106
TlI	103	123	103
CsBr	144.6	148	162
CsI	124	144	127

(a) From specific heat data, Tables I and II

(b) D = Debye specific heat only used in Eq. (6); D+E = Total specific heat

The Table III data reveal some interesting contrasts: (1) For TlCl and CsBr, there is excellent agreement with the calorimetric  $\theta_D$ 's if the Einstein modes are assumed not to carry heat, whereas (2) For TlBr, TlI, and CsI, the excellent agreement between  $\theta_D$  (calor.) and  $\theta_D(D+E)$  suggests

that the Einstein modes carry heat in these crystals. We remark that the analyses can discriminate easily between  $\theta_D(D)$  and  $\theta_D(D+E)$  in Table III because the Einstein term makes a large contribution to the specific heat above 10 K, particularly in the case of the cesium halides.

Strictly speaking, the Peierls relation Eq. (5) assumes that the Debye phonons are the dominant heat carriers, so the good agreement between the  $\theta_D$ 's in Table III for the case of the Einstein mode heat carriers (TlBr, TlI, and CsI) may be fortuitous. The clearer case is that of TlCl and CsBr where agreement between the  $\theta_D$ 's is achieved if the Einstein modes do not carry heat. Either way, the analyses distinguish between the two cases.

Turning next to the boundary scattering phenomena in these crystals, we shall employ Eq. (4) to find  $\lambda_C$ , the phonon mean free path in the  $T^3$  region of the thermal conductivity. We shall assume that the heat-carrying modes identified above in these crystals are correct, and the appropriate specific heats will be used in Eq. (4) (at the lowest temperatures involved the Einstein modes are almost frozen out so this assumption is not critical to our discussion). Finally, the Schottky term in the specific heat of the cesium halides is assumed to be localized and not a heat carrier.

The procedure is to solve Eq. (4) using (smoothed) C- and K-data at the lowest temperatures. The parameter values given above for  $\rho$  and  $\bar{v}$  were used, and the results are given in Table IV.

Table IV  
Boundary Scattering Mean Free Paths

Crystal	Smallest Sample Dimension (cm)	$\lambda_c$ (cm)
TlBr	0.145	0.016
TlBr	0.049	0.016
TlCl	0.155	0.0084
TlCl	0.064	0.0077
TlI(a)	0.169	0.0020
CsBr	0.172	0.063
CsBr	0.064	0.020
CsI	0.156	0.032

(a) Fused polycrystalline sample

The data in Table IV reveal two broad features: (1) The  $\lambda_c$  values in the cesium halides are generally much larger than in the thalious halides and scale with the sample dimension; and (2) In the thalious halides, the  $\lambda_c$  values are approximately independent of the sample dimension.

The clear indication is that in the cesium halides boundary scattering arises from the physical dimensions of the crystal, but in the thalious halides some small entity within the crystal is responsible for the boundary scattering. There is some evidence in the literature from low-angle x-ray diffraction<sup>10</sup> that the thalious halides develop a mosaic structure where the mosaics are  $\sim 100\mu\text{m}$  ( $\sim 0.01$  cm). The indication then is that the thermal conductivities of the thalious halides are limited at the lowest temperatures by boundary scattering at the boundaries of these mosaics.

## DISCUSSION

The specific heats of the thallos and cesium halides at low temperatures can be described very well by the simple models employed above, and we remark that the non-Debye phenomena described (e.g., the  $C/T^3$  maxima) are large and dominating effects. Moreover, there is a satisfying internal consistency in that the  $\theta_D$ 's from the two fitting regimes for the cesium halides (Tables I and II) are in excellent agreement.

Examination of the phonon mean free paths according to the Peierls relation Eq. (5) provides information on the nature of the heat-carrying modes in these crystals. It is clear that the Einstein modes in  $TlCl$  and  $CsBr$  do not carry heat whereas in the remaining halides these modes apparently are heat carriers. It is surprising that in these  $CsCl$ -type crystals some Einstein modes carry heat while others do not. This is made even more puzzling by observing that the Einstein frequencies are quite similar within the thallos halides ( $21.2 \pm 2.8\text{cm}^{-1}$ ) and the cesium halides ( $42.8 \pm 3.7\text{cm}^{-1}$ ). Finally, there is experimental evidence that the Einstein mode in  $TlCl$  is E-field independent (14 kV/cm) which suggests an acoustic mode, but the mean-free-path data indicate this mode doesn't carry heat.

The thermal conductivity data on these halides are understandable in a straightforward fashion: Boundary scattering in the cesium salts is due primarily to phonon scattering at the crystal surfaces, whereas in the thallos halides the boundary scattering is dominated by the mosaic structure. We remark in this regard that, in the former case, it is not unusual for  $\lambda_c$  to be  $\sim 3$ -5 times smaller than the crystal dimension as this bears on the diffuse/spectral scattering of phonons at the surface which in turn depends on the surface preparation.

In conclusion, we return to the suggestion that the Schottky term in the cesium halides may be due to an OH<sup>-</sup> concentration. It is known that OH<sup>-</sup> ions occupy halogen sites in NaCl-type crystals such as KCl and KBr and have six equilibrium orientations along [100].<sup>11</sup> The sixfold degeneracy of the ground state is tunneling split into a ground-state singlet A<sub>1g</sub> of energy -2δ, a triplet T<sub>1u</sub> of zero energy, and a doublet E<sub>g</sub> of energy δ, where δ is the zero-field splitting.<sup>7</sup> The Schottky contribution to the specific heat from these tunneling states is given by<sup>12</sup>

$$C_{\text{sch}} = \frac{6Nky^2(2e^{-2y} + 3e^{-3y} + e^{-5y})}{(1 + 3e^{-2y} + 2e^{-3y})^2}, \quad y = \delta/T \quad (7)$$

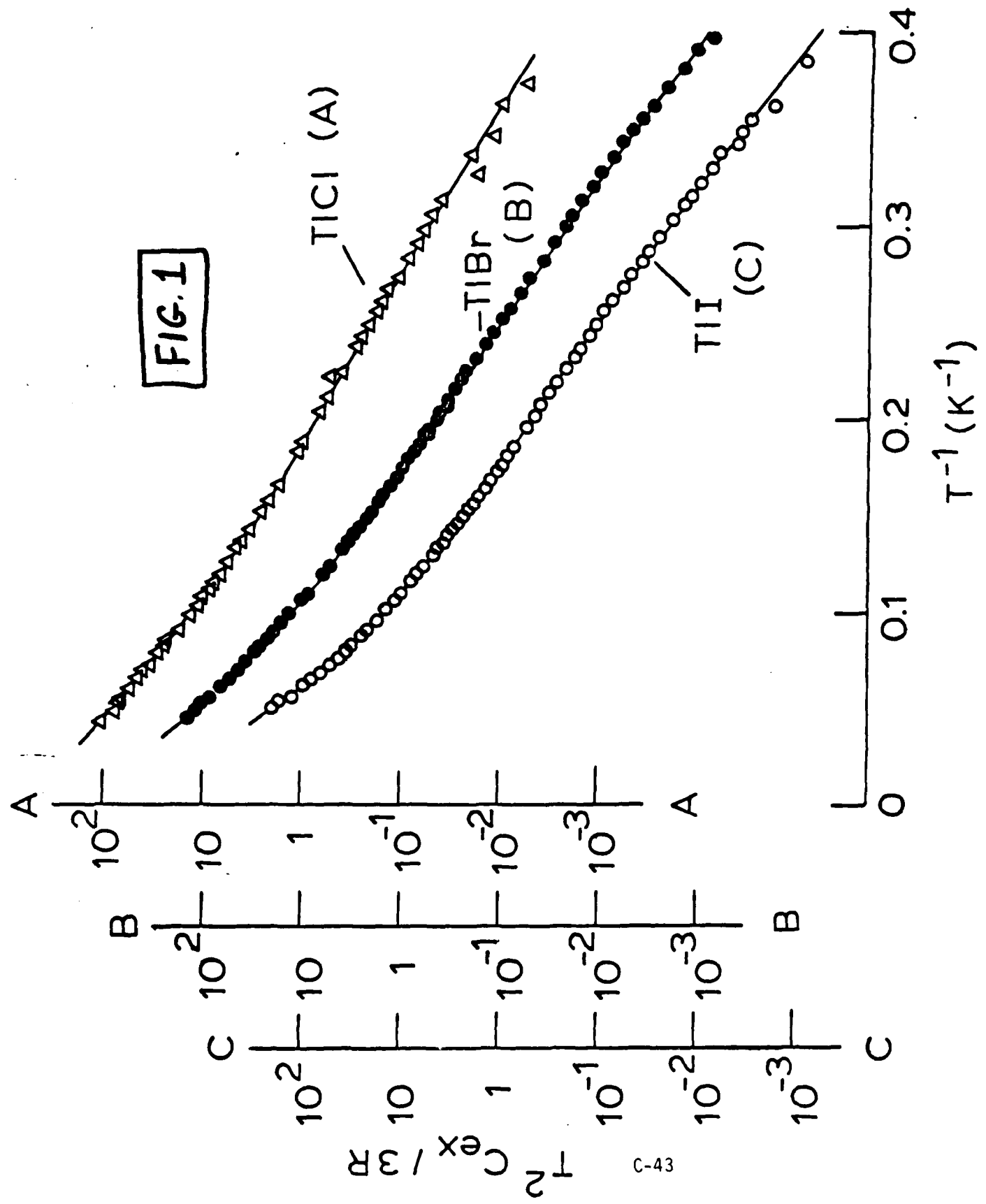
where N is the hydroxyl concentration in cm<sup>-3</sup>. Since OH<sup>-</sup> ions substituted in the CsCl lattice also have octahedral symmetry, Eq. (7) applies also to the cesium halides. The tunneling splittings in the NaCl-type lattices are δ ≈ 0.34 K,<sup>13</sup> and substituting this value into the T ≫ δ form of Eq. (7) and comparing with the fitted Schottky coefficients for the cesium halides, we find N ~ 10<sup>20</sup> cm<sup>-3</sup> for the two crystals. These concentrations are comparable to those found in KCl<sup>7</sup> and lend credence to the suggestion of significant OH<sup>-</sup> concentrations in the cesium halide crystals from Harshaw.

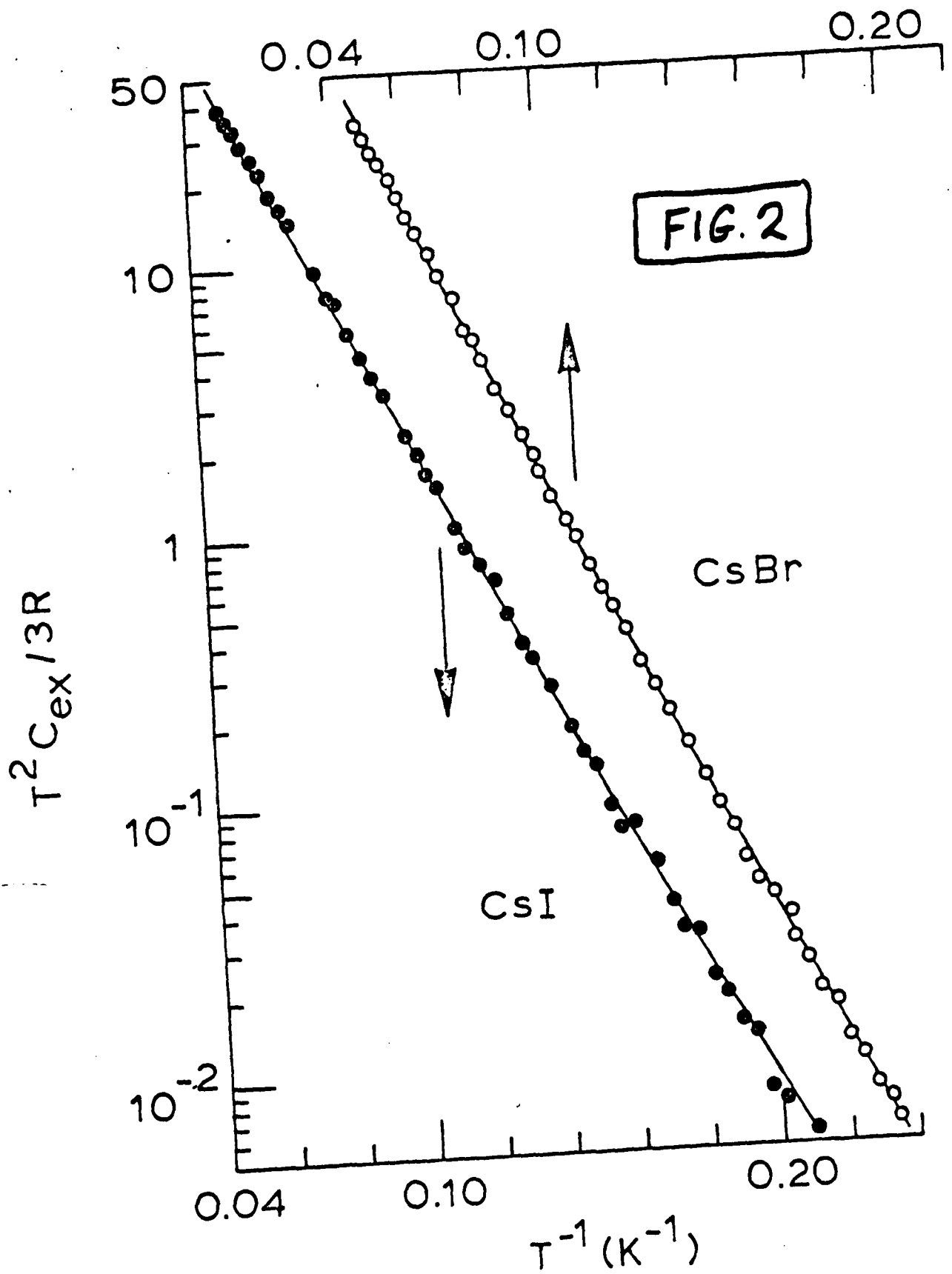
#### References

- <sup>1</sup>W.A. Phillips, *J. Non-Cryst. Solids* 31, 267 (1978).
- <sup>2</sup>W.N. Lawless, *Phys. Rev.* B14, 134 (1976).
- <sup>3</sup>E.S.R. Gopal, Specific Heats at Low Temperatures (Plenum, New York, 1966).

- <sup>4</sup> A.J. Bevolo, H.R. Shanks, P.H. Sidles, and G.C. Danielson, Phys. Rev. B9, 3220 (1974).
- <sup>5</sup> D.O. Pederson and J.A. Brewer, Phys. Rev. B16, 4546 (1977).
- <sup>6</sup> W.N. Lawless, Phys. Rev. B19, 3755 (1979).
- <sup>7</sup> I.W. Shepherd, J. Phys. Chem. Solids 28, 2027 (1967); J.P. Harrison, Rev. Sci. Instrum. 39, 145 (1968).
- <sup>8</sup> R. Peierls, Ann. Physik 3, 1055 (1929); C. Herring, Phys. Rev. 95, 954 (1954).
- <sup>9</sup> G.E. Morse and A.W. Lawson, J. Phys. Chem. Solids 28, 939 (1967).
- <sup>10</sup> A. Smakula and M.W. Klein, J. Opt. Soc. Am. 40, 748 (1950).
- <sup>11</sup> U. Kuhn and F. Lüty, Solid State Commun. 3, 31 (1965); F. Lüty, J. Phys. Suppl. 8-9, 28, C4-120 (1967).
- <sup>12</sup> W.N. Lawless, J. Phys. Chem. Solids 30, 1161 (1969).
- <sup>13</sup> G. Feher, I.W. Shepherd, and H. Shore, Phys. Rev. Lett. 16, 500 (1966).

**FIG. 1**





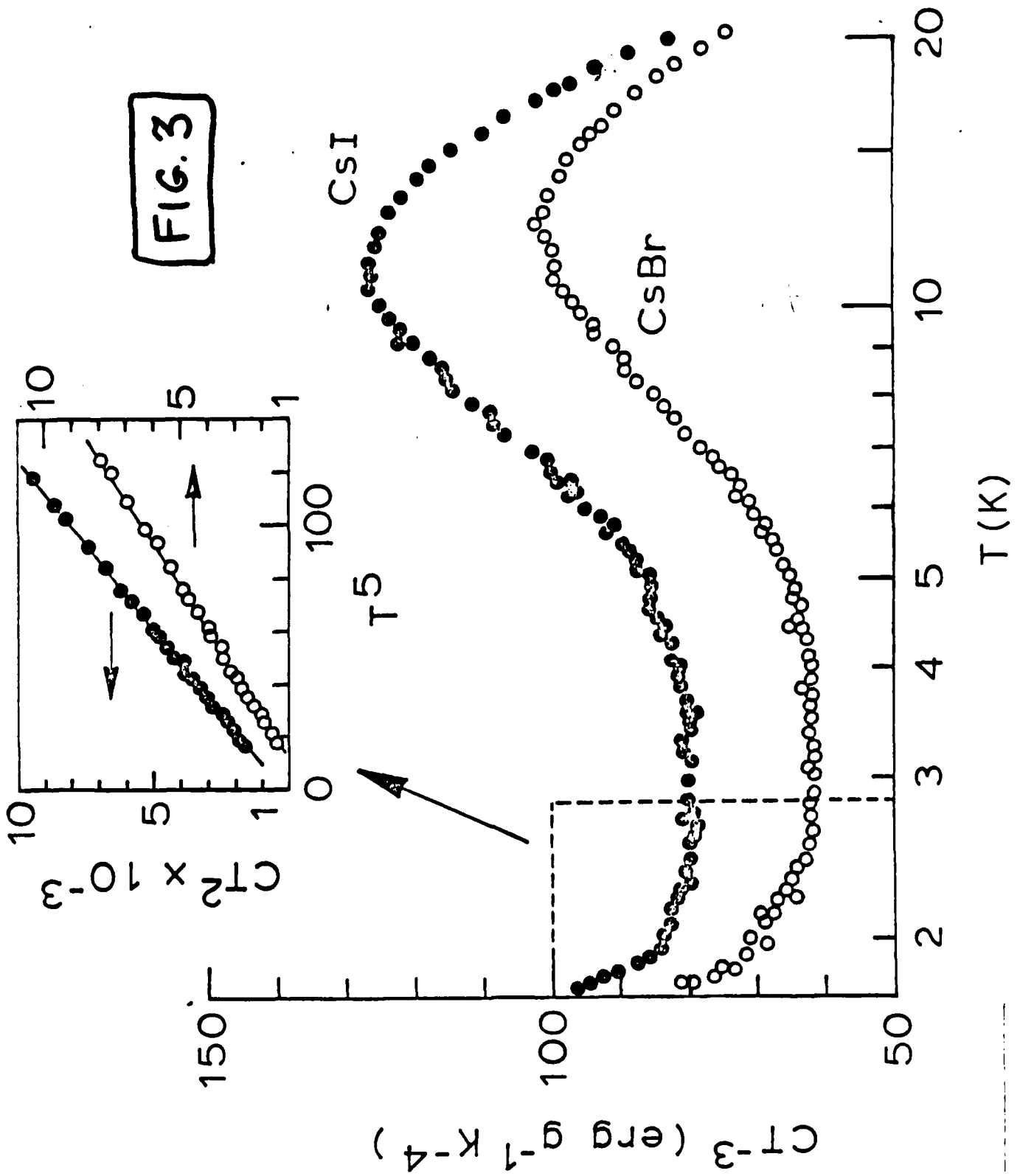
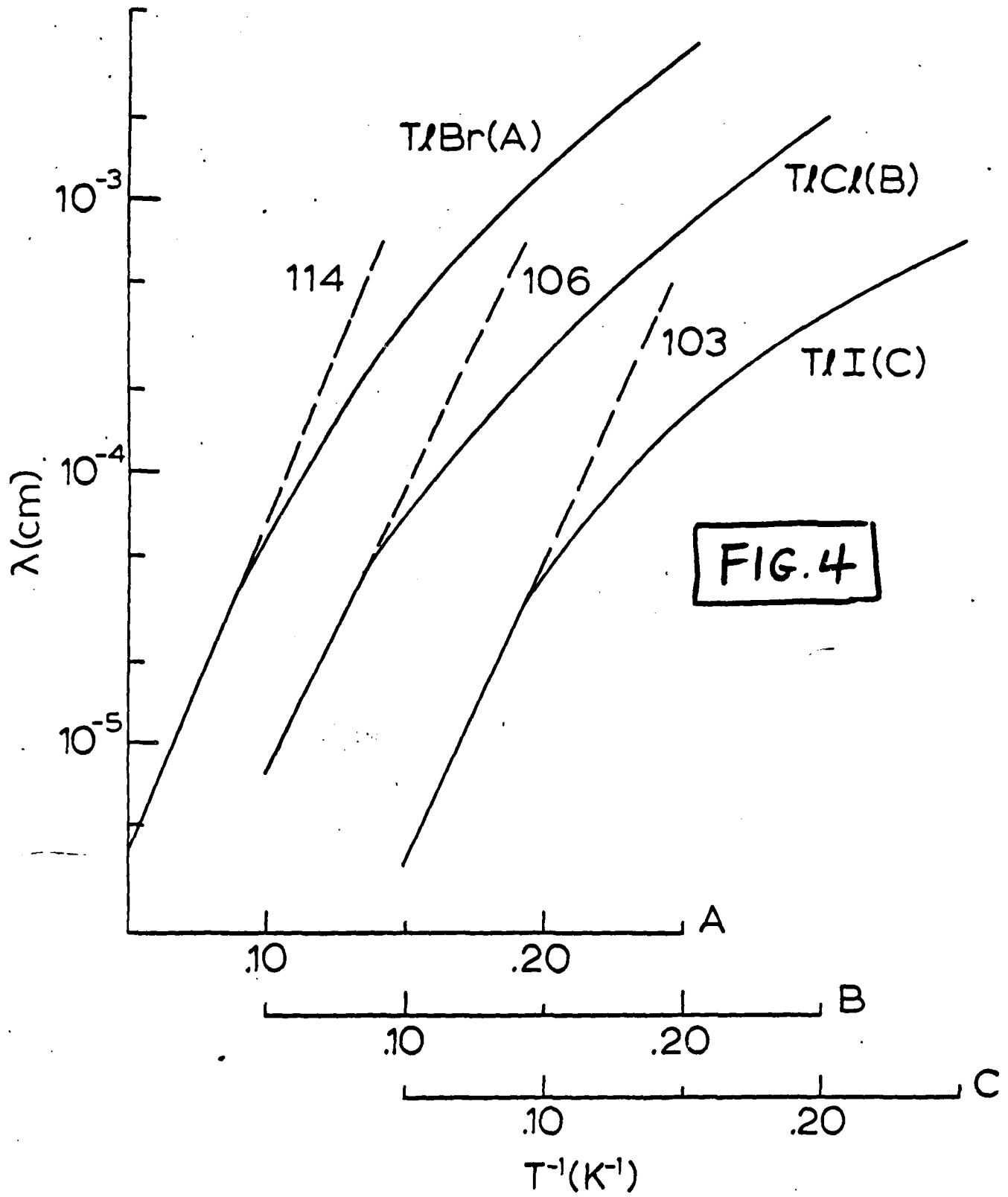
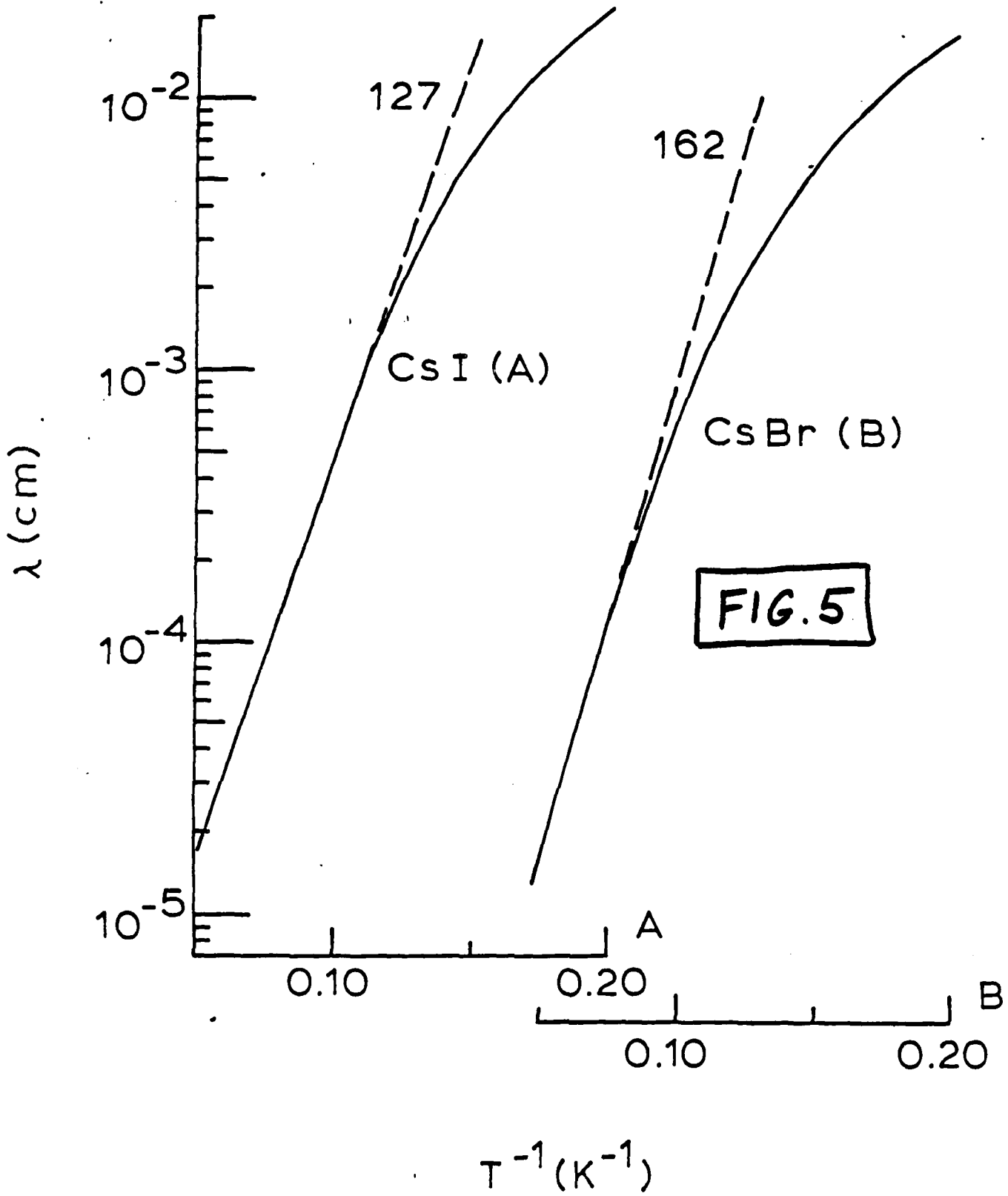


FIG. 3





Progress Report

AFOSR Contract #F49620-83-C-0129

Fundamental Physics Studies on High-Specific-Heat  
Dielectrics and Kapitza Resistance at Dielectric Boundaries

Alkali Halide Studies, III. Magnetolectric  
Measurements on CsBr at Low Temperatures

by

W.N. Lawless  
CeramPhysics, Inc.  
Westerville, Ohio 43081

*WNL*

July 31, 1984

Distribution:

J.H. Parker, Sr.

[REDACTED]

T.K. Gupta

M. Ashkin

C.F. Clark

B.R. Patton

This is the third in a series of reports dealing with the thallos and cesium halides at low temperatures. In the first report in this series, experimental data on the effect of intense magnetic fields on the thermal conductivities of  $TlCl$ ,  $TlBr$ , and  $CsBr$  at low temperatures were reviewed. All crystals were measured under identical conditions, and, although the thermal conductivities of the thallos halides showed small dependences on  $H$  (and were of opposite sign), the thermal conductivity of  $CsBr$  at 10.45 K underwent a large maximum at  $H \approx 8.5$  T. These data are reproduced here in Fig. 1. The temperature control in this experiment was  $\pm 0.04$  K, estimated from the quantifiable sources of error. The height of the maximum in Fig. 1 is so large ( $\Delta K/K \approx 35\%$ ) that in order to explain this as a spurious variation in the control temperature requires a temperature uncertainty  $\sim 1$  K.

The thermal conductivity is intimately related to the phonon modes and their density of states. Consequently, since both the thermal conductivity and the dielectric constant depend on these phonon modes, a magnetic-field effect in the former might also be manifested in the latter. The purpose of this report is to document measurements of the dielectric constant of  $CsBr$  in intense magnetic fields at low temperatures.

The  $CsBr$  sample was a crystal slice cut from a boule, and the slice was 0.072 cm thick with major electroded faces  $0.357 \text{ cm}^2$  in area (the orientation of the crystal was not determined). The crystal was suspended by its leads from posts within a simple immersion probe, and the probe was designed to fit into the high-field region of the tail-piece of the insertion dewar for the superconducting 15 T magnetic at the Francis Bitter National Magnet Laboratory (MIT). The probe was vented

to the atmosphere to avoid pressure buildup in the liquid helium of the insert dewar, and independent measurements of other samples with this arrangement indicated that isothermal conditions were maintained.

The capacitance and loss tangent of the crystal were measured at several field levels up to 15 T (150 kG) using a transformer ratio-arm bridge with associated oscillator (1 kHz) and detector in the three-terminal mode. The loss tangent of the crystal was so small ( $\sim 10^{-6}$ ) that the correction factor (i.e.,  $1 + \tan^2 \delta$ ) was ignored in calculating the dielectric constant at the various field levels. Moreover, the very small loss tangent of the sample indicates that the measured changes in  $\epsilon$  are intrinsic effects unrelated to any spurious conduction processes associated with impurities

The three-terminal mode of measurement eliminates all lead and stray capacitance, provided coaxial cables are used from the sample to the bridge. However, the leads within the probe were not fully coaxial, and for the position of the CsBr crystal the measured lead capacitance was 38.96 pF at room temperature. This was unfortunate because the total zero-field capacitance at 4.2 K was 40.313 pF (i.e., the lead capacitance constituted 96% of the total capacitance). The measured  $\epsilon$  at 4.2 K was 3.069, compared to the NIP Handbook value of 6.51 at room temperature. Consequently, it was suspected that the lead capacitance at 4.2 K was smaller than the measured value at 300 K, and the procedure used was to adjust the lead capacitance to yield  $\epsilon = 6.51$  at 4.2 K, 37.45 pF. These lead-capacitance considerations do not affect the changes in  $\epsilon$ . Moreover, we have firm experimental evidence that the lead capacitance at 4.2 K does not change with magnetic field

(i.e., similar measurements on SrTiO<sub>3</sub> and KTaO<sub>3</sub> in the same probe revealed very small changes in  $\epsilon$  of opposite sign for the two materials).

The results of these measurements on the CsBr crystal are shown in Fig. 2 where  $\epsilon$  is plotted vs. H; here  $\epsilon$  in zero field at 4.2 K has been selected as 6.51. The effect of a magnetic field on the dielectric constant is dramatic: At 15 T,  $\epsilon$  has decreased by about 4%, and this finding is qualitatively unaffected by the selection of  $\epsilon$  in zero field. We note that in Fig. 2 there is no apparent structure in  $\epsilon$  at 8.5 T as there is in the thermal conductivity at this field level, Fig. 1. However, based on the one data point 11.7 T,  $\epsilon$  appears to plateau between 9-12 T as indicated by the dashed line in Fig. 2.

The data in Fig. 2 are analyzed phenomenologically as follows: We construct the Gibbs free energy expansion for a simple cubic crystal, by selecting the polarization P and magnetization M as the independent variables,

$$A = A_0 + \frac{1}{2} \chi_0 P^2 + \frac{1}{4} \xi P^4 + \frac{1}{2} \alpha_0 M^2 + \frac{1}{2} \beta P^2 M^2 + \frac{1}{4} \gamma P^2 M^4 + \dots \quad (1)$$

where  $\chi_0$  and  $\xi$  are the dielectric coefficients,  $\alpha_0$  is the magnetic coefficient, and  $\beta$  and  $\gamma$  are the magnetoelectric coefficients. The temperature dependence is contained in the coefficients. The Gibbs free energy has the properties that the electric field is  $E = \partial A / \partial P$  and the magnetic field,  $H = \partial A / \partial M$ . The dielectric constant is defined by  $\epsilon = 1 + 4\pi \partial P / \partial E$ , so that the dielectric susceptibility is

$$\chi = 4\pi / (\epsilon - 1) = \partial E / \partial P = \partial^2 A / \partial P^2. \quad (2)$$

Solving,

$$\chi_H - \chi_o = (\beta/\alpha_o^2)H^2 + (\gamma/\alpha_o^4)H^4 + \dots \quad (2)$$

or

$$(\epsilon_H - 1)^{-1} - (\epsilon_o - 1)^{-1} = (\beta/4\pi\alpha_o^2)H^2 + (\gamma/4\pi\alpha_o^4)H^4 + \dots \quad (2')$$

The dielectric data are shown plotted in Fig. 3 according to Eq. (2'), and the region linear in  $H^2$  is resolved up to  $H^2 \sim 70 \text{ T}^2$  ( $H \sim 8.5 \text{ T}$ ). Not all the data shown in Fig. 2 are plotted in Fig. 3 because so few data points were measured above 10 T. Furthermore, it is probably coincidental that the upper limit of the linear range in Fig. 3 (8.5 T) coincides with the field of the maximum in  $K$  in Fig. 1; a plateau in  $\epsilon$  between 9-12 T is suggested by the data (dashed curve in Fig. 2) but this is prejudiced by the one point at 11.7 T.

The linear region in Fig. 3 yields from Eq. (2'),

$$\beta/\alpha_o^2 \approx 6.5 \times 10^{-4} \text{ (T}^{-2}\text{)} \quad (3)$$

Insufficient data were measured at fields about 10 T to resolve the fourth-order term in Eq. (2'), but a rough estimate yields

$$\gamma/\alpha_o^4 \sim -4 \times 10^{-7} \text{ (T}^{-4}\text{)}. \quad (4)$$

The Lyddane-Sachs-Teller relation for a simple diatomic cubic crystal relates the dielectric constant to the frequencies of the longitudinal and transverse optic modes,

$$\epsilon/\epsilon_\infty = (\omega_{LO}/\omega_{TO})^2 \quad (5)$$

where  $\epsilon_\infty$  is the infinite-frequency dielectric constant (i.e.,  $\epsilon_\infty = n^2 - 1$  where  $n$  is the refractive index). Assuming that the longitudinal optic mode is H-field dependent and combining with Eq. (2'), we find

$$\begin{aligned} \Delta \ln \omega_{LO} &= -\frac{1}{2} \epsilon \Delta(1/\epsilon) = -(\beta \epsilon / 8 \pi \alpha_o^2) H^2 + \dots \\ &= -1.7 \times 10^{-4} H^2 \quad (H \text{ in Tesla}) \end{aligned} \quad (6)$$

using Eq. (3). Consequently, at a field of 10 T [the approximate upper limit of validity for Eq. (3)], the change in  $\omega_{LO}$  is ~-2%.

#### DISCUSSION

The previous thermal conductivity measurements on CsBr established a marked dependence of  $K$  on  $H$  at 10.45 K, and the data reported here establish a dependence of  $\epsilon$  on  $H$  at 4.2 K. The basic problem here can be formulated as follows: The thermal conductivity is given by the integral

$$K = \frac{1}{3} \int_0^{\omega_D} C(\omega) \bar{v}(\omega) \lambda(\omega) d\omega \quad (7)$$

where  $C(\omega)$  is the specific heat,  $\bar{v}(\omega)$  is the phonon (group) velocity, and  $\lambda(\omega)$  is the phonon mean free path. The upper limit  $\omega_D$  is the Debye cutoff frequency. Only those phonon modes which transport heat are included in Eq. (7) (i.e., those modes for which  $\bar{v} \neq 0$ ), and these are generally recognized to be the long-wavelength, Debye acoustic phonons.

In fact, it will be recalled that in our previous studies of the  $H = 0$  thermal properties of CsBr, excellent agreement between the calorimetric  $\Theta_D$  and the  $\Theta_D$  derived from the Pierels relation for  $\lambda$  was obtained if the Debye acoustic phonons were assumed to be the only heat carriers. Thus one can safely say that the dependence of  $K$  on  $H$  derives from the magnetic-field dependence of the acoustic phonon spectrum in CsBr.

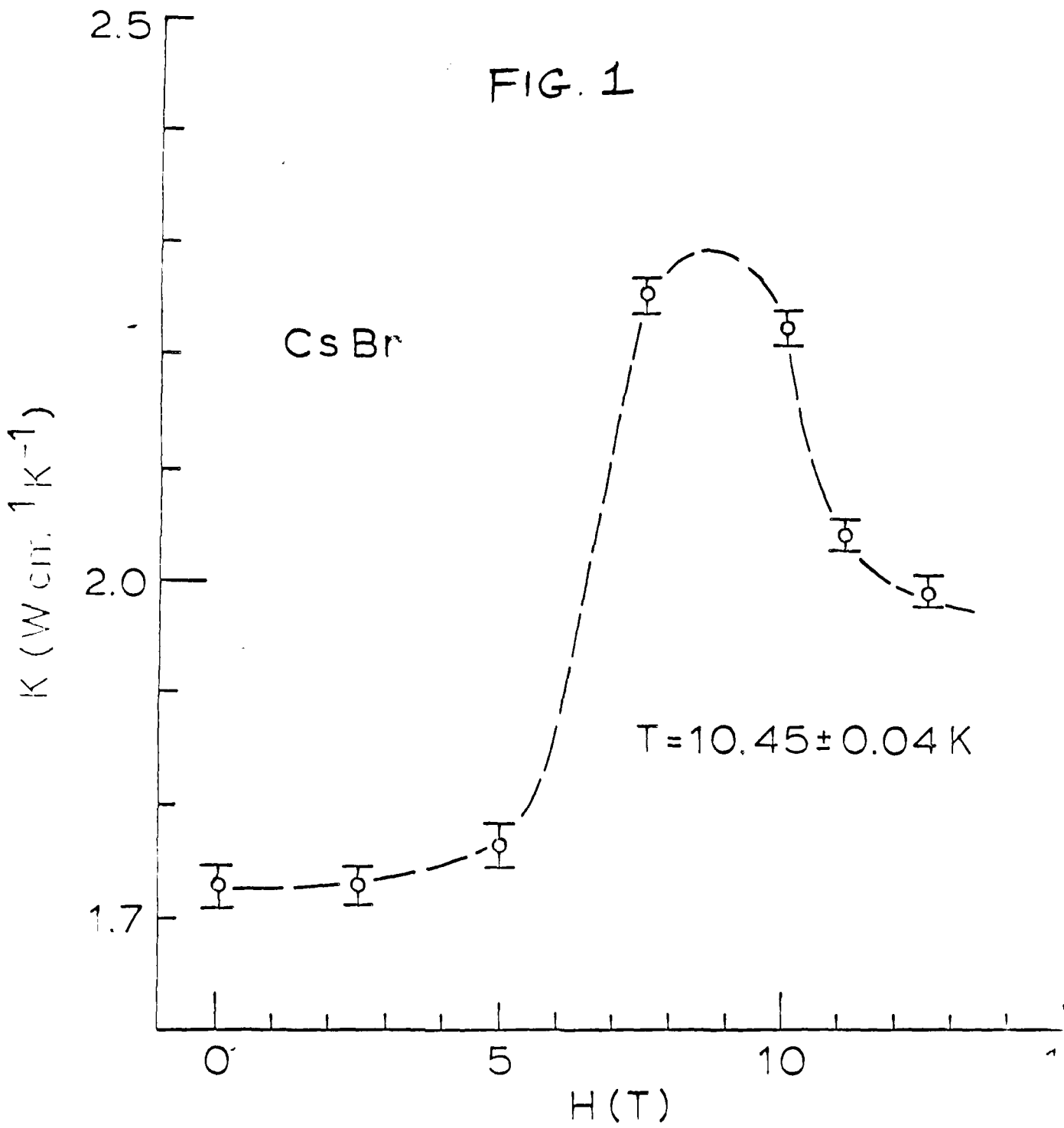
On the other hand, the  $\epsilon$ - $H$  data reported here clearly indicate via Eq. (5) that the optic phonon spectrum in CsBr is also influenced by a magnetic field. Going further, one can conjecture that the anharmonic interaction between the acoustic and optic branches in CsBr is much stronger than perturbative, although the origin of the microscopic interaction between the  $\text{Cs}^{+1}$  and/or  $\text{Br}^{-1}$  ions and an intense  $H$ -field is unclear.

Specific-heat measurements on CsBr in intense fields have been completed and are being data-reduced. These data when completed will say something about the  $C(\omega)$  term in Eq. (7).

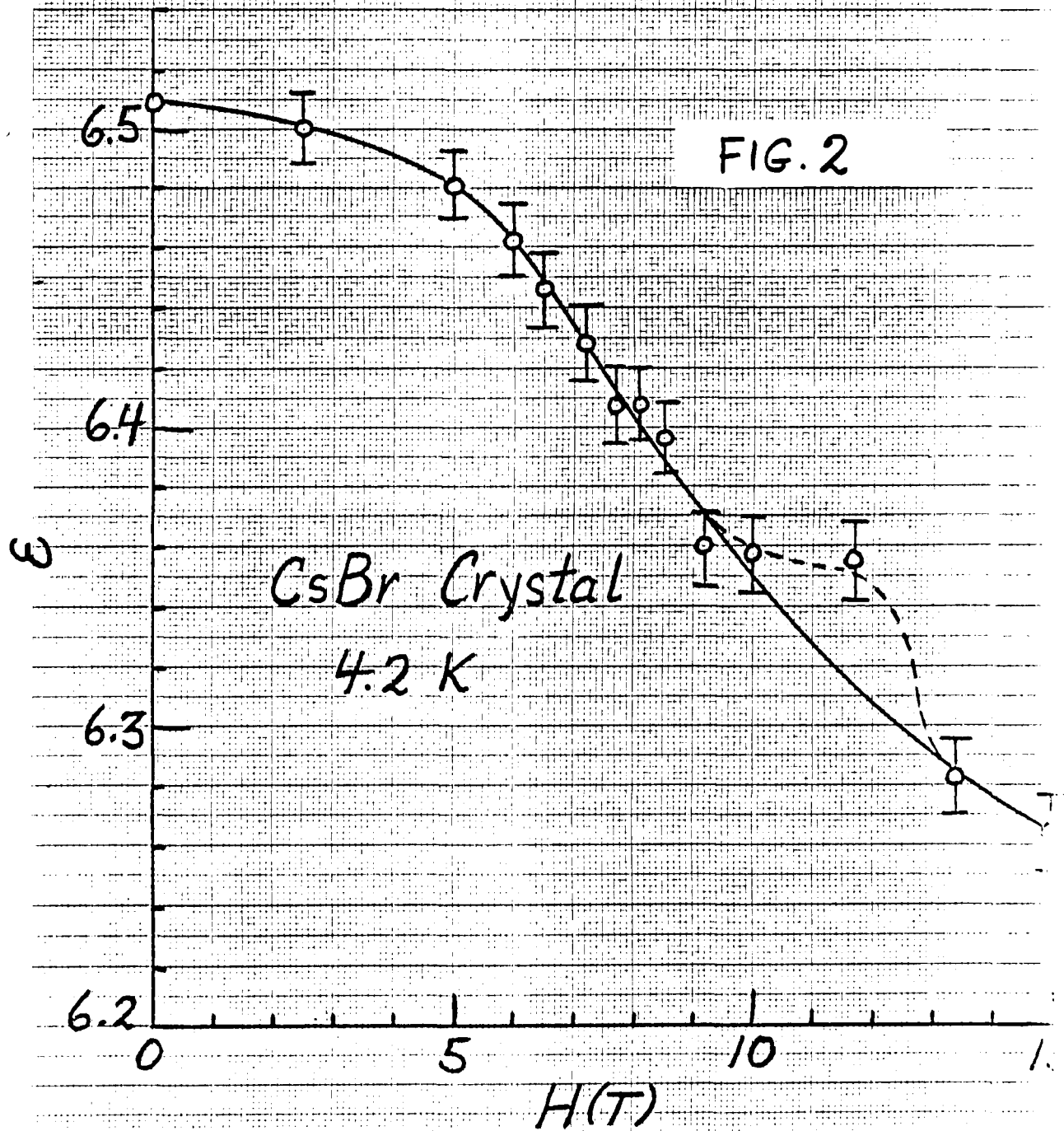
Thermal conductivity measurements in intense magnetic fields on CsBr in the  $T^3$  boundary-scattering regime would also be enlightening, because in this regime  $\lambda(\omega) = \text{constant}$  in Eq. (7). That is, from our previous studies,  $\lambda_C = d/3$ , where  $d$  is the smallest crystal dimension, in this regime.

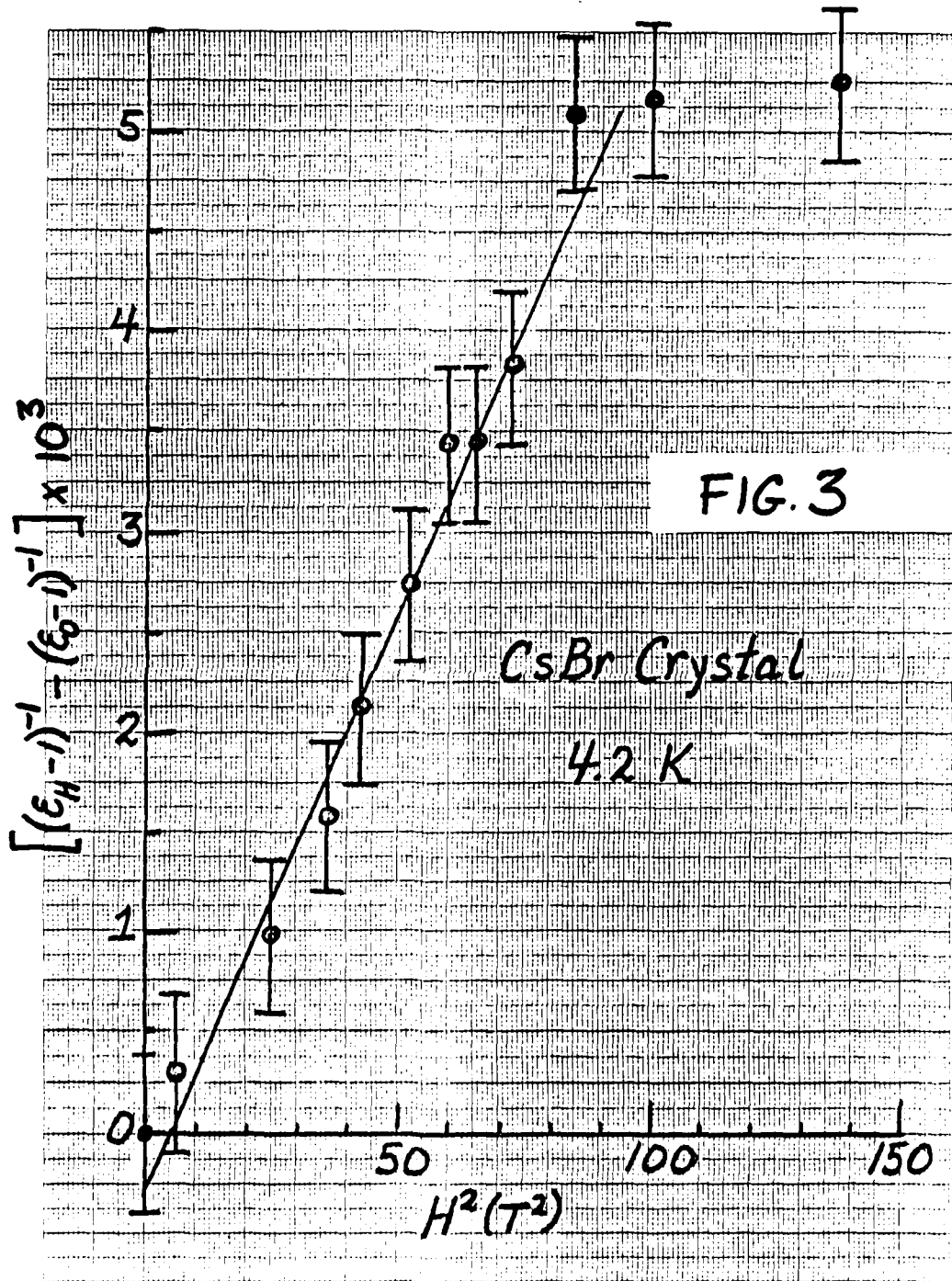
Finally, it would be worthwhile to repeat the dielectric measurements here under conditions where the lead capacitance is  $\approx 0$ . In particular,  $\epsilon$ - $H$  data measured with the magnetic field aligned along [100], [110], and [111] would indicate the possibility of vibronic effects in CsBr associated with hybrid orbitals.

FIG. 1



45 1113





Appendix D

SPINEL THERMAL PROPERTIES STUDIES

PROGRESS REPORT

AFOSR Contract #F49620-83-C-0129

Fundamental Physics Studies on High-Specific-Heat  
Dielectrics and Kapitza Resistance at Dielectric Boundaries

Spinel Studies, I. Broad Temperature  
Range Thermal Measurements

by

W.N. Lawless *WNL*  
CeramPhysics, Inc.  
Westerville, Ohio 43081

September 2, 1983

Distribution:

J.H. Parker, Jr.  
P.W. Eckels  
T.K. Gupta  
M. Ashkin  
C.F. Clark

## INTRODUCTION

A new ceramic material, variously referred to as SClC, C(9/1), or CCN (9/1), has been the subject of five applied programs owing to its enormous specific heat below 10 K. This ceramic displays a maximum in the specific heat at 8 K of  $\sim 2 \text{ J cm}^{-3} \text{ K}^{-1}$ ; for comparison, water at room temperature has a specific heat  $\sim 4 \text{ J cm}^{-3} \text{ K}^{-1}$  (note that the volumetric basis is the most demanding basis for comparison purposes). These applied programs have dealt with the use of this (and similar) material as regenerator-matrix materials<sup>1,2</sup> and as dielectric insulations for superconducting wires.<sup>3-5</sup>

These applied programs have raced far ahead of our basic understanding of this material, and one of the purposes of the present AFOSR program is to study the physics of this unusual, practical material.

This report is the first in a series of reports devoted to this material in general and to the spinels  $\text{CdCr}_2\text{O}_4$  and  $\text{ZnCr}_2\text{O}_4$  in particular. In this report we present a materials background and very accurate, broad-range measurements of specific heat and thermal conductivity.

## MATERIALS BACKGROUND

Ferroelectric crystals are excellent examples of soft-mode behavior wherein the frequency of an optic mode decreases with temperature,  $\omega_S^2 \propto T - T_0$ , above the Curie temperature, and below the ferroelectric transition this optic mode remains low-lying. The interaction of this mode with acoustic modes is much stronger than perturbative, and, consequently, it may be expected that ferroelectrics will have interesting thermal properties at low temperatures.

This concept led the author to measure the low-temperature properties of several ferroelectrics in the late 70's,<sup>6</sup> and one of the materials chosen for study was  $\text{Cd}_2\text{CrNbO}_6$  which had been reported in the Russian literature as a pyrochlore ferroelectric.<sup>7</sup> The specific heat of this material was so large that it proved difficult to measure, and a research program was started to explore this unusual material.

It was immediately noticed that when stoichiometric  $\text{Cd}_2\text{CrNbO}_6$  was batched, large weight losses occurred on ceramic firing. The ratios of  $\text{CdO}/\text{Cr}_2\text{O}_3/\text{Nb}_2\text{O}_5$  were varied in ceramic studies, and it was found that at certain ratios there was no weight loss. X-ray studies of these latter ceramics confirmed the presence of two phases: The spinel  $\text{CdCr}_2\text{O}_4$  and the columbite  $\text{CdNb}_2\text{O}_6$ . Moreover, re-examination of the ceramics displaying large weight losses revealed that the CdO vaporization loss was precisely the amount required to yield stoichiometric  $\text{CdCr}_2\text{O}_4 + \text{CdNb}_2\text{O}_6$  in various ratios. In fact, it was found that even small variations in stoichiometry resulted in small weight

losses to preserve the required stoichiometry. This result strongly suggested that there is negligible solid solubility between the spinel and columbite phases. This conclusion was later confirmed in specific-heat studies (see below).

The large specific heats of these spinel+columbite materials was believed due to the spinel phase, so attempts to make  $\text{CdCr}_2\text{O}_4$  were tried. It was found, however, that a ceramic body would not form, and it was unpredictable if the resultant powder was even the spinel due to  $\text{CdO}$  loss. The clear conclusion was that the columbite  $\text{CdNb}_2\text{O}_6$  had to be present for the  $\text{CdCr}_2\text{O}_4$  spinel to form predictably in a ceramic body.

The above studies were also performed on the analogous  $\text{ZnCr}_2\text{O}_4 + \text{ZnNb}_2\text{O}_6$  system with exactly the same results. The analogous Pb-containing system was tried with no success; apparently  $\text{Pb}^{2+}$  is too large an ion to form the spinel (note that  $\text{PbNb}_2\text{O}_6$  is rhombohedral rather than orthorhombic columbite<sup>9</sup>). The analogous Hg-containing system was avoided for toxicity reasons.

The above findings resulted in a patent<sup>9</sup> issued to the author.

Given that  $\text{CdNb}_2\text{O}_6$  (or  $\text{ZnNb}_2\text{O}_6$ ) must be present to form the spinel  $\text{CdCr}_2\text{O}_4$  (or  $\text{ZnCr}_2\text{O}_4$ ), the next question addressed was the minimum amount of the columbite that could be tolerated consistent with ceramic formation. In an NBS-funded program,<sup>1</sup> the spinel:columbite ratio was varied from 1/1 to 11/1 in these systems and the low-temperature specific heats of these ceramics were measured. A fortuitous result was found; namely, at the 9/1 molecular ratio a hard, strong ceramic was obtained which had the largest and most sharply peaked specific-heat maximum of all the samples. At the 11/1 ratio the mechanical properties were seriously degraded and there was evidence of incomplete crystallization of the spinel phase. Significantly, as the spinel/columbite ratio was increased across the series, the specific heat increased in direct proportion to the spinel content; this was further evidence of a lack of solid solubility between the spinel and columbite phases.

These findings apply to both the  $\text{CdCr}_2\text{O}_4/\text{CdNb}_2\text{O}_6$  and the  $\text{ZnCr}_2\text{O}_4/\text{ZnNb}_2\text{O}_6$  systems; hence, the terminology C(9/1), etc.

The volume %'s of the spinel phases in these two systems are easily calculated using X-ray densities ( $\text{CdCr}_2\text{O}_4$ , 5.862;<sup>10</sup>  $\text{ZnCr}_2\text{O}_4$ , 5.367;<sup>11</sup>  $\text{CdNb}_2\text{O}_6$ , 6.056;<sup>12</sup> and  $\text{ZnNb}_2\text{O}_6$ , 5.649<sup>12</sup>):

$$\text{C}(9/1) = \text{Cd-containing system} = 86.87 \text{ vol } \% \text{ CdCr}_2\text{O}_4$$

$$\text{D}(9/1) = \text{Zn-containing system} = 86.54 \text{ vol } \% \text{ ZnCr}_2\text{O}_4$$

The X-ray literature<sup>10,11</sup> indicates that both  $\text{CdCr}_2\text{O}_4$  and  $\text{ZnCr}_2\text{O}_4$  are cubic spinels, space group  $\text{O}_h\text{-Fd}3\text{m}$  with 8 molecules per unit cell. The reported lattice constants are  $8.595 \pm .011 \text{ \AA}$  and  $8.3275 \pm 0.0001 \text{ \AA}$ , respectively.

The dielectric properties of the Cd-containing system were briefly studied in the NBS program.<sup>1</sup> A 1/1 CdCr<sub>2</sub>O<sub>4</sub>/CdNb<sub>2</sub>O<sub>6</sub> sample was measured, and two significant results were found: (1) The dielectric constant, though large (~300), displayed no structure in the neighborhood of the maximum in the specific heat (8 K); and (2) The specific heat between 5-10 K was completely independent of electric fields up to 35.4 kV/cm. These findings suggest strongly that there is no ferroelectric nature to the 8 K specific-heat maximum and that magneto-electric effects are very weak or non-existent.

Thus, what began as a study of low-lying phonon modes in ferro-electrics has led to a non-ferroelectric, new material with ponderous practical applications, in the process invalidating some of the Russian literature.

Finally, a library search was done to see what publications existed on the CdCr<sub>2</sub>O<sub>4</sub> and ZnCr<sub>2</sub>O<sub>4</sub> spinels. This search, conducted in 1978, revealed the following (in addition to Refs. 10 and 11 above):

1. The enthalpy of formation of CdCr<sub>2</sub>O<sub>4</sub> was reported.<sup>13</sup>
2. The free energy of formation of ZnCr<sub>2</sub>O<sub>4</sub> was reported.<sup>14</sup>
3. The chemical-catalyst properties of ZnCr<sub>2</sub>O<sub>4</sub> have been studied.<sup>15</sup>
4. It has been claimed<sup>16</sup> that at 12.8 K ZnCr<sub>2</sub>O<sub>4</sub> undergoes a first-order transition from long-range to short-range magnetic order (We remark in this regard that our thermal measurements on ZnCr<sub>2</sub>O<sub>4</sub> show that the transition occurs at 10.6 K and that there is no latent heat associated with this transition).

A rather extensive literature has developed on the sulfochromite spinels, CdCr<sub>2</sub>S<sub>4</sub> and ZnCr<sub>2</sub>S<sub>4</sub>. This literature will be reviewed in a separate report.

#### THERMAL MEASUREMENTS

The above discussion shows that the 9/1 spinel-to-columbite materials probably represent the best experimental samples for studying the CdCr<sub>2</sub>O<sub>4</sub> and ZnCr<sub>2</sub>O<sub>4</sub> spinels. Note that the columbite phase constitutes only 13-14 volume % in these samples.

Since the dominant interest in these spinels centers on their thermal properties, it was decided to make accurate specific heat and thermal conductivity measurements over a broad temperature range (some measurements on 9/1 materials have been made in previous programs<sup>1</sup> but always over narrow temperature ranges).

Disc and bar samples of these ceramics were carefully made by standard techniques, and thermal measurements were made in the calorimeter described elsewhere.<sup>6</sup> Specific heat and thermal conductivity data on these materials in the range 1.7 to 30 K are shown in Figs. 1 and 2, respectively.

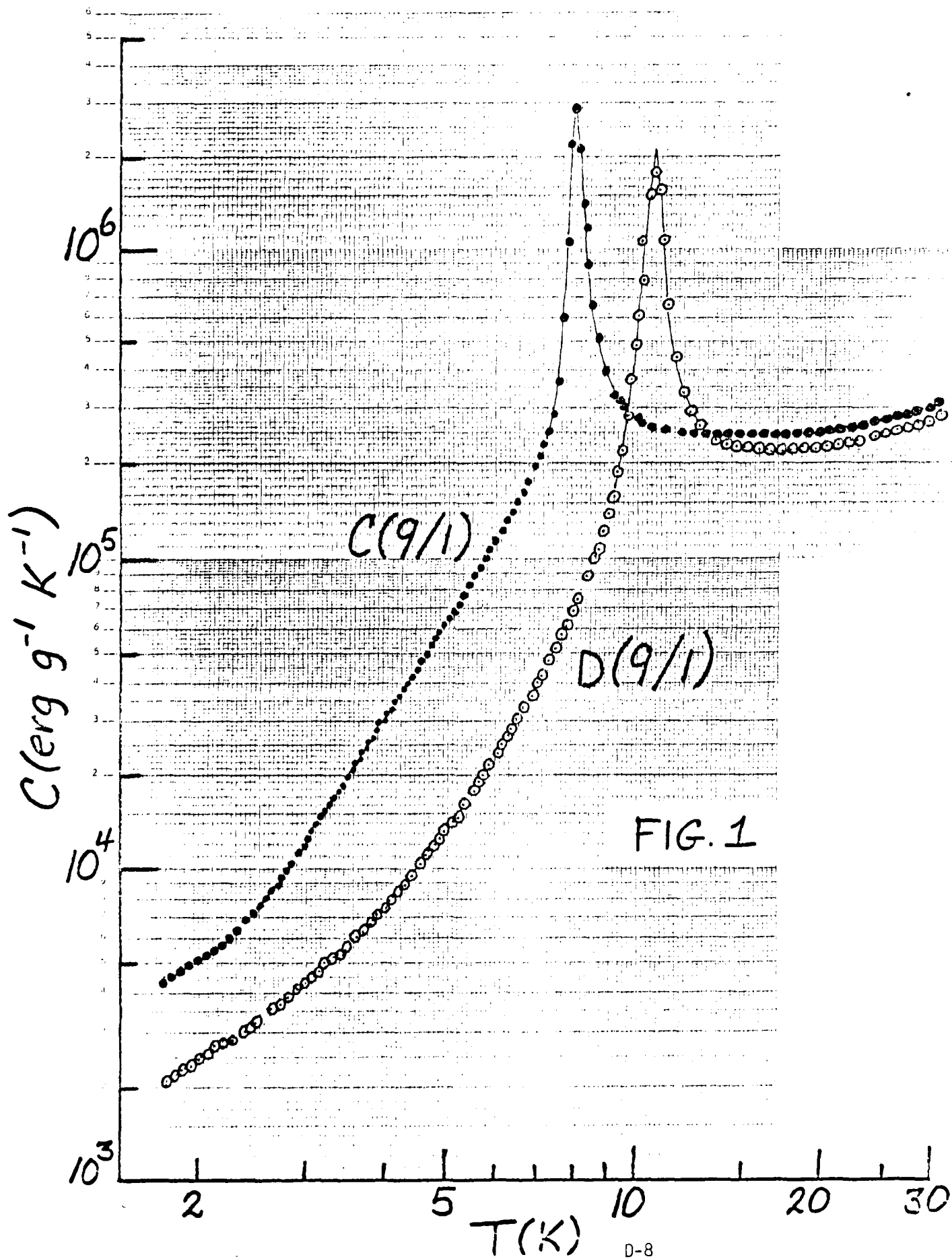
The specific heat data in Fig. 1 are plotted on a  $\log C$  vs.  $\log T$  basis and give the illusion that the data are more sharply peaked than they really are. The enormity of the specific heat maxima can be judged from Fig. 1; that is, using the densities quoted above, these maxima are  $\sim 1.2-2.0 \text{ J cm}^{-3} \text{ K}^{-1}$ , or roughly half the value of water at room temperature.

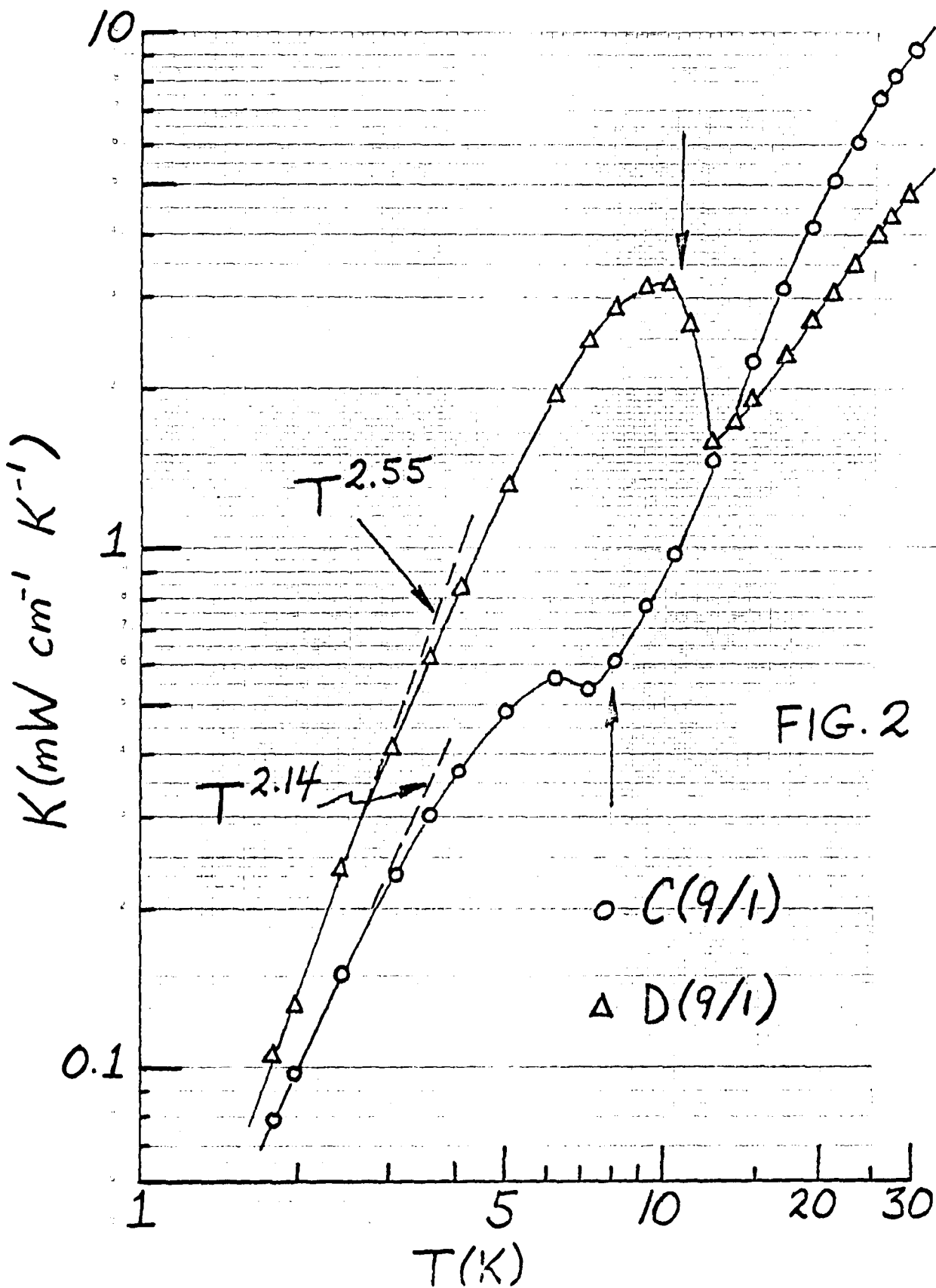
The thermal conductivity data in Fig. 2 display a very interesting feature: The conductivity makes a considerable "jump" as the transition is approached from above. The  $\log K$  scale in Fig. 2 somewhat obscures how large this discontinuity is; in particular, for the zinc-based material,  $K$  jumps by a factor of three. The arrows in Fig. 2 show the temperatures of the specific heat maxima. For  $\text{CdCr}_2\text{O}_4$ , the  $K$ -discontinuity takes place at a temperature below  $T_{\text{max}}$ ; for  $\text{ZnCr}_2\text{O}_4$ , above  $T_{\text{max}}$ . Note that at 86-87 volume % of spinel, the heat phonons are predominantly carried by the spinel phase.

At the lowest temperatures in Fig. 2,  $K \propto T^m$  with  $m = 2-2\frac{1}{2}$ , as shown. These exponents are very close to the  $m=2$  case of glassy materials, although no conclusions can be drawn here until the contribution of the heat-carrying phonons to the specific heat is determined.

## References

- <sup>1</sup>W.N. Lawless, Final Report, NBS Contract NB81RAC10007, "High Specific-Heat Ceramics for Cryocooler Regenerator Applications," Dec. 1981.
- <sup>2</sup>W.N. Lawless, Final Report, NBS Contract NB82RAC20013, "Part II. High Specific-Heat Ceramics for Cryocooler Regenerator Applications," May 1982.
- <sup>3</sup>W.N. Lawless, C.F. Clark, R.W. Arenz, Final Report, WPAFB Contract 33615-80-C-2022, "Enthalpy Improved Dielectric Insulation for Superconductors," March 1982.
- <sup>4</sup>WPAFB Contract F33615-82-C-2229, "Dielectric Insulation for Nb,Sn Superconducting Wire Incorporating Enthalpy Stabilization," in progress.
- <sup>5</sup>WPAFB Contract F33615-82-C-2227, "Dielectric Insulation for Superconductors," in progress.
- <sup>6</sup>W.N. Lawless, Phys. Rev. B14, 134 (1976); Phys. Rev. Lett. 36, 478 (1976); Phys. Rev. B16, 433 (1977); Phys. Rev. B18, 2394 (1978); Phys. Rev. B19, 3755 (1979).
- <sup>7</sup>D.G. Demurov and Yu. N. Venevtsev, Soviet Physics-Crystallography 16, 133 (1971); Yu. N. Venevtsev et al., J. Phys. Soc. Japan 28, 139 (1970); Yu. N. Venevtsev, Mat. Res. Bull. 6, 1085 (1971).
- <sup>8</sup>R.S. Roth, J. Res. Natl. Bur. Stand. 62, 27 (1959).
- <sup>9</sup>W.N. Lawless, U.S. Patent Nos. #4,231,231, #4,296,607, and #4,296,608.
- <sup>10</sup>NBS Monograph #25, Section 5, 1967, p. 16.
- <sup>11</sup>NBS Monograph #25, Section 9, 1971, p. 59.
- <sup>12</sup>S. Swartz, Penn State University, private communication.
- <sup>13</sup>F. Mueller, O.J. Kleppa, J. Inorg. Nucl. Chem. 35, 2673 (1973).
- <sup>14</sup>K.T. Jacob, Thermochem. Acta 15, 79 (1976).
- <sup>15</sup>O.N. Goroshko et al., Katal. Katal, 13, 92 (1975); V.L. Chernobrivets et al., Katal. Katal, 12, 60 (1974); T.P. Gaidei et al., Gos. Inst. Prikl. Khim. 68, 45 (1973); L. Ivanov et al., God. Vissh. Khim. Inst. Sofia 14, 257 (1970).
- <sup>16</sup>R. Plumier et al., J. Phys. (Paris) Lett. 38(6), 149 (1977).





PROGRESS REPORT

AFOSR Contract #F49620-83-C-0129

Fundamental Physics Studies on High-Specific-Heat  
Dielectrics and Kapitza Resistance at Dielectric Boundaries

Spinel Studies, II. Spinel Specific Heats

by

W.N. Lawless *WNL*  
CeramPhysics, Inc.  
Westerville, Ohio 43081

October 1, 1983

Distribution:

J.H. Parker, Sr.  
~~P.W. Eckels~~  
T.K. Gupta  
M. Ashkin  
C.F. Clark  
B.R. Patton

## INTRODUCTION

This is the second in a series of reports devoted to the  $\text{CdCr}_2\text{O}_4$  and  $\text{ZnCr}_2\text{O}_4$  spinels. In the first report, a materials background was presented and high-accuracy specific heat and thermal conductivity data were reported from 1.7 to 31 K. These data were measured on samples containing a 9/1 ratio of spinel:columbite phases, and it had been found that the columbite phase had to be present for the spinel phase to form.

In this report, the columbite specific heat will be subtracted to obtain the specific heat of the spinel phase for both  $\text{CdCr}_2\text{O}_4$  and  $\text{ZnCr}_2\text{O}_4$ . This separation will be made on an additivity basis because the ceramic studies discussed previously indicated that there was little, if any, solid solubility between the spinel and columbite phases in these materials. Once the specific heats of the  $\text{CdCr}_2\text{O}_4$  and  $\text{ZnCr}_2\text{O}_4$  spinels are obtained, these data will be analyzed according to various specific heat formalisms. These analyses will be presented in subsequent reports.

## SPECIFIC HEATS OF COLUMBITE PHASES

Disc samples of the  $\text{CdNb}_2\text{O}_6$  and  $\text{ZnNb}_2\text{O}_6$  columbites were prepared from the same grade of starting chemicals used to prepare the C(9/1) and D(9/1) samples reported previously. X-ray analyses confirmed that single-phase columbite materials had formed. Specific heat data on the  $\text{CdNb}_2\text{O}_6$  sample were published elsewhere<sup>1</sup> in a study of Cd- and Pb-containing materials. The specific heat of the  $\text{ZnNb}_2\text{O}_6$  sample was measured in the calorimeter reported elsewhere,<sup>2</sup> and specific heat data for both columbites are shown in Fig. 1.

The Fig. 1 data are plotted as  $C/T^3$  vs.  $T$  to illustrate the non-Debye nature of the data: (1) Below 5 K,  $C/T^3$  rises sharply with decreasing temperature; and (2) Above about 8 K,  $C/T^3$  rises slowly with increasing temperature (For a Debye solid,  $C/T^3$  is either flat or decreases with temperature.).

The commonality of the data in Fig. 1 suggests a similarity in phenomena for the two columbites. The lower temperature data were analyzed according to the high-T expansion of a two-level Schottky term,

$$C_{\text{Sch}} = Rg_0g_1(g_0+g_1)^{-2}(\delta/T)^2, \quad T \gg \delta$$

where  $g_0$ ,  $g_1$  are the degeneracies of the two-level system and  $\delta$  is the energy separation measured in absolute degrees. There is no reason to choose a two-level over, say, a three-level system; what is important is the  $T^{-2}$  dependence of Eq. (1) common to the general Schottky term. The addition of a  $T^3$  Debye background to Eq. (1) shows that a  $CT^2$  vs.  $T^5$  plot applies to the Schottky term, and in Fig. 2 are shown such plots for the two columbites. Excellent fits

to the experimental data are obtained, and the fitting parameters are given in Table I. In applying Eq. (1) we have arbitrarily set  $g_0 = g_1$ , and the Debye Temperatures  $\theta_D$  in Table I are simply derived from the slopes of the plots in Fig. 2.

Table I

Least-squares Fitting Parameters, Eq. (1)		
Columbite	$\theta_D$ (K)	$\delta$ (mK)
CdNb <sub>2</sub> O <sub>6</sub>	405.8	58.72
ZnNb <sub>2</sub> O <sub>6</sub>	442.2	64.61

The similarity of the level separations  $\delta$  in Table I leave little doubt that the same excitations are involved in both columbites. It is reasonable to attribute this Schottky effect to the electric quadrupole-moment of Nb<sup>5+</sup> interacting with the electric-field gradient at the Nb<sup>5+</sup> site in the columbite structure.<sup>1</sup>

The slow rise in  $C/T^3$  with increasing temperature in Fig. 1 was analyzed in terms of an Einstein model,

$$C = C_D(\theta_D/T) + 3Rrx^2 e^x / (e^x - 1)^2, \quad x = \theta_E/T, \quad (2)$$

where  $C_D$  and  $\theta_D$  are the Debye function and Debye temperature (normalized to one atom per lattice site, as above),  $r$  is the amplitude of the Einstein term (i.e., number of Einstein oscillators per formula weight), and  $\theta_E$  is the Einstein temperature. A three-level fitting procedure was used (i.e., for  $\theta_D$ ,  $\theta_E$ , and  $r$ ), and a tabulation<sup>3</sup> of the Debye function was incorporated. The  $T^{-2}$  contribution to the specific heat is negligible at the higher temperatures where the Einstein term is important, as seen in Fig. 1, and this term was ignored. The fit of the ZnNb<sub>2</sub>O<sub>6</sub> data to Eq. (2) are shown in Fig. 3; a similarly good fit for CdNb<sub>2</sub>O<sub>6</sub> has been published elsewhere.<sup>1</sup> The fitting parameters for these Einstein fits are given in Table II.

Table II

Fitting Parameters, Einstein Term, Eq. (2)			
Columbite	$\theta_D$ (K)	$\theta_E$ (K)	$r$
CdNb <sub>2</sub> O <sub>6</sub>	408.4 (a)	109.5 (a)	0.186 (a)
ZnNb <sub>2</sub> O <sub>6</sub>	444.4	106.7	0.283

(a) Taken from Ref. 1

There is very satisfactory agreement between the Debye temperatures in Tables I and II ( $407.1 \pm 0.45\%$  for CdNb<sub>2</sub>O<sub>6</sub>,  $443.3 \pm 0.35\%$  for ZnNb<sub>2</sub>O<sub>6</sub>) which lends confidence to the fitting schemes. It is also interesting to observe that the Debye temperatures of the two columbites scale very well with the square root of the molecular weights, as expected from the Lindemann equation.<sup>3</sup>

Although the physics of the specific heats of these two columbites are of interest in their own right, our goal here is to use these data to correct the specific heats of the C(9/1) and D(9/1) samples to arrive at the specific heats of the  $\text{CdCr}_2\text{O}_4$  and  $\text{ZnCr}_2\text{O}_4$  spinels. This we take up next.

#### SPECIFIC HEATS OF THE $\text{CdCr}_2\text{O}_4$ , $\text{ZnCr}_2\text{O}_4$ SPINELS

The above fitted data allow us to express the specific heats of the columbites  $\text{CdNb}_2\text{O}_6$  and  $\text{ZnNb}_2\text{O}_6$  in analytic forms, and these specific heat data are to be subtracted from the total specific heats of C(9/1) and D(9/1) reported previously.

The C(9/1) and D(9/1) materials are batched as:

$$\begin{aligned} \text{C(9/1)} &= 1 \text{ mole } \text{CdNb}_2\text{O}_6 + 9 \text{ moles } \text{CdCr}_2\text{O}_4 \\ \text{D(9/1)} &= 1 \text{ mole } \text{ZnNb}_2\text{O}_6 + 9 \text{ moles } \text{ZnCr}_2\text{O}_4 \end{aligned} \quad (3)$$

As discussed previously, all of the ceramic and specific heat studies to date indicate that there is negligible solid-solubility between the columbite and spinel phases in these systems. This in turn means that an additivity rule applies to the total specific heat of the two-phase material such that the specific heat of the spinel phase,  $C_s$ , can be expressed as

$$C_s = aC_t - bC_c \quad (4)$$

where  $C_t$  is the total specific heat,  $C_c$  is the specific heat of the columbite phase, and  $a$  and  $b$  are constants involving molecular weights according to Eq. (3).

The procedure is straightforward, if lengthy, the  $C_c$  data being given by the above fitting equations. Average Debye temperatures for the columbite phases were used (see above).

These separated spinel data are shown in Fig. 4. The data in Fig. 4 are plotted as  $C/T^3$  vs.  $T$  for convenience, and this plot reveals that at the lowest temperatures  $C/T^3$  rises sharply with decreasing temperature.

The data in Fig. 4 underscore the enormity of the maximum specific heats of these spinels: At 8 K, the  $\text{CdCr}_2\text{O}_4$  spinel has a maximum of  $2.3 \text{ J cm}^{-3}\text{K}^{-1}$ ; at 10.6 K, the  $\text{ZnCr}_2\text{O}_4$  spinel has a maximum of  $1.3 \text{ J cm}^{-3}\text{K}^{-1}$ .

As mentioned in the previous report, the C(9/1) and D(9/1) materials resulted from earlier studies where the spinel:columbite ratios were varied from 1/1 to 11/1. We therefore have specific heat data measured on old samples of C(9/1) and D(9/1) near the specific heat maxima from the earlier study,<sup>4</sup> and these data can be used to check on the reproducibility of the data. These previous data were

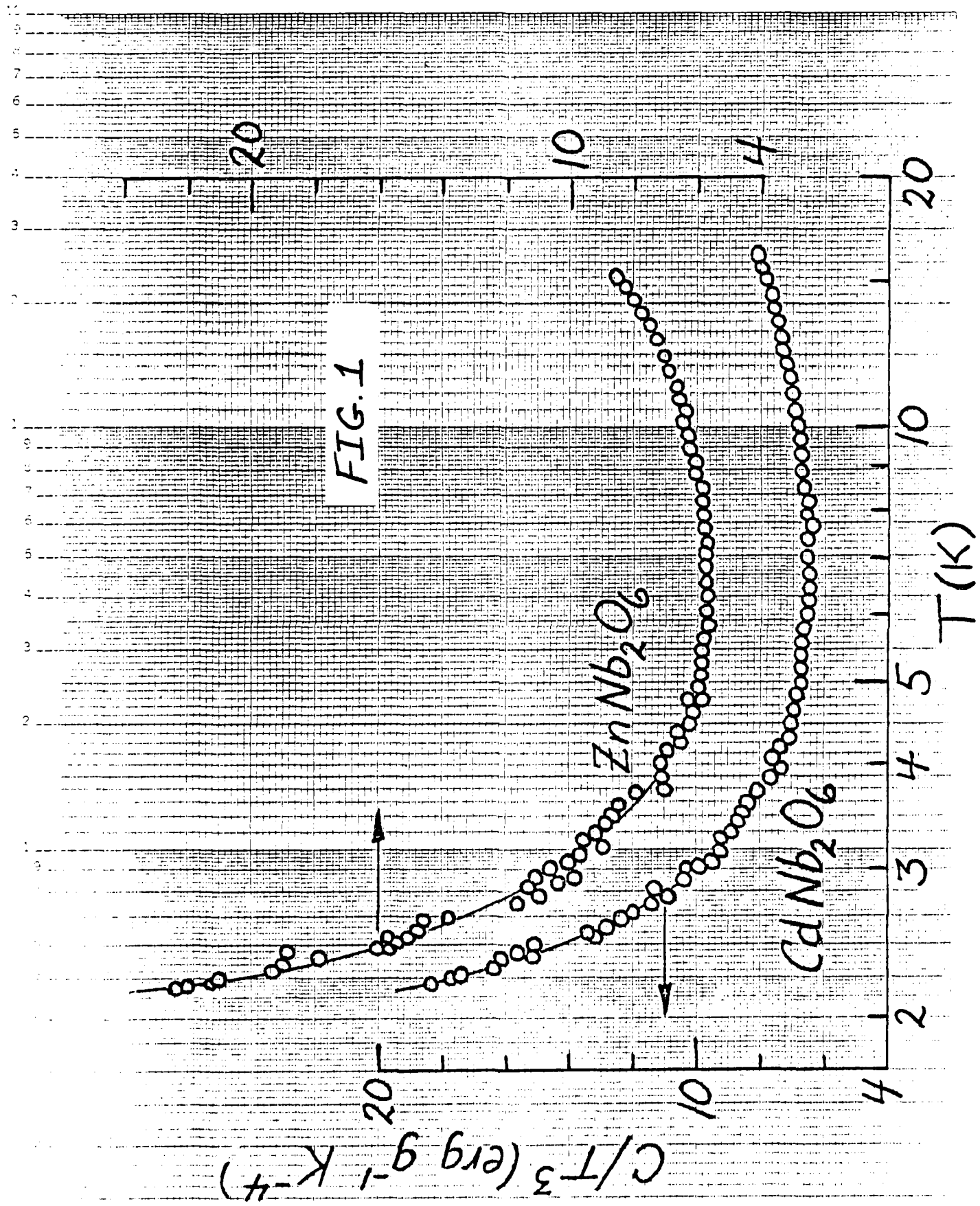
decomposed into the spinel data according to Eq. (4), and a comparison plot of the four data sets is shown in Fig. 5. As seen, there is a remarkable degree of agreement amongst the data sets, particularly near the maxima.

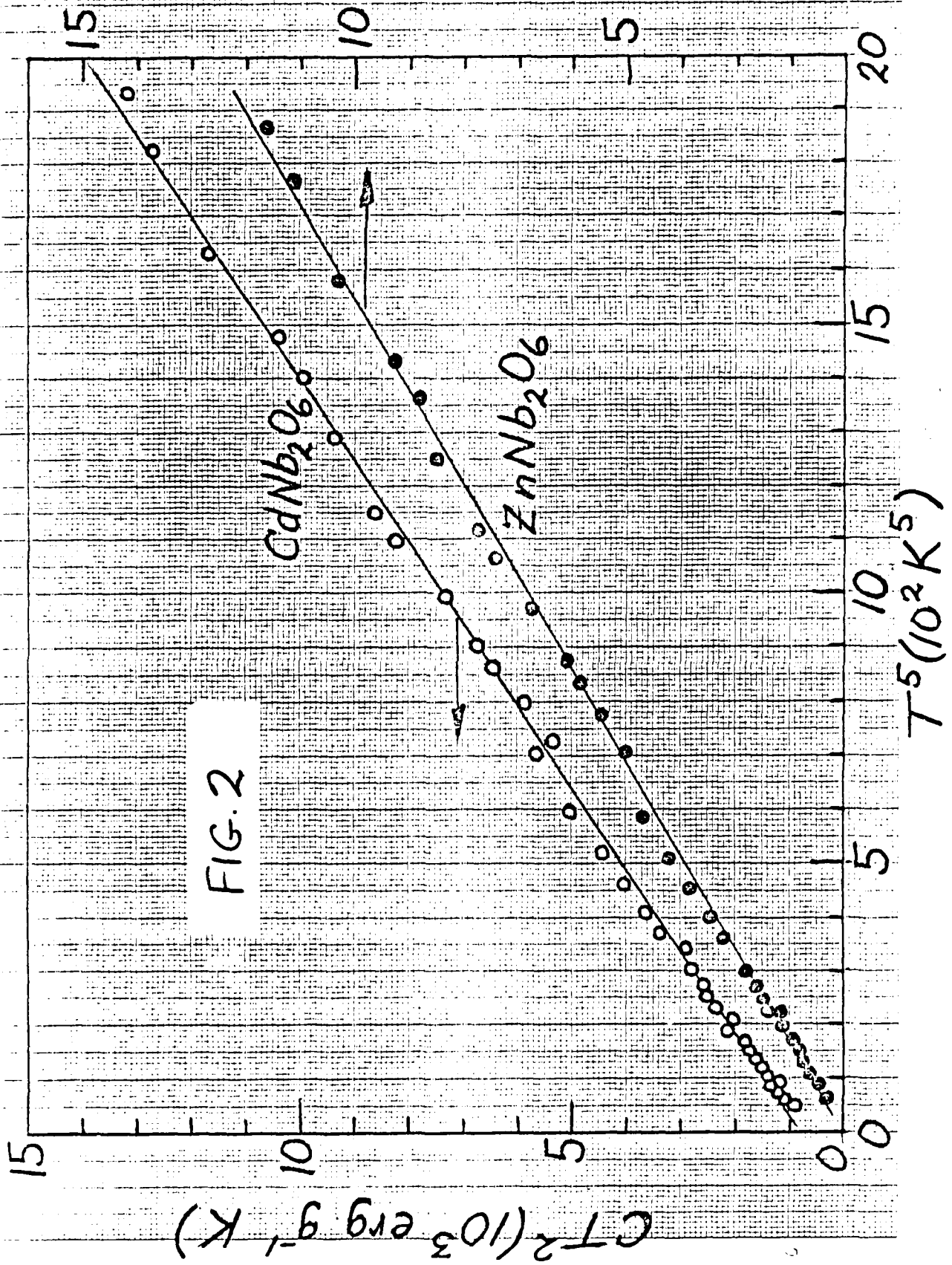
Finally, it is of interest to make a comparison between the two spinels. This is done by normalizing the specific heat data to the gas constant and normalizing the temperature to the transition temperatures  $T_N$ . These plots of  $C/3R$  vs.  $T/T_N$  are shown in Fig. 6. There is an interesting scaling of the data: The  $CdCr_2O_4$  data are 1.5-2 times larger than the  $ZnCr_2O_4$  data, and this scale factor is far too large to be attributed to experimental error or to the data-handling methods (e.g., the addenda contributed  $\sim 0.5\%$  in the experimental data, and the columbite phases contributed about 10% at most). This finding may suggest that different mechanisms are active in the two spinels. Note in this regard that the  $ZnCr_2O_4$  data in Figs. 4-6 are not as sharply peaked as the  $CdCr_2O_4$  data.

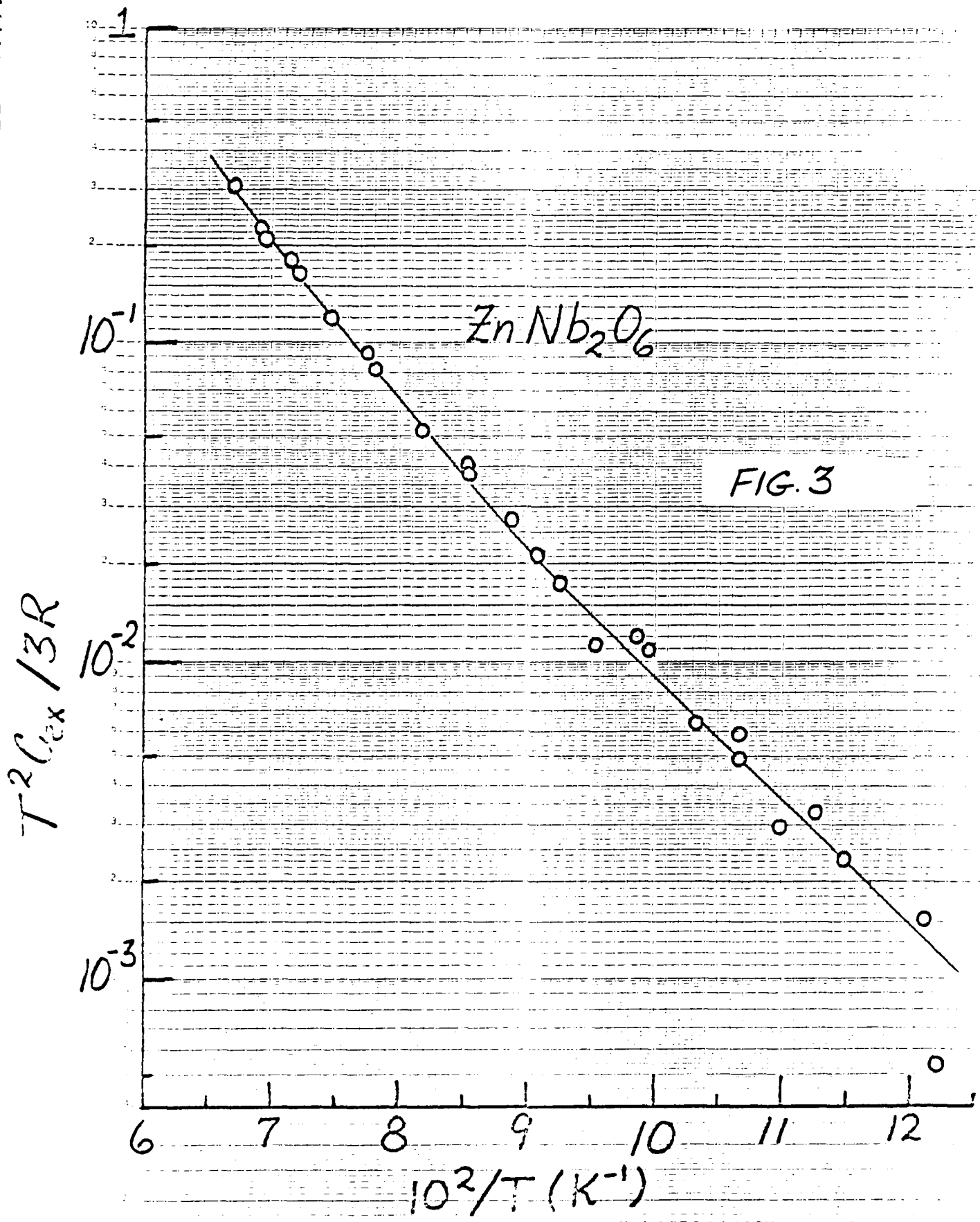
Our next studies will be devoted to analyzing the Fig. 4 data.

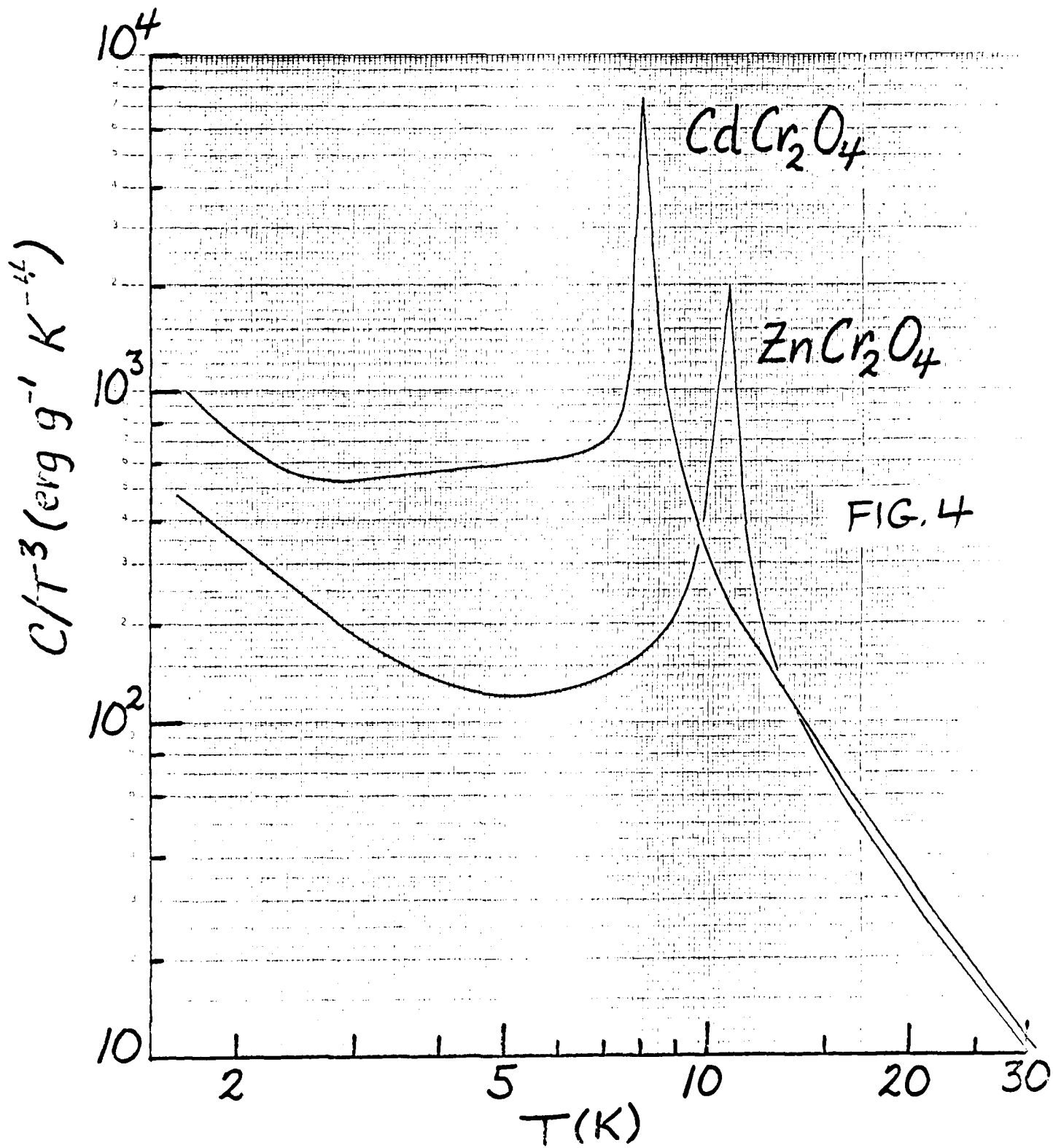
#### References

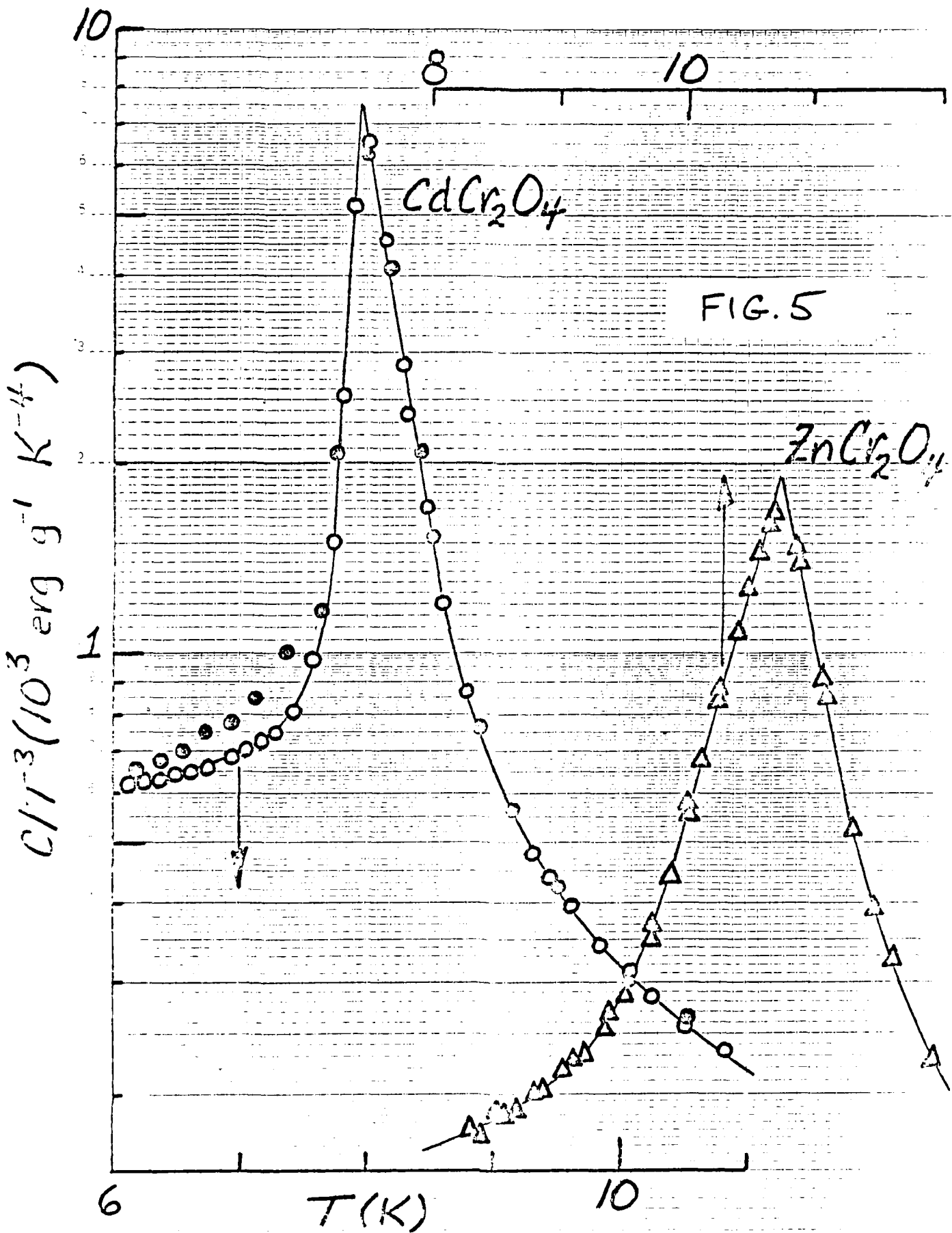
- <sup>1</sup>W.N. Lawless, Phys. Rev. B19, 3755 (1979).
- <sup>2</sup>W.N. Lawless, Phys. Rev. B14, 134 (1976).
- <sup>3</sup>E.S.R. Gopal, Specific heats at low Temperatures, (Plenum, New York, 1966).
- <sup>4</sup>W.N. Lawless, Final Report, NBS Contract NB81RAC10007, "High Specific-heat Ceramics for Cryocooler Regenerator Applications," Dec. 1981.



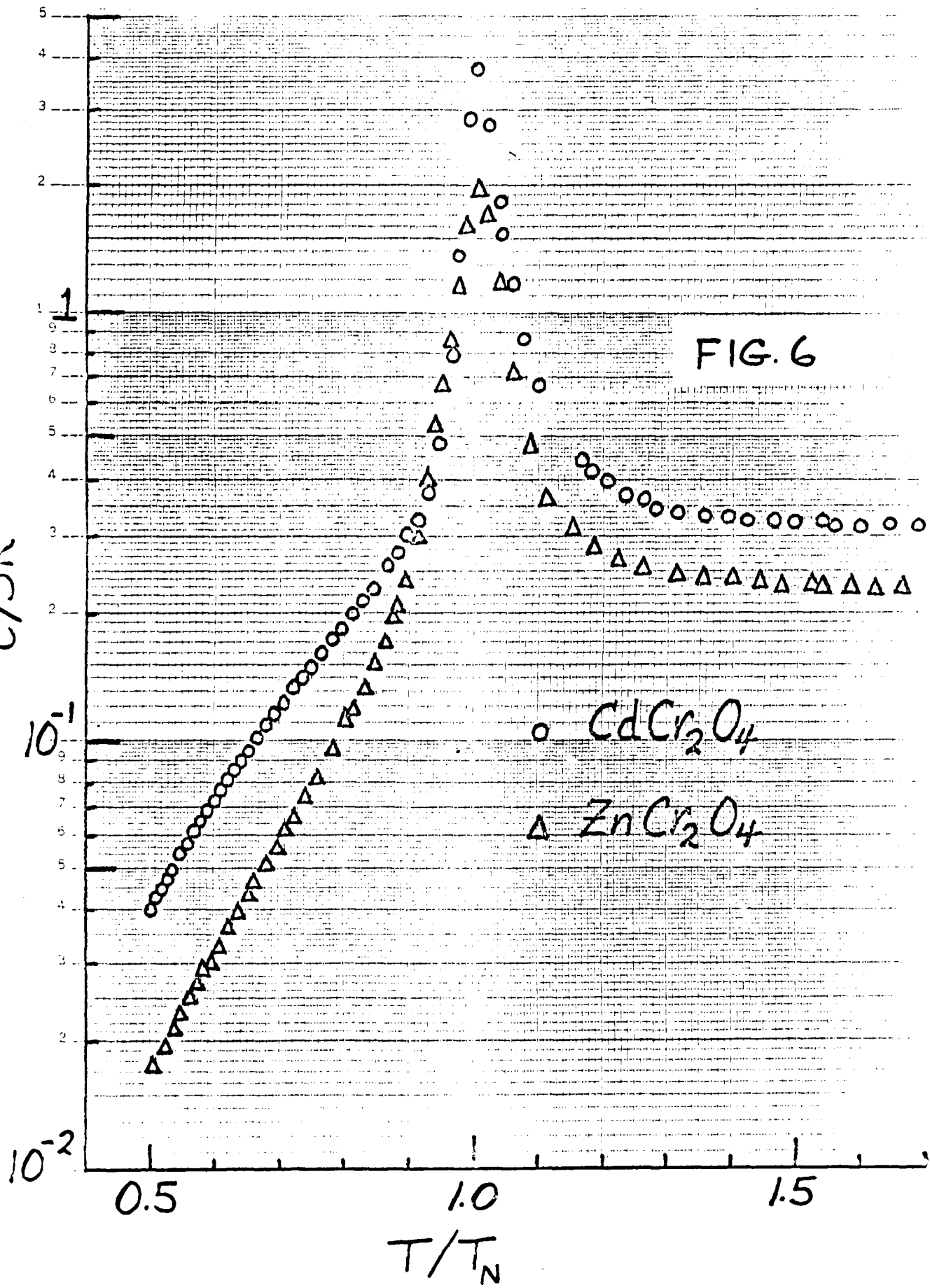








C/SR



PROGRESS REPORT

AFOSR Contract #F49620-83-C-0129

Fundamental Physics Studies on High-Specific-Heat  
Dielectrics and Kapitza Resistance at Dielectric Boundaries

Spinel Studies, III. Analyses of Spinel Specific Heats

by

W.N. Lawless *WNL*

CeramPhysics, Inc.

Westerville, Ohio 43081

*Jan. 23, 1984*

Distribution:

J.H. Parker, Sr.  
~~P.W. Eckels~~  
T.K. Gupta  
M. Ashkin  
C.F. Clark  
B.R. Patton

## INTRODUCTION

This is the third in a series of reports devoted to the thermal properties of the spinels  $\text{CdCr}_2\text{O}_4$  and  $\text{ZnCr}_2\text{O}_4$ . In the last report, the specific heats of these spinels, 1.7 to 30 K, were presented, and these data are reproduced in Fig. 1. In this report we present certain analyses of these data.

## LOWER TEMPERATURE DATA

At the lowest temperatures in Fig. 1, the  $C/T^3$  data increase with decreasing temperature, showing that some common mechanism has a temperature dependence stronger than the  $T^3$ -Debye background. Several straightforward functionals are suggested: (1) Ferrimagnetic spin waves contribute a  $T^{3/2}$  term;<sup>1</sup> (2) A disordered structure would contribute a glasslike tunneling term linear in temperatures;<sup>2</sup> and (3) Several mechanisms are possible which would give rise to a Schottky term, the  $T \gg \delta$  expansion of which varies at  $T^{-2}$ .<sup>1</sup>

Plots of the low temperature data according to the first two functionals (i.e.,  $C/T^{3/2}$  vs.  $T^{3/2}$  and  $C/T$  vs.  $T^2$ ) quickly showed that the excess specific heat has a stronger temperature dependence than  $T^m$ ,  $m > 0$ . However, excellent fits to the  $T \gg \delta$  form of the two-level Schottky term,

$$C_{\text{Sch}} = R g_0 g_1 (g_0 + g_1)^{-2} (\delta/T)^2, T \gg \delta \quad (1)$$

were obtained, and these are shown in Fig. 2. The important feature here is the  $T^{-2}$  behavior which is common to the general Schottky term. In Eq. (1),  $g_0$  and  $g_1$  are the degeneracies of the two-level system and  $\delta$  is the energy separation measured in absolute degrees. The lines in Fig. 2 represent least-squares fits, and the fitting parameters are given in Table I.

Table I

Lower Temperature Schottky Fitting Parameters <sup>(a)</sup>		
Spinel	$\theta_D$ (K)	$\delta$ (mK)
CdCr <sub>2</sub> O <sub>4</sub>	101.03	330.8
ZnCr <sub>2</sub> O <sub>4</sub>	162.43	367.6

(a) Two-level Schottky term

The energy separations  $\delta$  in Table I were obtained by setting  $g_0 = g_1$  in Eq. (1).

We note from Fig. 2 that the  $T^5$  fitting range is different for the two spinels and that the ZnCr<sub>2</sub>O<sub>4</sub> data tail off at the lower  $T^5$  values. Qualitatively, the  $T^{-2}$  approximation to the Schottky term tails off as  $T^{\delta}$ . The similarity of the  $\delta$ 's in Table I seems coincidental, since from Fig. 2 the CdCr<sub>2</sub>O<sub>4</sub> data do not show a deviation from the  $T^{-2}$  behavior. This appears to be another difference between the two spinels.

An attempt was made to fit the lower  $T^5$  data for ZnCr<sub>2</sub>O<sub>4</sub> by relaxing the condition  $g_0 = g_1$  and employing the full Schottky term,

$$C_{Sch} = R\rho x^2 e^x / (1 + \rho e^x)^2, \quad x = \delta/T, \quad \rho = g/g \quad (2)$$

The procedure was straightforward: The intercept in Fig. 2 relates  $\delta$  and  $\rho$  [i.e.,  $\delta = (1 + \rho)/\sqrt{\rho}$ ], and the excess specific heat (i.e., above the Debye background) is given by Eq. (2). However, the tailing off of the ZnCr<sub>2</sub>O<sub>4</sub> data could not be explained; obviously, the two-level system is not applicable to ZnCr<sub>2</sub>O<sub>4</sub> (and probably not to CdCr<sub>2</sub>O<sub>4</sub>, either).

We note that the Debye temperatures in Table I are suspiciously small for these hard, refractory spinels. For comparison, Pb has  $\theta_D \approx 110$ K. We shall return to this point below.

### HIGHER TEMPERATURE DATA

At temperatures well above the transition temperatures of  $\text{CdCr}_2\text{O}_4$  and  $\text{ZnCr}_2\text{O}_4$ , the spin fluctuations give rise to a Schottky-type contribution, and the specific heat in this region is expected to vary as  $mT^3 + b/T^2$  where  $m$  is simply related to the Debye temperature. This is a common procedure for determining the lattice specific heat.<sup>1,3</sup>

Appropriate plots for  $\text{CdCr}_2\text{O}_4$  and  $\text{ZnCr}_2\text{O}_4$  are shown in Fig. 3: Satisfactory linear regions are obtained prior to the tailing off of the Schottky terms. The significance of these plots is the determination of the lattice specific heats, and in Table II are given the Debye temperatures resulting from least-squares fittings of the Fig. 3 data.

Table II

#### Debye Temperatures of Spinel<sup>(a)</sup>

Spinel	$\theta_D$ (K)
$\text{CdCr}_2\text{O}_4$	420.06
$\text{ZnCr}_2\text{O}_4$	462.95

(a) c.f. High-Temp. Schottky fits

The note that the  $\theta_D$ 's in Table II are considerably larger than those given in Table I. As a point of comparison, the Lindemann equation<sup>1</sup> relates  $\theta_D$  to other properties,

$$\theta_D \cong B (T_m/MV^{2/3})^{1/2} \quad (3)$$

where  $T_m$  is the melting point,  $M$  is the molecular weight,  $V$  is the molecular volume, and  $B$  is a constant ( $\approx 115$ ). Adopting melting points for both spinels of  $1800^\circ\text{C}$ , Eq. (3) yields  $\theta_D = 414$  and  $469$  K for the  $\text{CdCr}_2\text{O}_4$  and  $\text{ZnCr}_2\text{O}_4$  spinels, respectively, in remarkably good agreement with the  $\theta_D$ 's in Table II. The actual

melting points  $T_m$  are unknown, and we have simply adopted the ceramic "rule of thumb" that  $T_m$  is about 50% larger than the sintering temperature (actually, changing  $T_m$  by  $\pm 200^\circ\text{C}$  affects  $\theta_D$  from Eq. (3) by only  $\pm 5\%$ ). Finally, we note that these Debye temperatures are large enough to justify the  $T^3$  limit up to the 30 K, which is implicit in the plots of Fig. 3.

### DISCUSSION

The excellent agreement with the predictions of the Lindemann equation lends credence to the fitted Debye temperatures in Table II for the lattice contribution.

The problem here is that the Debye temperatures in Table I are  $\sim 3-4$  times smaller than those in Table II. The explanation here may be that antiferromagnetic spin waves are involved at the lowest temperatures.

For antiferromagnets, the dispersion relation<sup>1</sup>

$$\omega = \alpha_a (2 J'sa^2/h)q$$

immediately leads to the low-T specific heat contribution,

$$C_M = C_a Nk(kT/2J's)^3 \propto T^3, \quad (4)$$

where the constant  $C_a$  depends on the lattice geometry and has been calculated for several lattice types. Consequently, the antiferromagnetic spin-wave specific heat has the same  $T^3$  dependence as the Debye acoustic-phonon background, and as such leads to a lower effective Debye temperature, as in Table I.

We have generated sufficient data in the above fittings to solve for the  $J$ 's values according to Eq. (4). At the lowest temperatures, the effective Debye coefficient is

$$m_e = m_D + C_a R(k/2J's)^3 \quad (5)$$

where  $m_D$  is obtained from the high-temperature fits (i.e., the  $\theta_D$ 's in Table II).

That is,  $m_e \propto \theta_{D1}^{-3}$  and  $m_D \propto \theta_{D1}^{-3}$ , where  $\theta_{D1}$  is taken from Table I,  $\theta_{D2}$  from Table II. Solving Eq. (5) using the appropriate parameters, we find:

$$\begin{aligned} \text{CdCr}_2\text{O}_4: \quad J's/C_a^{1/3} &= 5.943 \times 10^{-16} \text{ erg} \\ \text{ZnCr}_2\text{O}_4: \quad J's/C_a^{1/3} &= 9.651 \times 10^{-16} \text{ erg} \end{aligned} \tag{6}$$

The above fitting results now also allow us to calculate the magnetic entropy of these spinels; this we pursue next.

#### References

- <sup>1</sup>E.S.R. Gopal, Specific heats at low temperatures, (Plenum, New York, 1966).
- <sup>2</sup>W.A. Phillips, J. Non-Cryst. Solids, 31, 267 (1978).
- <sup>3</sup>See, for example, G.R. Stewart, J.A. Barclay, and W.A. Steyert, Solid State Comm. 29, 17 (1979).

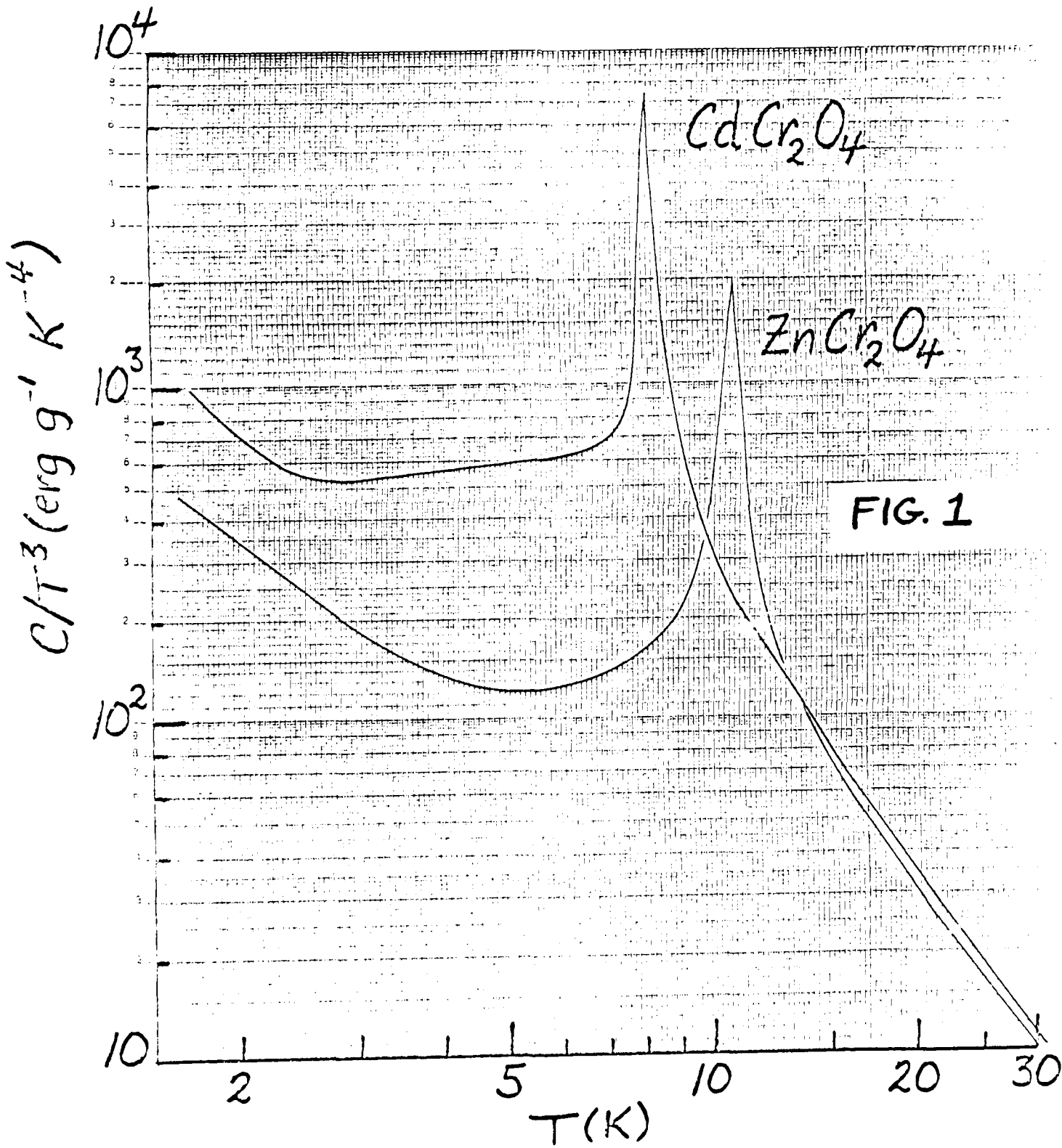


FIG. 1

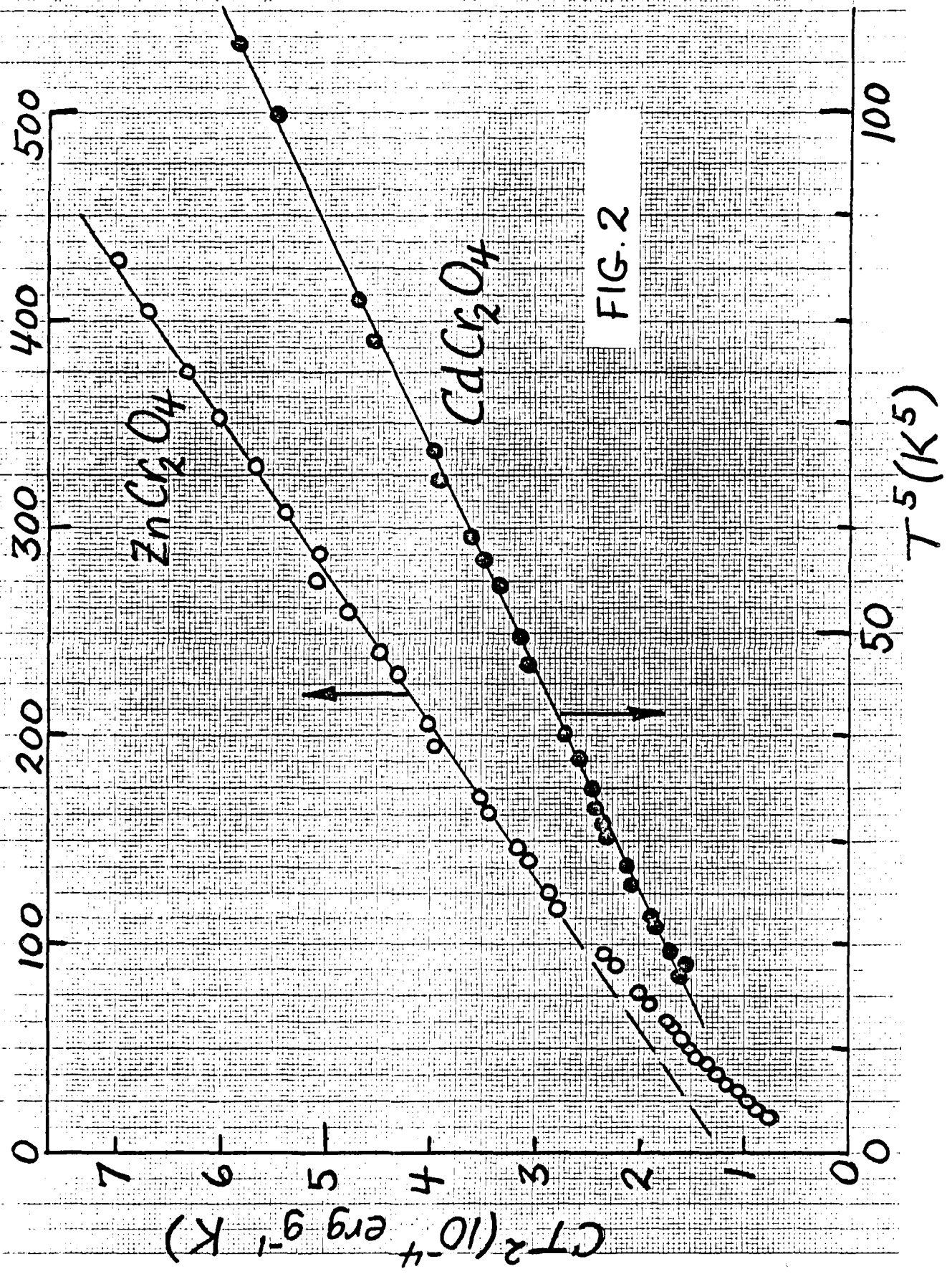


FIG. 2

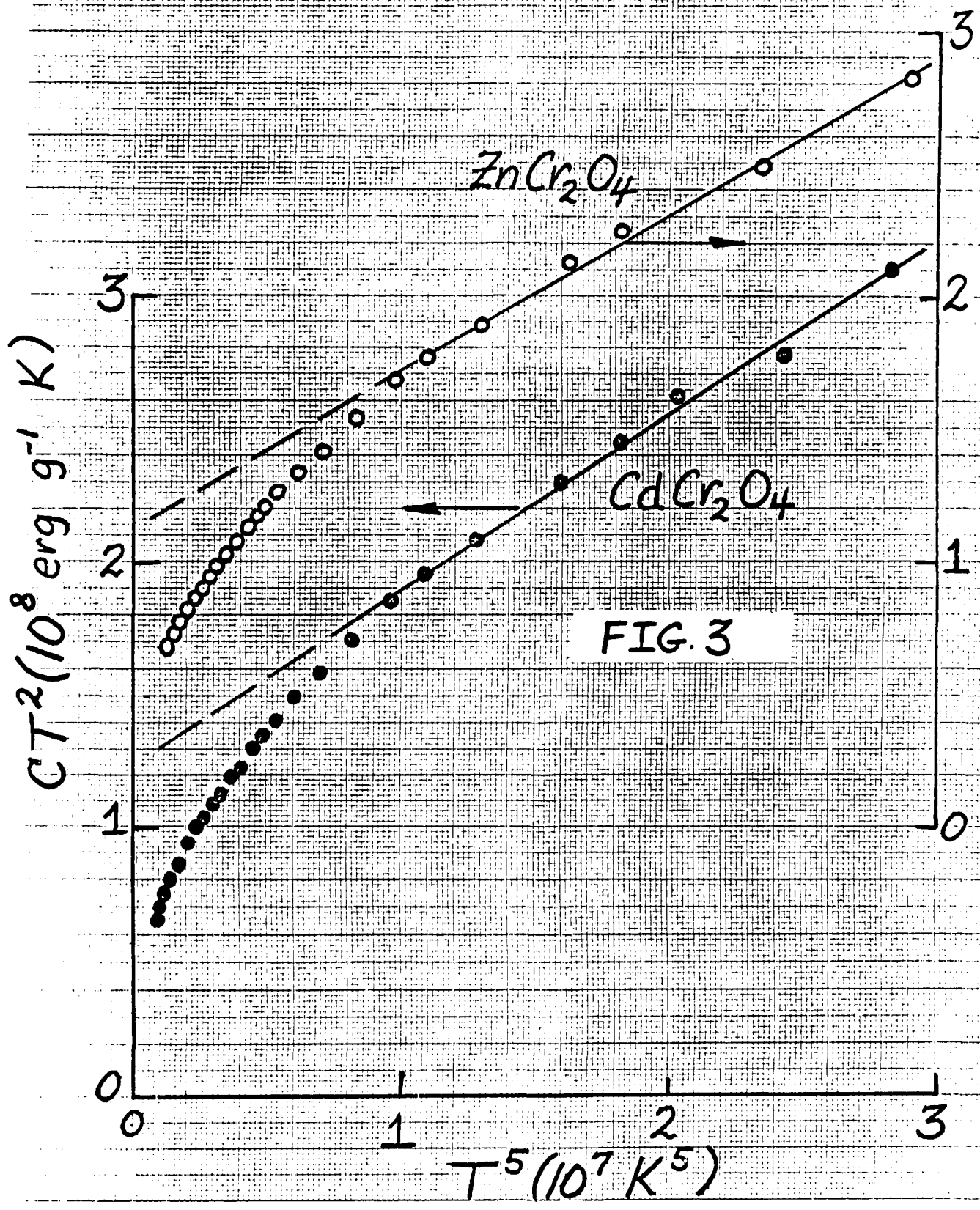


FIG. 3

PROGRESS REPORT

AFOSR Contract #F49620-83-C-0129

Fundamental Physics Studies on High-Specific-Heat  
Dielectrics and Kapitza Resistance at Dielectric Boundaries

Spinel Studies, IV. Magnetic Entropies and Enthalpies

by

W.N. Lawless



CeramPhysics, Inc.

Westerville, Ohio 43081

March 14, 1984

Distribution:

~~J.H.~~ Parker, Jr.  
P.W. Eckels  
T.K. Gupta  
M. Ashkin  
C.F. Clark  
B.R. Patton

## INTRODUCTION

This is the fourth report in a series devoted to the oxide spinels  $\text{CdCr}_2\text{O}_4$  and  $\text{ZnCr}_2\text{O}_4$  in an effort to understand the unusually large specific heats of these materials.

In previous reports, high-precision specific heat data, 1.7-31 K, on C(9/1) and D(9/1) were analyzed to determine the specific heats of the spinel phases, and further analyses of these spinel data revealed several significant findings:

1. From high-temperature (i.e.,  $T > 2T_N$ ) Schottky fits, Debye temperatures of 420 and 463 K were determined for the  $\text{CdCr}_2\text{O}_4$  and  $\text{ZnCr}_2\text{O}_4$  spinels, respectively. These Debye temperatures are in remarkably good agreement with predictions of the Lindemann relation based on melting temperatures and molecular weights.
2. From low-temperature (i.e.,  $T < 1/2 T_N$ ) Schottky fits, two-level excitations were identified with level splittings 0.33 and 0.37 K for the  $\text{CdCr}_2\text{O}_4$  and  $\text{ZnCr}_2\text{O}_4$  spinels, respectively. These fits also yielded unrealistically small Debye temperatures ( $\Theta_D \sim 100$ -160 K) for such hard, refractory materials, and the conclusion drawn was that antiferrimagnetic spin waves are contributing a  $T^3$  term to the specific heat, thus leading to very small effective Debye temperatures in this temperature range.

In this report, entropy and enthalpy data are reported for these spinels based on the above results.

## MAGNETIC ENTROPY OF SPINELS

The entropy (and enthalpy) of these two spinels are derived from the decomposed experimental data according to the following assumptions:

1. The lattice contributions are characterized by the Debye temperatures 420 and 463 K mentioned above because of the excellent agreement with the Lindemann relation.
2. Antiferromagnetic  $T^3$  spin-wave contributions are assumed (determined directly from the difference in the effective  $\Theta_D$ 's from the high- and low-temperature Schottky fits), and this  $T^3$  dependence is used down to 0 K. At the lowest temperatures, this  $T^3$  relation for spin waves becomes invalid, but the contribution to the entropy (and enthalpy) integrals at these lowest temperatures is so small that the error introduced is negligible.
3. The (assumed) two-level Schottky excitation for  $T < T_N$  is not identified but is assumed to be independent of the central specific heat peaks at 8 and 10.6 K for the  $\text{CdCr}_2\text{O}_4$  and  $\text{ZnCr}_2\text{O}_4$  spinels, respectively. Thus, this contribution to the specific heat is treated as a pseudo-lattice contribution rather than as a magnetic contribution. Also, a two-level Schottky term with equal degeneracies will be used to describe this pseudo-lattice contribution down to the lowest temperatures (this is a necessary assumption since the Schottky fit at the lowest experimental temperatures yields only the level splitting).
4. Above 31 K, the magnetic contribution to the specific heat will be extrapolated using the  $T^{-2}$  tail of the fitted high-temperature (i.e.,  $T > 2T_N$ ) Schottky term.

The total specific heat,  $C_t$ , is written as

$$C_t = C_l + C_m, \quad (1)$$

where  $C_l$  is the lattice contribution (including the pseudo-lattice term) and  $C_m$  is the magnetic contribution. We have  $C_t$ -data determined directly from the experimental data between  $T_1$  and  $T_2$  (i.e.,  $T_1 = 1.7$ ,  $T_2 = 31$  K), so the magnetic entropy is given by

$$S_m = \int_0^{T_1} C_m^{(sw)} d\ln T + \int_{T_1}^{T_2} C_t d\ln T + \int_{T_2}^{\infty} C_m^{(sch)} d\ln T - \int_{T_1}^{T_2} C_l d\ln T, \quad (2)$$

where  $C_m^{(sw)}$  is the spin-wave  $T^3$  term,  $C_m^{(sch)}$  is the Schottky-tail extension, and  $C_l$  comprises both the Debye contribution and the pseudo-lattice Schottky term. An advantage of Eq. (2) is that the pseudo-lattice term is not involved below  $T_1$  (see below).

The procedure now is straightforward: The first integral in Eq. (2) is evaluated using the  $T^3$  spin-wave approximation; the second integral, by numerical integration of the (decomposed) experimental spinel data; and the third integral, by using the fitted  $T^{-2}$  Schottky extension. The fourth integral in Eq. (2) involves the Debye term plus the pseudo-lattice Schottky term: Fortunately, the  $T^3$  Debye approximation is accurate to  $\pm 0.8\%$  uncertainty up to 31 K for the Debye temperatures involved, so that the Debye integral is trivial; the pseudo-lattice term was evaluated by numerically integrating the two-level schottky term.

The magnetic entropy  $S_m$  is simply related to the spin of the  $Cr^{3+}$  ion in these spinels: A particle with spin  $s\hbar$  has  $2s+1$  quantized orientations, and in the absence of a magnetic field there is a  $2s+1$  degeneracy in the state of the system, leading directly to

$$S_m = nR \ln(2s+1), \quad (3)$$

where  $n$  is the number of spins per formula weight (i.e.,  $n = 2$ ). The results of these calculations are summarized in Table I.

Table I  
Magnetic Entropies of Spinel

Spinel	$S_m(\text{erg g}^{-1} \text{K}^{-1})$	$S_m/R$	spin, $s$
$\text{CdCr}_2\text{O}_4$	$6.939 \times 10^5$	2.340	1.11
$\text{ZnCr}_2\text{O}_4$	$5.109 \times 10^5$	1.434	0.524

The various entropy contributions are evaluated as follows: (1) The magnetic entropy below  $T_1$  is calculable from the first integral in Eq. (2), and above  $T_2$ , from the third integral in Eq. (2); (2) The Debye lattice contribution is calculable from the  $T^3$  approximation up to  $\sim 35$  K, and from the Debye Table<sup>1</sup> above 35 K; (3) The pseudo-lattice contribution is obtained by direct numerical integration of the two-level Schottky term; and (4) The magnetic entropy between  $T_1$  and  $T_2$  is calculable from the difference between the total entropy and the lattice contributions.

These entropy calculations are summarized in Figs 1-3: Figs 1 and 2 summarize the entropy contributions for  $\text{CdCr}_2\text{O}_4$  and  $\text{ZnCr}_2\text{O}_4$ , respectively, where the lattice Debye and pseudo-lattice Schottky contributions are shown separately. And Fig. 3 compares the magnetic entropies in the two spinels.

## MAGNETIC ENTHALPY OF SPINELS

The enthalpies of the two spinels are calculated exactly along the lines of the above entropy calculations except that in Eq. (2) the integrations involve  $dT$  rather than  $d\ln T$ . The results of these calculations are given in Table II.

Table II  
Magnetic Enthalpies of Spinels

Spinel	$H_m(\text{erg g}^{-1})$	$H_m(\text{J per mole})$
$\text{CdCr}_2\text{O}_4$	$1.146 \times 10^7$	321.3
$\text{ZnCr}_2\text{O}_4$	$9.944 \times 10^6$	232.1

## DISCUSSION

There is an internal consistency in the manner in which the above magnetic entropies have been derived. That is, the Debye lattice contribution has been described by a Debye temperature in which we have confidence based on the Lindemann relation, and the magnetic entropy follows directly from experimental data. Both spinels have been treated identically. The lowest temperature Schottky term (i.e.,  $\delta \sim 0.3$  K), while unidentified, does not contribute significantly to  $S_m$  calculated from Eq. (2); that is, in the fourth integral in Eq. (2) the integrand of this term essentially varies as  $T^{-3}$  between  $T_1$  and  $T_2$ . Another way of seeing this is that the entropy of this term is essentially constant between  $T_1$  and  $T_2$  in Figs. 1 and 2.

The most significant findings from this study are the effective  $\text{Cr}^{3+}$  spin-values per molecule in Table I: For  $\text{CdCr}_2\text{O}_4$ ,  $s \approx 1$  and for  $\text{ZnCr}_2\text{O}_4$ ,  $s \approx 1/2$ .

These spin values allow us to evaluate the exchange constants in these spinels. That is, the antiferrimagnetic spin-wave contribution to the specific heat is<sup>1</sup>

$$C_m^{(sw)} = c_a R (k/2J's)^3 T^3 \quad (4)$$

where  $c_a$  is a constant depending on the lattice type,  $J'$  is the exchange constant, and  $s$  is the spin value. Assuming  $c_a = 1$  and using the spin values in Table I we find

$$\begin{aligned} J' (\text{CdCr}_2\text{O}_4)/k &= 3.88 \text{ K} \\ J' (\text{ZnCr}_2\text{O}_4)/k &= 13.34 \text{ K} \end{aligned} \quad (5)$$

in units of the Boltzman constant  $k$ . We have consistently found significant differences between these two spinels, and these spin and exchange values are yet another example.

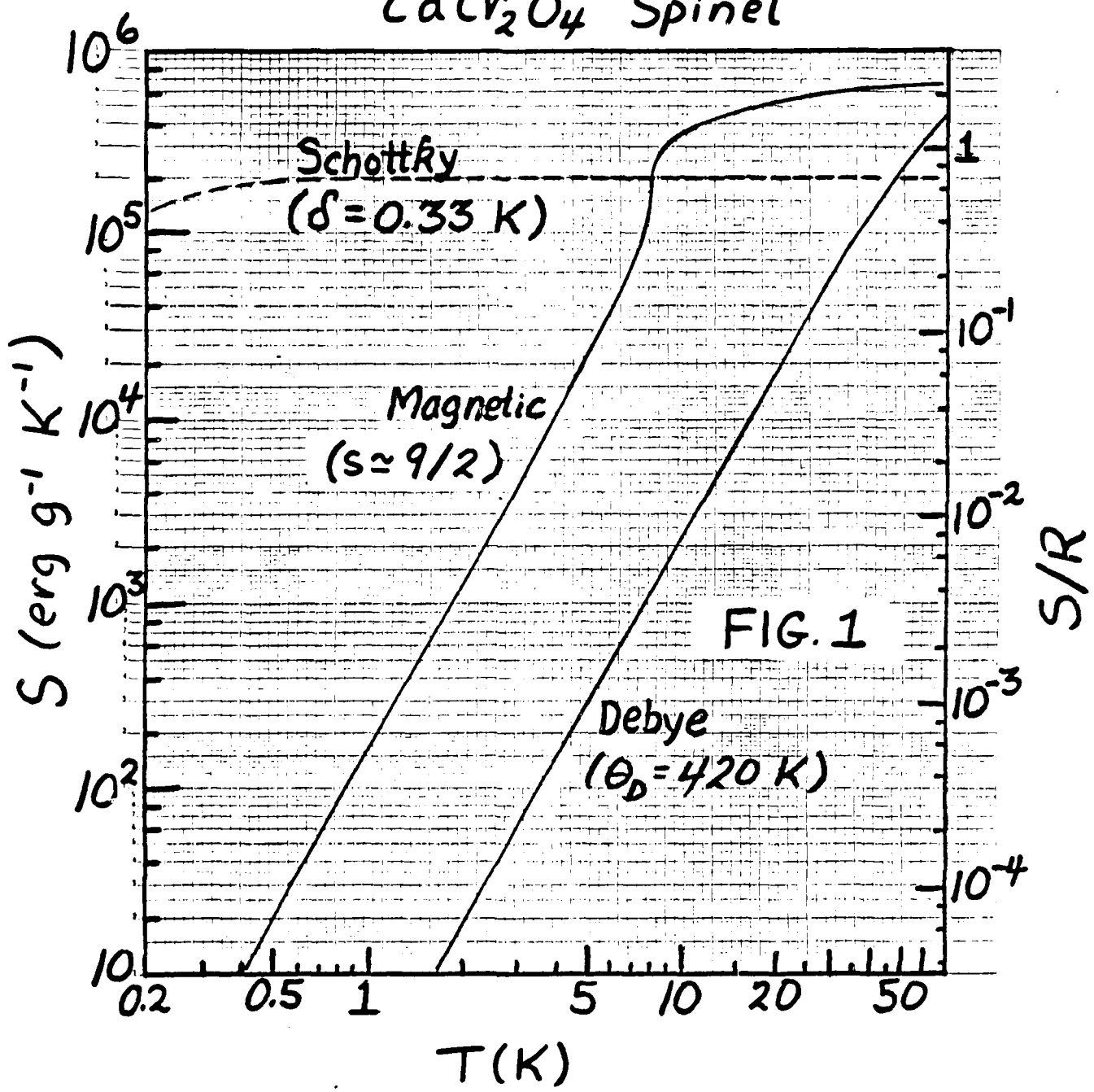
We are now in a position to make comparisons between the lattice and magnetic contributions to the specific heats of these spinels: At the lowest temperatures the antiferrimagnetic spin-wave contribution is about 71 times larger than the lattice contribution in  $\text{CdCr}_2\text{O}_4$ ; and about 22 times larger in  $\text{ZnCr}_2\text{O}_4$ . At the specific heat maximum at 8 K in  $\text{CdCr}_2\text{O}_4$ , the lattice contribution is only 0.10% of the total specific heat; stated differently, the total specific heat is about  $10^3$  times larger than the lattice contribution. At the specific heat maximum at 10.7 K in  $\text{ZnCr}_2\text{O}_4$ , the corresponding values are 0.35% and 287 times larger, respectively.

In conclusion, the specific heats of  $\text{CdCr}_2\text{O}_4$  and  $\text{ZnCr}_2\text{O}_4$  seem understandable in a straightforward fashion. The  $\text{Cr}^{3+}$  spin values are  $s \sim 1$  and  $s \sim 1/2$ , respectively, which are reasonable (the free-ion spin of  $\text{Cr}^{3+}$  is  $3/2$ ). These spin values are determined by assuming that all  $\text{Cr}^{3+}$  ions participate [i.e.,  $n = 2$  in Eq (3)]. The antiferromagnetic spin waves contribute at  $T^3$  term which is very large compared to the lattice term, but the exchange constants in Eq. (5) are reasonable values and compare favorably with values determined in similar spinels (e.g., in  $\text{CdCr}_2\text{S}_4$ ,  $J/k = 11.8$  K for ferromagnetic nearest-neighbor interactions.<sup>2</sup>) Finally, the lattice contributions are describable by Debye temperatures in excellent agreement with the predictions of the Lindemann relation.

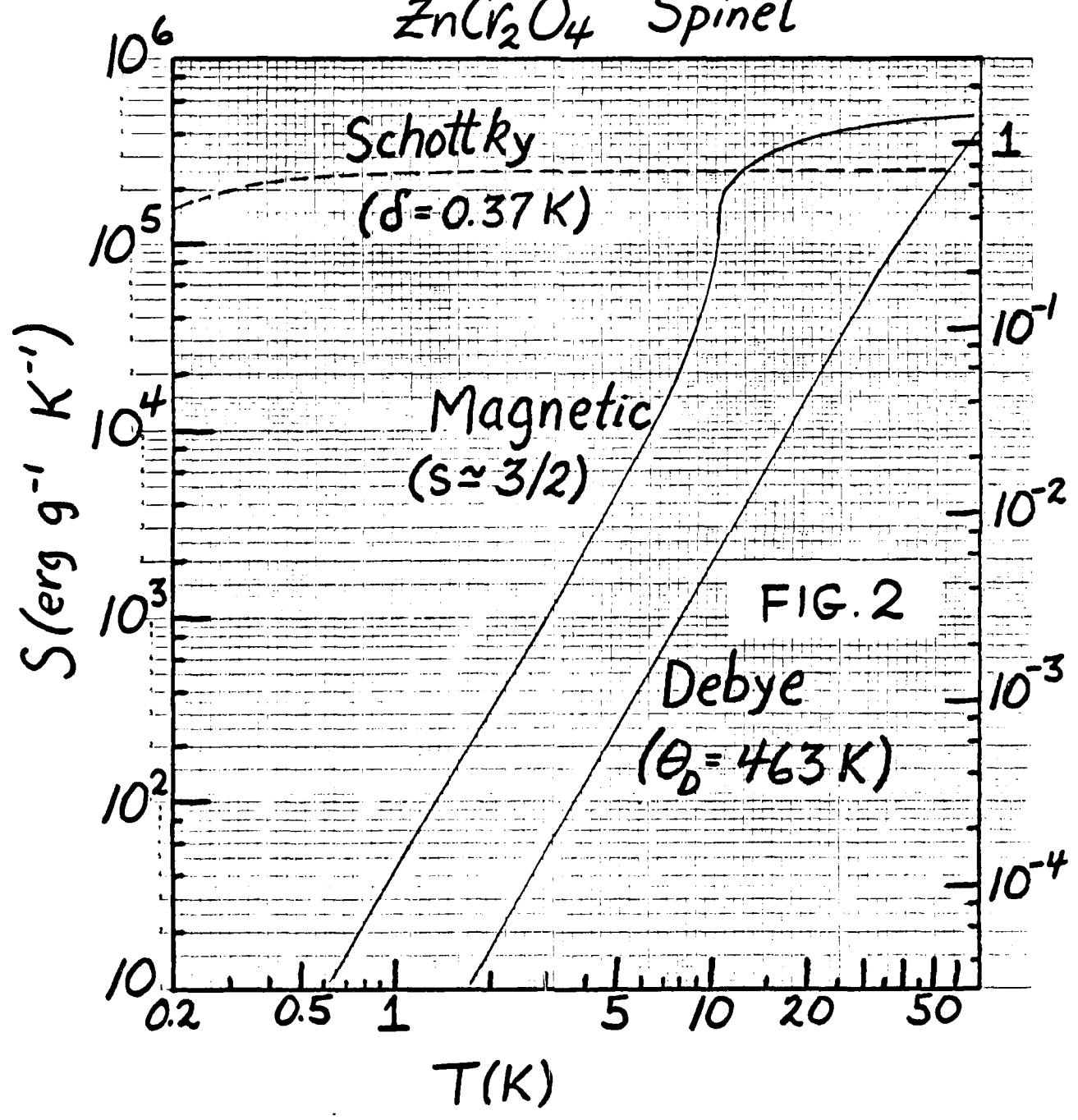
#### References

- <sup>1</sup>E.S.R. Gopal, Specific heats at low temperatures (Plenum Press, New York, 1966).
- <sup>2</sup>P.K. Baltzer, P.J. Wojtowics, M. Robbins, and E. Lopatin, Phys. Rev. 151, 367 (1966).

CdCr<sub>2</sub>O<sub>4</sub> Spinel



ZnCr<sub>2</sub>O<sub>4</sub> Spinel



PROGRESS REPORT

AFOSR Contract #F49620-83-C-0129

Fundamental Physics Studies on High-Specific-Heat  
Dielectrics and Kapitza Resistance at Dielectric Boundaries

Spinel Studies, V. Literature Survey

by

W.N. Lawless *WNL*

CeramPhysics, Inc.

Westerville, Ohio 43081

April 17, 1984

Distribution:

J.H. Parker, Jr.  
~~P.~~W. Eckels  
T.K. Gupta  
M. Ashkin  
C.F. Clark  
B.R. Patton

AD-A169 964

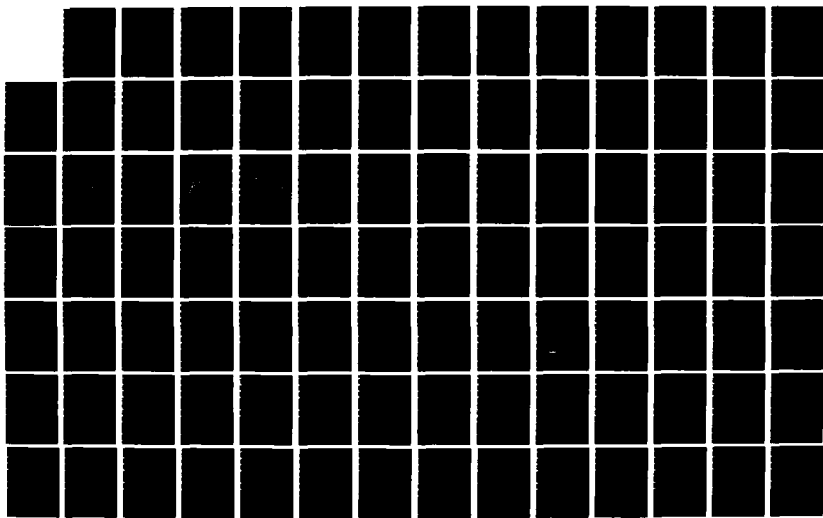
HIGH SPECIFIC HEAT DIELECTRICS AND KAPITZA RESISTANCE  
AT DIELECTRIC BOUND (U) WESTINGHOUSE RESEARCH AND  
DEVELOPMENT CENTER PITTSBURGH PA P W ECKELS ET AL

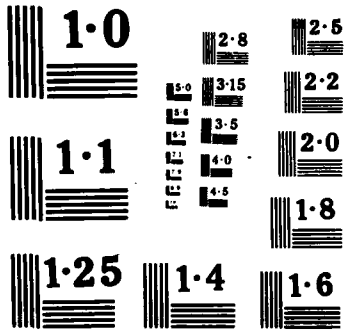
3/5

UNCLASSIFIED

30 SEP 85 AFOSR-TR-86-0477 F49620-83-C-0129 F/G 20/13

NL





## INTRODUCTION

This is the fifth report in a series devoted to the oxide spinels  $\text{CdCr}_2\text{O}_4$  and  $\text{ZnCr}_2\text{O}_4$  in an effort to understand the large specific heats of these materials.

By way of review, the  $\text{CdCr}_2\text{O}_4$  spinel has a specific heat maximum of  $C_{\text{max}}/3R = 4$  at 8 K, and the  $\text{ZnCr}_2\text{O}_4$  spinel has  $C_{\text{max}}/3R = 2$  at 10.7 K. On a volumetric basis, the specific heats of these spinels are comparable to that of water at room temperature.

Analyses of high-precision specific heat data, 1.7-31 K, strongly suggest antiferromagnetic transitions at 8.0 and 10.7 K in these spinels. Debye temperatures of 420 and 463 K for the Cd and Zn spinels were determined, and from the magnetic entropies of the transitions, effective  $\text{Cr}^{3+}$  spin values of 1.11 and 0.52 were deduced for the Cd and Zn spinels, respectively. From the antiferromagnetic spin-wave contributions to the specific heats at the lowest temperatures, exchange constants  $J/k = 3.88$  and  $13.34$  K were determined for the Cd and Zn spinels, respectively. Finally, it has been determined recently in drift experiments (to be described later) that there is no latent heat associated with the 8.0 K transition in the Cd spinel or with the 10.7 K transition in the Zn spinel, thus suggesting second-order transitions (That is, the Cd spinel, for example, was drifted slowly in temperature through the 8.0 K region; if a latent heat were involved, the sample temperature would remain constant at 8.0 K until this heat were dissipated, but such was not the case for either spinel).

The purpose of this report is to conduct a (limited) literature survey of these and similar spinels to see what insights might be gained into the  $\text{CdCr}_2\text{O}_4$  and  $\text{ZnCr}_2\text{O}_4$  spinels.

## LITERATURE SURVEY

A library search for papers on  $\text{CdCr}_2\text{O}_4$  and  $\text{ZnCr}_2\text{O}_4$  was conducted in 1978, and since then various abstracting journals have been followed for recent papers. These searches have been relatively fruitless: (1) The enthalpies of formation of the spinels have been reported;<sup>1</sup> and (2) The catalytic properties of  $\text{ZnCr}_2\text{O}_4$  have been reported.<sup>2</sup> The only paper bearing on the immediate problem reported<sup>3</sup> that at 12.8 K  $\text{ZnCr}_2\text{O}_4$  undergoes a first-order transition from long-range to short-range order; these authors, however, do not present evidence supporting the claim of a first-order transition (see above). Moreover, our considerable calorimetric studies of  $\text{ZnCr}_2\text{O}_4$  consistently place the transition at 10.7 K.

Thus, the literature data on these oxide spinels is very sparse. However, the literature data on the chromium chalcogenide spinels  $\text{MCr}_4\text{X}_2$  ( $\text{M} = \text{Zn}, \text{Cd}, \text{Hg}, \text{Cu}, \text{Fe}$  and  $\text{X} = \text{S}, \text{Se}, \text{Te}$ ) is quite voluminous, and in what follows below we will briefly review the literature on these spinels.

To begin, most all of these chalcogenide spinels are ferromagnetic, and in his 1967 book<sup>4</sup> Schieber lists the properties of these spinels (see Table I below).

The chromium chalcogenide spinels have generated considerable interest in recent years because, as semiconductors, they present the opportunity to study magnetic interactions in systems where the itinerant-electron population is accessible to experimental control.<sup>12</sup> In the case of  $\text{CdCr}_2\text{Se}_4$ , optically-induced changes in both the permeability and the magnetization have been observed.<sup>13</sup>

Table I  
Chalcogenide Spinel (Symmetry Fd3m)

Spinel	Lattice Constant (Å)	Curie Temp (K)	Reference
CdCr <sub>2</sub> S <sub>4</sub>	10.244	156 *	5
ZnCr <sub>2</sub> S <sub>4</sub>	9.21	18 **	5,6
CdCr <sub>2</sub> Se <sub>4</sub>	10.72	130 *	7,8
ZnCr <sub>2</sub> Se <sub>4</sub>	10.50	115 **	9,10
HgCr <sub>2</sub> S <sub>4</sub>	10.23	142 **	11
HgCr <sub>2</sub> Se <sub>4</sub>	10.75	200 *	11
CuCr <sub>2</sub> S <sub>4</sub>	9.82	390 *	9
CuCr <sub>2</sub> Se <sub>4</sub>	10.34	465 *	9
CuCr <sub>2</sub> Te <sub>4</sub>	11.14	400 *	9
FeCr <sub>2</sub> S <sub>4</sub>	9.97	234 *	6

\* Ferromagnetic

\*\* Antiferromagnetic

The semiconducting properties of Cd<sub>1-x</sub>Cu<sub>x</sub>Cr<sub>2</sub>Se<sub>4</sub> have been studied in detail.<sup>8</sup> Several authors have reported similar studies for CdCr<sub>2</sub>S<sub>4</sub>, CdCr<sub>2</sub>Se<sub>4</sub>, and HgCr<sub>2</sub>Se<sub>4</sub>,<sup>14</sup> and the remarkable phenomena are a decrease of the electronic conductivity and a giant negative magnetoresistance near the Curie temperature.

The semiconducting phenomena in Cd<sub>1-x</sub>Cu<sub>x</sub>Cr<sub>2</sub>Se<sub>4</sub> are explained along the lines of a model due to Goodenough:<sup>15</sup> The 3d copper electrons occupy the e<sub>g</sub><sup>4</sup>t<sub>2g</sub><sup>5</sup> orbital states, and one t<sub>2g</sub> orbital remains empty. The E<sub>g</sub> levels are located below the top of the valence band whereas the t<sub>2g</sub><sup>5</sup> states form a fairly shallow acceptor level. The top of the

valence band is due to the 4p states of the  $\text{Se}^{-2}$  ion, and the  $t_{2g}^3$  orbitals of the  $\text{Cr}^{3+}$  ions are located below the top of the valence band. Because the  $t_{2g}$  orbital in a tetrahedral environment forms strong  $\sigma$  bonds with the chalcogen ion, the localization of the  $t_{2g}$  electrons is disturbed by the cation-anion-cation interaction if the copper concentration is sufficiently large. For small copper concentrations, an electron is captured from the top of the valence band by the empty  $t_{2g}$  orbital and it then participates in the indirect exchange between the nearest  $\text{Cr}^{3+}$  ions, thereby forming a magnetic polaron. The conduction process is due to holes moving along the 4p states of the  $\text{Se}^{-2}$  ion near the top of the valence band. Some contribution to the conduction is also made by the drift of the magnetic polarons, but since their mobility is small compared to the hole mobility, this contribution is very small.

Calculations of the electronic band structures for  $\text{HgCr}_2\text{Se}_4$ <sup>16</sup> and for  $\text{CdCr}_2\text{S}_4$  and  $\text{CdCr}_2\text{Se}_4$ <sup>17</sup> by use of the discrete variational  $X_\alpha$  method have elucidated the semiconductor + magnetic properties of these materials.

In these spinels, the  $\text{Cr}^{3+}$  site has octahedral symmetry,<sup>18</sup> and in the many-electron representation the  $\text{Cr}^{3+}$  ground state has  $A_{2g}$  symmetry while the first excited state is either  $E_g$  or  $T_{2g}$ .<sup>19</sup> In ferromagnetic  $\text{CdCr}_2\text{Se}_4$  ( $T_C = 130$  K), the  $3d^3$  electrons of the  $\text{Cr}^{3+}$  ion occupy the up-spin  $t_{2g}$  nonbonding orbital, whereas the down-spin  $t_{2g}$  orbital remains empty. On the other hand, the  $e_g$  orbitals are considerably hybridized with the 4p orbitals on the  $\text{Se}^{2-}$  ion due to the covalency comprising both bonding and antibonding orbitals.<sup>20</sup> Since both  $\text{Zn}^{2+}$  and  $\text{Cd}^{2+}$  in these spinels have  $3d^{10}$  and  $4d^{10}$  outermost filled

shells, the band structures of  $\text{ZnCr}_2\text{X}_4$  and  $\text{CdCr}_2\text{X}_4$  are expected to be quite similar.<sup>17,21</sup> Yet, as seen in Table I, the Zn-chromium chalcogenide spinels tend to be antiferromagnetic, as contrasted with the ferromagnetic Cd spinels.

The explanation here might lie with the separation of the  $\text{Cr}^{3+}$  ions: The interaction between first nearest neighbor  $\text{Cr}^{3+}$  ions on octahedral sites in spinels are quite sensitive to distance, going from strongly antiferromagnetic in oxide spinels to strongly ferromagnetic in selenide spinels.<sup>22</sup>

Several details of these chromium chalcogenide spinels deserve mention:

The reflectance spectra measurements provide information on the covalency and band parameters through analyses of the inner-core optical spectra.<sup>23</sup> The reflectance spectra of  $\text{ZnCr}_2\text{Se}_4$  has been measured from 120 to 3000 Å and interpreted in terms of the covalency of the  $\text{Cr}^{3+}$  3d ( $e_g$ ) orbitals.<sup>20</sup>

The spiral-spin ground state of  $\text{ZnCr}_2\text{Se}_4$  suggests that at least one of the distant-neighbor interactions is ferromagnetic.<sup>24</sup>

The band gap  $E_g$  in  $\text{CdCr}_2\text{Se}_4$  (conduction to valence band transitions) determined from photoluminescence spectra is 1.8eV.<sup>25</sup> Similar measurements at high picosecond-laser intensities have established that  $\text{CdCr}_2\text{Se}_4$  is a direct-band-gap semiconductor.<sup>26</sup> The band-to-band absorption in  $\text{CdCr}_2\text{S}_4$  lies at 2.4 eV.<sup>27</sup>

In  $\text{CdCr}_2\text{S}_4$ , the exchange interactions with the six nearest-neighbor  $\text{Cr}^{3+}$  ions (via the intermediate sulfur ion) are ferromagnetic ( $J_1/k = 11.8$  K) while the interactions with 30 more distant neighbors are weaker and antiferromagnetic.<sup>22</sup> The anisotropy of  $\text{CdCr}_2\text{S}_4$  is very small down to the lowest temperatures,<sup>28</sup> but  $\text{Fe}^{2+}$  doping on the  $\text{Cd}^{2+}$

site raises the Curie point and introduces a strong anisotropy.<sup>29</sup> Ferromagnetic resonance studies at helium temperatures indicate that this anisotropy in  $\text{Cd}_{1-x}\text{Fe}_x\text{Cr}_2\text{S}_4$  can be explained by the single-ion anisotropy of the ferrous ion on the tetrahedral site.<sup>29</sup>

There are five first-order phonon lines in the Raman spectra of  $\text{CdCr}_2\text{X}_4$  ( $\text{X} = \text{S}, \text{Se}$ ), and the intensities of certain lines increase below the magnetic ordering temperatures.<sup>30</sup> Since the temperature dependence of the intensities varies like the spin-correlation function, this effect has been called spin-dependent phonon Raman scattering.<sup>30</sup> Two models have been proposed for this effect: (1) One model involves the dependence of the ion position on the superexchange interaction that couples the phonons to the spin system;<sup>31</sup> and (2) The second model interprets the effect as due to the variation of the d-electron transfer energy with lattice vibrations and/or non-diagonal exchange interactions.<sup>32</sup>

Finally, interesting speculations have been reported on the two transitions in  $\text{Cu}_{0.5}\text{In}_{0.5}\text{Cr}_2\text{S}_4$  at 160 and 35 K. The transition to paramagnetism takes place at 160 K, whereas neutron diffraction and calorimetric studies suggest a first-order transition from long-range magnetic ordering to a short-range ordering with correlations up to third nearest neighbors.<sup>33</sup>

#### DISCUSSION

It seems clear that, given the extensive literature developed on the chromium chalcogenide spinels the past twenty years, some serious attempts to make and study  $\text{CdCr}_2\text{O}_4$  and  $\text{ZnCr}_2\text{O}_4$  must have been made, since obviously the 2p states of  $\text{O}^{2-}$  are not greatly different than the 4p states of  $\text{Se}^{2-}$ . The lack of any reported studies on these oxide spinels strongly suggests that viable samples simply could not be made,

and this reinforces our results from ceramic studies -- namely, these spinels will not form unless the respective columbite phases are present (e.g.,  $\text{CdNb}_2\text{O}_6$  must be present for  $\text{CdCr}_2\text{O}_4$  to form). In any case, it is absolutely clear that the spinels  $\text{CdCr}_2\text{O}_4$  and  $\text{ZnCr}_2\text{O}_4$  are new materials to investigate, and apparently our ceramic techniques for making these materials are novel.

The above literature shows that there are consistent differences between the Cd- and Zn-containing chalcogenide spinels; for example,  $\text{CdCr}_2\text{S}_4$  and  $\text{CdCr}_2\text{Se}_4$  are ferromagnetic whereas  $\text{ZnCr}_2\text{S}_4$  and  $\text{ZnCr}_2\text{Se}_4$  are antiferromagnetic. We have noted consistent differences between  $\text{CdCr}_2\text{O}_4$  and  $\text{ZnCr}_2\text{O}_4$ , as reported previously. One set of experiments is noteworthy in this regard: In a previous program,<sup>34</sup> attempts were made to make the mixed spinel  $\text{Cd}_{1/2}\text{Zn}_{1/2}\text{Cr}_2\text{O}_4$ , and three mineralizers were tried:  $\text{ZnNb}_2\text{O}_6$ ,  $\text{CdNb}_2\text{O}_6$ ,  $\text{Cd}_{1/2}\text{Zn}_{1/2}\text{Cr}_2\text{O}_6$ . Good ceramic bodies were obtained in all cases, but subsequent specific heat measurements failed to show any specific heat maxima, 6-15 K. Still another attempt was tried where ceramic powders of C(9/1) and D(9/1) were independently made, then these powders were mixed in 50:50 ratios, cold-pressed into pellets and fired. Again, no specific heat maxima were observed at low temperatures. These studies clearly showed that substituting  $\text{Zn}^{2+}$  for  $\text{Cd}^{2+}$  in  $\text{CdCr}_2\text{O}_4$  (or  $\text{Cd}^{2+}$  for  $\text{Zn}^{2+}$  in  $\text{ZnCr}_2\text{O}_4$ ) destroyed the magnetic ordering. This was an unexpected result because: (1) The Fd3m lattice constants of  $\text{CdCr}_2\text{O}_4$  ( $8.595\text{\AA}$ ) and  $\text{ZnCr}_2\text{O}_4$  ( $8.328\text{\AA}$ )<sup>35</sup> are not much different; (2) The ionic radii of  $\text{Cd}^{2+}$  ( $0.97\text{\AA}$ ) and  $\text{Zn}^{2+}$  ( $0.74\text{\AA}$ ) are not much different; and (3) Both  $\text{Zn}^{2+}$  and  $\text{Cd}^{2+}$  in these spinels have  $3d^{10}$  and  $4d^{10}$  outermost filled shells, as mentioned above.

As reported earlier, the specific heat data for  $\text{CdCr}_2\text{O}_4$  and  $\text{ZnCr}_2\text{O}_4$  are consistent with antiferromagnetic transitions at 8.0 and 10.7 K,

respectively. This is consistent with the Table I data where in the  $M\text{Cr}_2\text{X}_4$  series ( $M = \text{Cd}, \text{Zn}, \text{X} = \text{S}, \text{Se}_4$ ) the trend is that the smaller the lattice constant, the lower the Curie temperature and the more favorable the antiferromagnetic state. Thus, judging simply from the above lattice constants for  $\text{CdCr}_2\text{O}_4$  and  $\text{ZnCr}_2\text{O}_4$ , one would expect antiferromagnetic transitions at temperatures below the Curie temperatures in Table I. However, this statement makes it even more puzzling why  $\text{ZnCr}_2\text{O}_4$  and  $\text{CdCr}_2\text{O}_4$  do not form an antiferromagnetic solid-solution series.

It is worth noting from Table I that the chalcogenide spinels have Curie temperatures well above the helium temperature range and as such are not as practical as the  $\text{CdCr}_2\text{O}_4$  and  $\text{ZnCr}_2\text{O}_4$  spinels. These latter spinels are, in fact, quite unique because of their low-temperature transitions.

As noted above,  $\text{Fe}^{2+}$  doping on the  $\text{Cd}^{2+}$  site in  $\text{CdCr}_2\text{S}_4$  raises the Curie point.<sup>29</sup> This is consistent with the trend in the ferromagnetic  $\text{CdCr}_2\text{X}_4$  spinels in Table I as regards the lattice constants. That is, as the lattice constant decreases (10.72 to 10.24Å) the Curie temperature increases (130 to 156 K). Thus, since the ionic radius of  $\text{Fe}^{2+}$  (0.75Å) is smaller than that of  $\text{Cd}^{2+}$  (0.97Å), the  $\text{Fe}^{2+}$  doping increases the lattice constant, thereby increasing the Curie temperature. Just the opposite effect takes place in antiferromagnetic  $\text{ZnCr}_2\text{X}_4$  spinels in Table I: Increasing the lattice constant (9.21 to 10.50Å) increases the Curie temperature (18 to 115 K).

Some doping studies in  $\text{CdCr}_2\text{O}_4$  were attempted in a previous program.<sup>34</sup> A 1%  $\text{Pb}^{2+}$  doping on the  $\text{Cd}^{2+}$  site slightly decreased the transition temperature, which argues for  $\text{CdCr}_2\text{O}_4$  being ferromagnetic by the above arguments based on the large ionic radius of  $\text{Pb}^{2+}$  (1.20Å).

Note that this study involved two-phase  $\text{CdNb}_2\text{O}_6 + \text{CdCr}_2\text{O}_4$  ceramics, and it is uncertain whether the  $\text{Pb}^{2+}$  dopant partitioned in the columbite or spinel phase.

A more definitive dopant was  $\text{Fe}^{3+}$  which progressively lowered the 8.0 K transition in  $\text{CdCr}_2\text{O}_4$  down to 6.4 K at 2%  $\text{Fe}^{3+}$ . At 3%  $\text{Fe}^{3+}$ , a broad transition centered at 5.95 K was obtained, and at 4.6 and 6.8% a flat, featureless specific heat was obtained. The  $\text{Fe}^{3+}$  ion (0.60Å) is smaller than  $\text{Cr}^{3+}$  (0.64Å), so the 8.0 → 6.4 K lowering of the transition temperature of  $\text{CdCr}_2\text{O}_4$  by the  $\text{Fe}^{3+}$  doping may be taken as an indication of an antiferromagnetic transition. The smearing of the specific heat peak at higher  $\text{Fe}^{3+}$  levels may indicate a disruption of the superexchange interactions.

Finally, our experimental studies to date do not suggest any significant semiconduction processes in  $\text{CdCr}_2\text{O}_4$ , based on two observations: (1) Measurements of the dielectric loss tangent, 3-16 K, revealed a small loss tangent (~1%) which did not show any structure around 8 K;<sup>34</sup> and (2) Mixtures of  $\text{CdCr}_2\text{O}_4 + \text{CdNb}_2\text{O}_6$  powders and glass powders have been fired onto copper wires to produce thin (~0.0005") coatings; coated wires have been twisted together pigtail-fashion, and breakdown field strengths ~2000 V/mil have been measured at 77 K.<sup>36</sup>

## REFERENCES

- <sup>1</sup> F. Mueller and O.J. Kleppa, *J. Inorg. Nucl. Chem.* 35, 2673 (1973); K.T. Jacob, *Thermochim. Acta* 15, 79 (1976).
- <sup>2</sup> O.N. Goroshko *et al.*, *Katal. Katal.* 13, 92 (1975); V.L. Chernobrivets *et al.*, *Katal. Katal.* 12, 60 (1974); T.P. Gaidei *et al.*, *Gos. Inst. Prikl. Khim.* 68, 45 (1973); L. Ivanov *et al.*, *God. Vissh. Khim. Inst. Sofia* 14, 257 (1970).
- <sup>3</sup> R. Plumier *et al.*, *J. Phys. (Paris) Lett.* 38(6), 149 (1977).
- <sup>4</sup> M.M. Schieber, *Experimental Magnetochemistry* (John Wiley & Sons, New York, 1967), Ch. 7.
- <sup>5</sup> N. Menyuk, K. Dwight, R. Arnott, and A. Wold, *J. Appl. Phys.* 37, 1387 (1966).
- <sup>6</sup> F.K. Lotgering, *Philips Res. Rept.* 11 (109), 337 (1956).
- <sup>7</sup> R.W.G. Wyckoff, *Crystal Structures* (Interscience Publ., New York, 1948).
- <sup>8</sup> K.P. Belov, L.I. Koroleva, M.A. Shalimova, V.T. Kalinnikov, T.G. Aminov, and G.G. Shabunina, *Sov. Phys. Solid State* 17, 2086 (1976).
- <sup>9</sup> F.K. Lotgering, *Solid State Commun.* 3, 347 (1965).
- <sup>10</sup> R. Plumier, *J. Appl. Phys.* 37, 964 (1966).
- <sup>11</sup> P.K. Baltzer, H.W. Lehman, and M. Robbins, *Phys. Rev. Lett.* 15, 493 (1965).
- <sup>12</sup> C. Haas, *CRC Crit. Rev. Solid State Sci.* 1, 47 (1970); W. Nolting, *Phys. Status Solidi (b)* 96, 11 (1979).
- <sup>13</sup> W. Lems, P.J. Rijerse, P.F. Bongers, and U. Enz, *Phys. Rev. Lett.* 21, 1643 (1968); V.E. Makhotkin, G.I. Vinogradova, and V.G. Veselago, *JETP Lett.* 28, 78 (1979); N.M. Salanskii and N.A. Drokin, *Sov. Phys. Solid State* 17, 205 (1975).

- <sup>14</sup> N. Koguchi and K. Masumoto, J. Phys. Chem. Solids 41, 1279 (1980).
- <sup>15</sup> J.B. Goodenough, Solid State Commun. 5, 577 (1967).
- <sup>16</sup> T. Oguchi, T. Kambara, and K.I. Gondaira, Phys. Rev. B24, 3441 (1981).
- <sup>17</sup> T. Oguchi, T. Kambara, and K.I. Gondaira, Phys. Rev. B22, 872 (1980);  
      , Jpn. J. Appl. Phys. Suppl. 19-3, 223 (1980).
- <sup>18</sup> P.K. Baltzer, H.W. Lehmann, and M. Robbins, Phys. Rev. Lett. 15,  
493 (1965).
- <sup>19</sup> S. Sugano, Y. Tanabe, and H. Kamimura, Multiplets of Transition-Metal  
Ions in Crystals (Academic Press New York, 1970).
- <sup>20</sup> S. Suga, S. Shin, M. Taniguchi, K. Inove, M. Seki, I. Nakada, S.  
Shibuya, and T. Yamaguchi, Phys. Rev. B25, 5486 (1982).
- <sup>21</sup> T. Kambara, T. Oguchi, and K. Gondaira, J. Phys. C. 13, 1493 (1980).
- <sup>22</sup> P.K. Baltzer, P.J. Wojtowics, M. Robbins, and E. Lopatin, Phys. Rev.  
151, 367 (1966).
- <sup>23</sup> M. Zvara, V. Prosser, A. Schlegel, and P. Wachter, J. Magn. Mater.  
12, 219 (1979).
- <sup>24</sup> K. Dwight and N. Menyuk, Phys. Rev. 163, 435 (1967); T. Watanabe,  
S. Endo, and A. Kasai, Jpn. J. Appl. Phys. Suppl. 19-3, 279 (1980).
- <sup>25</sup> S.S. Yao, F. Pellegrino, R.R. Alfano, W.J. Miniscalco, and A.  
Lempicki, Phys. Rev. Lett. 46, 558 (1981).
- <sup>26</sup> S.S. Yao and R.R. Alfano, Phys. Rev. B27, 1180 (1983).
- <sup>27</sup> S. Berger and L. Ekstrom, Phys. Rev. Lett. 23, 1499 (1969).
- <sup>28</sup> S. Berger and H.L. Pinch, J. Appl. Phys. 38, 949 (1967).
- <sup>29</sup> B. Hoekstra, R.P. van Stapele, and A.B. Voermans, Phys. Rev. B6,  
2762 (1972).
- <sup>30</sup> E.E. Steigmeier and G. Harbeke, Phys. Kond. Mater. 12, 1 (1970).

- <sup>31</sup> W. Baltensperger, J. Appl. Phys. 41, 1052 (1970).
- <sup>32</sup> N. Suzuki and H. Kamimura, J. Phys. Soc. Japan 35, 985 (1973).
- <sup>33</sup> R. Plumier, M. Sougi, M. Lecomte, Phys. Lett. 60A, 341 (1977).
- <sup>34</sup> W.N. Lawless, Final Report, NBS Contract NB81RAC10007, "High-Specific-Heat Ceramics for Cryocooler Regenerator Applications," Dec. 1981.
- <sup>35</sup> NBS Monograph #25, Section 5, 1967, p. 16, and Section 9, 1971, p. 59.
- <sup>36</sup> T.P. Gupta, private communication.

PROGRESS REPORT

AFOSR Contract #F49620-83-C-0129

Fundamental Physics Studies on High-Specific-Heat  
Dielectrics and Kapitza Resistance at Dielectric Boundaries

Spinel Studies, VI. Critical Exponents

by

W.N. Lawless *WNL*

CeramPhysics, Inc.

Westerville, Ohio 43081

*June 14, 1984*

Distribution:

J.H. Parker, Jr.

~~P.W. Eckels~~

T.K. Gupta

M. Ashkin

C.F. Clark

B.R. Patton

## INTRODUCTION

This is the sixth report in a series devoted to the oxide spinels  $\text{CdCr}_2\text{O}_4$  and  $\text{ZnCr}_2\text{O}_4$  in an effort to understand the unusually large specific heats of these materials.

This report deals with specific-heat measurements made very close to the peaks in the specific heats by an apparently novel calorimetric technique. Data analyses are presented along the lines of the renormalization group theory of critical exponents. The samples studied here are the same samples used in the "master" runs reported previously.

## EXPERIMENTAL METHODS AND RESULTS

The  $\text{CdCr}_2\text{O}_4$  and  $\text{ZnCr}_2\text{O}_4$  spinels have specific heat maxima at  $T_N=8.0$  and  $10.6$  K, respectively. The experiments here consisted of measuring the specific heats in the range  $T_N \pm 2$  K.

Similar measurements on  $\text{EuTe}$  and  $\text{EuSe}$  have recently been reported based on a pulse method.<sup>1</sup> There are two major drawbacks to the pulse method: (1) The temperature change  $\Delta T$  cannot be made arbitrarily small without introducing serious experimental constraints; and (2) More seriously, the pulse method necessarily involves times scales ( $\sim s$ ) which may be undesirably short to sample critical phenomena.

A drift method was adopted here wherein the sample slowly drifted in temperature over the range required. A variation of this method has been developed for measuring specific heats in intense magnetic fields.<sup>2</sup> A schematic illustration of the experimental arrangement is shown in Fig. 1. The sample (1) is notched to accept a carbon-resistor thermometer (2), and the sample is suspended from a copper pin (3) by two links (4 and 5). The manganin link (4) is simply for mechanical

support whereas the copper link (5) is the thermal link, and by varying the length of the latter link the sample drift rate can be adjusted (Note that the specific heats of the spinels are so large that even a copper link can yield a slow drift). The links (4 and 5) are indium-soldered to the pin (3) which in turn is bolted into a copper reservoir (6). This reservoir is mounted inside the adiabatic shield of the calorimeter<sup>3</sup> and is temperature-controlled.

The experiment consists of controlling the reservoir (6) at about  $T_N - 5$  K and using the sample heater (7) to bring the sample to about  $T_N + 2$  K. The  $dT/dt$  drift is initiated by de-activating the sample heater. Prior to the drift, the carbon resistor (2) is calibrated against a germanium thermometer mounted in the reservoir at several points in the range  $T_N \pm 3$  K. In the experiments here, the total drift time was adjusted to  $\sim 2$  hr; in the immediate neighborhood of  $T_N$  the drift rate was  $\sim 4$  mK/min. We remark that this is a major advantage of the technique --  $dT/dt$  slows considerably exactly in the range where the most data are desired.

All measurements were made by four-lead, dc potentiometric methods using battery supplies. The voltage signal from the carbon resistor ( $\sim 30$  mV) was bucked potentiometrically such that 1 mV was displayed on a chart recorder. Throughout the drift the exciting current was continuously monitored and adjusted to a constant value. The germanium thermometer on the reservoir was also monitored continuously, and it was found that the reservoir was controlled to  $\sim \pm 1$  mK. The  $dT/dt$  drift data were determined directly from the chart recorder using the carbon-resistor calibration.

The drift experiment is described<sup>2</sup>

$$mCdT/dt = - \int_{T_0}^T GdT \quad (1)$$

where  $G$  is the thermal conductance of the dominant thermal link (5 in Fig. 1) and  $T_0$  is the reservoir temperature. For copper,  $G \propto T$  so that the specific heat is given by

$$C \propto - (T^2 - T_0^2) / (dC/dt) \quad (2)$$

where the constant of proportionality in Eq. (2) involves the dimensions of the thermal link, the sample mass, and any scale factors involved in determining the  $\Delta t$ 's from the chart trace.

The specific heat in Eq. (2) includes the specific heats of the addenda and the columbite phase (i.e.,  $CdNb_2O_6$  or  $ZnNb_2O_6$ ). However, in the neighborhood of  $T_N$  these contributions are several orders of magnitude smaller than the specific heat of the spinel phase. The results of these drift experiments are shown in Fig. 2. More data were measured than are shown in Fig. 2, except for  $CdCr_2O_4$ ; the latter drift was terminated at 7.5 K due to helium loss which resulted in an unstable reservoir temperature. The data plotted in Fig. 2 are simply the rhs of Eq. (2), and both spinels display rounding at  $T_N$  which is more pronounced for the  $ZnCr_2O_4$  spinel.

The  $T_N$  values were determined graphically by plotting  $dT/dt$  vs.  $T$  above and below  $T_N$  and making a smooth extrapolation. The results are  $T_N = 7.958$  and  $10.637$  K for the  $CdCr_2O_4$  and  $ZnCr_2O_4$  spinels, respectively.

## DATA ANALYSES

The renormalization group theory of critical exponents suggests that<sup>1</sup>

$$C = (A/\alpha)|t|^{-\alpha} + Bt + E, T > T_N \quad (3)$$

where  $t = (T - T_N)/T_N$ . It is usual to denote a second set of parameters for  $T < T_N$ ,<sup>1</sup>

$$C = (A'/\alpha')|t|^{-\alpha'} + B't + E', T < T_N. \quad (4)$$

To gain some insight into the nature of these fits according to Eqs. (3) and (4), the drift data in Fig. 2 were first plotted according to the leading term (i.e.,  $\log C$  vs  $\log |t|$ ). The tacit assumption here is that near  $T_N$  the  $Bt + E$  terms may be small. These leading-term plots are shown in Figs. 3 and 4. The rounding of the drift data are particularly evident in Figs. 3 and 4; for  $ZnCr_2O_4$  the data are essentially flat for  $T_N \pm 0.4$  K. For  $CdCr_2O_4$  the data are noticeably skewed: the flatness sets in for  $T - T_N < 0.3$  K for  $T > T_N$ , but for  $T < T_N$  the flatness persists only up to  $|T - T_N| < 0.1$  K. This trend is also evident in the drift data for  $CdCr_2O_4$  in Fig. 2.

The  $\alpha$  and  $\alpha'$  values in Figs. 3 and 4 are unusually large ( $\sim 0.97$ - $1.5$ ) compared, say, to  $EuTe$  and  $EuSe$  ( $\sim 0.1$ ).<sup>1</sup> Correction for the  $Bt + E$  terms will only increase these critical exponents, as we shall see below.

In the next level of fittings, the  $Bt + E$  terms were taken into account as follows: The previously reported specific heat data for the  $CdCr_2O_4$  and  $ZnCr_2O_4$  spinels were plotted above  $T_N$  as shown in Fig. 5,

and in the temperature range  $2T_N$  to 30 K the data were fitted to  $Bt + E$ . These fits are also shown in Fig. 5, and both data sets follow the linear relation very well. The fitted parameters are

$$\begin{aligned}
 \text{CdCr}_2\text{O}_4: & \quad B = 1.188 \times 10^{-2} \text{ J mole}^{-1}\text{K}^{-2} \\
 & \quad E = 6.719 \text{ J mole}^{-1}\text{K}^{-1} \\
 \text{ZnCr}_2\text{O}_4: & \quad B = 7.498 \times 10^{-3} \text{ J mole}^{-1}\text{K}^{-2} \\
 & \quad E = 5.077 \text{ J mole}^{-1}\text{K}^{-1}
 \end{aligned}
 \tag{5}$$

These coefficients for the two spinels are quite similar. Also shown in Fig. 5 are two arrows indicating the minima in the specific heat data calculated from Eq. (3) using the fitting parameters. We shall return to this below.

The fitted  $Bt+E$  data were subtracted from the drift data to form

$$C_{ex} = C_S - Bt - E \tag{6}$$

where  $C_S$  is the total spinel specific heat. First, however, the drift data in Fig. 2 were scaled to the  $C_S$  data reported previously; since this scaling was done in the neighborhood of  $T_N \pm 2\text{K}$  the corrections due to the addenda and the columbite phase could be ignored.

The data plotted according to Eq. (6) with the parameters in Eq. (5) are shown in Figs. 6 and 7. In constructing these plots we have set  $B' = B$  and  $E' = E$ . We note immediately the similarity in the fitted critical exponents for  $t > 0$  -- i.e.,  $\alpha = 1.507, 1.502$  for the  $\text{CdCr}_2\text{O}_4$  and  $\text{ZnCr}_2\text{O}_4$  spinels, respectively. The fitted parameters for  $t > 0$  are:

$$\begin{aligned}
 \text{CdCr}_2\text{O}_4: \quad \alpha &= 1.507, \quad A = 86.74 \text{ J mole}^{-1} \text{ K}^{0.507} \\
 \text{ZnCr}_2\text{O}_4: \quad \alpha &= 1.502, \quad A = 100.2 \text{ J mole}^{-1} \text{ K}^{0.502}
 \end{aligned}
 \tag{7}$$

Again, it is striking how similar the fitted coefficients are for these two spinels.

As an internal check on the fitting parameters, we note from Eq. (4) that a minimum in  $C_S$  is predicted at  $t_m$  defined by

$$t_m^{\alpha+1} = (A/B) \tag{8}$$

Using the parameter data in Eqs. (5) and (7), the  $t_m$ 's for the two spinels are easily found, and these minimum temperatures are indicated by arrows in Fig. 5, as noted above. The predicted minima agree very well with the minima in the data, and we remark that the  $t_m$  values estimated from Eq. (8) are quite sensitive to  $\alpha$ .

Some attempts were made to vary  $T_N$  from the values given above, and it was found that  $\pm 10$  mK variations in  $T_N$  had little effect on  $\alpha = 3/2$  for both data sets. Moreover, there is a satisfying convergence in the  $C_{ex}$  data in Figs. 6 and 7 as  $|t| \rightarrow 0$  which lends confidence to the  $T_N$  values used.

The critical exponents for  $T < T_N$  in Figs. 6 and 7 seem unrealistically large (2.22 and 4.28), so the constraints  $B'=B$  and  $E'=E$  were relaxed and these  $T < T_N$  data were re-examined. However, the scaling-law constraint that  $\alpha'=\alpha$  was imposed for  $T < T_N$ .

Considering the  $\text{CdCr}_2\text{O}_4$  spinel first, we note from Fig. 3 that the uncorrected drift data have  $\alpha=1.492$ . The only way to satisfy the  $\alpha'=\alpha$  constraint is to impose  $B'=E'=0$  and allow  $A' \neq A$ . These data

are shown in Fig. 8 where the  $T > T_N$  data from Fig. 6 are duplicated. The parameters for  $\text{CdCr}_2\text{O}_4$  are then

$$\begin{aligned} \text{CdCr}_2\text{O}_4: \quad A' &= 31.11 \text{ J mole}^{-1} \text{ K}^{0.492} \\ \alpha' &= 1.492 = \alpha \end{aligned} \quad (9)$$

For  $\text{ZnCr}_2\text{O}_4$ , the Fig. 7 data clearly show that the  $B't+E'$  ( $=Bt+E$ ) term is too large (in fact,  $Bt+E$  becomes larger than  $C_S$  at about  $T_N-2$ ). The simplest solution is to set  $A'=A$ ,  $\alpha'=\alpha$  and to solve for  $B't+E'$  directly from the  $C_S$  data. Actually,  $B't+E' \approx E'$  since  $t$  is small and  $B \ll E$ , Eq. (5). This solution is shown in Fig. 9, and we find that

$$\text{ZnCr}_2\text{O}_4: \quad E' = 0.670 \text{ J mole}^{-1} \text{ K}^{-1}. \quad (10)$$

### DISCUSSION

The data in Figs. 8 and 9 are the summary plots from this study, and we find that the specific heat data near  $T_N$  for the two spinels can be adequately explained by Eqs. (3) and (4) except in the region of rounding very close to  $T_N$ .

The data analyses strongly suggest  $\alpha=3/2$  for the following reasons: (1) The region  $T > T_N$  yields very satisfying predictions of  $t_m$  from Eq. (8) considering that,  $A$ ,  $B$ , and  $\alpha$  are derived from two different fittings; (2) Both spinels are describable by  $\alpha=3/2$  in the region  $T > T_N$ ; and (3) The data in the region  $T < T_N$  for both spinels follow the constraint  $\alpha'=\alpha$  imposed in accordance with the scaling laws, provided certain conditions are imposed on the  $A'$ ,  $B'$ , and  $E'$  coefficients. It is perhaps significant that for both spinels,  $B't+E' < Bt+E$ , although this does indicate a discontinuity in the "background" specific heat.

It is unfortunate that the drift data display rounding for  $|T-T_N| < 0.3$  K as this prevents an examination of the scaling law over a wide range of  $|t|$  values. This rounding suggests unusually long correlation lengths in these spinels; that is, as the correlation length becomes commensurate with the ceramic grain size ( $\sim \mu\text{m}$ ), rounding of the specific heat near  $T_N$  is expected. Also, there may be some limited substitution of  $\text{Nb}^{5+}$  (ionic radius 0.69Å) on the  $\text{Cr}^{3+}$  (0.64Å) site in the spinel, although the previously reported studies indicate that the columbite phase is excluded from the spinel phase.

The magnitude of the critical exponent  $\alpha$  suggested by these studies is difficult to reconcile, since  $\alpha$  is related to the dimensionality. The scaling result  $(2-\alpha)(2-n) = \gamma d$  and Wilson's<sup>4</sup>  $\epsilon$ -expansion lead to

$$\alpha = (4-n)\epsilon/2(n+8) - (n+2)^2(n+28)\epsilon^2/4(n+8)^3. \quad (11)$$

For  $n=\epsilon=1$ ,  $\alpha=0.08$ , in reasonable agreement with the  $\alpha$  found for  $\text{EuTe}$  and  $\text{EuSe}$ .<sup>1</sup> However, in the limit  $n \rightarrow 0$ ,  $\alpha \rightarrow 0.20$ , as an upper limit.

Although we have found that  $\alpha=3/2$  satisfactorily fits the experimental data, it may be possible that critical phenomena are not involved in these new spinels. It is particularly significant that in zero magnetic field, the data reported here and elsewhere<sup>2</sup> show the rounding evident in Fig. 2. However, at 7.5 Tesla, the specific heat peak at 8 K in  $\text{CdCr}_2\text{O}_4$  does not show rounding.

### References

- <sup>1</sup> W.R. Johanson and D.C. McCollum, Phys. Rev. B22, 2435 (1980).
- <sup>2</sup> W.N. Lawless, C.F. Clark, and R.W. Arenz, Rev. Sci. Instrum. 53, 1647 (1982).
- <sup>3</sup> W.N. Lawless, Phys. Rev. B14, 134 (1976).
- <sup>4</sup> K.G. Wilson, Phys. Rev. Lett. 28, 548 (1972).

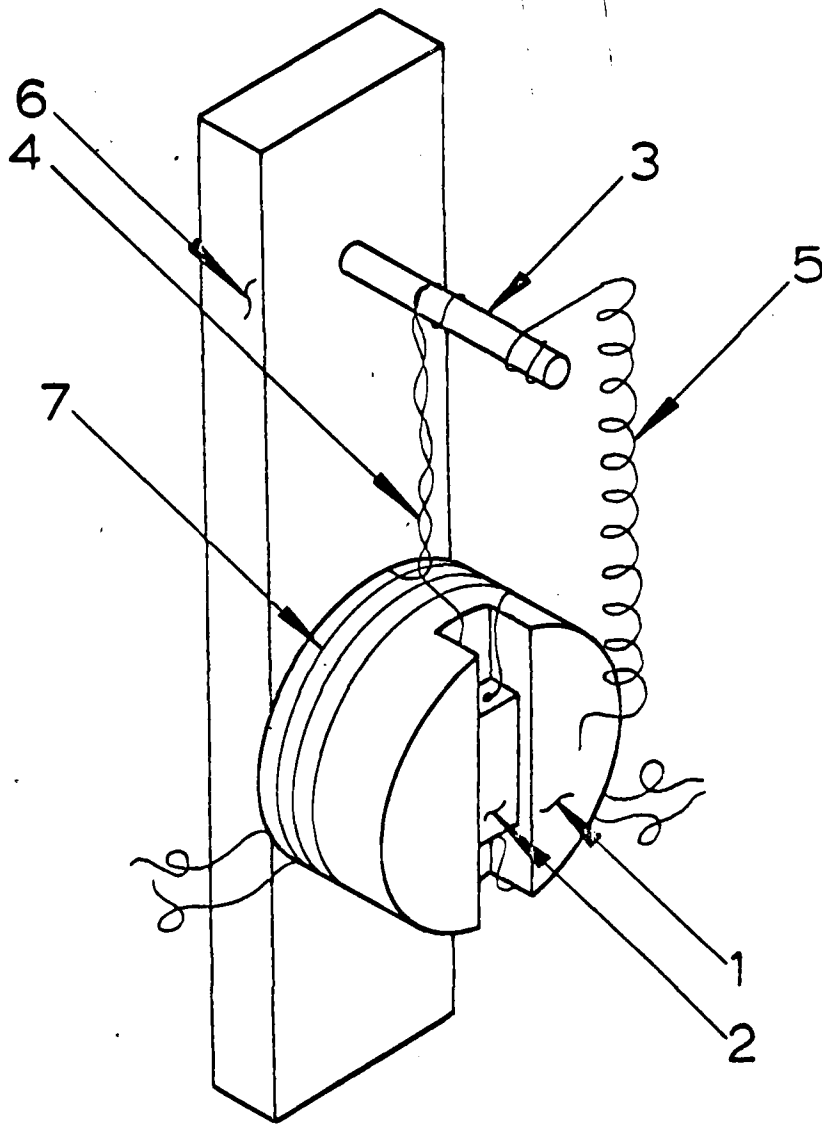
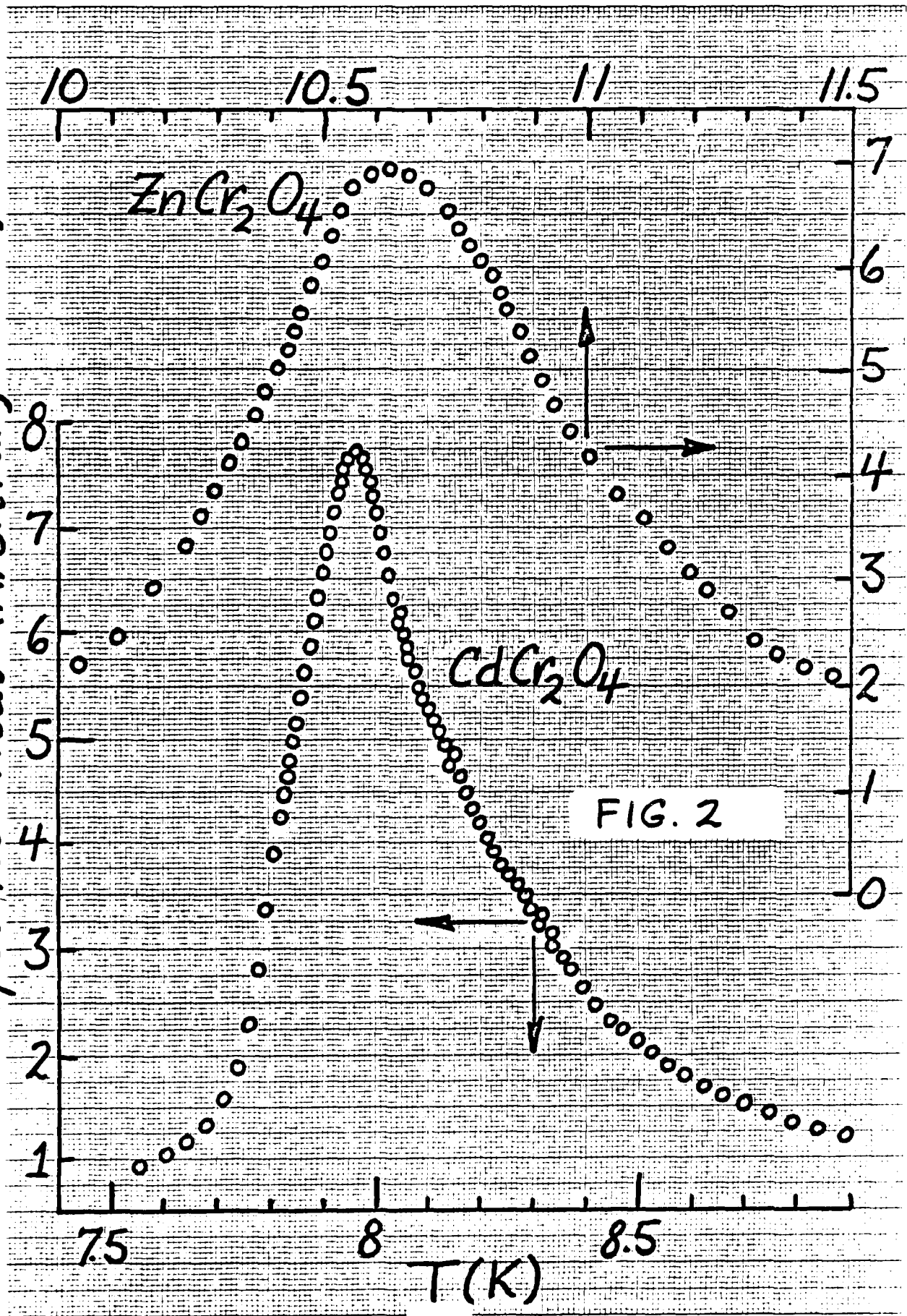
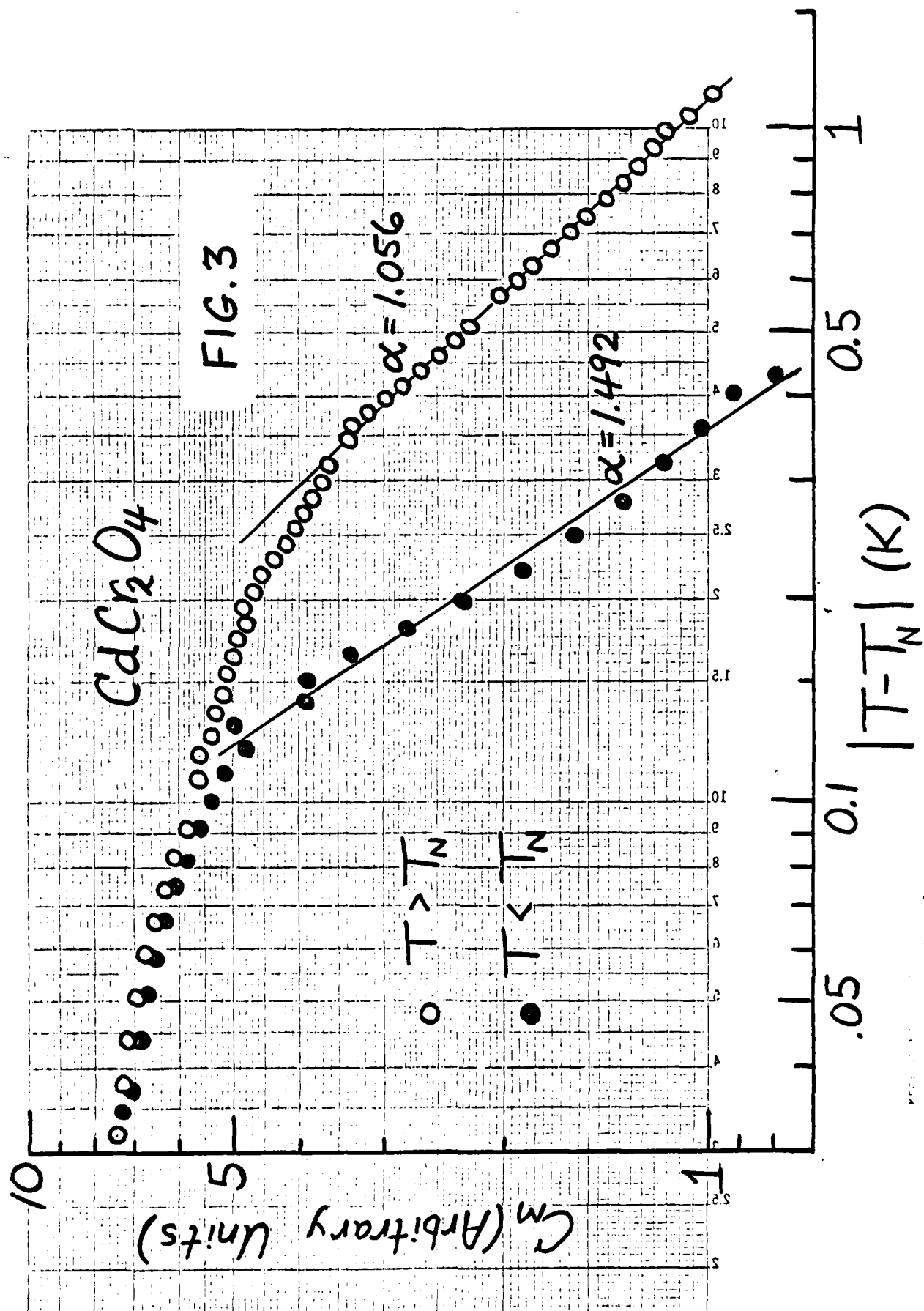


FIG. 1

Specific Heat (Arbitrary Units)





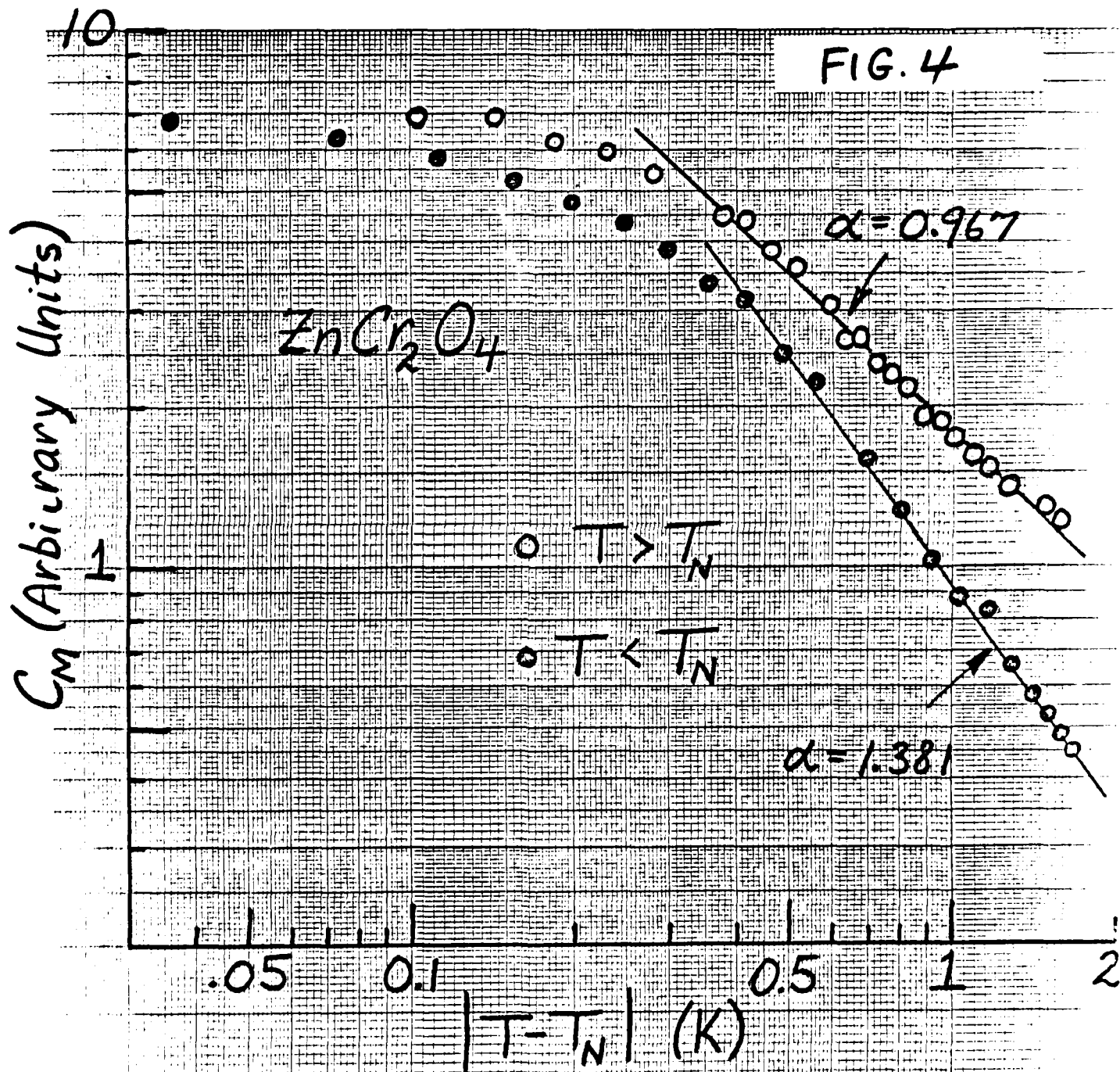


FIG. 5

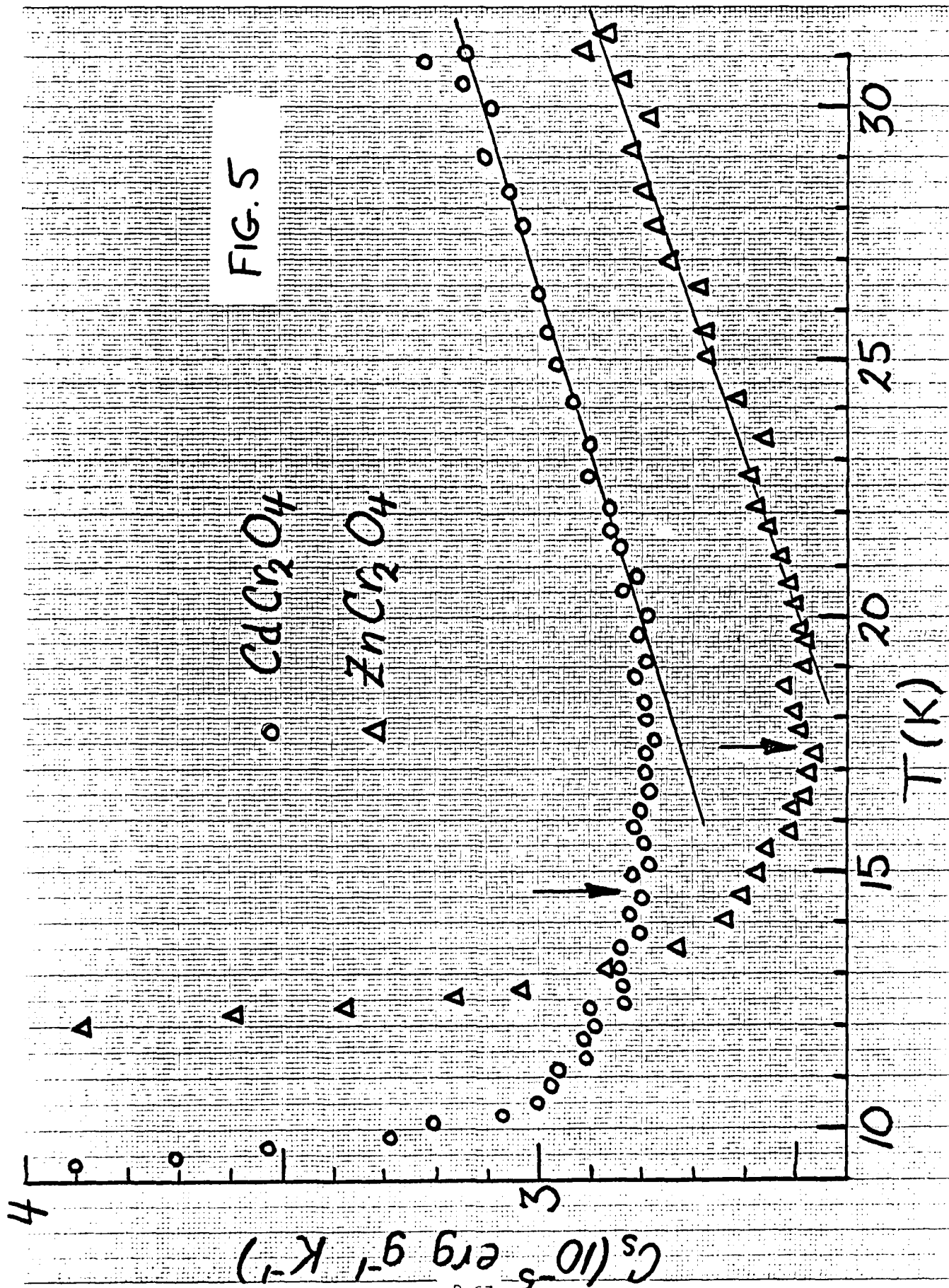
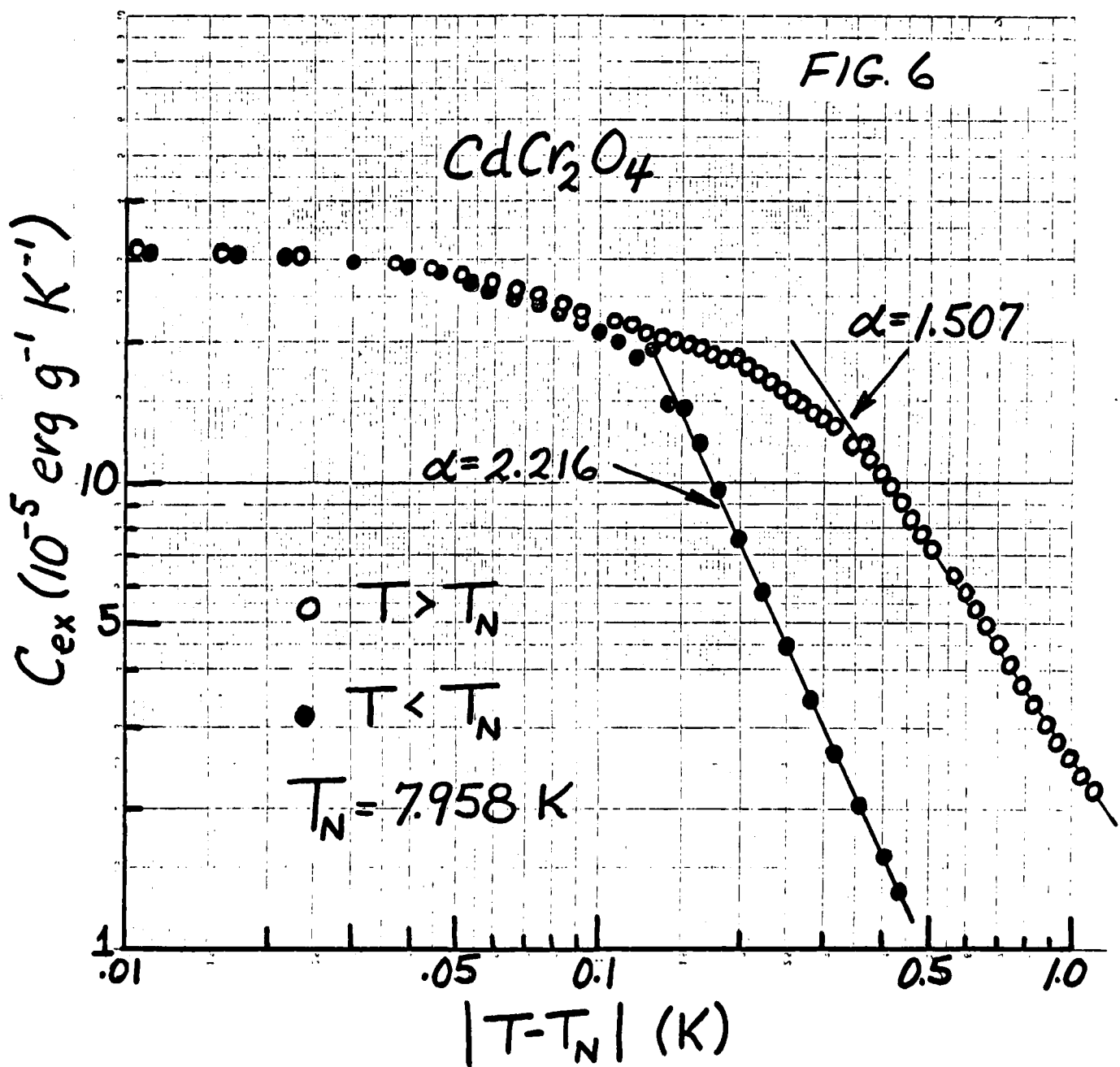
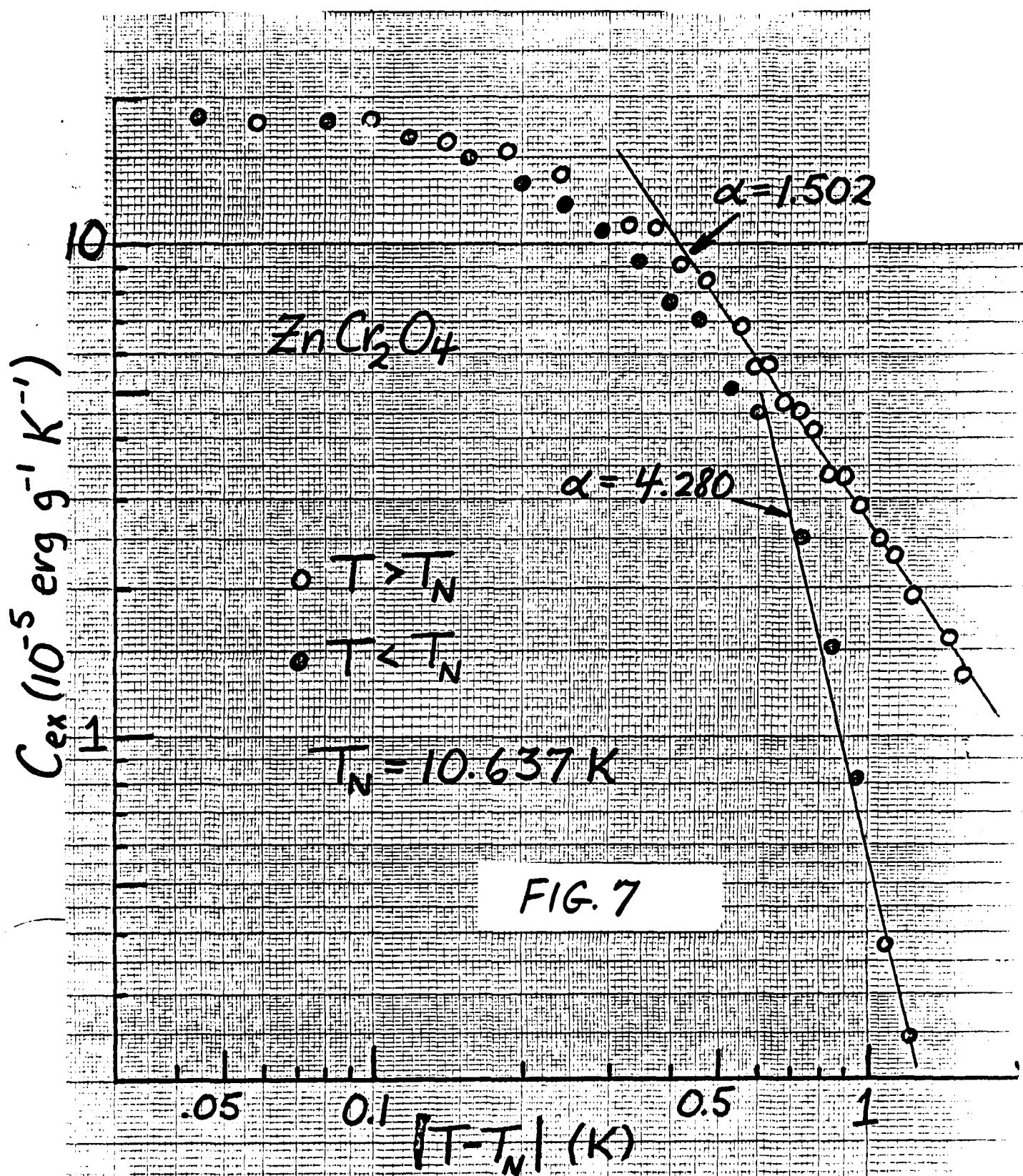


FIG. 6



QUALITY ASSURED  
1492 PRODUCTIONS 48 1083



2.5 3 4 5 6 7 8 9 10 1.5 2 2.5 3 4 5 6 7 8 9 10 1.5

FIG. 8

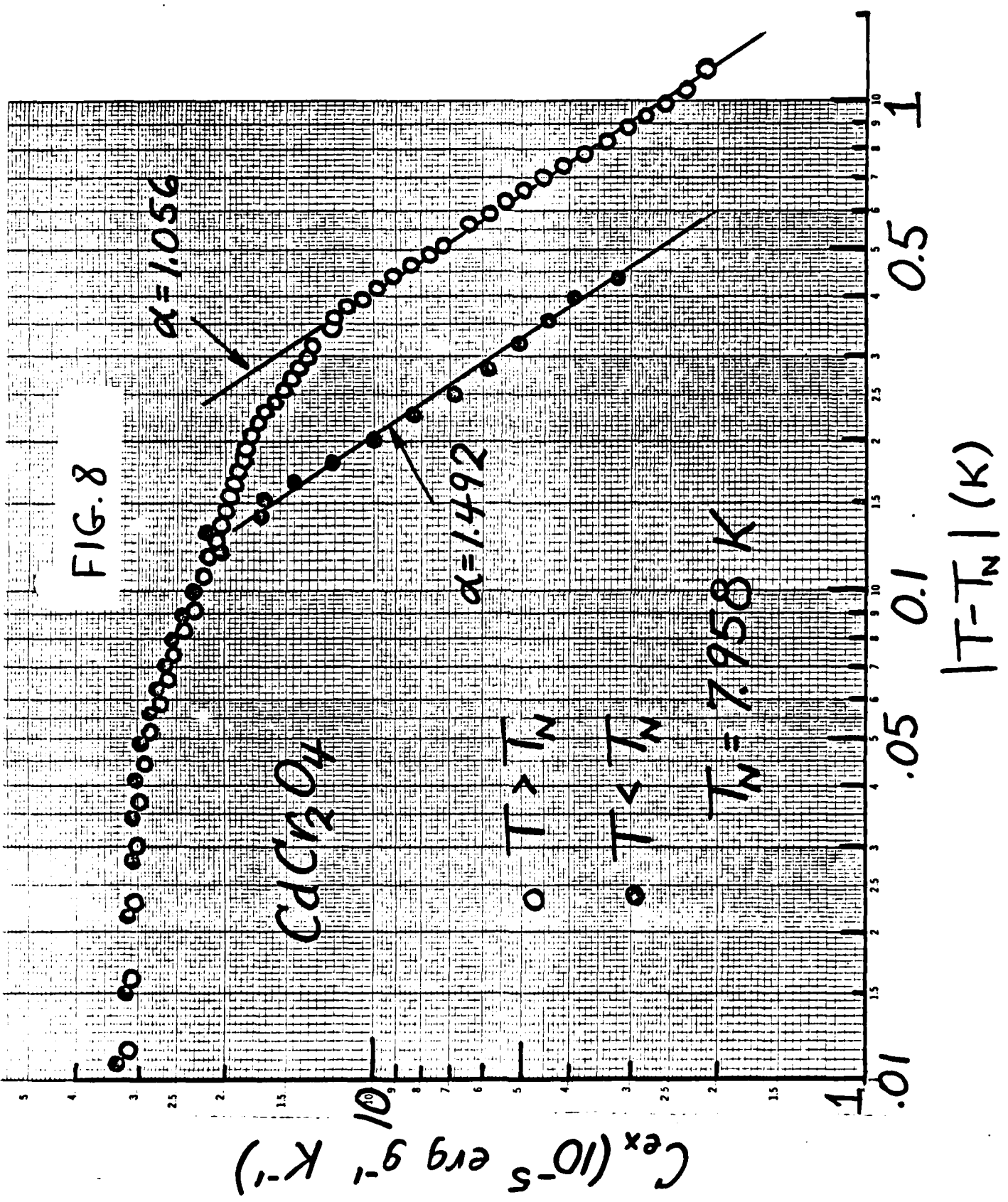
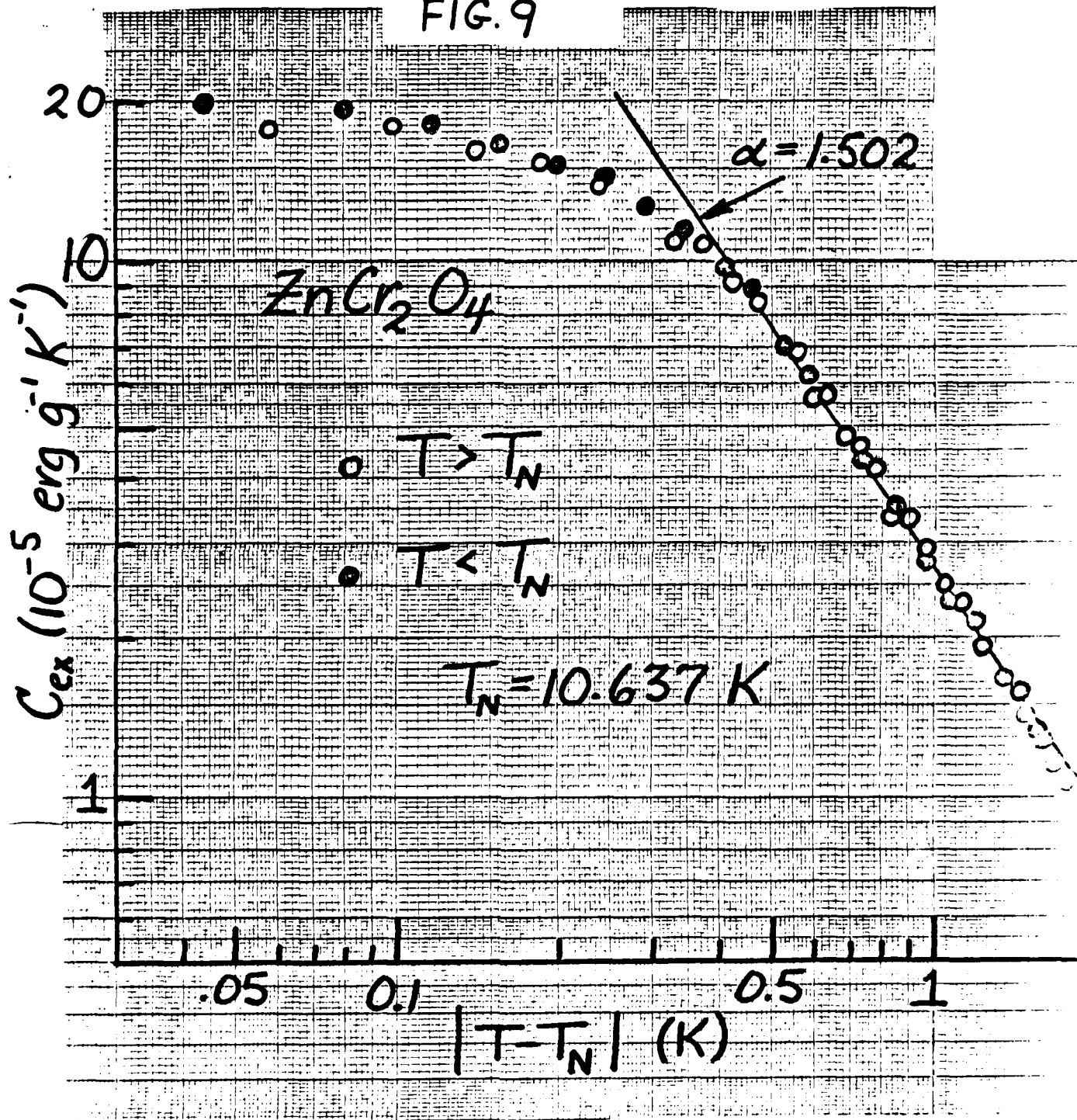


FIG. 9



PROGRESS REPORT

AFOSR Contract #F49620-83-C0129

Fundamental Physics Studies on High-Specific-Heat  
Dielectrics and Kapitza Resistance at Dielectric Boundaries

Spinel Studies VII. Magnetocaloric Effects

by

W.N. Lawless *WNL*

CeramPhysics, Inc.

Westerville, Ohio 43081

May 18, 1984

Distribution:

J.H. Parker, Jr.  
~~P.W.~~ Eckels  
T.K. Gupta  
M. Ashkin  
C.F. Clark  
B.R. Patton

## I. INTRODUCTION

In previous reports in this sequence, broad-range specific heat data on the two-phase ceramics C(9/1) and D(9/1) have been measured and analyzed. The analyses have focused on the dominant spinel phases,  $\text{CdCr}_2\text{O}_4$  and  $\text{ZnCr}_2\text{O}_4$ , respectively, which exhibit enormous specific heat maxima at 8 and 10.5 K. The specific heat analyses gave strong evidence for antiferrimagnetic phase transitions of lower than first order.

A critical test of this finding is to measure magnetocaloric effects well below the transition temperature: for an antiferrimagnet, one expects adiabatic-magnetization cooling and adiabatic-demagnetization heating. This report documents magnetocaloric measurements on these materials in the range 3-5 K and some analyses of these data along phenomenological lines, together with conclusions.

## II. EXPERIMENTAL METHODS AND RESULTS

The same ceramic samples of C(9/1) and D(9/1) were fixtured for the magnetocaloric measurements [performed at the National Magnet Lab (MIT)]. Carbon-chip thermometers were embedded in grooves in the two samples, and the samples were suspended from the reservoir on long time-constant thermal links ( $\tau = 10$  min. at  $\sim 4$  K). The Bitter magnet was ramped to and from fields  $< 10$  T in times  $< 30$  s, and since  $\Delta t/2\tau < 10^{-2}$ , the experiments were essentially adiabatic. The carbon thermometers were measured by the standard four-lead, d.c. - potentiometric method, and the magnetoresistance of the thermometers was taken into account using a CeramPhysics correction procedure.

The voltage output from the thermometer ( $\sim 30$  mV) was bucked using a battery-driven potentiometer ( $\sim 28$  mV), and the residual signal

(  
(~ 2 mV) was displayed on a calibrated strip-chart recorder. As the field was ramped 0 → H → 0, the corresponding changes in the thermometer voltage were measured on the chart recorder and subsequently converted to temperature changes. At higher H-fields, proportionally larger changes were recorded on the chart recorder (i.e., the bucking voltage was reduced and larger chart scales were used).

The experiments here were done at two fixed reservoir temperatures: 4.3 and 3.0 K. The former case corresponds to liquid-helium immersion, the latter case to pumping on the helium bath through a manostat. These conditions were chosen to avoid electronically controlling the reservoir temperature which is somewhat more difficult (but certainly possible for future measurements).

The temperature changes  $\Delta T$  were computed for both up-ramps (0 → H) and down-ramps (H → 0) for about 20 H-fields up to 10 T. Both samples at both temperatures displayed magnetization heating and demagnetization cooling.

There are two considerations in handling the  $\Delta T$ -data: (1) The addenda, and (2) The irreversible or hysteretic component. These were handled as follows:

The temperature change of the sample (i.e., the spinel CdCr<sub>2</sub>O<sub>4</sub>, for example), is given by

$$\Delta T_{\text{sample}} = \Delta T_{\text{meas}} (1 + C_a/C_s) \quad (1)$$

where  $C_a$  and  $C_s$  are the heat capacities of the addenda and of the sample, respectively. In this case, the columbite phase (e.g., CdNb<sub>2</sub>O<sub>6</sub>) is also included in the addenda. From our previous studies, the

columbite heat capacity is  $\sim 0.02\%$  of the spinel heat capacity, and the remaining addenda (thermometer, wires, varnish, etc.) constitute  $< 0.5\%$ . Therefore, the measured temperature changes are practically identical to the temperature changes of the spinel phase.

The temperature change has two components: the reversible part,  $\Delta T_{\text{rev}}$ , and the irreversible part,  $\Delta T_{\text{irrev}}$ , where  $\Delta T_{\text{rev}}$  depends on the sign of  $\Delta H$  whereas  $\Delta T_{\text{irrev}}$  does not. Therefore, the difference in the  $\Delta T$ 's for up and down ramps provides a measure of  $\Delta T_{\text{irrev}}$ , which then allows a determination of  $\Delta T_{\text{rev}}$ .

For both  $\text{CdCr}_2\text{O}_4$  and  $\text{ZnCr}_2\text{O}_4$ , the irreversible component was  $< 2\%$  of the reversible component and often  $\sim 0.2\%$ . Although  $\Delta T_{\text{irrev}}$  was always positive, there was no apparent scaling with  $H$  for either spinel, as expected if truly hysteretic behavior were involved. This small asymmetry may be inherent in the measurement since the sample temperature at the end of the down ramp did not return exactly to the value at the beginning of the up ramp (due to some decay in the temperature at full field while data were recorded).

For both spinels at both temperatures, the  $\Delta T$ 's were reproducible and were not influenced by the sample having seen much larger  $H$ -fields. The reversible temperature changes,  $\Delta T_{\text{rev}}$ , for the  $\text{CdCr}_2\text{O}_4$  and  $\text{ZnCr}_2\text{O}_4$  spinels are shown in Figs. 1 and 2, respectively. The average temperatures shown are the mean temperatures for all the events shown. For example, for  $\text{CdCr}_2\text{O}_4$  at 3.15 K, the average temperatures per event ranged from 2.83 K (at 0.8 T) to 3.39 K (at 9.2 T).

The fixturing of the samples for the magnetocaloric measurements lent itself to specific-heat measurements in intense magnetic fields by the drift method. In this technique, the reservoir is stabilized at

~ 2 K and the sample heater is used to bring the sample to ~ 6 K. The heater is then deactivated, and as the sample slowly drifts in temperature down to the reservoir temperature, the drift rate  $dT/dt$  is automatically monitored using a computerized data acquisition system.

Specific heat data as a function of magnetic field for  $\text{CdCr}_2\text{O}_4$  at 3.15 and 4.46 K (i.e., the average temperatures in Fig. 1) are shown in Fig. 3. The corresponding data for  $\text{ZnCr}_2\text{O}_4$  are shown in Fig. 4. These data are disappointing for a fundamental thermodynamic reason: The demagnetization-cooling data in Figs. 1 and 2 demand that the specific heat decrease in an intense magnetic field, yet this requirement is not obvious in Figs. 3 and 4. These results cast some doubt on our specific heat method. Nonetheless, it is clear that the effect of an intense magnetic on the specific heats of these spinels is relatively small since the method would certainly reveal gross effects.

The magnetizations of samples of C(9/1) and D(9/1) at 4.2 K were measured at the Westinghouse R&D Center, and the magnetization per unit mass of spinel is shown in Fig. 5 for the  $\text{CdCr}_2\text{O}_4$  and  $\text{ZnCr}_2\text{O}_4$  spinels. Here surprising results were obtained: both spinels are linear magnetic materials,  $M \propto H$  up to large fields (6.6 T).

### III. DISCUSSION

The thermodynamic relations can be sketched for these spinels, starting with the TdS equation

$$TdS = mC_H dT + \mu_0 m T (\partial M / \partial T)_H dH \quad (1)$$

where  $M$  is the magnetization per unit mass. The data in Fig. 5 show that the materials behave as linear paramagnets at 4.2 K.

$$M = kf(T)H \quad (2)$$

where  $k$  is a constant (see below) and the  $T$ -dependence is contained in  $f(T)$  [e.g., for a Curie material,  $f(T) \propto T^{-1}$ ]. The Fig. 5 data allow the convenient separation of the  $T$  and  $H$  variables given in Eq. (2).

Writing

$$C_H(T) = C_0(T)/g(H) \quad (3)$$

allows an integral separation of Eq. (1) under adiabatic conditions,

$$\int_{T_i}^{T_f} \frac{C_0 dT}{T f'(T)} = -\mu_0 k \int_{H_i}^{H_f} g(H) H dH \quad (4)$$

where  $f' = df/dT$ . Thus, in principle, the adiabatic magnetization/demagnetization data in Figs. 1 and 2 and the magnetization data in Fig. 5 can be correlated according to Eq. (4).

Several numerical attempts were made to solve Eq. (4) using the experimental data [e.g., by setting  $g(H) = 1$  and  $f(T) \propto T^n$ ], but these attempts led to inclusive results.

The following approach was therefore taken: The specific heat data in Figs. 3 and 4 suggest that  $g(H) = 1$  in Eq. (3), so that the differential form of Eq. (1) becomes

$$C_0 dT = -T k f' H dH \quad (5)$$

where  $\mu_0$  has been set equal to unity. If  $f(T)$  at 4.2 K is set equal to unity, then  $k$  can be evaluated directly from Fig. 5 for  $\text{CdCr}_2\text{O}_4$  ( $k = 1.40 \text{ emu g}^{-1} \text{ T}^{-1}$ ) and for  $\text{ZnCr}_2\text{O}_4$  ( $k = 0.521$ ).

Now, the  $\Delta T_{\text{rev}}$  data in Figs. 1 and 2 yield a set of  $T_f$  vs.  $H$  data, since  $T_i$  is essentially constant for each data set, and these data yield  $f'(T)$  from Eq. (5) using the previously reported  $C_0(T)$  data. That is, in each interval  $T_f = T_i + \Delta T_{\text{rev}}$  corresponding to  $\Delta H$  in Figs. 1 and 2,  $f'$  can be determined at the mean temperature of that interval using the appropriate  $C_0$  specific heat at that mean temperature. The  $f'(T)$  data determined in this fashion for both  $\text{CdCr}_2\text{O}_4$  and  $\text{ZnCr}_2\text{O}_4$  are shown in Fig. 6.

In judging the  $f'(T)$  data in Fig. 6, it must be realized that a great deal of experimental data were employed in arriving at these results (i.e., the mag/demag data in Figs. 1 and 2, the magnetization data in Fig. 5, and the specific heat data in Figs. 3 and 4 and reported previously). Moreover, in writing Eq. (2) we have assumed that  $f'(T)$  is the same for both  $\text{CdCr}_2\text{O}_4$  and  $\text{ZnCr}_2\text{O}_4$ .

The Fig. 6 data show three features: (1)  $f'(T)$  is approximately the same for both spinels; (2)  $f'(T)$  displays an extremely strong  $T$ -dependence, as illustrated in Fig. 6; and (3)  $f'(T)$  shows a strong discontinuity between the two temperature ranges in Fig. 6. This extreme discontinuity is relatively insensitive to assumptions made regarding  $g(H)$  in Eq. (3).

#### IV. CONCLUSIONS

The data presented here add to the mystery surrounding the physics of these spinels. First, both spinels have undergone transitions at

higher temperatures (8.0 and 10.5 for  $\text{CdCr}_2\text{O}_4$  and  $\text{ZnCr}_2\text{O}_4$ , respectively), and enormous specific heat maxima are associated with these transitions, suggesting that few degrees of freedom remain below these temperatures. Yet, at temperatures  $\sim 1/2 - 1/3$  of these transition temperatures, substantial degrees of freedom are available as evidenced by the magnetization/demagnetization temperature changes in Figs. 1 and 2.

Note in this regard that at 3-5 K the specific heats of these spinels are still very large, which limits the  $\Delta T$ 's by Eq. (5). For example, if these specific heats were on the order of magnitude of metallic Pb (which is still very large), the temperature drops would be  $\sim 100\%$  (i.e., to about absolute zero).

We had previously concluded for both of these spinels from analyses of specific heat data that antiferromagnetic transitions had occurred at 8.0 and 10.5 K. The evidence here was as follows: Debye temperatures determined at higher temperatures (20-40 K) were consistent with predictions from the Lindemann relation, and these Debye temperatures strongly indicated the presence of antiferromagnetic spin waves below  $\sim 5$  K. Yet, as mentioned above, if antiferromagnetic states were involved, magnetization cooling and demagnetization heating would have been observed, rather than the opposite as has been observed.

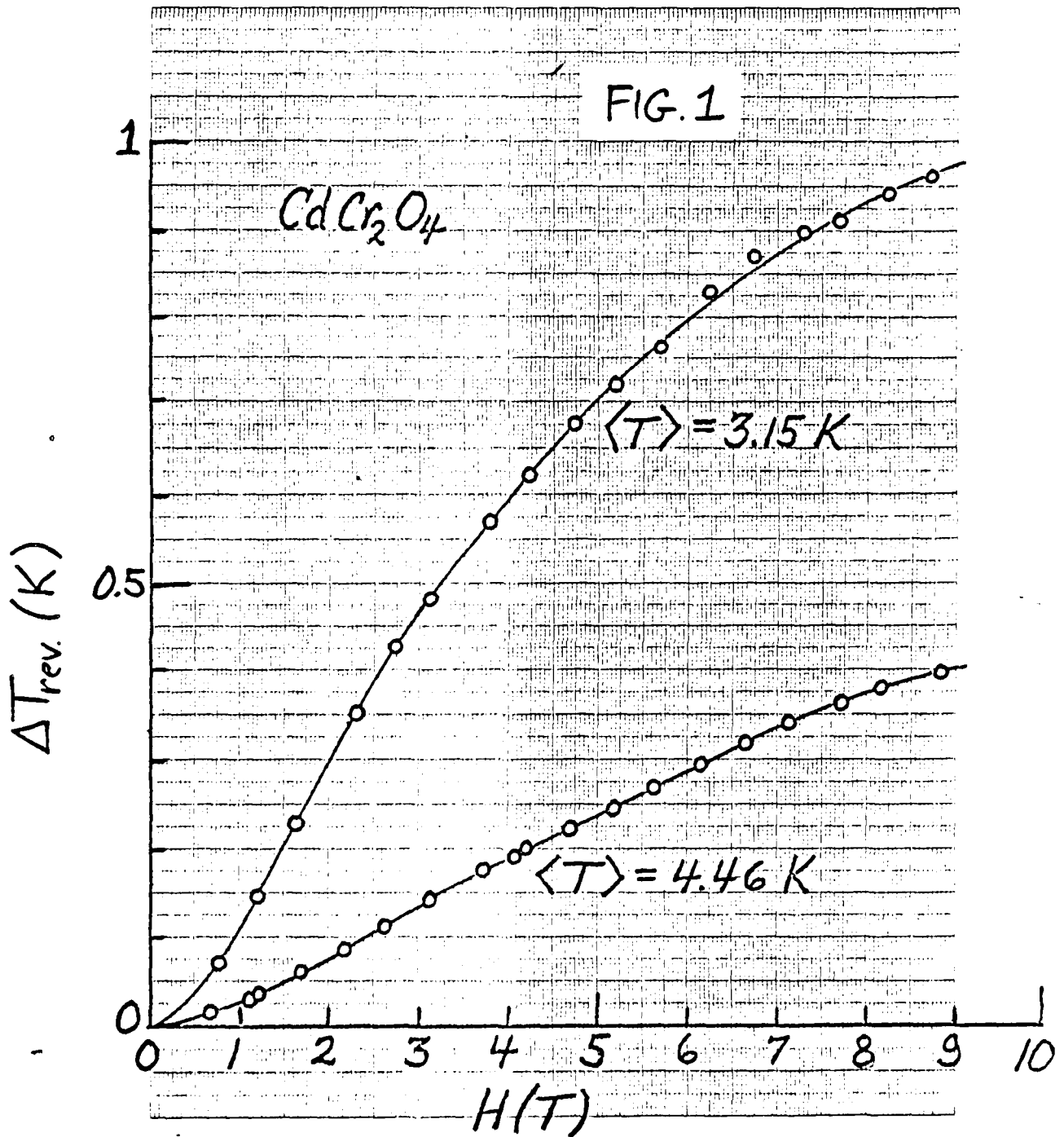
At 3-5 K, these spinels act as paramagnetics, as if the higher temperature transitions had not occurred: (1) The spinels are linear paramagnets with no evidence of hysteresis effects either in the M-H behavior (Fig. 5) or in the magnetization/demagnetization data (Figs. 1,2); and (2) The spinels display large, classic adiabatic-demagnetization cooling effects.

Our approach is, by necessity, an experimental approach, and it is clear that the next step is to sharpen the specific-heat data. Clearly, knowing  $g(H)$  in Eq. (3) would allow a closed-form solution of Eq. (4). The "noise" in the specific heat data can be reduced/eliminated by employing the following techniques: (1) Copper-wire thermal links have been employed, which require a magnetothermal resistance correction; using manganin thermal links would eliminate the correction factor but would require longer experimental times; (2) Using capacitance thermometry would eliminate the magnetoresistance correction for the carbon-chip thermometers, but only one sample at a time could be measured due to the unavoidable "cross-talk" noise between transformer-ratio-arm bridges; and (3) If small temperature ranges were focused on (e.g., 2-4 K), experimental accuracy would be greatly improved because thermometry calibrations would be simplified and scale changes would be avoided.

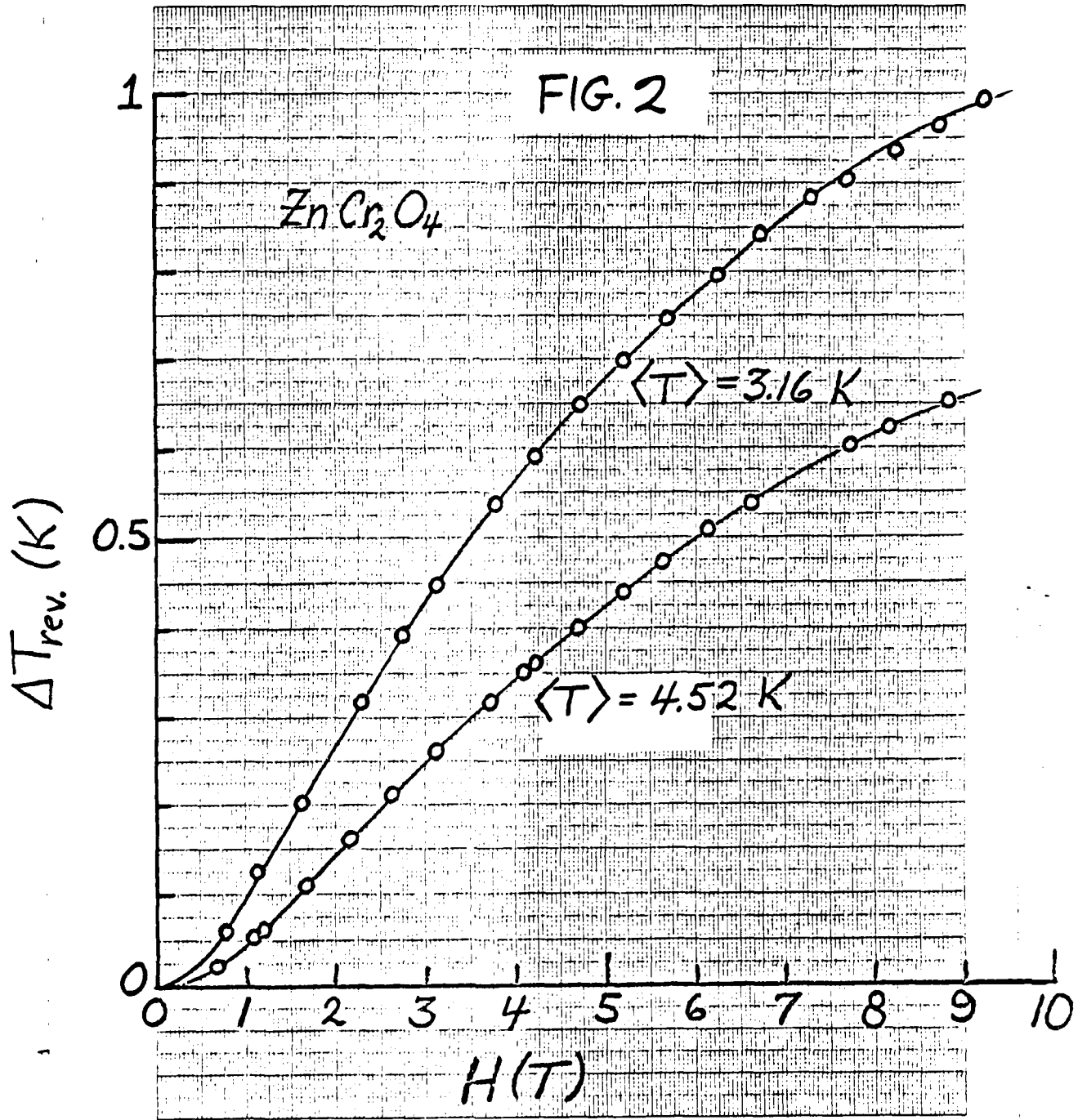
Nonetheless, it is doubtful if these minor experimental modifications will have much effect on the qualitative results in Fig. 6. Namely,  $f(T) \propto T^{-n}$  where  $11 < n < 27$ . This state-function temperature dependence is difficult to resolve in view of existing theories. Clearly, M-H magnetization data for a series of temperatures are needed to resolve these findings, since from Eq. (2)  $f(T)$  is found directly from magnetization data.

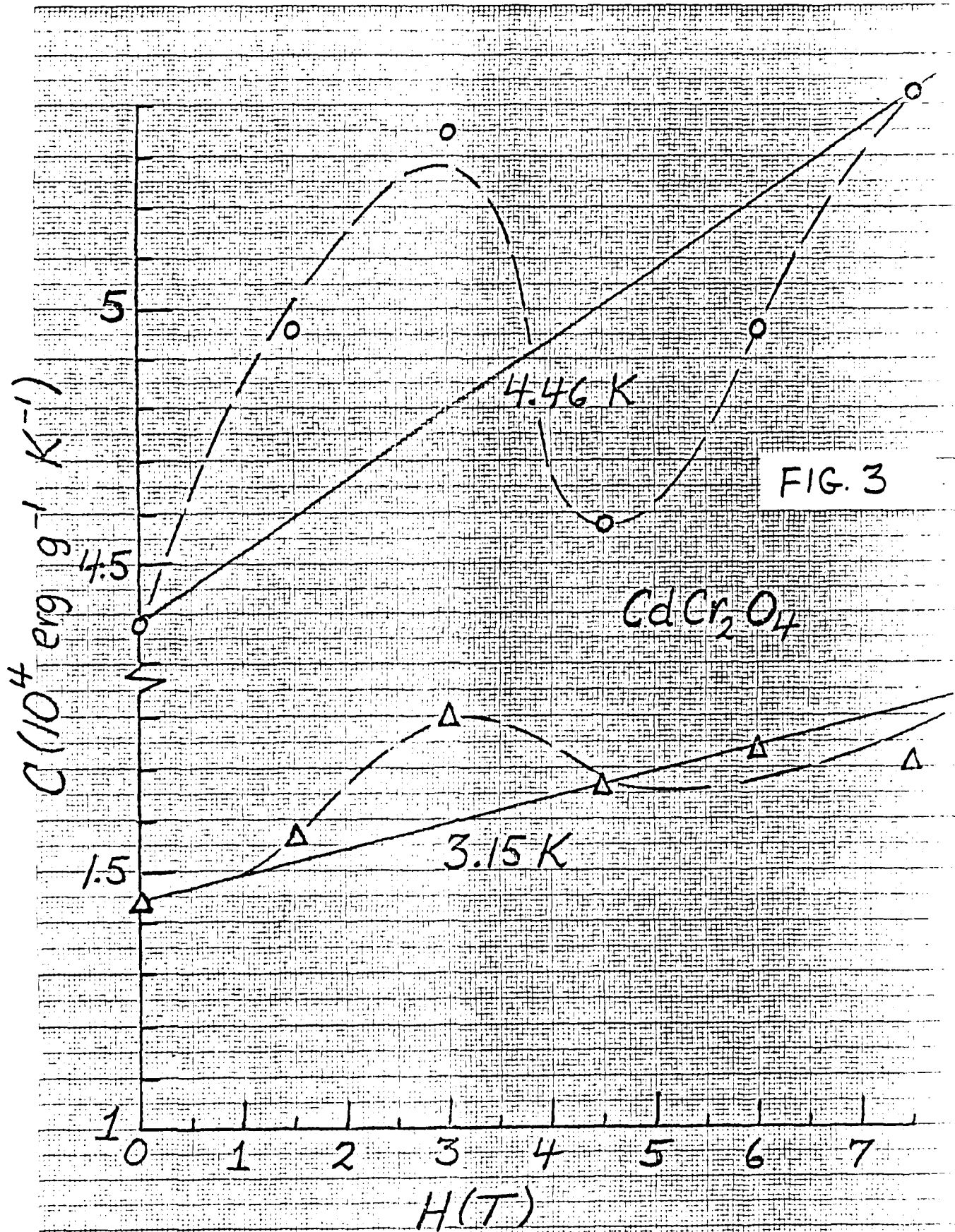
$\langle T \rangle = 3.15 \text{ K}$

FIG. 1



0 3.16





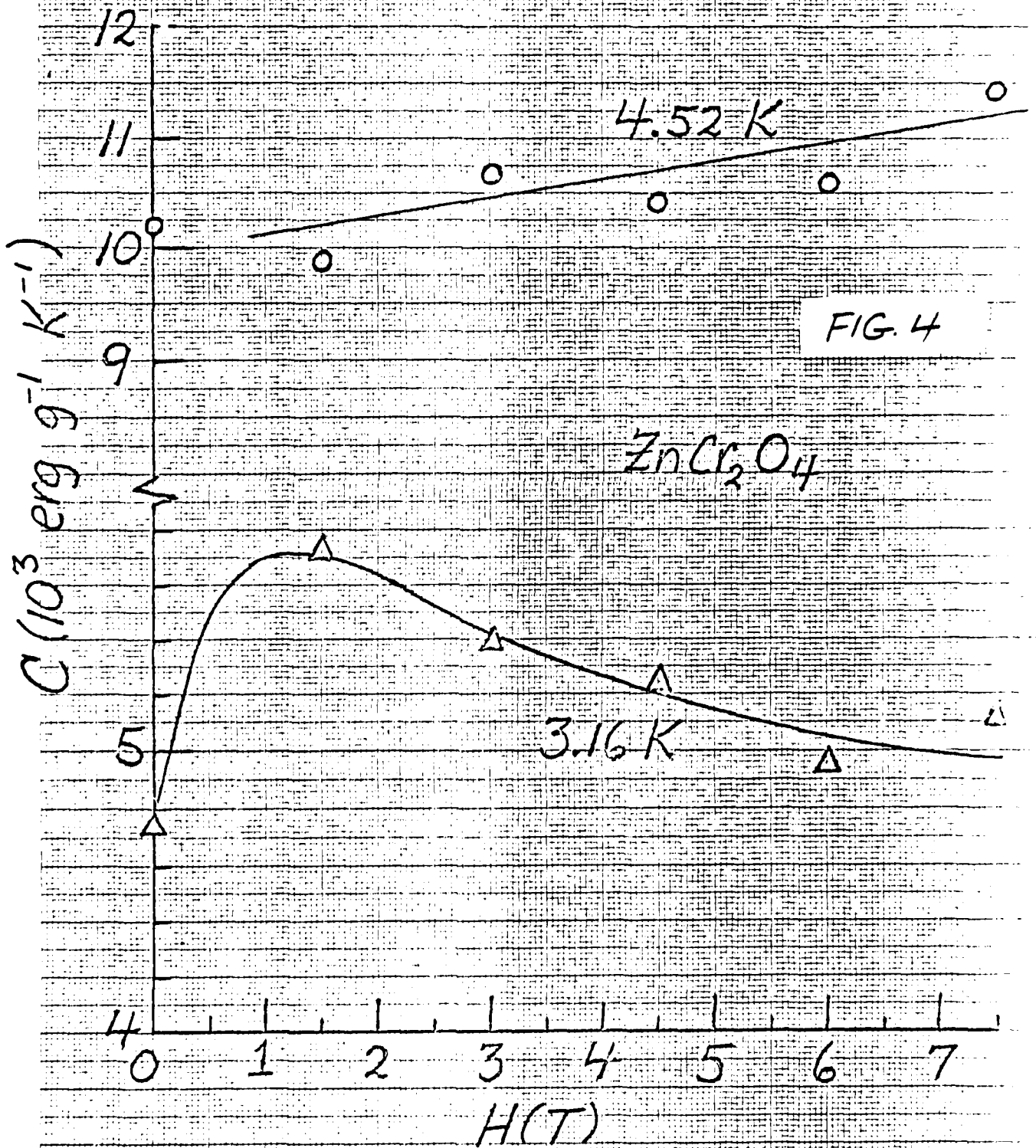
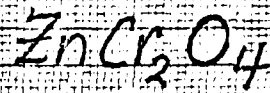
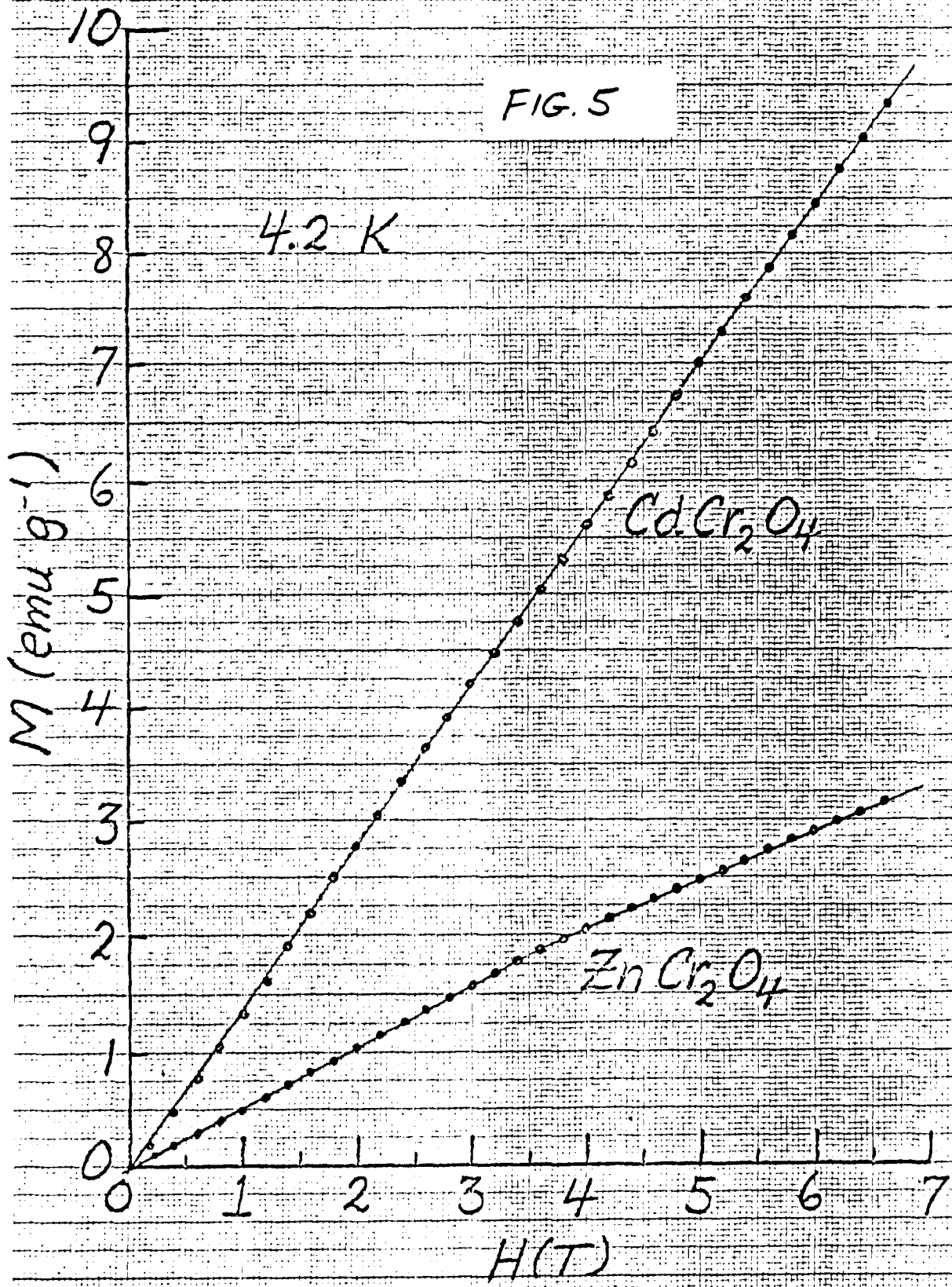
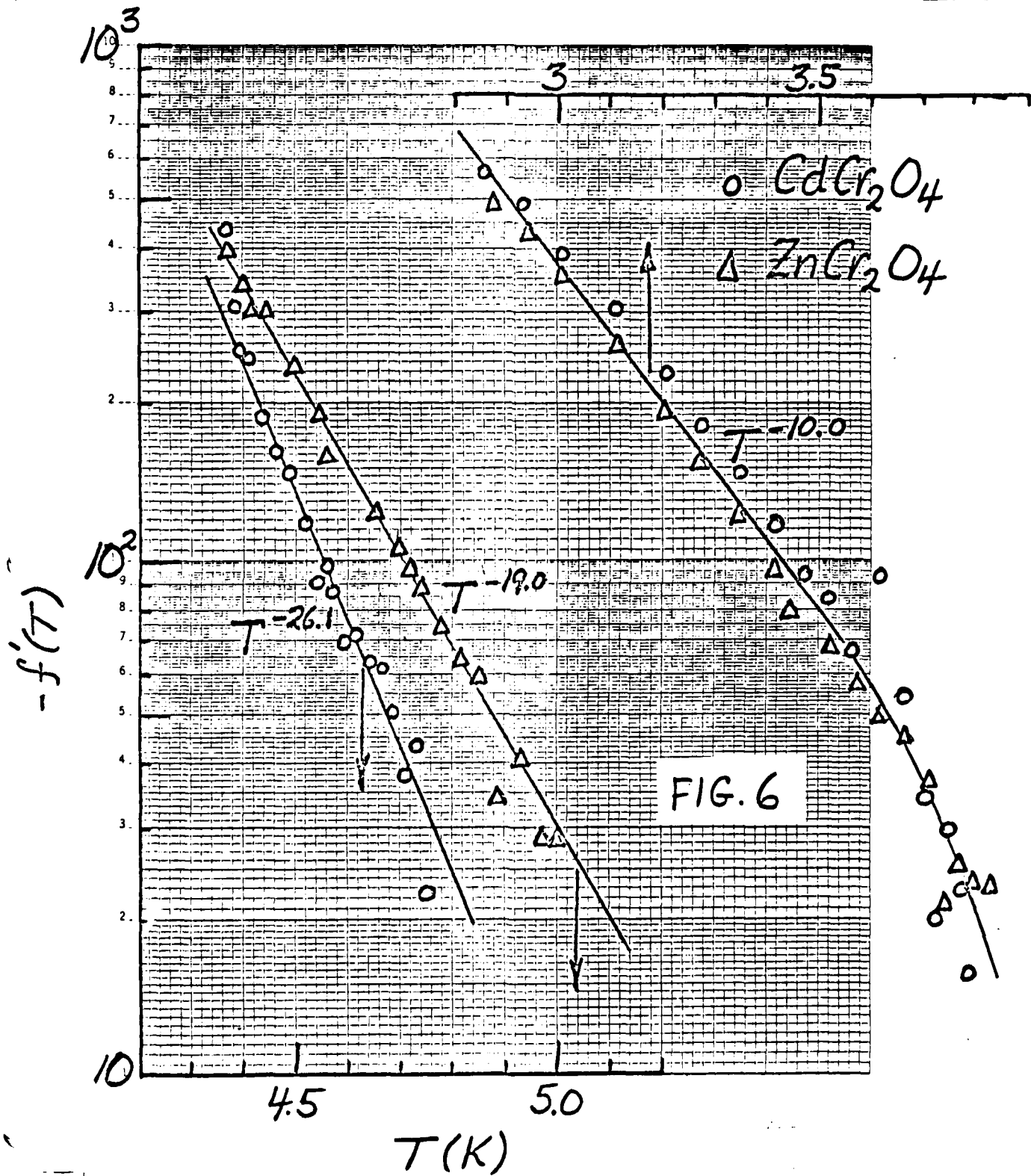


FIG. 4







Progress Report

AFOSR Contract #F49620-83-C0129

Fundamental Physics Studies on High-Specific-Heat  
Dielectrics and Kapitza Resistance at Dielectric Boundaries

Spinel Studies VIII. Thermal Conductivities in  
Intense Magnetic Fields

by

W.N. Lawless *WNL*  
CeramPhysics, Inc.  
Westerville, Ohio 43081

May 7, 1984

Distribution:

J.H. Parker, Jr.

~~P.W. Eckels~~

T.K. Gupta

M. Ashkin

C.F. Clark

B.R. Patton

In the first report in this series (Spinal Studies, I. Broad Temperature Range Thermal Measurements, Sept. 2, 1983), thermal conductivity measurements from 2-30 K were reported on the two-phase ceramics C(9/1) and D(9/1). The major phases in these materials are the spinels  $\text{CdCr}_2\text{O}_4$  and  $\text{ZnCr}_2\text{O}_4$ , respectively.

These thermal conductivity data are shown here in Fig. 1, and the major features are the maxima in K at 6.2 and 10.0 K in the  $\text{CdCr}_2\text{O}_4$  and  $\text{ZnCr}_2\text{O}_4$  spinels, respectively. The arrows in Fig. 1 indicate the transition temperatures (i.e., specific heat maxima). The tentative explanation put forward was that the excess thermal conductivity is associated with the magnetically ordered state.

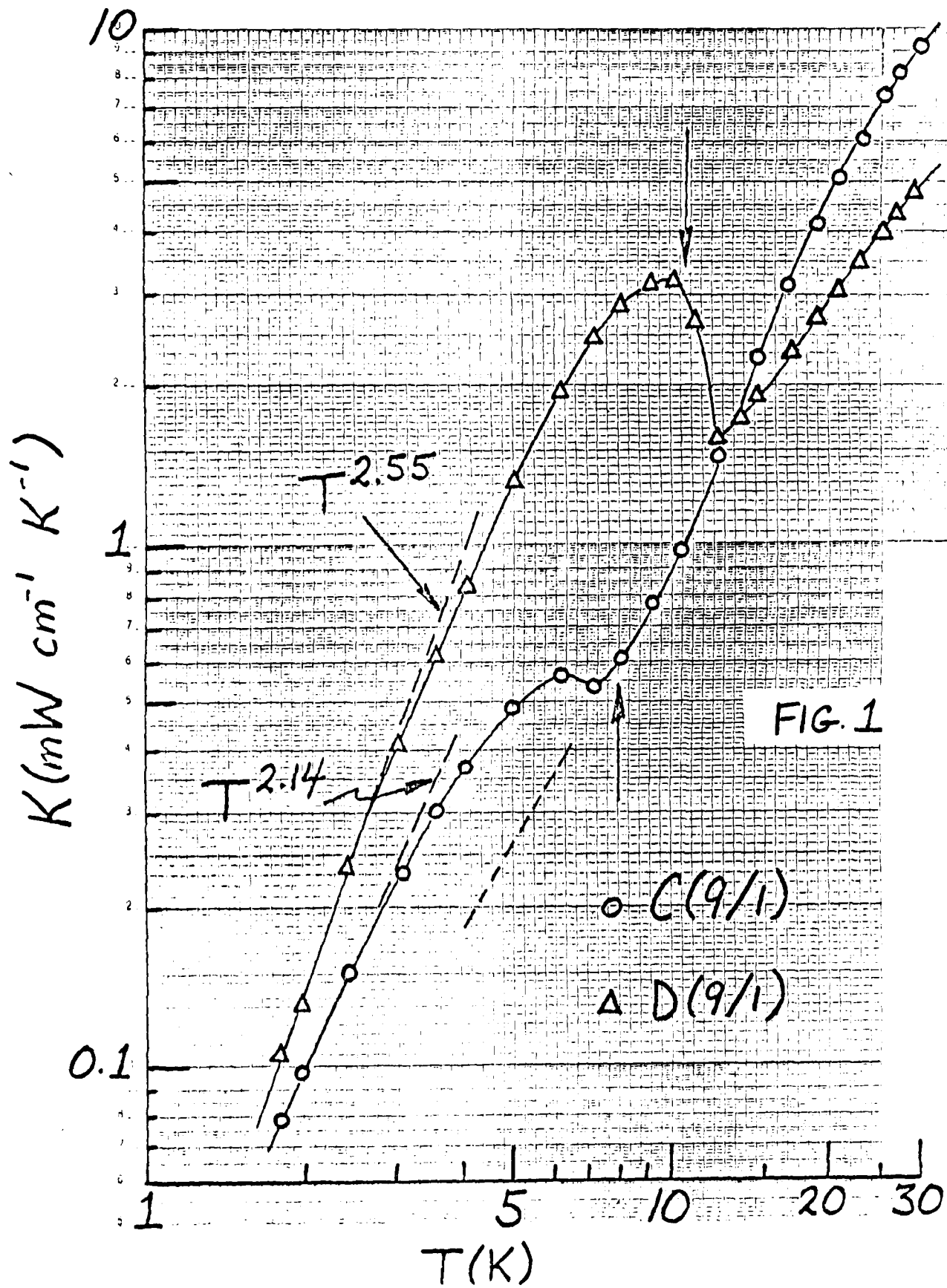
Pursuing this suggestion further, the magnetic-field dependence of this excess thermal conductivity was measured at the National Magnet Laboratory on the same samples used in the Fig. 1 measurements. The "two-heater, one-thermometer" method was employed which has the advantage that only one thermometer calibration is involved. Carbon-chip thermometers were attached to the free ends of the samples and were calibrated in situ at zero field against a calibrated Ge thermometer. The magnetoresistance of the thermometers was carefully taken into account, and both the heaters and thermometer leads were wrapped bifilarly on the samples. Four-lead, d.c. potentiometric methods were used to measure the thermometers.

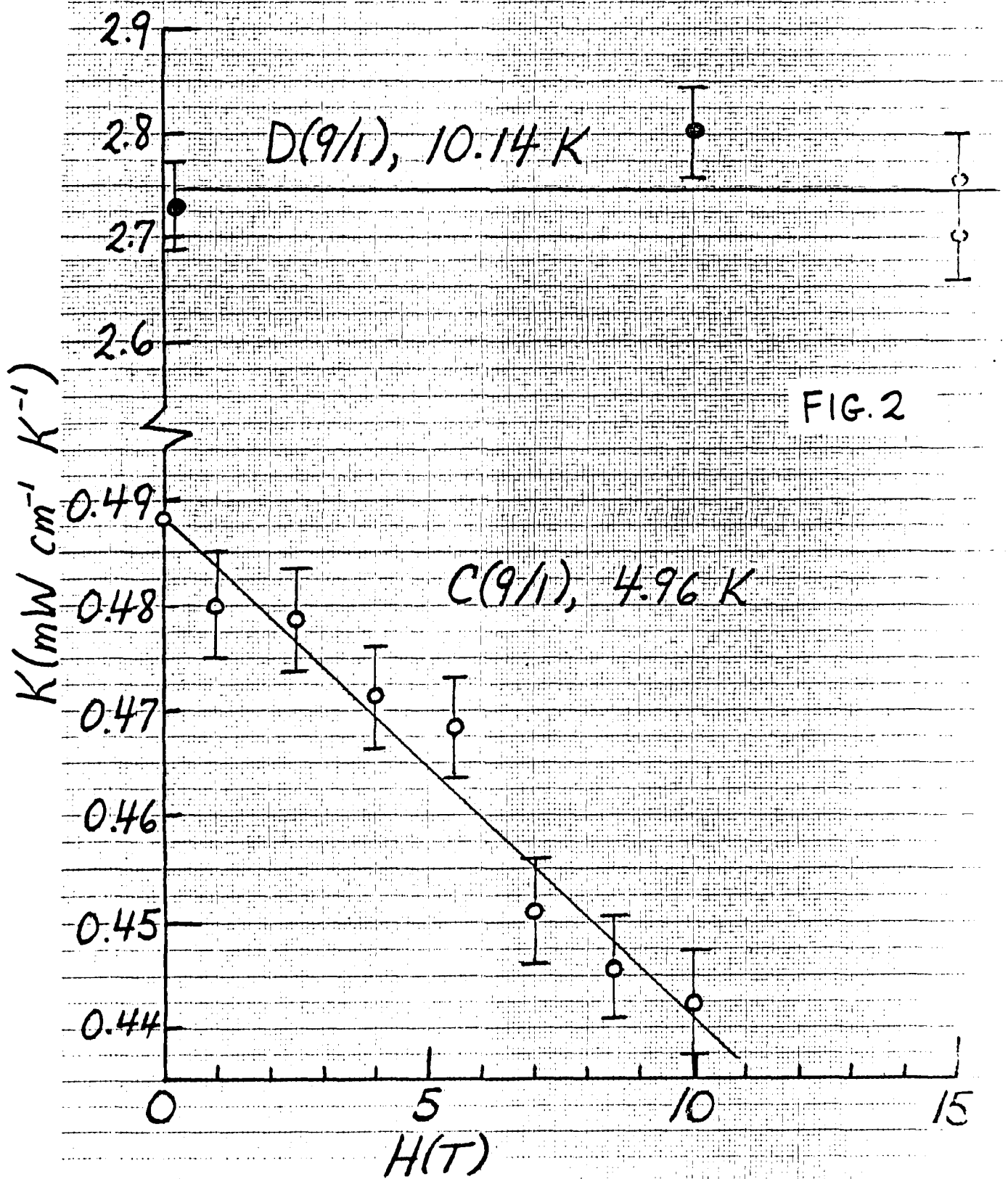
To examine the excess thermal conductivities in the  $\text{CdCr}_2\text{O}_4$  and  $\text{ZnCr}_2\text{O}_4$  spinels, thermal conductivity measurements in intense fields were performed at temperatures at, or slightly below, the temperatures of the maxima in K in Fig. 1. These data are shown in Fig. 2 where the  $\text{ZnCr}_2\text{O}_4$  was measured at 10.1 K, the  $\text{CdCr}_2\text{O}_4$  spinel at 5.0 K. The difference in the zero-field data between Figs. 1 and 2 ( $\sim \pm 10\%$ ) is due to the uncertainty in the  $A/\lambda$  ratio ( $\sim \pm 5\%$  for each set).

The thermal conductivity of  $\text{ZnCr}_2\text{O}_4$  is apparently insensitive to H-fields, and the average value is plotted in Fig. 2. By contrast, the K of  $\text{CdCr}_2\text{O}_4$  is linearly suppressed by a magnetic field, and the least-squares fit is shown in Fig. 2, according to which  $(\partial K/\partial H)_T = -4.73 \times 10^{-3} \text{ mW cm}^{-1} \text{ K}^{-1}$  (i.e.,  $(\partial \ln K/\partial H)_T = -1.02\% \text{ T}^{-1}$ ).

Experimental circumstances unfortunately preventing measuring more data on the  $\text{ZnCr}_2\text{O}_4$  spinel, but the existing data to 15 T definitely indicate a very minor, or non-existent, H-field dependence. For example, if  $\text{ZnCr}_2\text{O}_4$ , had the same relative dependence,  $\partial \ln K/\partial H$ , as  $\text{CdCr}_2\text{O}_4$ , then K would be suppressed from 2.75 to 2.35  $\text{mW cm}^{-1} \text{ K}^{-1}$  between 0 and 15 T (compare with Fig. 2).

The suppression of K with intense fields for  $\text{CdCr}_2\text{O}_4$  supports the suggestion that the excess thermal conductivity below the transition temperature is magnetic in origin. The picture then is that the thermal conductivity would follow the dashed line in Fig. 1 for  $\text{CdCr}_2\text{O}_4$  if no transition has occurred. From the dashed curve, the thermal conductivity at 5 K is  $\approx 0.26 \text{ mW cm}^{-1} \text{ K}^{-1}$ , so the excess thermal conductivity is  $\approx 0.23 \text{ mW cm}^{-1} \text{ K}^{-1}$ . From the slope of the K-H plot in Fig. 2, it is estimated that a field of  $\approx 50 \text{ T}$  would be required to "quench" this excess thermal conductivity in  $\text{CdCr}_2\text{O}_4$ .





columbite heat capacity is  $\sim 0.02\%$  of the spinel heat capacity, and the remaining addenda (thermometer, wires, varnish, etc.) constitute  $< 0.5\%$ . Therefore, the measured temperature changes are practically identical to the temperature changes of the spinel phase.

The temperature change has two components: the reversible part,  $\Delta T_{rev}$ , and the irreversible part,  $\Delta T_{irrev}$ , where  $\Delta T_{rev}$  depends on the sign of  $\Delta H$  whereas  $\Delta T_{irrev}$  does not. Therefore, the difference in the  $\Delta T$ 's for up and down ramps provides a measure of  $\Delta T_{irrev}$ , which then allows a determination of  $\Delta T_{rev}$ .

For both  $CdCr_2O_4$  and  $ZnCr_2O_4$ , the irreversible component was  $< 2\%$  of the reversible component and often  $\sim 0.2\%$ . Although  $\Delta T_{irrev}$  was always positive, there was no apparent scaling with  $H$  for either spinel, as expected if truly hysteretic behavior were involved. This small asymmetry may be inherent in the measurement since the sample temperature at the end of the down ramp did not return exactly to the value at the beginning of the up ramp (due to some decay in the temperature at full field while data were recorded).

For both spinels at both temperatures, the  $\Delta T$ 's were reproducible and were not influenced by the sample having seen much larger  $H$ -fields. The reversible temperature changes,  $\Delta T_{rev}$ , for the  $CdCr_2O_4$  and  $ZnCr_2O_4$  spinels are shown in Figs. 1 and 2, respectively. The average temperatures shown are the mean temperatures for all the events shown. For example, for  $CdCr_2O_4$  at 3.15 K, the average temperatures per event ranged from 2.83 K (at 0.8 T) to 3.39 K (at 9.2 T).

The fixturing of the samples for the magnetocaloric measurements lent itself to specific-heat measurements in intense magnetic fields by the drift method. In this technique, the reservoir is stabilized at

~ 2 K and the sample heater is used to bring the sample to ~ 6 K. The heater is then deactivated, and as the sample slowly drifts in temperature down to the reservoir temperature, the drift rate  $dT/dt$  is automatically monitored using a computerized data acquisition system.

Specific heat data as a function of magnetic field for  $\text{CdCr}_2\text{O}_4$  at 3.15 and 4.46 K (i.e., the average temperatures in Fig. 1) are shown in Fig. 3. The corresponding data for  $\text{ZnCr}_2\text{O}_4$  are shown in Fig. 4. These data are disappointing for a fundamental thermodynamic reason: The demagnetization-cooling data in Figs. 1 and 2 demand that the specific heat decrease in an intense magnetic field, yet this requirement is not obvious in Figs. 3 and 4. These results cast some doubt on our specific heat method. Nonetheless, it is clear that the effect of an intense magnetic on the specific heats of these spinels is relatively small since the method would certainly reveal gross effects.

The magnetizations of samples of C(9/1) and D(9/1) at 4.2 K were measured at the Westinghouse R&D Center, and the magnetization per unit mass of spinel is shown in Fig. 5 for the  $\text{CdCr}_2\text{O}_4$  and  $\text{ZnCr}_2\text{O}_4$  spinels. Here surprising results were obtained: both spinels are linear magnetic materials,  $M \propto H$  up to large fields (6.6 T).

### III. DISCUSSION

The thermodynamic relations can be sketched for these spinels, starting with the  $TdS$  equation

$$TdS = mC_H dT + \frac{1}{\mu_0} mT \left( \frac{\partial M}{\partial T} \right)_H dH \quad (1)$$

where  $M$  is the magnetization per unit mass. The data in Fig. 5 show that the materials behave as linear paramagnets at 4.2 K.

$$M = kf(T)H \quad (2)$$

where  $k$  is a constant (see below) and the  $T$ -dependence is contained in  $f(T)$  [e.g., for a Curie material,  $f(T) \propto T^{-1}$ ]. The Fig. 5 data allow the convenient separation of the  $T$  and  $H$  variables given in Eq. (2).

Writing

$$C_H(T) = C_0(T)/g(H) \quad (3)$$

allows an integral separation of Eq. (1) under adiabatic conditions,

$$\int_{T_i}^{T_f} \frac{C_0 dT}{T f'(T)} = -\mu_0 k \int_{H_i}^{H_f} g(H) H dH \quad (4)$$

where  $f' = df/dT$ . Thus, in principle, the adiabatic magnetization/demagnetization data in Figs. 1 and 2 and the magnetization data in Fig. 5 can be correlated according to Eq. (4).

Several numerical attempts were made to solve Eq. (4) using the experimental data [e.g., by setting  $g(H) \approx 1$  and  $f(T) \propto T^n$ ], but these attempts led to inclusive results.

The following approach was therefore taken: The specific heat data in Figs. 3 and 4 suggest that  $g(H) \approx 1$  in Eq. (3), so that the differential form of Eq. (1) becomes

$$C_0 dT = -T k f'(T) dH \quad (5)$$

where  $\mu_0$  has been set equal to unity. If  $f(T)$  at 4.2 K is set equal to unity, then  $k$  can be evaluated directly from Fig. 5 for  $\text{CdCr}_2\text{O}_4$  ( $k = 1.40 \text{ emu g}^{-1} \text{ T}^{-1}$ ) and for  $\text{ZnCr}_2\text{O}_4$  ( $k = 0.521$ ).

Now, the  $\Delta T_{\text{rev}}$  data in Figs. 1 and 2 yield a set of  $T_f$  vs.  $H$  data, since  $T_i$  is essentially constant for each data set, and these data yield  $f'(T)$  from Eq. (5) using the previously reported  $C_0(T)$  data. That is, in each interval  $T_f = T_i + \Delta T_{\text{rev}}$  corresponding to  $\Delta H$  in Figs. 1 and 2,  $f'$  can be determined at the mean temperature of that interval using the appropriate  $C_0$  specific heat at that mean temperature. The  $f'(T)$  data determined in this fashion for both  $\text{CdCr}_2\text{O}_4$  and  $\text{ZnCr}_2\text{O}_4$  are shown in Fig. 6.

In judging the  $f'(T)$  data in Fig. 6, it must be realized that a great deal of experimental data were employed in arriving at these results (i.e., the mag/demag data in Figs. 1 and 2, the magnetization data in Fig. 5, and the specific heat data in Figs. 3 and 4 and reported previously). Moreover, in writing Eq. (2) we have assumed that  $f'(T)$  is the same for both  $\text{CdCr}_2\text{O}_4$  and  $\text{ZnCr}_2\text{O}_4$ .

The Fig. 6 data show three features: (1)  $f'(T)$  is approximately the same for both spinels; (2)  $f'(T)$  displays an extremely strong  $T$ -dependence, as illustrated in Fig. 6; and (3)  $f'(T)$  shows a strong discontinuity between the two temperature ranges in Fig. 6. This extreme discontinuity is relatively insensitive to assumptions made regarding  $g(H)$  in Eq. (3).

#### IV. CONCLUSIONS

The data presented here add to the mystery surrounding the physics of these spinels. First, both spinels have undergone transitions at

higher temperatures (8.0 and 10.5 for  $\text{CdCr}_2\text{O}_4$  and  $\text{ZnCr}_2\text{O}_4$ , respectively), and enormous specific heat maxima are associated with these transitions, suggesting that few degrees of freedom remain below these temperatures. Yet, at temperatures  $\sim 1/2 - 1/3$  of these transition temperatures, substantial degrees of freedom are available as evidenced by the magnetization/demagnetization temperature changes in Figs. 1 and 2.

Note in this regard that at 3-5 K the specific heats of these spinels are still very large, which limits the  $\Delta T$ 's by Eq. (5). For example, if these specific heats were on the order of magnitude of metallic Pb (which is still very large), the temperature drops would be  $\sim 100\%$  (i.e., to about absolute zero).

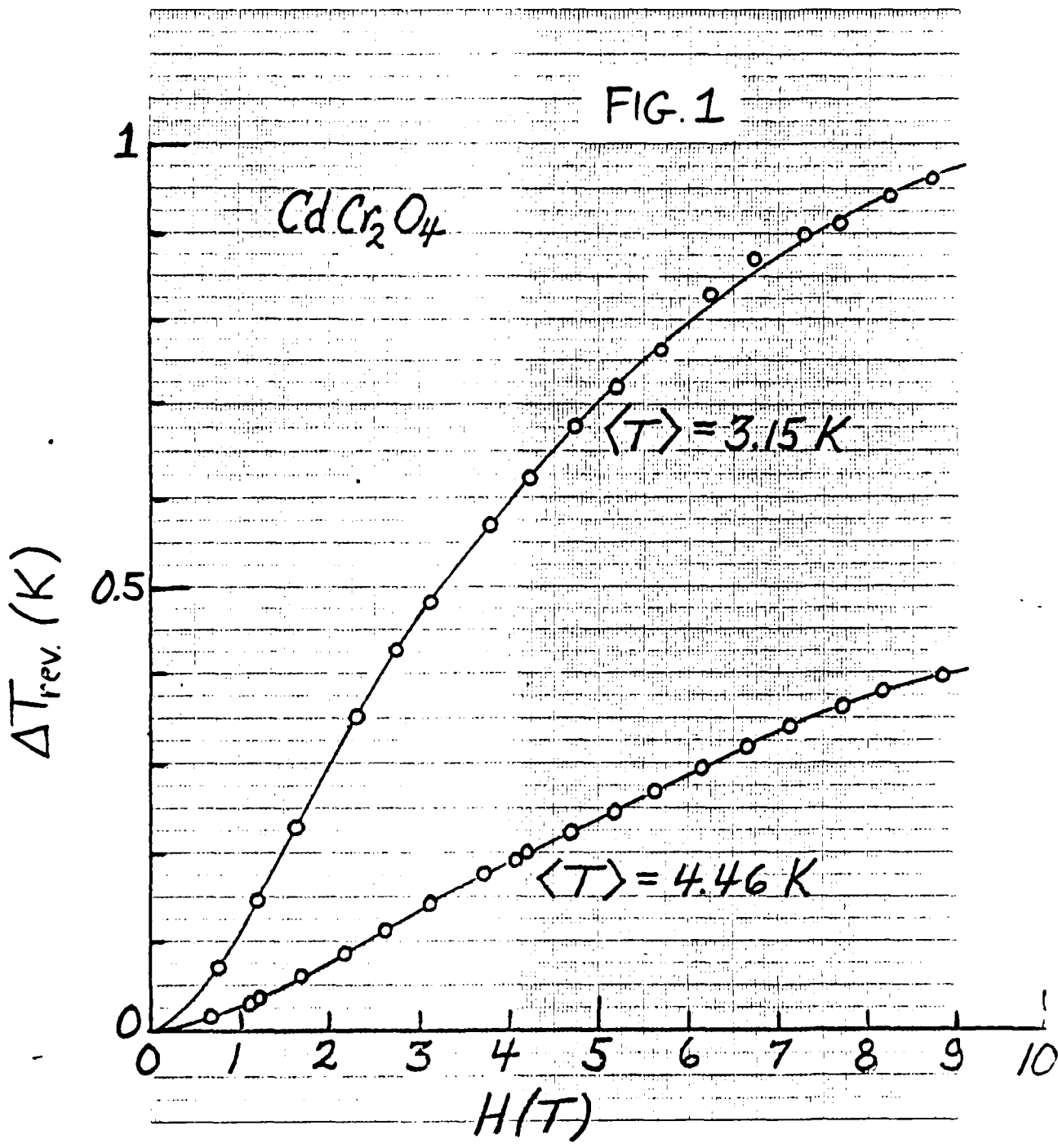
We had previously concluded for both of these spinels from analyses of specific heat data that antiferrimagnetic transitions had occurred at 8.0 and 10.5 K. The evidence here was as follows: Debye temperatures determined at higher temperatures (20-40 K) were consistent with predictions from the Lindemann relation, and these Debye temperatures strongly indicated the presence of antiferrimagnetic spin waves below  $\sim 5$  K. Yet, as mentioned above, if antiferrimagnetic states were involved, magnetization cooling and demagnetization heating would have been observed, rather than the opposite as has been observed.

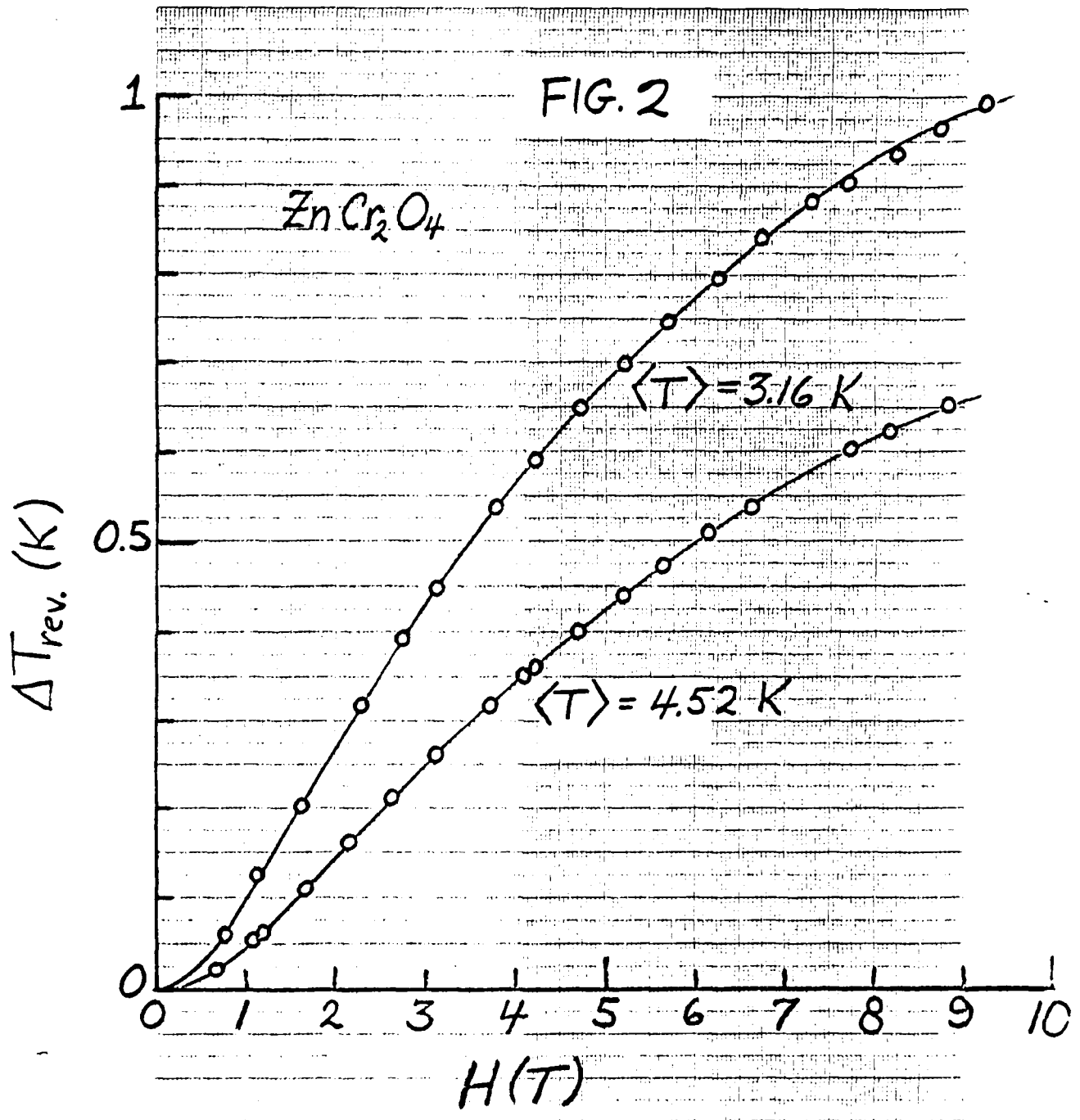
At 3-5 K, these spinels act as paramagnetics, as if the higher temperature transitions had not occurred: (1) The spinels are linear paramagnets with no evidence of hysteresis effects either in the M-H behavior (Fig. 5) or in the magnetization/demagnetization data (Figs. 1,2); and (2) The spinels display large, classic adiabatic-demagnetization cooling effects.

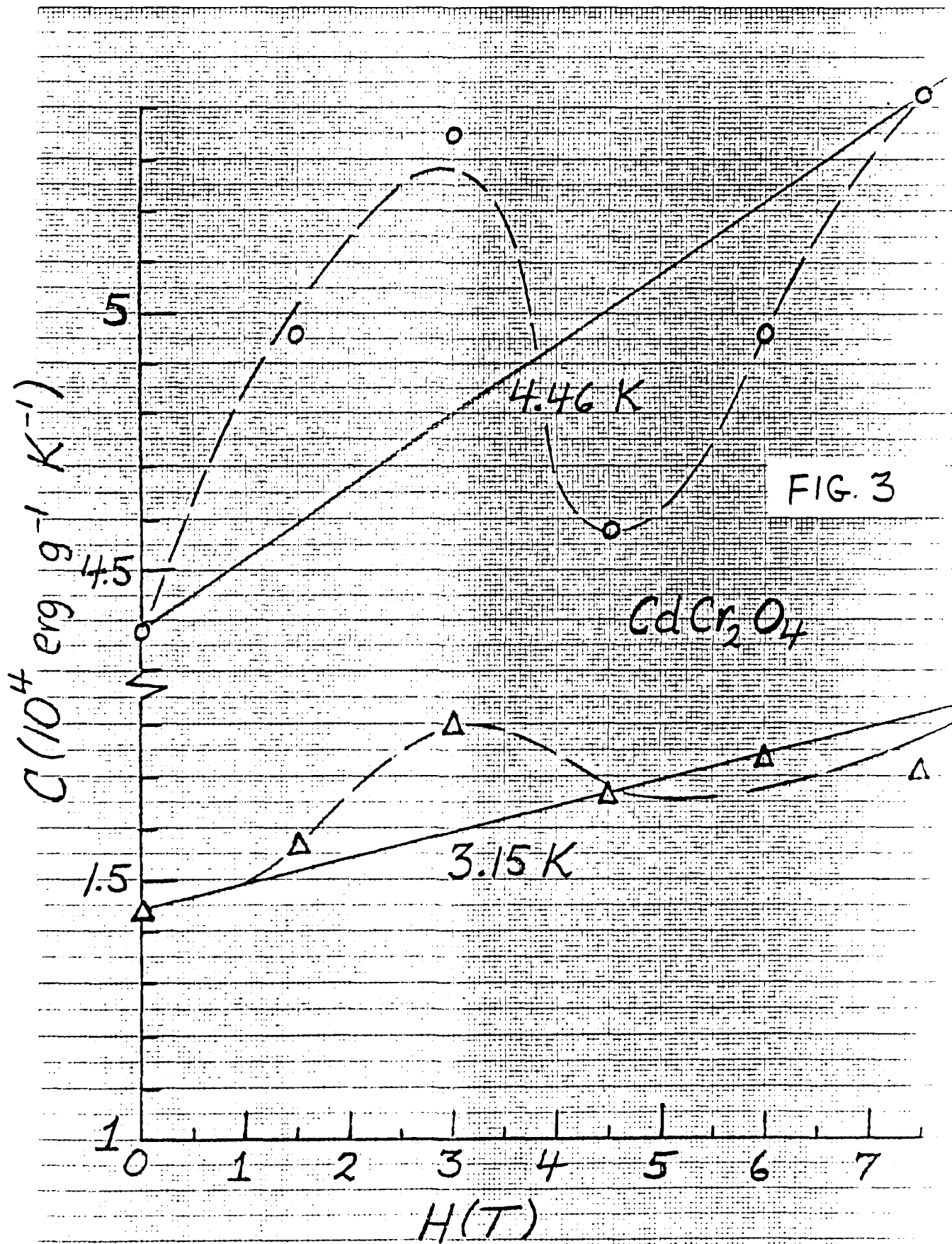
Our approach is, by necessity, an experimental approach, and it is clear that the next step is to sharpen the specific-heat data. Clearly, knowing  $g(H)$  in Eq. (3) would allow a closed-form solution of Eq. (4). The "noise" in the specific heat data can be reduced/eliminated by employing the following techniques: (1) Copper-wire thermal links have been employed, which require a magnetothermal resistance correction; using manganin thermal links would eliminate the correction factor but would require longer experimental times; (2) Using capacitance thermometry would eliminate the magnetoresistance correction for the carbon-chip thermometers, but only one sample at a time could be measured due to the unavoidable "cross-talk" noise between transformer-ratio-arm bridges; and (3) If small temperature ranges were focused on (e.g., 2-4 K), experimental accuracy would be greatly improved because thermometry calibrations would be simplified and scale changes would be avoided.

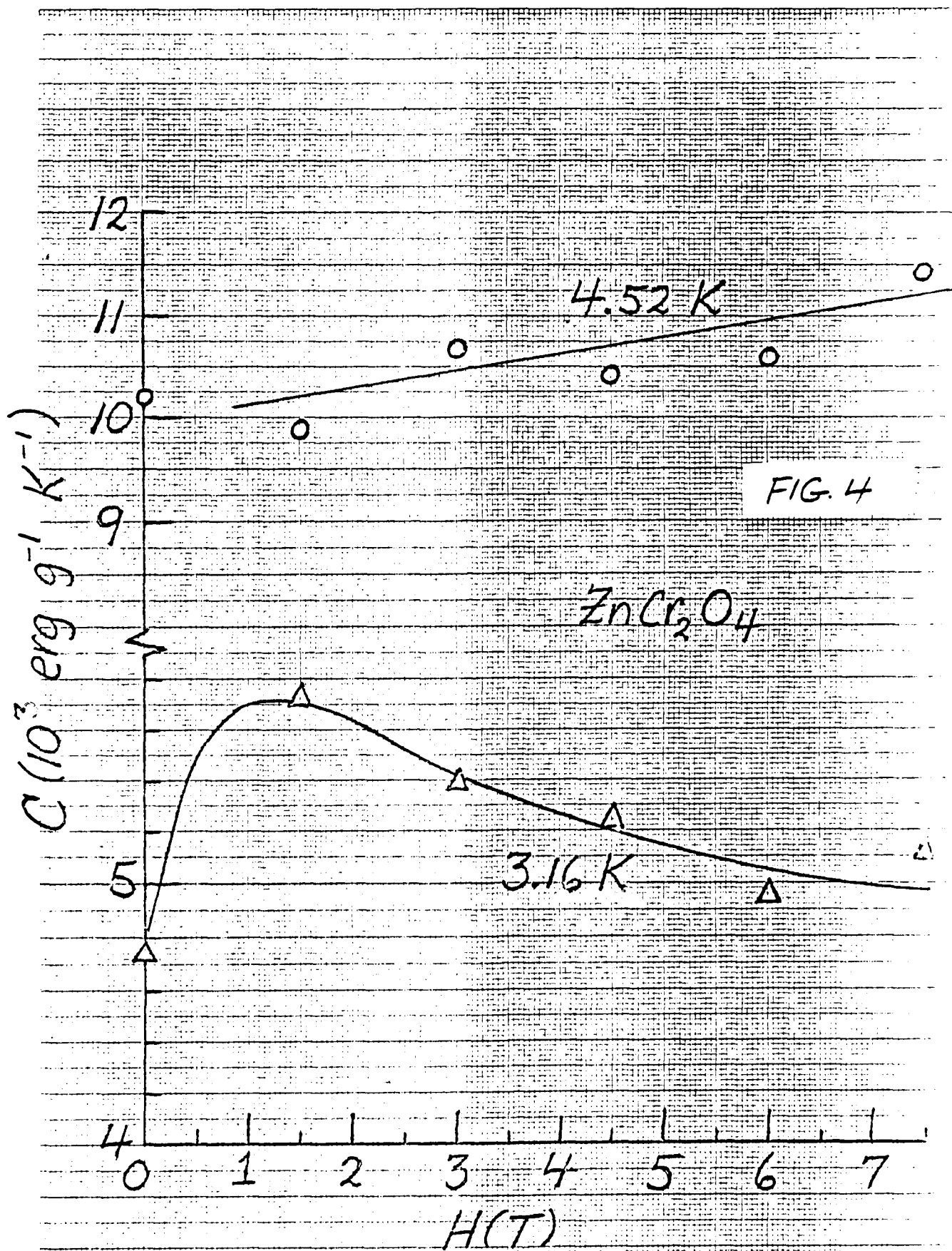
Nonetheless, it is doubtful if these minor experimental modifications will have much effect on the qualitative results in Fig. 6. Namely,  $f(T) \propto T^{-n}$  where  $11 < n < 27$ . This state-function temperature dependence is difficult to resolve in view of existing theories. Clearly, M-H magnetization data for a series of temperatures are needed to resolve these findings, since from Eq. (2)  $f(T)$  is found directly from magnetization data.

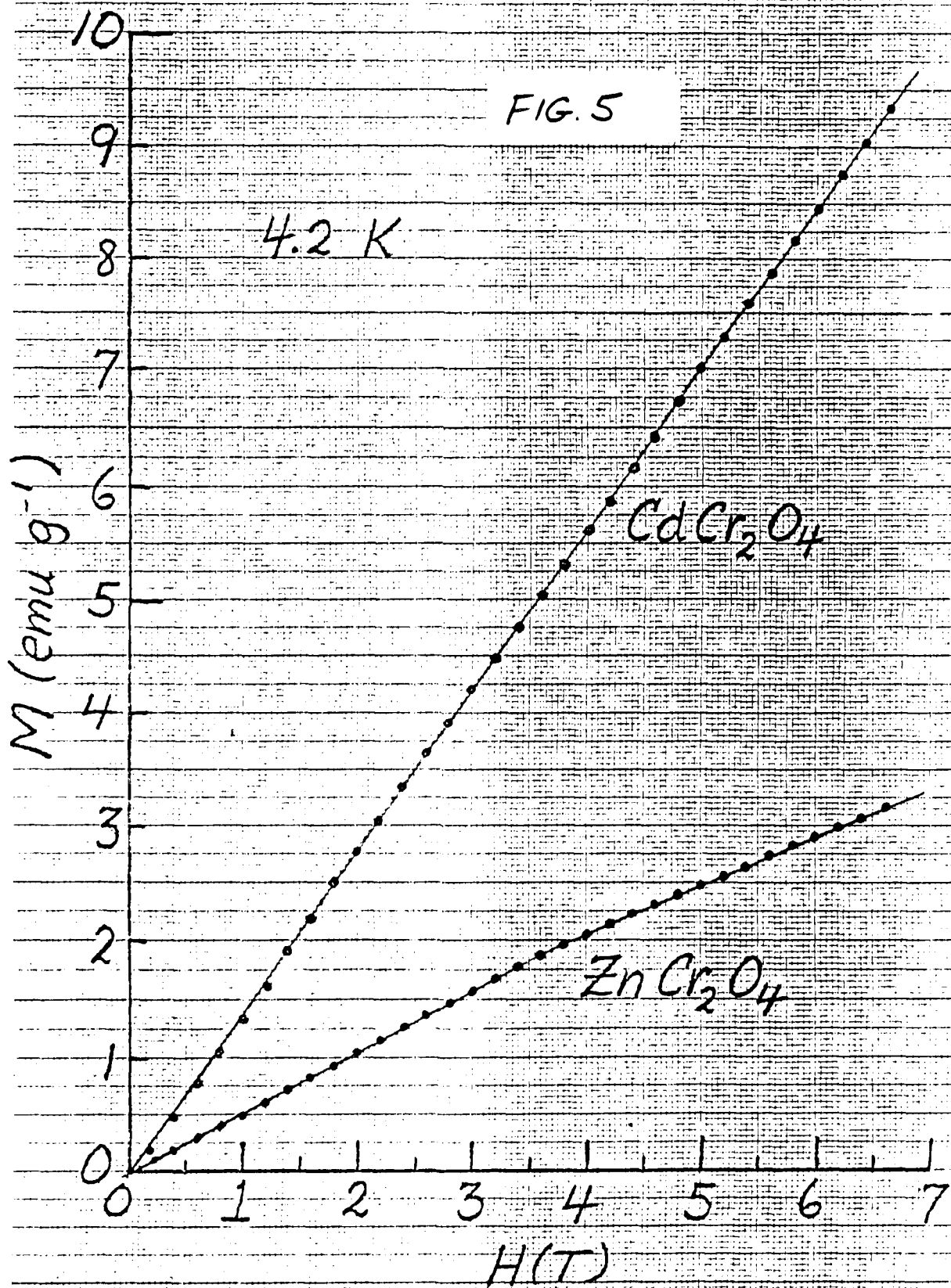
0-7-50 K

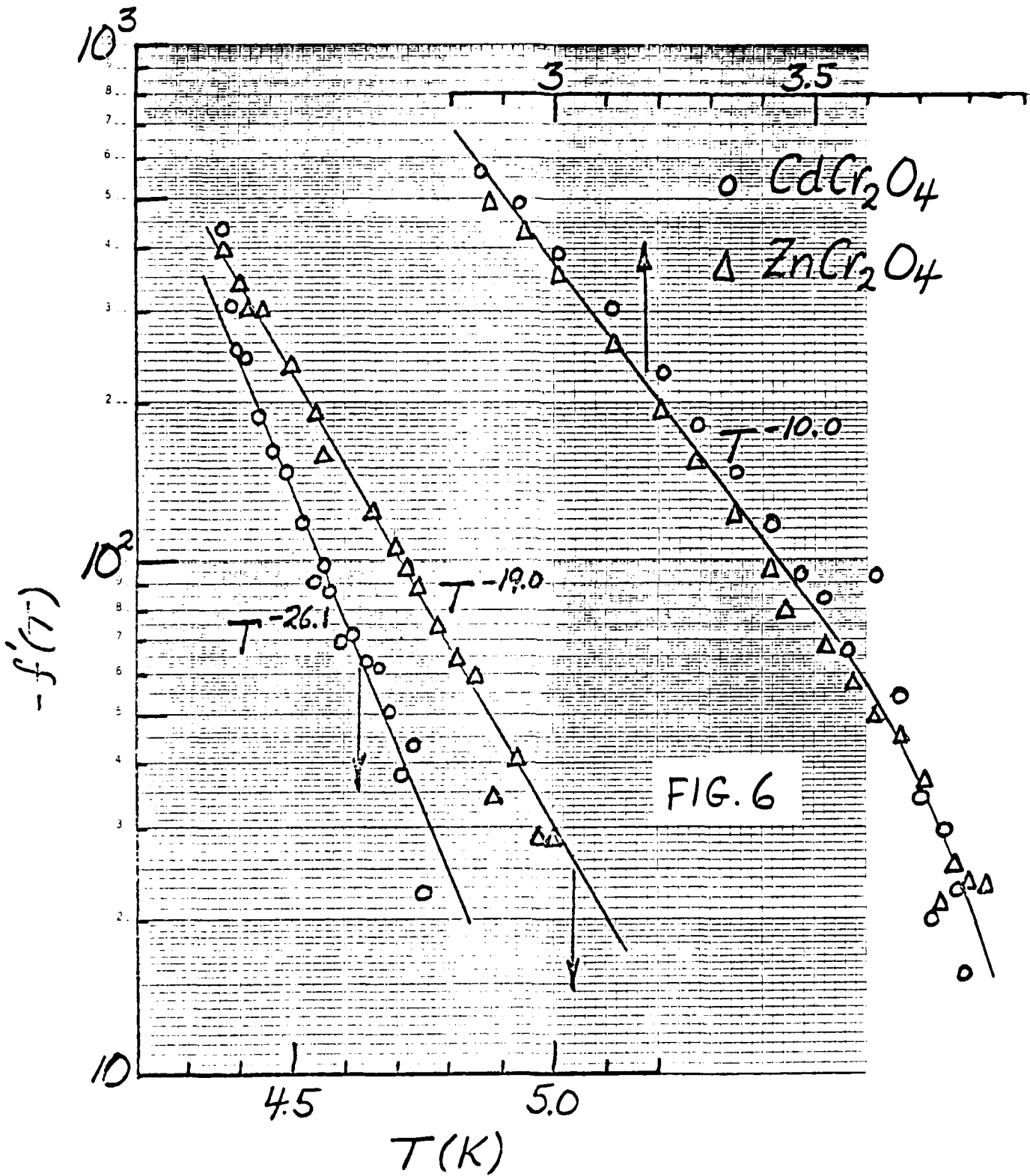












AFOSR Contract #F49620-83-C0129

Fundamental Physics Studies on High-Specific-Heat

Dielectrics and Kapitza Resistance at Dielectric Boundaries

Spinel Studies XI, Spin Densities

by

W.N. Lawless *WNL*

CeramPhysics, Inc.

Westerville, Ohio 43081

August 15, 1984

Distribution:

J.H. Parker, Jr.

  
T.K. Gupta

M. Ashkin

C.F. Clark

B.R. Patton

A. Menard

This is the eleventh report in a series of studies of the new spinels  $\text{CdCr}_2\text{O}_4$  and  $\text{ZnCr}_2\text{O}_4$ .

As these studies have progressed it has become increasingly clear that a serious contradiction exists in our basic concepts of these spinels. Namely, there is strong evidence that the huge specific heat maxima at 8 and 10.5 K are due to antiferrimagnetic ordering of  $\text{Cr}^{3+}$  spins; in contrast, the magnetocaloric data well below 8 K show definite paramagnetic behavior. These contradictory findings can be qualitatively resolved by assuming that some fraction of the  $\text{Cr}^{3+}$  spins partake in the antiferrimagnetic ordering and that the balance of the spins remain unordered and therefore paramagnetic.

This viewpoint is appealing theoretically, and the purpose of this report is to re-examine some of the experimental data according to this hypothesis. We state first the basic assumption: Each molecule of the spinel has two  $\text{Cr}^{3+}$  spins, and we write  $n_A$  for the fraction of antiferrimagnetically-ordered spins and  $n_p$  for the remaining, paramagnetic spins, where  $n_A + n_p = 2$ . This model ignores coupling between the two spin systems.

These two spin densities are obtained directly from the magnetic entropy associated with the specific heat maxima of the two spinels, which were determined previously from analyses of specific heat data:  $S_m = 6.939 \times 10^5$  and  $5.109 \times 10^5$  erg  $\text{g}^{-1}$   $\text{K}^{-1}$  for  $\text{CdCr}_2\text{O}_4$  and  $\text{ZnCr}_2\text{O}_4$ , respectively. Using the basic relation

$$S_m = n_A R \ln(2s + 1) \quad (1)$$

and the free-ion  $\text{Cr}^{3+}$  spin,  $s = 3/2$ , we immediately have

$$\begin{aligned} \text{CdCr}_2\text{O}_4: \quad n_A &= 1.688, \quad n_p = 0.312 \\ \text{ZnCr}_2\text{O}_4: \quad n_A &= 1.035, \quad n_p = 0.965 \end{aligned} \tag{2}$$

There is a good reason for using  $s = 3/2$  in Eq. (1); namely, it is commonly found in similar magnetic systems that the orbital angular momentum for  $d^3$  electrons is quenched by crystalline electric fields. We note also that if we set  $n_A = 2$  in Eq. (1), as was done previously, we obtain spins  $s = 1$  and  $1/2$  whereas one expects  $s > 3/2$  (i.e., if the orbital momentum is not quenched,  $s$  increases).

Thus, in this picture, 84.4% of the  $\text{Cr}^{3+}$  spins in  $\text{CdCr}_2\text{O}_4$  order at 8 K, 51.7 % in  $\text{ZnCr}_2\text{O}_4$  at 10.5 K, and this immediately explains why the height of the specific heat maximum for  $\text{CdCr}_2\text{O}_4$  is about 50% larger than that for  $\text{ZnCr}_2\text{O}_4$  (based on a C/3R comparison, see Fig. 6 of Spinel Studies, II).

Turning next to the antiferromagnetic spin-wave contribution to the specific heat resolved at the lowest temperatures,

$$C_{\text{SW}} = c_a n_A R (kT/2J's)^3, \tag{3}$$

it will be recalled that this term is experimentally indistinguishable from the  $T^3$  Debye term, and in our cases here was inferred from unrealistically small, fitted (effective) Debye temperatures. Setting the geometric factor  $c_a$  equal to unity in Eq. (3), using the  $n_A$ 's in Eq. (2) and  $s = 3/2$ , we find for the exchange constants

$$\begin{aligned} \text{CdCr}_2\text{O}_4: J'/k &= 3.419 \\ \text{ZnCr}_2\text{O}_4: J'/k &= 4.716 \end{aligned} \tag{4}$$

These results are very satisfying compared to our previously reported exchange constants which differed by a factor of 3 1/2 [i.e., calculated based on  $n_A = 2$  in Eq. (1)].

Turning next to the specific heat data well above the transition temperatures, these  $n_A$ -spin fluctuations follow a Schottky term very well,

$$C_{\text{Sch}} = n_A R g_0 g_1 (g_0 + g_1)^{-2} (\delta/T)^2 \tag{5}$$

where previously we had ignored the parameters in Eq. (5) (Recall that the purpose of these fits was to obtain the Debye temperatures which agreed very well with predictions of the Lindemann relation). The form of Eq. (5) is for a two-level system (although we have no reason for selecting this form other than for simplicity), and we can now evaluate the level splittings (setting  $g_0 = g_1$ ),

$$\begin{aligned} \text{CdCr}_2\text{O}_4: \delta &= 31.5 \text{ K} \quad T > T_N \\ \text{ZnCr}_2\text{O}_4: \delta &= 35.0 \text{ K} \end{aligned} \tag{6}$$

Once again, the use of the  $n_A$ -densities in Eq. (2) bring these specific heat parameters in line.

A second Schottky term was resolved in both spinels for temperatures well below  $T_N$ , and it is natural to ascribe this feature to the

paramagnetic spins. Using these previously reported data with the appropriate  $n_p$  values in Eq. (5) we find that (again setting  $g_0 = g_1$ ),

$$\begin{aligned} \text{CdCr}_2\text{O}_4: \quad \delta &= 0.592 \text{ K} \\ \text{ZnCr}_2\text{O}_4: \quad \delta &= 0.374 \text{ K} \end{aligned} \quad T < T_N \quad (7)$$

The agreement here (~ 50%) is poorer than reported previously (~ 10%), but this may not be too surprising in view of the simple model used here to describe the  $n_p$ -spin fluctuations within the ordered  $n_A$ -spin ordered lattice.

The thermal conductivities of  $\text{CdCr}_2\text{O}_4$  and  $\text{ZnCr}_2\text{O}_4$  display significant jumps in the neighborhood of  $T_N$ , the effect in  $\text{ZnCr}_2\text{O}_4$  being the more pronounced (see Fig. 2 of Spinel Studies, I). Correspondingly, the  $n_p$  density in  $\text{ZnCr}_2\text{O}_4$  is three times larger than in  $\text{CdCr}_2\text{O}_4$ , Eq. (2), so in this picture the jump in  $K$  appears associated with the paramagnetic spins. A contradiction arises, however; namely, the  $K$ -jump in  $\text{CdCr}_2\text{O}_4$  is far more affected by intense magnetic fields than in  $\text{ZnCr}_2\text{O}_4$  (see Fig. 2 of Spinel Studies, VIII).

We turn next to the magnetization data measured on these spinels at 4.2 K. Beginning with the simple quantum theory of paramagnetism, the number of magnetic moments per unit volume is

$$M_p = N_p p^2 \mu_B^2 H / 3kT \quad (8)$$

where  $p = g \sqrt{J(J+1)} = 2 \sqrt{s(s+1)}$  if orbital momentum is quenched. Here  $N_p$  is the number of paramagnetic spins per  $\text{cm}^3$ ,

$$N_p = n_p A_0 \rho_s / M_W \quad (9)$$

where  $A_0$  is Avogadro's number,  $\rho_s$  is the spinel density, and  $M_W$  is the molecular weight. Simplifying,

$$M_p = \sigma_p n_p (\rho_s / M_W) H / T \quad (10)$$

where  $\sigma_p$  is a constant common to the  $n_p$ -densities of both spinels.

The  $n_A$ -densities have a finite susceptibility, and it is reasonable to write

$$M_A = \sigma_A n_A (\rho_s / M_W) H g(T) \quad (11)$$

where  $g(T)$  is the T-dependence associated with the antiferrimagnetically-ordered spin system. Combining,

$$M = M_p + M_A = (\rho_s / M_W) [\sigma_p n_p / T + \sigma_A n_A g(T)] H \quad (12)$$

which follows the linear magnetizations measured on both spinels at 4.2 K (see Fig. 5 of Spinel Studies VII).

It is found experimentally that at constant H

$$M(\text{CdCr}_2\text{O}_4) = 2.65 M(\text{ZnCr}_2\text{O}_4).$$

Correcting for the densities (6.056, 5.649) and molecular weights (280.43, 233.40) of the spinels ( $\text{CdCr}_2\text{O}_4$ ,  $\text{ZnCr}_2\text{O}_4$ ), we find that

$$[\sigma_p n_p / T + \sigma_A n_A g(T)]_{\text{CdCr}_2\text{O}_4} = 2.97 [\sigma_p n_p / T + \sigma_A n_A g(T)]_{\text{ZnCr}_2\text{O}_4} \quad (13)$$

This relation has only one solution, assuming that the  $\sigma$ 's and  $g(T)$  are the same for both spinels; namely,  $n_p$  and  $n_A$  for  $\text{CdCr}_2\text{O}_4$  are three times larger than for  $\text{ZnCr}_2\text{O}_4$ . Curiously, from Eq. (2)  $n_p$  for  $\text{ZnCr}_2\text{O}_4$  is almost exactly three times larger than  $n_p$  for  $\text{CdCr}_2\text{O}_4$  (were the magnetization samples interchanged?).

We are left with two possibilities: (1) The samples were interchanged and the  $n_A$ -contribution to  $M$  is very small compared to the  $n_p$ -contribution for both spinels; or (2) The differences in the  $\sigma$ 's and  $g(T)$  for the spinels are large enough to overwhelm the differences in  $n_p$  and  $n_A$ .

Turning next to the magnetocaloric data, the basic thermodynamic relation is

$$T dS = m C_0 dT + v \mu_0 T (\partial M / \partial T)_H dH \quad (14)$$

where  $m$  and  $v$  are the sample weight and volume, and, as before, we ignore the  $H$ -field dependence of the specific heat ( $C_0$ ) based on our specific heat measurements of these spinels in intense magnetic fields.

Combining Eqs. (12) and (14) for adiabatic conditions ( $dS = 0$ ), we have

$$C_0 dT = T (\mu_0 / M_w) [\sigma_p n_p / T^2 - \sigma_A n_A g'(T)] H dH \quad (15)$$

where  $\rho_s = m/v$  has been used and  $g'(T) = dg/dT$ .

Equation (15) describes the adiabatic temperature changes  $dT$  corresponding to field changes  $dH$ , and the picture here is that the paramagnetic spins  $n_p$  show demagnetization cooling (i.e.,  $dT < 0$  if  $dH < 0$ ) whereas the antiferrimagnetic spins  $n_A$  show demagnetization heating. Note that it is a property of antiferrimagnetically ordered spins that  $g'(T) > 0$ .

Experimentally, the net magnetocaloric effect is demagnetization cooling in both spinels, so that in this picture the  $n_p$ -spin system overwhelms the  $n_A$ -spin system. That is, from Eq. (15)

$$\sigma_p n_p > \sigma_A n_A T^2 g'(T) \quad (16)$$

We found experimentally that the reversible temperature changes  $\Delta T_{rev}$  in  $ZnCr_2O_4$  were larger than in  $CdCr_2O_4$  at both 4.5 and 3.2 K (see Figs. 1 and 2 in Spinel Studies, VII). However, the specific heat of  $ZnCr_2O_4$  at these temperatures is smaller than that of  $CdCr_2O_4$ , so for a meaningful comparison of the rhs of Eq. (15) for the two spinels the specific heats should be factored out. Consequently,  $C_0 \Delta T_{rev}$  data were constructed for the two spinels, and these data are shown in Fig. 1 (the  $T$ -dependence of  $C_0$  was taken into account in constructing these plots). Two features are immediately apparent: (1) The  $C_0 \Delta T_{rev}$  data for  $CdCr_2O_4$  in Fig. 1 are about three times larger than for  $ZnCr_2O_4$ , a value suspiciously in agreement with the magnetization results, Eq. (13); and (2) The  $T$ -dependence of the rhs of Eq. (15) is rather small, the trend being for the rhs at 3.2 K to be smaller than at 4.5 K.

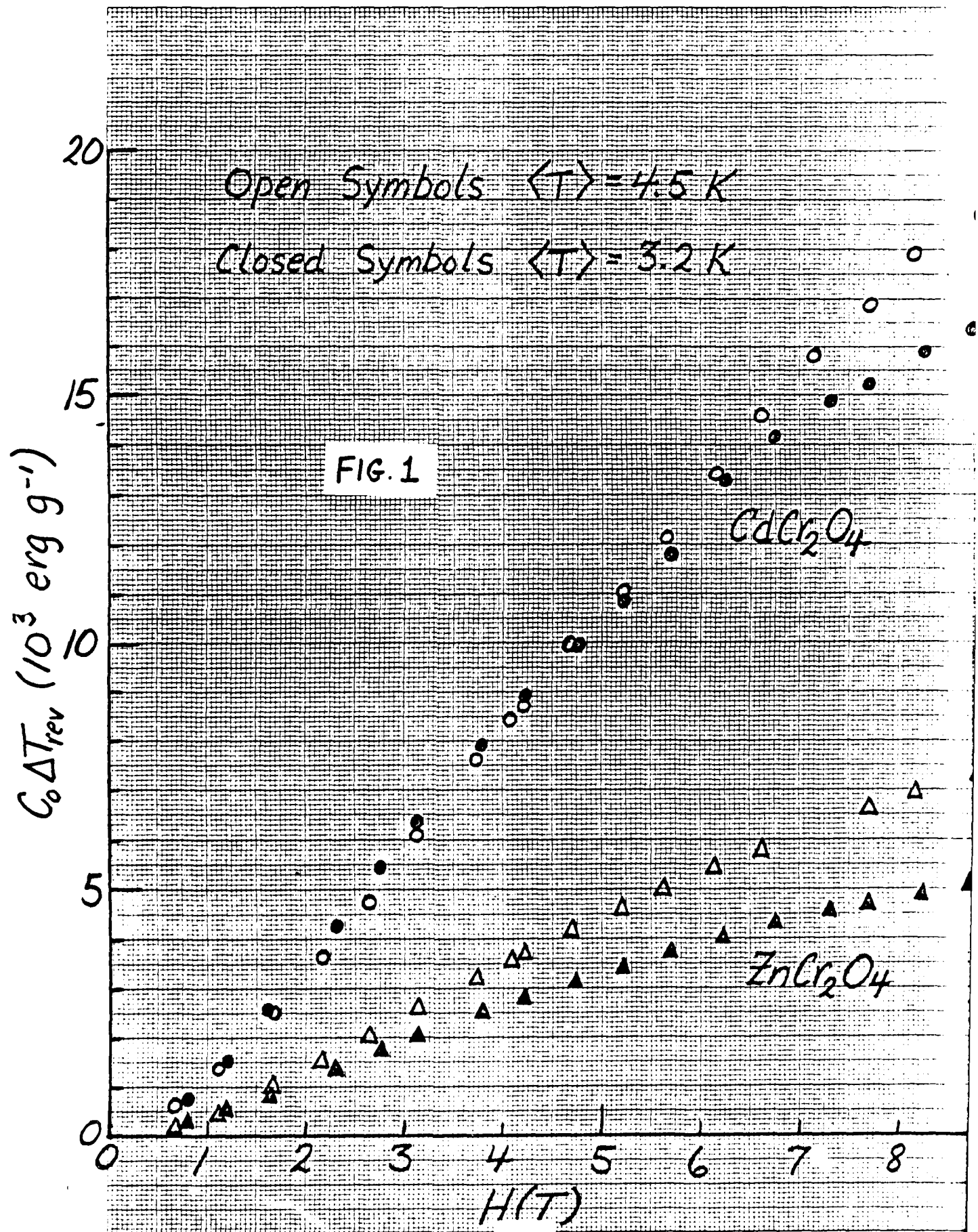
Thus, we are faced with a confusing problem: Analyses of specific heat data indicate that  $n_p(\text{CdCr}_2\text{O}_4) < n_p(\text{ZnCr}_2\text{O}_4)$ , but the magnetization and magnetocaloric data suggest the opposite. We also note another puzzling feature: The  $n_p$ -contribution to the magnetocaloric effect clearly overwhelms the  $n_A$ -contribution, suggesting from Eq. (15) that  $C_0\Delta T_{\text{rev}} \propto T^{-1}$ ; but the opposite trend is seen in Fig. 1.

Finally, we discuss our previous numerical integration of Eq. (15). To review, the  $\Delta T_{\text{rev}}$  data were measured by cycling the field  $0 \rightarrow H_1 \rightarrow 0$ ,  $0 \rightarrow H_2 \rightarrow 0$ , etc. where the sample always returned to a baseline temperature  $T_0$  at zero field. Considering just the magnetization half of the cycle, these data were used to construct a  $T$  vs.  $H$  plot; e.g.,  $T_1 = T_0 + \Delta T_1$  at  $H_1$ ,  $T_2 = T_0 + \Delta T_2$  at  $H_2$ , etc. This curve was numerically integrated according to Eq. (14) by assuming it represented an equivalence experiment: Namely, when the field changed  $0 \rightarrow H_1$ , the temperature changed  $T_0 \rightarrow T_1$ ; on  $H_1 \rightarrow H_2$ ,  $T_1 \rightarrow T_2$ ; on  $H_2 \rightarrow H_3$ ,  $T_2 \rightarrow T_3$ , etc. This numerical integration yielded an extremely strong temperature dependence for the quantity in brackets in Eq. (15) for both spinels (see Fig. 6 of Spinel Studies VII), in marked contrast to the Fig. 1 data here.

In summary, splitting the spins into  $n_A$ - and  $n_p$ -components leads to several appealing results, and the rationale for this decomposition is straightforward: (1) A  $T^3$  antiferromagnetic spin-wave contribution to the specific heat at the lowest temperatures, and (2) Adiabatic demagnetization cooling effects indicating paramagnetic spins. However, the specific heat results are at seemingly wide variance with the magnetization and magnetocaloric results for both spinels according to this picture.

We remark here that we have seen qualitative evidence for the two spin systems in magnetocaloric experiments. That is, competition between  $n_A$ -heating and  $n_p$ -cooling spins upon demagnetization have been observed in certain temperature ranges, and this competition was evidenced by different spin-phonon relaxation times such that the sample temperature first showed heating, then cooling. However, it is believed that in all the data reported to date the experimental waiting times were long compared to these relaxation times so that net effects were measured (e.g., Fig. 1 here).

The results here suggest some future experimental directions: (1) The magnetization results should be checked to answer the question of sample mixup; (2) Magnetization measurements at several temperatures 1.5 - 20 K are needed; and (3) Magnetocaloric measurements at several temperatures are also needed. In particular, we need to develop T vs. H data sets by changing  $0 \rightarrow H_1 \rightarrow H_2 \rightarrow H_3$ , etc. to compare with the results of the  $0 \rightarrow H_1 \rightarrow 0$ ,  $0 \rightarrow H_2 \rightarrow 0$ ,  $0 \rightarrow H_3 \rightarrow 0$ , etc. data sets.



PROGRESS REPORT

AFOSR Contract #F49620-83-C-0129

Fundamental Physics on High-Specific-Heat  
Dielectrics and Kapitza Resistance at Dielectric Boundaries

Spinel Studies XII

Re-examination of Critical Exponents

by

W.N. Lawless and R.W. Arenz

*WNL, RWA*

CeramPhysics, Inc.  
Westerville, Ohio 43081

March 1, 1985

Distribution:  
J.H. Parker, Sr.  
P.W. Eckels  
T.K. Gupta  
M. Ashkin  
C.F. Clark  
B.R. Patton

In the June 14, 1984, progress report for this contract, critical-exponent analyses were made of data gathered near the peaks in the specific heats of the oxide spinels  $\text{CdCr}_2\text{O}_4$  and  $\text{ZnCr}_2\text{O}_4$ . The data used were measured using a novel calibrated-link drift method of calorimetry in which a sample weakly linked to a thermal reservoir was heated above the reservoir temperature, the heating was removed, and the sample was allowed to drift slowly toward equilibrium with the reservoir. A time-temperature record was generated by monitoring with a chart recorder the voltage drop across a carbon resistor thermometer attached to the sample; specific heats were derived from this record by reduction of the  $T$  and  $dT/dt$  information.

The analysis of the derived specific heat data then proceeded along the lines of the renormalization group theory of critical exponents in which the specific heat in the peak region is described by equations of the form:

$$C = (A/\alpha)t^{-\alpha} + Bt + E, \quad (1)$$

where

$$t = |T - T_N/T_N|, \quad (2)$$

where  $\alpha$ ,  $B$ , and  $E$  are constants and  $T_N$  is the temperature corresponding to the specific heat peak. From the data gathered in the experiment reported in June,  $\alpha$ 's on the order of  $3/2$  were determined. These values seemed unusually large in the light of work performed on  $\text{EuTe}$  and  $\text{EuSe}$ <sup>1</sup> and in the light of the scaling result  $(2 - \alpha)(2 - n) = \gamma d$  and Wilson's<sup>2</sup> epsilon-expansion. For both materials the data gathered also displayed a "rounding" in the  $C_{\text{ex}}$  vs.  $|T - T_N|$  curves at  $|T - T_N| < 0.3$  K. The reality of this "rounding" was suspect in the light of the methods of reducing the data from the chart recorder record, and it was bothersome in that it did not allow an examination of the scaling law over a wider range of  $t$  values (i.e.,  $t \rightarrow 0$ ).

Because of these observations and results, we have repeated

the drift experiments reported in June, 1984, utilizing a different data collection method and longer drift times. In this latest work we have continuously recorded the sample and reservoir temperatures digitally during the drift using a digital voltmeter/computer interface, thus generating a directly computer-reducible time-temperature record. This eliminated the human factors involved in reducing the chart-recorder record by hand.

In the revised experiment the carbon resistor sample thermometer, the germanium resistor reservoir thermometer and the current (i.e., the voltage drop over a standard 1 K ohm resistor) common to both were sampled simultaneously at regular intervals using three Keithly Model 181 nano-volmeters. The sampling and recording of measurements was controlled by a Digital Equipment Corporation Professional 350 computer via an IEEE 488 interface. The sampling rate and drift times for the  $\text{CdCr}_2\text{O}_4$  and  $\text{ZnCr}_2\text{O}_4$  were 5 seconds over 56 minutes and 10 seconds over 166 minutes, respectively. Temperature drift between consecutive data points were on the order of 1 mK over the specific heat peaks.

The recorded voltages were converted to temperatures using previously determined thermometer calibrations, and the temperature-time records were "smoothed" using a computer routine which did a least squares fitting analysis of each point based on the point and an interval about the point.  $dT/dt$ 's were computed for each pair of points in the smoothed T record and then the  $dT/dt$ 's themselves were smoothed. Arbitrarily scaled C's were computed from the smoothed T and  $dT/dt$  records, and the link calibration was then determined by adjusting the arbitrary C curves to optimally correspond to C values determined previously by pulse calorimetric techniques. The final results of this procedure are shown in Figures 1 and 2.

From these C records the  $T_N$  values for  $\text{CdCr}_2\text{O}_4$  and  $\text{ZnCr}_2\text{O}_4$  were determined to be 7.9405 K and 10.6222 K, respectively. In the June, 1984 report, values for the constants B and E in equation (1) above were determined which should be reliable; these were applied to give a  $C_{ex}$

$$C_{ex} = C - Bt - E \quad (3)$$

where  $t$  is given by Equation (2) above. These  $C_{ex}$ 's are plotted against  $\log |t|$  in Figures 3-6 with Figures 3 and 4 showing the full range of  $C_{ex}$  data for the two materials and Figures 4 and 6 showing the data for  $|T - T_N/T_N| < 0.005$ . Some of the data for  $\log |t| < -1$ ,  $T < T_N$  branch, have been excluded from Figure 3 ( $CdCr_2O_4$ ) as the  $Bt - E$  correction was larger than the  $C$  value (i.e., the correction was too large). In both Figures 3 and 4 the  $T < T_N$  branch of the data is the "lower" or "leftmost" and the  $T > T_N$  branch of the data is the "upper" or "rightmost" branch.

As may be seen, the "rounding" effect noted in the June, 1984, report is again evident; thus it seems that this effect is real. If the information in the region of the "rounding" is not an artifact, then it may be valid to compute  $\alpha$ 's based upon data very near  $T_N$ . This has been done using linear least squares fittings and the results are shown in Figures 4 and 6. The values determined are 0.0098 for  $CdCr_2O_4$  and 0.0078 for  $ZnCr_2O_4$ .

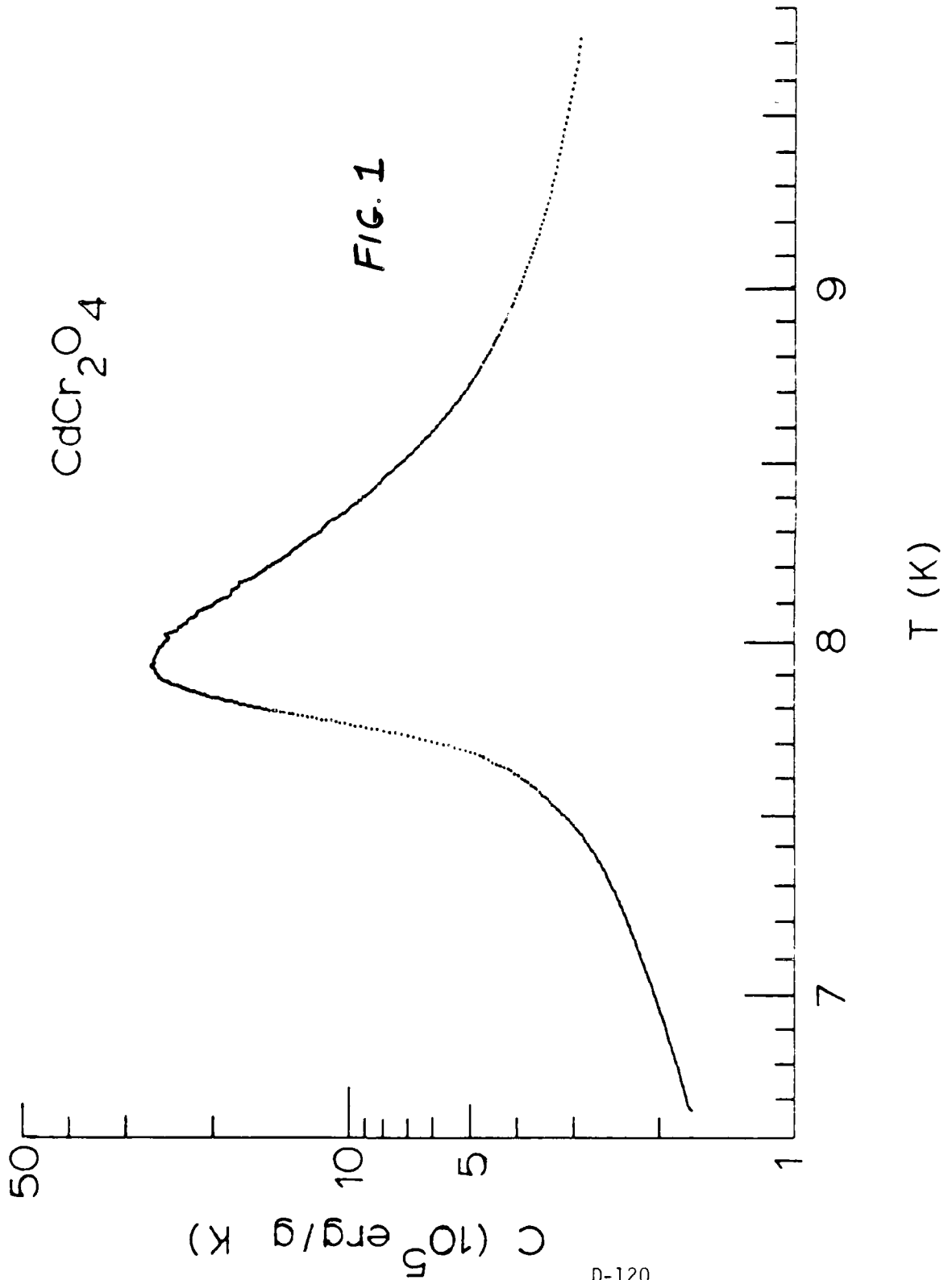
If the information very near  $T_N$  is somehow fallacious while data further away is more trustworthy, we again encounter the assymetries in the  $C_{ex}$  curve noted in the previous report. This latest experiment tended to confirm the  $\alpha$  values derived for  $CdCr_2O_4$ : least squares fittings of the regions shown in Figure 3 produce  $\alpha$ 's of 1.79 and 2.41, roughly comparable to the earlier determinations of 1.51 and 2.22. This, unfortunately, is not the case for the  $ZnCr_2O_4$  sample as the values determined were 4.91 and 0.736 for the  $T > T_N$  and  $T < T_N$  regions, respectively. These are to be compared to earlier values of 1.50 and 4.28. There are two possible reasons for this discrepancy: First, there is a problem with determining which part of the rather smoothly curved legs of the  $ZnCr_2O_4$  data to use in determining  $\alpha$ . Second, there was a difficulty fitting the drift  $C$  data to previously determined pulse data points, and in fact a skewing between the two data sets was seen in the  $T > T_N$  regions. This was most likely due to some uncertainty in the carbon resistance thermometer calibration.

It is remarkable that the  $\alpha$  values determined for the two materials for T values very near  $T_N$  are quite similar.

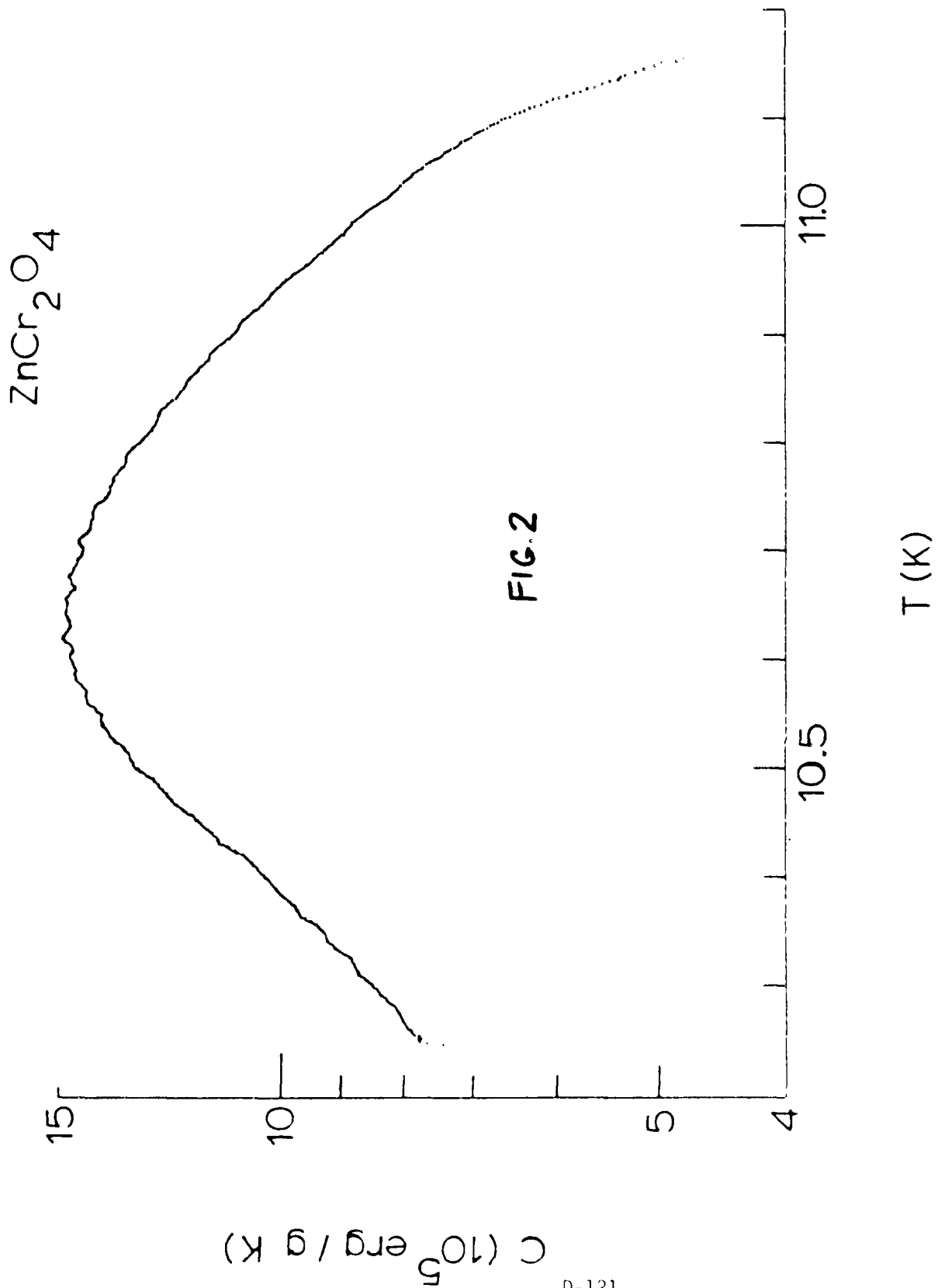
References

- <sup>1</sup> W.R. Johanson and D.C. McCollum, Phys. Rev. B22, 2435 (1980).
- <sup>2</sup> K.G. Wilson, Phys. Rev. Letter. 28, 548 (1972).

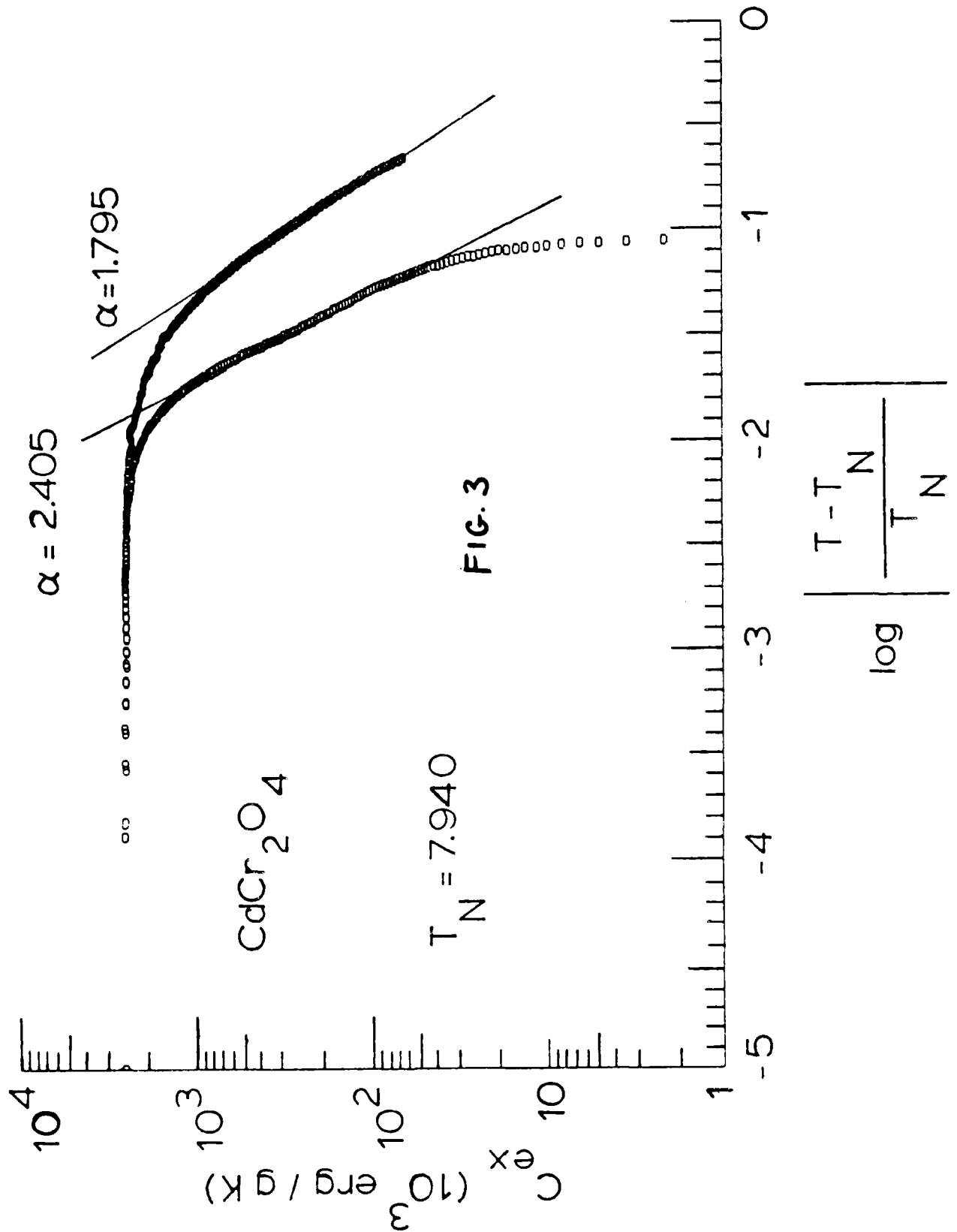
.....  
.....  
(19/1) DRIFT CRITICAL EXPONENTS 11/28/84  
A = 2.3948061E+00 B = 3.2994988E+00 P = 7.0499444E-01 LEAD RESISTANCE = 0.0000  
ADDITIONAL AND SAMPLE WEIGHTS:  
SAMPLE = 1.7290000E+00  
SLOPE = 7.8900002E+01 INTERCEPT = 0.0000000E-01 TIME STEP (SECS) = 5.00  
XMIN = 6.60000E+00 XMAX = 9.80000E+00 YMIN = 1.00000E+05 YMAX = 5.00000E+06  
THE Y VALUES ARE CONVERTED TO LOG 10 IN PLOTTING



.....  
 ZN(9/1) THIRD DRIFT NOV 20, 1984 CRITICAL EXPONENTS EXP.  
 A = 2.0383507E+00 B = 2.7465701E+00 P = 4.3296078E-01 LEAD RESISTANCE = 0.0000  
 ACCURACY AND SAMPLE HEIGHTS:  
 SAMPLE = 2.0123000E+00  
 SLOPE = 0.4600000E+00 INTERCEPT = 0.0000000E-01 TIME STEP (SECS) = 10.00  
 MIN = 1.02000E+01 MAX = 1.12000E+01 MIN = 4.00000E+05 MAX = 1.56000E+06  
 THE Y VALUES ARE CONVERTED TO LOG 10 IN PLOTTING



C(9/1) DRIFT CRITICAL EXPONENTS 11/28/84  
 A = 2.3548061E+00 B = 3.2994988E+00 P = 7.0499444E-01 LEAD RESISTANCE  
 ADDONUM AND SAMPLE HEIGHTS:  
 SAMPLE = 1.7290000E+00  
 SLOPE = 7.8900002E+01 INTERCEPT = 0.0000000E-01 TIME STEP (SECS) = 5.00  
 TN = 7.9405 KELVIN, B = 4.23700E+02 E = 2.39600E+05  
 AMIN = -5.00000E+00 AMAX = 0.00000E-01 YMIN = 1.00000E+03 YMAX = 1.00000E+07  
 THE Y VALUES ARE CONVERTED TO LOG 10 IN PLOTTING



A = 2.0387307E+00 B = 2.7463701E+00 F = 4.3236070E-04 LEAD RESISTANCE  
 ADJUDUM AND SAMPLE WEIGHTS:  
 SAMPLE = 2.0123000E+00  
 SLOPE = 8.4600000E+00 INTERCEPT = 0.0000000E-01 TIME STEP (SECS) = 10.00  
 TN = 10.6222 KELVIN, B = 3.21300E+02 L = 2.17600E+05  
 YMIN = -5.00000E+00 YMAX = -1.00000E+00 YMIN = 2.00000E+05 YMAX = 1.50000E+06  
 THE T VALUES ARE CONVERTED TO LOG 10 IN PLOTTING

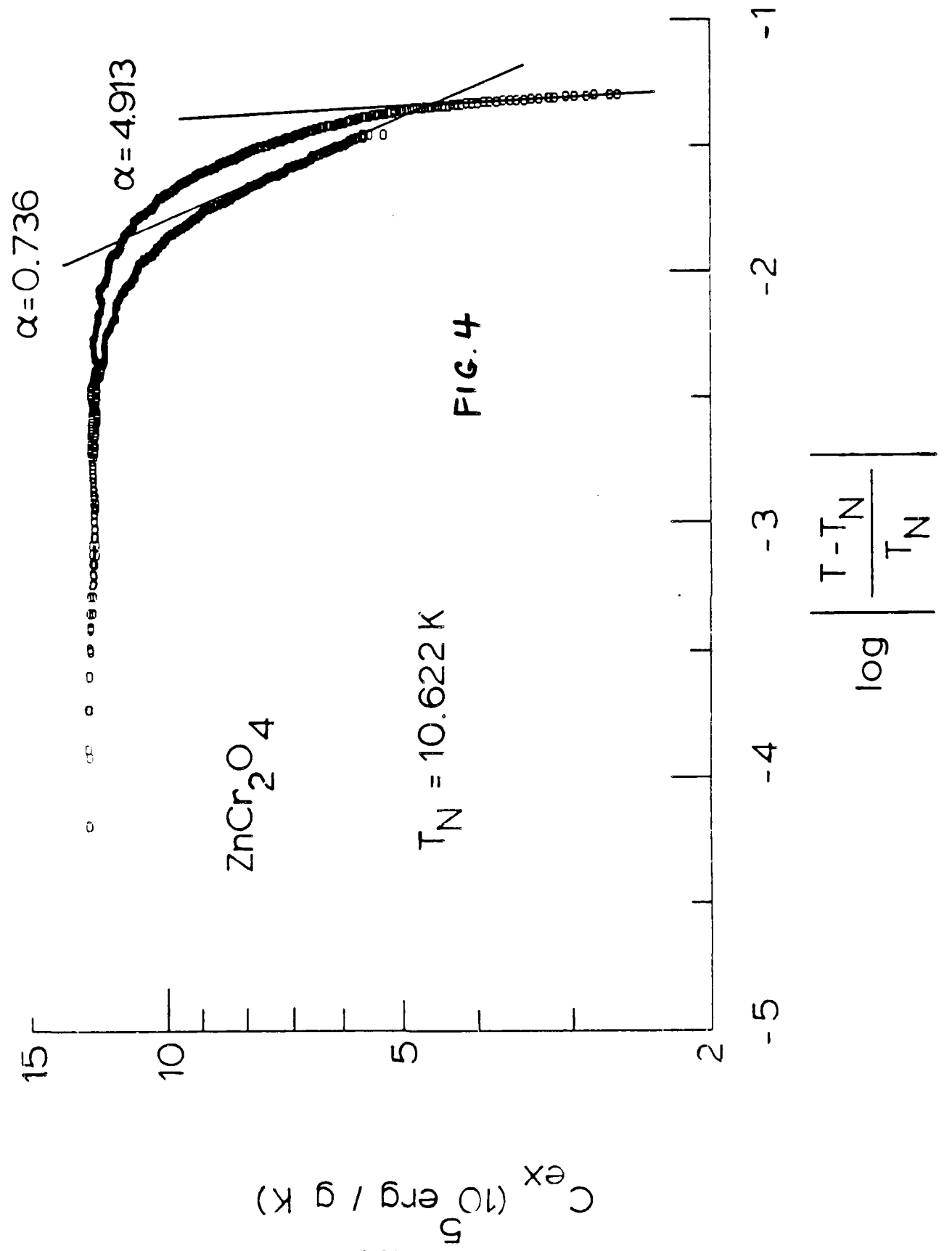
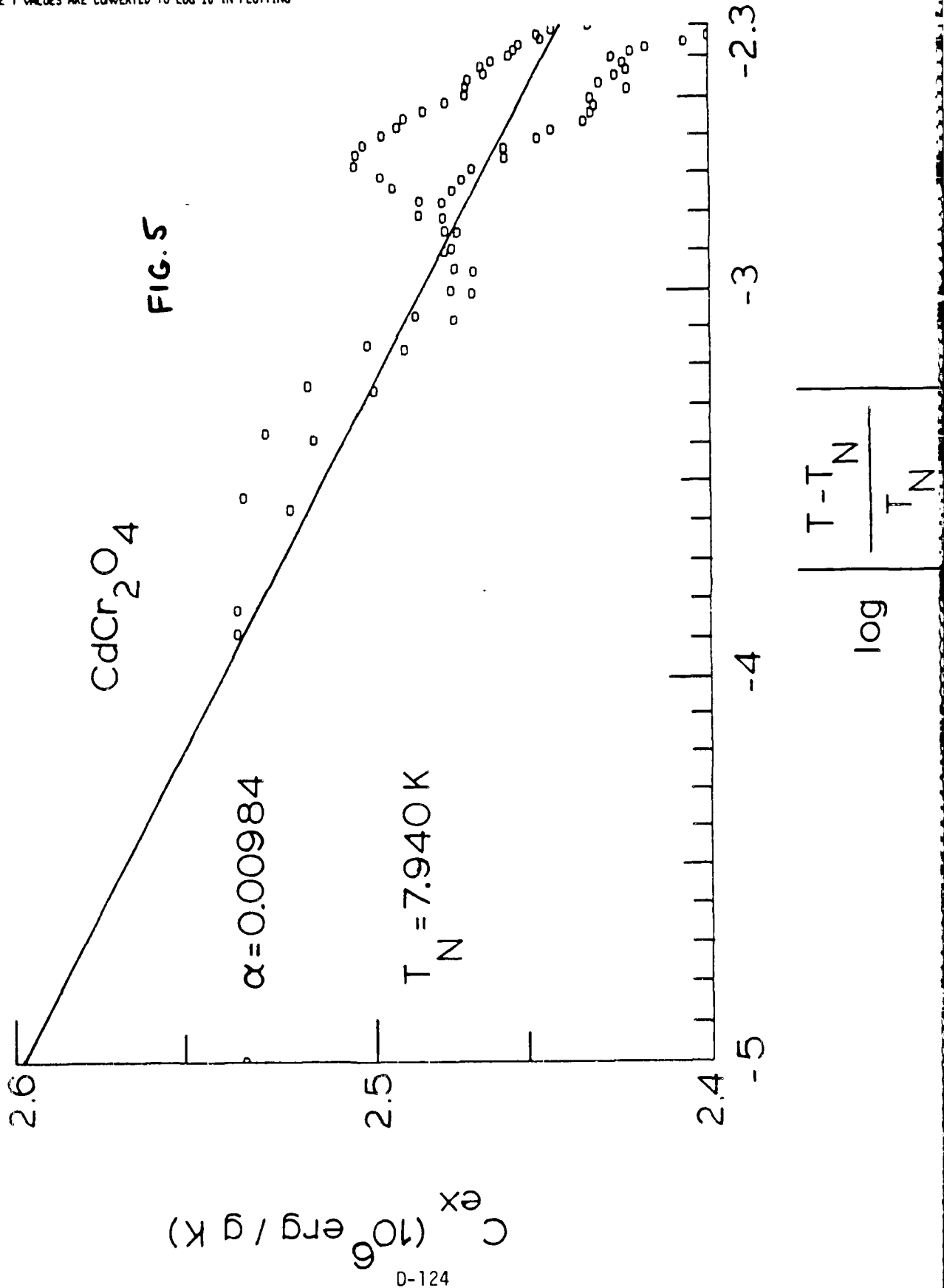
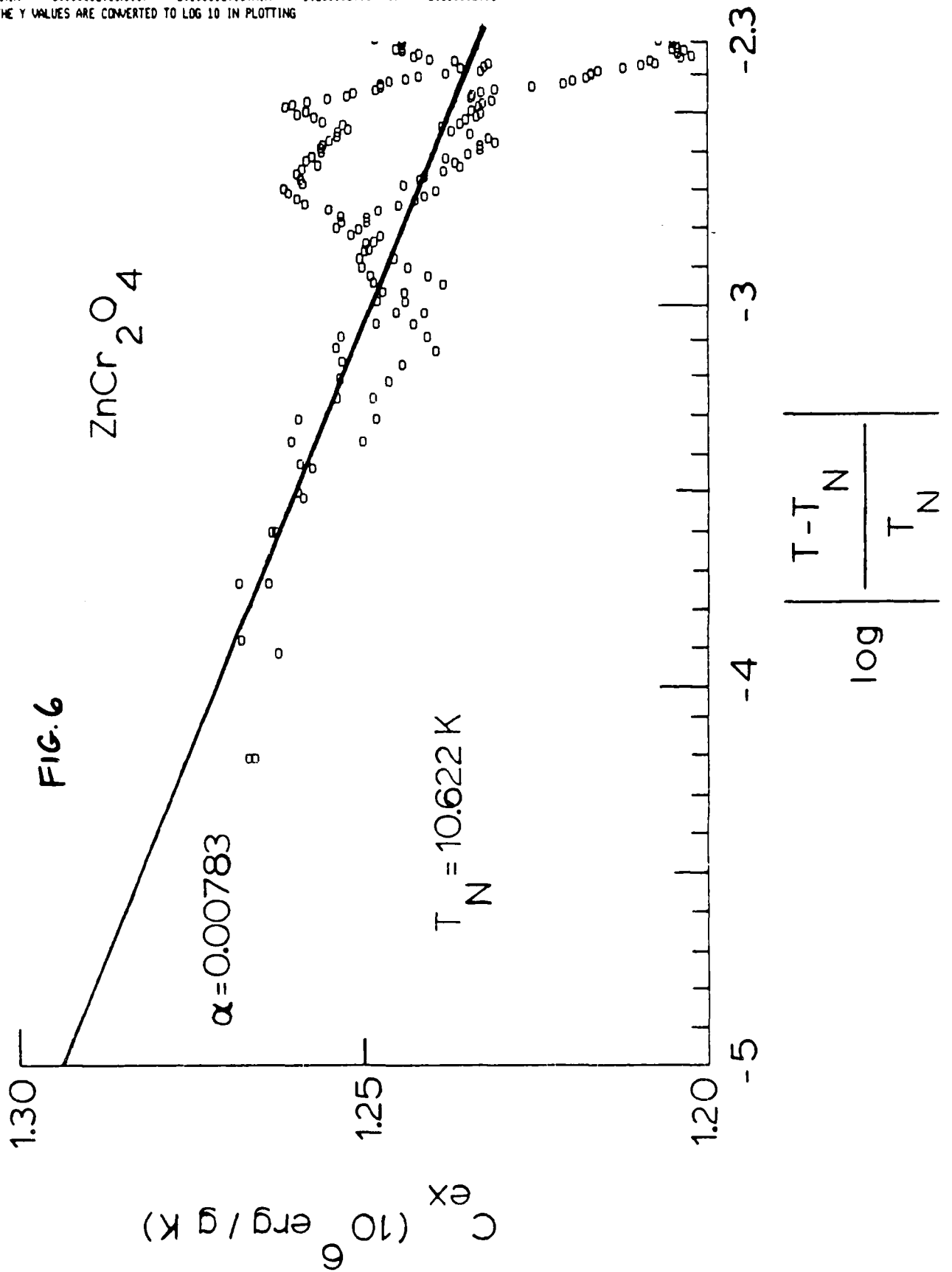


FIG. 4

61373 DRIFT CRITICAL EXPONENTS 11/28/64  
 A = 2.3948061E+00 B = 3.2994988E+00 P = 7.0499444E-01 LEAD RESISTANCE  
 ADDENDUM AND SAMPLE HEIGHTS:  
 SAMPLE = 1.7290000E+00  
 SLOPE = 7.8900002E+01 INTERCEPT = 0.0000000E-01 TIME STEP (SECS) = 5.00  
 TN = 7.9405 KELVIN, B = 4.23700E+02 E = 2.39600E+05  
 XMIN = -5.00000E+00 XMAX = -2.30000E+00 YMIN = 2.40000E+06 YMAX = 2.60000E+06  
 THE Y VALUES ARE CONVERTED TO LOG 10 IN PLOTTING



A = 2.0389507E+00 B = 2.7465701E+00 P = 4.3296076E-01 LEAD RESISTANCE  
 ADDENDUM AND SAMPLE WEIGHTS:  
 SAMPLE = 2.0123000E+00  
 SLOPE = 8.4600000E+00 INTERCEPT = 0.0000000E-01 TIME STEP (SECS) = 10.00  
 TN = 10.6222 KELVIN, B = 3.21300E+02 E = 2.17600E+05  
 XMIN = -5.00000E+00 XMAX = -2.30000E+00 YMIN = 1.20000E+06 YMAX = 1.30000E+06  
 THE Y VALUES ARE CONVERTED TO LOG 10 IN PLOTTING



AFOSR Contract #F49620-83-C0129  
Fundamental Physics Studies on High-Specific-Heat  
Dielectrics and Kapitza Resistance at Dielectric Boundaries

Spinel Studies XIII, Doping Studies

by

W.N. Lawless

CeramPhysics, Inc.  
Westerville, Ohio 43081  
April 1, 1985

Distribution:

J.H. Parker, Jr.  
P.W. Eckels  
T.K. Gupta  
M. Ashkin  
C.F. Clark  
B.R. Patton  
A. Menard

Previously reported experimental work on the new spinels  $\text{CdCr}_2\text{O}_4$  and  $\text{ZnCr}_2\text{O}_4$  has dealt with the thermal and magnetothermal properties at low temperatures. These have been derivative data based on measurements of the ceramic samples C(9/1) and D(9/1), where C(9/1) is a mixture of 9 moles  $\text{CdCr}_2\text{O}_4$  + 1 mole  $\text{CdNb}_2\text{O}_6$ , and similarly for D(9/1). It will be recalled that these spinels form only in the presence of the columbite mineralizers.

Theoretical progress in this program suggests that the anti-ferrimagnetic ordering temperatures of these new spinels,  $T_N$ , might be susceptible to doping on the A- or B-sites. This Report documents some initial studies in this area.<sup>1</sup> Specifically, three types of studies were undertaken:

1. Mixed spinels,  $(\text{Zn,Cd})\text{Cr}_2\text{O}_4$
2. Doping on the B-site in  $\text{CdCr}_2\text{O}_4$  with  $\text{Fe}^{3+}$  and  $\text{Gd}^{3+}$
3. Doping on the A-site in  $\text{CdCr}_2\text{O}_4$  with  $\text{Pb}^{2+}$

We emphasize at the outset that there is an unfortunate uncertainty in knowing how the added dopant partitions between the spinel phase, the columbite phase, and the grain boundary--to answer these questions would require a considerable diagnostic effort. By necessity, our approach was simply to make ceramic samples (noting weight gain/loss) and measure the low temperature specific heats.

#### Mixed Spinels

The studies here were limited to 50:50 compositions,  $\text{Zn}_{1/2}\text{Cd}_{1/2}\text{Cr}_2\text{O}_4$ , and three mineralizers were studied-- $\text{CdNb}_2\text{O}_6$ ,  $\text{ZnNb}_2\text{O}_6$ , and  $\text{Zn}_{1/2}\text{Cd}_{1/2}\text{Nb}_2\text{O}_6$ . These batched powders were thoroughly mixed and processed in the usual fashion (negligible weight loss), and the resulting specific heat data are shown in Fig. 1.

The Fig. 1 data show that in all three cases a specific heat maximum failed to develop between 6-12 K [specific heat data for C(9/1) and D(9/1) are shown for comparison]. In fact, the "mixed spinel" data in Fig. 1 appear to form the background data for C(9/1) and D(9/1).

One possible explanation for the Fig. 1 data is the forma-

tion of complex phases in the ceramic processing. A second attempt was pursued by first reacting the C(9/1) and D(9/1) powders separately (at 1000°C) and then mixing and sintering these powders together (1350°C) in a 50:50 ratio. Here one relies on a diffusion interchange of Zn and Cd on the A-site.

A subtlety is involved here in mixing the reacted powders. Namely, the reacted powders are fine-grained,  $\sim 1 \mu\text{m}$ , and wet-milling further reduces the grain size which could lead to unwanted phase formation. On the other hand, dry-milling the powders will not reduce the grain size but may not lead to complete mixing. Consequently, samples were prepared by both mixing methods.

Good ceramic samples were formed in both cases with negligible weight loss, and the resulting specific heat data are shown in Fig. 2. Again, no structure in the specific heat is seen.

These studies conclusively prove that a complete poisoning of the spin ordering occurs at the 50:50 ratio, and the frustration here may follow by analogy with the ferrimagnet  $\text{CdCr}_2\text{S}_4$  and the antiferrimagnet  $\text{ZnCr}_2\text{S}_4$ . However, our previous spin wave studies clearly showed that the new spinels here are both antiferrimagnets below  $T_N$ , and this conclusion was later supported by the magnetocaloric and magnetization measurements. Finally, we note that the ionic radii of  $\text{Zn}^{2+}$  (0.74 Å) and  $\text{Cd}^{2+}$  (0.97 Å) are quite different.

#### Doping Studies

In the first set of experiments here, a doping with 1%  $\text{Pb}^{2+}$  on the A site and 1% of  $\text{Fe}^{3+}$  and  $\text{Gd}^{3+}$  on the B site of  $\text{CdCr}_2\text{O}_4$  were attempted. These compositions were batched as if all of the dopant would enter the desired site, but, as cautioned above, there was no way to verify this.

The results of these three doping studies are shown in Fig. 3, and it is seen that the  $\text{Pb}^{2+}$  and  $\text{Gd}^{3+}$  dopings have relatively small effects compared to the  $\text{Fe}^{3+}$  dopings. One explanation here may be the close ionic radii match between  $\text{Fe}^{3+}$  (0.60 Å) and  $\text{Cr}^{3+}$  (0.64 Å) compared to  $\text{Gd}^{3+}$  (0.97 Å) or  $\text{Pb}^{2+}$  (1.32 Å). If the

ionic radius tolerance factor is only marginally favorable, the dopant could mainly partition in the columbite phase or grain boundary.

The  $\text{Fe}^{3+}$  doping was pursued further by preparing and measuring samples with 2, 3, 4.6, and 6.8%  $\text{Fe}^{3+}$  on the B site. These data are shown in Fig. 4, and it is seen that the effect of increasing the  $\text{Fe}^{3+}$  content is to suppress  $T_N$  and lower  $C_{\text{max}}$ . However, by 4.6% the specific heat maximum is quenched. The 3% ceramic was remeasured, and the data in Fig. 4 represent the data from both runs.

The results of these  $\text{Fe}^{3+}$  doping studies are summarized in Table I.

Table I

Fe <sup>3+</sup> Doping Studies in CdCr <sub>2</sub> O <sub>4</sub>			
Fe <sup>3+</sup>	Level	T <sub>N</sub>	C <sub>max</sub> (erg g <sup>-1</sup> K <sup>-1</sup> )
0		7.95	2.8x10 <sup>6</sup>
1		7.05	1.5x10 <sup>6</sup>
2		6.50	1.05x10 <sup>6</sup>
3		5.95	0.45x10 <sup>6</sup>

### Discussion

The Fig. 4 data suggest that the  $\text{Fe}^{3+}$  dopant enters the B-site preferentially in  $\text{CdCr}_2\text{O}_4$ , and it is of practical significance that this dopant has the effect of increasing the specific heat of C(9/1) at 4.2 K. This may be of importance for superconductor insulations, and it would be interesting to study magnetocaloric effects in, say, the 2% ceramic.

These doping studies are also of interest from the theoretical viewpoint, since understanding the effect of the  $\text{Fe}^{3+}$  dopant would provide guidelines for other dopants which may raise  $T_N$  into the hydrogen temperature range for cryoconductor-insulation applications.

<sup>1</sup>Some preliminary doping studies were performed under National Bureau of Standards Contract #NB81RAC10007

FIG. 1

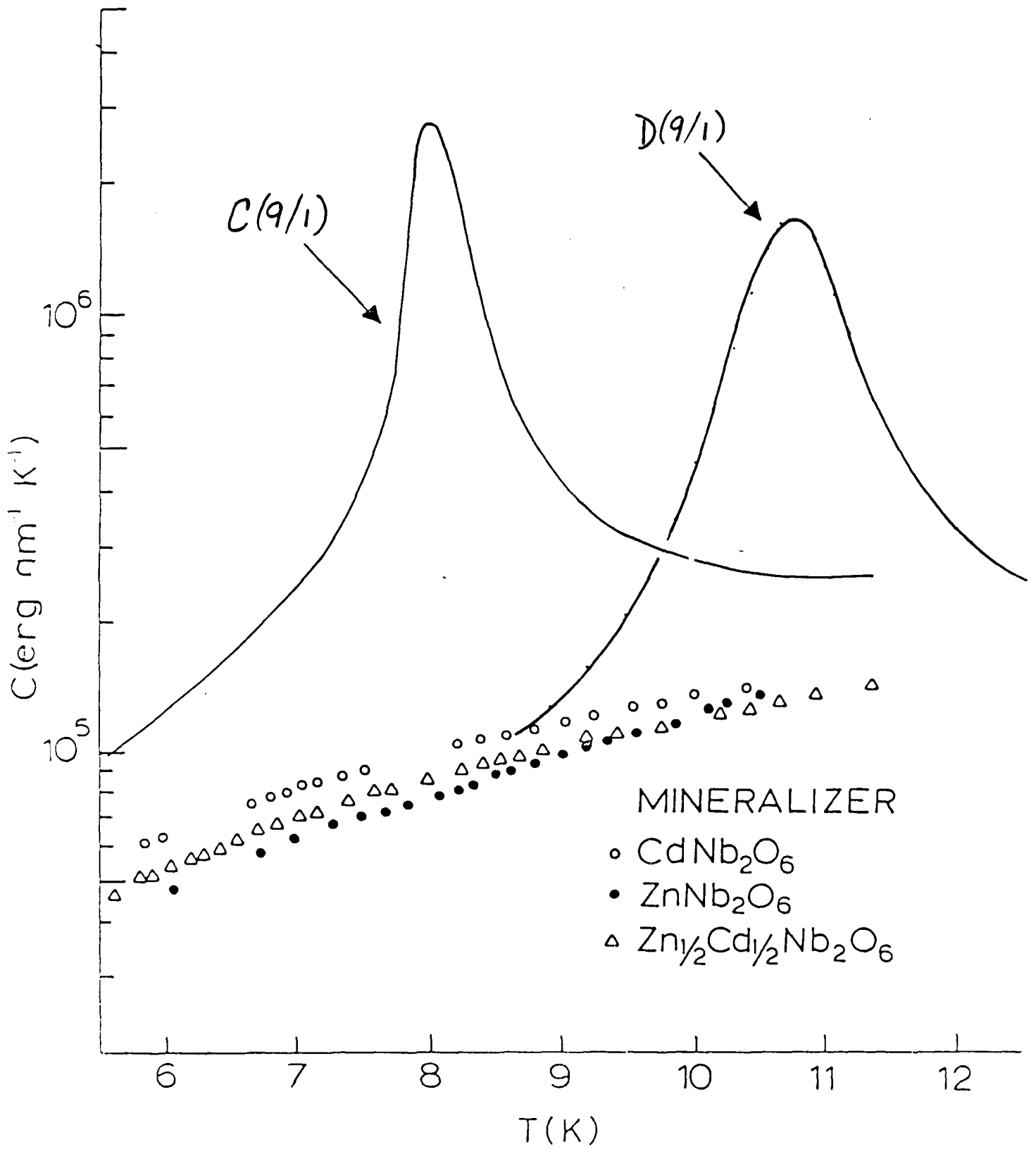


FIG. 2

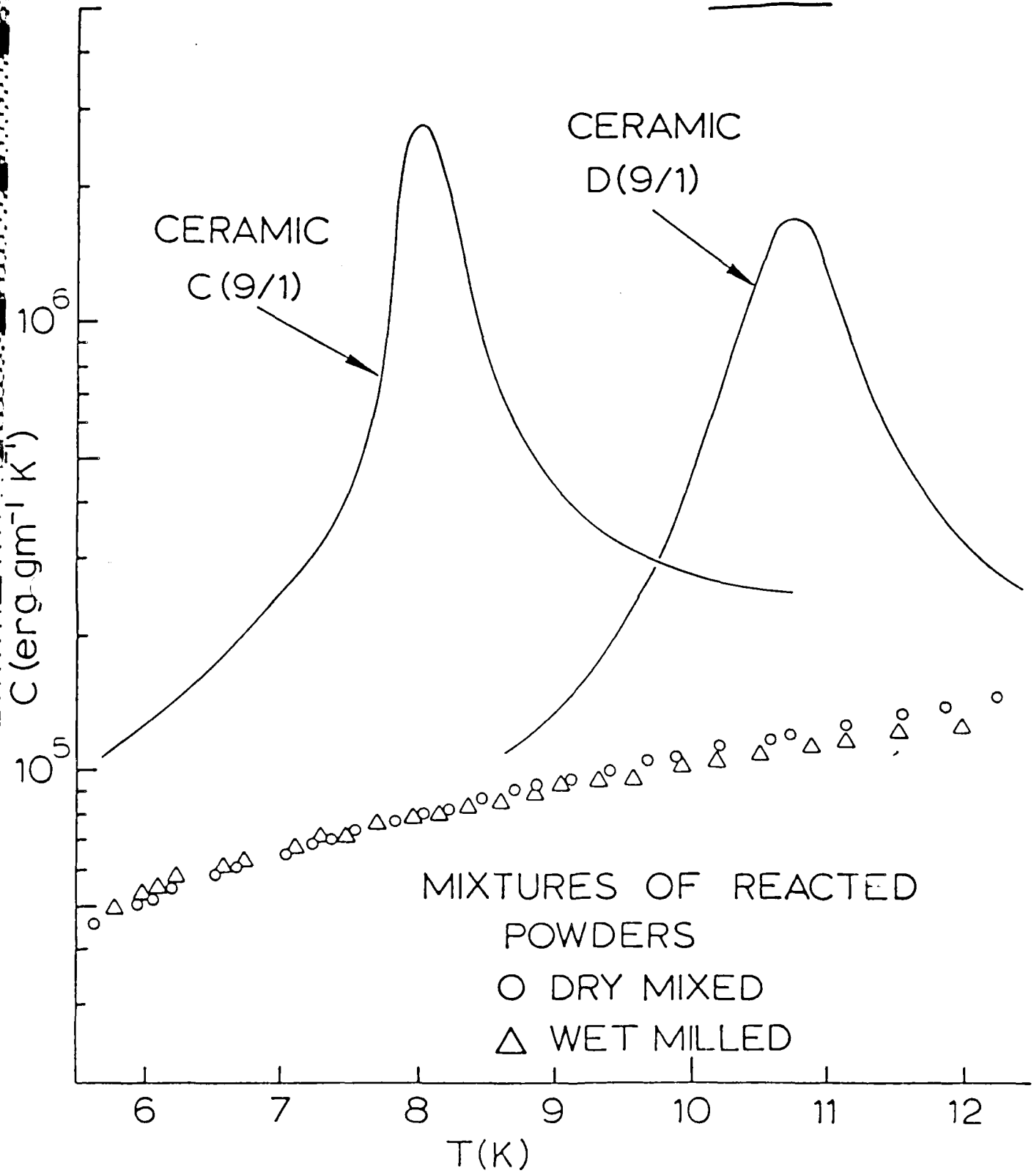


FIG. 3

DOPING IN CERAMIC C(9/1)

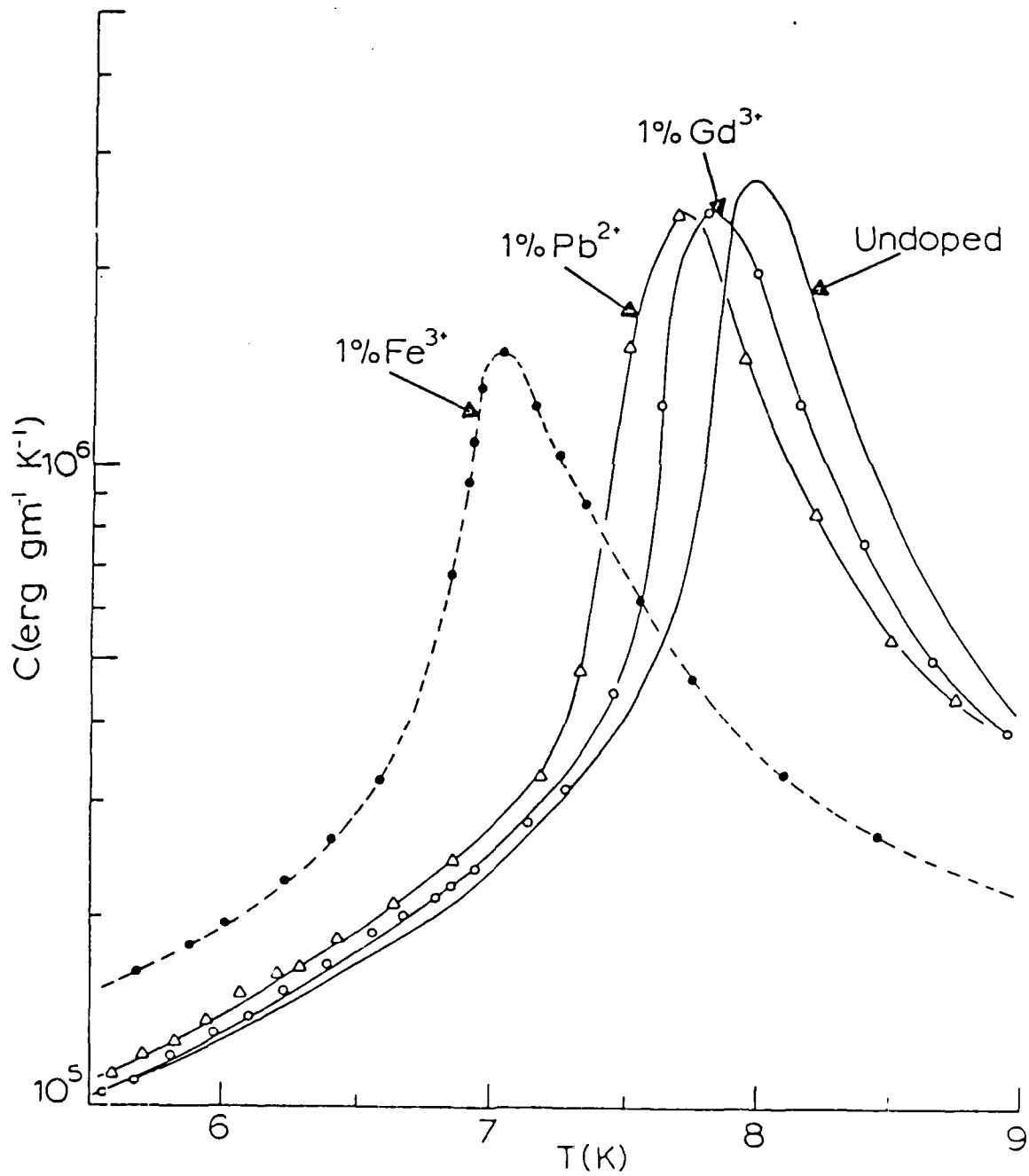
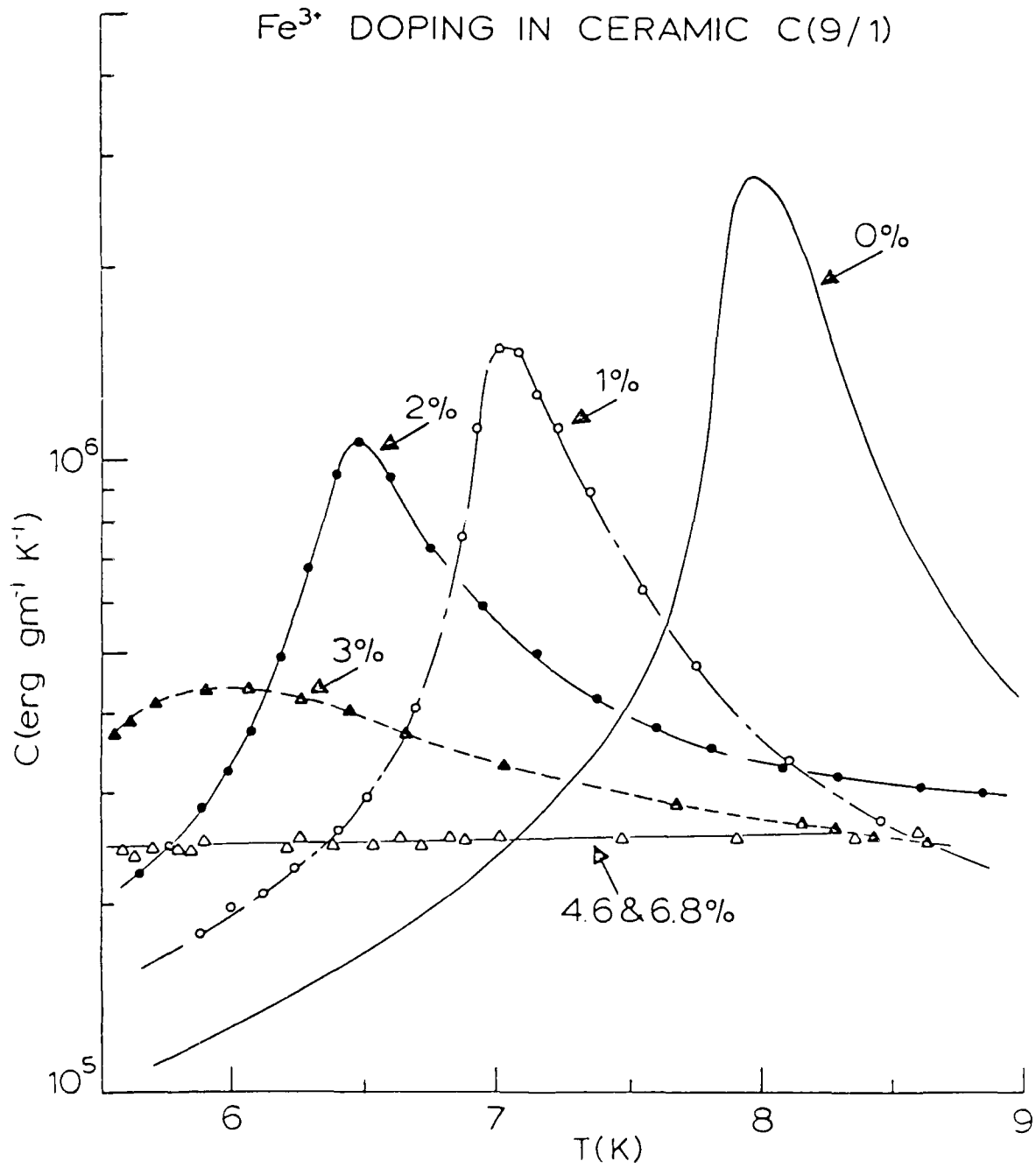


FIG. 4



Progress Report  
AFOSR contract #F49620-83-C0129

Fundamental Physics Studies on High-Specific-Heat  
Dielectrics and Kapitza Resistance at Dielectric Boundaries

Spinel Studies XIV. Careful Measurements of Thermal  
Conductivities in the Neighborhood of  $T_N$

by

W.N. Lawless *ANZ*  
CeramPhysics, Inc.  
Westerville, Ohio 43081  
May 3, 1985

Distribution:

J.H. Parker, Jr.  
P.W. Eckels  
T.K. Gupta  
M. Ashkin  
C.F. Clark  
B.R. Patton

We had previously reported broad range (1.7-30 K) thermal conductivity data ( $\kappa$ ) on C(9/1) and D(9/1), and these data are reproduced here in Fig. 1. Although these ceramics are two-phase mixtures of spinel + columbite, there is no doubt that the Fig. 1 data reflect heat flow in the spinel phase because the columbite phase represents a minor phase volumetrically (~ 10%). Stated differently, there is connectivity between the spinel grains.

A number of features are evident in Fig. 1: At the lowest temperatures a definitive  $T^3$  boundary-scattering region is not achieved, and one explanation may be Kapitza-limiting phenomena. In fact, one might suppose that the C(9/1) material is more Kapitza-limited than the D(9/1) material simply from the magnitudes of the  $\kappa$ -data in Fig. 1. However, this acoustic-mismatch explanation cannot easily be reconciled with the closeness of the Debye temperatures in the spinel phase (420, 463 K) and columbite phase (407, 433 K) in C(9/1) and D(9/1), respectively. A more satisfactory correlation for the suppression of the C(9/1) data relative to the D(9/1) data comes from previous estimates that ~ 80% of the  $\text{Cr}^{3+}$  spins in  $\text{CdCr}_2\text{O}_4$  order at  $T_N$  compared to ~ 50% of the spins in  $\text{ZnCr}_2\text{O}_4$ . Thus, it appears that the spin fluctuation term plays a significant role in limiting the thermal conductivity.

Along this line we also found previously that an intense magnetic field suppresses  $\kappa$  in C(9/1) below  $T_N$  but  $\kappa$  in D(9/1) was unaffected.

The most significant feature in Fig. 1 is the maximum in  $\kappa$  below  $T_N$  for both materials, and this is particularly evident in the case of D(9/1). However, there are actually very few data points in the neighborhood of this feature in Fig. 1, although the log-log plot tends to give the opposite illusion. Since this feature is of considerable theoretical interest, it was decided to measure the thermal conductivity at several points in the neighborhood of  $T_N$  for these materials, and this report documents these measurements.

Bars of C(9/1) and D(9/1) were fixtured with carbon-chip thermometers and heaters pursuant to the linear-flow method in

the usual fashion, and the carbon-chip thermometers were calibrated over narrow temperature ranges [e.g., 5-10 K for C(9/1)] during the course of the run (correlation coefficients > 0.9999). The thermal conductivity is given by

$$\kappa = i^2 R_{300} (a+bT) \ell / A \Delta T \quad (1)$$

where  $i$  is the heater current,  $R_{300}$  is the heater resistance at 300 K,  $(a+bT)$  corrects for the small temperature dependence of the heater wire,  $\ell$  is the separation of the thermometers,  $A$  is the cross-section area of the bar, and  $\Delta T$  is the temperature difference between the two thermometers ( $\Delta T/T < 2\%$  was maintained in these experiments). Since  $T$ ,  $\Delta T$ , and  $i$  were measured very accurately, we consider Eq. (1) in the form

$$\kappa = ci^2 (a+bT) / \Delta T \quad (2)$$

where the constant  $c$  is to be determined by carefully scaling the new data to the previous, Fig. 1 data. This is a relative procedure, and the motivation is to arrive at a precise comparison of  $\kappa$ -data. There is always the problem of comparing run-to-run data because the quantity  $R_{300} \ell / A$  can vary by as much as 5-7% between setups, due primarily to the uncertainty in  $\ell$ . Our scaling procedure eliminated this scale factor, and the results of these measurements are shown in Figs. 2 and 3 for C(9/1) and D(9/1), respectively. Here, the circles are the Fig. 1 data, and the triangles represent the new data points.

There is excellent agreement with the previous data sets (note linear scales), and the  $\kappa$ -features have been carefully mapped out. The critical experimental data are summarized in Table I.

Table I  
Thermal Conductivity Features ( $\text{mW cm}^{-1} \text{K}^{-1}$ )

Spinel	$T_N$	$T_{\min}$	$T_{\max}$	$\kappa_{\min}$	$\kappa_{\max}$
$\text{CdCr}_2\text{O}_4$	7.95 K	7.15 K	6.25 K	0.54	0.56
$\text{ZnCr}_2\text{O}_4$	10.73	12.3	10.1	1.59	3.22

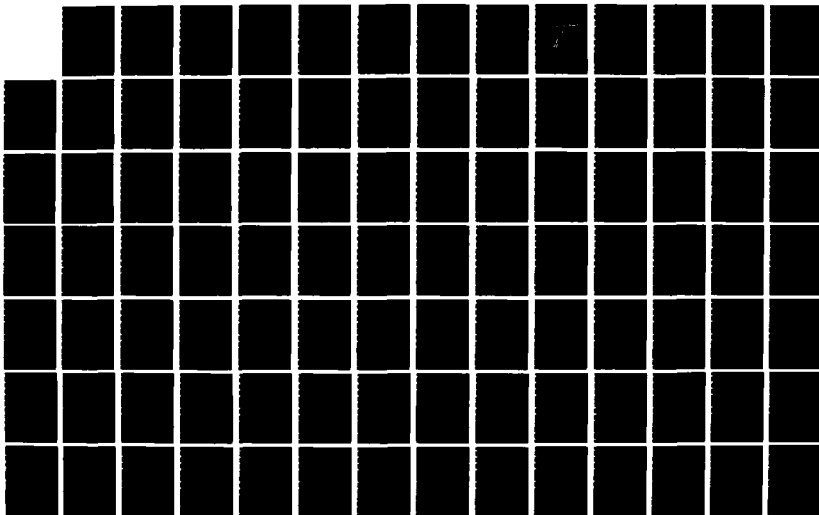
AD-A169 964

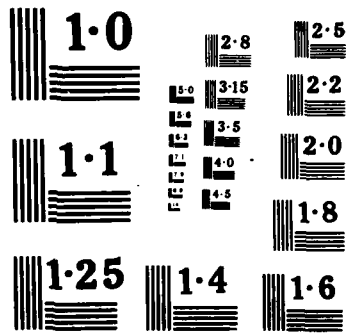
HIGH SPECIFIC HEAT DIELECTRICS AND KAPITZA RESISTANCE  
AT DIELECTRIC BOUND (U) WESTINGHOUSE RESEARCH AND  
DEVELOPMENT CENTER PITTSBURGH PA P W ECKELS ET AL  
30 SEP 85 AFOSR-TR-86-0477 F49620-83-C-0129 F/G 20/13

4/5

UNCLASSIFIED

ML





We note that distinct differences exist between the two spinels. For  $\text{CdCr}_2\text{O}_4$ , both  $T_{\text{min}}$  and  $T_{\text{max}}$  are below  $T_N$ , and  $\kappa_{\text{min}}$  and  $\kappa_{\text{max}}$  differ by only 4%. However, for  $\text{ZnCr}_2\text{O}_4$ ,  $T_{\text{max}}$  is slightly below  $T_N$ , and  $\kappa_{\text{min}}$  and  $\kappa_{\text{max}}$  differ by a factor of two (exactly). We conclude that the antiferrimagnetic spin wave contribution to  $\kappa$  in  $\text{ZnCr}_2\text{O}_4$  is huge compared to that in  $\text{CdCr}_2\text{O}_4$ .

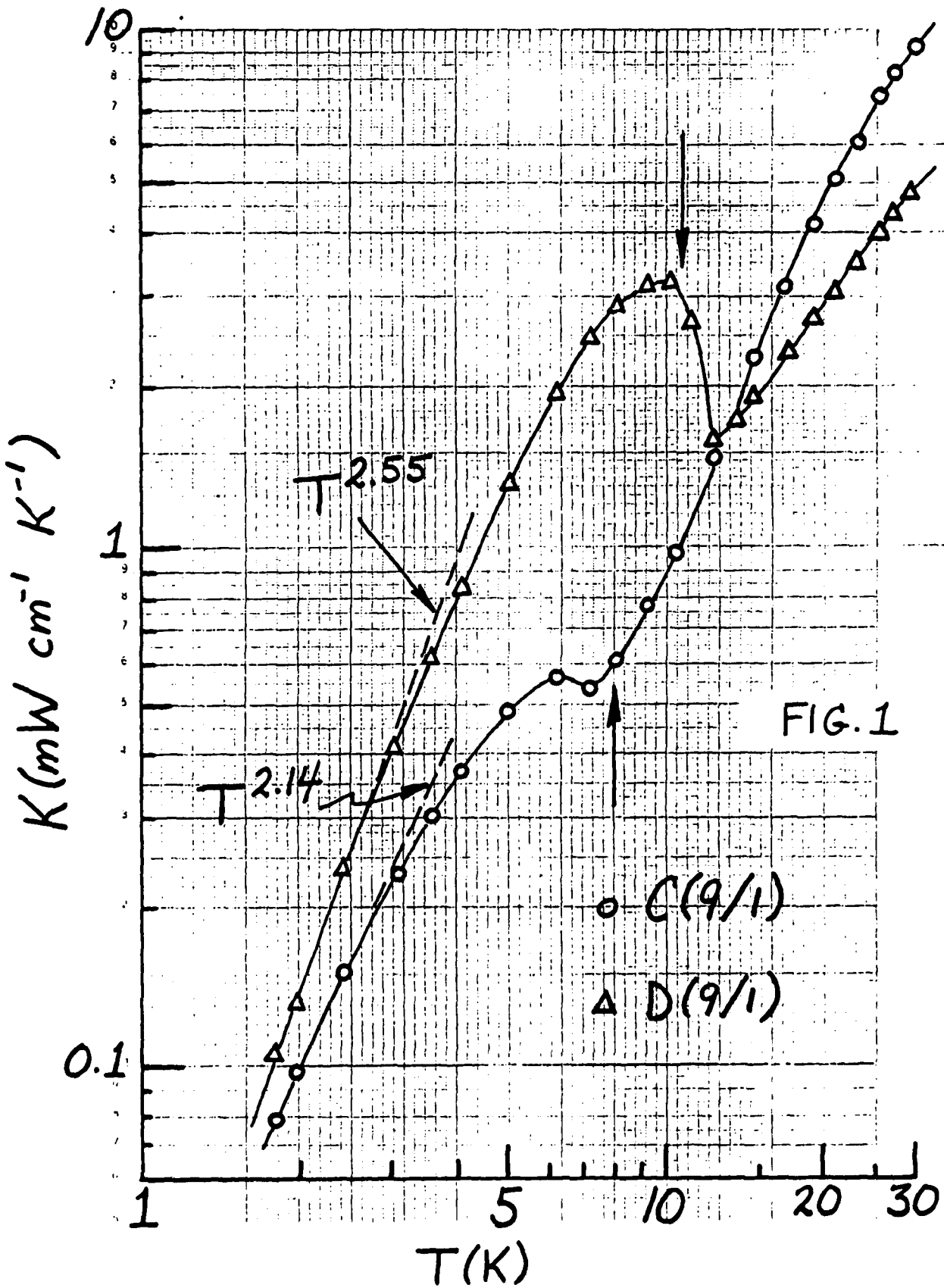
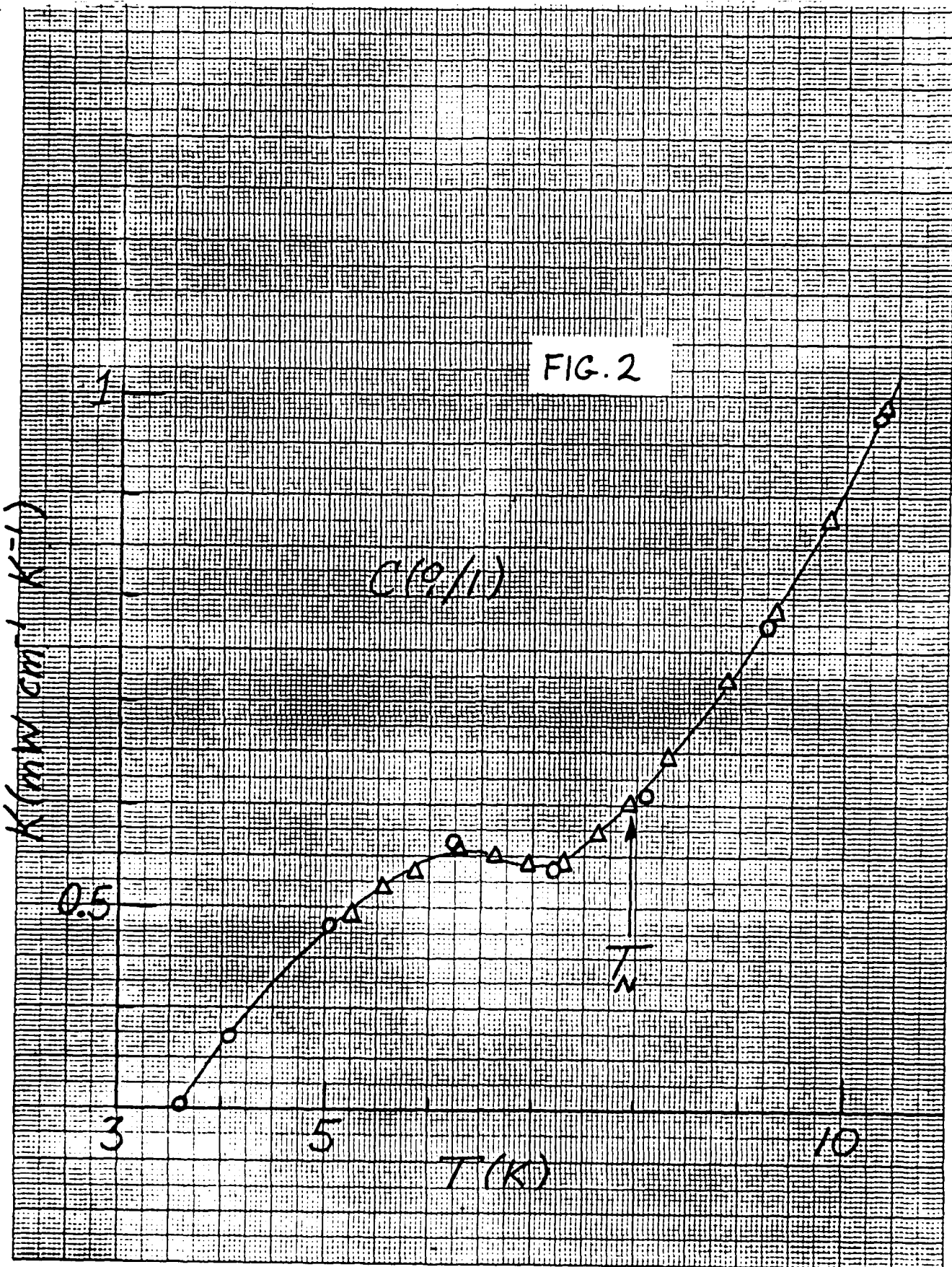
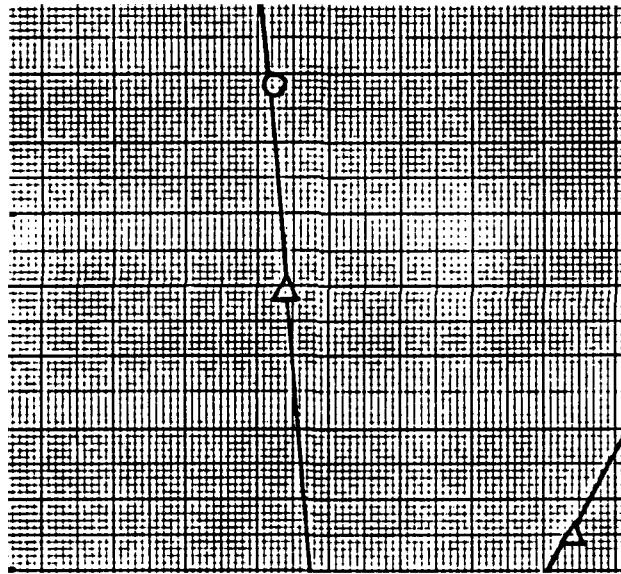


FIG. 1





AFOSR Contract #F4962C-83-CO129  
Fundamental Physics Studies on High-Specific-Heat  
Dielectrics and Kapitza Resistance at Dielectric Boundaries

Spinel Studies, XV.  $\text{Fe}^{3+}$  Doping  
in C(9/1)--Specific Heat Measurements

by

W.N. Lawless *WNL*

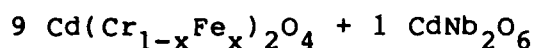
CeramPhysics, Inc.  
Westerville, Ohio 43081  
July 17, 1985

Distribution:

J.H. Parker, Jr.  
P.W. Eckels  
C.F. Clark  
B.R. Patton  
A. Menard

Some preliminary measurements several years ago indicated that  $\text{Fe}^{3+}$  doping in C(9/1) not only entered the  $\text{CdCr}_2\text{O}_4$  spinel but also had a dramatic effect on the specific heat properties. It was found that 1-3% of  $\text{Fe}^{3+}$  in C(9/1) depressed both the height and temperature of the specific heat peak, and above 4.6% the specific heat peak was missing. These previous measurements spanned a limited temperature range, ~ 4-10 K. The purpose of this Report is to document specific heat measurements on 2 and 5%  $\text{Fe}^{3+}$ -doped samples over the range 1.8-20 K.

Two pellets were prepared according to the composition



with  $x = 0.020$  and  $0.050$ . The usual ceramic processes were used, and the final firing was at  $1275^\circ\text{C}$  for 2 h.

In the specific heat measurements, the addenda constituted 1.5-1.6 wt % and contributed 1.3% at most to the total heat capacity.

The results of these measurements are shown in Fig. 1 where the data for undoped C(9/1) are shown for comparison. Four features are evident in Fig. 1: (1) The 2% doping lowers the peak temperature to 6.34 K from 7.99 K in the undoped case; (2) The 5% doping eliminates the specific heat peak; (3) There are no additional specific heat features in the 2 and 5% samples in the range 1.8-25 K; and (4) The 5% sample has the largest specific heat below 5.5 K.

These features are shown in Fig. 2 from 3-12 K plotted linearly. Here the doping progression is seen somewhat more clearly than in Fig. 1; in particular, the 2%  $\text{Fe}^{3+}$  doping broadens the specific heat peak and decreases the maximum value. In both Figs. 1 and 2 the specific heat data converge above about 10 K, which is a satisfying check on the experimental methods.

### Discussion

The results here confirm the earlier findings and show that no additional specific heat features are induced by the  $\text{Fe}^{3+}$

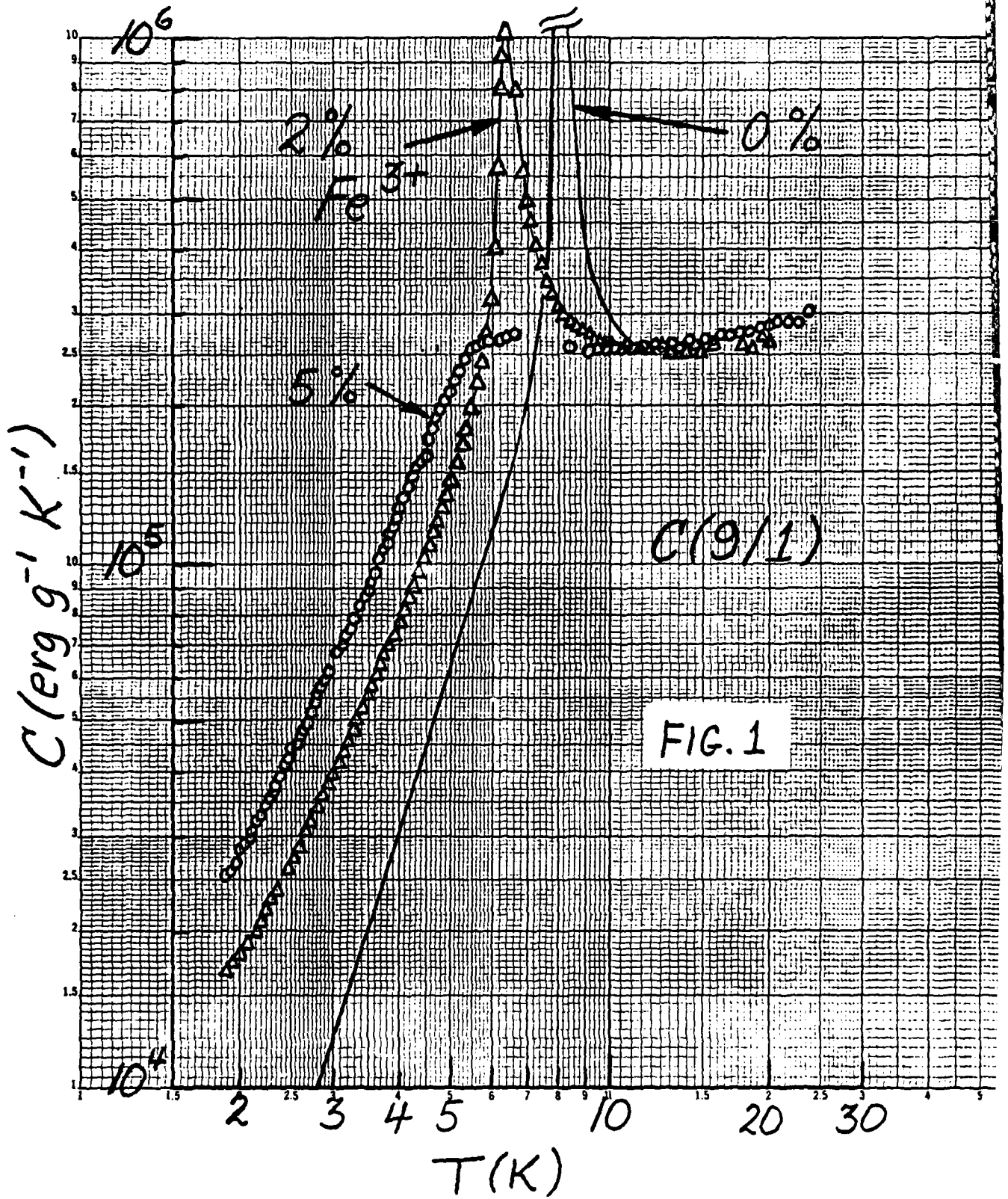
doping (e.g., a peak at, say, 20 K). Previous studies have shown that only some fraction of the  $\text{Cr}^{3+}$  spins order at 8 K in  $\text{CdCr}_2\text{O}_4$ , and the results here suggest that a small amount of  $\text{Fe}^{3+}$  doping further frustrates this ordering so that by 5%, complete frustration has occurred. This in turn suggests that the 5% doping should lead to larger magnetocaloric effects.

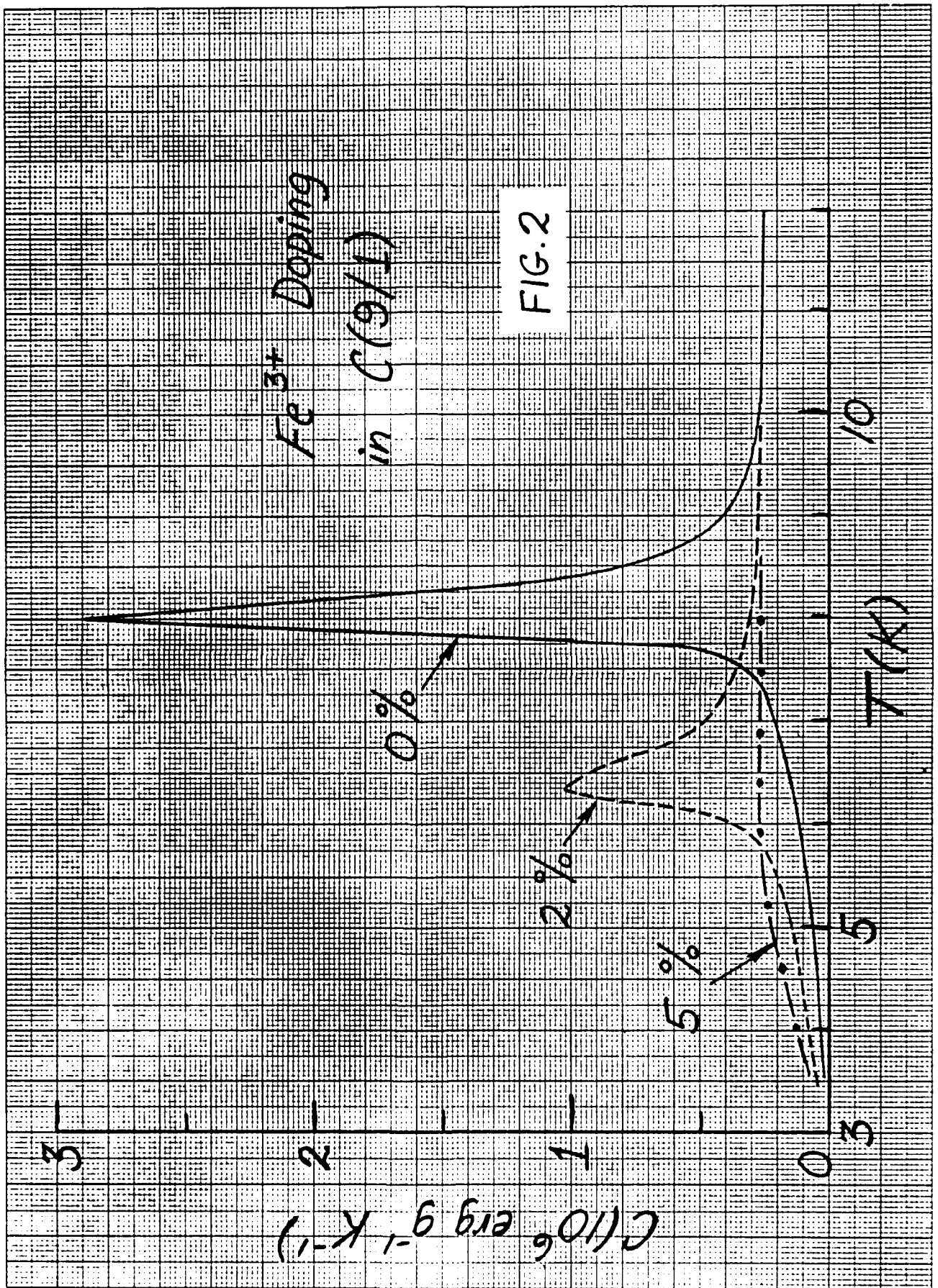
Spin resonance studies are needed to prove that all the  $\text{Fe}^{3+}$  added to the ceramic is indeed entering the spinel phase at the  $\text{Cr}^{3+}$  site.

For regenerator applications it is interesting to note that between 5.8 and 7.5 K the 2% doping yields the largest specific heat, whereas below 5.8 K the 5% doping yields the largest specific heat. It would be particularly interesting to develop a dopant that would raise the peak temperature of C(9/1).

Thermal conductivity measurements on these 2 and 5%-doped C(9/1)'s are in progress.

K&E LOGARITHMIC 46 7083  
5 1/2 CYCLES  
RUFFEL & SEBER CO.





AFOSR Contract #F49620-83-CO129  
Fundamental Physics Studies on High-Specific-Heat  
Dielectrics and Kapitza Resistance at Dielectric Boundaries

Spinel Studies, XVI.  $\text{Fe}^{3+}$  Doping  
in C(9/1)--Thermal Conductivity Measurements

by

W.N. Lawless



CeramPhysics, Inc.  
Westerville, Ohio 43081  
August 8, 1985

Distribution:

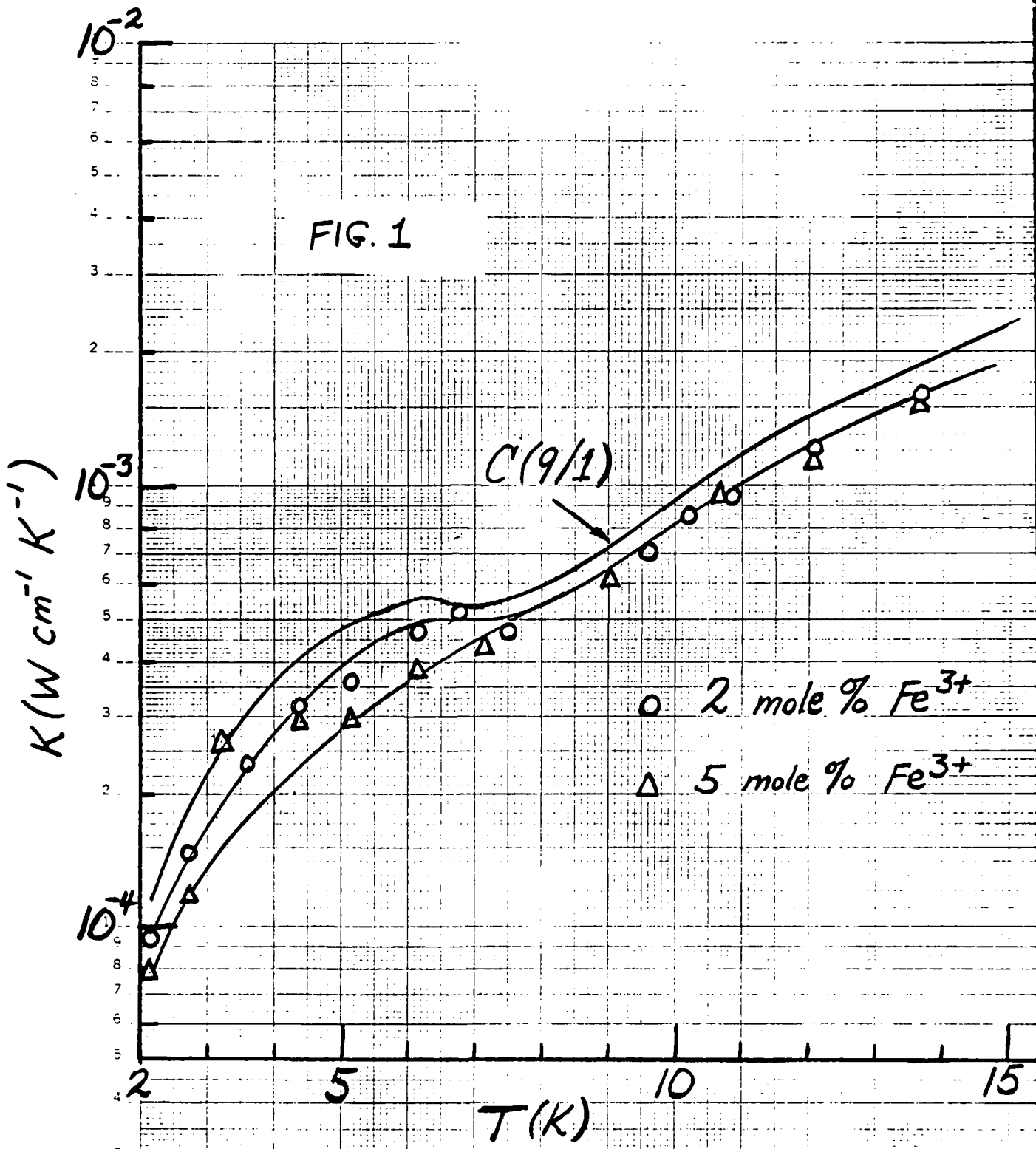
J.H. Parker, Jr.  
P.W. Eckels  
C.F. Clark  
B.R. Patton  
A. Menard

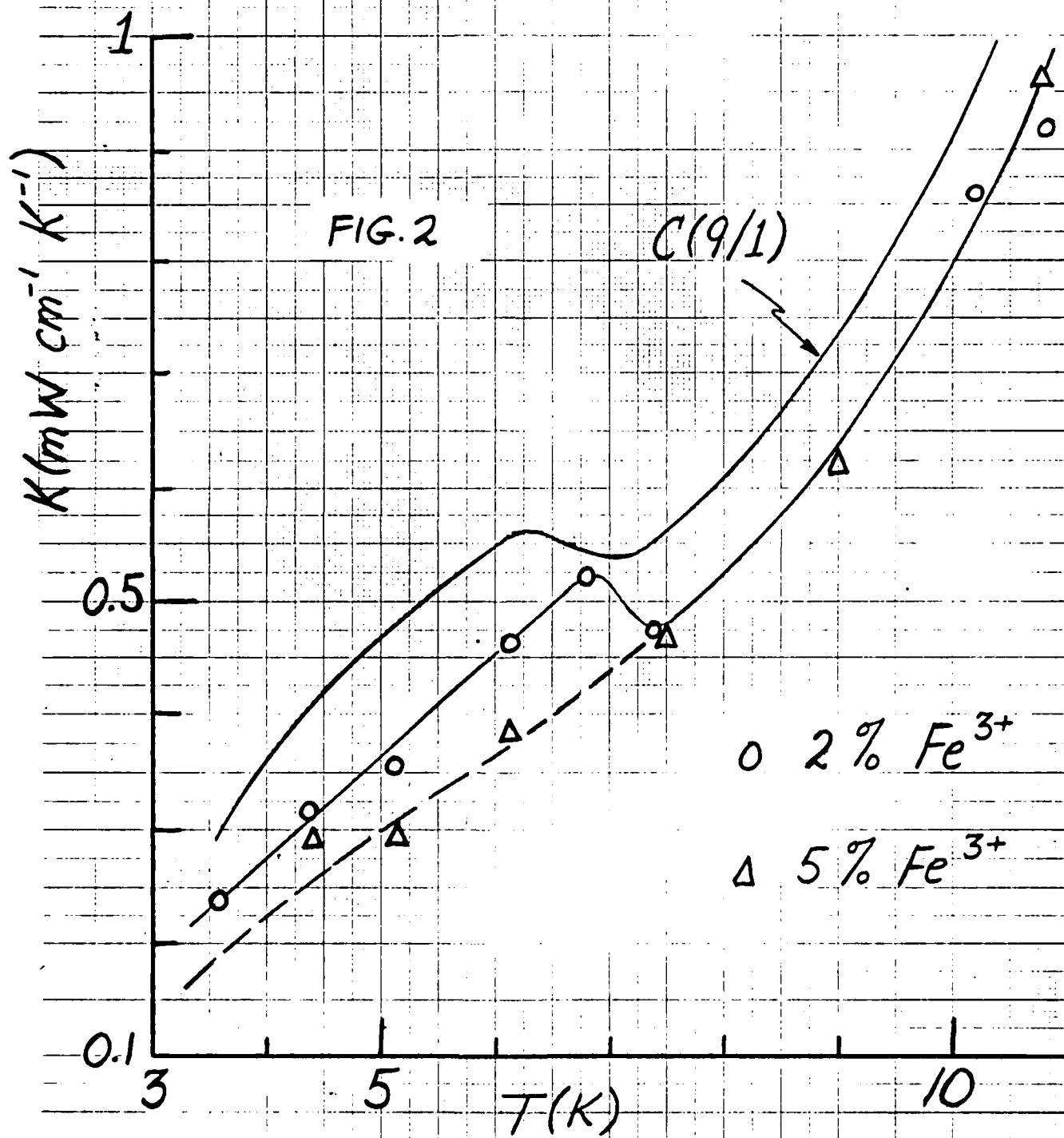
In the last Letter Report on Spinel Studies, we documented specific heat measurements on C(9/1) doped with 2 and 5 mole %  $\text{Fe}^{3+}$  (i.e., assuming the  $\text{Fe}^{3+}$  enters the B-site of the spinel). At the 2% level the specific heat maximum is shifted from 8.0 to 6.35 K, and the height of the maximum is depressed from 2.9 to 1.05 ( $10^5 \text{ erg g}^{-1} \text{ K}^{-1}$ ). At the 5% level, the specific heat maximum is totally suppressed, and no other specific heat structure appears in the range 1.8 to 30 K. Above 10 K all specific heat data converge (including the undoped case).

The purpose of this Letter Report is to document thermal conductivity data on these 2 and 5 %  $\text{Fe}^{3+}$ -doped C(9/1) compositions. The thermal conductivity bars here were fabricated side by side with the specific heat pellets previously measured. Thermal conductivity measurements were made by the two-thermometer linear flow method, and very long waiting times were required to reach equilibrium due to the very low thermal conductivities.

Thermal conductivity data in the range 2-15 K are shown in Fig. 1 together with data on undoped C(9/1) which show the jump in the thermal conductivity. A similar jump appears in the 2%-doped data, but the 5%-doped data display no structure. The data above 9 K for the 2- and 5%-doped ceramics are identical but are suppressed compared to the undoped case.

These thermal conductivity data are shown in more detail in Fig. 2. Surprisingly, the data for the 2% case show a jump at a higher temperature than the undoped case, although the ordering of the respective specific heat maxima is just the opposite. The data for the 5% case appear to represent the background data for the 2% case but not for the undoped case. For example, the experimental uncertainty in the measurements is  $\sim \pm 5\%$  (due predominantly to the uncertainty in measuring the separation of the thermometers). Consequently, at say 10 K, the thermal conductivities of the doped and undoped ceramics are  $0.92 \pm 0.05$  and  $0.80 \pm 0.04 \text{ mW cm}^{-1} \text{ K}^{-1}$ , respectively. Thus, the separation of the curves in Fig. 2 above 8 K is not due to experimental uncertainty.





AFOSR Contract #F49620-83-C0129  
Fundamental Physics Studies on High-Specific-Heat  
Dielectrics and Kapitza Resistance at Dielectric Boundaries

Columbite Studies I. Critical Exponents

by

R.W. Arenz and W.N. Lawless

*AW*

*WNL*

CeramPhysics, Inc.  
Westerville, Ohio 43081  
June 3, 1985

Distribution:

J.H. Parker, Jr.  
P.W. Eckels  
C.F. Clark  
B.R. Patton  
A. Menard

Previous studies in this program have been devoted exclusively to the new spinels ( $\text{CdCr}_2\text{O}_4$  and  $\text{ZnCr}_2\text{O}_4$ ) and to the heavy-metal halides (e.g., CsI). There is, however, a third category of important materials, namely the new columbites  $\text{NiNb}_2\text{O}_6$  and  $\text{MnNb}_2\text{O}_6$ .

To review briefly, Fig. 1 is a plot of specific heat data on refractory ceramics compared both to helium gas at three pressures and to Pb. These data are plotted on a volumetric basis, and the curves labelled  $C^1$  and D refer to  $C(9/1)$  and  $D(9/1)$ , respectively, which we have studied extensively in this program. The curves labelled A and B refer to  $\text{MnNb}_2\text{O}_6$  and  $\text{NiNb}_2\text{O}_6$ , respectively.

The Fig. 1 data show that these columbites have technologically important transition temperatures,  $\sim 4.2$  and  $\sim 5.5$  K, and that very large specific heat maxima are attained,  $\sim 0.2 \text{ J cm}^{-3} \text{ K}^{-1}$ . Going further, these single-phase ceramics have relatively large thermal conductivities, as shown in Fig. 2 (note here that the thermal conductivity for both columbites varies smoothly and monotonically through the transition region, in contrast to the spinels).

For these reasons, both of these columbites have been introduced into the applied Air Force programs aimed at developing dielectric insulations for superconductors. Specifically:

1. Both ceramics A and B (alternately referred to in the applied programs as SClA and SClB) have been studied in the form of composites with various glasses, and viable ceramic/glass composites have been demonstrated. In particular, an SClA/3072 composite has been identified as a possible candidate insulation for  $\text{Nb}_3\text{Sn}$ .
2. The A ceramic displays very interesting magnetocaloric properties at 4.2 K: Adiabatic demagnetization cooling in fine particle size, adiabatic magnetization cooling in coarse particle size. No magnetocaloric studies have been made on ceramic B.

3. Powders of ceramic A have been added to an impregnating epoxy, and it was found that both the specific heat and the thermal conductivity were markedly improved.

Given the applied significance of these two new columbites, it was decided to devote a limited effort in the present program to these materials. Certainly one of the most interesting items to explore here is the critical exponent associated with the sharply peaked specific heat (Fig. 1). CeramPhysics has recently developed a sophisticated, computer-interfaced method for measuring specific heats by a slow-drift technique, and the purpose of this Letter Report is to document these critical-exponent studies on  $\text{MnNb}_2\text{O}_6$  and  $\text{NiNb}_2\text{O}_6$ .

Samples of  $\text{MnNb}_2\text{O}_6$  (1.026 g) and  $\text{NiNb}_2\text{O}_6$  (1.841 g) were grooved to accept carbon-chip thermometers, the purpose of the grooves being to minimize the thermal diffusion path. The samples were fixtured with thermometers, heaters, and long (15 cm) thin copper-wire thermal links. These links were designed to provide overall drift rates  $\sim 10$  mK/sec, but of course the drift method "slows" considerably in the neighborhood of  $T_N$ . The addenda constituted 3.1 and 1.8 wt % to the samples and contributed  $< 0.1$  % to the total heat capacity, respectively.

The experiments were carried out in the adiabatic calorimeter, and the first step was to calibrate the carbon-chip thermometers in situ in the range  $T_N \pm 2.5$  K. About 6-7 calibration points each were taken and fitted to  $\log R = A + BT^{-P}$  (correlation  $> 0.9999$ ). Next the sample heater was used to bring the sample to  $T_N + 2$  K, the heater was de-activated, and the drift record started. Data points were taken every 5 s by the automated data-collection system, and three quantities were recorded: (1) The common thermometer current, (2) The carbon-chip thermometer voltage; and (3) The voltage of a germanium standard mounted in the reservoir. Computer analysis of this information yields temperature records coincident in time for the sample and reservoir, which are then further reduced to yield specific heat information per the scheme outlined in the March 1,

1985, Letter Report. In the present work, one drift of  $\text{NiNb}_2\text{O}_6$  and two drifts of  $\text{MnNb}_2\text{O}_6$  were performed; the drifts were 53.5 minutes, 65 minutes, and 73.5 minutes, respectively. In all three drifts, the temperature changed  $\sim 3$  mK per sampling step over the specific heat peaks. The resultant specific heat data are presented in Figs. 3 and 4 (only the result of the second of the two  $\text{MnNb}_2\text{O}_6$  drifts is shown).

Critical exponent information is extracted from the specific heats using the methodology presented in the March 1 report. At the time of these reductions for  $\text{MnNb}_2\text{O}_6$  and  $\text{NiNb}_2\text{O}_6$  an error was found in the March 1 results for  $\text{CdCr}_2\text{O}_4$  and  $\text{ZnCr}_2\text{O}_4$ . To be consistent with the methods actually used, the equations 1-3 listed in that report should be written

$$C = (A/\alpha)t^{-\alpha} + B\tau + E \quad (1)$$

$$t = |T - T_N / T_N| \quad \tau = T - T_N \quad (2)$$

$$C_{\text{ex}} = C - B\tau - E \quad (3)$$

The B and E terms for  $\text{CdCr}_2\text{O}_4$  and  $\text{ZnCr}_2\text{O}_4$  given these redefinitions are (in appropriate cgs units):

$$\begin{array}{ll} \text{CdCr}_2\text{O}_4: & B = 3.3710 \times 10^3 \quad E = 2.3960 \times 10^5 \\ \text{ZnCr}_2\text{O}_4: & B = 3.4173 \times 10^3 \quad E = 2.1751 \times 10^5. \end{array}$$

Recomputation of the  $\text{CdCr}_2\text{O}_4$ ,  $\text{ZnCr}_2\text{O}_4$  data yields  $C_{\text{ex}}$  results quite close to those reported March 1. Both materials showed less than 0.05% change in the specific heat peak region  $C_{\text{ex}}$  values, thus  $\alpha$  values for these regions may stand without correction.

Variations between originally reported  $C_{\text{ex}}$  values and the recomputed values become greater as one moves from the specific heat peak to temperatures higher and lower. At the extremes of temperatures reported for  $\text{ZnCr}_2\text{O}_4$  this variation was still less than 1%. For  $\text{CdCr}_2\text{O}_4$  the greatest variation was higher,  $\sim 5\%$ . However, if the new results are plotted upon March 1 figs. 3 and 4, these variations are nearly unnoticeable in the regions where the  $\alpha$  values for the wings were determined. Again, we conclude it is unnecessary to recompute new  $\alpha$  values for the March 1

report.

The calculation of  $C_{ex}$  for  $NiNb_2O_6$  and  $MnNb_2O_6$  requires B and E coefficients which are determined in the manner reported June 14, 1984; Fig. 5 diagrams the process. Note in the present study that specific heat data for  $MnNb_2O_6$  above  $T-T_N = 10$  K were not available, and that the E term had to be estimated upon the basis of B assumed the same for both  $NiNb_2O_6$  and  $MnNb_2O_6$ . The values determined in this manner are (in appropriate cgs units):

$$\begin{array}{lll} NiNb_2O_6: & B = 1.3136 \times 10^3 & E = 6.9893 \times 10^4 \\ MnNb_2O_6: & B = 1.3136 \times 10^3 & E = 6.2714 \times 10^4. \end{array}$$

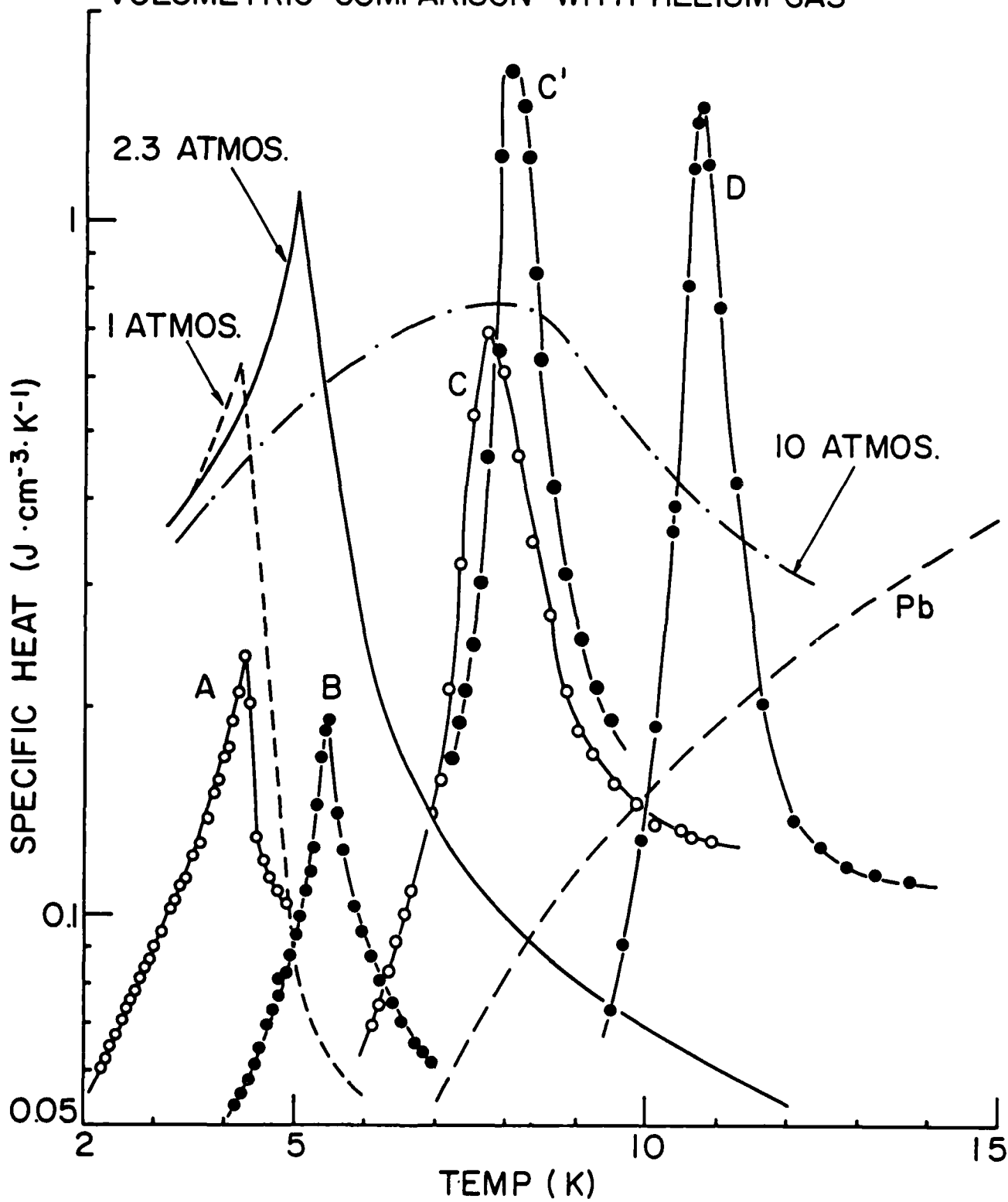
The  $T_N$  values adopted from the specific heat records were 5.49704 K for  $NiNb_2O_6$  and 4.3324 K for  $MnNb_2O_6$ . The latter value is an average between the two records for  $MnNb_2O_6$  which differed by 8.8 mK in  $T_N$ .

Figures 6-8 present the reduced  $C_{ex}$ 's versus  $\log t$ . The peaks are asymmetric for both materials; in our opinion no consistent alpha values are defined in the wings around the specific heat peaks. Thus, alpha's were computed only for the "flat" regions immediately around the peaks using least squares techniques (Figs. 9-11). The alpha determined for  $NiNb_2O_6$  was  $1.45 \times 10^{-3}$ . The alpha determined from one drift of  $MnNb_2O_6$  was  $1.19 \times 10^{-2}$ , from the other drift was  $5.32 \times 10^{-3}$ . All of these values are roughly on the same order as those determined for  $CdCr_2O_4$  and  $ZnCr_2O_4$ .

Differences between the two runs on  $MnNb_2O_6$  indicate something about the repeatability of the experimental method. Though there were no great differences in the experimental details between the two drifts of the sample and reduction was handled exactly the same for the two samples, there was a difference in the specific heat values generated. The two curves were rather parallel to one another, but separated by ~ 8% at the peaks. The alpha's determined differed by a factor of 2. As may be guessed from Figs. 10 and 11, the least squares fitting is quite sensitive to the grouping of data about  $T_N$  and is particularly sensitive to the  $\log \left| (T-T_N)/T_N \right|$  value for the point nearest to  $T_N$ . That is, if T is very close to  $T_N$ , the point will

lie quite far from the main body of points in the fitting and will decrease the apparent alpha. If the  $t = -4.5$  point is eliminated in Figure 11 the alpha becomes  $9.70 \times 10^{-3}$ , much nearer the alpha of Figure 10. We intend to do further studies upon the repeatability of the results from drift to drift.

VOLUMETRIC COMPARISON WITH HELIUM GAS



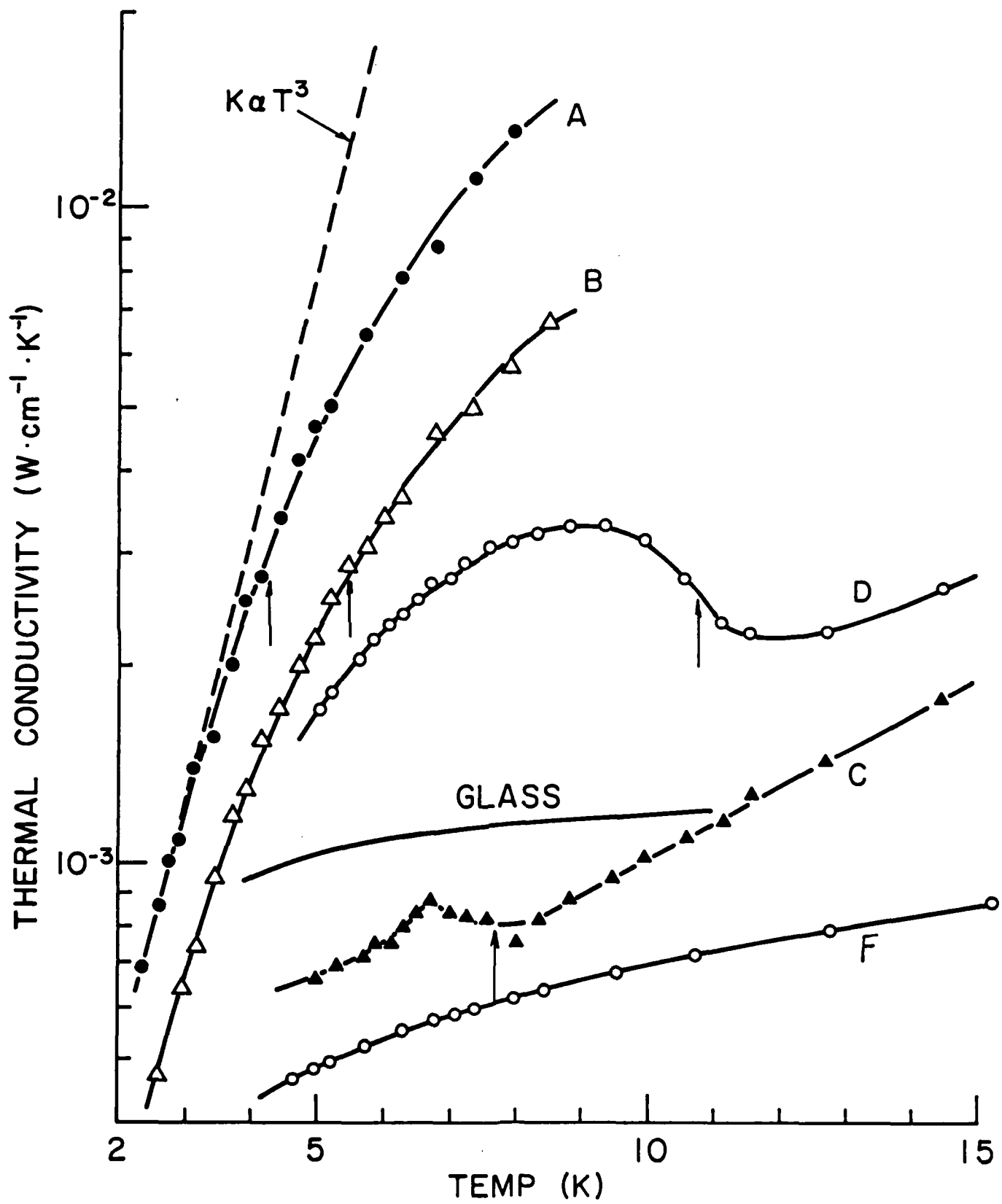
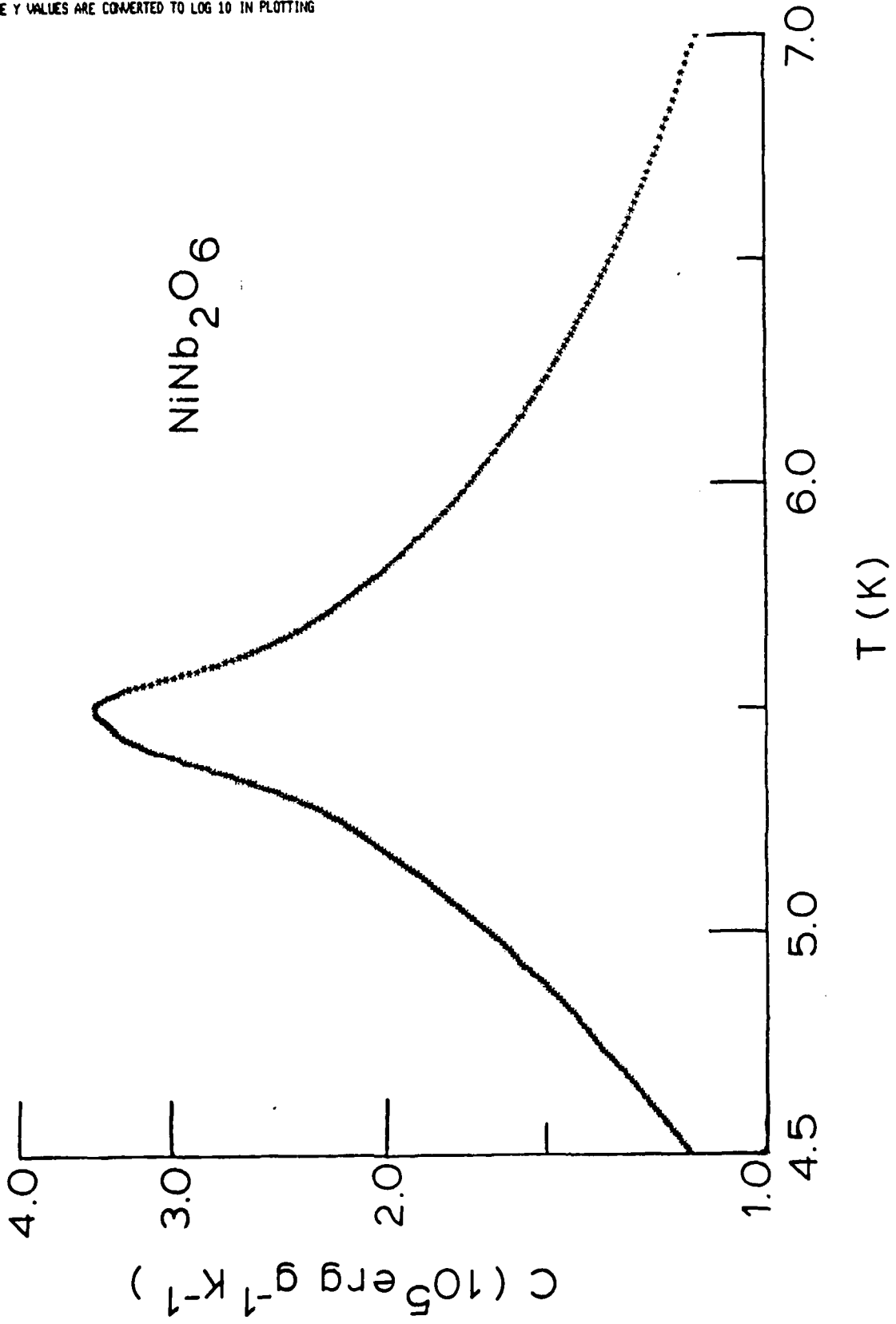


Fig. 2

\*\*\*\*\*  
 NIN DRIFT FOR CRITICAL EXPONENTS 3/28/85  
 A = 2.4976324E+00 B = 3.5018778E+00 P = 8.0261737E-01 LEAD RESISTANCE = 0.0000  
 ACCORDION AND SAMPLE HEIGHTS:  
 SAMPLE = 1.8408000E+00 GRAPHITE = 9.3000000E-03 GE7031 = 1.4000000E-03 METAL = 2.2000000E-02  
 ALPHA = 3.8696100E+02 BETA = 2.0025700E+01 GAMMA = 0.0000000E-01  
 SLOPE = 5.4122799E+01 INTERCEPT = -2.6710873E+01 TIME STEP (SECS) = 5.00  
 XMIN = 4.50000E+00 XMAX = 7.00000E+00 YMIN = 1.00000E+05 YMAX = 4.00000E+05  
 THE Y VALUES ARE CONVERTED TO LOG 10 IN PLOTTING



MIN 240 DRIFT FOR CRITICAL EXPS. 3/28/85  
 A = 2.5470545E+00 B = 3.5369631E+00 P = 8.1599224E-01 LEAD RESISTANCE = 0.0000  
 AGGENDUM AND SAMPLE WEIGHTS:  
 SAMPLE = 1.3259000E+00 GRAPHITE = 8.5000005E-03 GE7031 = 7.9999998E-04 METAL = 2.5900000E-02  
 ALPHA = 4.0145999E+02 BETA = 2.0679001E+01 GAMMA = 0.0000000E-01  
 SLOPE = 5.6500000E+01 INTERCEPT = -7.0048500E+01 TIME STEP (SECS) = 5.00  
 XMIN = 3.50000E+00 XMAX = 6.00000E+00 YMIN = 1.50000E+05 YMAX = 5.50000E+05  
 THE Y VALUES ARE CONVERTED TO LOG 10 IN PLOTTING

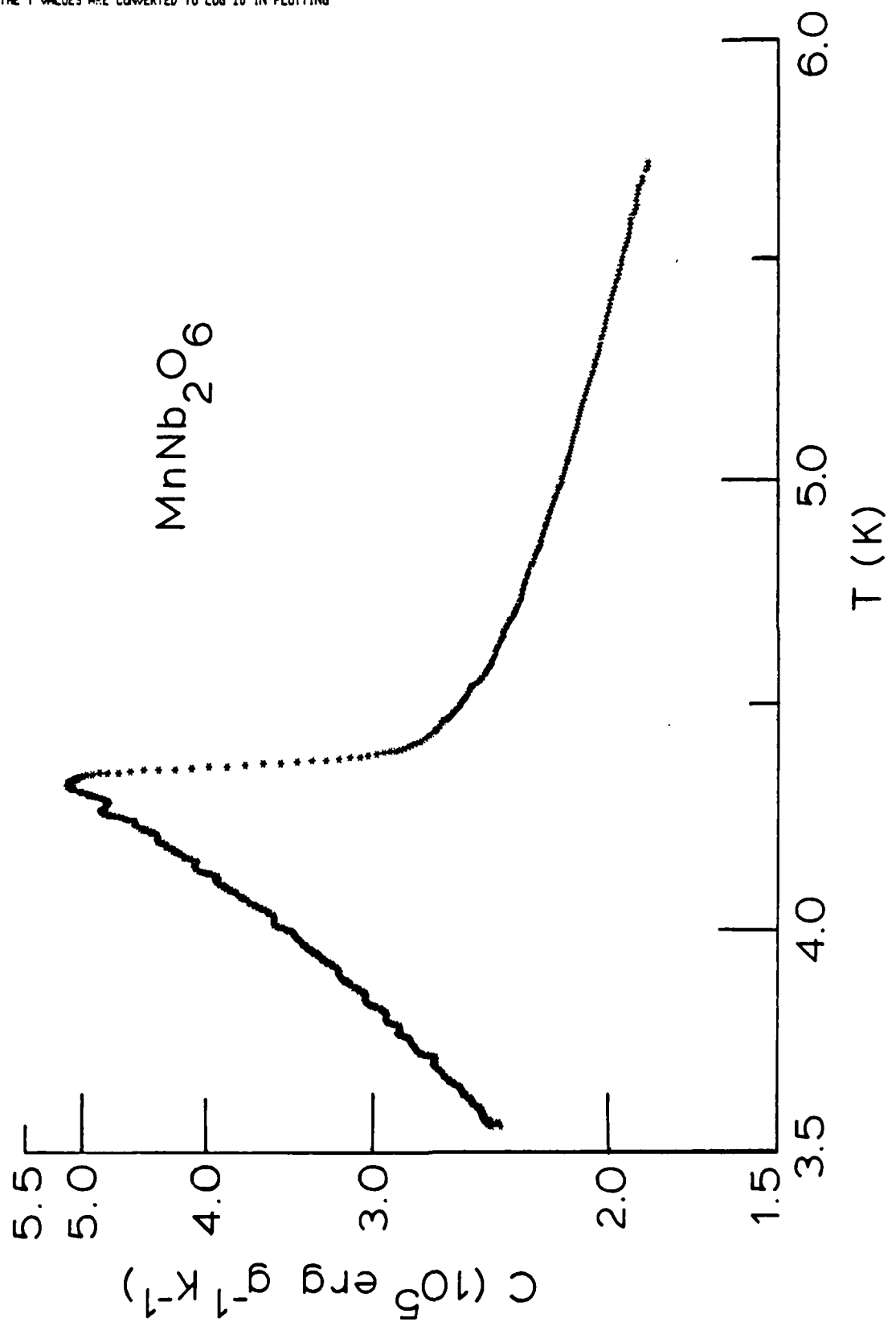
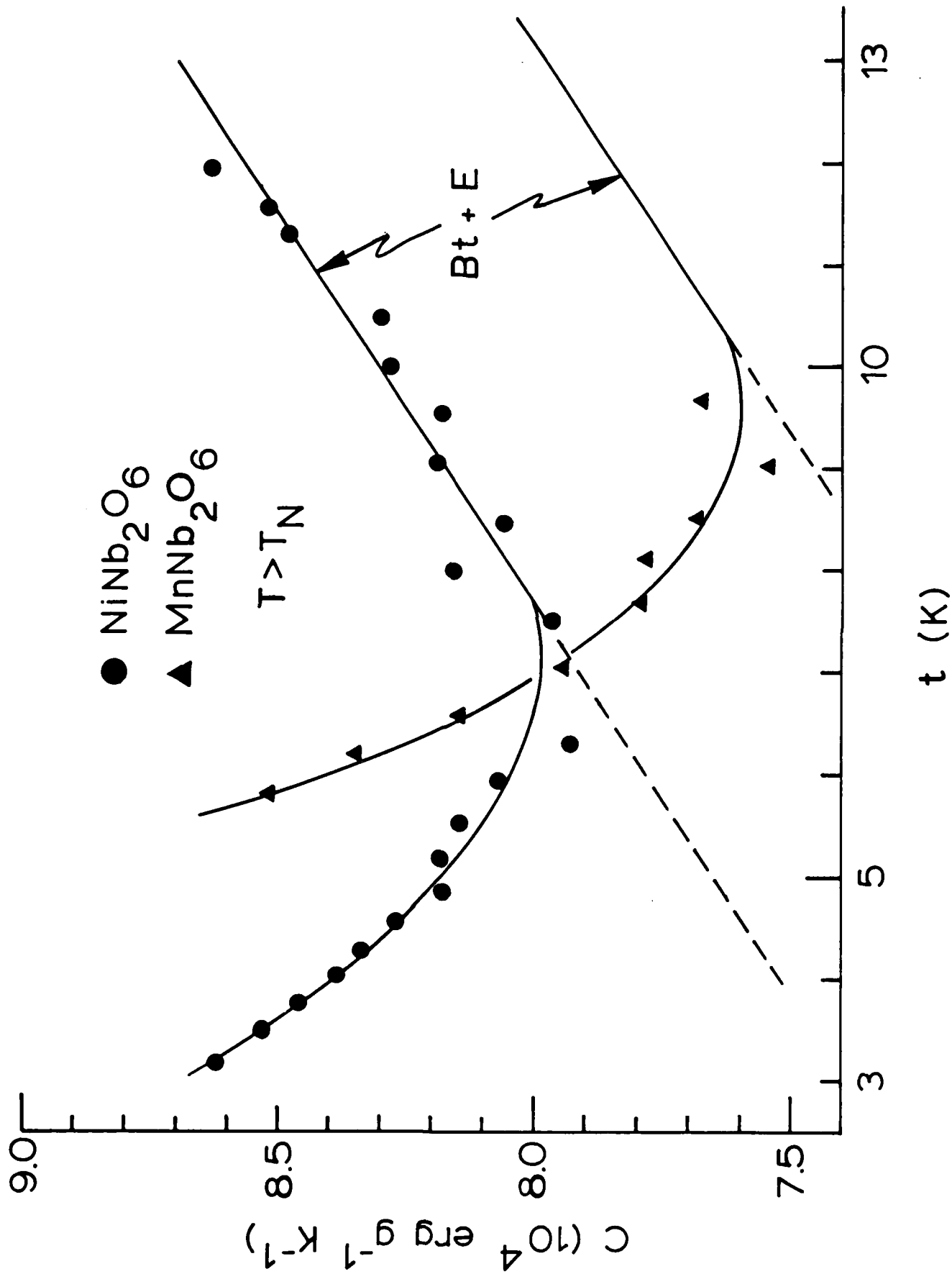


Fig. 4



D-160

00000  
 N SLOPE = 5.4122799E+01 INTERCEPT = -2.6710873E+01 TIME STEP (SECS) =  
 A = 2.4970324E+00 B = 3.5018778E+00 P = 8.0261737E-01 LEAD RESISTANCE  
 SAMPLE = 1.8408000E+00 GRAPHITE = 9.3000000E-03 GE7031 = 1.4000000E-03 ME  
 ALPHA = 3.8696100E+02 BETA = 2.0025700E+01 GAMMA = 0.0000000E-01  
 SLOPE = 5.4122799E+01 INTERCEPT = -2.6710873E+01 TIME STEP (SECS) =  
 TN = 5.4970 KELVIN, B = 1.31360E+03 E = 6.99330E+04  
 AMIN = -3.50000E+00XMAX = -8.00000E-01YMIN = 5.00000E+04YMAX = 3.00000E+05  
 THE Y VALUES ARE CONVERTED TO LOG 10 IN PLOTTING

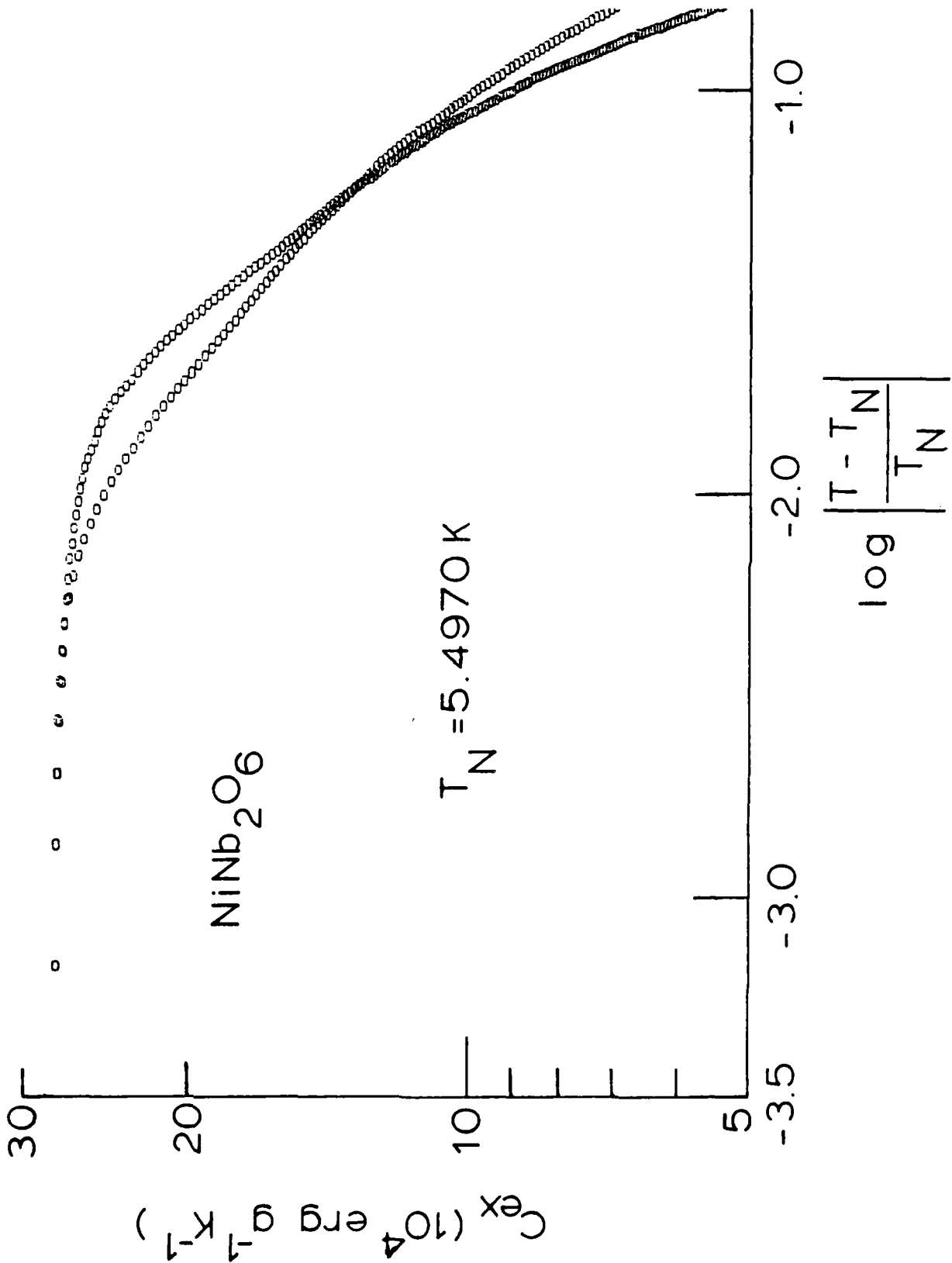
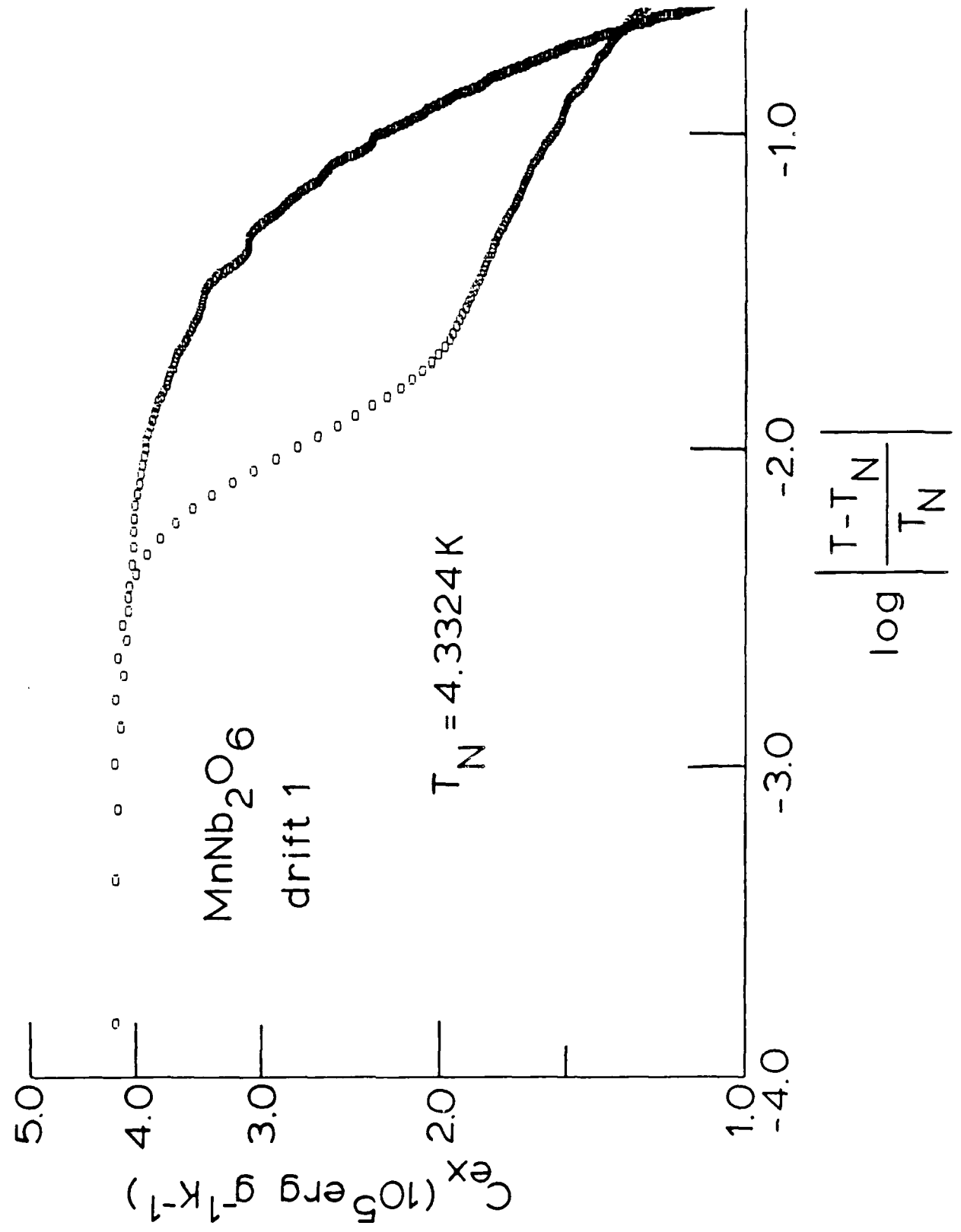


Fig. 6

00000  
 H SLOPE = 5.650000E+01 INTERCEPT = -7.004850E+01 TIME STEP (SECS) =  
 A = 2.5470545E+00 E = 3.5389931E+00 P = 8.1539224E-01 LEAD RESISTANCE  
 SAMPLE = 1.0253000E+00 GRAPHITE = 8.5000005E-03 GE7031 = 7.9999996E-04 ME  
 ALPHA = 4.0145399E+02 BETA = 2.0679001E+01 GAMMA = 0.0000000E-01  
 SLOPE = 5.6500000E+01 INTERCEPT = -7.0048500E+01 TIME STEP (SECS) =  
 TN = 4.3324 KELVIN, B = 1.31360E+03 E = 6.27140E+04  
 AMIN = -4.00000E+00/AMAX = -6.00000E-01/MIH = 1.00000E+05/IMAX = 5.00000E+05  
 THE Y VALUES ARE CONVERTED TO LOG 10 IN PLOTTING



00000

M SLOPE = 5.650000E+01 INTERCEPT = -7.004850E+01 TIME STEP (SECS) =  
A = 2.5470545E+00 B = 3.5389831E+00 P = 8.1599224E-01 LEAD RESISTANCE  
SAMPLE = 1.0259000E+00 GRAPHITE = 8.500000E-03 GE7031 = 7.999998E-04 ME  
ALPHA = 4.0145999E+02 BETA = 2.0679001E+01 GAMMA = 0.000000E-01  
SLOPE = 5.650000E+01 INTERCEPT = -7.004850E+01 TIME STEP (SECS) =  
TN = 4.3324 KELVIN, B = 1.31360E+03 E = 6.27140E+04  
AMIN = -4.00000E+00 AMAX = -6.00000E-01 YMIN = 1.00000E+05 YMAX = 5.00000E+05  
THE Y VALUES ARE CONVERTED TO LOG 10 IN PLOTTING

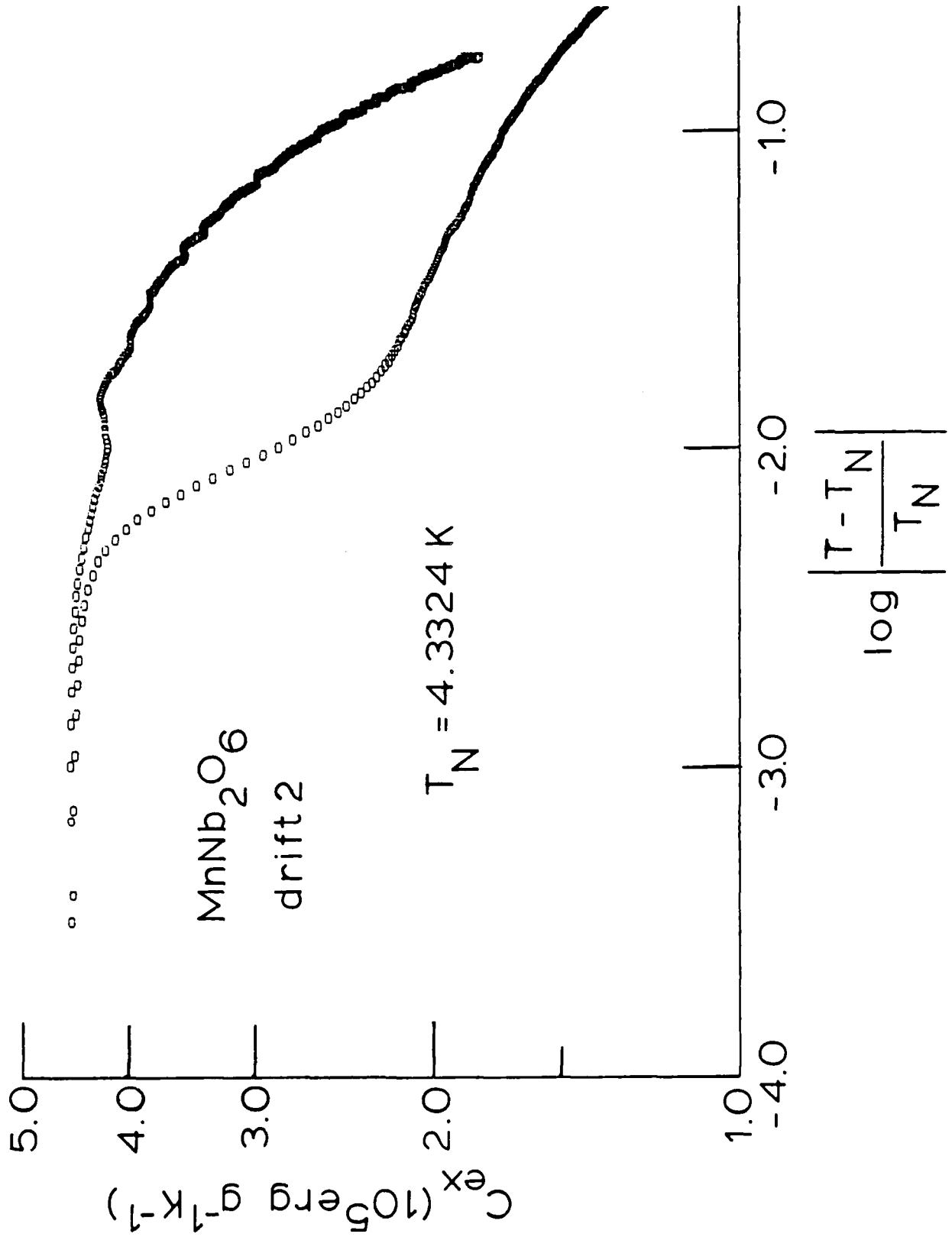
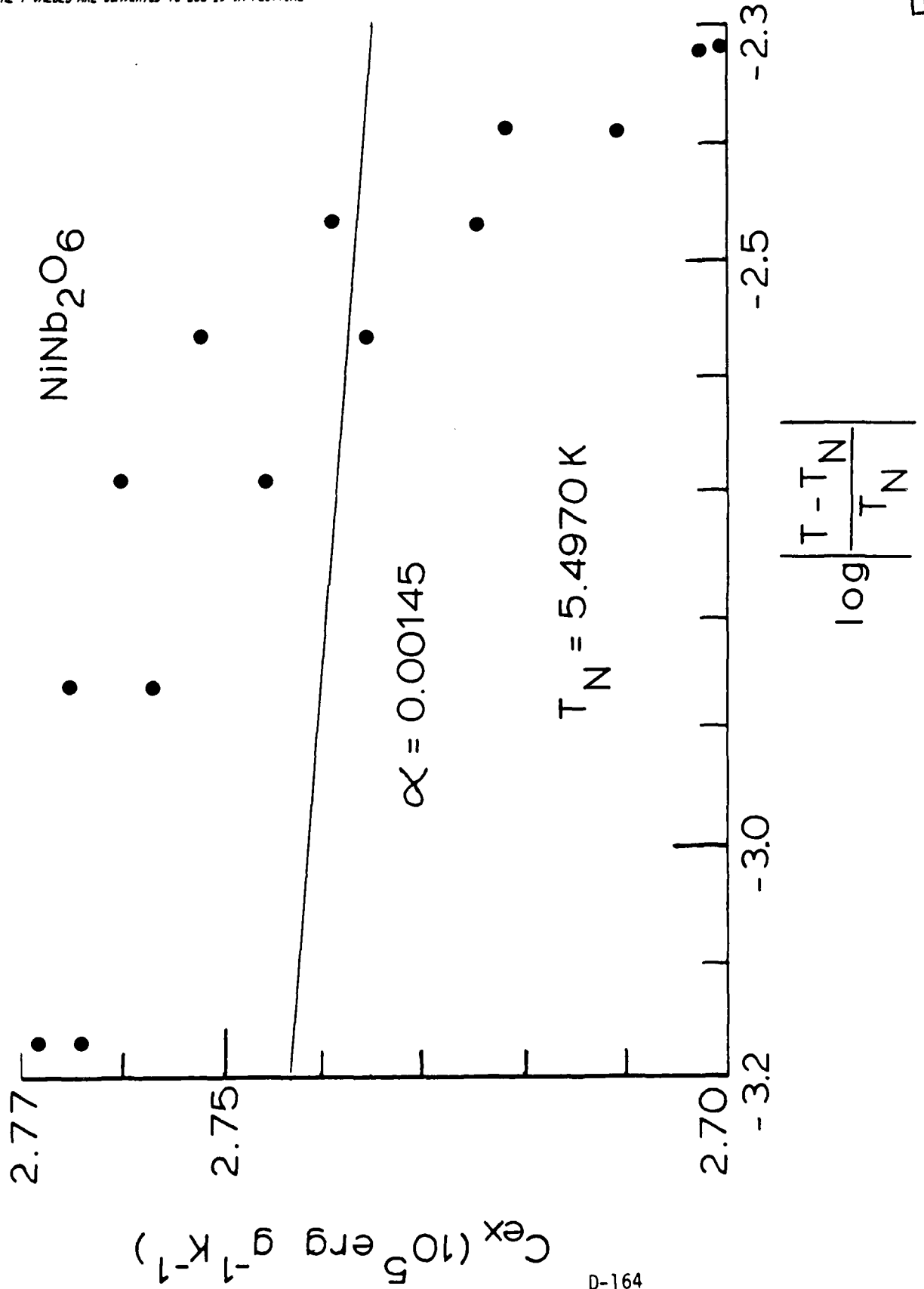
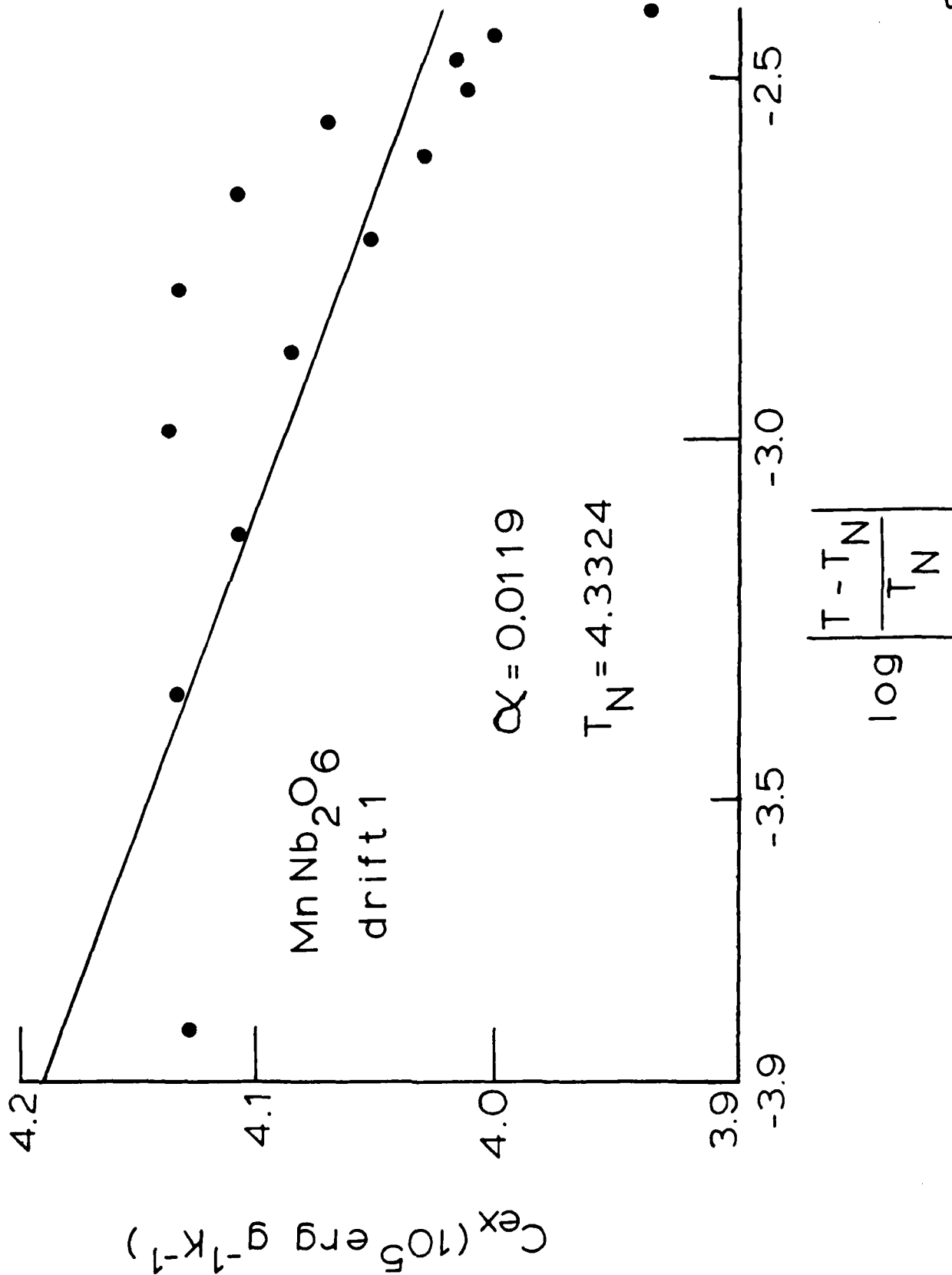


Fig. 8

\*\*\*\*  
 N SLOPE = 5.4122799E+01 INTERCEPT = -2.6710873E+01 TIME STEP (SECS) =  
 A = 2.4970324E+00 B = 3.5018778E+00 P = 8.0261737E-01 LEAD RESISTANCE  
 SAMPLE = 1.8408000E+00 GRAPHITE = 9.3000000E-03 GE7031 = 1.4000000E-03 ME  
 ALPHA = 3.8696100E+02 BETA = 2.0025700E+01 GAMMA = 0.0000000E-01  
 SLOPE = 5.4122799E+01 INTERCEPT = -2.6710873E+01 TIME STEP (SECS) =  
 TN = 5.4970 KELVIN, B = 1.31360E+03 E = 6.98930E+04  
 XMIN = -3.20000E+00 XMAX = -2.30000E+00 YMIN = 2.70000E+05 YMAX = 2.77000E+05  
 THE Y VALUES ARE CONVERTED TO LOG 10 IN PLOTTING



\*\*\*\*  
 M SLOPE = 5.650000E+01 INTERCEPT = -7.0048500E+01 TIME STEP (SECS) =  
 A = 2.5470545E+00 B = 3.5389831E+00 P = 8.1599224E-01 LEAD RESISTANCE  
 SAMPLE = 1.0259000E+00 GRAPHITE = 8.5000005E-03 GE7031 = 7.9999998E-04 ME  
 ALPHA = 4.0145999E+02 BETA = 2.0679001E+01 GAMMA = 0.0000000E-01  
 SLOPE = 5.6500000E+01 INTERCEPT = -7.0048500E+01 TIME STEP (SECS) =  
 TN = 4.3324 KELVIN, B = 1.31360E+03 E = 6.27140E+04  
 XMIN = -3.90000E+00 XMAX = -2.40000E+00 YMIN = 3.90000E+05 YMAX = 4.20000E+05  
 THE Y VALUES ARE CONVERTED TO LOG 10 IN PLOTTING



\*\*\*\*  
 M SLOPE = 5.650000E+01 INTERCEPT = -7.004850E+01 TIME STEP (SECS) =  
 A = 2.547054E+00 B = 3.5389831E+00 P = 8.1599224E-01 LEAD RESISTANCE  
 SAMPLE = 1.025900E+00 GRAPHITE = 8.5000005E-03 GE7031 = 7.9999998E-04 ME  
 ALPHA = 4.0145999E+02 BETA = 2.0679001E+01 GAMMA = 0.000000E-01  
 SLOPE = 5.650000E+01 INTERCEPT = -7.004850E+01 TIME STEP (SECS) =  
 TN = 4.3324 KELVIN,  $\theta$  = 1.31360E+03 E = 6.27140E+04  
 XMIN = -4.60000E+00 XMAX = -2.40000E+00 YMIN = 4.30000E+05 YMAX = 4.50000E+05  
 THE Y VALUES ARE CONVERTED TO LOG 10 IN PLOTTING

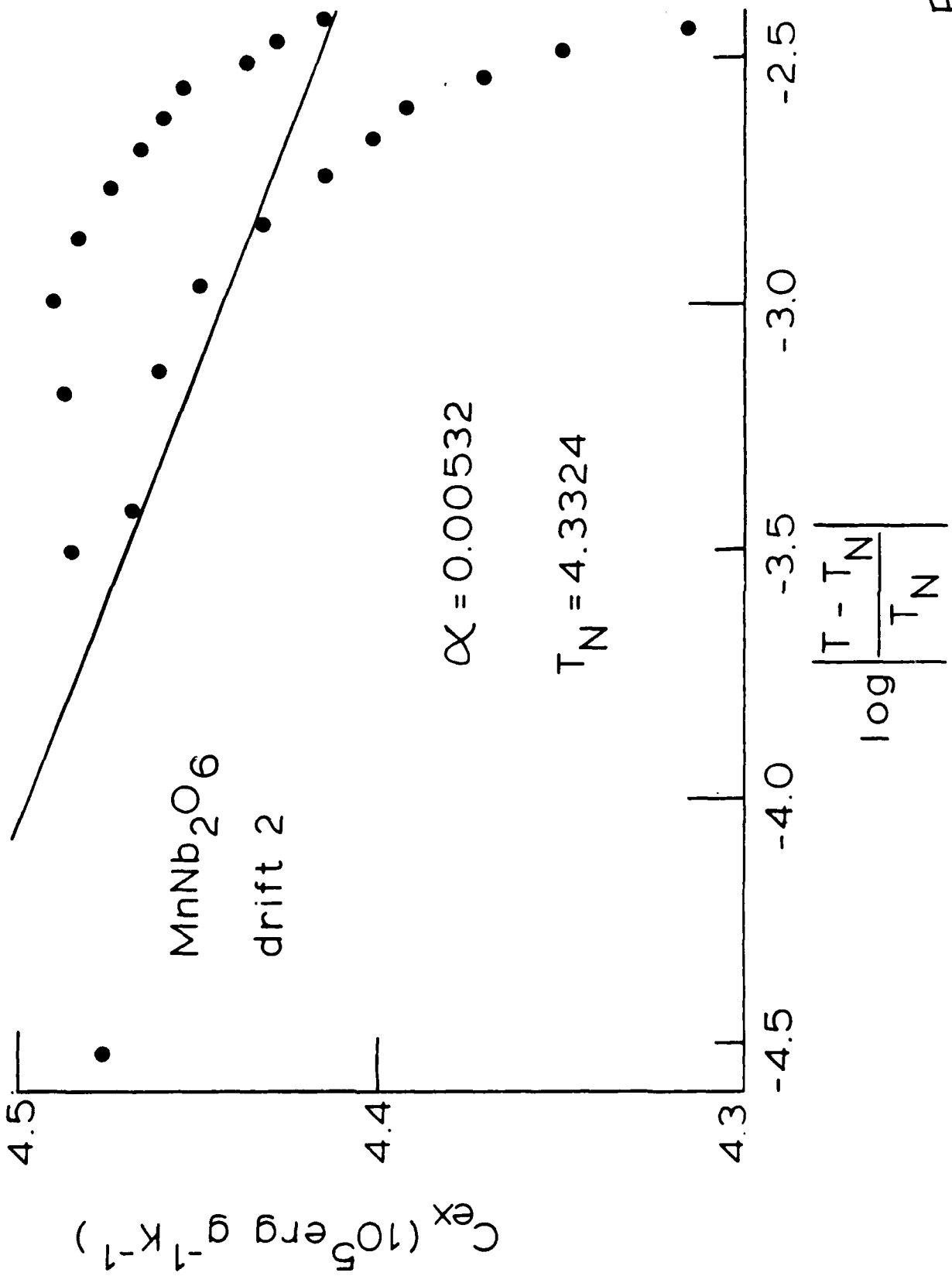


Fig 11

Appendix E

THEORETICAL THERMAL PROPERTIES STUDIES

PROGRESS REPORT

AFOSR Contract #F49620-83-C-0129

Fundamental Physics Studies on High-Specific-Heat  
Dielectrics and Kapitza Resistance at Dielectric Boundaries

Spinel Studies I. Structural Studies

by

Bruce R. Patton  
Department of Physics  
The Ohio State University  
Columbus, Ohio 43210

BRP  
#772

May 7, 1984

Distribution:

J.H. Parker, Jr.

P.W. Eckels

T.K. Gupta

M. Ashkin

C.F. Clark

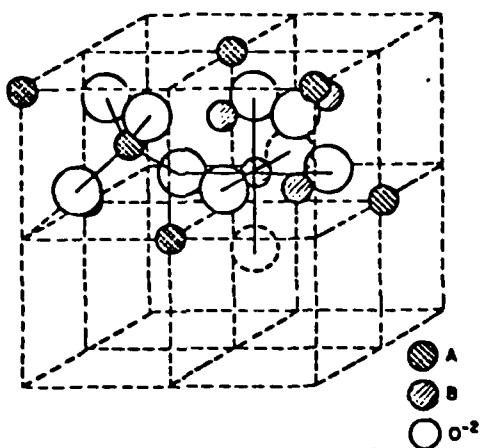
W.N. Lawless

## INTRODUCTION

The materials of interest in this study are zinc and cadmium chromite, with the formulae  $\text{ZnCr}_2\text{O}_4$  and  $\text{CdCr}_2\text{O}_4$ , respectively. These compounds are members of the spinel class of ferrite materials,<sup>1</sup> which has the generic formula  $\text{XY}_2\text{R}_4$  where X and Y are metal cations, at least one of which is magnetic, and R is a chalcogenide anion,  $\text{R} = \text{O}, \text{S}, \text{Se}, \text{or Te}$ .<sup>2</sup> In the following we will be primarily interested in the (2-3) spinels, where the X cations are divalent and the Y are trivalent, with the formula  $\text{X}^{2+}(\text{Y}^{3+})_2(\text{R}^{2-})_4$ .<sup>3,5</sup>

The spinel lattice is shown in Fig. 1.<sup>4</sup> The structure is a face-centered cubic array of  $\text{R}^{2-}$  ions, with the X and Y metal ions occupying interstices between the R ions. The properties of the spinel depend critically on how the X and Y ions are distributed among the interstices, which involves the choices of the X and Y metals as well as the method of preparation of the material (for example, rapid quenching produces a more random distribution of the ions). The unit cell contains eight formula units. The interstitial sites are of two types, tetrahedral (or A) sites where the metal ion is surrounded by four R anions in the form of a tetrahedron, and octahedral (or B) sites where the metal ion sits at the center of six R anions in the form of an octahedron. The unit cell, however, has only 8 of the 64 tetrahedral sites and 16 of the 32 octahedral sites filled. From consideration of just the charge state of the cations and anions, it is clear that the divalent X ion would prefer to sit in a tetrahedral A site, while the more highly charged Y trivalent ion

would sit at the octahedral B site where it can take advantage of the two extra negative R anions. A (2-3) spinel in which the  $X^{2+}$  metal ions occupy the A sites and the  $Y^{3+}$  metal ions the B sites is called a normal spinel. In an inverse spinel the divalent X ions occupy half of the B sites, while half of the trivalent Y ions sit on the A sites and the other half on B sites.



Two octants of the spinel unit cell. A ions are on tetrahedral sites and B ions on octahedral sites of the O<sup>2-</sup> anion packaging.

Fig. 1. Spinel unit cell

Inverse spinels may be favored when the bonding anisotropy of the 3d transition metal orbitals is taken into account; thus  $d^0$ ,  $d^5$  and  $d^{10}$  ions prefer tetrahedral sites, while  $d^3$  and  $d^8$  ions prefer octahedral B sites.<sup>4</sup> From this we conclude that the materials we are interested in,  $ZnCr_2O_4$  and  $CdCr_2O_4$ , are strong normal spinels, with the magnetic  $Cr^{3+}$  ( $d^3$ ) ions sitting only on B sites. This in turn, as we will see shortly, implies that the

magnetic transitions in the Zn and Cd spinels occur at a magnitude lower temperature than in spinels in which a magnetic ion sits at both the A and B sites.

In order to clarify patterns in these materials, we analyze trends in the (2-3) normal spinels with a non-magnetic metal ion on the A site. In other words we look at compounds which are iso-structural and iso-electronic with  $ZnCr_2O_4$  and  $CdCr_2O_4$  as we replace the Zn or Cd by other non-magnetic divalent metals, the Cr by other 3d transition metals, and the O by the other members of its column, S, Se, or Te. In Table 1 the lattice constants and magnetic transition temperatures of compounds of the form  $XCr_2R_4$  are presented (i.e., we fix  $Y = Cr$ ), while in Table 2

Table 1. Lattice constants and magnetic transition temperatures of  $XCr_2R_4$  (t = tetragonal distortion at  $T_N$ , f = ferromagnetic, af = anti-ferromagnetic)

	X = Mg	Zn	(CuIn) <sub>5</sub>	(AgIn) <sub>5</sub>	Cd	Hg
a. Lattice constant (in Angstroms)						
R = O	8.333 <sub>t</sub>	8.3275 <sub>t</sub>			8.595	
R = S			10.06	10.24	10.244	10.237
R = Se		10.44 <sub>t</sub>	10.583	10.72	10.755	
b. Magnetic transition temperature (in degrees Kelvin)						
R = O	15 <sub>af</sub>	16 <sub>af</sub>			9 <sub>af</sub>	
R = S		18 <sub>af</sub>	40 <sub>af</sub>	17 <sub>af</sub>	84.5 <sub>f</sub>	42 <sub>af</sub>
R = Se		129.5 <sub>f</sub> 21 <sub>af</sub>	<4.2	60 <sub>f</sub>	129.5 <sub>f</sub>	

similar data for the oxygen compounds ( $R = O$ ) of the form  $XY_2O_4$  are shown. The data are from references 3 and 6.

Table 2. Lattice constants and magnetic transition temperatures of  $XY_2O_4$

	Y = V	Cr	Mn	Fe	Co	Ni
a. Lattice constant						
X =	Mg	8.418 <sub>t</sub>	8.333 <sub>t</sub>			
	Zn	8.41 <sub>t</sub>	8.3275 <sub>t</sub>	8.10=a 9.25=c	8.416	
	Cd		8.595 <sub>?</sub>			
	Ge <sup>4+</sup>				8.317	8.221
b. Magnetic transition temperature						
X =	Mg	45 <sub>af</sub>	15 <sub>af</sub>			
	Zn	45 <sub>af</sub>	16 <sub>af</sub>		9-17 <sub>af</sub>	
	Cd		9 <sub>af</sub>			
	Ge <sup>4+</sup>					20 <sub>af</sub>

Several features become clear when the compounds are analyzed systematically as shown in Tables 1 and 2. First of all, these systems are characterized by a low temperature magnetic transition, at a temperature of order 20K for an anti-ferromagnetic case and of order 100K for the ferromagnetic; the interesting case of  $ZnCr_2Se_4$  has both transitions. The ferromagnetic transitions occur only for the larger R atoms, sulfur and selenium, and are never associated with a tetragonal

distortion. We note that the lattice size depends primarily on the R atom, weakly on the non-magnetic atom X, and is virtually independent of the magnetic atom Y. This results from the fact that the spinel lattice is basically a close packed array of R (oxygen) atoms with the smaller X and Y metal atoms fitting easily into the interstices. The lattice constant is independent of the transition metal Y since the atomic size is almost unchanged across the 3d transition metal series from V to Ni; the added electrons go into the closely bound d shell instead of filling up orbitals of larger radius. These observations also explain the tendency toward a tetragonal distortion below the anti-ferromagnetic transition  $T_N$  for the smaller metal ions. In this case the metal ions rattle around on their sites, providing little stabilization energy for the lattice. We shall see later that the anti-ferromagnetic spin lattice in the spinels is highly frustrated (for symmetry reasons not all spins can order anti-ferromagnetically at the same time); thus, below  $T_N$  the spin ordering energy may be increased by distorting the lattice to reduce the frustration, much like a Jahn-Teller distortion. This occurs more readily in an easily deformable lattice, i.e., with the smaller X and Y atoms. We will return to consider this coupling between the lattice and the spins in later reports, since it is likely that it is very important in determining the large specific heats of these compounds and the ability to transmit heat through the lattice as seen in the large thermal conductivities.

We consider now the nature of the magnetic ordering in this

series.<sup>6</sup> We consider first one of the simpler cases in which the spins order anti-ferromagnetically along the c-axis, the vanadium-oxygen compounds. Fig. 2 shows a plot of the unit cell in the a-b plane;<sup>6</sup> the spins point in and out of the page, in the c direction. Only the vanadium ions are shown. It can be seen that a given spin is surrounded by equivalent up and down spin

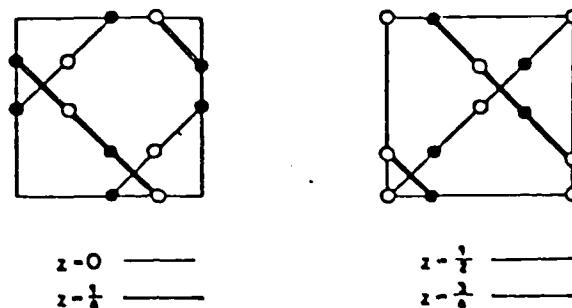


Fig. 2. Magnetic structure of  $MgV_2O_4$  and  $ZnV_2O_4$  (solid dot=spin out, open dot=spin in, Ref. 6)

neighbors; the tetragonal distortion changes the c lattice constant with respect to the a=b lattice constant, in order to allow the spin to interact more strongly with its oppositely directed neighbors, and less strongly with its similarly directed ones. The case of  $ZnCr_2O_4$  is shown in Fig. 3. It is clear that this compound has a much more complicated anti-ferromagnetic spin structure, however, it is physically reasonable that the spin energy is favor by distorting the lattice.

Finally, we consider the question of why the transition

temperatures are so low in all these compounds, and why they are mostly anti-ferromagnetic (note that we have not distinguished the case of ferrimagnetic ordering, which typically occurs when the opposing moments on different sublattices do not completely cancel, usually because the spins or their number differ on one sublattice; we consider this case in detail in our next study on the thermodynamic properties, but for the present considerations the distinction is not necessary). The answer to these questions

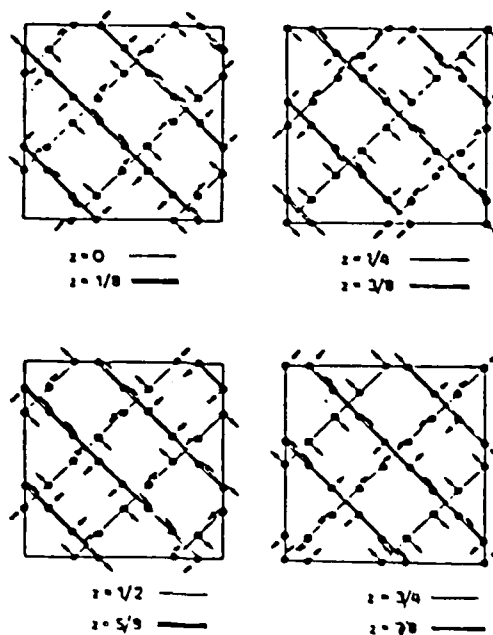


Fig. 3. Magnetic structure of  $ZnCr_2O_4$  (spins in  $a-b$  plane, Ref. 6)

lies in the nature of the exchange interaction in magnetic oxide materials. To start with, the reason these materials are good insulators is that they consist of a lattice of alternating

charged ions, not unlike sodium chloride,  $\text{Na}^+\text{Cl}^-$ , which binds the electrons to the ions. The interaction between two magnetic ions must then take place via an indirect exchange involving an intervening oxygen (or  $\text{R}^{2-}$ , in general) ion, usually called superexchange. This interaction, to the extent that it takes place via the O p-orbitals, is strongly angular dependent; it is strongest when the metal-oxygen-metal unit lies in a straight line, i.e., when the angle between the bonds is 180 degrees. It is weakest when the angle is 90 degrees, directly reflecting the symmetry of the p-orbital. In Fig. 4 we show the metal ion

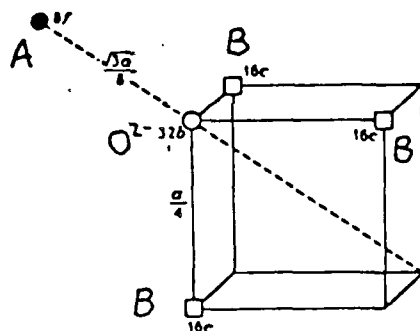


Fig. 4 A and B site nearest neighbors of an oxygen ion in perfect spinel lattice

configuration around an oxygen ion in the spinel lattice.<sup>2</sup> The B sites are at the corners of a perfect cube, while the A site lies on the diagonal. In compounds like  $\text{Fe}_3\text{O}_4$  or  $\text{NiFe}_2\text{O}_4$ , magnetic ions occupy both the A and B sites, and, although the angle is less than  $180^\circ$ , it is still large and the superexchange

interaction is near its maximum, resulting in transition temperatures of order 1000K. A second possibility is that the transition metal ions occupy only the A sites, as in  $\text{FeAl}_2\text{O}_4$  or  $\text{CoAl}_2\text{O}_4$ . In this case, as can be seen from Fig. 5, the interaction via an intermediate O ion involves even longer distances than the exchange interaction between two B sites. This is confirmed by the fact that these two compounds have even lower Néel transitions ( $T_N = 8\text{K}$ , and  $4\text{K}$  respectively) than all the materials in Tables 1 and 2, in which the magnetic ions sit on the B sites. Both the A-A and B-B systems have much weaker

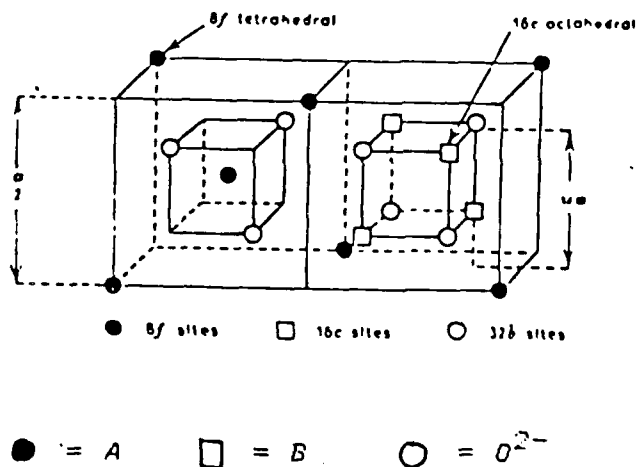


Fig. 5. Two octants of perfect spinel unit cell (ref. 2) interactions because the bond angle is close to  $90^\circ$ , unlike the case of the A-B interaction. Furthermore, as mentioned above and visible from Fig. 5, if the interaction is ferromagnetic in character between the B sites, then the spins are frustrated in the sense that if all the neighbors of a given spin are aligned anti-parallel to it, then the neighbors are unfavorably aligned,

namely, parallel. This requires either the spins to align in a complex pattern that does not take maximum advantage of the anti-ferromagnetic interaction or the lattice to distort to remove the frustration.

From the trends revealed above it would appear that a number of the normal spinels with non-magnetic A site ions, and small metal ions should give rise to interesting low temperature anomalies such as anti-ferromagnetic ordering and lattice distortions. We note that it may well be possible to fine tune the properties of a spinel of this type by use of an alloy of the A site metal, as in the CuIn and AgIn compounds.

#### REFERENCES

1. C. Kittel, *Introduction to Solid State Physics*, Wiley, 1971.
2. K.J. Standley, *Oxide Magnetic Materials*, Oxford, 1962.
3. R.S. Tebble and D. J. Craik, *Magnetic Materials*, Wiley-Interscience, 1969.
4. P.I. Slick, "Ferrites for Non-microwave Applications", in *Ferromagnetic Materials*, vol. 2, E.P. Wohlfarth, ed., North Holland, 1980.
5. S.V. Vonsovskii, *Magnetism*, vol.2, Wiley, 1974.
6. A. Uleś, F. Kajzar, M. Kucab, and W. Sikora, *Magnetic Structures Determined by Neutron Diffraction*, Państwowe Wydawnictwo Naukowe, Warsaw, 1976.

PROGRESS REPORT

AFOSR Contract #F49620-83-C-0129

Fundamental Physics Studies on High-Specific-Heat  
Dielectric and Kapitza Resistance at Dielectric Boundaries

Spinel Studies II Theoretical Models

by

Bruce R. Patton  
Department of Physics  
The Ohio State University  
Columbus, Ohio 43210

July 12, 1984

Distribution:

J.H. Parker, Jr.

~~P.~~W. Eckels

T.K. Gupta

M. Ashkin

C.F. Clark

W.N. Lawless

## INTRODUCTION

In the last report of our series on the theory of the B-site spinels, the structure of the spinel class of ferrite materials was considered. In particular, the two materials of interest in these studies, zinc chromite,  $ZnCr_2O_4$ , and cadmium chromite,  $CdCr_2O_4$ , were shown to fit into a pattern of magnetic and structural instabilities at low temperatures. To summarize briefly our findings, we recall that the two metal ions occupy two distinct types of sites in the spinel lattice, denoted by A and B.<sup>1</sup> When magnetic ions sit on both the sites, a strong interaction occurs between the two sublattice spins, of an antiparallel nature. This leads to a high temperature transition to a generally ferrimagnetic state; since the A and B sites are inequivalent, the moments on the A and B sites, although oppositely aligned, do not cancel completely.

The situation is rather different for the case we are interested in, when the A site is occupied by the non-magnetic ion Zn or Cd.<sup>2</sup> In this case there is no large magnetic interaction between the A and B sites; instead a much weaker, right-angle bond between the magnetic ions on neighboring B sites becomes the dominant interaction. We shall call the spinels in which no magnetic ion sits on an A site, B-site spinels, for brevity. The B-site spinels are characterized by much lower magnetic instability temperatures, of order 10 Kelvin, due to the weaker interaction; and by the presence of "frustration" in the arrangement of bonds in the B sublattice. Frustration occurs,

for example, when two neighbors of a given spin are also neighbors; all three spins cannot then be aligned in an antiparallel configuration. As a result there is a tendency for the lattice to distort in order to reduce the frustration and increase the spin ordering energy. The spin ordering of the B-site spinels can therefore be very complex and is often coupled to a lattice transformation, giving rise in general to a very rich set of low temperature phenomena.

In the present study we attempt to find the important variables that are necessary to describe the behavior of the zinc and cadmium chromites. Proceeding from an analysis of the structure of these materials, we write down a first principles Hamiltonian that characterizes the interaction of the moments with each other, the lattice, and the external fields. Then we proceed to extract the relevant order parameters that enable a theory of a more phenomenological Ginsberg-Landau nature to be obtained. From comparison with some of the experiments, the characteristic interactions in the theory may be determined and some of the unusual properties of these materials understood.

The microscopic Hamiltonian describes the interaction between the spins  $S_i$  on various sites  $i$ . The lattice of B-sites where the spins sit in the spinel structure is shown in Fig.1.<sup>3</sup> The interaction between two neighboring B-spins occurs via superexchange through the A ion. Since this B-A-B bond may be seen to form a  $90^\circ$  angle, the magnitude of the interaction is very weak. Denoting this interaction by  $J_{ij}$ , the Hamiltonian has the form

$$H = \sum J_{ij}^{\alpha\beta} S_{\alpha i} S_{\beta j} + \sum K_{ijk}^{\alpha\beta\delta} S_{\alpha i} S_{\beta j} \phi_{\delta k} - \sum S_{\alpha i} H_{\alpha} \quad (1)$$

where the Greek indices denote Cartesian coordinates  $x, y, z$ , while the indices  $i, j, k$  run over  $B$  lattice sites, and repeated indices are summed over. The interaction  $K$  denotes the coupling of the spins to the lattice distortion  $\phi$ , and  $H_{\alpha}$  is the external magnetic field. Although Eq. (1) is quite general, we will for the present ignore next-nearest neighbor interactions and consider  $i, j$ , and  $k$  to run only over nearest neighbors. Then roughly speaking, the magnetic transition temperature is given by the magnitude of  $J$ , while the magnitude of  $K$  determines the extent of the lattice distortion in the magnetic phase.

The above Hamiltonian contains too much information for present purposes. We really only need a description involving the averaged quantities, the sublattice magnetizations,

$$M_1(r) = \sum_{i \in l} S_i \quad (2)$$

where the sum is over all sites  $i$  on the sublattice  $l$  in a small volume around the point  $r$  in the crystal.  $M_1(r)$  thus represents the sublattice magnetization which may vary slowly in space throughout the material. An expression for the free energy  $F$  of the system expressed in terms of  $M_1(r)$  may be formally obtained by integrating out the degrees of freedom associated with the motion of the individual spins:

$$e^{-F[M_1]/kT} = \text{Tr} \cdot e^{-H(S_1)/kT} \quad (3)$$

where the trace is carried out over all spin degrees of freedom

except for the slowly varying envelope function  $M(r)$ .

The result of this process is to obtain a free energy functional of the Ginsberg-Landau<sup>4</sup> type which describes the possible phases of the material in terms of the order parameters, the sublattice magnetizations.<sup>5</sup> The expression for the free energy functional has the form

$$F = \int d^3r \left[ \sum A_{ln}^{\alpha\beta} M_{l\alpha} M_{n\beta} + \sum B_{lmnp}^{\alpha\beta\sigma\mu} M_{l\alpha} M_{m\beta} M_{n\sigma} M_{p\mu} + \sum C_{ln}^{\alpha\beta\sigma\mu} \frac{dM_{l\beta}}{dr_\alpha} \frac{dM_{n\mu}}{dr_\sigma} + \sum M_{l\alpha} H_\alpha \right] \quad (4)$$

The first term in  $F$  is the energy of the sublattice magnetization mode; the matrix  $A$  has all positive eigenvalues at high temperatures, one of which approaches zero first as the temperature is lowered. That temperature defines the point at which the normal phase becomes unstable. The eigenvector corresponding to the first zero eigenvalue characterizes the nature of the magnetic order below the transition. In the B site spinels, this is usually an antiferromagnetic state. The second term in (4) is the interaction energy of the modes and  $B$  must be positive to stabilize the system when  $A$  goes negative. The third term is the spin wave energy associated with a deformation of a uniform configuration of the magnetization modes. Finally, the last term represents the coupling of the total magnetization to the external magnetic field.

It is difficult, if not impossible, at this time to predict from first principles which combinations of sublattice magnetizations will become favored below the transition; however,

from neutron scattering experiments (as shown in Report I of this series, Figs. 2 and 3, reproduced in this report) the ordering pattern of the spins on the various sublattices may be readily deduced. It is clear that the ordering in  $\text{ZnV}_2\text{O}_4$  and  $\text{MgV}_2\text{O}_4$  (Fig. 2) is much simpler than that in  $\text{ZnCr}_2\text{O}_4$  (Fig. 3). In the former case the spins point only in the c direction and involve a simple sublattice, while in the latter case the spins point in various directions in the a-b plane and sit on a much more complicated set of sublattices.

In order to clarify the physics involved, we will start with a simpler sublattice than that actually involved in  $\text{ZnCr}_2\text{O}_4$ . In effect, as a first approximation we keep only the minimum number of combinations of the sublattice magnetizations: the antiferromagnetic combination,  $l_\alpha = \sum_{i,j} (M_{i\alpha} - M_{j\alpha})$ , summed over all pairs of oppositely ordered sublattices, i and j, and the total magnetization  $m_\alpha = \sum_i M_{i\alpha}$ . The free energy functional then takes the form

$$F = \int d^3r \left[ \alpha |l|^2 + \frac{\beta}{2} |l|^4 + \delta |d_r l|^2 + a |m|^2 + \frac{b}{2} |m|^4 + \Gamma |l|^2 |m|^2 - m \cdot H \right] \quad (5)$$

where  $l$  denotes the antiferromagnetic vector order parameter, the sublattice magnetization, which becomes finite below  $T_N$ , and  $\alpha = \text{const} \cdot (T - T_N)$ . The coefficients  $\beta$  and  $b$  are positive for stability, while  $a$ , unlike  $\alpha$ , remains positive at all temperatures (assuming no spontaneous magnetization occurs). The coupling  $\Gamma$  represents the interaction between the two vector order parameters  $l$  and  $m$  and may be positive or negative in

principle. It should be noted that there are no linear couplings between  $l$  and  $m$  (i.e.,  $l \cdot m$ ) since they would require  $\langle m \rangle$  to be finite when  $\langle l \rangle$  was finite, in contradiction of the assumption of no spontaneous magnetization.

We consider first the mean field solution for the order parameters which is obtained by setting the variation of the functional (5) with respect to  $l$  equal to zero and similarly for  $m$ :

$$\frac{\delta F}{\delta l} = 0 = \alpha l + \beta |l|^2 l + \Gamma |m|^2 l \quad (6a)$$

$$\frac{\delta F}{\delta m} = 0 = a m + b |m|^2 m + \Gamma |l|^2 m - H \quad (6b)$$

In examining the nature of the solution of these equations, we will first assume that the coupling  $\Gamma$  is weak and thus may be neglected. In that case, when the external magnetic field vanishes, the only solution for  $m$  is zero since all terms in Eq. (6b) are positive. Eq. (6a) then implies that there are two solutions for  $l$ , depending on the sign of  $\alpha$ . To summarize, for weak coupling and no magnetic field the solutions are:

$$m_0 = 0 \quad \text{for } H = 0 \text{ and } \Gamma \geq 0 \quad (7a)$$

$$l_0 = \begin{cases} 0 & \text{for } \alpha > 0 \quad (T > T_N) \end{cases} \quad (7b)$$

$$l_0 = \begin{cases} \left[ \frac{-\alpha}{\beta} \right]^{1/2} & \text{for } \alpha < 0 \quad (T < T_N) \end{cases} \quad (7c)$$

In the presence of a finite magnetic field, the magnetization  $m$  will become nonzero. To consider this situation, we examine Eq. (6b) again. Firstly, as long as  $m$  remains small we may neglect the term involving the coefficient  $b$ , since that term is

proportional to  $m^2$ . Secondly, we use the solutions (7b) and (7c) for  $l$ ; this is equivalent to assuming that the interaction between  $l$  and  $m$  has a weak effect on the antiferromagnetic order. Solving Eq. (6) gives

$$m_0 = \frac{H}{a} \quad \text{for } T > T_N \quad (8a)$$

$$m_0 = \frac{H}{a + \frac{\Gamma|\alpha|}{\beta}} \quad \text{for } T < T_N \quad (8b)$$

From Eqs. (8a) and (8b) we see that the magnetization is linear in the applied field, however, the susceptibility,  $X \equiv m/H$  changes as the temperature is lowered below the Néel point

$$X = \frac{1}{2a} \quad \text{for } T > T_N \quad (9a)$$

$$X = \frac{1}{2a + \frac{2\Gamma|\alpha|}{\beta}} \equiv \frac{1}{2\tilde{a}} \quad \text{for } T < T_N \quad (9b)$$

As noted above the assumption of an absence of spontaneous magnetization implies that the parameter  $a$  is positive and non-vanishing, with a weak temperature dependence in the vicinity of  $T_N$ , whereas  $|\alpha|$  increases linearly below  $T_N$ . Therefore we expect the susceptibility to be weakly temperature dependent above  $T_N$ , but to have a strong temperature dependence below  $T_N$ . From the experimental observation<sup>4</sup> that the susceptibility increases as the temperature is lowered below  $T_N$ , we conclude that the interaction parameter  $\Gamma$  is negative, i.e., the occurrence of the antiferromagnetic order enhances the tendency toward ferromagnetic order. In Eq. (9b) we have defined the parameter  $\tilde{a}$ , which plays the role of a renormalized ferromagnetic mode

energy. The temperature dependence of the susceptibility is manifested in the temperature dependence of  $\chi$  which arises from the coupling to the antiferromagnetic mode.

We now proceed to calculate the specific heat due to the various modes in the system. First we calculate the specific heat in the mean field approximation; in our next report we will evaluate corrections to the mean field result due to fluctuations. This should give us a reasonable overall picture for the specific heat near the antiferromagnetic transition in our system, although we do not expect the results to necessarily be quantitatively accurate unless the material has long range interactions which justify the mean field approximation. From thermodynamic arguments the specific may be obtained from the free energy\*

$$C = -T \frac{d^2 F}{dT^2} \quad (10)$$

where the thermodynamic free energy is given in terms of the free energy functional  $F[l,m]$ , integrated over the degrees of freedom  $l$  and  $m$  (see Eq. (3), for example). Thus

$$e^{-F/kT} = \int Dl Dm e^{-F[l,m]/kT} \quad (11)$$

where the angular integral sign denotes an integral over the functions  $l(r)$  and  $m(r)$ . The mean field approximation estimates the functional integral in (11) by simply replacing the integral by the value of the integrand at its maximum value. The effect of fluctuations may then be included by integrating gaussian fluctuations around the maximum value. The maximum value of the

exponential is given by the minimum value of the functional  $F[l,m]$ ; however the minimum value of  $F[l,m]$  corresponds to the equilibrium solutions for the order parameters  $l_0$  and  $m_0$  found in Eqs. (7) and (8). Thus

$$\begin{aligned} F[l,m]_{\min} &= F[l_0,m_0] \\ &= -\frac{|\alpha|^2}{2\beta} - \frac{H^2}{4\beta} \end{aligned} \quad (12)$$

The temperature dependence of the free energy arises from the dependence of  $\alpha$  on temperature. As noted above,  $\alpha$  varies linearly with temperature in the vicinity of  $T_N$ , however, at low temperatures  $\alpha$  must become independent of temperature in order to be consistent with the third law of thermodynamics. We assume the following form for  $\alpha$ , which gives a typical temperature dependence for the order parameter:

$$\alpha = \alpha_0 \cdot \left[ \frac{T^2 - T_c^2}{2T_c^2} \right] \quad (13)$$

Combining Eqs. (10), (12), and (13), gives for the specific heat

$$C = C_N \quad \text{for } T > T_N \quad (14a)$$

$$C = \left[ \frac{T}{T_c} \right]^3 \frac{\alpha_0^2}{\beta T_c} \left[ 1 + \frac{2\Gamma^2}{\beta \alpha^3} H^2 \right] + C_N \quad \text{for } T < T_N \quad (14b)$$

where  $C_N$  is the specific heat in the normal phase. The first term in (14b) is the jump in the specific heat at the transition, while the second term represents the change in the specific heat in a finite magnetic field. We see that the specific heat

increases in a magnetic field, although this result, it should be noted, only holds for fields such that  $\Gamma|m_0| \ll |\alpha|$  or

$$H \ll H_c \equiv 2\alpha \cdot \left[ \frac{|\alpha|}{\Gamma} \right]^{1/2} \quad (15)$$

In summary, we have examined the microscopic models for the description of the B-site spinels, and have derived predictions for the susceptibility and the specific heat in the leading approximation. The results show a very interesting and unexpected behavior, namely, the linear dependence of the magnetization on external magnetic field associated with a strongly temperature dependent susceptibility below the Néel transition, and the related phenomena of the increase of the specific heat in the external field. In our next report in this series we will include fluctuations in the calculation, extend the results to more complex magnetic sublattice structures, and undertake some detailed comparisons with the experimental data.

## REFERENCES

1. K.J. Standley, *Oxide Magnetic Materials*, Oxford, 1962.
2. S.V. Vonsovskii, *Magnetism*, vol. 2, Wiley, 1974.
3. J.E. Thompson, *The Magnetic Properties of Materials*, Newnes, 1968.
4. L.D. Landau and E.M. Lifshitz, *Statistical Physics, Part 1*, Pergamon, 1980.
5. E.A. Turov, *Physical Properties of Magnetically Ordered Crystals*, Academic, 1965.
6. W.N. Lawless, "Spinel Studies VII. Magnetocaloric Effects", Progress Report - AFOSR Contract F49620-83-C0129.

Fig. 1. Spinel crystal structure.

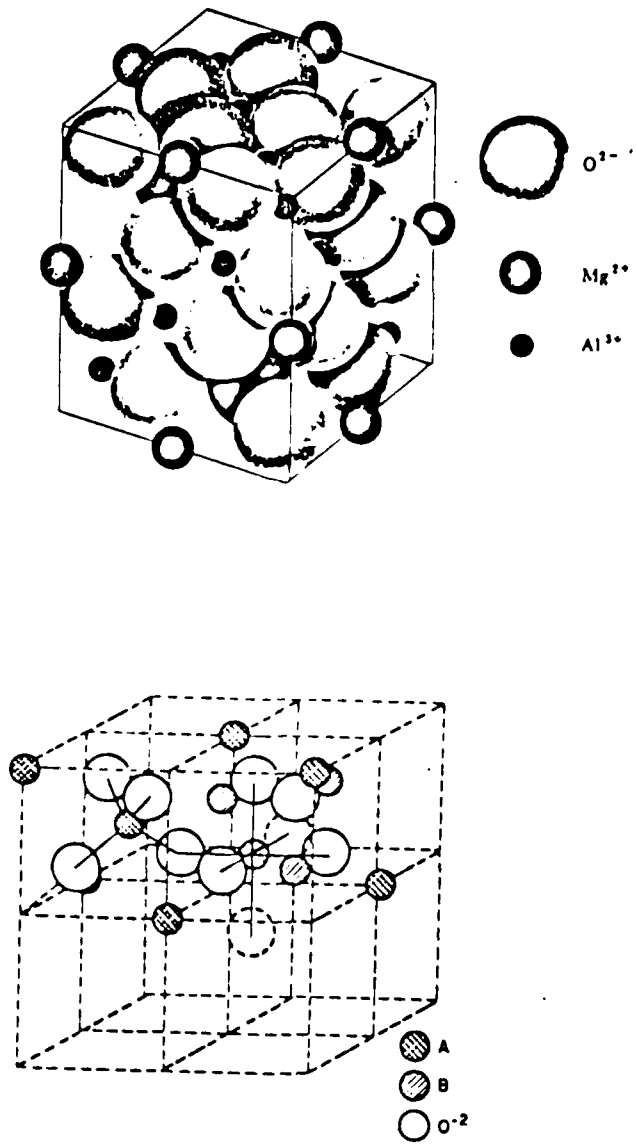
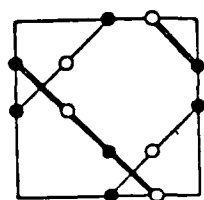
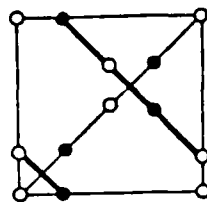


Fig. 2. Magnetic structure of  $\text{MgV}_2\text{O}_4$  and  $\text{ZnV}_2\text{O}_4$ : spins in c direction, from Ref 2.

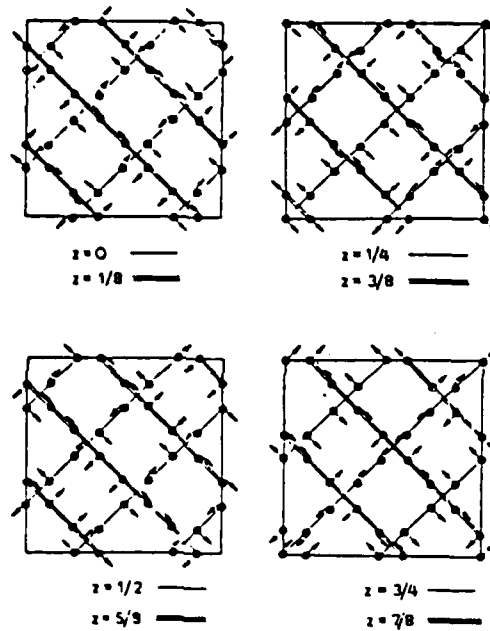


$z=0$  ———  
 $z=\frac{1}{4}$  ———



$z=\frac{1}{2}$  ———  
 $z=\frac{3}{4}$  ———

Fig. 3. Magnetic structure of  $\text{ZnCr}_2\text{O}_4$ : spins in the a-b plane, from Ref. 2.



PROGRESS REPORT

AFOSR Contract #F49620-83-C-0129

Fundamental Physics on High-Specific-Heat  
Dielectrics and Kapitza Resistance at Dielectric Boundaries

Theoretical Research Program

Spinel Studies

III. Thermal Properties

by

*B.R.P.*

Bruce R. Patton

Department of Physics

The Ohio State University

Columbus, Ohio 43210

Distribution:

J.H. Parker, Jr.  
P.W. Eckels  
T.K. Gupta  
M. Ashkin  
C.F. Clark  
B.R. Patton  
A. Menard

## INTRODUCTION

In our previous reports on our research on the B-site spinel phases, we have developed a theoretical model for compounds of the type represented by zinc chromite,  $\text{ZnCr}_2\text{O}_4$ , and cadmium chromite,  $\text{CdCr}_2\text{O}_4$ . The magnetic properties of these materials were characterized by weak interactions among the magnetic ions, compared to ordinary magnetic materials, and consequently low magnetic transition temperatures.<sup>1,2,3,5</sup> In addition, the arrangement of the magnetic ions on the lattice leads to a high degree of frustration in the mutual antiferromagnetic ordering of the spins. As a first step in treating these materials theoretically, we derived a Ginzburg-Landau<sup>4</sup> free energy which involved two order parameters. The first was the sublattice magnetization  $l_\alpha = \sum_{i,j} (M_{i\alpha} - M_{j\alpha})$ , representing the antiferromagnetically ordered spins, and the second was total magnetization  $m_\alpha = \sum_i M_{i\alpha}$ , corresponding to the component of ferromagnetically ordered spins. We noted that the ferromagnetic order never developed in  $\text{CdCr}_2\text{O}_4$  and  $\text{ZnCr}_2\text{O}_4$ , but that the paramagnetic spins influenced the other order parameter and gave rise to a temperature dependent magnetic susceptibility. The free energy as a functional of these two order parameters is

$$F = \int d^3r \left[ \alpha |l|^2 + \frac{\beta}{2} |l|^4 + \delta |\nabla \cdot l|^2 + a |m|^2 + \frac{b}{2} |m|^4 + c |\nabla \cdot m|^2 + \Gamma |l|^2 |m|^2 - m \cdot H \right] \quad (1)$$

Since we will be dealing with fluctuations in the report, Eq. (1) has been generalized to include the gradient energy associated

with deformations of the magnetization  $m$ . In our last report we found the solutions to (1) in mean field theory

$$l_0 = \begin{cases} 0 & T > T_N \\ \left[ \frac{-\alpha}{\beta} \right]^{1/2} & T < T_N \end{cases} \quad (2)$$

$$m_0 = \begin{cases} \frac{H}{2a} & T > T_N \\ \frac{H}{2a + \frac{2\Gamma|\alpha|}{\beta}} & T < T_N \end{cases} \quad (3)$$

In the present report we evaluate the corrections to mean field due to fluctuations. Since the fitted exponents for the specific heat exponent are large, it may be of quantitative interest to consider the fluctuations in the Gaussian or weak fluctuation limit. The large exponents indicate that the transitions may possibly have a reasonably large region over which classical exponents are an accurate fit. We will consider later the critical region and the need for a renormalization group approach.

To obtain the fluctuation corrections to the mean field behavior we expand the partition function

$$e^{-F/k_B T} = \int Dl Dm e^{-F[l,m]/k_B T} \quad (4)$$

about the mean field solutions given by Eqs. (2) and (3), and then carry out the functional integral over gaussian fluctuations away from the mean values. The free energy functional becomes

$$F(l,m) = -\frac{H^2}{4a} + \sum_k (\alpha' + \delta k^2) |l_k|^2 + \sum_q (a + cq^2) |m_q|^2 \quad (5)$$

for  $T > T_N$ , where  $\alpha' = \alpha + \Gamma H^2/4a^2$ . Inserting the result (5) in the functional integral (6) and carrying out the integration gives

$$\begin{aligned}
 F &= - k_B T \ln \left[ \int \prod_k \prod_q D l_k D m_q e^{-F(1,m)/k_B T} \right] \\
 &= - \frac{H^2}{4a} - k_B T \sum_k \ln \left[ \frac{k_B T}{\alpha' + \delta k^2} \right]^{3/2} - k_B T \sum_q \ln \left[ \frac{k_B T}{a + cq^2} \right]^{3/2}
 \end{aligned}
 \tag{6}$$

The specific heat (per unit volume) may now be directly obtained from the free energy in the usual fashion

$$\begin{aligned}
 C &= - T \frac{d^2 F}{dT^2} \\
 &= \frac{3}{16\pi} \frac{k_B}{\xi_1^3} \left[ \frac{T}{T_c} \right]^2 \frac{1}{t_1^{1/2}} + \frac{3}{16\pi} \frac{k_B}{\xi_m^3} \left[ \frac{T}{T_c} \right]^2 \left[ \frac{\Gamma \alpha_0 T_c}{\beta a} \right]^2 + C_N
 \end{aligned}
 \tag{7}$$

where the coherence length for the antiferromagnetic order parameter is defined by  $\xi_1 \equiv \delta/\alpha_0 T_c$ , and the ferromagnetic one by  $\xi_m \equiv c/a$ , and  $t_1 \equiv t + \Gamma H^2/4a^2 \alpha_0 T_c$ ,  $t_m \equiv 1 - \Gamma \alpha/a\beta = 1 - |\Gamma \alpha|/a\beta$ , where the reduced temperature  $t \equiv (T - T_N)/T_N$ . This gives the specific heat above the Néel temperature. To find the specific heat in the region below the transition, the functional integral is expanded around the mean field solution below  $T_N$  and a similar integration carried out. The result after straightforward manipulations is

$$C = \frac{3}{4\pi} \frac{k_B}{\xi_1^3} \left[ \frac{T}{T_c} \right]^4 \frac{1}{t_1^{1/2}} + \frac{3}{4\pi} \frac{k_B}{\xi_m^3} \left[ \frac{T}{T_c} \right]^4 \left[ \frac{\Gamma \alpha_0 T_c}{\beta a} \right]^2 \frac{1}{t_m^{1/2}}$$

$$+ \left[ \frac{T}{T_c} \right]^3 \frac{\alpha_0^2}{\beta} \left[ 1 + \frac{2\Gamma^2}{\beta a'^3} H^2 \right] + C_N \quad \text{for } T < T_N \quad (8)$$

where below  $T_N$ , the reduced temperature  $t'$  is given by  $t' \equiv 2|t| + \Gamma H^2 / 4a^2 \alpha_0 T_c$ , and  $a' \equiv a + \Gamma|\alpha|/\beta = a - |\Gamma\alpha|/\beta$ . We will return to these equations when we compare them to the experimental data on  $\text{CdCr}_2\text{O}_4$  and  $\text{ZnCr}_2\text{O}_4$ .

We consider now the possibility for large exponents  $\alpha$  for the specific heat critical exponent. We give a simple argument that the exponent  $\alpha$  cannot exceed one for thermodynamic consistency, but then explore a non-thermodynamic situation in which an effective exponent does exceed unity, and, in fact, where  $\alpha = 3/2$ .

The specific heat critical exponents are defined by

$$\begin{aligned} C &\approx t^{-\alpha} \quad \text{as } t \rightarrow 0^+ \\ C &\approx |t|^{-\alpha'} \quad \text{as } t \rightarrow 0^- \end{aligned} \quad (9)$$

Since the free energy is related to the specific heat upon taking two derivatives with respect to temperature it follows that the free energy contains the contribution

$$F \approx \begin{cases} t^{2-\alpha} & \text{as } t \rightarrow 0^+ \\ |t|^{2-\alpha'} & \text{as } t \rightarrow 0^- \end{cases} \quad (10)$$

Now, however, it follows from the basic relation between the free energy and the entropy,  $S = -dF/dT$ , that the entropy must contain the term

$$S \approx \begin{cases} t^{1-\alpha} & \text{as } t \rightarrow 0^+ \\ |t|^{1-\alpha'} & \text{as } t \rightarrow 0^- \end{cases} \quad (11)$$

Thus it follows that in order for the entropy to be finite at the transition, we must have

$$\begin{aligned} \alpha &< 1 \\ \alpha' &< 1 \end{aligned} \quad (12)$$

Another way to see the same result is to consider the entropy above the transition<sup>6</sup>

$$S_\infty - S_c = \int_{T_c}^{\infty} \frac{C}{T} dT \Rightarrow \frac{C_1}{T_c} \int_0^{\infty} \frac{t^{-\alpha}}{t+1} dt = \frac{C_1}{T_c} \frac{\pi}{\sin(1-\alpha)\pi} \quad (13)$$

if the specific heat has a contribution of the form  $C = C_0 + C_1 t^{-\alpha}$  and  $\alpha$  satisfies  $0 < \alpha < 1$ . Again, as  $\alpha \rightarrow 1$  the entropy may be seen to diverge.

We now consider an argument which in a disordered material can produce an exponent larger than unity. This does not violate the thermodynamic constraint discussed above since the system is in a quenched disordered state rather than one of thermodynamic equilibrium. Consider the free energy above for just one order parameter, either  $l$  or  $m$ , in principle. We assume that the order parameter couples to locally random fields  $H_r$  which average to zero,  $\langle H_r \rangle = 0$ , thus  $m$  satisfies the equation

$$m \hat{q} = \frac{H_r}{a + c \hat{q}^2} \quad (14)$$

and therefore the average of  $m$  vanishes due to the effect of the

random fields acting on it

$$\langle m_q \rangle = \frac{\langle H_r \rangle}{a + cq^2} = 0 \quad (15)$$

However, the square of the local fields does not vanish,  $\langle H_r^2 \rangle = \sigma \neq 0$ , and square of the order parameter exists

$$\langle m^2 \rangle = \sum_q \frac{\sigma}{(a + cq^2)^2} \quad (16)$$

To calculate a specific heat we recall that C is related to the order parameter in a simple way

$$\langle m^2 \rangle = \frac{dF}{da} \quad (17)$$

$$C \approx - \frac{d^2 F}{da^2} \approx - \frac{d\langle m^2 \rangle}{da}$$

Combining Eqs. (16) and (17) gives the following result for the specific heat

$$C \approx \int d^3 q \frac{\sigma}{(a + cq^2)^3} \approx a^{-3/2} \quad (18)$$

In just what sense the last relationship (17) represents the actual specific heat remains to be investigated. We plan to return to this question when we examine in detail the role of disorder in these materials.

In our next two reports we will complete the study of the thermal properties by considering the thermal conductivity, and then apply the various theoretical results we have obtained to attempt to fit the experimental data on  $\text{CdCr}_2\text{O}_4$  and  $\text{ZnCr}_2\text{O}_4$ .

## REFERENCES

1. K.J. Standley, *Oxide Magnetic Materials*, Oxford, 1962.
2. S.V. Vonsovskii, *Magnetism*, vol. 2, Wiley, 1974.
3. J.E. Thompson, *The Magnetic Properties of Materials*, Newnes, 1968.
4. L.D. Landau and E.M. Lifshitz, *Statistical Physics, Part 1*, Pergamon, 1980.
5. E.A. Turov, *Physical Properties of Magnetically Ordered Crystals*, Academic, 1965.
6. D. H. Martin, *Magnetism in Solids*, Iliffe, 1967, p. 382.

PROGRESS REPORT

AFOSR Contract #F49620-83-C-0129

Fundamental Physics on High-Specific-Heat  
Dielectrics and Kapitza Resistance at Dielectric Boundaries

Theoretical Research Program

Spinel Studies

IV. Thermal Conductivity

by

Bruce R. Patton

*BRP*

Department of Physics

The Ohio State University

Columbus, Ohio 43210

Distribution:

J.H. Parker, Sr.

P.W. Eckels

T.K. Gupta

M. Ashkin

C.F. Clark

B.R. Patton

*November 15, 1984*

## INTRODUCTION

In our last report on our research on the B-site spinel phases, we applied our theoretical model for compounds of the type represented by zinc chromite,  $\text{ZnCr}_2\text{O}_4$ , and cadmium chromite,  $\text{CdCr}_2\text{O}_4$ , to the calculation of the thermal properties such as the specific heat. We recall that the magnetic properties of these materials were characterized by weak interactions among the magnetic ions and consequently low magnetic transition temperatures.<sup>1,2,3,5</sup> An important feature was the fact that the arrangement of the magnetic ions on the lattice leads to a high degree of frustration in the mutual antiferromagnetic ordering of the spins. Our first approach to the theory of these materials was to derive a Ginzburg-Landau<sup>4</sup> free energy which involved two order parameters, the first being the sublattice magnetization  $l_\alpha = \sum_{i,j} (M_{i\alpha} - M_{j\alpha})$ , representing the antiferromagnetically ordered spins, and the second the total magnetization  $m_\alpha = \sum_i M_{i\alpha}$ , corresponding to the component of ferromagnetically ordered spins. The ferromagnetic order never fully develops in  $\text{CdCr}_2\text{O}_4$  and  $\text{ZnCr}_2\text{O}_4$ , but the paramagnetic spins influence the other order parameter and gave rise to a temperature dependent magnetic susceptibility. The specific heat showed the singularity at  $T_N$  due to the ordering of the antiferromagnetic spins, but, in a very interesting feature, the specific heat was also enhanced below  $T_N$  by the effect of the fluctuations in the remaining unordered paramagnetic spins. Reasonable fits of the experimental data on  $\text{CdCr}_2\text{O}_4$  and  $\text{ZnCr}_2\text{O}_4$  have been made and will

be discussed in our next report. In the present report we wish to consider the thermal conductivity of these materials.

#### THERMAL CONDUCTIVITY

The simplest kinetic theory argument gives the result that the excitations or particles of a system carry heat in proportion to their specific heat  $C$ , velocity  $v_0$ , and mean free path  $\lambda$ <sup>8</sup>

$$\kappa = \frac{1}{3} C v_0 \lambda = - C v_0^2 \tau \quad (1)$$

where the mean free path is related to the scattering time  $\tau$  by  $\lambda = v_0 \tau$ . For phonons in crystals at low temperatures the specific heat is proportional to the number of phonons, which goes as  $T^3$ , while the scattering rate has contributions that arise from boundary (or impurity) scattering which are temperature independent as well as phonon scattering terms which vary as  $T^{3.6}$ . In magnetic systems, both the specific heat as well as the scattering rate depend on the type of excitations in the material. In ferromagnetic systems, the spin wave excitation energies have a quadratic wave number dependence,  $\omega(q) \approx q^2$ . Consequently, the specific heat varies as  $T^{3/2}$  well below the Curie temperature, and the spin wave scattering rate has a similar temperature dependence. In an antiferromagnet, however, the spin waves have a linear dispersion,  $\omega(q) \approx q$ , like phonons, and thus give rise to  $T^3$  contributions to both the specific heat and scattering rates.

The general formula for the thermal conductivity may be expressed in terms of the Green's functions  $G(k, \omega)$  describing the

fundamental excitations of the system:<sup>7</sup>

$$\langle \kappa_{\mu\nu} \rangle = \frac{2K}{\pi k_B T^2 V} \int_0^\infty d\omega \frac{\omega^2 e^{-\hbar\omega/k_B T}}{[e^{\hbar\omega/k_B T} - 1]^2} \text{Tr} \langle v_\mu \text{Im}G(\omega) v_\nu \text{Im}G(\omega) \rangle \quad (2)$$

In the materials of interest here,  $\text{CdCr}_2\text{O}_4$  and  $\text{ZnCr}_2\text{O}_4$ , there are at least two types of excitations contributing to the thermal conductivity, the phonons and the spin waves; the latter contribute as propagating modes well below  $T_N$  and as diffusive modes in the vicinity of  $T_N$ . The scattering of the phonons is determined by fluctuations in the local crystalline density, such as those caused by impurities, boundaries, or other phonons. The effect of spin fluctuations on the phonon scattering depends on the coupling of the spins to deformations of the lattice; as we have noted in our first report in this series on structural properties of these spinels, in the pure phase there is usually a small tetragonal lattice distortion accompanying the anti-ferromagnetic transition. Thus we have strong experimental evidence of a significant spin-lattice coupling, which implies a term in the fundamental hamiltonian of the form

$$H_{\text{sp-ph}} = \int d^3r g |\mathbf{l}|^2 |\nabla \cdot \mathbf{q}|^2 \quad (3)$$

where  $\mathbf{q}$  is the displacement of the lattice. With this interaction, and using some simplifying assumptions,<sup>7</sup> the thermal conductivity expression (2) reduces to the form

$$\langle \kappa \rangle = \frac{1}{V} \sum_{\mathbf{k}, i} C[\omega_i(\mathbf{k})] |v_i(\mathbf{k})|^2 \tau_i(\mathbf{k}) \cos^2 \theta \quad (4)$$

where  $C[\omega_i(\mathbf{k})]$  is the specific heat contribution of a mode with

energy  $\omega_i(k)$ ,  $v_i(k)$  is the velocity of the mode,  $\tau_i(k)$  its relaxation time, and  $V$  is the volume. Eq. (4) shows that all modes contribute to the thermal conductivity in the form of the simple Eq. (1), but that the contributions are summed over the type of mode  $i$  and its wavenumber  $k$ .

We consider first the contribution of the phonons to the thermal conductivity. For temperatures well above the Debye temperature, the specific heat is constant and equal to  $3Nk_B$ . The velocity  $v$  is the sound velocity, while the mean free path may be obtained from the following argument. The scattering is proportional to the local variation in the velocity, which arises from fluctuations in the local density:

$$\frac{1}{\tau_{ph}} = \frac{v}{\lambda_{ph}} \cong \frac{v}{a} \overline{\left[ \frac{\delta v}{v} \right]^2} \cong \frac{v}{a} \gamma^2 \overline{\left[ \frac{\delta \rho}{\rho} \right]^2} \quad (5)$$

where  $\rho$  is the density,  $\gamma$  is Grüneisen's constant, and  $a$  is the lattice constant. The thermal average of fluctuations in the density (or volume) may be obtained from the equipartition theorem,

$$\overline{\left[ \frac{\delta V}{V} \right]^2} = k_B T \frac{K}{V} \cong \frac{N k_B T}{V \rho v^2} \quad (6)$$

where  $K$  is the isothermal compressibility. Thus the thermal conductivity becomes

$$\kappa \cong \frac{\rho v^3 a}{\gamma^2 T} \quad (7)$$

which shows the well-known inverse temperature dependence of the

conductivity at high temperatures, arising from scattering from lattice fluctuations having a probability proportional to the temperature. As the temperature is lowered, for a pure crystalline material the umklapp scattering processes (those with momentum change larger than  $2\pi/a$ ) become the determining factor since small angle scattering preserves the momentum and energy of the phonon heat current. Since these processes involve an exponential of the debye energy over the temperature, the thermal conductivity drops rapidly until the scattering length becomes limited by the boundaries of the sample for a pure specimen, or the average spacing between impurities or lattice imperfections for disordered samples.

We consider now the analogous situation for the scattering of spin waves. Below  $T_N$  a good fraction of the heat may be carried by spin waves in the ordered magnetic phase. At low temperatures the fluctuations in the magnetic ordering are small and the spin waves propagate freely. As the temperature increases toward  $T_N$ , however, fluctuations increase and the spin wave scattering also increases, thus tending to decrease the spin wave contribution to the thermal conductivity. The spin wave modes give a large contribution to the specific heat near  $T_N$ , though, and the net effect on the thermal conductivity reflects the competition between these effects.

We first estimate the spin wave scattering. Following the argument given above for phonons, we expect a contribution to the scattering proportional to the fluctuations in the order parameter  $l$ , since the spin wave velocity depends on the

stiffness of the magnetic order. Thus the spin wave fluctuation scattering should be given by

$$\frac{1}{\tau_{fl}} = \frac{v}{\lambda_{fl}} \cong \frac{v}{a} Y_1^2 \left[ \frac{\delta l}{l} \right]^2 \quad (8)$$

where  $Y_1$  is an effective Grüneisen constant. From the free energy, for the antiferromagnetic state described in the second report of this series we may calculate the fluctuations in the order parameter  $l$

$$\langle |\delta l|^2 \rangle = \begin{cases} 3 \sum_q \frac{k_B T}{\alpha + \xi^2 q^2} \cong 3k_B T (c_0 - c_1 \alpha^{1/2}) & T > T_N \\ \sum_q \frac{k_B T}{2|\alpha| + \xi^2 q^2} = k_B T [c_0 - c_1 (2|\alpha|)^{1/2}] & T < T_N \end{cases} \quad (9)$$

The scattering rates for the different mechanisms are additive if the scattering is not too strong, thus the total scattering rate can be written

$$\begin{aligned} \frac{1}{\tau} &= \frac{1}{\tau_{imp}} + \frac{1}{\tau_{ph+afsw}} + \frac{1}{\tau_{fl}} \\ &= a_1 + a_2 T^3 + (a_3 - a_4 |\alpha|^{1/2}) T \end{aligned} \quad (10)$$

where  $a_1$ ,  $a_2$ , and  $a_3$  and  $a_4$  are constants proportional to the amount of boundary/impurity, phonon/antiferromagnetic spin wave, and spin fluctuation scattering, respectively. To illustrate the nature of our results for the thermal conductivity we use the scattering rate (10) in Eq. (4), together with the result for the specific heat from our previous report

$$\begin{aligned}
C_{>} &= \frac{3}{16\pi} \frac{k_B}{\xi_1^3} \left[ \frac{T}{T_c} \right]^2 \frac{1}{t_1^{1/2}} + \frac{3}{16\pi} \frac{k_B}{\xi_m^3} \left[ \frac{T}{T_c} \right]^2 \left[ \frac{\Gamma \alpha_0 T_c}{\beta a} \right]^2 + C_N \\
C_{<} &= \frac{3}{4\pi} \frac{k_B}{\xi_1^3} \left[ \frac{T}{T_c} \right]^4 \frac{1}{t_1^{1/2}} + \frac{3}{4\pi} \frac{k_B}{\xi_m^3} \left[ \frac{T}{T_c} \right]^4 \left[ \frac{\Gamma \alpha_0 T_c}{\beta a} \right]^2 \frac{1}{t_m^{1/2}} \\
&\quad + \left[ \frac{T}{T_c} \right]^3 \frac{\alpha_0^2 T_c}{\beta} \left[ 1 + \frac{2\Gamma^2}{\beta a^3} H^2 \right] + C_N
\end{aligned} \tag{11}$$

where  $C_{>}$  and  $C_{<}$  indicate the specific heat above and below  $T_N$ , respectively, and the other parameters are defined in our last report. Figs. 1 and 2 show plots of the specific heat and the thermal conductivity, using the above equations with a typical set of parameters for  $\text{ZnCr}_2\text{O}_4$ . The same values of the fitting constants have been used for both the specific heat and the thermal conductivity. It may be noted that the specific heat has a large increase at the transition, approximately a factor of seven, while the thermal conductivity has an increase of only about a factor of two. The difference comes from the increase in the scattering of spin fluctuations near the transition. In our next report we will extend this numerical analysis to a detailed comparison with the data for the specific heat and thermal conductivity of both  $\text{ZnCr}_2\text{O}_4$  and  $\text{CdCr}_2\text{O}_4$ .

## REFERENCES

1. K.J. Standley, *Oxide Magnetic Materials*, Oxford, 1962.
2. S.V. Vonsovskii, *Magnetism*, vol. 2, Wiley, 1974.
3. J.E. Thompson, *The Magnetic Properties of Materials*, Newnes, 1968.
4. L.D. Landau and E.M. Lifshitz, *Statistical Physics, Part 1*, Pergamon, 1980.
5. E.A. Turov, *Physical Properties of Magnetically Ordered Crystals*, Academic, 1965.
6. J. M. Ziman, *Electrons and Phonons*, Oxford, 1960.
7. R. J. Elliott and P. L. Leath, in *Dynamical Properties of Solids*, edited by G. K. Horton and A.A. Maradudin, North Holland, 1975, vol. 2, p. 416.
8. Neil W. Ashcroft and N. David Mermin, *Solid State Physics*, Holt, Rinehart, and Winston, 1976, chap. 25.

Fig. 1. Specific heat vs. temperature.

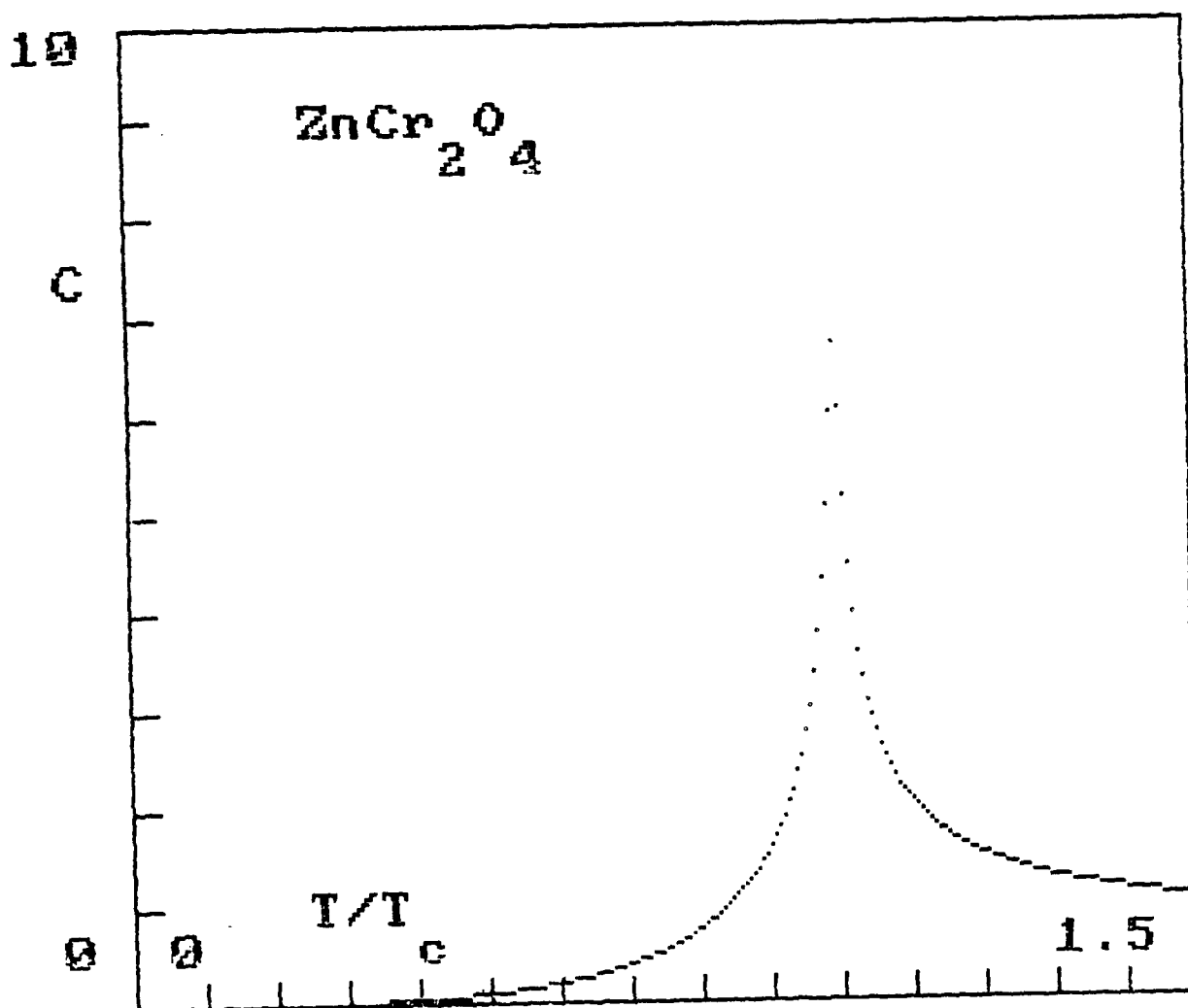
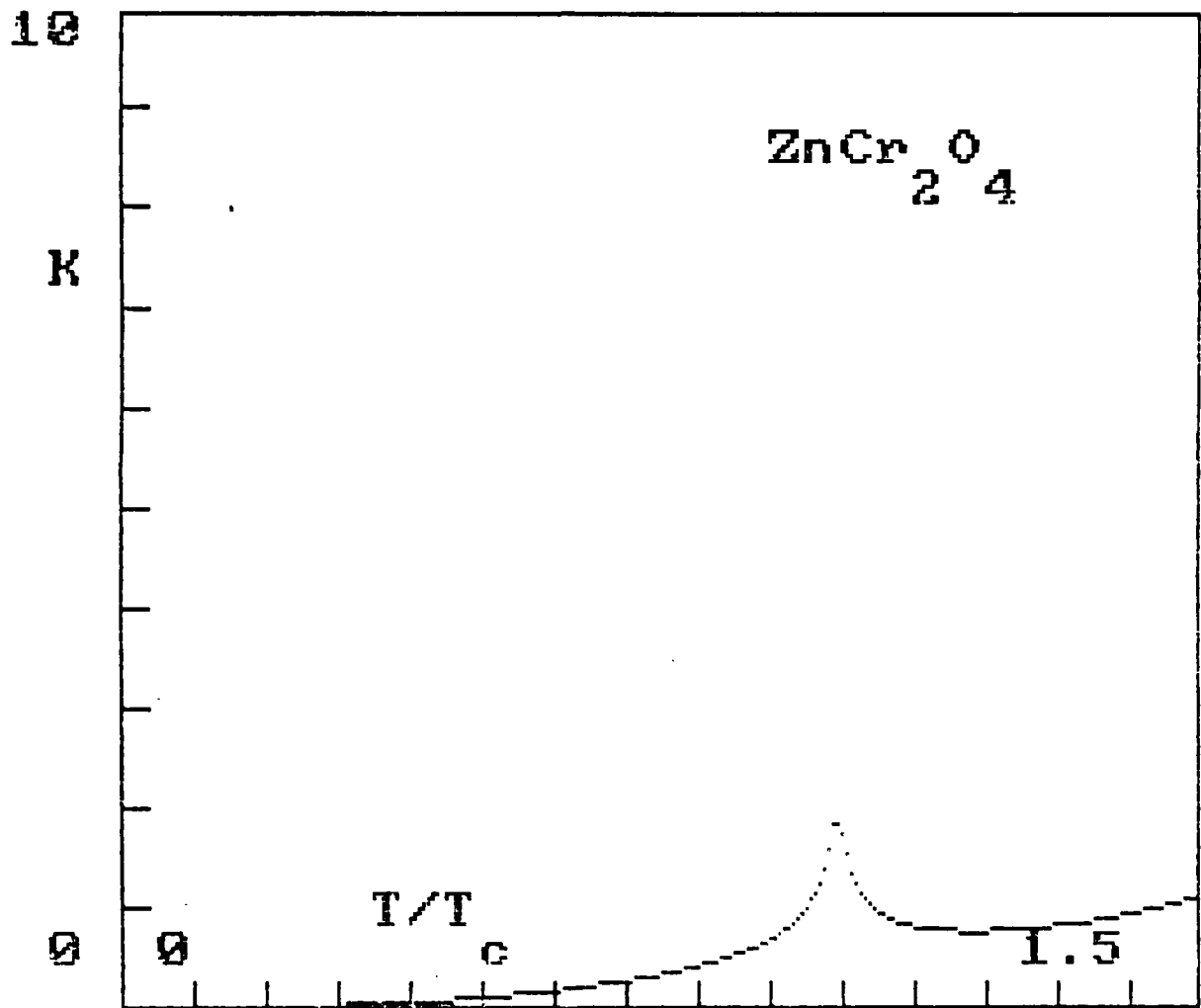


Fig. 2. Thermal conductivity vs. temperature.



PROGRESS REPORT

AFOSR Contract #F49620-83-C-0129

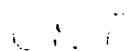
Fundamental Physics on High-Specific-Heat  
Dielectrics and Kapitza Resistance at Dielectric Boundaries

Theoretical Research Program

Spinel Studies

V. Comparison with Experiment: Specific Heat

by



Bruce R. Patton

Department of Physics

The Ohio State University

Columbus, Ohio 43210

August 15, 1985

E-48

## INTRODUCTION

Our previous reports in this series on research on the B-site spinel phases developed a theoretical model for compounds of the type represented by zinc chromite,  $ZnCr_2O_4$ , and cadmium chromite,  $CdCr_2O_4$ . We found that the magnetic properties of these materials arose from weak interactions among the magnetic ions, which explained the low magnetic transition temperatures of order 10 to 20K.<sup>1,2,3,4</sup> The other characteristic feature of these materials was the frustrated arrangement of the magnetic ions on the lattice with respect to the mutual antiferromagnetic ordering of the neighboring spins. A Ginzburg-Landau<sup>5</sup> free energy involving two order parameters was proposed. One order parameter was the sublattice magnetization  $l_a = \sum_{i,j} (M_{i,a} - M_{j,a})$ , representing the anti-ferromagnetically ordered spins, while the second was total magnetization  $m_a = \sum_i M_{i,a}$ , corresponding to the component of ferromagnetically ordered spins. We noted that the ferromagnetic order never developed in  $CdCr_2O_4$  and  $ZnCr_2O_4$ , but that the paramagnetic spins influenced the other order parameter and gave rise to a temperature dependent magnetic susceptibility.

## THEORY

The free energy as a functional of these two order parameters  $l_a$  and  $m_a$  is

$$F = \int d^3r \left[ \alpha |l|^2 + \frac{\beta}{2} |l|^4 + \delta |\nabla \cdot l|^2 + a |m|^2 + \frac{b}{2} |m|^4 + c |\nabla \cdot m|^2 + \Gamma |l|^2 |m|^2 - m \cdot H \right] \quad (1)$$

In our third report we evaluated the specific heat in the Gaussian limit. We summarize briefly here the results of that calculation. The partition function is given by the functional integral over the order parameter variables  $l$  and  $m$

$$e^{-F/k_B T} = \int Dl Dm e^{-F[l,m]/k_B T} \quad (2)$$

The functional integral was performed for gaussian fluctuations away from the mean values, yielding the thermodynamic free energy. The specific heat then follows from the free energy by taking two derivatives with respect to temperature.

$$C_{>} = \frac{3}{16\pi} \frac{k_B}{\xi_1^3} \left[ \frac{T}{T_N} \right]^2 \frac{1}{t_1} \frac{1}{2} + \frac{3}{16\pi} \frac{k_B}{\xi_m^3} \left[ \frac{T}{T_N} \right]^2 \left[ \frac{\Gamma \alpha_0 T_N}{\beta a} \right]^2 \frac{1}{t_m} \frac{1}{2} + C_N \quad \text{for } T > T_N \quad (3a)$$

$$C_{<} = \frac{3}{4\pi} \frac{k_B}{\xi_1^3} \left[ \frac{T}{T_N} \right]^4 \frac{1}{t'_1} \frac{1}{2} + \frac{3}{4\pi} \frac{k_B}{\xi_m^3} \left[ \frac{T}{T_N} \right]^4 \left[ \frac{\Gamma \alpha_0 T_N}{\beta a} \right]^2 \frac{1}{t_m} \frac{1}{2} + \left[ \frac{T}{T_N} \right]^3 \frac{\alpha_0^2}{\beta T_N} \left[ 1 + \frac{2\Gamma^2}{\beta a^2} H^2 \right] + C_N \quad \text{for } T < T_N \quad (3b)$$

where the coherence length for the antiferromagnetic order parameter is defined by  $\xi_1 \equiv \delta/\alpha_0 T_N$ , and the ferromagnetic one by  $\xi_m \equiv c/a$ .  $C_{>}$  is the specific heat above the Néel temperature,  $t_1 \equiv t + \Gamma H^2/4a^2 \alpha_0 T_N$ , and  $t_m \equiv 1 - \Gamma \alpha/a\beta = 1 + \Gamma|\alpha|/a\beta$ , where the reduced temperature  $t \equiv (T - T_N)/T_N$ . The specific heat in the region below the transition is given by  $C_{<}$ , where below  $T_N$ , the reduced temperature  $t'$  is given by  $t' \equiv 2|t| + \Gamma H^2/4a^2 \alpha_0 T_N$ , and  $a' \equiv a + \Gamma|\alpha|/\beta = a + |\Gamma\alpha|/\beta$ . We will return to these equations

when we compare them to the experimental data on  $\text{CdCr}_2\text{O}_4$  and  $\text{ZnCr}_2\text{O}_4$ .

#### COMPARISON WITH EXPERIMENT

Figs. (1) to (4) show the results of fits to the data of Lawless<sup>6</sup> on  $\text{CdCr}_2\text{O}_4$ , while Figs. (5) through (8) give the fits for the  $\text{ZnCr}_2\text{O}_4$  data. Fig. (1) shows the experimental specific heat data<sup>6</sup> for  $\text{CdCr}_2\text{O}_4$  for a temperature range from zero to 15K; the transition is at about 8K. To fit the theoretical expression (3) to the experimental data, we must rewrite the theoretical formula in a clarified parametric form. However, we need to first address a limitation of our original result (3a). In the present case we are interested in temperatures well above the transition, and in that case, we need a formula that is accurate at higher temperatures, unlike (3a) which is valid for  $t-1 \ll 1$ . In Appendix A we give the details of a more accurate derivation; the result, however, is simply to remove the factors of  $(T/T_N)^2$  from Eq. (3a). These factors make an insignificant change near the transition, but clearly have a large effect for  $T \lesssim 2T_N$ . The result is the following form for the specific heat

$$C_p = C t + B + \frac{A}{(t-1)^\alpha} \quad \text{for } T > T_N \quad (4a)$$

where the first term is the normal specific heat, B is a background term arising from paramagnetic fluctuations and corrections to scaling, and the last term is the singular contribution from the anti-ferromagnetic fluctuations.

The specific heat below  $T_N$  is rewritten in a similar

fashion; in this case it is important to take into account thermodynamic relations that hold for the entropy. In Appendix B we show that these relations lead to a form for the specific heat, given by the formula

$$C_{\downarrow} = 3C t^3 + \frac{A t^4}{[(t-1)]^\alpha} + \frac{B t^4}{[1+D(1-t)]^{1/2}} \quad \text{for } T < T_N \quad (4b)$$

where  $A = 3k_B/(4\pi\xi_1^3)$ ,  $B = 3k_B D^2/(4\pi\xi_m^3)$ ,  $C$  is proportional to the density of states,  $t \equiv T/T_N$ , and  $D = \Gamma\alpha_0 T_N/\beta a$ . We have generalized the result using a scaling argument to the case of critical fluctuations;  $\alpha$  may then take on values different from  $1/2$ . The paramagnetic fluctuations (the last term in (4b)) are presumably never critical since those degrees of freedom do not order, thus the mean field exponent of  $1/2$  accurate. Finally, since the experimental data does not diverge to infinity, we convolve Eqs. (4) with a finite temperature resolution  $\delta t$ , which is determined by fitting the height of the peak at  $T = T_N$ .

From Fig. 2, it is clear that the mean field value for  $\alpha$ , namely,  $\alpha = 0.5$ , is not a very good fit to the specific heat data for  $\text{CdCr}_2\text{O}_4$ . In Fig. 3, a value of  $0.667$  is tried for  $\alpha$ ; the fit is better. However, the best fit is obtained for  $\alpha = 1.5$ , as shown in Fig. 4. (See also Ceramphysics Report VI: Critical Exponents.) A possible explanation for such a large value of  $\alpha$  was given in our third report, and involved an essential role of disorder. It should be noted that in the scaling region very close to the transition, a careful analysis of the specific heat data finds small exponents,<sup>7</sup> consistent with theoretical expectations for scaling behavior in the critical region. In our

analysis here we are interested not just in the critical fluctuations near the transition, but rather in the full range of temperature, from  $T = 0$  to  $T \approx 2T_N$ , which involves a possible mean-field region and corrections to scaling, and what the general form of the specific heat reveals about the internal structure and degrees of freedom of the material.

The data on  $ZnCr_2O_4$  is compared with theory in the second series of figures. The data is shown in Fig. 5, and the theory is plotted for  $\alpha = 0.5$  in Fig. 6. As with the cadmium material, the fit is not very good. A plot for  $\alpha = 0.667$  is shown in Fig. 7, and Fig. 8 gives a fit using  $\alpha = 1.5$ . Again it may be seen that the value of  $\alpha = 1.5$  gives a better characterization.

The fits to the data on  $CdCr_2O_4$  and  $ZnCr_2O_4$  are summarized in Table I where the values of the fitted parameters are given.

#### SUMMARY

The value  $\alpha = 1.5$  clearly gives the best fit for both  $ZnCr_2O_4$  and  $CdCr_2O_4$ . This appears to indicate that a significant role for disorder must occur in these B-site spinel materials. Another interesting feature that may be extracted from the analysis we have done is that the best fits occur for a positive sign of  $D$ , as may be seen from Table I. The values of  $D$  must be greater than  $-1$ , otherwise a transition to a ferromagnetic state would occur at some temperature, which has not been observed. Although it was not possible to determine  $D$  with a great deal of precision, the value of  $+1$  for  $D$  is distinctly better than a

value of  $-1$ . Since the sign of  $D$  depends on the sign of  $\Gamma$ , this result indicates that the interaction between the anti-ferromagnetic and incipient ferromagnetic order parameters is repulsive, i.e., the two types of ordering tend to inhibit each other. This has important consequences for the effect of doping on these materials as we will show on our report on disorder effects.

#### REFERENCES

1. K.J. Standley, *Oxide Magnetic Materials*, Oxford, 1962.
2. S.V. Vonsovskii, *Magnetism*, vol. 2, Wiley, 1974.
3. J.E. Thompson, *The Magnetic Properties of Materials*, Newnes, 1968.
4. L.D. Landau and E.M. Lifshitz, *Statistical Physics, Part 1*, Pergamon, 1980.
5. E.A. Turov, *Physical Properties of Magnetically Ordered Crystals*, Academic, 1965.
6. W.N. Lawless, "Spinel Studies II: Spinel Specific Heats", Progress Report - AFOSR Contract #F49620-83-C-0129.
7. W.N. Lawless, "Spinel Studies XII: Re-examination fo Critical Exponents", Progress Report - AFOSR Contract #F49620-83-C-0129.

## Appendix A

In this appendix we derive the relation between the specific heat above and below the transition. In the mean field approximation the results for the specific heat must be consistent with the third law of thermodynamics; the entropies of the normal and the ordered state must be the same at the transition. This requires

$$S_M(T_N) = \int_0^{T_N} \frac{C_N}{T} dT = S_N(T_N) = \int_0^{T_N} \frac{C_M}{T} dT \quad (A1)$$

The free energy is given by

$$F_M = F_N - \frac{\alpha^2}{2\beta} \quad (A2)$$

where we choose a temperature dependence for  $\alpha$  which is accurate at both low temperature and near the transition in the mean field approximation

$$\alpha = \alpha_0 \cdot \frac{T^2 - T_N^2}{2T_N} \quad (A3)$$

Eq. (A3) shows that  $\alpha$  and therefore the square of sublattice magnetization,  $|m_a|^2 = -\alpha/\beta$ , is linear in  $(T-T_N)$  near the transition, while at low temperatures the order parameter saturates at a maximum value. Calculating the entropy,  $S = -\partial F/\partial T$ , gives

$$S = S_N + \frac{\alpha_0^2}{2\beta} \left[ \frac{T^2}{T_N^2} - 1 \right] T \quad (A4)$$

From the requirement that the entropy must vanish as  $T \rightarrow 0$ , in accordance with the third law of thermodynamics, we find that

$$S_N = \frac{\alpha_0^2}{2\beta} \cdot T \quad \text{as } T \rightarrow 0 \quad (\text{A5})$$

The normal specific heat is then

$$C_N = T \frac{\partial S_N}{\partial T} = \frac{\alpha_0^2}{2\beta} T \quad (\text{A6})$$

while the specific heat in the magnetic phase is

$$C_M = \frac{3\alpha_0^2}{2\beta T_N^2} T^3 = 3C_N \left[ \frac{T}{T_N} \right]^2 \quad (\text{A7})$$

Using the results (A6) and (A7), it is easily verified that the relationship for the entropies (A1) is satisfied.

## Appendix B

In this appendix we derive a more accurate form for the fluctuation specific heat in the region above the transition temperature:  $T_N \leq T \leq 2T_N$ . The basic result is that the factors of  $T^2$  in the expression (3a) for  $C_>$  are removed in a more accurate treatment. Near the transition temperature  $T_N$  the factor  $(T/T_N)$  is unity so there is no difference close to the transition. However, further above the transition, the factor causes the fluctuation specific heat to increase in an unphysical fashion.

The starting point of a more careful treatment is the observation that a microscopic treatment of the fluctuations yields an expression for  $\alpha$  that is valid over a larger temperature range:

$$\alpha = \alpha_0 T_N \ln \left[ \frac{T}{T_N} \right] \quad (B1)$$

From Eq. (III.6) (Eq. (6) in our third report), the free energy in zero magnetic field is

$$\begin{aligned} F &= -k_B T \ln \left[ \prod_k \prod_q D l_k D m_q e^{-F(1,m)/k_B T} \right] \\ &= -k_B T \sum_k \ln \left[ \frac{k_B T}{\alpha + \delta k^2} \right]^{3/2} - k_B T \sum_q \ln \left[ \frac{k_B T}{a + cq^2} \right]^{3/2} \quad T > T_N \end{aligned} \quad (B2)$$

Evaluating the specific heat,  $C = -T \partial^2 F / \partial T^2$ , gives the result

$$C_> = \frac{3}{16\pi} \frac{k_B}{\xi_1^3} \frac{\lambda}{t_1^{1/2}} + B + C_N \quad (B3)$$

where  $t_1 \equiv \ln(T/T_w)$ ,  $\lambda = 1 + t_1$ , and  $B$  is a constant that is independent of temperature which arises both from the  $l$  fluctuations and from the  $m$  fluctuations. Not too far above the transition temperature the factor  $\lambda$  is essentially equal to one.

Table I. Theoretical Parameters Deduced From Experiment.

	$T_N$	$\alpha$	A	B	C	D	$\delta t$
	8.05	.50	1.55	.25	.45	1	.0020
CdCr <sub>2</sub> O <sub>4</sub>	8.05	.667	.90	.30	.40	1	.0030
	8.05	1.5	.09	1.7	.55	1	.020
	10.75	.50	1.3	.35	.15	1	.0045
ZnCr <sub>2</sub> O <sub>4</sub>	10.75	.667	.70	.96	.25	1	.0027
	10.75	1.5	.082	1.9	.20	1	.026

Parameters extracted from fits of the theory Eqs. (4) to the experimental data.

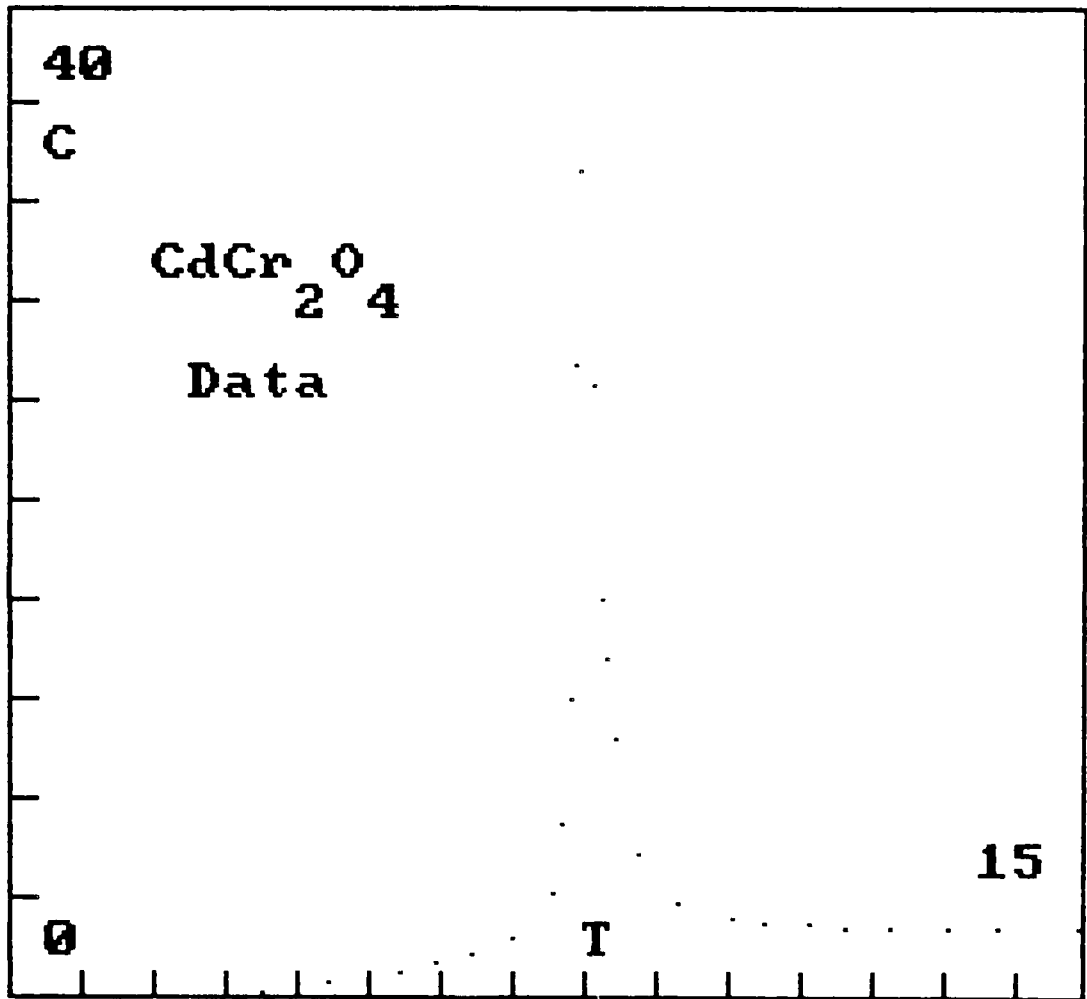


Fig. 1. Experimental data on CdCr<sub>2</sub>O<sub>4</sub>.

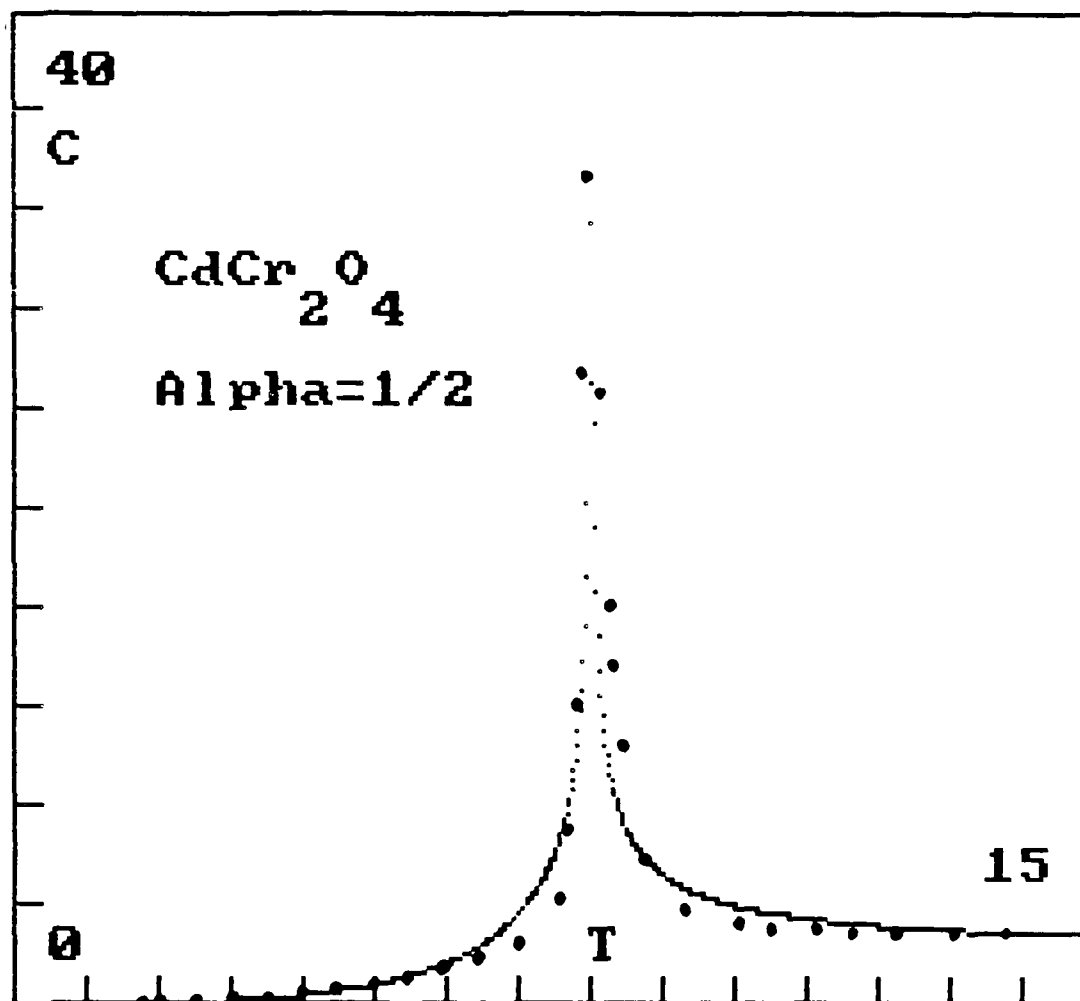


Fig. 2. Comparison of theory for  $\alpha = 0.5$  with data on  $\text{CdCr}_2\text{O}_4$ .

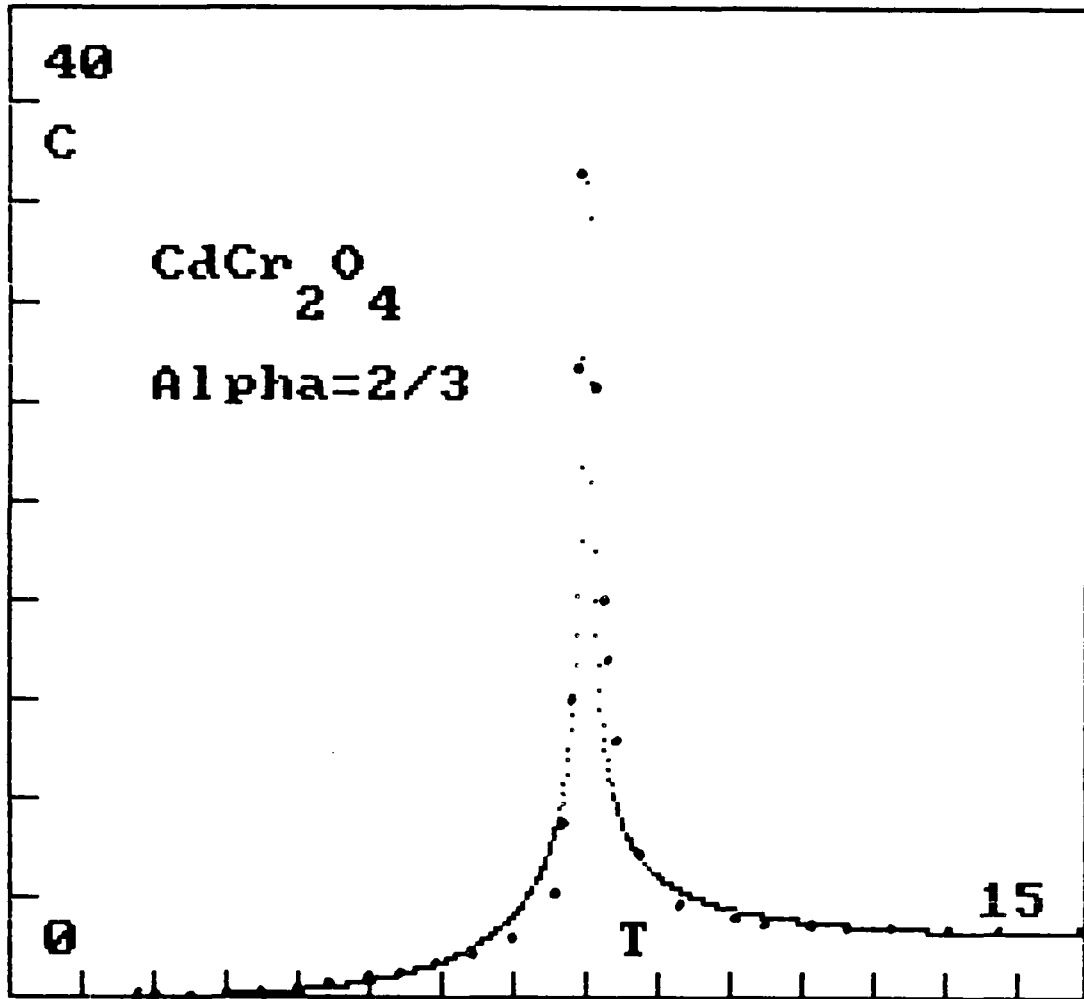


Fig. 3. Comparison of theory for  $\alpha = 0.667$  with data on  $\text{CdCr}_2\text{O}_4$ .

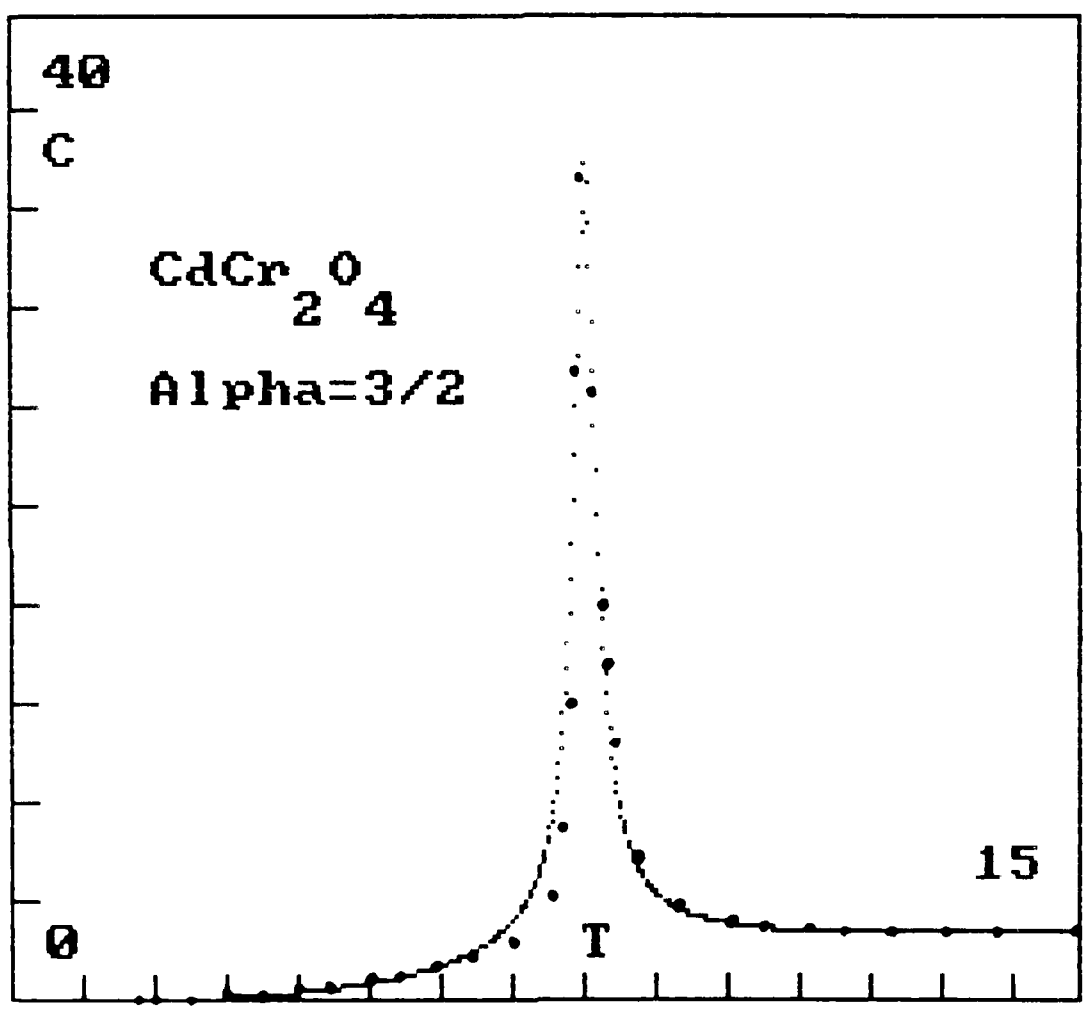


Fig. 4. Comparison of theory for  $\alpha = 1.5$  with data on  $\text{CdCr}_2\text{O}_4$ .

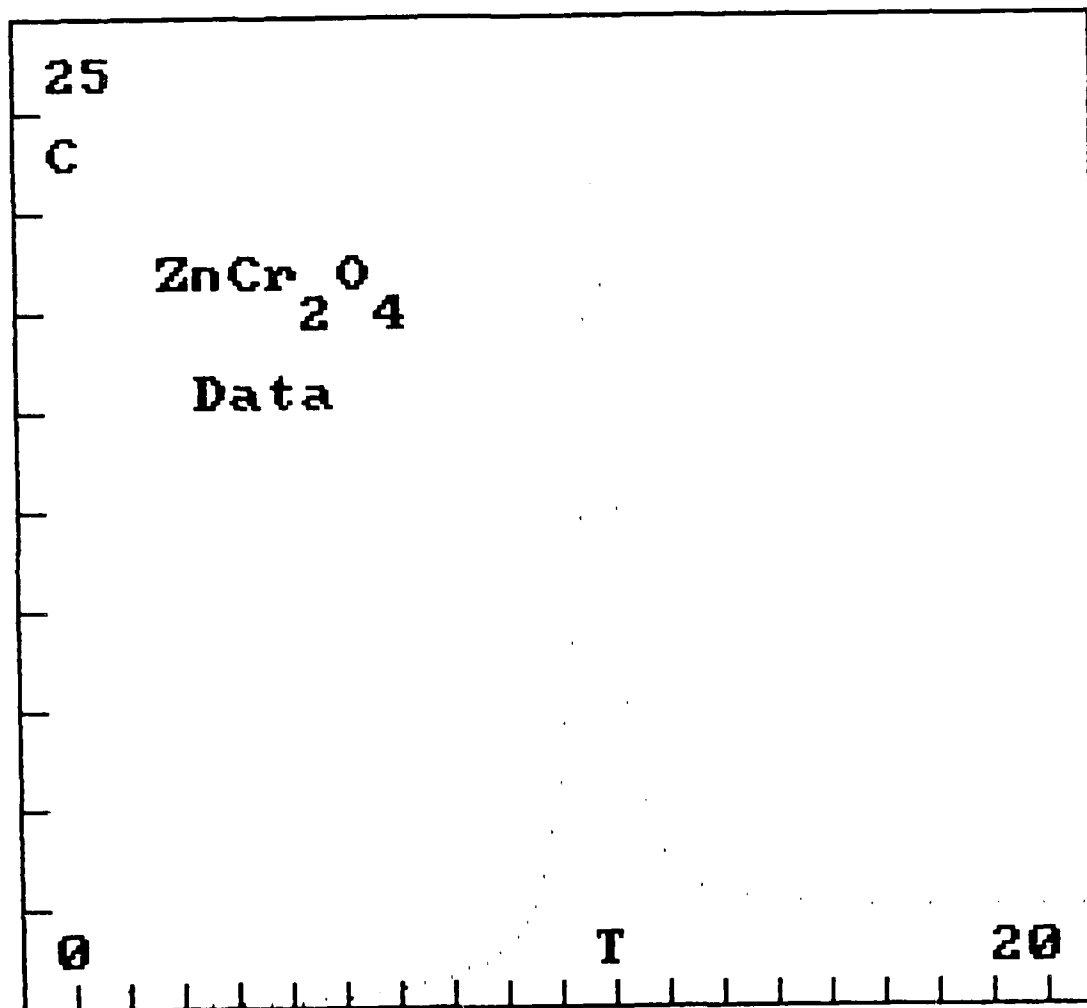


Fig. 5. Experimental data on  $\text{ZnCr}_2\text{O}_4$

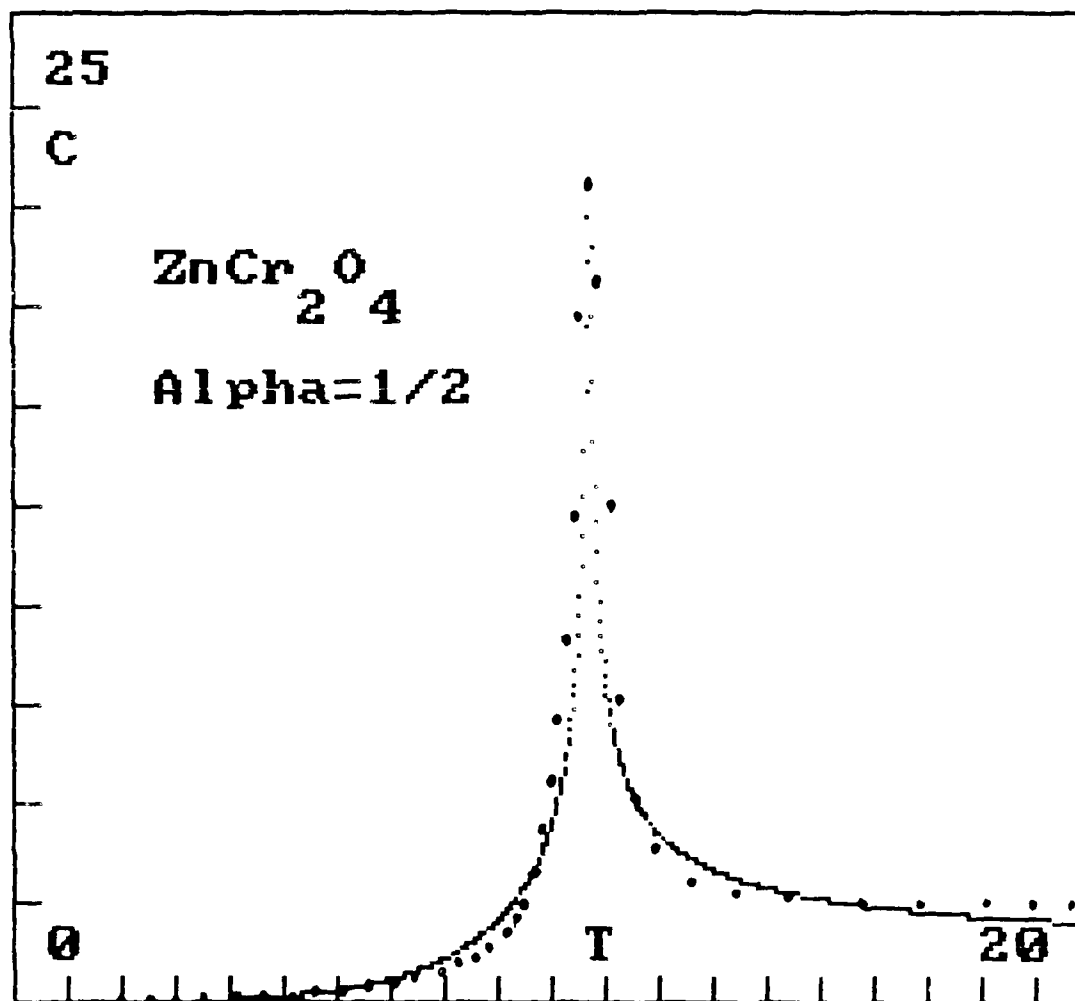


Fig. 6. Comparison of theory for  $\alpha = 0.5$  with data on  $\text{ZnCr}_2\text{O}_4$

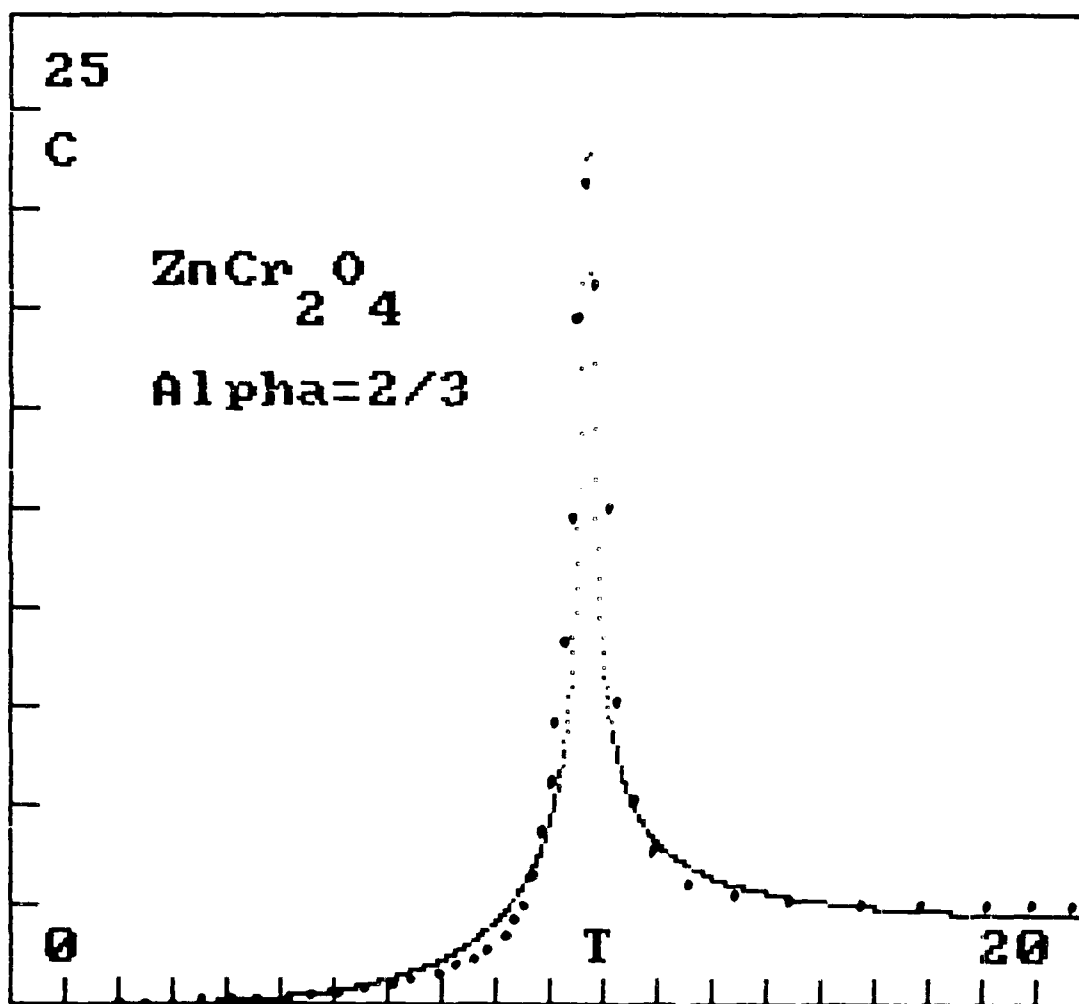


Fig. 7. Comparison of theory for  $\alpha = 0.667$  with data on  $\text{ZnCr}_2\text{O}_4$

AD-A169 964

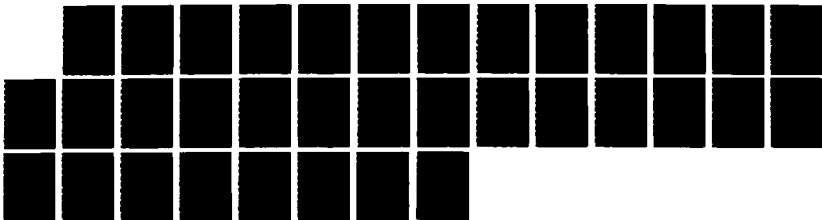
HIGH SPECIFIC HEAT DIELECTRICS AND KAPITZA RESISTANCE  
AT DIELECTRIC BOUND (U) WESTINGHOUSE RESEARCH AND  
DEVELOPMENT CENTER PITTSBURGH PA P W ECKELS ET AL

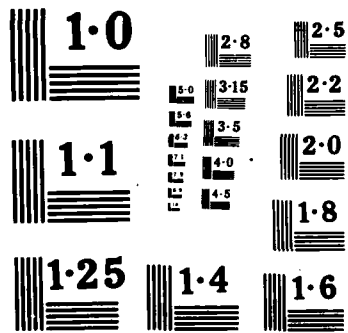
5/5

UNCLASSIFIED

30 SEP 85 AFOSR-TR-86-0477 F49620-83-C-0129 F/G 20/13

NL





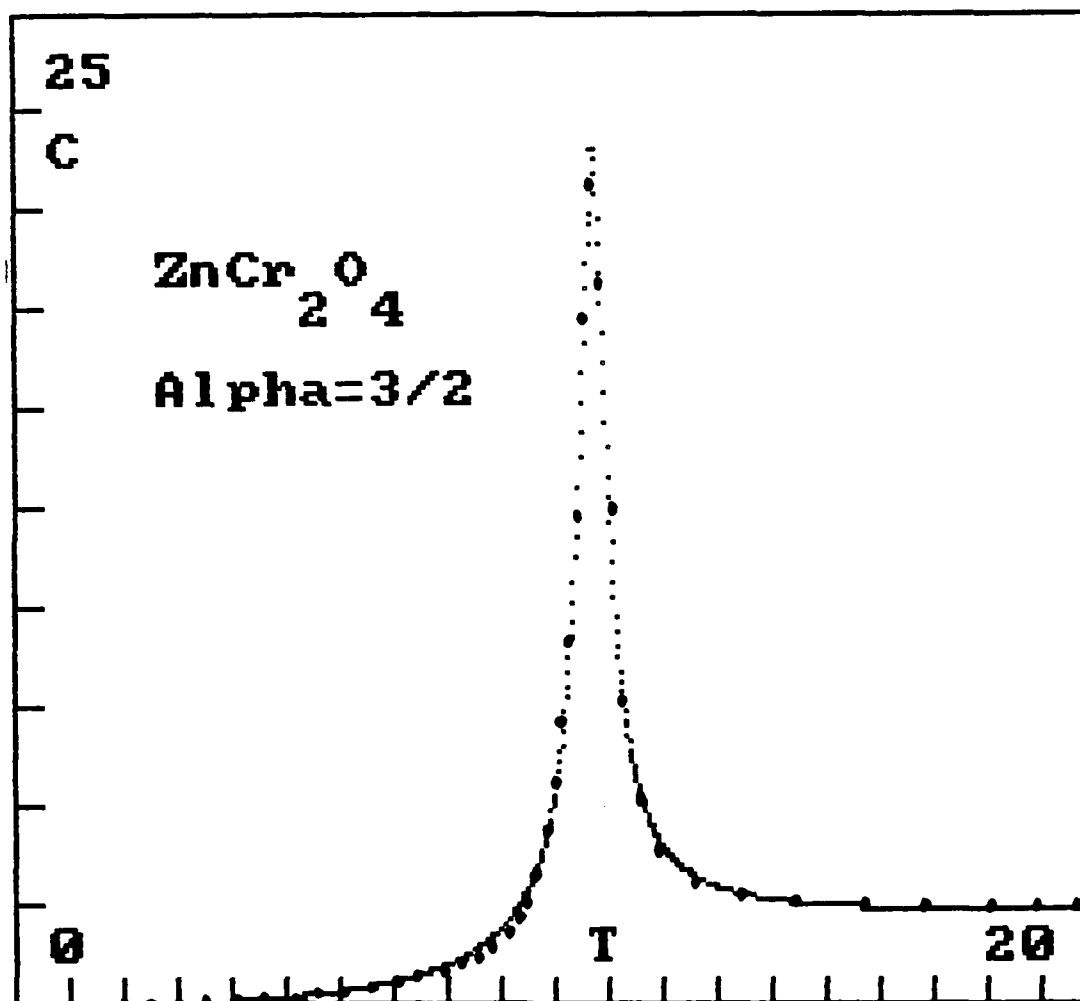


Fig. 8. Comparison of theory for  $\alpha = 1.5$  with data on  $\text{ZnCr}_2\text{O}_4$ .

PROGRESS REPORT

AFOSR Contract #F49620-83-C-0129

Fundamental Physics on High-Specific-Heat  
Dielectrics and Kapitza Resistance at Dielectric Boundaries

Theoretical Research Program

Spinel Studies

VI. Comparison with Experiment: Thermal Conductivity

by

Bruce R. Patton

BR.P.

Department of Physics

The Ohio State University

Columbus, Ohio 43210

August 30, 1985

## INTRODUCTION

In our last report on our research on the B-site spinel phases, we used our theoretical model for compounds of the type represented by zinc chromite,  $ZnCr_2O_4$ , and cadmium chromite,  $CdCr_2O_4$ , to fit experimentally thermal properties such as the specific heat. In the present report we continue this comparison with experiment by analyzing the experimental data on thermal conductivity.

We recall that the magnetic properties of the B-site spinels were characterized by weak interactions among the magnetic ions and consequently low magnetic transition temperatures.<sup>1,2,3,5</sup> An important feature was the fact that the arrangement of the magnetic ions on the lattice leads to a high degree of frustration in the mutual antiferromagnetic ordering of the spins. Our first approach to the theory of these materials was to derive a Ginzburg-Landau<sup>4</sup> free energy which involved two order parameters, the first being the sublattice magnetization  $l_\alpha = \sum_{i,j} (M_{i\alpha} - M_{j\alpha})$ , representing the antiferromagnetically ordered spins, and the second the total magnetization  $m_\alpha = \sum_i M_{i\alpha}$ , corresponding to the component of ferromagnetically ordered spins. The ferromagnetic order never appears to fully develop in  $CdCr_2O_4$  and  $ZnCr_2O_4$ , but the paramagnetic spins influence the other order parameter and gave rise to a temperature dependent magnetic susceptibility. The specific heat showed the singularity at  $T_N$  due to the ordering of the antiferromagnetic spins, but, in a very interesting feature, the specific heat was

also enhanced below  $T_N$  by the effect of the fluctuations in the remaining degrees of freedom.<sup>6</sup> Finally, in a transport property like the thermal conductivity, we found that the fluctuations in the spin ordering gave rise to characteristic scattering effects.<sup>7</sup> In the present report we wish to consider detailed fits of our theory to the thermal conductivity of these materials.

#### REVIEW OF THEORETICAL RESULTS

We summarize briefly here the theoretical formulae derived in our fourth report on thermal conductivity. The fundamental starting point in calculating the thermal conductivity is the Kubo formula:<sup>7</sup>

$$\langle \kappa_{\mu\nu} \rangle = \frac{2h}{\pi k_B T^2 V} \int_{-\infty}^{\infty} d\omega \frac{\omega^2 e^{-h\omega/k_B T}}{[e^{h\omega/k_B T} - 1]^2} \text{Tr} \langle v_{\mu} \text{Im}G(\omega) v_{\nu} \text{Im}G(\omega) \rangle \quad (1)$$

Because of the difficulty of directly exploiting this result in the absence of detailed knowledge of the microscopic Green's function  $G(\omega)$ , we transformed this result to a form which could be related to our phenomenological Ginzberg-Landau hamiltonian.<sup>8</sup> The thermal conductivity expression (1) reduces to the form<sup>7</sup>

$$\langle \kappa \rangle = \frac{1}{V} \sum_{k,i} C[\omega_i(k)] |v_i(k)|^2 \tau_i(k) \cos^2 \theta \quad (2)$$

where  $C[\omega_i(k)]$  is the specific heat contribution of a mode with energy  $\omega_i(k)$ ,  $v_i(k)$  is the velocity of the mode,  $\tau_i(k)$  its relaxation time, and  $V$  is the volume. A kinetic theory argument gives the result that the excitations of a system carry heat in proportion to the specific heat  $C$ , velocity  $v_0$ , and mean free

path  $\lambda$

$$\lambda = \frac{1}{3} C v_0 \lambda = - C v_0^2 \tau \quad (3)$$

where the mean free path is related to the scattering time  $\tau$  by  $\lambda = v_0 \tau$ . Eq. (2) shows that all modes contribute to the thermal conductivity in the form of the simple Eq. (3), but that the contributions are summed over each type of mode  $i$  and its wavenumber  $k$ .

In the spinels, we are concerned with the contributions which come primarily from two types of modes: phonons and spin waves. The phonon modes provide a background contribution to the thermal conductivity, while the spin waves give a contribution which varies strongly in the vicinity of the Néel transition temperature and decreases at lower temperatures. The reason for the latter is that below  $T_N$  a good fraction of the heat may be carried by spin waves in the ordered magnetic phase. At low temperatures the fluctuations in the magnetic ordering are small and the spin waves propagate freely. As the temperature increases toward  $T_N$ , however, fluctuations increase and the spin wave scattering also increases, thus tending to decrease the spin wave contribution to the thermal conductivity. It is important to note that the spin wave modes give a large contribution to the specific heat near  $T_N$ , though, and the net effect on the thermal conductivity reflects the competition between the specific heat and the scattering effects.

A proper evaluation of Eq. (3) for the thermal conductivity would involve the separate estimation of the contributions of

each mode to the specific heat. Unfortunately, all that is experimentally accessible is the total specific heat. Examination of (3), however, shows that when a large contribution, from the spin waves, for example, dominates, the thermal conductivity is well approximated by dividing the total specific heat by the total scattering rate. Similarly, far above the transition, when the spin wave effect is small, the same approximation is valid. We may then combine our successful fit of the specific heat from our last report<sup>9</sup> with our calculation of the scattering rate.

We estimated the contribution of the spin waves in a previous report<sup>7</sup> using a calculation of the scattering rate of the magnetic modes. In Appendix A we recalculate the expression for the scattering of spin waves in order to obtain a result which is valid over an extended temperature range. The result reduces to the formula we obtained in Report IV for temperatures near  $T_N$ , but gives an accurate form for the scattering also further away from the transition. The result we obtain in Appendix A has the form

$$\frac{1}{\tau} = \frac{1}{\tau_{\text{imp}}} + \frac{1}{\tau_{\text{fl}}} + \frac{1}{\tau_{\text{afsw}}}$$

$$= \begin{cases} a_1 + a_2 \frac{3R^3}{[3^{\frac{1}{2}}R + (t-1)^{\frac{1}{2}}]^2} & T > T_N \\ a_1 + a_2 \frac{tR^3}{[R + [2(1-t)]^{\frac{1}{2}}]^2} + a_3 t^3 & T < T_N \end{cases}$$

(4a)

(4b)

We combine these results with the fits of the specific heat

that we made in our last report.<sup>6</sup> For completeness we include here the formulae used to characterize the specific heat. The general result we obtained in Reports III and IV was

$$C_{>} = \frac{3}{16\pi} \frac{k_B}{\xi_1^3} \frac{1}{\epsilon_1^{1/2}} + \frac{3}{16\pi} \frac{k_B}{\xi_m^3} \left[ \frac{\Gamma \alpha_0 T_N}{\beta a} \right]^2 \frac{1}{\epsilon_m^{1/2}} + C_N \quad \text{for } T > T_N \quad (5a)$$

$$C_{<} = \frac{3}{4\pi} \frac{k_B}{\xi_1^3} \frac{t^4}{\epsilon_1^{1/2}} + \frac{3}{4\pi} \frac{k_B}{\xi_m^3} \left[ \frac{\Gamma \alpha_0 T_N}{\beta a} \right]^2 \frac{t^4}{\epsilon_m^{1/2}} + \frac{\alpha_+^2}{\beta T_N} t^3 + C_N \quad \text{for } T < T_N \quad (5b)$$

where the coherence length for the antiferromagnetic order parameter is defined by  $\xi_1 \equiv \delta/\alpha_0 T_N$ , and the ferromagnetic one by  $\xi_m \equiv c/a$ .  $C_{>}$  is the specific heat above the Néel temperature,  $\epsilon_1 \equiv \epsilon$ , and  $\epsilon_m \equiv 1 - \Gamma\alpha/a\beta = 1 + \Gamma|\alpha|/a\beta$ , where the dimensionless temperature  $t \equiv T/T_N$ , and the reduced temperature  $\epsilon \equiv t - 1$ . The specific heat in the region below the transition is given by  $C_{<}$ , where below  $T_N$ , the reduced temperature  $\epsilon'$  is given by  $\epsilon' \equiv 2|\epsilon|$ , and  $a' \equiv a + \Gamma|\alpha|/\beta$ .

In our fifth report in this series<sup>6</sup> we cast the equations for the specific heat in a parametric form which could be fit to experiment:

$$C_{>} = C t + B + \frac{A}{(t-1)^\alpha} \quad \text{for } T > T_N \quad (6a)$$

where the first term is the normal specific heat,  $B$  is a background term arising from paramagnetic fluctuations and corrections to scaling, and the last term is the singular contribution from the anti-ferromagnetic fluctuations.

The specific heat below  $T_N$  is rewritten in a similar fashion:

$$C_{<} = 3C t^3 + \frac{A t^4}{[(t-1)]^\alpha} + \frac{B t^4}{[1+D(1-t)]^{1/2}} \quad \text{for } T < T_N \quad (6b)$$

where  $A = 3k_B/(4\pi\xi_l^3)$ ,  $B = 3k_B D^2/(4\pi\xi_m^3)$ ,  $C$  is proportional to the density of states, and  $D = \Gamma\alpha_0 T_N/\beta a$ .

#### COMPARISON WITH EXPERIMENT

Using Eqs. (2), (4), and (6) we fit the thermal conductivity data on  $\text{CdCr}_2\text{O}_4$  and  $\text{ZnCr}_2\text{O}_4$ .<sup>9</sup> We use the  $\alpha = 1/2$  fit for the specific heat; although it does not give quite as good a fit as  $\alpha = 1.5$ , it is adequate for the present purpose, and it is not as clear how to use a scaling argument for a transport property to generalize to non-mean-field exponents. The values of the constants  $A$ ,  $B$ ,  $C$ ,  $D$ ,  $\delta t$ , and  $T_N$  were determined from the specific heat data, while the constants  $a_1$ ,  $a_2$ ,  $a_3$ , and  $R$  were determined from the best fit to the thermal conductivity. The fitted value of the parameters is given in Table I.

We note some interesting features of the results. The fact that the structure in the thermal conductivity in  $\text{CdCr}_2\text{O}_4$  is much weaker than in  $\text{ZnCr}_2\text{O}_4$  may be attributed to weaker spin fluctuations, together with a larger  $T^3$  background due to both phonon and spin wave contributions. The structure in the  $\text{ZnCr}_2\text{O}_4$  data is nicely reproduced, and depends essentially on two features of the theory: (1), the factor of three in the fluctuation scattering rate above  $T_N$ , which represents the fact that three components of the sublattice magnetization contribute

above compared to only one below, the other two components giving rise to propagating spin waves below  $T_N$ , and (2), the factor of two in the temperature dependence below  $T_N$ . It is not possible to fit the thermal conductivity data with significantly different values of these two constants, which are basic ingredients of the theory we have developed, and depend on general features, like the dimensionality of the order parameter.

From comparing the two fits, several general conclusions regarding the difference between the two spinels are possible. The greater structure in the thermal conductivity of the Zn material comes from: (1), a smaller impurity ( $a_1$ ) contribution, possibly because of larger microstructural domains, (2), a somewhat larger coherence length ( $\xi^3 \approx 1/a_2$ ), and (3), a much smaller spin-wave/phonon background ( $a_3$ ), seventy times smaller in  $ZnCr_2O_4$  than in  $CdCr_2O_4$ . Evidence of a larger phonon contribution in the Cd compound is clear from the way the theory drops below the experimental thermal conductivity at higher temperatures, while in the Zn material, the spin modes appear much more dominant.

## REFERENCES

1. K.J. Standley, *Oxide Magnetic Materials*, Oxford, 1962.
2. S.V. Vonsovskii, *Magnetism*, vol. 2, Wiley, 1974.
3. J.E. Thompson, *The Magnetic Properties of Materials*, Newnes, 1968.
4. L.D. Landau and E.M. Lifshitz, *Statistical Physics, Part 1*, Pergamon, 1980.
5. E.A. Turov, *Physical Properties of Magnetically Ordered Crystals*, Academic, 1965.
6. B.R. Patton, "Theoretical Spinel Studies V: Comparison with Experiment - Specific Heat", Progress Report - AFOSR Contract #F49620-83-C-0129.
7. B.R. Patton, "Theoretical Spinel Studies IV: Thermal Conductivity", Progress Report - AFOSR Contract #F49620-83-C-0129.
8. B.R. Patton, "Theoretical Spinel Studies II: Theoretical Models", Progress Report - AFOSR Contract #F49620-83-C-0129.
9. W.N. Lawless, "Spinel Studies I: Broad Temperature Range Thermal Measurements", "Spinel Studies VIII: Thermal Conductivities in Intense Magnetic Fields", and "Spinel Studies XIV: Careful Measurements of Thermal Conductivities in the Neighborhood of  $T_N$ ", Progress Reports - AFOSR Contract #F49620-83-C-0129.

## Appendix A

In this appendix we calculate the spin fluctuation scattering for a wider range of temperatures than in Report IV<sup>7</sup>. The contribution to the scattering is proportional to the fluctuations in the order parameter  $l$ , since the spin wave velocity depends on the stiffness of the magnetic order. From our earlier report, the spin wave fluctuation scattering rate is given by

$$\frac{1}{\tau_{fl}} = \frac{v}{\lambda_{fl}} \cong \frac{v}{a} \gamma_1^2 \left[ \frac{\delta l}{l} \right]^2 \quad (A1)$$

where  $\gamma_1$  is an effective Grüneisen constant. From the free energy for the antiferromagnetic state described in the second report<sup>8</sup> of this series we calculated the fluctuations in the order parameter  $l$

$$\langle |\delta l|^2 \rangle = \begin{cases} 3 \int \frac{k_B T}{\alpha + \xi^2 q^2} = 3k_B T (c_0 - c_1 \alpha^{1/2}) & T > T_N \\ \int \frac{k_B T}{2|\alpha| + \xi^2 q^2} = k_B T [c_0 - c_1 (2|\alpha|)^{1/2}] & T < T_N \end{cases} \quad (A2)$$

The result (A2) is valid only for  $c_1 |\alpha|^{1/2} \ll c_0$ , which is essentially equivalent to  $(T - T_N) \ll T_N$ . However, in comparing with experiment, a larger range of temperature is needed, namely,  $T \approx 2T_N$ . The difficulty with evaluating Eqs. (A2) is that in three dimensions the integrals are formally divergent. In fact, the Ginzberg-Landau theory has implicit in it a cutoff at length scales shorter than a distance of order  $\xi_0$ , the zero temperature coherence length. In order to obtain an proper expression for

the fluctuations, we introduce the cutoff  $R$  explicitly

$$\langle |\delta l|^2 \rangle = \begin{cases} 3 \int_0^R \frac{k_B T}{\alpha + \xi^2 q^2} \left[ \frac{R^2}{R^2 + \xi^2 q^2} \right]^2 & T > T_N \\ \int_0^R \frac{k_B T}{2|\alpha| + \xi^2 q^2} \left[ \frac{R^2}{R^2 + \xi^2 q^2} \right]^2 & T < T_N \end{cases} \quad (A3)$$

The form of the cutoff introduced in (A3) insures that  $\langle |\delta l|^2 \rangle \approx 1/\alpha$  as  $\alpha \rightarrow \infty$ , as it should. Carrying out the integrals gives

$$\langle |\delta l|^2 \rangle = \begin{cases} \frac{\pi^2}{\xi^3} \cdot \frac{3R^3}{(R + \sqrt{\alpha})^2} & \text{for } T > T_N \\ \frac{\pi^2}{\xi^3} \cdot \frac{R^3}{[R + (2|\alpha|)^{1/2}]^2} & \text{for } T < T_N \end{cases} \quad (A4)$$

Combining this equation with the expression for the scattering rate (A1) and writing the result in terms of the temperature and various fitting parameters gives Eq. (4), where we have imposed the requirement that the scattering rates approach the same limiting value at  $T_N$  from both above and below, which introduces a  $\sqrt{3}R$  in the denominator of (4a).

Table I. Theoretical Parameters Deduced From Experiment.

## A. From fits to the specific heat.

	$T_N$	$\alpha$	A	B	C	D	$\delta t$
$\text{CdCr}_2\text{O}_4$	8.05	.50	1.55	.25	.45	1	.0020
$\text{ZnCr}_2\text{O}_4$	10.75	.50	1.3	.35	.15	1	.0045

## B. From fits to the thermal conductivity.

	$a_1$	$a_2$	$a_3$	R
$\text{CdCr}_2\text{O}_4$	.0001	80	.70	.082
$\text{ZnCr}_2\text{O}_4$	.00001	17	.011	.12

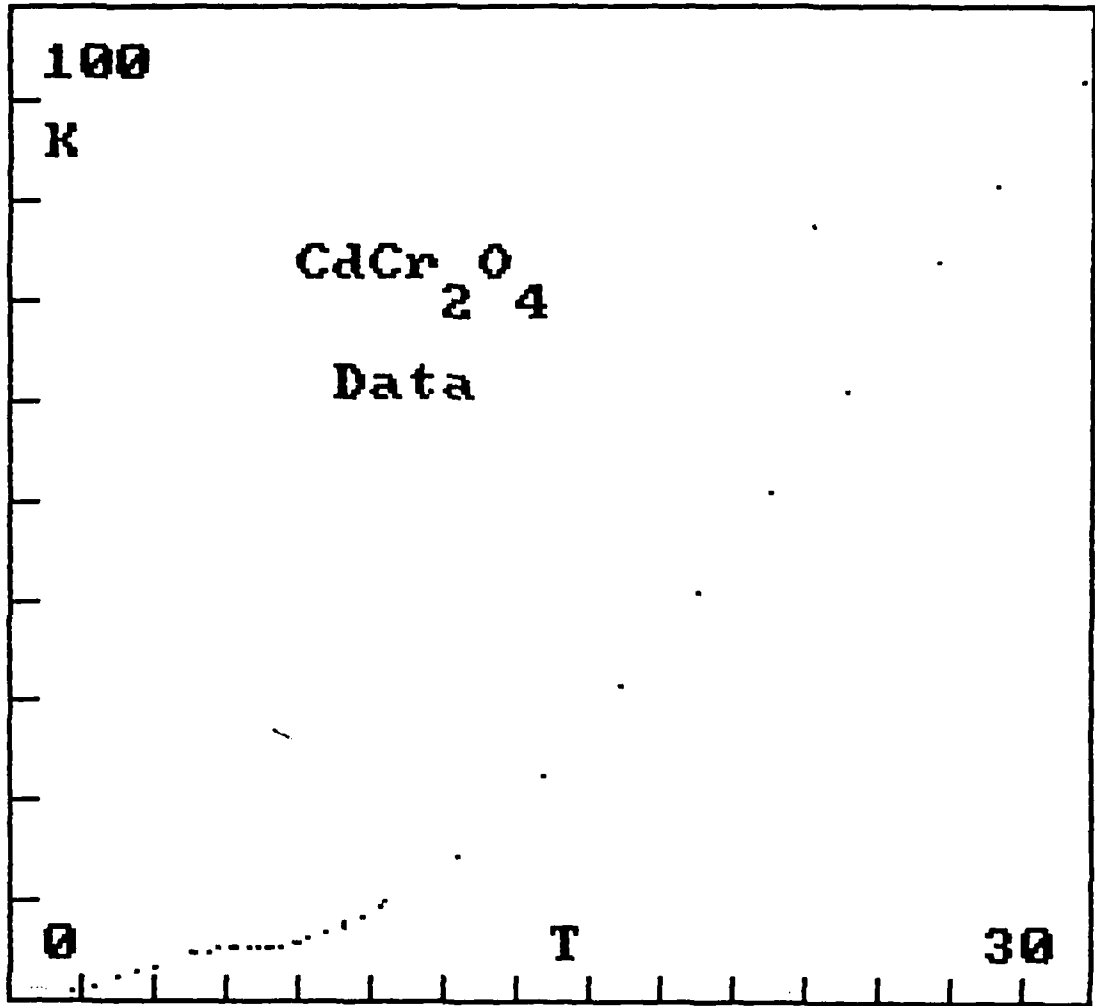


Fig. 1. Thermal conductivity data on CdCr<sub>2</sub>O<sub>4</sub>.

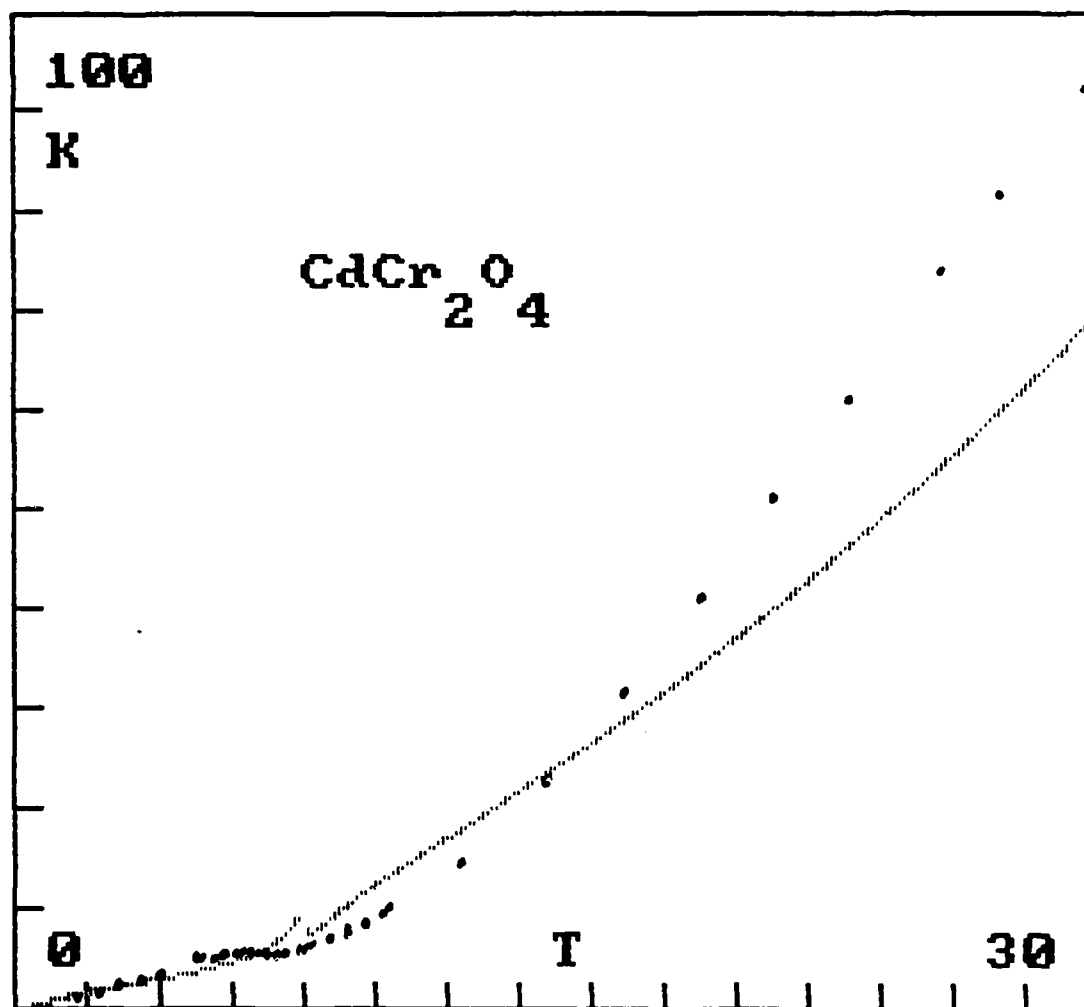


Fig. 2. Comparison of theory with thermal conductivity data on  $\text{CdCr}_2\text{O}_4$ .

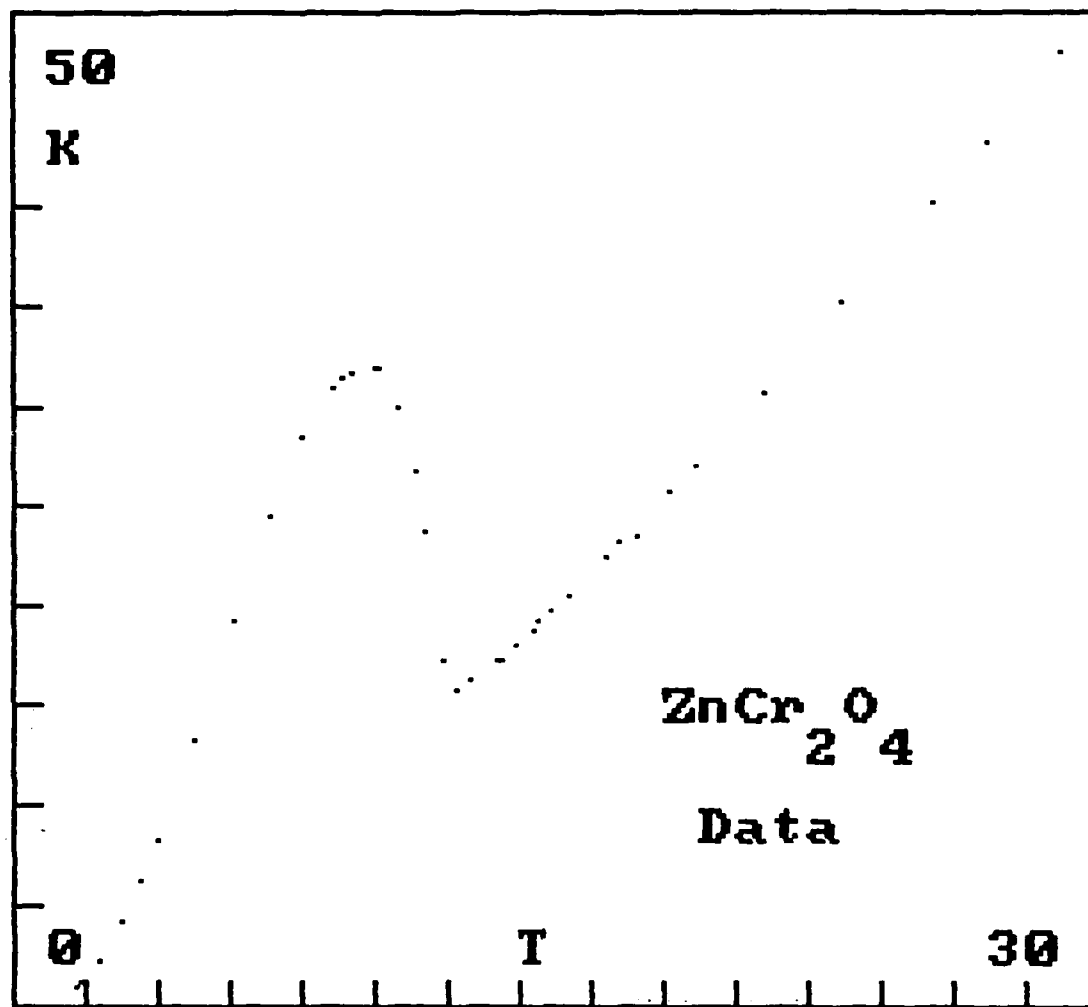


Fig. 3. Thermal conductivity data on  $\text{ZnCr}_2\text{O}_4$ .

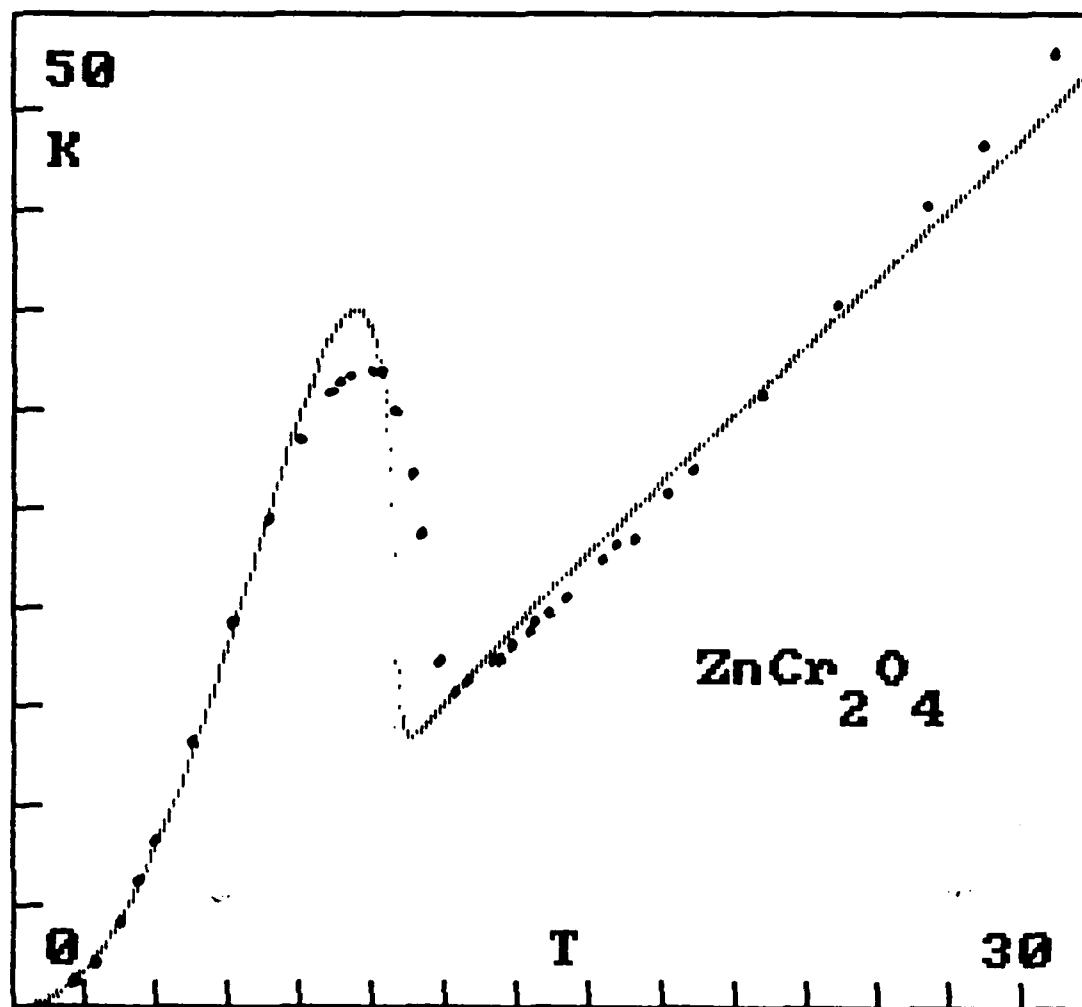


Fig. 4. Comparison of theory with thermal conductivity data on  $ZnCr_2O_4$ .

PROGRESS REPORT  
AFOSR Contract #F49620-83-C-0129  
Fundamental Physics on High-Specific-Heat  
Dielectrics and Kapitza Resistance at Dielectric Boundaries

H6-

Theoretical Research Program

Spinel Studies

VII. Impurity Models

by

Bruce R. Patton

B.R.P.

Department of Physics  
The Ohio State University  
Columbus, Ohio 43210  
September 7, 1985

## INTRODUCTION

In our previous reports on our research on the B-site spinels represented by cadmium chromite,  $\text{CdCr}_2\text{O}_4$ , and zinc chromite,  $\text{ZnCr}_2\text{O}_4$ , we analyzed the structure of the spinel lattice,<sup>1</sup> developed a theoretical model,<sup>2</sup> and calculated thermal<sup>3</sup> and transport<sup>4</sup> properties of the materials. In our last two reports, the theoretical calculations were compared with experimental data on the specific heat<sup>5</sup> and thermal conductivity.<sup>6</sup> In this report we extend the theory to include effects of doping impurities.

A number of interesting effects arise when impurities are substituted into the B-site spinel lattice. In the simplest picture substitution of a different spin in the lattice should change the magnetic transition temperature in proportion to the difference of its magnetic moment from the host lattice moment: a larger spin should increase the transition temperature, while a smaller moment should decrease it. Precisely the opposite result is found in Ceramphysics doping experiments<sup>7</sup>, indicating that a more complex situation exists. In this report we first consider the chemical and structural effects of various dopants, then examine the change the spin impurities induce in the complex ordering patterns of the B-site spinels, and finally develop a theory of the effect of substitutional impurities on the transition temperature which explains the drop in  $T_N$ .

## IMPURITIES IN THE SPINEL STRUCTURE

In our first report of our series on the theory of the B-site

spinel, the structure of the spinel class of ferrite materials was considered.<sup>1</sup> In particular, the two materials of interest in these studies, zinc chromite,  $ZnCr_2O_4$ , and cadmium chromite,  $CdCr_2O_4$ , were shown to fit into a pattern of magnetic and structural instabilities at low temperatures. We summarize briefly those conclusions as a starting point toward understanding the role of impurities. The metal ions may occupy two distinct types of sites in the spinel lattice, denoted by A and B as shown in Fig. 1.<sup>8</sup> When magnetic ions sit on both the sites, a strong interaction occurs between the two sublattice spins, of an antiparallel nature. This leads to a high temperature transition usually to a ferrimagnetic state; since the A and B sites are inequivalent, the moments on the A and B sites, although oppositely aligned, do not cancel completely.

The matter is rather different for the situation where the A site is occupied by the non-magnetic ion Zn or Cd.<sup>9</sup> In this case there is no large magnetic interaction between the A and B sites; instead a much weaker, right-angle bond between the magnetic ions on neighboring B sites is the dominant interaction. The B-site spinels are characterized by much lower magnetic instability temperatures of order 10 Kelvin due to the weaker interaction, and by the presence of "frustration" in the arrangement of bonds in the B sublattice. As shown in Fig. 2, frustration occurs because two neighbors of a given spin are also neighbors; all three spins cannot then be aligned in an antiparallel configuration. As a result there is a tendency for the lattice to distort in order to reduce the frustration and decrease the

energy. The spin ordering of the B-site spinels can therefore be very complex and is often coupled to a lattice transformation, giving rise in general to a very rich set of low temperature phenomena.<sup>1</sup>

The introduction of impurities into the spinel lattice has several consequences. The first question concerns the location of the iron ion. As noted in our first report,  $\text{CdCr}_2\text{O}_4$  and  $\text{ZnCr}_2\text{O}_4$  are both strong normal spinels; the  $\text{Cr}^{3+}$  ion with a  $d^3$  configuration has a major preference for the B site. An iron  $\text{Fe}^{3+}$  ion, however, with a  $d^5$  configuration, has a preference for a tetrahedral A site. Thus it is not clear where the iron ion actually goes in the doped materials, so we will consider the possibility of both the A and B sites. A major effect of the iron impurity, wherever it sits, is the introduction of a magnetic moment on the iron ion which is appreciably larger than that on the chromium ion. Table I gives the effective magnetic moments  $\mu_{\text{eff}}$  for a number of 3+ ions.

Ion	$\text{V}^{3+}$	$\text{Cr}^{3+}$	$\text{Mn}^{3+}$	$\text{Fe}^{3+}$	$\text{Gd}^{3+}$
$\frac{\mu_{\text{eff}}}{\mu_B}$	2.8	3.7	5.0	5.9	8.0

Table I. Effective Experimental Magnetic Moments<sup>10</sup>

We consider the modifications introduced by the impurities to

the microscopic Hamiltonian which describes the interaction between the spins on various sites. A Cr spin on a B site  $i$  is denoted by  $s_i$ , while a Fe spin on a site  $j$  which may be either an A or a B site is labeled  $S_j$ . From the diagram of the spinel structure shown in Fig.1, it is clear that the interaction between two neighboring B-site spins occurs via superexchange through the A ion. Since this B-A-B bond forms a  $90^\circ$  angle, the magnitude of the interaction is very weak. However, the angle between an A and a B site is  $135^\circ$ , resulting in a much larger interaction. Thus the interaction  $J_{ij}$  between the Cr spins is always weak, while the size of the Cr-Fe spin interaction  $I_{ij}$  depends crucially on where the Fe spin is located. If the Fe ion is on a B site, the magnitude of  $I_{ij}$  should be comparable to  $J_{ij}$ . The hamiltonian with impurity spins included thus has the form

$$H = \sum J_{ij}^{\alpha\beta} s_{\alpha i} s_{\beta j} + \sum I_{ik}^{\alpha\beta} s_{\alpha i} S_{\beta k} \quad (1)$$

where the Greek indices denote Cartesian coordinates  $x, y, z$ , while the indices  $i$  and  $j$  run over B lattice sites,  $k$  over either A or B sites depending on the location of the Fe impurities, and repeated indices are summed over. We have not included direct Fe-Fe interactions, since we are assuming the concentration of Fe is low.

We now examine the connectivity of the lattice sites that are coupled by (1). Fig. 2 gives a topological representation of the B lattice sites of the host lattice. Considering first the case where an iron ion goes into a B site, we see that the result is that a large spin replaces a Cr one at the corner of one of the

coupled tetrahedra. The iron ion interacts with the spins in each of the two tetrahedra that it is connected to. The spins in each tetrahedra are coupled antiferromagnetically to each other, the primary source of the frustration in this lattice. However, if the iron goes into an A site, then the large interaction with the B-site Cr spins insures that all the Cr spins align antiferromagnetically with respect to the Fe spin, thus removing frustration within the tetrahedron.

The simplest mean field argument says that the transition temperature, to whatever kind of magnetic order, occurs for

$$k_B T_c \approx Z \cdot \langle J_{ij} s_i s_j \rangle \quad (2)$$

where  $Z$  is the number of nearest neighbors of a spin. Although not always quantitatively accurate, this equation often gives the correct qualitative result, for example, the drop in  $T_c$  in a diluted spin lattice. For our problem, this mean field argument predicts that if the Fe goes into B sites and the Fe-Cr interaction is comparable in magnitude to the Cr-Cr interaction, then  $T_c$  would go up because the spin moment of Fe is almost twice as large as that of Cr (Table I). The fact that this does not happen indicates that more complex phenomena are involved. The main thing neglected in the above argument is the role of frustration in the ordering.

It appears likely that the Fe goes into the B sites, otherwise the large exchange interaction between the A-B sites would give an increase in  $T_N$ , or a transition to some other kind of magnetic state at a temperature of order hundreds of degrees

or more. Considering the Fe on the B site then, we calculate the lowest energy configuration for an Fe ion surrounded by two neighboring tetrahedra of Cr spins as shown in Fig. 3. Denoting the Cr-Cr interaction energy by  $E_0 = Js^2$ , and the Cr-Fe energy by  $E_1 = IsS$ , an undoped crystal has the lowest energy for two up and two down spins in each tetrahedra, with a total energy  $E = -4E_0$ . With the iron substituted, that configuration energy becomes  $E = -2E_0 - 2E_1$ . Since  $S > s$ , from Table I, then  $E_1 > E_0$ . However, if the Cr-Fe interaction is large enough, the energy may instead be minimized by aligning all the Cr spins antiparallel to the Fe spin, a state which has an energy  $E = -6E_1 + 6E_0$ . This second configuration has a lower energy if  $E_1 \geq 2E_0$ . Using the values in Table I gives  $E_1 \approx 1.6E_0$ , indicating that the host spin configuration remains preferred, but that the second configuration is close enough to it in energy to contribute possible destabilizing fluctuation effects.

#### GINZBERG-LANDAU THEORY OF DISORDER

As discussed above, the insertion of a larger spin into the spinel lattice serves to polarize the surrounding spins. Since the large spin does not fit into the natural antiferromagnetic order of the lattice without leaving its moment partially uncanceled, the net effect is to produce a local net magnetization; the antiferromagnet has locally been converted into a ferrimagnet, with incomplete cancellation of the sublattice magnetizations. From the point of view of our Ginzberg-Landau hamiltonian, the  $Fe^{3+}$  impurity act like a local

contribution to the magnetization order parameter  $m$ , which interacts with the antiferromagnetic order parameter  $l$  primarily involved in the transition. We recall the free energy introduced in our second report,<sup>2</sup> which involves the two order parameters, the antiferromagnetic combination,  $l_\alpha = \sum_{i,j} (M_{i\alpha} - M_{j\alpha})$ , summed over all pairs of oppositely ordered sublattices,  $i$  and  $j$ , and the total magnetization  $m_\alpha = \sum_i M_{i\alpha}$ :

$$F = \int d^3r \cdot \left[ \alpha |l|^2 + \frac{\beta}{2} |l|^4 + \delta |\nabla \cdot l|^2 + a |m|^2 + \frac{b}{2} |m|^4 + \Gamma |l|^2 |m|^2 - m \cdot H \right] \quad (3)$$

where  $l$  denotes the antiferromagnetic order parameter which becomes finite below  $T_N$ , and  $\alpha = \alpha_0 \cdot (T - T_N) / T_N$ . The coefficients  $\beta$  and  $b$  are positive for stability, while  $a$ , unlike  $\alpha$ , remains positive at all temperatures since no spontaneous magnetization occurs. The coupling  $\Gamma$  is the interaction between the two vector order parameters  $l$  and  $m$  and, from the discussion in the preceding section, represents the destabilizing effect of paramagnetic fluctuations on the antiferromagnetic spin ordering.

We examined the mean field solutions for the order parameters obtained by setting the variation of the functional (3) with respect to  $l$  and  $m$  equal to zero

$$\frac{\partial F}{\partial l} = 0 = \alpha l + \beta |l|^2 l + \Gamma |m|^2 l \quad (4a)$$

$$\frac{\partial F}{\partial m} = 0 = a m + b |m|^2 m + \Gamma |l|^2 m - H \quad (4b)$$

For weak coupling  $\Gamma$  and zero magnetic field the solutions were:

$$m_0 = 0 \quad \text{for } H = 0 \text{ and } \Gamma \geq 0 \quad (5a)$$

$$l_0 = \begin{cases} 0 & \text{for } \alpha > 0 \quad (T > T_N) \\ \left[ \frac{-\alpha}{\beta} \right]^{1/2} & \text{for } \alpha < 0 \quad (T < T_N) \end{cases} \quad (5b)$$

$$(5c)$$

The addition of  $\text{Fe}^{3+}$  impurities gives rise to a local value of  $m$ , even though the thermal average of  $m$  remains zero,  $\langle m \rangle = 0$ , because, on average, the impurity spin moments, randomly located in the lattice, have no net long range orientational order. However, the square average  $\langle m^2 \rangle$  is finite. The equation for  $l$  then becomes

$$0 = \alpha l + \beta |l|^2 + \Gamma \langle |m|^2 \rangle l \quad (6)$$

where

$$\langle |m|^2 \rangle = c [S - s]^2 \quad (7)$$

where  $c$  is the concentration of  $\text{Fe}^{3+}$  spin impurities, and  $S$  is the  $\text{Fe}^{3+}$  spin moment and  $s$  the  $\text{Cr}^{3+}$  moment. Solving Eq. (5) for the sublattice magnetization  $l$  gives

$$|l|^2 = \frac{-\alpha - \Gamma \langle |m|^2 \rangle}{\beta} \quad (8)$$

which is valid for  $\alpha + \Gamma \langle |m|^2 \rangle \leq 0$ . The transition temperature  $T_N$  is given by the requirement that  $l$  just vanish, which occurs for

$$\alpha = -\Gamma \langle |m|^2 \rangle \quad (9)$$

which may be rewritten in the more revealing form

$$\begin{aligned} \frac{T_N - T_{No}}{T_{No}} &= - \frac{\Gamma}{\alpha_o} c \langle [S - s]^2 \rangle \\ &= - \frac{\Gamma \mu_B^2}{\alpha_o} (5.9 - 3.7)^2 c \end{aligned} \quad (10)$$

where we have inserted the experimental values for the effective 3+ ion magnetic moments from Table I. The striking thing about Eq. (10) is that the change in  $T_N$  depends linearly on the concentration (for small concentration) and that the sign of the effect depends on the sign of the interaction  $\Gamma$ .

In Fig. 4 we have plotted Eq. (10) against the data<sup>7</sup> on the suppression of  $T_N$ . From the experimental slope, we may extract the value of  $\Gamma \approx 1.9 \cdot \alpha_o / \mu_B^2$ , a value which is reasonably large indicating a strong interaction between the ferromagnetic and antiferromagnetic ordering. A drop in  $T_N$  as seen in the doping experiments<sup>7</sup> clearly means that  $\Gamma$  is positive, a result which is consistent with the value of  $\Gamma$  needed to fit the specific heat in our fifth report.<sup>5</sup> Another interesting feature is that the transition extrapolates to zero around an impurity concentration of 10%, a value at which the nearest neighbor tetrahedra of Fig. 3 would begin to have two  $Fe^{3+}$  impurities present. Thus complete disruption of the antiferromagnetic order of the host corresponds to the onset of direct Fe-Fe interactions, and presumably another type of magnetic phase.

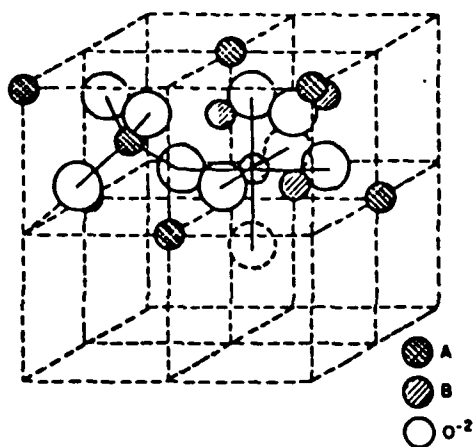
#### SUMMARY

The comparison of our disorder theory with experiment is

satisfactory and gives an explanation for the puzzling feature of a larger spin causing a drop in the transition temperature. The rich spin ordering properties of these spinels are clearly responsible for the complex behavior observed in the experimental work under this contract. However, further work would be of interest in order to understand the precise mechanism for the effect on the transition temperature, for example, whether the transition temperature could be raised by reducing the frustration in the lattice through impurities with smaller spins or through stabilization of lattice distortions.

## REFERENCES

1. B.R. Patton, "Theoretical Spinel Studies I: Structural Studies", Progress Report - AFOSR Contract #F49620-83-C-0129.
2. B.R. Patton, "Theoretical Spinel Studies II: Theoretical Models", Progress Report - AFOSR Contract #F49620-83-C-0129.
3. B.R. Patton, "Theoretical Spinel Studies III: Thermal Properties", Progress Report - AFOSR Contract #F49620-83-C-0129.
4. B.R. Patton, "Theoretical Spinel Studies IV: Thermal Conductivity", Progress Report - AFOSR Contract #F49620-83-C-0129.
5. B.R. Patton, "Theoretical Spinel Studies V: Comparison with Experiment - Specific Heat", Progress Report - AFOSR Contract #F49620-83-C-0129.
6. B.R. Patton, "Theoretical Spinel Studies VI: Comparison with Experiment - Thermal Conductivity", Progress Report - AFOSR Contract #F49620-83-C-0129.
7. W.N. Lawless, "Spinel Studies XIII: Doping Studies", "Spinel Studies XI: Fe<sup>3+</sup> Doping in C(9/1)--Specific Heat Measurements", and "Spinel Studies XVI: Fe<sup>3+</sup> Doping in C(9/1)--Thermal Conductivity Measurements", Progress Reports - AFOSR Contract #F49620-83-C-0129.
8. K.J. Standley, *Oxide Magnetic Materials*, Oxford, 1962.
9. S.V. Vonsovskii, *Magnetism*, vol. 2, Wiley, 1974.
10. N.W. Ashcroft and N.D. Mermin, *Solid State Physics*, Holt, Rinehart, and Winston, 1976, p. 657-8.



Two octants of the spinel unit cell. A ions are on tetrahedral sites and B ions on octahedral sites of the O<sup>2-</sup> anion packaging.

Fig. 1. Spinel Lattice Structure

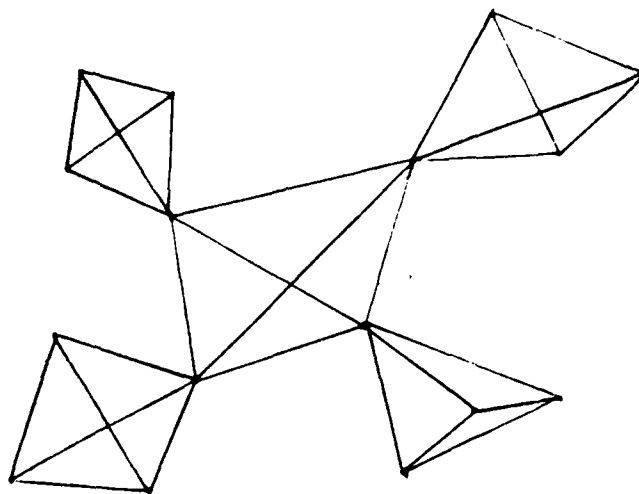
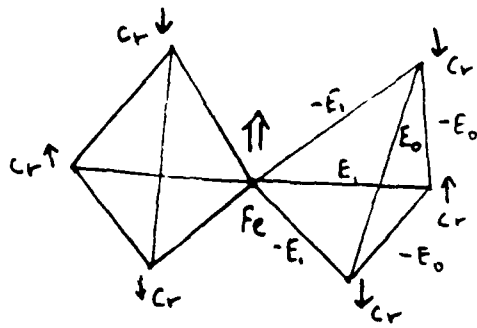
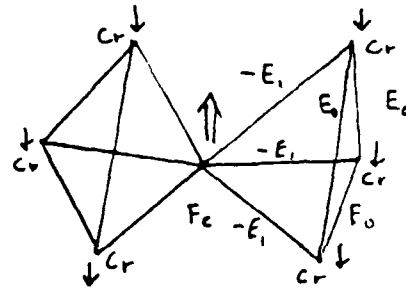


Fig. 2. Topological structure of spin interactions on B sites of spinel lattice.



$$E = -2E_1 - 2E_0$$



$$E = -6E_1 + 6E_0$$

Fig. 3. Impurity spin configurations.

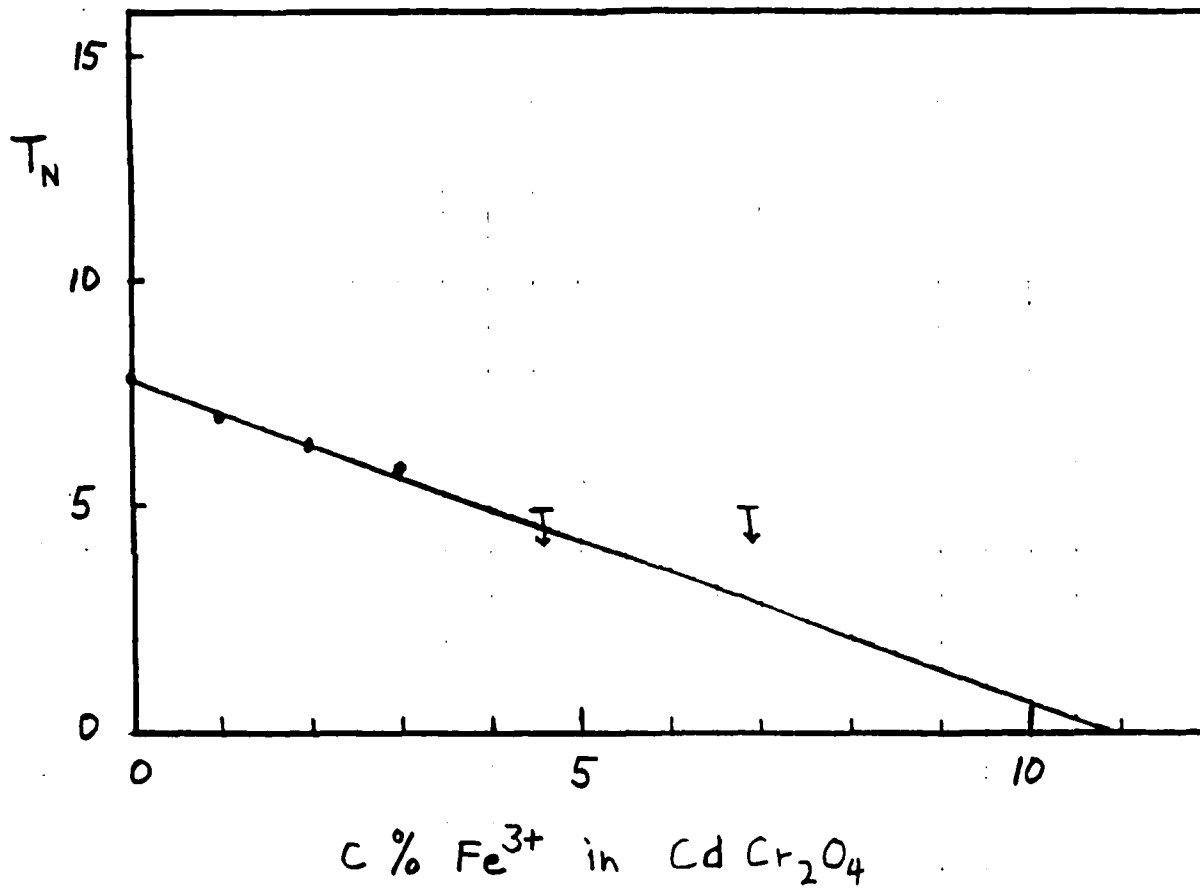


Fig. 4. Suppression of  $T_N$  with  $\text{Fe}^{3+}$  doping concentration in  $\text{CdCr}_2\text{O}_4$ .

END

DTIC

9-86